Surface Science Reports 66 (2011) 185–297

Contents lists available at ScienceDirect

Surface Science Reports

journal homepage: www.elsevier.com/locate/surfrep

A surface science perspective on TiO_2 photocatalysis

Michael A. Henderson *

Institute for Interfacial Catalysis, Pacific Northwest National Laboratory, P.O. Box 999, MS K8-87, Richland, WA 99352, United States

ARTICLE INFO

Article history:
Received 9 February 2010
Accepted 25 January 2011
editor: W.H. Weinberg

Keywords:
TiO_2 photocatalysis

ABSTRACT

The field of surface science provides a unique approach to understanding bulk, surface and interfacial phenomena occurring during TiO_2 photocatalysis. This review highlights, from a surface science perspective, recent literature that provides molecular-level insights into photon-initiated events occurring at TiO_2 surfaces. Seven key scientific issues are identified in the organization of this review. These are: (1) photon absorption, (2) charge transport and trapping, (3) electron transfer dynamics, (4) the adsorbed state, (5) mechanisms, (6) poisons and promoters, and (7) phase and form. This review ends with a brief examination of several chemical processes (such as water splitting) in which TiO_2 photocatalysis has made significant contributions in the literature.

Contents

* Tel.: +1 509 371 6527; fax: +1 509 371 6242.
E-mail address: ma.henderson@pnl.gov.

0167-5729/$ – see front matter © 2011 Elsevier B.V. All rights reserved.
doi:10.1016/j.surfrep.2011.01.001

0. Introduction

Interest in TiO_2-based photocatalysis has been remarkable since Fujishima and Honda's first reports in the early 1970's of UV-induced redox chemistry on TiO_2 [1]. Recently, Fujishima et al. [2] highlighted the astonishing number of publications involving heterogeneous photochemical studies (in general) and those specifically involving TiO_2. As shown in Fig. 2.4 of their 2008 Surface Science Reports review, the number of publications have increased dramatically over the last decade to the extent that of the ~2400 heterogeneous photochemistry papers published in 2008, roughly 80% involved TiO_2-based materials! This remarkable level of publication activity reflects the potential for new applications emerging from research in this field. Numerous reviews exist on the subjects of: **heterogeneous photochemistry** [3–12], and **TiO_2-based photochemistry** [2,13–42] that blend in chemistry, physics and engineering perspectives to the field. There are reviews involving the role of TiO_2-based materials in such subjects as: **photocatalytic water splitting and hydrogen production** [3,10,43–60], **photoelectrochemistry** [58,61–63], **dye sensitization and solar energy conversion** [46,64–77], **reactor design and process kinetics** [7,78–80], and **photochemical air and water treatments** [13,20,48,81–96]. Most TiO_2 photocatalysis reviews adopt an application-driven perspective, but a few approached the field from a **surface science perspective**. As examples of the latter, the Yates group, drawing from their extensive work in the field, has published several reviews [97–100] that focus on molecular-level

List of acronyms and symbols

2PPE	two photon photoemission
A	anatase
AFM	atomic force microscopy
ATR	attenuated total reflectance
B	brookite
CB	conduction band
CT	charge transfer
DFT	density functional theory
DOS	density of states
DSSC	dye sensitized solar cell
e^-/h^+	electron–hole pair
EDTA	ethylenediaminetetraacetic acid
EELS	electron energy loss spectroscopy
EMA	effective mass approximation
EPR	electron paramagnetic resonance
ESR	electron spin resonance
EXAFS	extended X-ray absorption fine structure
FTIR	Fourier transform infrared spectroscopy
HOMO	highest occupied molecular orbital
HREELS	high resolution electron energy loss spectroscopy
HRTEM	high resolution transmission electron microscopy
IEP	isoelectric point
IPA	isopropyl alcohol
IPS	inverse photoemission spectroscopy
IR	infrared
LDA	local density approximation
LUMO	lowest unoccupied molecular orbital
m_0	electron rest mass
m_e	electron effective mass
m_h	hole effective mass
MBE	molecular beam epitaxy
MD	molecular dynamics
ML	monolayer
N_{int}	interstitial N
N_{sub}	substitutional N
NEXAFS	near-edge X-ray absorption fine structure
NMR	nuclear magnetic resonance
NRA	nuclear reaction analysis
O_{vac}	oxygen vacancy
OH_{br}	bridging OH group
OH_t	terminal OH group
OPAMBE	oxygen plasma assisted MBE
P-25	Degussa P-25, mixed anatase and rutile commercial TiO_2 standard
PED	photoelectron diffraction
PSD	photon stimulated desorption
QMMD	quantum mechanical molecular dynamics
R	rutile
RH	relative humidity
RHEED	reflection high energy electron diffraction
SEM	scanning electron microscopy
SFG	sum frequency generation
SHG	second harmonic generation
STM	scanning tunneling microscopy
TCE	trichloroethylene
TEM	transmission electron microscopy
TMA	trimethyl acetate
TMAA	trimethyl acetic acid
TOF	time of flight
TPD	temperature programmed desorption
UHV	ultrahigh vacuum
UPS	ultraviolet photoelectron spectroscopy
UV	ultraviolet
UV–vis	ultraviolet–visible optical absorption spectroscopy
VB	valence band
XANES	X-ray absorption near-edge structure
XAS	X-ray absorption spectroscopy
XES	X-ray emission spectroscopy
XPS	X-ray photoelectron spectroscopy
XRD	X-ray diffraction
⟨abc⟩	family of vectors equivalent to the [abc] vector
[abc]	specific crystal vector
{abc}	family of surfaces equivalent to that defined by the normal vector [abc]
(abc)	specific surface termination defined by the vector [abc]

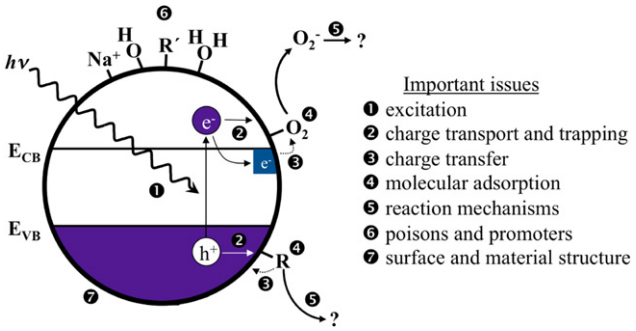

Fig. 1. Schematic model illustrating the seven fundamental issues associated with TiO_2 photocatalysis addressed in the review.

phenomena occurring as a result of photon irradiation of TiO_2 single crystal surfaces. In these reviews, Yates and coworkers explored the relationships between a surface's properties (e.g., reactivity, structure, electronic properties, etc.) and various observed photochemical events (e.g., O_2 photodesorption). This approach allows the researcher to understand and control for many variables (such as coverage, surface structure, temperature, etc.) while examining in detail various fundamental aspects of photon-initiated events. The surface science approach typically utilizes well-defined materials (e.g., single crystals) and ultrahigh vacuum (UHV) techniques to understand physical and chemical phenomenon occurring at interfaces. It is the aim of this review to motivate readers to approach the subject of TiO_2 photocatalysis from the same perspective.

The structure of this review was developed using an expanded version of the common TiO_2 photocatalysis cartoon shown in Fig. 1. This cartoon shows a TiO_2 nanoparticle with superimposed on it a simple electronic structure of the TiO_2 valence band (VB) states, the conduction band (CB) states and the bandgap. The cartoon illustrates seven key issues (labeled 1 through 7) that will be considered in discussing the fundamental processes important to TiO_2 photocatalysis. The first of these is photon absorption (Section 1). Much effort has been aimed at understanding and altering the optical properties of TiO_2, particularly for enhancing visible light absorption. In contrast, much less is known about the optical properties of TiO_2 *surfaces* or about how alterations of bulk optical properties affect surfaces. The second issue involves the behaviors of charge carriers after their creation (Section 2), in particular how these carriers reach surfaces and what happens to them there prior to being involved in transfer chemistry. Since the essential characteristic of TiO_2 photocatalysis is the electron transfer event, the third subject is dedicated to reviewing various electron transfer processes at TiO_2 surfaces (Section 3), with the focus on the dynamics of single electron transfer events. In order for electron transfer to occur, donor and acceptor molecules must approach the TiO_2 surface, and in many cases, become

chemisorbed (Section 4). The binding site, structure and stability of these molecules set the stage for electron transfer and the desired catalytic behavior of the TiO_2 surface. The mechanistic aspects of coupling sequential, single electron transfer events with thermal reaction steps to constitute a catalytic process involving both redox half reactions is the focus of the fifth topic (Section 5). Just as in thermal heterogeneous catalysis, the presence of poisons, promoters and spectators can have important influences on TiO_2 photocatalysis, so the sixth topic (Section 6) will review how these additives affect the electron transfer and catalytic aspects of TiO_2 photocatalysis. Finally, TiO_2 photocatalysts are not, as the cartoon in Fig. 1 might imply, round balls devoid of surface (or bulk) structure. Section 7 will review literature that illustrates how the phases and forms of TiO_2 surfaces impact chemical and electron transfer processes occurring during photocatalysis. In conclusion, Section 8 will take a brief look at several TiO_2 photochemical applications from a surface science perspective.

1. Photon absorption

The photon absorption step in a photocatalytic reaction typically is viewed as a bulk (i.e., subsurface) process. However, two issues make this topic relevant to surfaces. First, as a consequence of lattice truncation and formation of surface 'dangling' bond states, the electronic structures of surfaces are distinctly different than those of the bulk. Unique excitation events can arise from surface states or surface charge transfer complexes. Second, surface photon absorption processes can provide significant contributions to the overall photon absorption capacity of a TiO_2 nanoparticle. For example, with a nominal radius of ~3–4 nm, the ratio of 'surface' atoms to 'bulk' atoms in a TiO_2 nanoparticle in on the order of 1 in 10. In this situation, the surface region of a TiO_2 nanoparticle could account for ~10% (or more) of the optical absorptivity of the material.

1.1. Pure TiO_2

The bulk optical properties of TiO_2 anatase (A) and rutile (R) are well-documented in the literature [101–107]. Insights into the optical absorptivity of TiO_2 have been obtained from a variety of optical techniques, including photoconductivity and photoacoustic spectroscopy [108–113]. The absorption thresholds of TiO_2 are well-known (see below), however the maxima in the bulk optical absorption spectra of A and R are not frequently discussed. The lowest photon energy at which the greatest probability exists for generating charge carriers can be visualized as the coupling of the highest density of states (DOS) near the VB maximum with the highest DOS near the CB minimum. This point occurs at ~4.0 eV for both polymorphs of TiO_2 [106,107,114].

It is generally held that in the bulk limit, the bandgaps in A and R are indirect and direct, respectively. Recent measurements [101,115,116] concur with past analyses that the energies for these transitions are at ~3.2 and 3.0 eV, respectively. The threshold for the direct bandgap transition in A is reported to be at ~3.8–4.0 eV [115,117]. As shown by Tang and coworkers [114,118, 119], the absorption behavior of A at threshold exhibits Urbach behavior, where the absorption coefficient increases exponentially with increasing photon energy (at all temperatures). In contrast, the absorption coefficient of R increases more-or-less linearly above the threshold. The optical absorption edges decrease with increasing temperature for both polymorphs (see Fig. 1.1). Tang et al. have shown that the dichromic behavior of A (i.e., the difference in the absorption properties perpendicular to versus parallel to the *c*-axis) increases with increasing temperature, but disappears in R as room temperature is approached. These authors attribute these differences to excitonic states in A being 'self-trapped' whereas those in R are considered 'free'. Although the reason for this difference is not clear, the authors proposed it likely has to due with structural differences between A and R, in particular that the R unit cell is neighbored by 10 other unit cells whereas it is only neighboring by 8 in A. Based on first-principle plane wave calculations, Asahi et al. [120] concluded that the optical anisotropy in the absorption cross section of A at onset was due to the presence of a significant contribution from the non-bonding d_{xy} orbitals at the bottom of the A CB which are preferentially oriented perpendicular to the *c*-axis in A. These observations regarding the bulk absorptivity of TiO_2 sets the stage for considering how surfaces alter the absorptive properties of TiO_2. This subject will be continued in Section 7, where surface electronic structure measurements and theory in the literature reveal differences between the surfaces of A and R that impact photon absorption.

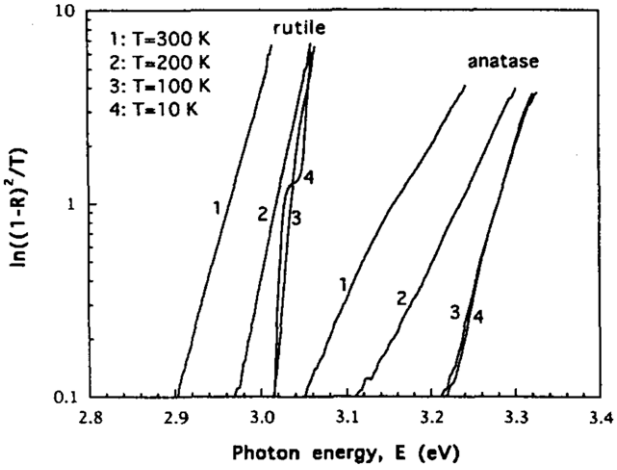

Fig. 1.1. The optical absorption onsets (plotted on a log scale) versus photon energy for anatase and rutile crystals at 4 different sample temperatures. 'R' signifies the fraction reflected and 'T' the fraction transmitted.
Source: From Tang et al. [114].

In contrast to A and R, the optical properties of brookite (B) are not well-understood, primarily because of the lack of reliable samples on which to work. As an example of optical absorptivity work being done on B, Zallen and Moret [121] indicate that mineral samples of B are always colored (in contrast to pure A or R which are nearly colorless), possessing an indirect bandgap of ~1.9 eV. The low bandgap for this B sample was likely due to the presence of impurities. Koelsch et al. estimated the B bandgap to be ~3.8–4 eV based on measurements of synthetic particles [122].

1.2. Nanoscaled TiO_2

Numerous groups [113,123–135] have observed or proposed that quantum confinement in TiO_2 nanoparticles in the <10 nm size range results in a blueshift of the absorption threshold as the particles become more 'molecular' in character. For example, Fig. 1.2 from the work of Satoh et al. [124] shows blueshifting in the absorption thresholds of TiO_2 nanoparticles as the centroid of the particle size distribution was decreased (through synthetic means) from ~2.8 nm (blue trace) to ~1.9 nm (red trace) to ~1.5 nm (green trace). (The inset shows the thresholds in electron volts.) Similar effects have been seen in TiO_2 materials that would not normally be considered for quantum confinement. Lee et al. [126], and Enright and Fitzmaurice [127] have each reported absorption blueshifts in TiO_2 films composed of nanoparticles, despite the many particle interconnections that one might expect to negate true quantum confinement. Similarly, Joo et al. [128] proposed

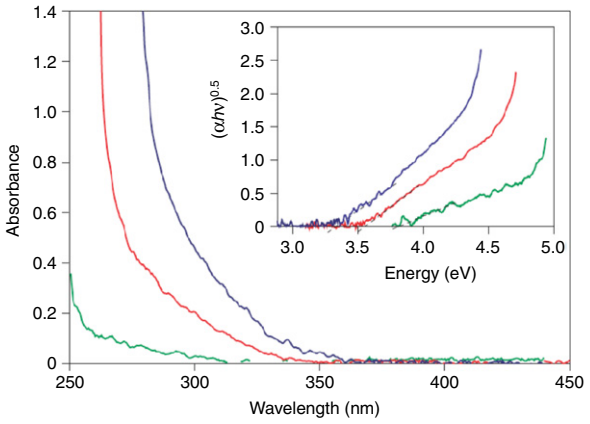

Fig. 1.2. Optical absorption measurements of three size distributions (peaked at ∼2.8 nm (blue) to ∼1.9 nm (red) to ∼1.5 nm (green)) for hydrolyzed TiO_2 nanoparticles. (For interpretation of the references to color in this figure legend, the reader is referred to the web version of this article.)
Source: Reprinted by permission from Satoh et al. [124].
© 2008, Macmillan Publishers Ltd. Nature Nanotechnology.

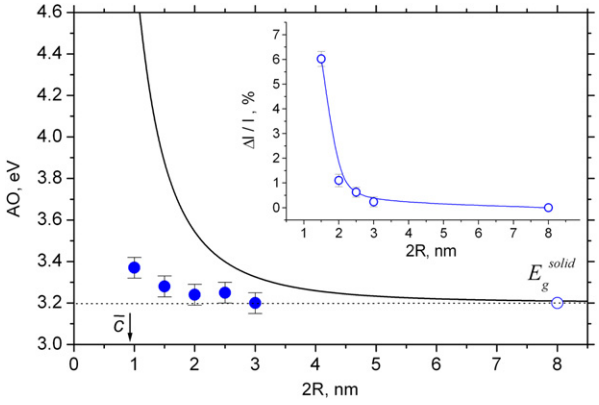

Fig. 1.3. The optical absorption onset energy for anatase nanoparticles (circles) as a function of particle size. The solid curve represents a theoretical assessment based on the EMA, and the dashed line is the bulk bandgap value. The inset shows the relative change of the (101) lattice constant with particle size.
Source: From Monticone et al. [137].

that an increase in the bandgap of ∼0.13 eV resulted from the nanoscaled lateral dimensions of A nanorods, despite the fact that the dimension along the rods was well outside the scale for quantized behavior.

There have been attempts to model the effect of nanoscaling on the optical properties of TiO_2. Qu and Kroes [123] used density functional theory (DFT) to calculate an increase in the effective bandgap in $(TiO_2)_n$ clusters as n was decreased from 9 (3.84 eV) to 1 (4.89 eV). Satoh et al. [124] observed blueshifts in the absorption threshold of A with decreasing particles sizes below 2 nm that matched their calculations based on the effective mass approximation (EMA), with values for the electron effective mass obtained from the literature. (See Section 2 for details on the EMA.) In contrast, Serpone et al. [136] did not observe blueshifting for nanoscaled A particles down to 2 nm. These authors proposed that the blueshifts observed below 2 nm were due instead to changes from indirect to direct bandgap excitation as their A particles became smaller and geometric distortions in the coordination spheres of Ti became more prevalent. In agreement with these conclusions, Monticone and coworkers [137] examined the optical properties of small A nanoparticles as a function of a tight particle size distribution controlled by varying the concentration of acetylacetone (as binder) during preparation. As shown in Fig. 1.3, these authors observed little or no blueshift for particles with diameters ("2R") ≥2 nm and only slight blueshifting (≤0.2 eV) for particles ≤1 nm. Their data did not fit the EMA (using literature values for the electron and hole effective masses). Instead, the significant changes that they observed in the oscillator strengths of optical transitions in the 3.5–4.5 eV range with decreasing particle size were attributed to increased lattice strain in the particles arising from nanoscaling. These authors argued that the EMA becomes invalid when the electronic structure of TiO_2 departs from a band structure model (in this case, when at the nanoscale).

1.3. Surface absorption effects

This section attempts to address how the optical absorption properties can be influenced by surfaces. However, in most cases, surface photon 'absorptivity' and how it can be altered (e.g., by doping) can only be inferred based on bulk studies. In order to fully understand the potential involvement of TiO_2 surfaces in absorbing light, one should have an understanding of the electronic structures of those surfaces (see Section 7).

1.3.1. Surface states

Absorptivity at TiO_2 surfaces may be altered from that of the bulk in terms of changes in transition energies and/or oscillator strengths of transitions due to formation of surface states. Truncation of a bulk lattice invariably results in the formation of new electronic states associated with surface reconstructions or surface dangling bonds that are different from those in the bulk. The extent to which surface states resulting from these 'non-bulk-like' structures play a role in the light absorption properties of TiO_2 is unclear. Kobayashi et al. [138,139] proposed the latter based on second harmonic generation (SHG) and sum frequency generation (SFG) to explore the optical properties of the R TiO_2(110) surface. These authors observed variations in the angular dependence of the SHG signal as a function of photon energy and polarization that indicated strong anisotropic optical absorptivity and energy dependence in the electronic states of this surface (Fig. 1.4). The angular dependence and polarization behaviors were significantly different above and below the near-threshold photon energy region (∼3.5 eV) suggesting the presence of surface states near the threshold. These results support the notion that surface states on well-ordered TiO_2 surfaces (such as the R TiO_2(110) surface) may provide unique, non-bulk-like optical properties for TiO_2. This supposition is also supported by work on the prototypical Degussa P-25 (hereafter referred to as P-25). Hurum et al. [140] proposed that interfacial states between A and R may be responsible for the appearance of photochemical "hot spots" in mixed A + R materials (like P-25) leading (for example) to visible light excitation.

1.3.2. Surface modification

Numerous groups have shown that the optical properties of TiO_2 can be altered by surface modifiers. In most cases, modification of the optical properties of TiO_2 results simply from inclusion of the optical transitions of the surface modifier; however, in other cases the electronic states of TiO_2 can be affected by the modifier. For example, when the TiO_2 surface is decorated with: UV/vis-active oxides (such as WO_3 [141–144], SnO_2 [145], and Fe_2O_3 [146] among many), metal clusters (such as Ag [147–152], Au [153–157] or Pt [154,158–162]) possessing visible light active plasmonic transitions, or certain molecules (such as sensitizing dyes [163–166], stearic acid [167] or chlorophenols [168–172]) in which charge transfer (CT) states are generated from adsorption. The case of chlorophenols provides an example of how the absorptive properties of TiO_2 surfaces can be modified by molecular adsorption. In Fig. 1.5, Kim and Choi [168] show that new excitations result from the creation

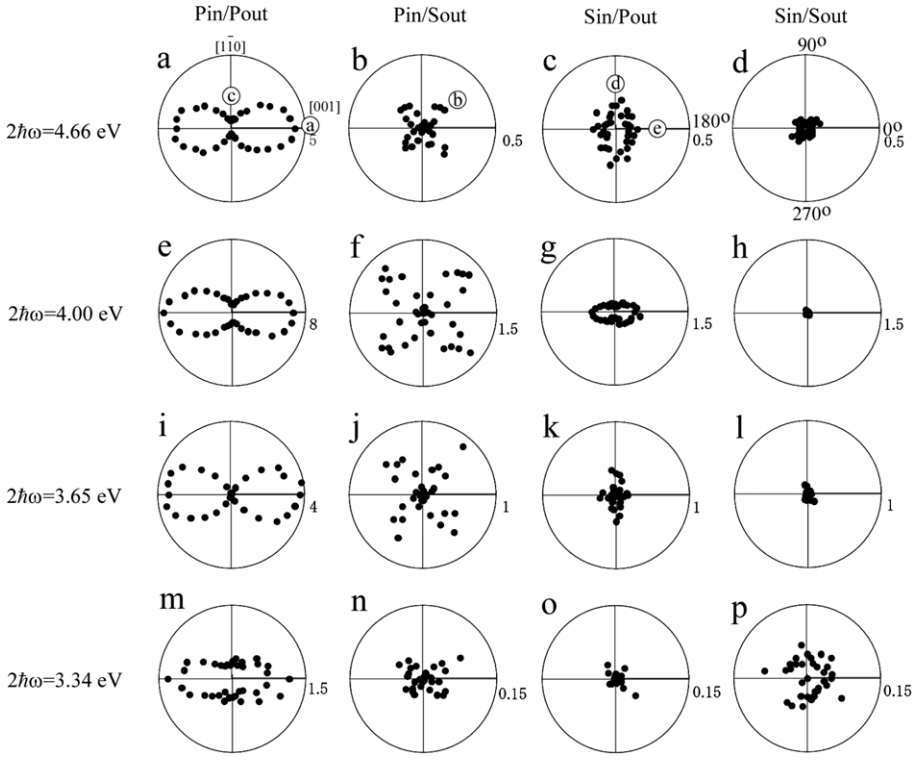

Fig. 1.4. The azimuthal angle dependence of the second harmonic intensity from rutile TiO_2(110) at 4 fundamental photon energies in various combinations of 'P/S-in' and 'P/S-out' polarization configuration.
Source: From Kobayashi et al. (139b).

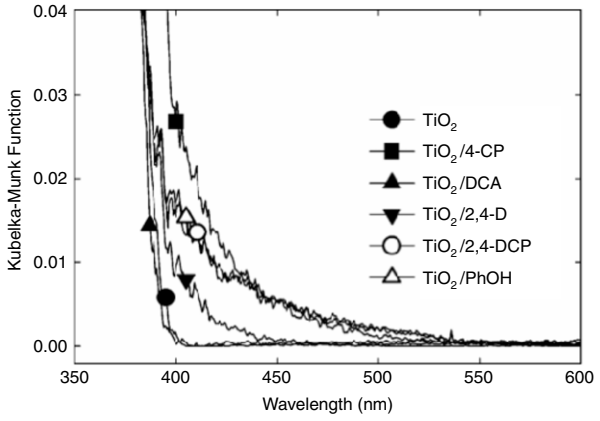

Fig. 1.5. Diffuse reflectance UV–vis absorption spectra of various charge transfer molecules (4-CP = 4-chlorophenol; DCA = dichloroacetate; 2,4-D = 2,4-dichlorophenoxyacetate; 2,4-DCP = 2,4-dichlorophenol; PhOH = phenol) adsorbed on anatase TiO_2 powder.
Source: Adapted with permission from Kim and Choi [168].

of charge transfer states during adsorption of various phenolic compounds on TiO_2. In each case, the authors found that charge carriers were generated from excitation of these charge transfer states. In contrast, adsorbed dichloroacetate (DCA in Fig. 1.5) did not produce a new CT state (at least not in the visible) and it did not undergo any detectable visible light photochemistry.

1.3.3. Doping

In the context of this section, doping involves inclusion or substitution of a foreign atom into the TiO_2 lattice in such a way as to induce new electronic states and new optical transitions not seen in pure TiO_2. There is much ambiguity in the literature with regard to the atomic-level details of doping, particular as to where the limits of solubility lie for a particular dopant state (e.g., substitutional or interstitial) and what changes occur in the optical properties when the limits are crossed. The degree of 'local' versus 'extended' influence of a dopant also plays a role in the optical properties of TiO_2 and the 'usefulness' of the resulting charge carriers [173,174]. Few TiO_2 studies have been able to specify the dopant location in and impact on the TiO_2 lattice with a high degree of certainty, what the dopant spatial distributions are, and how dopants alter the physical and electronic structures of TiO_2. Most studies focus on how dopant preparation methods affect the photochemical behavior of some reaction. There is also considerable uncertainty in many studies as to whether the dopant resides in the TiO_2 bulk or surface (or both). Some surface studies have utilized photoemission techniques to examine how adsorbates (e.g., organics or noble metals) affect the VB states of TiO_2 single crystal surfaces [175], however little is known about how optical transitions are affected. As a consequence, the discussion here will focus broadly on the issue of bulk doping with the hope of stimulating surface science studies aimed at understanding surface doping as well.

Self-doped TiO_2 (reduced)

The most common example of doping in TiO_2 involves self-doping. In both A and R, self-doping is n-type, resulting from a stoichiometric imbalance in which oxygen is lost and reduced cation sites are incorporated into the lattice [176–183]. Conceptually, this imbalance can manifest itself in several ways, for example, formation of isolated point defects such as oxygen vacancies or titanium interstitials, or formation of networks of such point defects. Bulk defects in TiO_2 appear to result in occupied gap states located below the CB edge that are predominately Ti 3d related. There appear to be no examples of p-type self-doping in A or R in which

unoccupied VB states are seen to form in the bandgap as a result of deviations from the ideal TiO_2 stoichiometry.

The blue color in reduced TiO_2 is derived from optical absorption in the near-IR region of the visible spectrum resulting from excitation events associated with Ti^{3+}-related bulk defects. Efforts to calculate the absorption spectra of Ti^{3+} sites in bulk TiO_2 have been few (as an example, see work of Lin et al. [184] for oxygen vacancies in A). Khomenko et al. [185] have examined the optical transitions and electron paramagnetic resonance (EPR) properties of reduced R single crystals. These authors detected optical transitions in reduced samples between 0.75 and 0.9 eV which were assigned to excitations of Ti^{3+} sites via small polaron electron transfer processes. These authors also observed much weaker transitions between 2.3 and 2.9 eV which they assigned to d–d transitions associated with Ti^{3+}. Their EPR results showed multiple Ti^{3+} states, but the most intense signals resulted from interstitial Ti^{3+} sites. These results suggest that the main sub-bandgap optical transitions in reduced TiO_2 result from localized excitations of Ti^{3+} (i.e., from localized to localized states). The lifetimes of these excitation states are not known, but are believed to be very short-lived. In contrast to localized excitations of Ti^{3+}, some groups envision optical excitations of Ti^{3+} centers to involve transitions into the TiO_2 CB (i.e., from localized to delocalized states). For example, Komaguchi et al. [186] proposed that visible light excitation of Ti^{3+} was associated with transitions of localized electrons at Ti^{3+} sites into the TiO_2 CB (which should be EPR-silent) because the EPR signal corresponding to Ti^{3+} in reduced P-25 disappeared at 77 K when exposed to sub-bandgap light but reappeared when the light was turned off.

The presence of reduced cation sites at the surface (or near-surface region) of TiO_2 offers the potential for new optical excitation events that may result in new avenues of photochemistry. Several groups have observed visible light photoactivity for slightly reduced TiO_2 materials [187–191]. For example, Martyanov et al. [191] found that near-stoichiometric TiO_2 prepared by oxidation of TiO or Ti_2O_3 was able to photocatalyze acetaldehyde oxidation with visible light. Similarly, Justicia et al. [188–190] found that sub-stoichiometric A films exhibited visible photoactivity for methylene blue degradation. These authors attributed the observed photoactivity directly to excitation of Ti^{3+} sites. They also proposed that sub-stoichiometry in A changes the bandgap of this material from indirect to direct, and increases the absorptivity at threshold.

While the most well-characterized TiO_2 single crystal surface, that of the R TiO_2(110) surface, is known for the chemical properties of its 'sub-stoichiometric' defects (i.e., oxygen vacancy sites [175]), there are no published accounts of visible light photocatalysis on this surface resulting from excitations of these defects. However, two groups have observed transient signatures for excitation of electrons in defect states on the TiO_2(110) surface, in both cases using two photon photoelectron spectroscopy (2PPE). Petek's group [192–197] has shown that excitations of occupied gap states in the R TiO_2(110) surface (i.e., oxygen vacancy sites) are too short-lived to measure, but become longer lived (>10 fs) when the surface is covered with protonic solvents (such as H_2O or CH_3OH). This effect was not observed if the surface was oxidized prior to water adsorption (see Fig. 1.6). As shown in Fig. 1.7, the intensity and temperature dependence of the 2PPE signal from the vacancy excited state correlated with the H_2O (or CH_3OH) coverage suggesting to the authors an excited state that involved solvent-like behavior (i.e., a "wet electron" state). The lifetime of this intermediate excited state was longer in the case of CH_3OH (>30 fs) than for H_2O (<20 fs). These data suggest that excitations of surface electronic defect states should play a part in affecting the dynamics of electronic states at TiO_2 surfaces during photocatalysis. Similar observations have been made with 2PPE studies of reduced TiO_2(110) by Ino et al. [198], although these authors did not conduct time-resolved measurements.

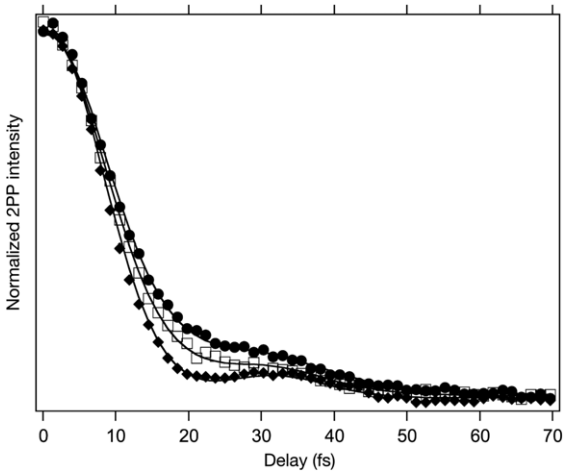

Fig. 1.6. Signals from 2PPE as a function of time delay between excitation and ionization pulses for the reduced R TiO_2(110) surface (solid diamonds), this surface exposed to 0.7 L H_2O (open squares) and 1.6 L H_2O (solid circles) at 100 K. Solid lines represent fits to the decay signal. (1 L = 1×10^{-6} Torr s).
Source: From Onda et al. [194]. Reprinted with permission from AAAS.

The 2PPE technique provides useful information regarding the surface initial state and the dynamics of the initial excitation event (when used in a time-resolved fashion); it does not, however, provide a spectrum of initial excitation events unless a tunable 'pump' excitation source is utilized. Surface electron energy loss spectroscopy (EELS) [199–202] provides spectral information regarding surface electronic excitations similar to what is seen in bulk studies using other energy loss approaches (e.g., from electron transmission imaging; see work of Khomenko et al. [185]). In the scattering mode, the EELS technique preferentially detects optical transitions available at the surface. Fig. 1.8(a) shows the EELS spectrum for the reduced R TiO_2(110) surface (possessing ~8% oxygen vacancies). Band-to-band transitions are evident at energies above 3 eV, with a peak at slightly above 4 eV (consistent with optical absorptivity results; see above). The most prominent feature in the spectrum is that of the Ti^{3+} excitation feature at ~0.8 eV (~1550 nm) associated with surface oxygen vacancy sites. The energy of this transition is consistent with what is seen from optical (UV–vis) measurements of reduced TiO_2 powders (see Section 2.4). Section 5 provides more details on the reactivity of oxygen vacancy sites on the R TiO_2(110) surface to molecules like O_2 (Fig. 1.8(b)–(d)), and Section 7 delves into the electronic structure of these sites. (For example, see work by Komiyama and Li [203,204].)

Cation-doped TiO_2

Studies that examine the photochemical properties of cation-doped single crystal TiO_2 surfaces are few (as an example, see the work of Bechstein et al. [205,206]). Studies on cation doping of powdered TiO_2 surfaces are more abundant. Many groups have examined how cation doping shifts the TiO_2 absorption properties into the visible. A variety of metals on TiO_2 have been explored, including: Fe [207–216], Cr [41,212–222], V [212,213,215,216,223–226], Ni [213,216,227], Nb [107,213,219,228], Na [229], Mn [212], Cu [216,230], Al [231] and Co [215,216]. Taking Cr^{3+} as an example, the Anpo group ([41] and references therein) has shown that cation doping of TiO_2 results in both visible light absorptivity (see Fig. 1.9) and photoactivity toward NO. The latter was only observed for TiO_2 samples doped by ion implantation and not for those whose surfaces were chemically doped with Cr^{3+}. This suggests that the chemical and/or structural environments of the Cr^{3+} dopant will impact its utility as a promoter of visible light activity

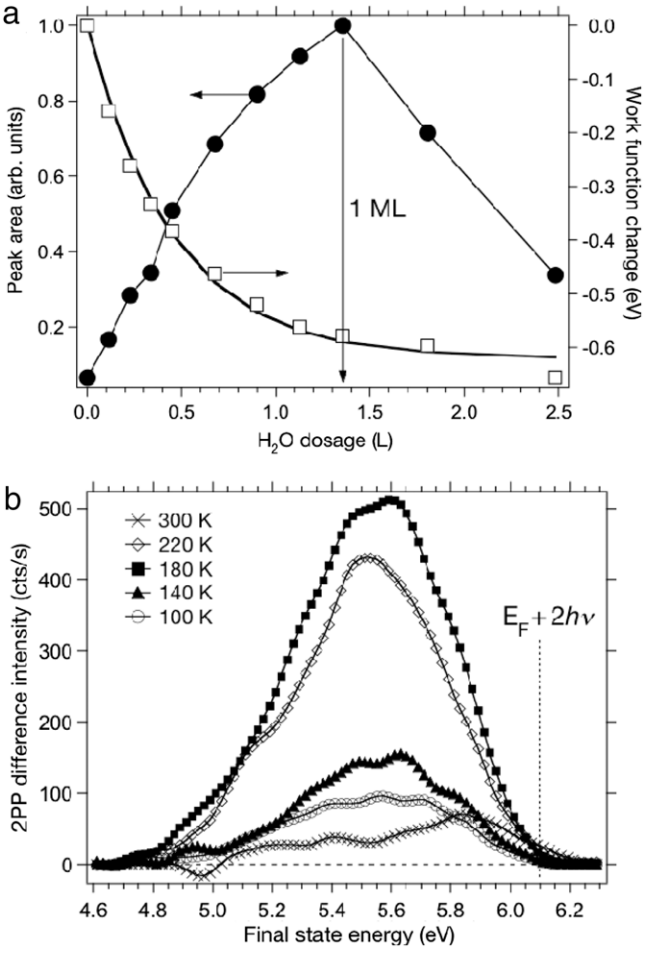

Fig. 1.7. (a) Integrated signals from 2PPE (solid circles) and work function change (open squares) as a function of water exposure on the reduced R TiO_2(110) surface. The approximate exposure point corresponding to 1 ML is indicated. (c) 2PPE difference spectra for a 1.35 L H_2O exposure at 100 K followed by various heating treatments. (1 L = 1×10^{-6} Torr s and 1 ML = 5.2×10^{14} cm^{-2}).
Source: From Onda et al. [194]. Reprinted with permission from AAAS.

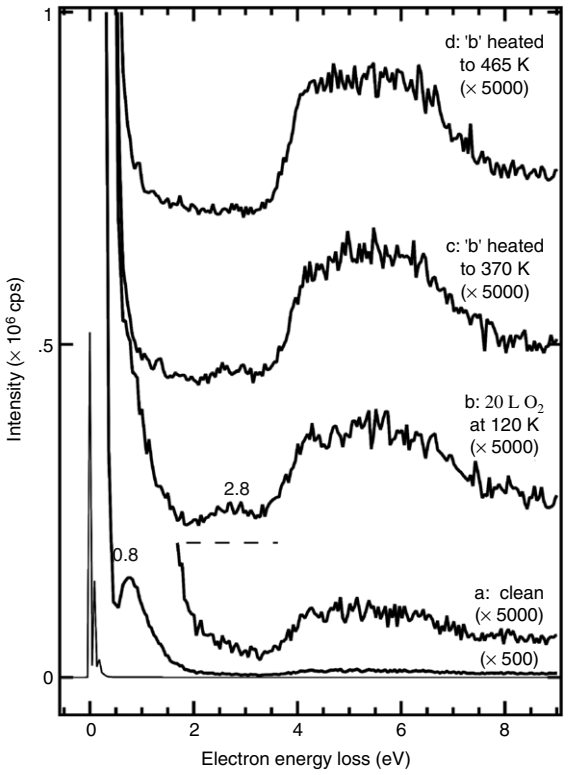

Fig. 1.8. EELS spectra from the reduced R TiO_2(110) surface (a), followed by exposure to 20 L O_2 at 120 K (b), and heated to 370 K (c) and 465 K (d). (1 L = 1×10^{-6} Torr s).
Source: Reprinted with permission from Henderson et al. [200].
© 1999, American Chemical Society.

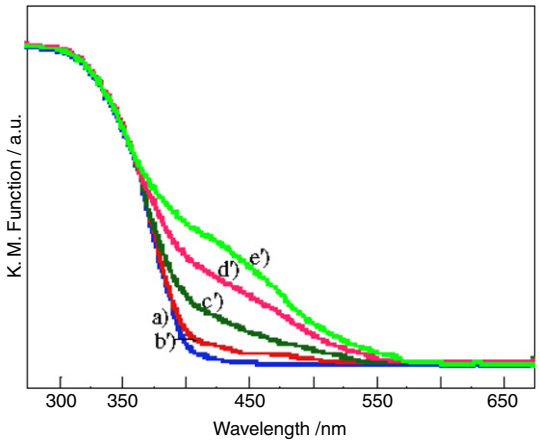

Fig. 1.9. UV–vis absorption spectra for TiO_2 (a) and for various weight percent levels of Cr^{3+} ion doped into TiO_2 (b': 0.01, c': 0.1, d': 0.5, e': 1). A 0.1 wt% equals ~4.9 μmol/g − TiO_2.
Source: From Iino et al. [41].

in TiO_2. Based on DFT calculations for substitutional Cr doping in bulk R, Umebayashi et al. [232] proposed that visible excitations should result from either excitation of TiO_2 VB electrons into unoccupied Cr mid-gap states (labeled 'c' in Fig. 1.10) or from excitation of partially filled Cr mid-gap states ('c') into the TiO_2 CB ('d'). These authors proposed that the position of the dopant's t_{2g} state in the R lattice's octahedral field (for substitutional 1st row metal cation dopants) is key to whether optical transitions result from the dopant into TiO_2 states or from TiO_2 states into the dopant. While both types of transitions may occur using visible light, both do not have the same potential for redox. In contrast, V dopant states were located near the CB edge (labeled 'a' and 'b' in Fig. 1.10) so transitions from the TiO_2 VB to unoccupied V states are likely. Excitations of mid-gap for Mn and Fe dopant states to the TiO_2 CB should be important. (Metals such as Co and Ni which have t_{2g} states at the top of TiO_2 VB may not exhibit much visible activity.)

Aside from the studies of the Anpo group, several other groups suggest that visible excitations in Cr-doped TiO_2 can promote surface photochemistry. For example, Zhu et al. [221] prepared Cr^{3+} doped A (by sol–gel methods) that absorbed in the visible. This photocatalyst exhibited enhanced photodegradation in the UV for an azoic yellow dye, as well as activity in the visible. Similarly, Lee and coworkers [213] observed redshifted absorption thresholds for A sol gels doped with Cr^{3+}, Ni^{2+} and Fe^{3+}. These also showed greater activity in the visible than pure TiO_2 for CH_3OH photodecomposition, although pure A outperformed all doped samples in the UV. Surface complexes of Cr^{6+} on P-25 have shown visible activity in promoting 4-chlorophenol oxidation not seen with other high valent cations (e.g., Cu^{2+}, Fe^{3+}, Mn^{4+}, Ce^{4+} or V^{5+}) according to Sun et al. [233]. However, the authors concluded that these photoreactions were not catalytic.

In contrast, other groups have not observed that visible light absorptivity in metal-doped TiO_2 translated into photochemistry. For example, Salmi et al. [214] used transient absorption spectroscopy to study Cr- and Fe-doped A. These samples showed longer lived trapped holes than for undoped A, but increased hole lifetimes did not result in increased UV photoactivity for either acetaldehyde or

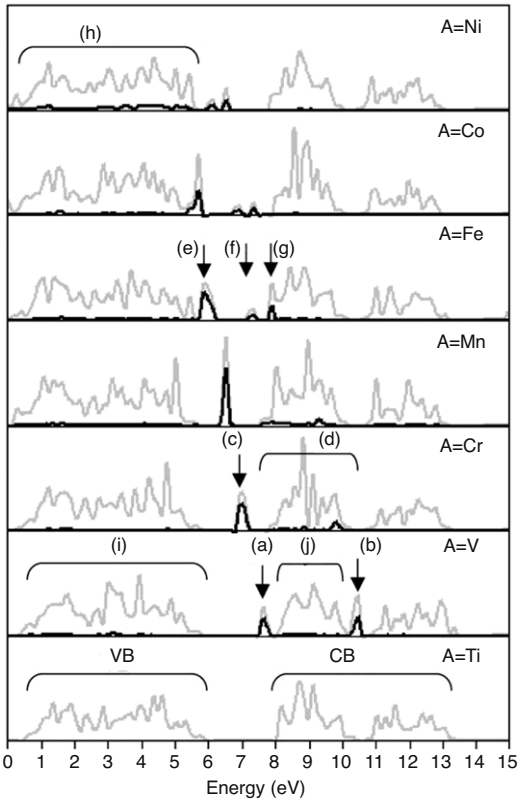

Fig. 1.10. Calculated DOS for various substitutionally doped cations in the R TiO_2 lattice. The black traces represent the portion of the DOS due to the cation dopant. VB and CB regions are labeled on the relative energy scale.
Source: From Umebayashi et al. [232].

toluene photooxidation. Similarly, Gracia et al. [215] observed redshifts in the absorption thresholds with Cr, V, Fe and Co doping, but no enhancement in photocatalytic activity for these doped samples over pure TiO_2. They also detected evidence for metal oxide segregation on TiO_2 after annealing, which suggests that bulk doping with these cations was susceptible to thermal degradation.

According to Choi and coworkers [216], the optimum dopant concentration balances the ability of these centers to act as traps for effective charge separation with the adverse tendency of these sites to also promote charge recombination. The dopants most active for redshifting TiO_2 photochemistry into the visible were those with open shells, whereas no photochemical benefit was derived from closed shell cation dopants. These conclusions were reached by examining a wide variety of metal cation dopants at 0.1–0.5 at.% concentrations in 2–4 nm sized TiO_2 colloidal particles using transient absorption spectroscopy as a diagnostic. Some cation dopants (such as Fe^{3+} and TV^{4+}) exhibited much longer lived carrier lifetimes than in undoped TiO_2, whereas other cations (e.g., Al^{3+}) resulted in shorter lifetimes.

Anion-doped TiO_2

There has been an explosion of papers in the literature on anion-doping of TiO_2 since Asahi and coworkers' 2001 *Science* report of visible light activity in nitrogen-doped TiO_2 [234]. By far, the most extensively studied anion dopant has been N [184,191,229,234–322], but other anion dopants (e.g., C [191,234,245,246,254,305,314,315,323–336], S [234,237,245,246,261,305,335,337–347], halides [272,278,348–355], P [234,337,356] and B [357–359]) have also been examined, both experimentally (references above) and theoretically [184,229,234,236,249–251,258,260,272,276,278,283,288,298,305,306,309,310,314,320,325,334,337,338,343,348,357,358]. The general idea is that anions which are less electronegative than O, when substitutionally doped into the lattice will have some of their valence p-states pushed up out of the TiO_2 VB into the bandgap. The question as to whether these new gap states are localized or are part of the VB structure remains unresolved [174]. The issue of how non-substitutional anion dopant behave also remains an important issue.

Fujishima et al. [2] have briefly described some of the preparation methods and general characteristics of anion-doped TiO_2, so these will not be repeated here. It should be emphasized that doping preparation methods (in general) are very diverse, ranging from dry methods (e.g., ion implantation or incomplete oxidation of Ti nitrides, carbides, etc.) to wet methods (e.g., sol–gel synthesis). There is, at present, little understanding of how these preparation methods produce consistency in the characteristics of the doped material. (This statement applies equally to cation doping of TiO_2, discussed above.) Discussion from this point will center on N-doped TiO_2 because of the greater amount of attention paid to this anion dopant.

As mentioned above, Asahi et al. [234,236] were the first to synthesize high surface area N-doped TiO_2 (mixed A + R) and to study its properties for visible light photochemistry. These authors sputter-deposited TiO_2 in Ar/N_2 gas mixtures and observed a redshift in the optical absorption spectrum of the resulting films. Based on theory (see below) and a 396 eV X-ray photoelectron spectroscopy (XPS) feature in the N 1s region, they assigned the N dopant to a substitutional site. These films exhibited methylene blue decolorization and acetaldehyde photooxidation in visible light. There have been many subsequent reports of N-doped TiO_2 powders or films exhibiting activity in the visible. For example, Wang et al. [304] prepared N-doped A by wet methods that absorbed in the visible but had a N 1s feature at ~400 eV (instead of ~396 eV) that was stable up to 400 °C, but largely disappeared after 600 °C. Their N-doped A promoted photooxidation of phenol in the visible under aqueous conditions. Joung et al. [267,268] prepared N-doped A by annealing pure TiO_2 in an NH_3 gas stream. XPS showed a N 1s feature at 400 eV and a Ti 2p region resembling pure TiO_2 (i.e., with little or no Ti^{3+}), although EPR was able to detect Ti^{3+} spins and no N-related spins. Their N-doped A absorbed light in the visible and promoted trichloroethylene (TCE) photodegradation in the visible. Other examples of visible light activity for N-doped TiO_2 can be gleaned from the extensive list of papers cited above.

While a variety of techniques have been employed to characterize the N dopant in high surface area TiO_2 samples, at present the most commonly used diagnostic tool for characterizing the state of the dopant is XPS. In general, groups have assigned the dopant's site location based on this technique, where features at ~396 eV are attributed to substitutional N and features at ~400 eV are due to interstitial N [282]. Features above 400 eV are typically attributed to either embedded N_2 or to nitrate/nitrite species. These assignments are by no means firm in the literature, as will be discussed below. Also, the concentration and preparation method dependences leading to these different N 1s features have not been well-established.

Confusion about the photochemical properties of different forms of N in high surface area TiO_2 is compounded by observations in which N-doping does not lead to visible light photochemistry. For example, Irie et al. [264] observed a N 1s feature at 396 eV and absorption at wavelengths greater than 400 nm for N-doped TiO_2 prepared heating the pure phase in NH_3 gas. While these samples exhibited visible activity for isopropanol photooxidation, the relative quantum efficiencies were lower for visible light irradiation of the N-doped samples than was observed for band-to-band excitation (see Fig. 1.11). The quantum efficiencies also decreased as the N concentration was increased suggesting to the authors that N centers in TiO_2 acted not only as light-absorbing centers but also as charge recombination sites. Lower quantum

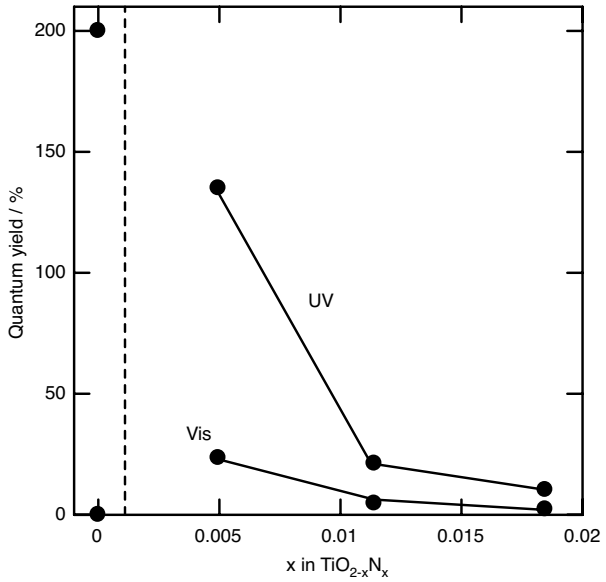

Fig. 1.11. Quantum yields for isopropanol photodecomposition using visible and UV light as a function of nitrogen–dopant level in TiO_2.
Source: Reprinted with permission from Irie et al. [264].
© 2003, American Chemical Society.

yields relative to UV values were also obtained from visible light photooxidation of CO over N-doped TiO_2 prepared by wet methods [294]. The assertion that N dopants act as recombination centers was also offered by the Hoffmann group [238] based on a comparison of formate photodecomposition on N-doped and undoped A. The same group [285] raised an additional issue of concern regarding N-doping. These authors prepared N-doped A through wet ($N(C_2H_5)_3 + Ti(i\text{-}OC_3H_8)_4$) and dry (powder treated with NH_3 at 550 °C) methods, both of which absorbed visible light. However, neither sample promoted photooxidation of formate or ammonium ions in the visible. These authors concluded that the oxidative power of holes trapped at dopants were noticeably less than those thermalized to the VB edge in pure TiO_2. Dopant-trapped holes were unable to oxidize (by direct or indirect means) adsorbates whose donor levels were at or below the VB maximum. Consistent with this conclusion, Fu et al. [259] used EPR data to propose that many examples of visible light photodecomposition of organics on N-doped TiO_2 actually proceeded via electron-mediated reactions involving O_2^- and not through holes generated at N dopant sites. (What happened to the trapped holes in this case was a mystery.) More than likely, as Mrowetz and coworkers suggest, there are some adsorbate-to-hole electron transfer events that would normally proceed with VB holes but not with N dopant holes.

Finally, Tachikawa et al. [35,300] used time-resolved diffuse reflectance (pump pulse in the UV or visible followed by probe pulse at 700 nm) to study photodecomposition of ethylene glycol on pure and N-doped A prepared by dry methods. (See Section 2 for a discussion of wavelengths for the transient probing of holes versus electrons in photoexcited TiO_2.) N dopant concentrations ranged from 0.2% to 0.7% based on the intensity of the N 1s feature at 396 eV in XPS. These authors found evidence in their transient signal decays for hole transfer to ethylene glycol after a 355 nm pump of undoped TiO_2, with the same occurring for N-doped A except that the transient signals were much weaker. As expected, there was no evidence for hole transfer (or electron trapping) with the 460 nm pump on undoped A, but only weak signals were detected for N-doped A. These latter signals were ascribed to hole trapping at dopant sites. Nevertheless, the authors observed visible light activity for ethylene glycol photodegradation over anion-doped TiO_2 *and* hole trapping in their transient spectra. Based on these results, Tachikawa et al. proposed that UV photodegradation of ethylene glycol occurred via both electron and hole pathways, but that the degradation observed via visible light irradiation of anion-doped TiO_2 occurred predominately via reactive species generated in the reduction half reaction, in agreement with the conclusions of Fu et al. [259]. A synopsis of these effects is shown in Fig. 1.12 from the work of Tachikawa and coworkers.

Based on these high surface area TiO_2 studies, it would appear that more information is needed regarding the physical and chemical state of N dopants generated by various preparation methods. Direct correlations between the optical properties of these forms of N dopants and electron transfer reactions occurring at the surfaces of N-doped TiO_2 are also needed. These needs have spawned studies examining N-doping of TiO_2 from more fundamental perspectives. For example, the first theoretical examinations of N-doped TiO_2 were conducted by Asahi et al. [234]. These authors obtained DOS information from linearized augmented plane wave calculations in the local density approximation (LDA). These calculations indicated that anion dopant levels for substitutional N, C, S and P occurred, just above the O 2p-dominated VB, whereas F 2p states resided within the energy range of the O 2p VB. These observations are consistent with the electronegativities of the various anions relative to that of O. More recently, Di Valentin and coworkers [249] employed spin-polarized DFT to calculate the electronic structures of substitutional N in A and R. In the absence of charge compensation from a donor state, they predicted that substitutional N^{2-} would result in an apparent redshift in the absorption threshold of A, with N states residing at top of VB, but an apparent blueshift for doping in R. With one exception (see below), this prediction of a blueshift for N-doped R is inconsistent with experimental work on the subject. Di Valentin and coworkers suggested that allowing charge compensation of the N^{2-} dopant (e.g., from a Ti^{3+} donor state) would alter this effect. While this group has not returned to the subject of N-doped R, they have shown in subsequent papers [250,251,258,276] that the presence of bulk Ti^{3+} donor states (e.g., those associated with oxygen vacancies) in A resulted in charge compensation of N^{2-} to N^{3-}. This is schematically shown in Fig. 1.13. In turn, N-doping in seen to significantly lower the formation energy of bulk oxygen vacancies in A. Their theory also showed that both interstitial and substitutional N were thermodynamically favorable, depending on the oxidative chemical potential during the doping process, and that both types of N dopant resulted in gap states, although those for N_{sub} appeared closer to the VB edge. These authors also indicated that the doping process did not result in a shift of the VB edge (i.e., a shift in the energy of the predominant O 2p states), but in more-or-less localized N 2p states whose energies were located in the gap. These conclusions are in general agreement with other theoretical groups that have examined N-doped TiO_2 [260,288, 309,310,320], although there are some differences. For example, Graciani et al. [260] predicted that no bandgap narrowing would be exhibited for N^{3-} doping in R TiO_2(110) even with stabilization by O vacancies. Yang et al. [309,310] predicted that the total energy of the A system significantly increased for N_{sub} concentrations $>1\%$ indicating increased destabilization of the lattice. However, they also predicted that both N_{sub} and N_{int} in R should show gap states.

Di Valentin and coworkers [250,251,276] complimented their theory (discussed above) with EPR and XPS results on A in which they found evidence for hole trapping on the N dopant site and degradation of methylene blue in the visible at rates that were slightly greater for N-doped A than for undoped A. Their estimate of the number of N-related spins detected per gram of TiO_2 ($\sim 10^{17}$

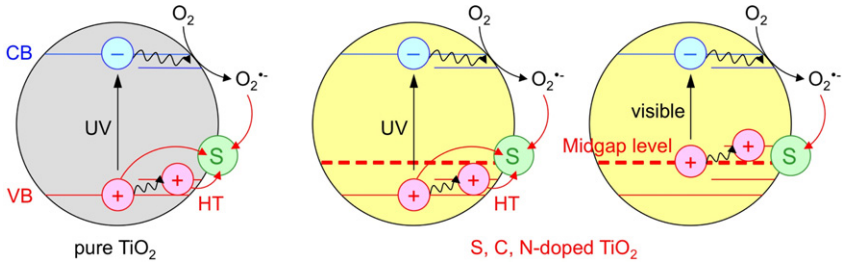

Fig. 1.12. Schematic models for photooxidation of an adsorbed species (designated as 'S') on undoped TiO_2 (left) and anion-doped TiO_2 by hole transfer (HT) and by O_2^- mediated processes (middle and right, respectively).
Source: Reprinted with permission from Tachikawa et al. [35].
© 2004, American Chemical Society.

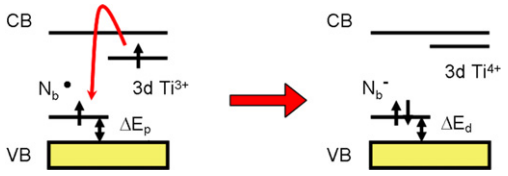

Fig. 1.13. Schematic model for the donor state (Ti^{3+}) charge compensation process that transforms a N^{2-} dopant into N^{3-}.
Source: From Di Valentin et al. [251].

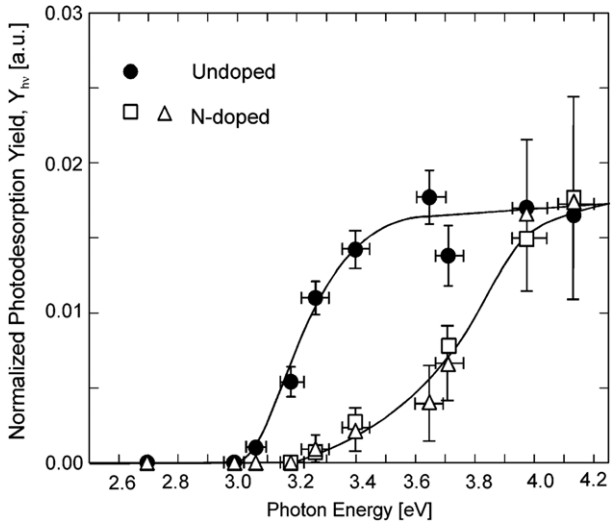

Fig. 1.14. Normalized O_2 photodesorption yields as a function of wavelength from saturation O_2 exposed to undoped R TiO_2(110) (solid circles) and to N_2^+ implanted in R TiO_2(110) (open squares and triangles).
Source: Reprinted with permission from Diwald et al. [253].
© 2004, American Chemical Society.

or ~6 × 10^{-4}% of available lattice O) suggested that most of the incorporated N was spin silent (N^{3-}) [250].

The Yates group [252,253] was the first to consider experimentally the issue of N-doping in single crystal TiO_2. They used two means of N-doping: sputter implantation using 3 keV N_2^+ ions and annealing in flowing NH_3 at 870 K. Both methods showed the characteristic 396-7 eV N 1s feature ascribed in the literature to N_{sub}, although the latter method also showed a N 1s feature at ~400 eV typically assigned to N_{int}. These authors, however, assigned the 400 eV feature to N-H_{int} sites. Rutile TiO_2(110) doped by heating in flowing NH_3 exhibited visible light absorptivity (down to 2.4 eV) and visible light photoactivity for Ag^+ reduction in solution. In contrast, these authors did not observe visible light activity for O_2 photodesorption on the implanted sample. Instead, a significant blueshift was observed relative to the typical UV activity on the undoped surface (see Fig. 1.14). These authors proposed that N-doping of TiO_2(110) resulted in a partial filling of the TiO_2 CB that prevented low energy indirect band-to-band excitations, requiring higher photon energies to accomplish band-to-band excitation. This conclusion has not yet been substantiated in the literature (see below). It is possible that their results of an apparent blueshift for N_2^+-implanted TiO_2(110) can be explained in terms of hole trapping effects (see above) since O_2 photodesorption is a hole-mediated processes (see Section 5). Other studies have reported results on the electronic and/or physical structures of single crystal TiO_2 doped by N_2^+ implantation [239,240,288], with high surface Ti^{3+} concentrations detected with XPS as a result. As shown in Fig. 1.15, Batzill et al. [239,240] observed formation of high concentrations of (1 × 2) domains on R TiO_2(110) in STM and undefined protrusions with increased surface roughening on A TiO_2(101) as a result of N_2^+ implantation and subsequent annealing. These authors concluded that high concentrations of near-surface Ti^{3+} resulted from a combination of sputtering and ion implantation, and that these became manifested on the surface as extended, sub-stoichiometric defects. This effect was reversed by sputter removal of the N-implanted region, resulting in a return of the nearly perfect surface integrity after annealing. The impact of these sub-stoichiometric regions on surface photochemistry has not yet been explored. Batzill et al. also observed large regions of high contrast in images of N-doped A TiO_2(101) (Fig. 1.15(f)) that were not seen in images of the clean surface (Fig. 1.15(g)). These authors speculated that these high contrast regions in the doped surface might arise from modification of the TiO_2 CB states (since their images are from tunneling to the surface from the tip) by surface or subsurface N dopants.

In an effort to prepare highly ordered N-doped films, Okato et al. [291] used pulsed laser deposition from a mixed R and TiN target to deposit N-doped A on the lattice-matched $LaAlO_3$(100) surface. Their films were deemed highly crystalline based on X-ray diffraction (XRD), and exhibited a redshifted absorption threshold with optimum N concentrations of 1–2%. XPS showed N_{sub} at 396 eV, but also a Ti–O–N species at 400 eV due to N_{int} or an oxynitride phase. Significant defect formation was observed based on XRD for N concentrations above 2%, with these films exhibiting instability toward R formation. More recently, Chambers and coworkers [244,248,322,360,361] extended the approach of Okato, et al. by employed O_2 plasma assisted molecular beam epitaxy (OPAMBE) to the preparation of single crystal films of doped and undoped TiO_2. (More details on the utility of this approach in preparing highly order oxide films on lattice-matched substrates may be found elsewhere [362,363].) Using commercially available R single crystals and lattice-matched single crystal oxides ($LaAlO_3$ or $SrTiO_3$), they were able to prepare highly ordered N-doped R or A films, respectively. In both cases, the solubility limit of N_{sub} incorporation was found to be ≤2%, in agreement with Okato and coworkers. XPS showed the dopant to be N^{3-} state (at 396 eV), presumably compensated by donor states incorporated during

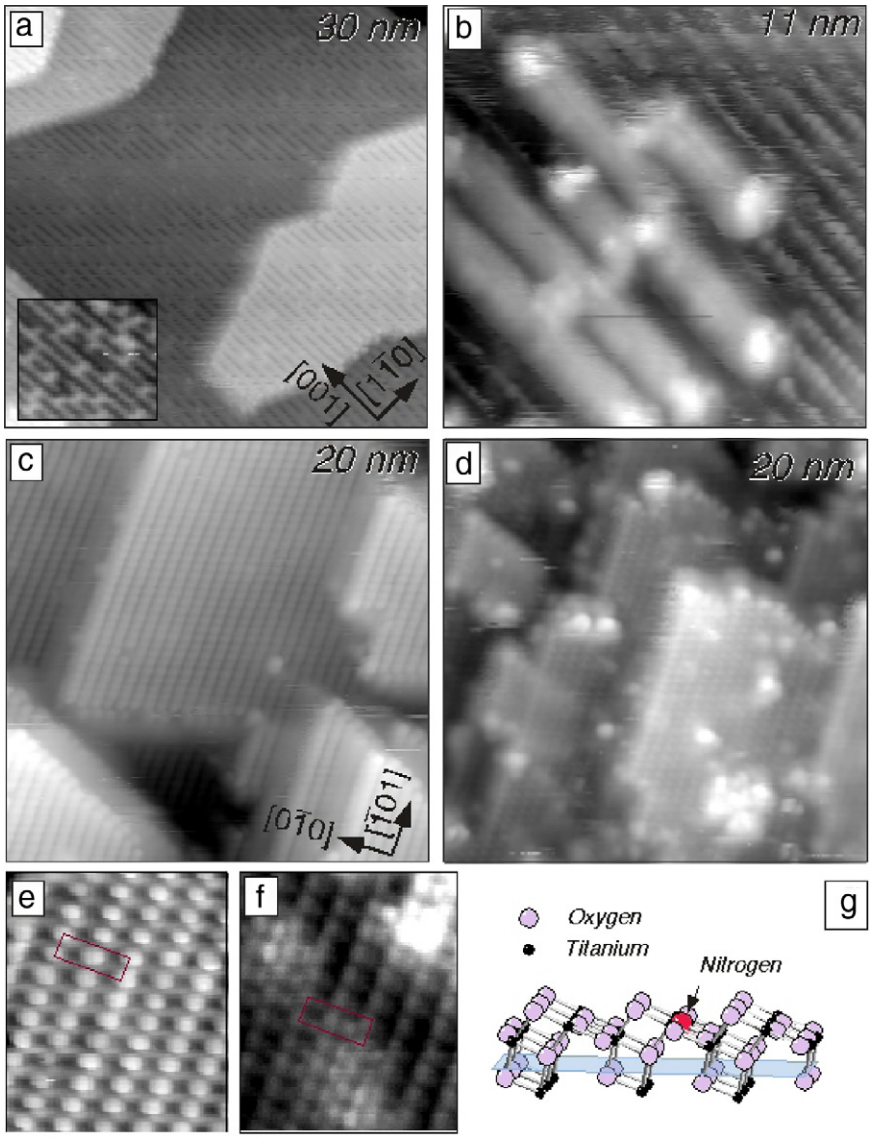

Fig. 1.15. STM images from annealed R TiO_2(110) (a) and A TiO_2(101) (c), and after N_2^+ implantation (and mild annealing) into R TiO_2(110) (b) and A TiO_2(101) (d). High resolution images in (e) and (f) show regions of the clean (with the unit cell indicated) and the N-doped A TiO_2(101) surfaces, respectively, with a ball-and-stick model shown in (g).
Source: Reprinted with permission from Batzill et al. [239].

growth. Despite careful control of the growth conditions, p-type N-doped surfaces were never formed even under the most stringent of oxidation conditions. This suggests that compensated N-doped films were thermodynamically more stable, in agreement with results from Di Valentin and coworkers [250,251,258,276]. Under ideal N-doped conditions, a small Ti 3p feature was observed at ~458 eV, shifted by ~1 eV from the main Ti 2p feature. This feature was not due to Ti^{3+}, especially since a Ti^{3+} gap state was not observed in ultraviolet photoelectron spectroscopy (UPS), but instead was due to a Ti^{4+}–N^{3-} species. This assignment is in agreement with results by Takahashi et al. [301] who prepared N-doped R TiO_2(110) by heating in flowing NH_3 at 600 and 700 °C. After annealing at 600 °C, they observed a N 1s feature at ~396 eV assigned to substitutional N^{3-} and a broad Ti 2p feature at ~458 eV (shifted from the main Ti 2p feature) similar to that seen by Chambers and coworkers. The new Ti 2p feature was also assigned to a Ti–N chemical shift and not to Ti^{3+} since their UPS did not show bandgap states typically seen if Ti^{3+} were present. In contrast, preparation at 700 °C yielded an additional N 1s feature at ~399 eV and evidence for Ti^{3+} in both XPS and UPS. Both groups observed a slight extension of the VB toward lower energies in UPS indicating new N states in the gap.

Chambers and coworkers [244,248,322,360] also performed transmission UV–vis measurements on their N-doped films and observed an apparent bandgap narrowing by ~0.6 eV. Under these conditions, EPR did not detect N-related spins, and only a weak Ti^{3+} was observed for a homoepitaxial N-doped film on R TiO_2(110) likely resulting from the substrate itself. However, the most useful structural information was obtained using MeV D^+ nuclear reaction analysis (NRA). When used in the channeling mode, this technique is extremely sensitive to species residing in non-lattice positions. Fig. 1.16 compares the channeling profiles for collisions of D^+ with lattice O (blue) and doped N (red). These profiles are presented as a ratio of the NRA signal obtained from a 'random' (non-channeling) direction for the purposes of normalization. In the channeling direction (normal to the surface), the majority of MeV D^+ ions passed through the 1 mm thick crystal with no collisions, however as the incident trajectory of the ions

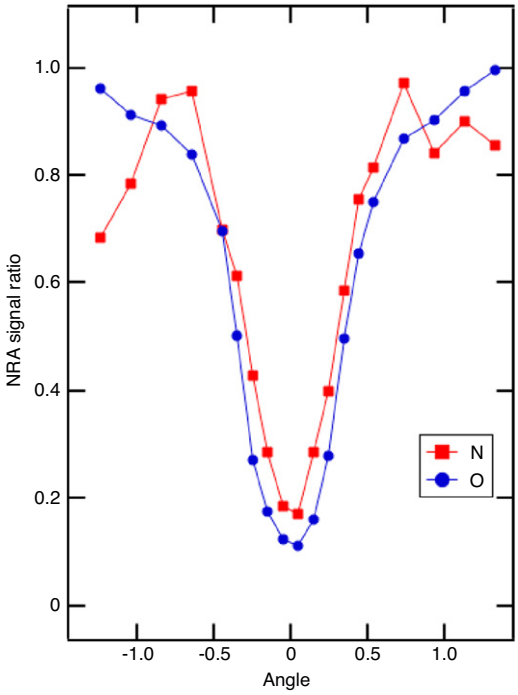

Fig. 1.16. Normalized NRA rocking curves from collisions of ∼1 MeV D^+ with lattice O (blue) and doped N (red) in a 500 Å homoepitaxial film of ∼2% N-doped R TiO_2(110). The 0.0° point corresponds to the surface normal. (For interpretation of the references to color in this figure legend, the reader is referred to the web version of this article.)
Source: From Henderson et al. [360].

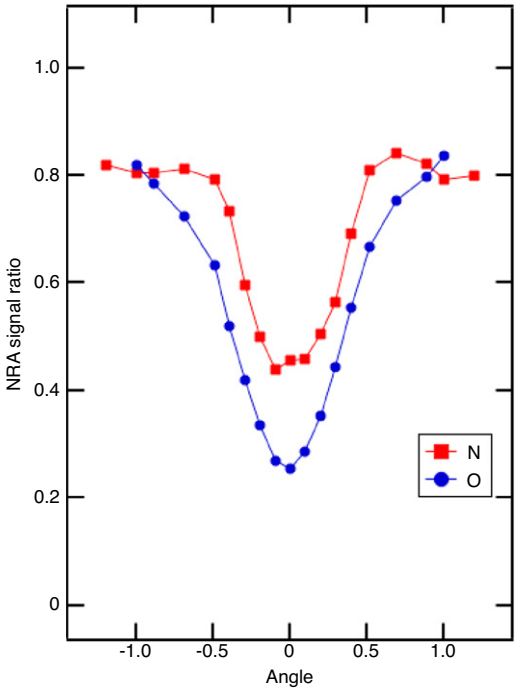

Fig. 1.17. Normalized NRA rocking curves from collisions of ∼1 MeV D^+ with lattice O (blue) and doped N (red) in a 500 Å homoepitaxial film of ∼2.4% N-doped R TiO_2(110). The 0.0° point corresponds to the surface normal. (For interpretation of the references to color in this figure legend, the reader is referred to the web version of this article.)
Source: From Henderson et al. [360].

deviated from the surface normal by as little as 0.5°, the likelihood of collision approached that of the 'random' orientation as the beam traversed the width of the crystal. At a N dopant level of <2%, the D^+ NRA profile for N was essentially the same as that for O, indicating that the N dopant resided in the same crystallographic position as O. (The narrower profile for N suggests that the position of N was slightly displaced from the ideal anion lattice position.) In contrast, Fig. 1.17 shows that the D^+ profile for both N and O were significantly diminished when the N dopant concentration in the ∼200 Å film was increased to ∼2.4%. These data suggest that N resided substitutionally in R for N concentrations below ∼2%, but non-substitutionally for some N as the concentration exceeded ∼2%. Commensurate with the degraded NRA signals, UPS showed the appearance of a Ti^{3+} gap state, XPS showed a large Ti^{3+} 2p signal, and surface order was lost in reflection high energy electron diffraction (RHEED) images, all three suggestive of formation of a disordered surface phase. Surprisingly though, the N 1s XPS feature only shifted by ∼0.4 eV to higher binding under these conditions. Taken in the absence of other data, this N 1s BE might be assigned to N_{sub} sites, but clearly in this case (and possibly in others) the N 1s BE cannot be used as an indicator of the N dopant location as previously thought. The transition from well-ordered, N_{sub}-doped films to poorly structured and heterogeneously composed films occurred in both R and A at N concentrations above 2%, suggesting that the solubility limit of N in TiO_2 is ∼2%.

The photochemistry of these well-characterized N-doped A and R films grown by OPAMBE was explored by Ohsawa et al. [290,322] using STM and photon stimulated desorption (PSD). As a probe of hole-mediated activity, these authors examined the photodecomposition of trimethyl acetate (TMA) on ∼1% N-doped R TiO_2(110) and A TiO_2(001) single crystal films. (As indicated above, at this N concentration the dopant was only in substitutional sites and compensated by Ti^{3+} donor states in the form of N^{3-}.) The upper portion of Fig. 1.18 shows CO_2 PSD signals resulting from UV photodecomposition of TMA on undoped R TiO_2(110) and on various levels of N-doped R TiO_2(110) films. The photodecomposition of TMA with UV light was nearly completely suppressed by N-doping in R TiO_2(110), and no visible light activity was observed despite the fact that the film was shown to absorb in the visible [244,248]. In contrast, the lower portion of Fig. 1.18 shows that the UV activity for A TiO_2(001) was only mildly affected by N-doping. This N-doped A TiO_2(001) film showed nearly the same photoactivity per incident photon in the visible as in the UV. While the PSD techniques provided a 'global' assessment of the influence of N-doping on the photoactivities of R TiO_2(110) and A TiO_2(001), STM was used to provide a local perspective on the influence of N-doping. As shown in Fig. 1.19, TMA molecules were clearly discernible on the ridge-and-trough reconstructed structure of A TiO_2(001) [175]. Progressing through images labeled 'b' to 'f', the STM data of Fig. 1.19 clearly shows that TMA molecules decomposed on the N-doped A TiO_2(001) surface during visible light irradiation. The kinetics for removal of TMA based on the local picture derived from STM were consistent with the 'global' measurements derived from PSD, providing a consistent picture of the hole-mediated activity of the N-doped A TiO_2(001) surface with visible light. Ohsawa and coworkers proposed that while the structural integrity and electronic properties of N-doped R TiO_2(110) and A TiO_2(001) were similar (for N concentrations below 2%), the difference in photoactivity likely resulted from differences in the hole trapping/detrapping and neutralization rates in the two N-doped polymorphs. (Note from Fig. 1.18 that the 'per-molecule' activity of undoped R TiO_2(110) was higher than that of A TiO_2(001), suggesting that the differences in activity in the doped films was not due to VB or CB effects, but due the N dopant states.) These data suggest that hole trapping and detrapping rates along the ⟨001⟩ direction of A were unaffected by N substitution

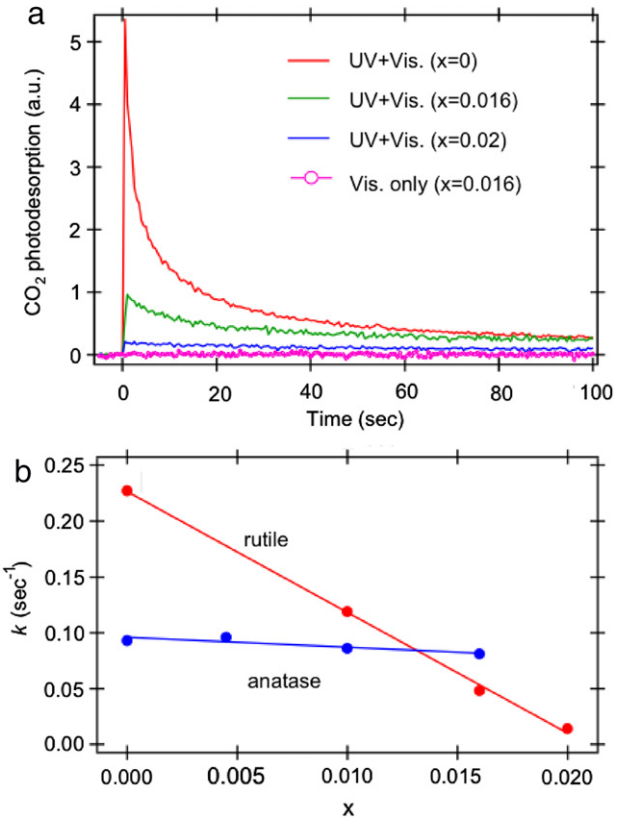

Fig. 1.18. CO_2 photodesorption traces from UV and/or visible light exposures to adsorbed TMA on R $TiO_{2-x}N_x$(110) with various 'x' levels of substitutional N-doping. (b) Comparisons of TMA photodecomposition rate constants (k) as a function of the level of N-doping into R TiO_2(110) and A TiO_2(001). (For interpretation of the references to color in this figure legend, the reader is referred to the web version of this article.)
Source: Reprinted with permission from Ohsawa et al. [290].

for O, but that hole trapping and neutralization were promoted in R TiO_2(110) by N-doping. These data also suggest that trapping and detrapping rates are critically important in anion-doped TiO_2, and that strong anisotropic behavior in the rates of hole mobility exists in the different polymorphs of TiO_2.

Co-doping

Although much confusion still exists regarding the structural and photochemical properties of doped TiO_2, numerous groups are exploring the general properties of co-doped TiO_2 [222,272,274,364–374], particularly with more than one cation or anion doped into the lattice, or with a cation and anion co-doped into the lattice. The behavior of self-compensation of anion dopants in R and A (see above), suggest that the electronic structures of co-doped TiO_2 can be manipulated with cation doping to achieve desired activities. The objective in many of these studies is to advance the material engineering of TiO_2 by altering the optical properties through specially designing trap sites for both electrons and holes.

2. Charge transport and trapping

In order for photon absorptivity in a semiconducting photocatalyst to translate into surface photoactivity, generated charge carriers must reach the surface with high probability and be stabilized at the surface for electron/hole transfer processes (and not for recombination events). This situation invokes questions about how charge carriers move through a lattice to a surface. What are the relative timescales for charge separation, thermalization, transport and trapping? What are the typical charge trapping surface sites and should trapping at the surface be considered to be good or bad? Literature on these and other related questions will be reviewed in this section.

2.1. Exciton transport and trapping

Bandgap excitation of TiO_2 should result in separated charge carriers in order to be of use from a photocatalytic or photoelectrocatalytic perspective. While the majority perspective in the literature is that photocatalysis is best understood in terms of electron transfer events involving 'independent' charge carriers (i.e., separated CB electrons and VB holes), the properties of excitonic states are not understood well enough to exclude their influence, particularly in nanoscaled materials. Excitation of A TiO_2 is typically thought to pass through an excitonic state (where the electron is bound as a quasi-particle by the hole) prior to charge separation. Not much is known about the relationship between the excitonic properties and the photochemical properties of TiO_2. Luminescence is perhaps the most commonly used approach to studying excitons in TiO_2 (see below). Characterizations of exciton thermalization, lifetimes, transport kinetics, trapping and quenching are all difficult tasks. There is also the added complication of singlet to triplet conversions in excitonic states [375].

Excitons in A are generally thought to be 'self-trapped' [101,110,114,118,119,167,376–381,381–384]. Exciton self-trapping in A stems from a large lattice relaxation in the excitonic state that hinders quenching or charge separation [110]. In bulk A, Murakami et al. [101] have shown that the self-trapped exciton is stable from 5 to 200 K, and does not exhibit photoluminescence above 200 K (probably due to recombination). Watanabe and coworkers [381–383] suggest that the self-trapped state in A is preferentially generated with excitations near the A bandgap threshold, whereas self-trapping is less likely with supra-bandgap energies because the excess energy is above the self-trapping energy gain. Carrier separation in A appears to occur predominately during thermalization. In contrast, excitons in R are considered 'free' [114,118]; that is, the lattice site at and around the exciton is not sufficiently altered by the exciton so that its creation generates its own, lower energy, trapping site. One explanation for this is that the size of the exciton in R is much larger than the lattice unit cell, so lattice distortions are minimal and charge separation or recombination takes precedence.

As a consequence of the different excitonic properties of A and R, exciton quenching is more frequently radiative in A and almost exclusively non-radiative in R (see below). These characterizations apply to the 'bulk' situation; it is expected that the surfaces and interfaces of A and R should provide different environments. For example, Zou and coworkers [167] found that the photoluminescence of self-trapped excitons in A nanoparticles could be stabilized to room temperature through the influence of a stearate 'coating' on the nanoparticles. Their results support the idea that suitable interfacial dipole layers can be used to stabilize excited states on the surface of A. In the R case, Nilius and coworkers [385] found evidence for radiative decay of excitons (generated via energy transfer events from de-excitation of plasmons in supported Ag nanoparticles) on reduced R TiO_2(110) with near-bandgap energies (Fig. 2.1). In these experiments, an STM tip was used to excite plasmons in supported Ag particles, and photon emission was probed as an indicator of de-excitation processes. While, no emission signal was detected on the clean TiO_2(110) surface, addition of Ag resulted in emission intensity that increased with the Ag particle size but did not shift in energy as one would expect for the particle size dependence of the Ag plasmon energy. Nilius and coworkers interpreted this to be a consequence of energy transfer from the excited Ag particles to the R TiO_2(110) surface where recombination resulted in a constant energy of emission (at and below the R bandgap energy).

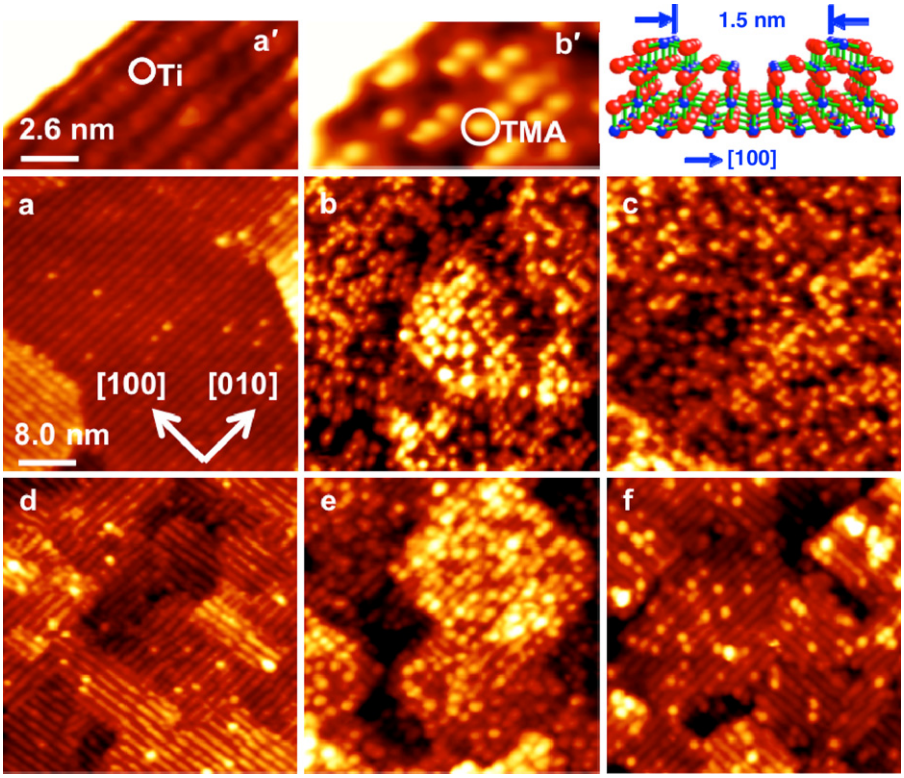

Fig. 1.19. STM images of: (a and a') the clean A TiO_2(001) surface, (b and b') the same surface with a saturation coverage of TMA at 300 K, and (c) the surface in 'b' after a visible light exposure of ~5.6 × 10^{20} photons cm^{-2}. Images 'd', 'e' and 'f' are the same as 'a', 'b' and 'c', except for 1% N-doped A TiO_2(001). (A ball-and-stick model of the reconstructed A TiO_2(001) surface is shown in the upper right.)
Source: Reprinted with permission from Ohsawa et al. [290].

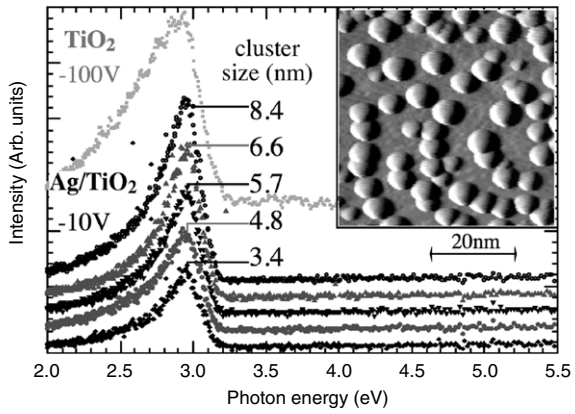

Fig. 2.1. Photon emission spectra from variously sized Ag clusters on reduced R TiO_2(110) obtained by injection electron stimulation (−10 or −100 V bias and 2 nA current) of the clusters. Inset shows STM image of Ag on R TiO_2(110).
Source: From Nilius et al. [385].

There do not appear to be any examples in the literature in which excitonic energy in A or R resulted in *direct* energy transfer to an adsorbate or supported material. In concept, an exciton may transfer its energy directly (e.g., via phonon coupled quenching) across the TiO_2 interface. Particularly on A, where a radiative diagnostic exists, it should be possible to follow the fate of excitonic energy to learn the extent to which this form of energy transfer (in contrast to electron transfer) plays a role in photocatalysis on TiO_2.

2.2. Charge separation and thermalization

The majority of excitation events in 'ideal' TiO_2 generate charge carriers that must be spatially separated in order to be used in electron transfer processes. These charge carriers are not (initially) in their lowest energy state when created, but rapidly 'thermalize' to their respective band edges, as discussed below. In this section, charge separation and thermalization processes in TiO_2 are reviewed as critical components in charge transport.

Charge separation: A variety of approaches exist in the photocatalytic literature for promoting charge separation in TiO_2. In general, these approaches employ either an interfacial (e.g., a heterojunction or supported charge trap) or a bulk (e.g., a dopant) charge trapping agent specifically designed for separating one carrier from the other. TiO_2 surfaces, themselves, can also be thought of as charge trapping agents (e.g., see the work of Tamaki et al. [386]). Details concerning the chemical and structural methods for promoting charge separation are discussed in Sections 6 and 7. This section considers the general issue of charge separation in un-modified TiO_2. The roles that surfaces have in stabilizing (trapping) separated charges will be discussed below, in Section 2.4. A key issue in charge separation relates to the energy of the charge carriers formed from the excitation event. 'Hot' electrons and deep holes are more likely to separate than charge carriers generated with near-bandgap energy light [382]. Conversely, higher temperatures can negate the charge separation effectiveness of some trapping sites (e.g., see work of Berger et al. [387]). Also, the DOS at the energy of the charge carrier affects mobility (see below). The high dielectric constant of TiO_2 greatly assists in separation as point charges moving away from each other become screened from their counter charges by the lattice. An imposed electric field [388,389]

can also assist in charge separation, just as establishment of a space charge region can.

Charge thermalization: In an ideal scenario, all excitation energy invested into generation of charge carriers would be made available for redox chemistry. The higher the potential energy of the electron (hole) the more reductive (oxidative) capability there is. Being able to tune a carrier's energy could be useful in promoting desired electron transfer reactions. For example, a given photon energy in excess of the TiO_2 bandgap could be used to selectively generate shallow VB hole states and 'hot' electrons high in the TiO_2 CB with high reductive power, or (conversely) make deep VB holes (with high oxidative power) by excitation to the TiO_2 CB edge. In reality, charge carrier thermalization is rapid. The 'excess' potential energy is lost to the lattice via strong coupling with phonon modes and there is no potential for taking advantage of specificity in the absorption event. A deeper understanding of charge carrier thermalization could provide insights into means of utilizing the energy of 'hot' electrons and deep holes before thermalization occurs.

Methods for following the thermalization of CB electrons are fairly common. For example, electron thermalization rates can be obtained by monitoring the dynamics of charge injection from an optically excited sensitizer. Such photodynamic studies provide detailed information into the thermalization of 'hot' electrons in the TiO_2 CB. For example, Gundlach and coworkers used 2PPE to track electron injection thermalization from two dyes adsorbed on R TiO_2(110) [390,391]. Fast initial decay of the 2PPE signal resulting from thermalization of the injected electron occurred on the 10 fs timescale. The thermalization process may not be as rapid in nanoparticles based on work by Turner et al. [392] who used time-resolved terahertz spectroscopy to monitor the photoconductivity of CB electrons injected into P-25 from an adsorbed R535 dye excited with 100 fs pulses of 400 nm light. They found that injected electrons thermalized to the CB edge on the ~300 fs timescale. Similarly, van de Lagemaat and Frank [393] found evidence for non-thermalized electron transport in porous TiO_2 coated electrodes, particularly for electron injected into particles near the surface of the collecting electrode. For charge injection at particles in contact with the electrode, ~80% of the injected electrons were not completely thermalized before transfer to the collector.

Measurements of hole thermalization in TiO_2 come mainly from direct bandgap excitation studies (since optically initiated 'hole injectors' are not available that readily couple with the TiO_2 VB). In band-to-band excitation studies, hole thermalization in the VB is accompanied by electron thermalization in the CB making it difficult to differentiate the two processes. Nevertheless, several groups have proposed that hole transfer [394–398] or hole trapping [386,399,400] can precede hole thermalization in TiO_2. For example, Grela and coworkers [396–398] were among the first to consider whether hole transfer (to an adsorbate) could compete on the same timescale with hole thermalization in the VB of TiO_2. For example, these authors examined the rate of salicylate photooxidation on suspended TiO_2 nanoparticles ($\leq$5 nm) as a function of excitation energy to show that higher Q (quantum yield) values resulted from higher excitation energies. In another study, the Q values for 3-nitrophenol photooxidation were shown to be greater for higher energy photons (see Fig. 2.2). These results were also consistent with this group's use of action spectroscopy to follow 'hot' hole oxidation of various aromatic molecules on colloidal TiO_2 [397].

Other groups have used time-resolved techniques to track hole thermalization in TiO_2. Morishita et al. [394] used changes in transient reflectivity (on the 110–690 fs timescale) to show that hole transfer to adsorbed SCN^- involved non-thermalized holes in the TiO_2 VB. Similarly, Tamaki et al. [386,399,400] used transient absorption spectroscopy (with excitation at 266 or 355 nm) to track electron and hole trapping lifetimes in nanocrystalline films of A (particles of $\leq$20 Å). Based on their assignments of the optical properties of trapped holes, they proposed that in some cases hole trapping preceded hole thermalization by up to 100 ps. Using a transient grating technique, Shen and coworkers [401,402] found that hole thermalization in A was a first order process occurring on the picosecond timescale. This technique, however, is not charge carrier specific. The authors attributed the fast relaxation component of their observed signals to VB holes based on assumptions regarding the relative effective masses of VB holes and CB electrons.

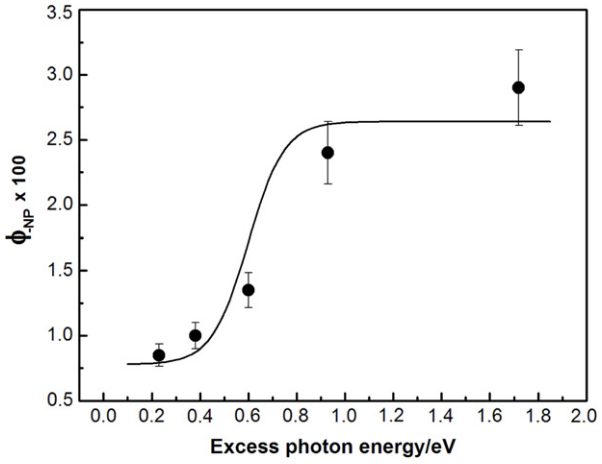

Fig. 2.2. Quantum yields for photooxidation of 3-nitrophenol over suspended TiO_2 as a function of 'excess photon energy' (defined as the photon energy in excess of the TiO_2 bandgap energy).
Source: Reprinted with permission from Grela and Colussi [398].
© 1999, American Chemical Society.

2.3. Charge transport

The concepts of charge diffusion and mobility are macroscopic properties associated with motion in a concentration gradient and an applied field, respectively. In contrast, charge transport (or charge "hopping") can be thought of as a site-to-site phenomenon deriving meaning from the local properties of the 'sites'. In this section, studies of the transport of point charges in TiO_2 will be reviewed to provide a better understanding of surface photocatalytic processes on TiO_2.

2.3.1. Carrier effective mass

An integral part of charge carrier transport in a semiconductor is the effective mass of the carrier (relative to that of a free electron), with the EMA method [403,404] often employed as a convenient tool in such descriptions. To the extent that carriers can be treated as semi-classical particles, the larger the effective mass of the particle, the more localized it is and the less likely it is to move from lattice site to lattice site. Charge carrier effective masses are frequently used to determine the influence of nanoscaling on the optical properties of TiO_2 [113,124–127,405–411]. For example, the work by Kormann et al. [125] is a much-cited reference for experimental-derived effective mass values in A. The EMA is not without its critics. Monticone and coworkers [137] point out that the EMA appears to break down when dealing with nanoscale particles, and its usefulness for determining carrier effective mass values or changes in optical properties is limited. Similarly, Serpone et al. [136,412] indicate that confusion in the TiO_2 literature regarding the effective mass

values for electrons and holes is largely due to questionable use of the EMA. Experimentally, care must be taken in determining effective masses in TiO_2 because of trapping effects. Theoretical estimates based on the degree of curvature at the bottom/top of the CB/VB obtained from DFT calculations provides a more reasonable, single-particle perspective of the effective mass of a charge carriers in TiO_2 (for example, see work of Thulin and Guerra [413]). With these issues as backdrop, this section reviews literature estimations of charge carrier effective masses in TiO_2.

Electrons: Many reports modeling carrier dynamics in R utilize effective mass values for electrons (m_e) obtained from other studies. Actual measurements for 'free' CB electrons in R can be dominated by the character of electron trap states. Yagi et al. [414] determined the m_e of the electron trap state in slightly reduced, single crystal R using resistive and Hall measurements. At oxygen-deficient levels between 3.7 and 13×10^{18} cm^{-3} (i.e., between 6 and 20 parts per 100,000), point defects in R that described the donor character of the material were comprised only of interstitial Ti^{3+} based on the author's EPR measurements. The m_e value of these donor electrons at temperatures below 20 K was ~7–8 m_0, with significant anisotropy in exhibited in the lattice. For example, the m_e value along the ⟨001⟩ direction was 2–4 times the electron rest mass (m_0), but roughly 10–15 times m_0 along ⟨100⟩ directions. As the crystal temperature was raised above 50 K, Yagi et al. found that the m_e values of the donor state in R increased further due to increases in phonon scattering. In agreement with these results, Hendry et al. [415,416] examined the diffusion (as opposed to transport) of electrons in porous R films. They found that the effective mass of electron polarons (essentially trapped electron states) in R was 3–10 times larger than that of the 'free' electron effective mass. Both free and trapped electrons showed anisotropic diffusional behavior, with values of the diffusion coefficient being greater along the ⟨001⟩ direction. In response to an applied electric field, the 'mobility' of electrons in porous TiO_2 was several orders of magnitude less than that in bulk TiO_2 due to screening of the electric field locally by the porous media, as well as due to trapping and lattice anisotropy effects. Given that electron trapping in R occurs on the sub-picosecond time scale (see below), it seems likely that electron effective mass measurements of free electrons in the R CB may be complicated by trapping.

The situation in A is less clear. Tang et al. [110] estimated an m_e of ~m_0 for the shallow donor level in A, which they ascribed to band-like (metallic) conductivity. In contrast, these authors indicated that conductivity in R was through excitations of small polaronic states (see below), resulting in m_e values of ~$20m_0$ (based on references in [110]). Their assessment of m_e in A being ~m_0 is consistent with measurements by other groups [417,418] for thin A films and by DFT theory [413], although one report places $m_e > 10m_0$ for A [127]. As yet, there appear to be no measurements reported on high quality single crystal A.

Holes: In general, the effective mass of a hole in R is thought to be less than that of the CB electron [2], however there are few determinations available for holes in R. Several groups have assessed the effective mass of a hole in A, with the EMA being used in each case. For example, Toyoda and Tsuboya [113] estimated a hole effective mass of $0.01m_0$ in A nanoparticles, a value they attributed to delocalization of the hole over the A particle. However, this was done by assuming $m_e = m_0$. Kormann et al. [125] calculated an m_h of $2m_0$ (assuming that $m_e = 9m_0$) based on a blueshift of 0.15 eV in the absorption threshold for 2.4 nm diameter A particles. Enright and Fitzmaurice [127] estimated m_h to be $0.8 \pm 0.2m_0$ for A using a similar approach.

Thulin and Guerra [413] recently calculated the impact of lattice strain (as might be encountered in nanoscaling of TiO_2 or in mixed-phase situations) on the electronic properties of A.

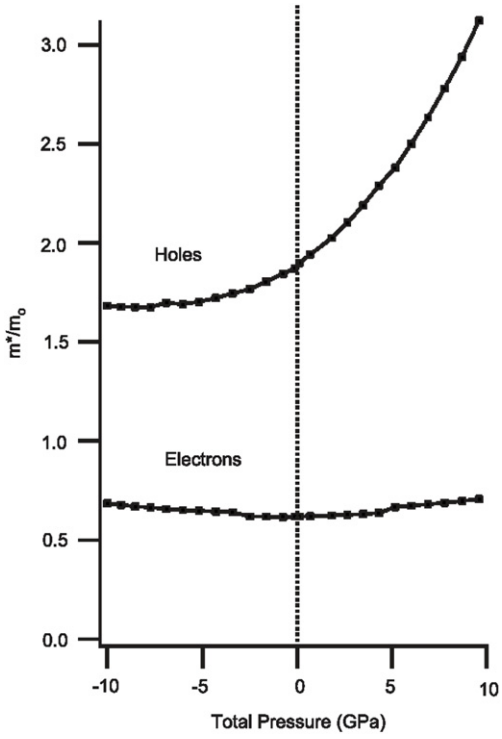

Fig. 2.3. Calculated electron and hole effective masses as a function of compressive (+) and expansive (−) lattice strain in anatase.
Source: Reprinted with permission from Thulin and Guerra [413].

They found that the A bandgap increased with compressive lattice strain. The opposite was seen for an expansive strain. In terms of effective mass, Fig. 2.3 shows that the authors' calculations predict that the electron effective mass should be fairly flat with +/− lattice strain (at ~$0.7m_o$), but that the hole's effective mass should be very sensitive to compressive strain, resulting in greater localization and potentially more recombination. In contrast, expansive strain (negative values in Fig. 2.3) caused the hole effective mass to minimize at ~$1.7m_o$. Based on these findings, Thulin and Guerra proposed that engineering tensile strain ('expansive strain') into TiO_2 materials should lower the bandgap and increase photoefficiencies.

2.3.2. Electron transport

The issue of CB electron transport in TiO_2 is of significance to any photochemical process that utilizes electrons injected into or excited to CB states. Electron transport is of particular importance in dye sensitized solar cell (DSSC) applications where an excited electron is transferred from an anchored dye into the CB of TiO_2 and traverses many TiO_2 unit cells (and often across many TiO_2–TiO_2 interfaces) to a collector [392,393,419–452]. Because the performance of such devices can be limited by electron transport, many groups have examined the transport of electrons through various forms of TiO_2, including nanoporous films of A particles [393,423,424,429,438,441,442,445,449–451,453–462], nanoporous films of mixed polymorphic TiO_2 (e.g., P-25): [392,430,443,446,463–470], miscellaneous amorphous or undefined TiO_2 films [421,422,427,433–435,444,471,472], and R single crystals [109,415,473,474]. Considerable work has been invested in theoretical and kinetic modeling of electron transport [419,420,425,426,428,431,432,436,437,439–442,444,445,447,448,452,471,475–477]. There is much debate in the literature as to how electron transport in TiO_2 depends on trapping and detrapping processes [392,393,435,440,446,449–451,456,468,478–483], as well as to the chemical and

structural (electronic and physical) properties of TiO_2 surfaces. Trapping is most frequently considered as a surface or interfacial phenomenon. In DSSC applications, where there are no VB holes in TiO_2 (the hole is on the dye), electron trapping is generally viewed as an undesired event. In contrast, electron trapping in band-to-band excitation events (i.e., redox photocatalysis) can be considered as a favorable event if it facilitates charge separation.

Measurements of an electron 'drift' velocity in TiO_2, done by Salafsky [470] for a mixed-phase sample, provide a value of $\sim 4 \times 10^3$ cm/s. Estimates of thermal velocities of CB electrons in TiO_2 based on an assumed m_e value of $\sim 10 m_0$ are roughly two orders of magnitude faster [392,423,426], illustrating that electron transport in TiO_2 may be limited by sample-related (e.g., interfaces) issues. The behavior of electron transport in nanoporous networks will be different than in crystalline nanowires/rods, which will be different than in single crystals. With the exclusion of amorphous TiO_2 materials, the existence of surfaces and interfaces become key limiting factors in influencing electron transport. Electron transport in porous TiO_2 was initially thought to be controlled by trapping and detrapping processes. For example, de Jongh and Vanmaekelbergh [468] used modulated photocurrent spectroscopy to study electron transport in nanoporous electrode-coated films of P-25 using 350 nm light to excite carriers. Analysis of their data suggests that transport was limited by electron trapping and detrapping in surface states on particles or at the boundaries between particles. Similarly, Wahl and Augustynski [449] proposed that electron transport through porous TiO_2 networks used in DSSC applications was facilitated in early stages of illumination by a "self-doped" insulator-to-conductor transition in TiO_2 resulting from electron trapping. These authors estimated that the electron number density needed for this self-doping to occur was $\sim 10^{19}$ cm^{-3}, with charge compensation coming from adjustment of the cation concentration in the Helmholtz layer about each particle. For P-25 with a mean particle size of 25 nm, this corresponded to a change in the cation charge at the surface of only $\sim 10^{13}$ cm^{-2} or a few percent of a monolayer (ML).

van de Lagemaat and Frank [482] initially characterized electron transport through porous TiO_2 networks by a trapping/detrapping model involving a distribution of surface trap states because of an observed power law dependence in the photocurrent (i.e., the collection rate increased as the ~ 2.6 power of the injected electron concentration in TiO_2 films). More recently, Frank and coworkers [393,450,451] have shown that electron transport in nanoporous TiO_2 films does not fit a trap model because a photon flux dependence was not observed in the activation energy (E_a) for transport (which varied from 0.19 to 0.27 eV depending on the sample preparation). Their E_a values for transport were consistent with values from other groups [446,456,484]. (The need for thermal activation is also seen indirectly through the influence of temperature on the back-electron transfer (i.e., from the surface back to the ionized dye) rates, which are higher at low temperatures [433].) One would expect that the E_a values for electron transport would vary with the trap occupancy, with the deeper traps being preferentially filled at low injection currents, but this was not observed. Instead, Frank et al. [393,450,451] proposed that structural disorder in their porous films (particularly at interfaces) had a greater influence on electron transport than did the trap population energy distribution. One way to interpret this conclusion is to say that the integrity of TiO_2–TiO_2 interfaces and the degree of circuitous transport through a porous network of interfaces both play a greater role in electron transport than does many trapping/detrapping cycles. This conclusion is mirrored in time-resolved terahertz spectroscopy measurements by Turner et al. [392] for injected electrons from R535 dye into P-25. They observed fast short-range transport of electrons within particles. In contrast, long-range transport (particle-to-particle) was hindered by disorder in their films and not by trapping/detrapping processes.

Other groups have also found that the 'trapping/detrapping' model was inadequate in describing electron transport in TiO_2. Boschloo and Hagfeldt [446] examined electron transport in TiO_2 P-25 films sensitized with a Ru-based dye. In agreement with Frank's group, they found that electron transport into TiO_2 was thermally activated with E_a values of ~ 0.1–0.15 eV. A trapping/detrapping model based on an exponential distribution of trap sites (as a function of trapping energy) did not fit their data. Instead, they proposed that models are needed that take into account localized barriers between connecting particles, electrostatics associated with high electron concentrations per particle and between electron and counter ions at interfaces, and Fermi level pinning and unpinning effects. Other issues affecting electron transport include the effect of electrolyte 'drag' on electron transport (e.g., via ambipolar diffusion) [393,456,483] and the presence of chemical species that initiate unwanted electron transfer depletion (e.g., trace electron scavengers like O_2 [461]).

The transport of electrons in the bulk of TiO_2 is influenced mostly by strong electron–phonon coupling [415]. Groups have shown that anisotropy exists in electron transport in both R and A, presumably reflected in the directional dependence of this coupling. For example, the Batista group [447,448] modeled electron transport in A $TiO_2(101)$ resulting from excited catechol charge injection. Fig. 2.4 shows that the injected electron charge was distributed into the bulk anisotropically, being faster along the surface normal and the lateral $\langle 010 \rangle$ directions, but slower along the lateral $\langle -101 \rangle$ directions. Thermal fluctuations in the lattice helped alleviate much of this anisotropy. Dupuis and coworkers [475–477,485] examined the transport of electrons and holes in bulk A and R using Marcus theory for polaron hopping (illustrated in Fig. 2.5 for the electron case). Results from their modeling efforts for electrons and holes in A and R are shown in Table 2.1. They found that hole hopping in R was adiabatic with E_a values roughly twice that for electron hopping. Lattice distortions around the holes were more significant than those around the electrons. Electron and hole hopping to the R $TiO_2(110)$ surface (from the bulk) required higher E_a than in the bulk because the surface tended to repel these charges, presumably due to a lower dielectric constant of the interface compared to the bulk. Dupuis et al. also predicted that electron hopping should be more facile in R than in A, particularly along the R $\langle 001 \rangle$ direction, whereas hopping in A (and other R directions) was more diabatic in nature. This conclusion is consistent with 4-point probe measurements performed by Byl and Yates [474] on the $TiO_2(110)$ surface.

2.3.3. Hole transport

At present, the best picture regarding hole transport in TiO_2 is found from the theoretical Marcus transfer studies of Dupuis and coworkers (see literature discussed above). On a macroscopic scale, not enough is known about the relationship between hole trapping and hole transport. Experimental studies of hole transport in TiO_2 are few, despite the obvious importance of holes in a host of photocatalytic applications. Two tidbits of data shed some light on this issue. First, as mentioned above, Grela et al. [396] proposed that holes were transported to the surface of <5 nm TiO_2 particles without complete thermalization, suggesting that coupling to phonons may not be as efficient as in the case with electrons. (This is in contrast to results by Duzhko et al. [466] who suggest that the diffusion coefficients for electron transport in the CBs of A or R are generally greater than those for holes in the VB of either polymorph.) Second, Lantz and Corn [486] used time-resolved SHG to probe hole mobility in R $TiO_2(001)$ photoelectrodes. They

Table 2.1
Tabulated kinetic parameters for electron (top) and hole (bottom) polaron hopping events along various crystal directions in R and A obtained from Marcus theory. Top: reprinted with permission from Deskins and Dupuis [475]. © 2007, by the American Physical Society. Bottom: adapted with permission from Deskins and Dupuis [476]. © 2009, American Chemical Society.

Phase	Direction	ΔG^* (eV)	κ	Transfer mode	k_{et} (s^{-1})	D (cm^2/s)	μ ($cm^2/V\,s$)
Rutile	[001]	0.09	1.00	Adiabatic	$7.65 \cdot 10^{11}$	$1.35 \cdot 10^{-3}$	$5.24 \cdot 10^{-2}$
	[111]	0.31	0.02	Non-adiabatic	$3.66 \cdot 10^{6}$	$1.91 \cdot 10^{-8}$	$7.42 \cdot 10^{-7}$
Anatase	[100]	0.30	0.17	Non-adiabatic	$3.68 \cdot 10^{7}$	$2.71 \cdot 10^{-7}$	$1.06 \cdot 10^{-5}$
	[201]	0.30	0.45	Non-adiabatic	$1.73 \cdot 10^{8}$	$1.27 \cdot 10^{-6}$	$4.96 \cdot 10^{-5}$

Phase/Direction (see (476) for details)	ΔG^* (eV)	κ	Transfer mode	k_{et} (s^{-1})	D (cm^2/s)	μ ($cm^2/V\,s$)
Rutile/A	0.55	0.00	Non-adiabatic	$3.75 \cdot 10^{2}$	$6.60 \cdot 10^{-13}$	$2.57 \cdot 10^{-11}$
B	0.25	1.00	Adiabatic	$1.41 \cdot 10^{9}$	$9.22 \cdot 10^{-7}$	$3.59 \cdot 10^{-5}$
C	0.16	1.00	Adiabatic	$4.17 \cdot 10^{10}$	$1.32 \cdot 10^{-4}$	$5.13 \cdot 10^{-3}$
D	0.25	1.00	Adiabatic	$1.36 \cdot 10^{9}$	$4.18 \cdot 10^{-6}$	$1.63 \cdot 10^{-4}$
E	0.62	0.30	Non-adiabatic	$2.13 \cdot 10^{2}$	$3.45 \cdot 10^{-13}$	$1.34 \cdot 10^{-11}$
Anatase/A	0.59	0.00	Non-adiabatic	$2.04 \cdot 10^{-4}$	$3.25 \cdot 10^{-19}$	$1.27 \cdot 10^{-17}$
B	0.51	0.00	Non-adiabatic	$5.40 \cdot 10^{-2}$	$1.03 \cdot 10^{-16}$	$4.01 \cdot 10^{-15}$
C	0.52	0.04	Non-adiabatic	$1.43 \cdot 10^{3}$	$4.14 \cdot 10^{-12}$	$1.61 \cdot 10^{-10}$
D	0.17	1.00	Adiabatic	$3.91 \cdot 10^{10}$	$4.77 \cdot 10^{-5}$	$1.85 \cdot 10^{-3}$
E	0.59	0.69	Non-adiabatic	$4.63 \cdot 10^{3}$	$1.34 \cdot 10^{-11}$	$5.22 \cdot 10^{-10}$

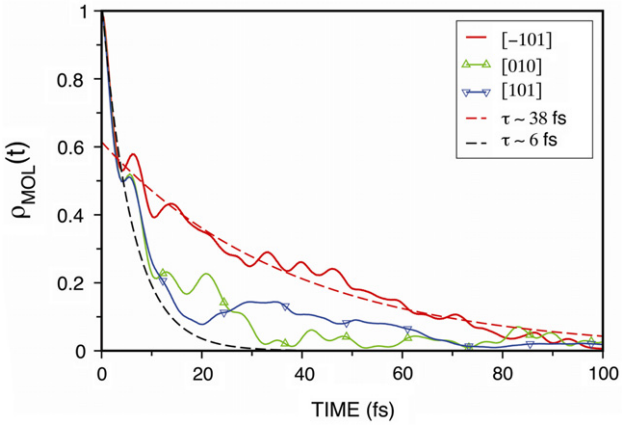

Fig. 2.4. Time-dependent survival probabilities of electrons injected into the A TiO_2(101) surface from excitation of bound catechol. Survival probabilities are shown for electron trajectories along the (101) surface normal (blue), and in two lattice directions, [−101] and (010), in the surface (red and green, respectively). (For interpretation of the references to color in this figure legend, the reader is referred to the web version of this article.)
Source: Reprinted with permission from Rego and Batista [447].
© 2003, American Chemical Society.

observed an average timescale of 25 ps for hole diffusion from the bulk to the surface that was independent of applied potential or electrolyte conditions. From their measurements, they estimated an average hole 'drift velocity' of ~4 × 10^4 cm/s (assuming an average depth-of-origin to be ~10 nm and that the motion of holes was strictly normal to the surface). This value is roughly an order of magnitude faster than the drift velocity of electrons in mixed-phase TiO_2 measured by Salafsky [470].

2.4. Charge trapping

Trapping and detrapping (of electrons or holes) are important issues in electron transfer (to or from TiO_2) and in charge stabilization. The previous section highlighted some of the debate regarding the influence of charge trapping on charge transport in TiO_2. The field is still sorting out how these phenomena impact photocatalytic performance. For example, trapping could be considered beneficial if it localized charge carriers at important electron transfer sites on TiO_2 surfaces or if it promoted charge carrier separation. Conversely, trapping could be considered detrimental if trap sites were far from preferred electron transfer sites or led to recombination. (Based on these contrasting arguments, similar assessments could be made regarding detrapping.) Trapping ener-

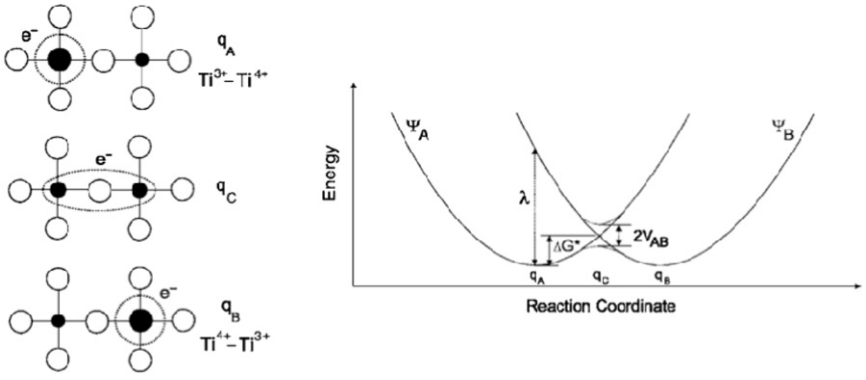

Fig. 2.5. Schematic models for electron polaron hopping in a TiO_2 lattice (left) and for the hopping event from the perspective of Marcus theory (right). Designations 'q_A', 'q_B' and 'q_C' correspond to the initial, final and transition state site configurations, with Ψ_A and Ψ_B representing the state descriptions of the initial and final, respectively. The terms 'λ', ΔG^* and $2V_{AB}$ refer to the reorganization energy, diabatic activation energy and electronic coupling factor, respectively. (The transition driving force, ΔG°, is not shown, but is the energy difference between the minima which ideally is zero.)
Source: Reprinted with permission from Deskins and Dupuis [475].
© 2007, by the American Physical Society.

gies, if too large, could diminish the redox power of a charge carrier or inhibit rapid transport. However, if the trapping energy were not large enough any benefits of trapping would be inconsequential. The trapping timescales and detrapping rates, resulting from either thermal or non-thermal processes, also come into play. This section attempts to provide some background to charge carrier trapping in TiO_2 to assist in clarifying the role of trapping in photocatalysis.

2.4.1. Electron trapping

Electron traps are believed to be localized in the TiO_2 lattice as Ti^{3+} sites, although the degree of localization remains unclear. Topics discussed here include the trapping site, energy, kinetics and concentration, and methods for detection of traps in/on TiO_2.

Trapping energy: Electrons lower their energy by trapping. Reports of the electron trapping energy of range between 0.1 and 1 eV [111,487–491], consistent with photoemission results for electronic defects on the surface of TiO_2 single crystal surfaces [175]. The energies of surface electron trap states can be affected by applied potential (in an electrochemical system) [492] by local structure and dielectric properties [411] or by the presence of adsorbates. The trapping event likely entails structural relaxation that contributes to localization. Frequently, a distribution of trapping energies is observed arising from an ensemble average of different trap sites present [420,422,423,432,435,438,446,468,478,493–501]. The lifetimes and reactivities of these will also depend on the local properties. It is not well-understood what causes the energy distribution in trap sites, but site heterogeneity appears to be the most likely cause.

Trapping site: One means of identifying trap sites has been to determine which sites gain the most stabilization by having electrons localized in their unoccupied CB states. The general consensus in the field is that electrons prefer trapping at the surfaces of TiO_2 (irrespective of the polymorph) [51,133,202,488,492,493,502–516]. However, there are reports of electron trap sites being located in the bulk [457,512–514,517–521], and theoretical studies predict bulk (subsurface) trapping over surface trapping [477,485,522,523]. Other theoretical work. [123] proposes that the most stable electron trap sites should be under-coordinated Ti cation sites located at surfaces. Studies by two separate experimental groups [513,514] suggest that bulk electron trap sites mainly arise from heat treatments and not from any inherent structural property of an ideal bulk TiO_2 structure. Similarly, other groups suggest that electron traps occur at TiO_2-TiO_2 particle interfaces [429,518,524] or at grain boundaries [525]. Pore size, which affects the electrostatics at pore walls, can have a significant influence on electron trap stabilities based on work by Planelles and Movilla [411]. These authors calculated the dependence of nanopore sizes in semiconductors on their ability to trap electrons using a model that examines the self-polarization induced charge stabilization at the pore walls for single electron wavefunctions. For TiO_2, they calculated that electron trapping induced by nanopores occurred for pores <14 nm in diameter, with the trapping stability depending mostly on the pore diameter and the chosen dielectric constant.

Based on Fourier transform infrared (FTIR) analysis, Szczepankiewicz et al. [508,510] proposed that photoexcited electrons are preferentially trapped at surface OH groups on TiO_2. Fig. 2.6 shows the effect on the O–H stretching region as a result of UV irradiation. Spectrum 'a' is of a partially dehydrated surface and 'b' is after UV irradiation. The most noticeable effect is the appearance of a sharp feature at 3716 cm^{-1} that was assigned to an isolated Ti^{3+}–OH^-. These authors proposed that Ti^{4+}–OH^- species were preferred as electron traps because the trapping energy ($\sim$0.5 eV $\approx$ 4000 cm^{-1}) matched the O–H stretching excitation energy. They also proposed that

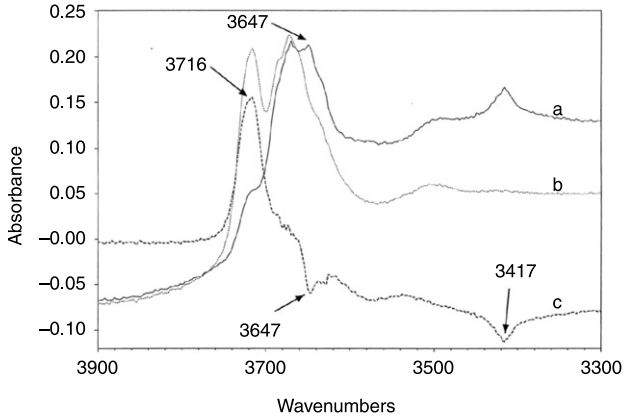

Fig. 2.6. Effect of UV irradiation on the FTIR spectrum of P-25: (a) partially dehydrated P-25 under vacuum, (b) 'a' after UV irradiation, and (c) difference spectrum, 'b'-'a'.
Source: Reprinted with permission from Szczepankiewicz et al. [510].
© 2000, American Chemical Society.

the matching of the O–H stretching energy to the trapping energy facilitated energy dissipation during the trapping process. Luminescence measurements on A TiO_2 nanoclusters [133] and studies on single crystal R TiO_2(110) [202,515] have also suggested that electrons prefer surface OH groups as trap sites. Perhaps the easiest means of differentiating between bulk and surface trapping is by employing an electron scavenger, such as O_2, to titrate off the surface traps [51,202,488,492,503,506,508–511,513,515,517]. This, however, is not a fool-proof approach since one could argue that the degree of delocalization in the electron wavefunction associated with a subsurface trap could be sufficient to allow a surface species (such as O_2) to interact with a subsurface electron trap state. Based on STM data for R TiO_2(110), Wendt et al. [526] recently proposed that subsurface charge associated with Ti^{3+} interstitial sites can be available at the surface to a degree sufficient to promote O_2 dissociation. The depth at which these electronic states can no longer participate in surface chemistry not known.

The degree of electron localization in surface (and bulk) traps remains an elusive issue, predominately because of the lack of experimental probes to address this issue and uncertainties associated with DFT methods. Recently, Minato et al. [527] used STM to examine the electronic signature of surface defect states on R TiO_2(110). While the extent to which oxygen vacancy sites on R TiO_2(110) can be used as models for electron trap sites remains to be seen, the similarities between their energies and chemical reactivities make surface vacancies a reasonable model for fundamental studies of electron traps. As shown in Fig. 2.7(a), Minato and coworkers found that the 'unoccupied' electronic states associated with vacancies were localized (to the extent revealed by STM contrasts), but clearly appeared delocalized when imaged by the occupied states (b). In the latter case, the images correspond to tunneling from the surface (occupied states) and show electron density on cation sites adjacent to vacancies. Occupancy of the vacancy sites by OH groups did not significantly change the degree of electron delocalization. These data suggest that electrons confined in shallow donor sites at TiO_2 surface sites are delocalized.

The site preference for an excited ('excess') electron was explored theoretically by Deskins et al. [485] using DFT + U calculations on the R TiO_2(110) surface. As shown in Fig. 2.8 (left), these authors found that subsurface Ti sites were energetically more favorable for trapping electrons than the Ti sites located below bridging O sites (O_b), which were highly unfavorable for electron trapping. Their results also found that deeper sites ($\geq$2 lattice spacings down) were unfavorable and that surface five-

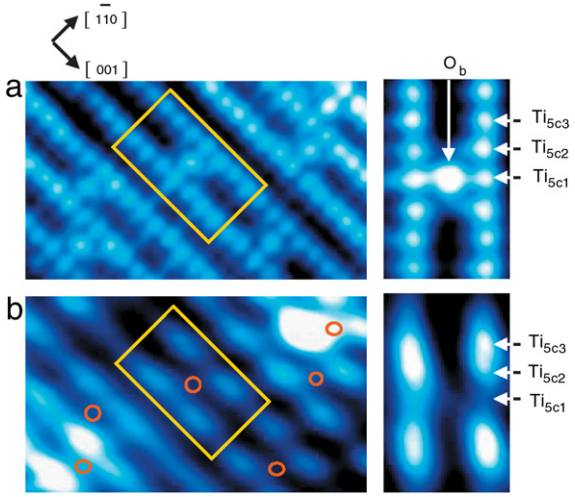

Fig. 2.7. Constant current STM images from the R TiO_2(110) surface at 78 K. (a) Unoccupied state image ($V_s = +0.6$ V; $I_t = 0.6$ nA), and (b) occupied state image ($V_s = -1.1$ V; $I_t = 0.1$ nA). Images on the left are 3.4×5.8 nm and those on the right (from the boxes on the left) are 2.1×1.3 nm. Circles in 'b' indicate oxygen vacancies in 'a'.
Source: Reprinted with permission from Minato et al. [527].

coordinate Ti^{4+} sites (labeled 'Ti_{5c}') were favorable trapping sites. Similar calculations for hydroxylation of the O_b sites (Fig. 2.8, right) did not alter the preference for subsurface cation sites but did make Ti cation sites below the OH sites slight more favorable as surface traps.

Trapping time scale and trap stability: Much is known about electron trapping in TiO_2 from DSSC studies, where localization of a hole on an anchored dye molecule permits examination of the behavior of the injected electron in the TiO_2 CB in the absence of a VB hole. One of the major findings from studies using ultrafast spectroscopies, is that the trapping timescale of an injected electron is quite short. Most groups concur that trapping of an injected electron occurs on a sub-picosecond time scale [111,386,399,488,512,528–534] and possibly shorter than 100 fs [535] depending on the conditions. These observations indicate not only rapid thermalization of the injected electron within the CB, but also that the electron rapidly finds and localizes in particular Ti 3d electronic states, which then 'falls out' of the TiO_2 CB into a shallow donor state (see below).

While the trapping timescales are very short, many groups have observed that the trapping lifetimes can be very long, particularly in the absence of electron scavengers (such as O_2). Various research groups [133,488,495,506,508,509,536–540] have determined electron trap lifetimes over a wide timescale (from hundreds of picoseconds [488] to months [540]) as a result of (intentional or unintentional) manipulation of hole scavenger concentrations. For example, Peiró et al. [509] used ethanol as a hole scavenger to study electron trapping in synthesized nanocrystalline TiO_2 films, and in films of commercial P-25 and P-90 (which has smaller particles and greater A content than P-25) with transient absorption spectroscopy. Fig. 2.9 shows that in the absence of ethanol and O_2, the transient signal at 800 nm (associated with excitation of trapped electrons) had a long half-life (~25 μs), reflective of slow e^-/h^+ pair recombination at trap sites. This is in agreement with an earlier conclusion by Rabani et al. [538] that electron trapping competes well with e^-/h^+ pair recombination even in the absence of a suitable hole scavenger. Peiró and coworkers further observed that in the presence of ethanol (but still no O_2), electron trapping lifetimes were even longer (~0.5 s) (see Fig. 2.9). The opposite was seen with O_2 present but ethanol not present (not shown).

As mentioned above, the electronic state associated with surface Ti^{3+} sites on single crystal TiO_2 surfaces has been shown to mimic the chemical properties of trapped electrons on TiO_2 powders [199]. These Ti^{3+} sites are stable on single crystal TiO_2 surfaces indefinitely at room temperature under UHV conditions [175] (i.e., under the best controlled conditions that exclude the influence of scavengers). These observations highlight the ability of TiO_2 surfaces to rapidly stabilize CB electrons in trap sites, and accounts for why this material can sustain hole-mediated photochemistry (e.g., organic photooxidation) in the absence of electron scavengers [202,515,541–543]. It would appear that TiO_2 surfaces have a built-in mechanism for dealing with excess electrons (charge) when the electron scavenger concentration wanes or when scavenger access to the surface becomes temporarily blocked by other adsorbates.

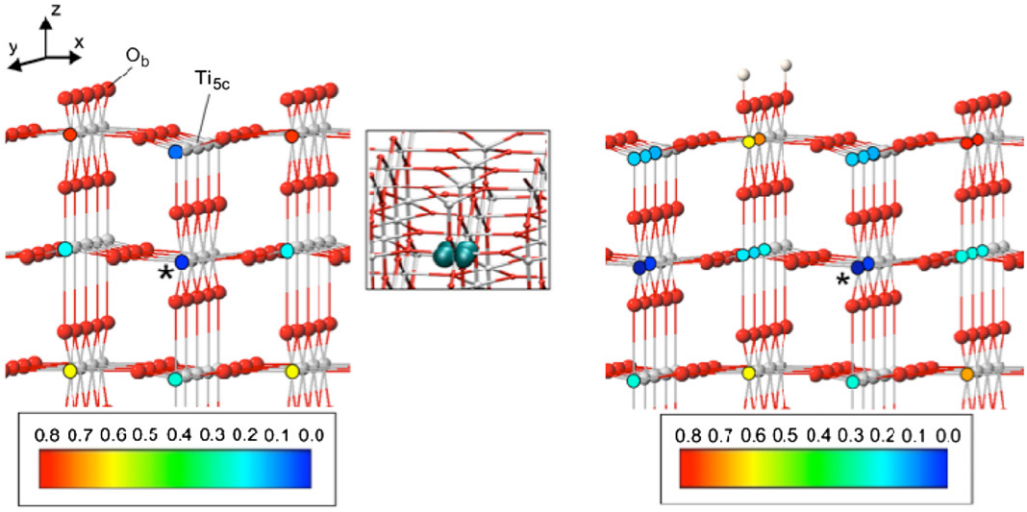

Fig. 2.8. Relative energies for electron polaron structures in R TiO_2(110) resulting from addition of an excess electron. The colored scale and corresponding colored circles are for specific trapping sites of the excess electron. Left: ideal surface; right: partially hydroxylated surface. The asterisks show the preferred trapping site in each case, with the spin density profile of the associated Ti d_{xy} state shown on the left. (For interpretation of the references to color in this figure legend, the reader is referred to the web version of this article.)
Source: Reprinted with permission from Deskins et al. [485].

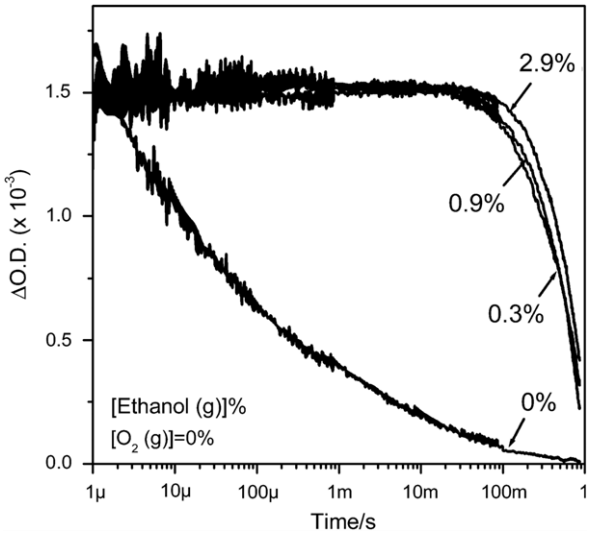

Fig. 2.9. Transient absorption spectra (excitation at 337 nm and probe at 800 nm) of excited electrons in nanocrystalline TiO_2 films under anaerobic conditions at various gas phase concentrations of ethanol (in N_2).
Source: Reprinted with permission from Peiro et al. [509].
© 2006, American Chemical Society.

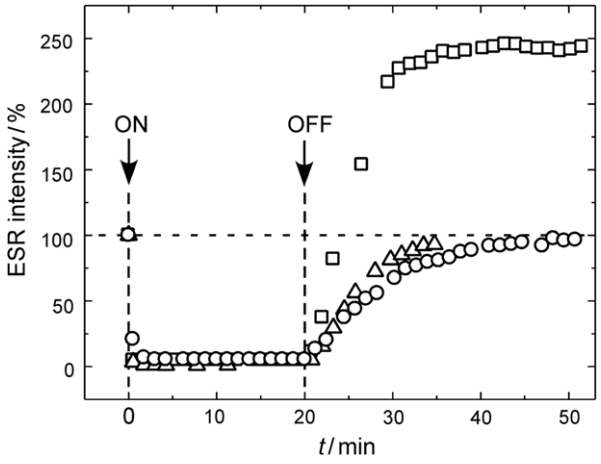

Fig. 2.10. Relative changes in the EPR (ESR) signals associated with trapped electrons in anatase (circles), rutile (triangles) and P-25 (squares) resulting from visible light irradiation in air.
Source: From Komaguchi et al. [186].

Electron detrapping: Electron detrapping [186,393,435,440,446, 456,468,478,484,498,539,544–547] is of importance in applications that rely on rapid electron transport (e.g., photovoltaic applications). Detrapping of electrons can be viewed from two perspectives: polaronic hopping, which can be envisioned as 'trap-to-trap' hopping [475], and complete detrapping, which involves conversion of a localized electron state to a delocalized ('free') electron. Detrapping can be initiated via thermal activation [440,446, 456,484,546], where the barriers are thought to be on the order of 0.1–0.3 eV [446,456,484], or via non-thermal activation [186, 539,547], particularly by means of sub-bandgap light. In concept, both polaronic hopping and CB detrapping should be accessible thermally. At room temperature, thermal detrapping on TiO_2 is rapid, occurring at a rate of 10^8 events per sec based on sensitization studies by van de Lagemaat and Frank [393]. In contrast to thermal detrapping, non-thermal detrapping via optical excitation will be governed by the optical properties of the trap state. Shkrob and Sauer [539] found that electron detrapping in colloidal A TiO_2 resulted from either 532 nm or 1064 nm light. They observed charge recombination as a result of optical detrapping on a timescale faster than 3 ns (pulse width limited), with Q efficiencies of 0.28 and 0.024, respectively. Interestingly, these Q values did not match the relative absorption intensities at the respective wavelengths suggesting that not all absorption events at 1064 nm led to detrapping. Beerman et al. [547] and Komaguchi et al. [186] also showed that visible light absorption could enhance electron detrapping in TiO_2. For example, in Fig. 2.10, Komaguchi and coworkers tracked Ti^{3+} electron spin resonance (ESR — essentially the same technique as EPR) signals for thermally reduced A (circles), R (triangles) and P-25 (squares) during and after visible light irradiation. In both the A and R cases, attenuation of the ESR signals to near zero during irradiation was attributed to detrapping (since 'free' CB electrons give no ESR signal). The ESR signals then returned to previous levels after the light was turned off. The exception to this was P-25, where the ESR signal increased to a level greater than in the initial case. Analysis of the spectral features led the authors to conclude that electrons were detrapped from the A component of P-25 and 'retrapped' on the R component (which happens to gives more intense Ti^{3+} ESR signals than does A). Reduced P-25 exposed to air (which removes surface Ti^{3+} sites but not bulk sites) showed evidence for surface Ti^{3+} signals after irradiation, indicating retrapping of bulk electrons at surface sites.

Trapped electron detection: Many groups [5,140,186,387,457, 499,513,519–521,548–559] have used EPR (ESR) to detect and characterize trapped electrons (and holes) on/in TiO_2, with surface and subsurface trap sites distinguished using chemistry (e.g., O_2). The spin state environments allow researchers to differentiate between paramagnetic features associated with Ti (trapped electrons) and O (trapped holes), as well as their populations and reactivities. Although EPR is an extremely powerful tool for characterizing trap states in TiO_2, it is not convenient for many researchers, for example, because of its low temperature requirement of operation. Other techniques have been sought for detection and characterization of trapped electrons in TiO_2.

A number of groups have used optical spectroscopies for detecting trapped electrons [51,386,399,488,489,506,528–531, 540,560–563]. The real challenge here is correlating absorption events at specific wavelengths, which are typically very broad, with specific sites in or on TiO_2. Identification of the excited state level of an optical transition is another challenge, as excitation of a trapped electron could be via a polaronic excited state or into a delocalized (CB) state. As illustrated by the schematic model of Yamakata et al. [51] (Fig. 2.11), many of the authors above have proposed two types of optical transitions for excited electrons: those associated with 'free' CB electrons and those associated with trapped electrons (which the authors depicted as being excited into the CB, although localized excitations are as likely). Spectral features ranging from the IR to the near-UV have been associated with these transitions, with assignments made either by titrating trapped holes or trapped electrons with appropriate scavengers (e.g., organics or O_2, respectively). Ikeda et al. [488] differentiated optical transitions due to trapped holes from those of trapped electrons resulting from band-to-band excitation of colloidal TiO_2 suspended in deaerated solutions using hole scavengers (methanol or triethanolamine). These authors assigned transitions at ~600 nm to excitations of trapped electrons, in agreement with other studies [506,528–531,563]. Other groups found that trapped electrons resulting from injection or direct excitation were excited in the IR [51,560–562], a region of optical absorption otherwise interpreted to 'free' CB electrons. For example, Fig. 2.12 shows optical absorption spectra of van't Spijker et al. [560] for electrons trapped in nanoporous A films following electron injection from various Ru-based dyes. The broad absorption feature above ~1000 nm was attributed to excitation of trapped electrons

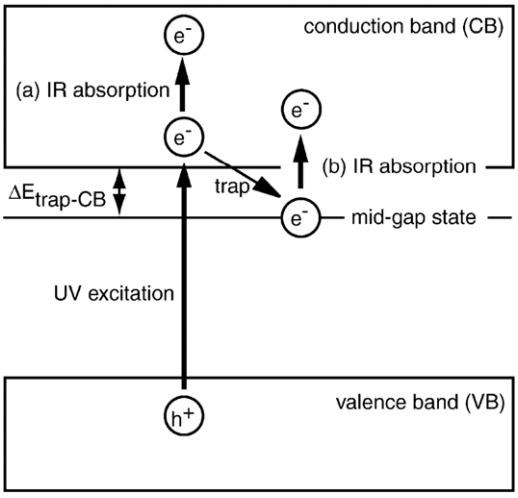

Fig. 2.11. Schematic illustration of possible optical transitions associated with excited electrons following band-to-band transitions in TiO_2. (a) CB electrons and (b) trapped electrons.
Source: From Yamakata et al. [51].

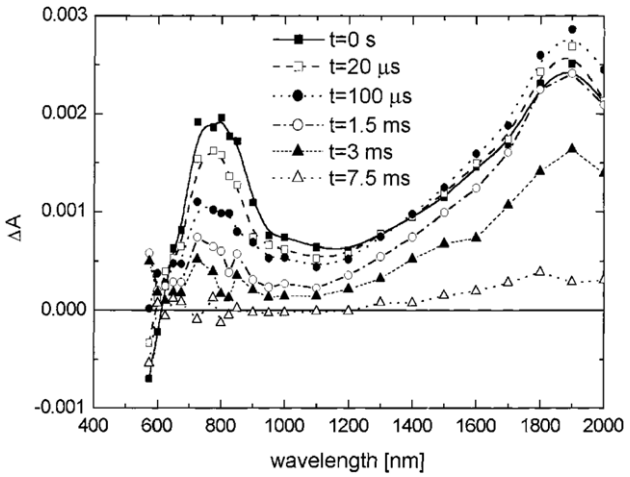

Fig. 2.12. Transient absorption signal as a function of probe wavelength following excitation of dye sensitized TiO_2 with 532 nm light.
Source: Reprinted with permission from van't Spijker et al. [560].
© 2001, American Chemical Society.

and the absorption at ~800 nm was due to the dye cation. The authors used these data to characterizing the lifetimes of the trapped electron and the dye cation. On the other hand, Boschloo and Fitzmaurice [489] proposed that optical transitions at ~400 nm were more likely to involved trapped electrons. Kuznetsov et al. [540] observed a broad absorption continuum for trapped electrons that spanned the range from 350 nm to 2.5 μm. Clearly better identification is needed of what these transitions are (i.e., from what state to what state), as well as what they are associated with (e.g., electrons or holes).

Not much work has been done on characterizing trapped charges on single crystal TiO_2 surfaces by means of their electronic transitions. As mentioned above, EELS is both surface sensitive and provides insights into optically excited transition by means of similar selection rules for inelastic electron scattering [564,565]. As shown in Fig. 1.8, EELS analysis of the R TiO_2(110) surfaces shows band-to-band excitations above ~3 eV, the R bandgap region, and an intense feature at ~0.8 eV that tails into the bandgap region [199,201,202]. The latter is due to excitations of Ti^{3+} centers on the R TiO_2(110) surface. It is important to keep in mind that EELS, like optical spectroscopies, does not provide information about the *positions* of initial and final electronic states, but only the transition energies. The 0.8 eV energy values for the defect state's position relative to the Fermi level that is obtained from photoemission [175,566] and the 0.8 eV EELS feature seen in Fig. 1.8 are purely coincidental. The 0.8 eV EELS feature does not correspond to excitations from Ti^{3+} sites into the TiO_2 CB for two reasons. First, the DOS at the CB edge is near zero, as seen by the weak signal for band-to-band excitations at ~3 eV, so there should be little EELS signal at 0.8 eV based on photoemission. Second, transitions to the CB from the trap state, if possible, would result in a continuum of excitation energies from ~1 to 5 eV based on the electronic DOS in the CB (see Section 7). Instead, excitation of surface Ti^{3+} on R TiO_2(110) appear localized in energy consistent with a polaron excitation model. These data show that the surface optical transition intensity (as probed by specularly scattered electrons in the EELS technique) of the defect state is intense relative to band-to-band excitations. In agreement with many studies, exposure of the surface to O_2 oxidizes the surface oxygen vacancies and removes the vacancy-related Ti^{3+} excitation feature at 0.8 eV (see Fig. 1.8(d)). The population of trapped electrons on the TiO_2(110) surface, as gauged by the ~0.8 eV transition, has been shown to track the degree of hole-mediated photochemistry on R TiO_2(110), and was not susceptible to water chemistry [199].

TiO_2 trap capacities: The capacity of TiO_2 surfaces to trap photogenerated electrons is an important issue for photochemical applications. The ability of TiO_2 surfaces to trap high coverages of electrons has a significant impact on sustaining photooxidation rates under 'lean' oxygen conditions or when surfaces become covered with strongly bound organics that block access of oxygen [515]. Alternatively, surface traps can be viewed as electron 'storage' sites. To the extent that transport depends on trap filling, then the number and energy of traps are both important. One of the earliest studies on the electron trapping capacity by TiO_2 was done by Kormann et al. [125], who suggested that up to 10% of the cation sites in a nanoparticle could be occupied as electron traps when ethanol was used as a hole trap and O_2 was absent. Similarly, the Kanaev group [537,540,567,568] measured trapping capacities of 7%–14% in TiO_2 gels. Ikeda et al. [488] examined a variety of TiO_2 powders under colloidal conditions, and measured the electron trapping capacity using methylviologen (which readily reacts with Ti^{3+} sites) in deaerated solutions rich in hole scavengers (methanol or triethanolamine). With this approach only surface traps were quantified. From analysis of the authors' data, the coverage of trapped electrons per unit surface area of each powder varied from $\sim 1 \times 10^{13}$ to $\sim 3 \times 10^{14}/cm^2$. The authors also observed that the maximum coverage of trapped electrons varied more with particle size than with polymorph type, with the large particles sustaining more charge per unit surface area than small particles. This is in agreement with results by Kopidakis and coworkers [502] who showed that the electron trapping capacity in porous TiO_2 films was proportional to surface area. In contrast, results by Katoh et al. [505] showed that, after normalizing for surface area, 20 nm sized TiO_2 particles trapped more electrons than did 300 nm particles. Wang et al. [516] have shown that the electron trap populations on nanoporous A TiO_2 vary with pH (indicating surface trapping) from $\sim 4 \times 10^{11}/cm^2$ at pH = 4.7 to $\sim 5 \times 10^{13}/cm^2$ at pH = 13. This is consistent with measurements by Boschloo and Fitzmaurice [489] for electron trapping levels on the surface of an A film of $\sim 3 \times 10^{12}/cm^2$. Berger et al. [387] have shown that irradiation of A nanoparticles of ~13 nm average diameter resulted in ~10 charge traps per nanoparticle with only one electron–hole (e^-/h^+) pair per particle surviving to ~298 K. Two other reports [393,538] indicate that the electron trapping

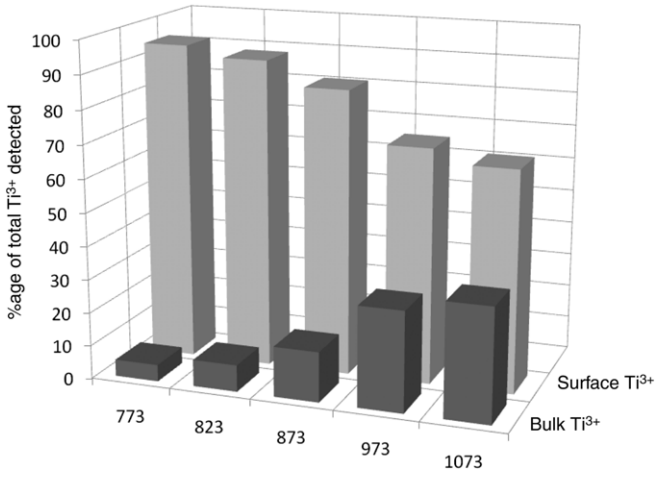

Fig. 2.13. Variations in the surface-to-bulk ratio of Ti^{3+} states in rutile powder measured by EPR as a function of thermal reduction temperature.
Source: Adapted with permission from Jenkins and Murphy [514].

capacity of nanoparticulate TiO_2 is on the order of one electron per nanoparticle.

One way of considering relative electron trap capacities in the surface versus the bulk would be to ask how the polymorphs of TiO_2 respond to reduction because, to some extent, a photogenerated trapped electron resembles reduction [175]. As shown in Fig. 2.13, Jenkins and Murphy [514] used EPR and O_2 titration to show that the level of bulk Ti^{3+} sites (generated by vacuum reduction) in R exhibited an increase relative to the surface concentration as a function of heating in vacuum to >823 K. However, the R surface still possessed ~95% of the Ti^{3+} signal up to this temperature. (Surface versus bulk Ti^{3+} signals were differentiated by O_2 exposure.) While intriguing, more work is needed to verify the similarities and differences between Ti^{3+} sites generated by vacuum reduction with those formed when an excited electron becomes trapped. Nevertheless, these data suggest that from a thermodynamic perspective, R surfaces can stabilize more Ti^{3+} states than can the bulk. In agreement with Jenkins and Murphy, numerous studies on single crystal R surfaces have shown large capacities for stabilizing reduction, particularly compared to the levels that can be achieved in the bulk prior to the onset of bulk reconstruction (see citations in [178]). It is well-known that the R TiO_2(110) surface can stabilize oxygen vacancy concentrations on the order of 10% or more [175,566]. Much higher concentrations of surface reduction have been achieved on R TiO_2(110) during aerobic photochemistry [202,515]. As yet, there does not appear to be examples in the literature for electron trapping at A single crystal surfaces under similar aerobic photochemistry conditions [542]. (See Section 7 for discussion on the reducibility of A versus R surfaces.)

2.4.2. Hole trapping

Unlike the case of electron trapping studies conducted through sensitization, there are no convenient means to inject holes into the VB of TiO_2. Still, much work has been invested toward understanding hole trapping during band-to-band excitation processes because of its importance in understanding photocatalytic redox processes on TiO_2.

Trapping site: Numerous groups have explored hole trapping at A and R surfaces [386,399,412,457,476,477,504,513,518–521,534,549,552,559,569–572], particularly by means of hole scavenging chemicals such as SCN^-, organics or I^-. EPR results by several groups [457,518–521,549,552,559,570,571] indicate that the most likely hole trap site is a surface Ti^{4+}–O^- site, where the hole resides on an under-coordinated (surface) oxygen atom. However, it is unclear what the preferred coordination of such a site should be (e.g., bridged or oxo type). Thurnauer's group [518,520,552] examined hole trapping on the surfaces of P-25 and R using various EPR techniques. They found that replacement of H in surface OH groups with D did not change the observed O^- lineshape, but enrichment of the surface with ^{17}O did, leading them to conclude that holes did not trap at surface oxygen anion sites that were protonated. Additionally, some groups have also found evidence for subsurface hole traps [386,399,503,569,573]. Kerisit and coworkers [477] performed electrostatic calculations on hole (and electron) trapping at the unrelaxed R TiO_2(110) surface. Their results, shown in Fig. 2.14, suggest that holes preferred trap

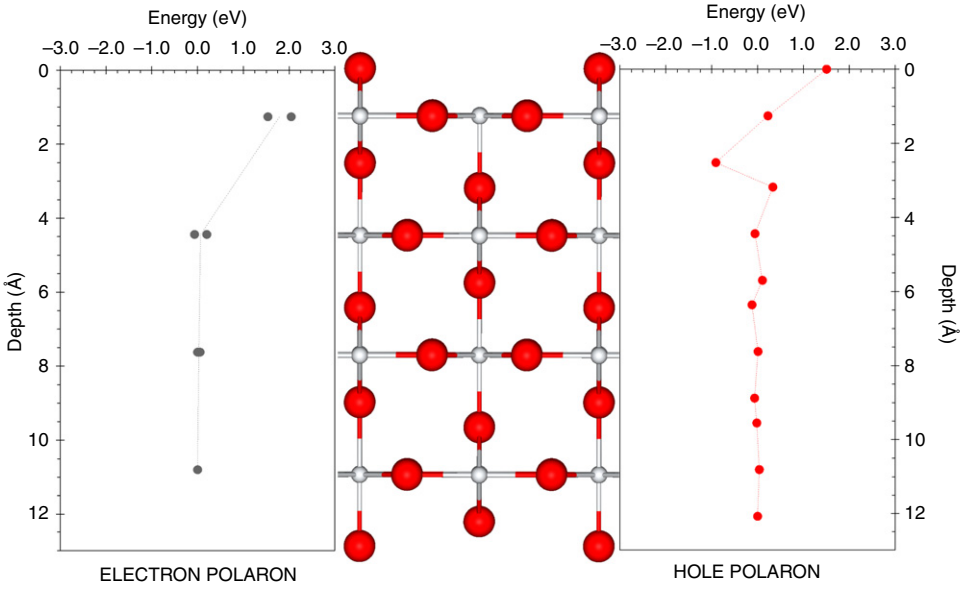

Fig. 2.14. Electron (left) and hole (right) polaron free energy profiles at and near the R TiO_2(110) surface. A model of the R TiO_2(110) surface (middle) provides reference locations for each trap site.
Source: Reproduced with permission from Kerisit et al. [477].

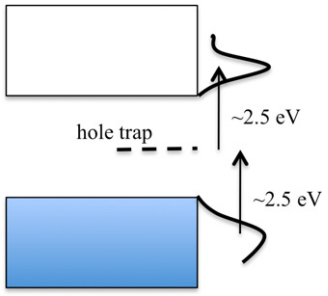

Fig. 2.15. Schematic model for possible optical transitions associated with a partially occupied mid-gap state in TiO_2. Conceptualized occupied VB (bottom) and unoccupied CB (top) DOS are based on approximate maxima in each being ~1 eV below/above the respective band edges (see text).

sites in the near-surface region, as opposed to in the bulk or on surface sites. (In contrast, electrons preferred subsurface sites.) Their findings are consistent with results by Shapovalov et al. [522] using an *ab initio* embedded cluster approach.

Trapped hole detection: Compared to the case of trapped electrons, there are fewer accounts regarding the optical properties of trapped holes [386,399,402,412,504,534,569,574]. Although absorption events in specific spectral regions have been assigned based on comparisons before and after exposure to hole scavengers, the exact nature of the optical transitions (from what state to what state) is not known. Furube's group [386,399,504,569] used transient absorption spectroscopy and CH_3OH as a scavenger to track hole trapping in nanocrystalline films of A (comprised of particles $\leq$20 Å). They assigned the spectral region at ~500 nm to excitation events associated with trapped holes. Similarly, Yang and Tamai [534] observed a broad transient absorption signal at ~520 nm evolving immediately on excitation of colloidal A with a 200 fs 360 nm pulsed laser source. This absorption was assigned to excitation of trapped holes because it was not observed if the hole scavenger SCN^- was present. Features in this spectral regime (~2.5 eV) are difficult to assign because they can correspond to transitions from the maximum DOS in the VB (~1 eV below the VB edge) to a gap state, as well as transitions from a partially occupied gap state to the maximum DOS in the CB (~1 eV above the CB edge), as shown in the cartoon of Fig. 2.15. The latter transition would correspond to excitation from a doublet O 2p state (O^-) in the gap to the CB. While this is optically allowed, it likely results in a highly unstable O state. The former possibility would correspond to excitation from the VB into the same O 2p gap, which may not be optically allowed.

There are no studies quantifying the capacity of TiO_2 surfaces to trap holes or spectroscopic observations of trapped holes at specific surface sites on a single crystal TiO_2 surface. However, Thompson and Yates [573] were able to quantify hole trap densities in the near-surface region of a R TiO_2(110) surface by varying the photon flux and using O_2 PSD as a gauge of the hole concentration reaching surface (see Fig. 2.16). (PSD of chemisorbed O_2 is a hole-mediated process in which a hole neutralizes an adsorbed $O_2^{\delta-}$ species resulting in neutral O_2 and subsequent desorption; see Section 5 for more details.) These authors observed two domains in the relationship between the photon flux and the O_2 PSD yield. At low fluxes, they found that the O_2 PSD yield was significantly less than at high fluxes and proposed that this was due to preferential trapping of holes away from adsorbed O_2 molecules, presumably in the subsurface. As the photon flux exceeded a critical threshold (labeled in Fig. 2.16), the flux of holes reaching the surface eclipsed that being trapped and the rate of O_2 PSD increased. These authors estimated a hole trap density of ~2.5×10^{18} cm^{-3} (~0.004%), which is comparable to typical electron donor concentrations in vacuum reduced R single crystals (see the work of Aono

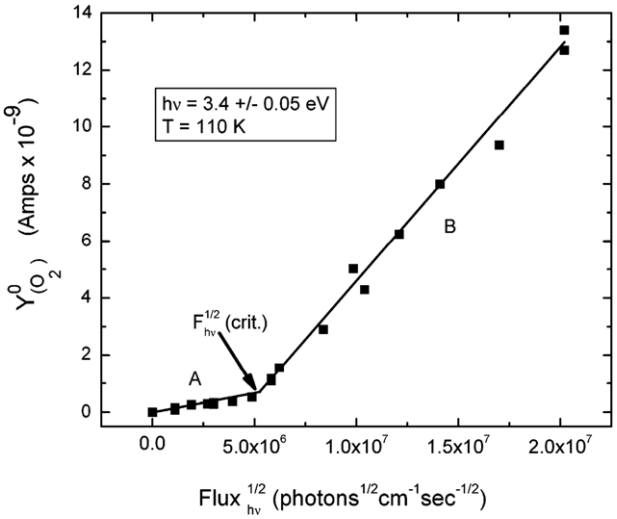

Fig. 2.16. Dependence of the $^{18}O_2$ photodesorption yield on the incident UV photon flux for $^{18}O_2$ adsorbed on the R TiO_2(110) surface at 110 K.
Source: Reprinted with permission from Thompson and Yates [573].
© 2005, American Chemical Society.

et al. [575]). Although characterization of the actual hole traps was not part of their study, these authors determined that the observed hole trapping was dynamic and not static. That is, the hole trap sites were readily regenerated via neutralization, allowing the trap sites to participate in multiple trapping/neutralization events during the course of the measurements. Studies on vacuum reduced A TiO_2 powder which show less surface hole trapping than with unreduced samples suggest that these bulk traps are related to reduced centers arising from vacuum processing [559].

The stability of surface trapped holes in TiO_2 powders may be different from that of the near-surface traps in R TiO_2(110) probed by Thompson and Yates. If the accompanying excited electron is removed (with an electron scavenger), lifetimes on the order of milliseconds to minutes have been estimated for holes trapped at TiO_2 surfaces in the absence of hole scavengers (static trapping) [386,398–400]. EPR studies show that when the electron is not scavenged, the surface trapped holes were stable up to ~180 K, above which electron detrapping and neutralization occurs [457, 519,549,552].

Hole trapping on the surfaces of TiO_2 appears to occur as rapidly as does electron trapping. Yang and Tamai [534] estimated a hole trapping timescale at the surface of colloidal A particles of ~50 fs using transient absorption signal at ~520 nm after excitation at 360 nm. This transient feature was not observed if the hole scavenger SCN^- was present, indicating that trapping does not compete well with electron transfer from SCN^-. Similarly, Tamaki et al. [386,399,400] estimated a hole trapping timescale of ~200 fs for 'hot' holes resulting from band-to-band excitation at either 266 or 355 nm. The trapped holes then thermalized over the next 100+ ps. As with Yang and Tamai, the presence of a hole scavenger (in this case, CH_3OH) precluded these observations. Shen and coworkers [401] also found that the lifetimes of trapped holes in R were longer than in A. These authors used a 'lens-free' heterodyne (LF-HD) transient grating technique to follow the lifetimes of charge carriers in A and R films constituted from nanoparticles. This technique essentially monitors the change in reflectivity of light resulting from generation of charge carriers in the near-surface region. Fig. 2.17(a) shows that over 60% of the initial transient signal (attributed to holes) attenuated in A within ~2 ps of excitation, but >95% of the same signal in R persisted beyond 50 ps (Fig. 2.17(b)). Although the authors did not provide some experimental details in their paper (e.g., the

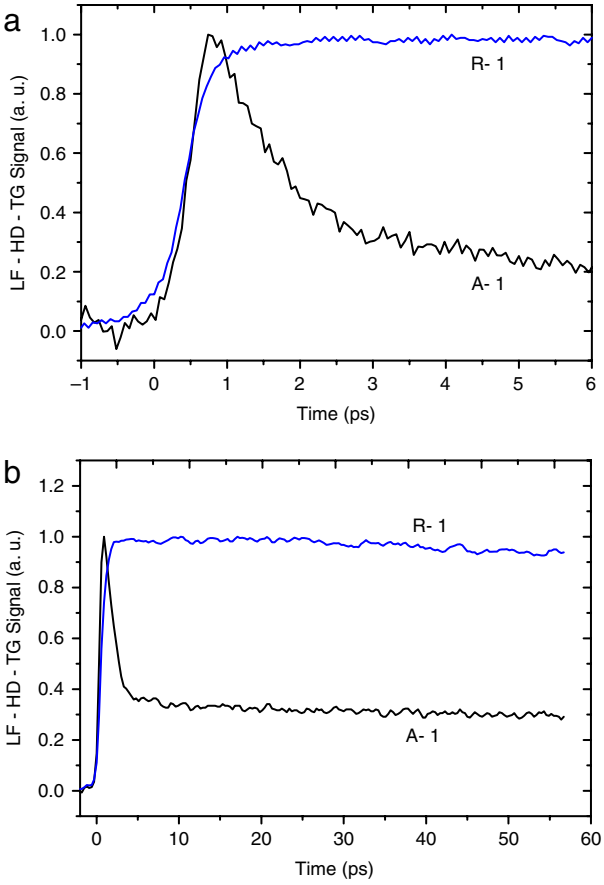

Fig. 2.17. Transient grating optical responses following band-to-band excitations of R and A films over time periods of (a) 6 ps, and (b) 60 ps. (The *y*-axis label 'LF-HD-TG' corresponds to 'lens-free heterodyne detection transient grating' — see text.) *Source:* From Shen et al. [401].

atmospheric conditions) and presented their data as normalized signals (preventing quantitative comparisons between A and R), their data clearly shows that charge carrier stability in their R films exceeded that of A. Assuming their measurements were specific to surface trapped holes, the findings of Shen et al. were consistent with theoretical work by Deskins et al. [476] who predict that holes should be more stable in R than in A.

2.5. Charge recombination

The all-to-common outcome of e^-/h^+ pair creation is recombination. While this is an undesirable event in photoconversion, much can be learned about charge carrier dynamics in TiO_2 by studying recombination. The two major outcomes of recombination are radiative and non-radiative energy release. The proportion of radiative versus non-radiative recombination events in TiO_2 is generally believed to be skewed toward the latter. The actual proportion is difficult to assess because the extents of absorption and recombination are not easy to determine. Additives such as dopants, supported metal particles, or interfacial heterojunctions have been employed by many groups to suppress (or even enhance) recombination. Details of these studies will be discussed in Section 6.

2.5.1. Radiative

Radiative decay (photoluminescence) of excitation events in TiO_2 has been the subject of growing interest in the field [17,101,110,114,117–119,132,136,377,379,383,384,412,576–590] because it reflects an avenue, albeit an unproductive one, in which energy from light absorption is dissipated in TiO_2. Photoluminescence is generally at sub-bandgap energies due to carrier relaxation (thermalization) and trapping. As a result, photoluminescence events provide insights into the dynamics and structural properties of TiO_2 in relation to thermalization and trapping. Photoluminescence can also result from exciton quenching (as opposed to charge carrier recombination). As shown in Fig. 2.18 [110], photoluminescence in A occurs at ∼2.3 eV (∼540 nm) via decay of a self-trapped exciton [17,101,110,114,119,377,379,383,384,581,582,587,591]. Surface modification or nanoscaling of A can shift this emission energy (see Section 1). The more distorted Ti–O octahedral structure in A facilitates exciton binding as opposed to the less distorted structure in the R lattice that favors 'free' excitons [114,118,119,582]. The R lattice is also slightly more dense (4.25 g/cm^3) than the A lattice (3.89 g/cm^3) which somewhat contributes to inhibiting distortions in the former relative to the latter. Self-trapped exciton photoluminescence in A has a strong emission component in directions perpendicular to the *c*-axis and weak component parallel to the *c*-axis [101,114,379]. The timescale for photoluminescence in A is typically on the order of nanoseconds [577,578], which reflects the self-trapping timescale and the resulting stability of the self-trapped exciton. Using epitaxial films of A TiO_2(001) on $LaAlO_3$(100), Murakami et al. [101] observed that photoluminescence from self-trapped excitons was significantly quenched at sample temperatures above 200 K, suggesting that recombination events at higher temperature became non-radiative due to increased lattice motions. Bulk defects or dopants in A have been shown to have an effect on the self-trapped luminescence state [119,377,587], as one might expect. Surfaces have also been shown to exert unique influences on the quenching of excitons in A [577]. For example, Zhu et al. [588,589] observed that surface sites on ∼4 nm diameter A particles associated with —OH or —OCH_2CH_3 groups gave rise to luminescence at ∼475 nm. Removal of these groups (e.g., by plasma treatment) resulted in disappearance of the 475 nm feature. In another example, Yoon et al. [591] showed that liposome templated A nanoparticles with disk-like shapes exhibited the main luminescence at 420 nm, with weaker features at 470 and 550 nm, indicative of three excitonic states, all interface related. Changes in time-resolved fluorescence of A nanostructures in various solid matrices (e.g., zeolites) resulting from thermal removal of OH/water suggests that emission is from surface and/or interfacial features [133]. Systems with other TiO_2-related interfaces (with SiO_2 [592] and supported Ag [385] or Pt [162] nanoparticles) have also been shown to play a role in photoluminescence following bandgap excitation of TiO_2 indicating radiative recombination at those interfaces. These studies indicate that surface structure and the presence of adsorbates on A surfaces play an important role in guiding neutralization events towards emission.

Photoluminescence in R TiO_2 is not as well-studied as it is for A. However, several groups have observed and explored this issue. Defects, surfaces and impurities are the likely sources of photoluminescence in R [577,579,580,584,585]. For example, Nakamura et al. [584,585] have shown that photoluminescence at single crystal R surfaces (namely, (100) and (110)) was observed on atomically smooth surfaces, but not from surfaces that had been photoetched (in $HClO_4$). Fig. 2.19 correlates atomic force microscopy (AFM) images for various surface conditions (left) with the photoluminescence (right) from these surfaces. As-received R TiO_2(100) and TiO_2(110) were rough ((a) and (b) on the left) and exhibited little or no photoluminescence ((c) and (d) on the right). After a mild HF etch, both 'as-received' surfaces became smooth with well-defined step structures ((c) and (d) on the left) and exhibited photoluminescence signal ((a) and (b) on the right) during potential controlled illumination with 365 nm light. These observations may indicate that well-

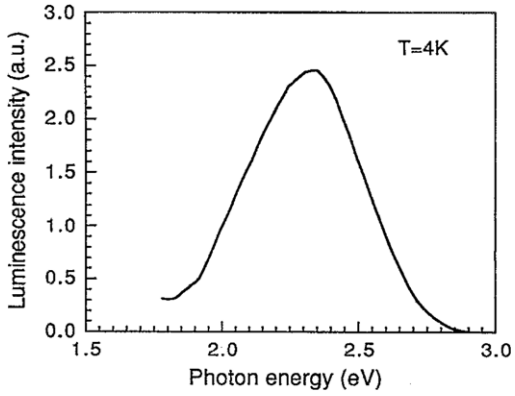

Fig. 2.18. Photoluminescence spectrum from an A film prepared by reactive sputter deposition.
Source: Reprinted with permission from Tang et al. (110).
© 1994, American Institute of Physics.

ordered sites or surface species (as in the A case) are key to photoluminescence on R surfaces. Amorphous surface structures may readily promote charge recombination events that do not lead to photoluminescence. As such, time-resolved studies on single crystal TiO_2 surfaces that correlate emission and photochemistry can provide unique insights into the dynamics of charge carrier recombination relative to that of electron transfer.

2.5.2. Non-radiative

The vast majority of recombination events in TiO_2 are believed to be non-radiative in nature [111,112,140,386,400,412,457,488,512,518,528–531,533,538,539,546,549,559,562,568,570,573,593–602]. As suggested by the results of Nakamura et al. [584,585] above, and as will be discussed in Section 7, the degree of crystallinity in TiO_2 plays a major role in promoting charge recombination events. Because non-radiative recombination events are difficult to directly detect, indirect measures such as the heat generated or the impact on charge carrier processes become the best metrics. For example, Leytner and Hupp [111] used time-resolved photoacoustic measurements to estimate that ~60% of excitation events in their colloidal A samples experienced recombination within 25 ns of excitation and that ~150 kJ/mol of energy was released (as heat) by these recombination events. (Band-to-band, non-radiative quenching of all absorption events would have corresponded to ~310 kJ/mol of heat.) In contrast, radiative recombination events are not expected to contribute significantly to heat generation. The two numbers (60% quenching and 150 kJ/mol released) form a self-consistent picture that most recombination events in their TiO_2 samples were non-radiative in nature.

The issue at hand is not just the loss of charge carriers in TiO_2 due to recombination, but the details of the relationship between recombination and the TiO_2 structure. As in the case of photoluminescence, surfaces, defects and impurities likely play roles in promoting recombination. As yet, there do not appear to be any systematic studies in the literature that correlate actual recombination rates with the concentrations, locations or types of recombination sites involved. There have been correlations between charge carrier densities and recombination rates [596,597], but these correlations do not directly provide insights into the nature of the TiO_2 recombination sites. Various studies have probed the timescales and dynamics of charge carrier recombination in TiO_2 on a global scale. Recombination events in colloidal or particulate systems span large timescales [111,400,412,512,531,533,594]. Rationalizing a wide range of recombination timescales starts with a better understanding of the surface and bulk structural conditions, including the influence of adsorbates and impurities. As an example, Rabani et al. [538] found that in the absence of an electron scavenger (an adsorbate), electron trapping competed well with recombination when the level of e^-/h^+ pairs per particle was kept at ~1, but greatly favored recombination as the 'density' of pairs increased. They also found that the presence of a scavenger decreased the amount of recombination (as one would expect). These results are consistent with what one would expect for the carrier concentration dependence of the recombination process. Several studies [528,531,533,599,603] observed 2nd order recombination kinetics, as one would expect. However, there is some disagreement on this issue. Grela and Colussi [604] used a random walk diffusional model to described the rates of charge recombination

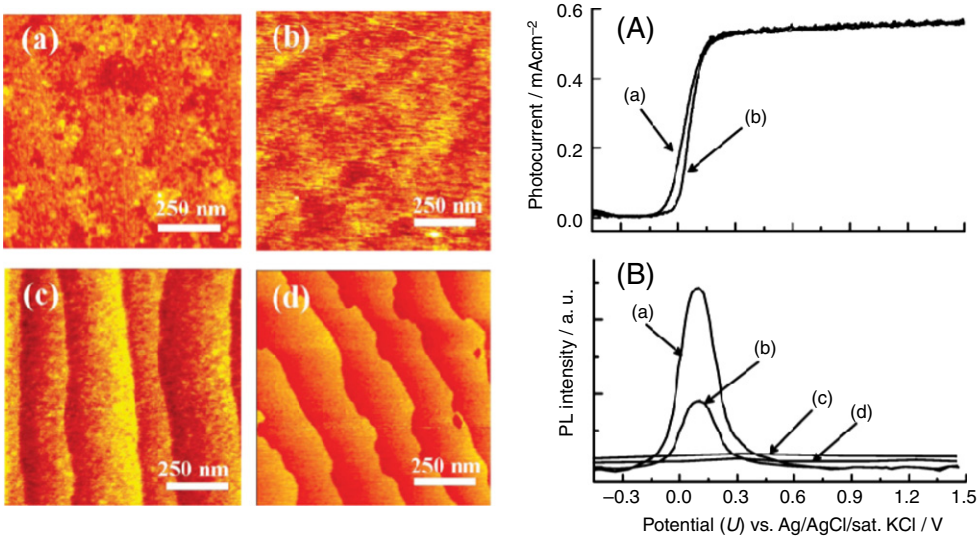

Fig. 2.19. Left: AFM images from (a) as-received R TiO_2(100) and (b) as-received R TiO_2(110), and those after treatment of these surfaces in 20% HF solution, followed by annealing in air at 600 °C ((c) and (d), respectively). Right: Photocurrent versus potential (A) and photoluminescence signal (>800 nm) versus potential (B) in 0.1 M $HClO_4$ solution. Traces 'a' and 'b' are for the HF-treated R TiO_2(100) and TiO_2(110) surfaces, respectively, and traces 'c' and 'd' are for the as-received R TiO_2(100) and TiO_2(110) surfaces, respectively.
Source: Reprinted with permission from Nakamura et al. [584].
© 2005, American Chemical Society.

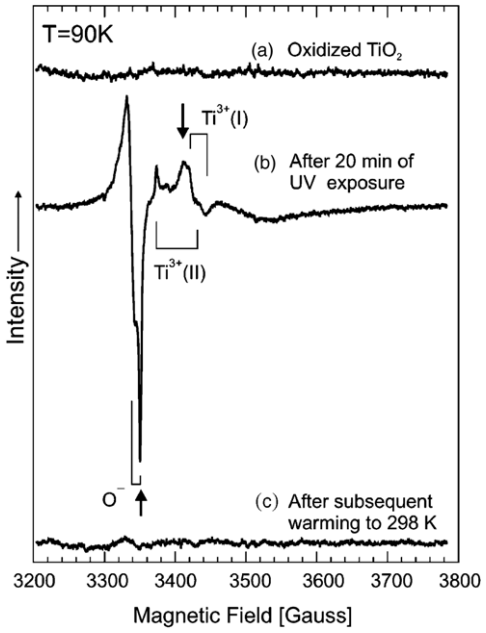

Fig. 2.20. EPR spectra from oxidized A nanoparticles (a), followed by: (b) UV exposure at 90 K, and (c) subsequent heating to 298 K.
Source: Reprinted with permission from Berger et al. [559].
© 2005, American Chemical Society.

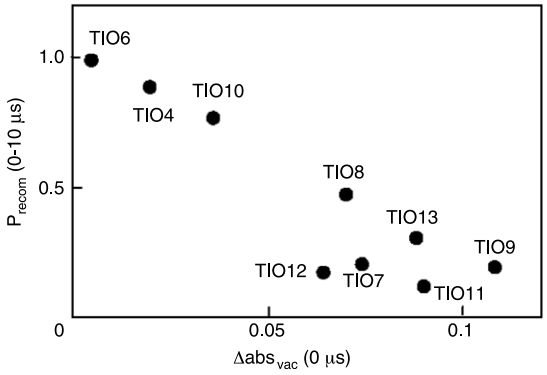

Fig. 2.21. Magnitude of the initial transient IR absorption response (at 2000 cm^{-1}) versus percent absorption of a 10 ns pulse of 335 nm light exposure to various TiO_2 nanoparticles samples (e.g., sample 'TIO4' is Degussa P-25) in vacuum.
Source: From Yamakata et al. [593].

in competition with the rates of electron transfer (for electron to O_2 and for hole to an electron donor) occurring on an A nanoparticle. They observed that the kinetics of recombination did not follow a 2nd order process. Exciton annihilation is first order but becomes 2nd order with rate asymptotically approaching a $t^{-1/2}$ dependence (characteristic of fractal kinetics) as a result of the exciton–exciton proximity in promoting recombination. The kinetics were still not second order if one carrier was strongly trapped and the other was free. Tamaki et al. [400] observed multi-exponential decay kinetics which they attributed to a distribution of diffusion-related rates influencing recombination.

Several studies have explored the relationship between surface trapped charges and charge recombination. For example, Hurum et al. [518] used EPR to characterize spin states generated from bandgap irradiation of P-25. Based on their EPR observations, they proposed that the majority of recombination events in P-25 occurred at the surface or at the interfaces between particles or phases. Most often recombination was the result of 'free' hole states reacting with electron trap states. Berger et al. [549, 559,570] also detected non-radiative decay of charge carriers through the disappearance of trapped charges in EPR, specifically during heating pre-irradiated TiO_2 from 90 K to room temperature (see Fig. 2.20). The activation energy required in this case for recombination was associated with detrapping of a charge carrier (most likely the electron) that enabled recombination. These authors [570] also detected local temperature changes (on the order of ~30 K) in EPR due to energy released from repeated e^-/h^+ pair recombinations.

Other groups have examined the relationship between recombination and the TiO_2 particle attributes (such as surface area). Du and Rabani [602] found that recombination rates did not depend on particle size, per se, but on the surface-to-volume ratio because the bulk density influenced absorptivity and the surface influenced recombination. Using transient spectroscopy, Yamakata et al. [593] estimated the probability of recombination within the first 20 μs of excitation on various TiO_2 samples. Fig. 2.21 shows that the extent of recombination varied greatly from ~10% to 100 % across samples. The variation in recombination had no apparent correlation to surface area or phase composition. Instead, these authors observed a correlation between the absorptivity and the recombination rate, with highest absorbing samples having the lowest recombination rates. Finally, Serpone et al. [412] found that the kinetics for recombination depended on the number density of e^-/h^+ pairs generated, in agreement with results of Rabani et al. [538]. The recombination rates also varied with particle size, but more accurately with the ability of O_2 to access the surface and scavenge electrons before charge recombination could occur. For example, the recombination rate was $\sim 1 \times 10^{-11}$ cm^3/s in 2 nm diameter A particles but $\sim 3 \times 10^{-7}$ cm^3/s in 27 nm particles. In all, Serpone and coworkers found that ~85% of excitation events in their samples led to recombinations within the first 10 ns after excitation. Katoh et al. [505] have estimated that the rate of e^-/h^+ recombination ($\sim 5 \times 10^{-13}$ cm^2/s) in single crystal rutile was ~4 orders of magnitude slower than the hopping rate, which suggests that many hops precede recombination in an infinitely large, well-ordered lattice. It seems likely then that charge recombination (in rutile at least) is governed predominately by particle surfaces and their inherent structural heterogeneity.

3. Electron transfer dynamics

In the context of heterogeneous photocatalysis, electron transfer is an interfacial phenomenon between a surface and a chemisorbed (or physisorbed) species. The interaction is essentially a donor/acceptor (D/A) relationship initiated by a photoabsorption event. This is not to say that other processes (e.g., thermal reactions) are not also important, but that electron transfer across the interface is at the heart of TiO_2 photocatalysis. Starting with the TiO_2 VB and CB in mind, the common types of electron transfer are illustrated in the cartoon of Fig. 3.1. The first form considered in this section involves electron transfer from a donor into the TiO_2 CB ('1' in Fig. 3.1); the second ('2' in Fig. 3.1) involves hole transfer from the TiO_2 VB to a hole acceptor (i.e., electron transfer from an electron donor into a VB hole state); the third ('3' in Fig. 3.1) is electron transfer from the TiO_2 CB to an acceptor; and the fourth ('4' in Fig. 3.1), which is not commonly observed for TiO_2, involves hole transfer from a donor into the TiO_2 VB (i.e., electron transfer from a TiO_2 VB state to an unoccupied state of an acceptor). The phrase 'hole transfer' implies electron transfer in the opposite direction and is used for convenience in expressing electron transfer into vacated valence states, whether it be in TiO_2 or in an adsorbate. (While not shown in Fig. 3.1, transfer processes involving gap states could be included, although these generally involve dopants, defects or impurities.) Two forms of electron transfer deal with excitation events in TiO_2

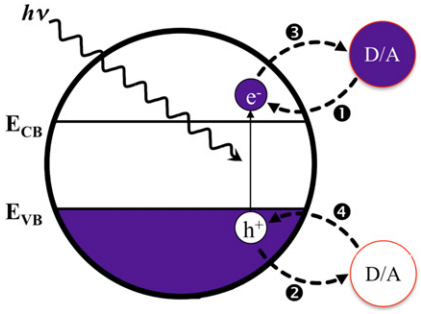

Fig. 3.1. Schematic illustration of four possible charge (electron or hole) transfer processes involving TiO_2. 'D' and 'A' correspond to 'donor' and 'acceptor', respectively.

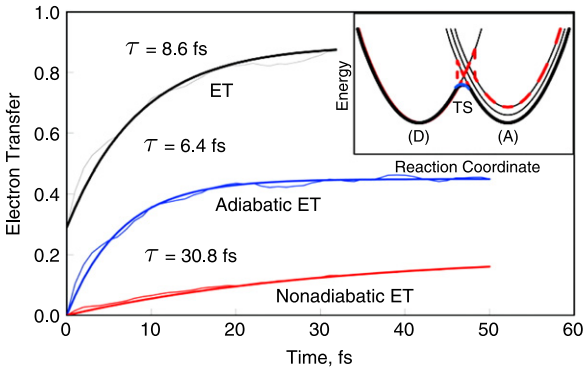

Fig. 3.2. Electron transfer (ET) between adsorbed alizarin and R TiO_2 showing time-dependent variations in the initial state (labeled 'ET'), as well as for adiabatic and non-adiabatic ET processes. The inset shows the difference between the adiabatic process (blue line passing through a transition state (TS)) and the non-adiabatic process (red dashed lines involving transitions to/from non-ground state configurations of the donor (D) and acceptor (A)). (For interpretation of the references to color in this figure legend, the reader is referred to the web version of this article.)
Source: Reprinted with permission from Prezhdo et al. [72].

('2' and '3') and two deal with excitation events in an adsorbed or attached entity ('1' and '4'). These four forms of electron transfer are discussed here with an emphasis on dynamics. Chemical (mechanistic) evidence for electron transfer to and from TiO_2 is abundant in the literature, and is discussed in more detail in Section 5. Examples discussed in this section will involve molecular systems (for convenience), but there are numerous examples of electron transfer dynamics across heterojunctions containing TiO_2. (For example, Evans et al. [605] observed that electron transfer from excitation of CdS nanoparticles into TiO_2 occurred on a ~2 ps timescale.) Keep in mind also that not all electron transfer events result in chemistry (i.e., bond-forming and bond-breaking events) or involve ground state configurations. Finally, the phrase 'electron transfer' is distinguished from the phrase 'charge transfer' because the latter is frequently used in the literature in the context of complexation, which is a ground state phenomenon.

3.1. Excited electron donor to TiO_2 conduction band

The dynamics of electron injection from an electronically excited dye molecule into the CB of TiO_2 has become an intensely studied phenomenon in the field of heterogeneous photochemistry [71,163,164,198,390,391,447,448,494,497,511,532,535,536,601,606–670]. The underlying utility of TiO_2 (or other similar semiconductors) in dye sensitization is its ability to accept into its CB excited electrons with high efficiency and transport these

Adiabatic electron transfer:
- Slow
- Passing through a transition state
- System adjusts during transfer
- E.g.: Marcus theory

Non-adiabatic electron transfer:
- Fast
- State-to-state
- System does not have time to adjust
- E.g.: Fermi's golden rule

Scheme 3.1.

electrons away from the sensitizer. In this situation, the molecular sensitizer is the 'photocatalyst', efficiently absorbing light and generating charge carriers, and the TiO_2 surface is the electron acceptor, facilitating charge separation. While much discussion in the literature has focused on optimizing the properties of the dye and the redox couples, attention here will be on the properties of TiO_2 as an electron acceptor. Coupling between the excited dye's electronic structure and the TiO_2 CB states is so strong that injection yields approaching 100% have been measured for many different dyes [610,612,622,623,631,633,636,638,640,652]. Another reflection of the strong coupling is that electron injection typically occurs on the sub-picosecond timescale [390,494,601,613,624,628,629,637,638,640,641,643,647,667,669], and in some cases faster than 100 fs [163,198,391,532,536,606,607,609,617,618,625,632,649–651,655,656,662,666]. The kinetics for injection often compete well with those for thermalization of the excited dye [649,656].

The majority of DSSC work in the literature has been conducted on high surface area TiO_2 because these materials maximize areal densities of dye and facilitate study under typical operational conditions. However, several groups have examined electron transfer between an excited dye and a single crystal TiO_2 surface [116,390,391,626,633,655,671–674]. Schnadt et al. [655] were one of the first groups to use the R TiO_2(110) surface to study the dynamics of electron injection, albeit in their case from resonant core–hole excitation of adsorbed isonicotinic and bi-isonicotinic acids rather than via visible light absorption. These authors observed electron injection occurring in less than 5 fs. More recently, Gundlach and coworkers used 2PPE to examine electron injection from visible light excitation of a perylene chromophore rigidly held with a 'tripod' anchoring system [390] and from adsorbed catechol [391], both on the R TiO_2(110). In the perylene case, they observed two electron injection times (~700 fs and ~7 ps) attributed to injection from two possible adsorption geometries in which the chromophore was ~0.75 and 1 nm (respectively) from the surface. From this example, the adsorption state of the dye played a major role in the injection dynamics. Dyes with chromophoric centers far from the surface or isolated by non-conducting linkages exhibit slower injection times (and slower back-electron transfer times). In the catechol case, Gundlach et al. described the electron injection process as being "instantaneous" (i.e., on the 20 fs timescale of their initial 440 nm pump pulse).

Electron injection into TiO_2 from excited dyes has also been the subject of numerous theoretical modeling efforts [72,447,448,614–616,630,639,642,644,648,653,654,661,664,665]. One of the main aims in these studies has been to accurately described the electron transfer in terms of adiabatic versus non-adiabatic characteristics of transfer (see Scheme 3.1). For example, Stier and Prezhdo [654] performed molecular dynamics (MD) simulations of both adiabatic electron transfer (in which the excited system 'relaxes' on the timescale of electron transfer) and non-adiabatic electron transfer (in which electron transfer is fast compared to

relaxation of the excited system) between excited isonicotinic acid (adsorbed as isonicotinate) and the unreconstructed A TiO_2(001) surface. They determined average electron transfer trajectories of ~40 and ~19 fs for the adiabatic and non-adiabatic contributions, respectively. Their simulations indicated that the non-adiabatic process dominated at short times, but became less important at longer times, as one might expect. The result of both, though, was a complex, multi-exponential profile for electron injection. Similarly, the Batista group [447,448] simulated electron transfer in the catechol — A TiO_2(101) system using quantum mechanical MD and *ab initio* DFT MD simulations. They determined electron transfer timescales on the order of 6 fs timescale, and found that thermal fluctuations in the A lattice provided variations in the initial state that increased the rate of electron transfer by opening up non-adiabatic pathways, similar to that shown by Stier and Prezhdo. Perzhdo's group [72,615,616] has also shown fast injection (~8 fs) from alizarin to R TiO_2(100) using *ab initio* MD simulations, but occurring predominately through adiabatic pathways, as shown in Fig. 3.2. Non-adiabatic electron transfer through the lowest energy excited state of alizarin was unique (in its 'slowness') in this case because it involved a singlet excited state positioned roughly at the R CB edge. In this situation, thermal fluctuations in the lattice had only a minor impact on increasing the injection rate. Their results of fast injection and predominately adiabatic transfer were consistent with experimental findings on the alizarin-TiO_2 system [625]. Finally, Nilsing et al. [639] calculated electron injection rates for a series of perylene derivatives adsorbed on R TiO_2(110) using the Newns–Anderson approach in which lifetimes were determined from the broadening of dye unoccupied states resulting from interactions with the TiO_2 CB continuum. These authors found that rates were faster for carboxylate-anchored dyes than for phosphate-anchored dyes. Aliphatic spacers between the anchor and the dye tended to decrease the injection rate.

Aside from localized excitations in adsorbed dyes, there is also the possibility of excitation (and subsequent electron transfer into TiO_2) of charge transfer complexes that result from dye adsorption. However, it is not altogether straightforward to determine if such complexes exist and if their excitations (as opposed to excitation of an inherent local transition in the dye) contribute to electron injection. Taking the alizarin-TiO_2 system as an example, both Ramakrishna et al. [675], and Shoute and Loppnow [657] proposed that a charge transfer complex between alizarin and the TiO_2 surface formed on adsorption and excitation of this complex led to the observed electron injection. The latter authors estimated that the TiO_2 nanoparticle surface used in their studies experienced the majority of the observed reorganization energy (~0.32 eV total) that resulted from this process based on a fluorescence Stokes shift seen after excitation. In contrast, Huber et al. [625] used femtosecond transient spectroscopy to examine electron injection in the alizarin-TiO_2 system. They characterized the transfer as adiabatic and not resulting from excitation of a charge transfer state but from a localized dye excitation event.

Electron transfer processes between catechol and TiO_2 were attributed to excitation of a charge transfer complex. This is shown in Figs. 3.3 and 3.4 from the work of Wang, et al. [670] for excitation of catechol adsorbed on TiO_2 nanoparticles. Fig. 3.3 shows the optical absorption spectra of catechol alone (a), of catechol chelated to a Ti^{4+} complex (b), of suspended TiO_2 nanoparticles (c), and of catechol adsorbed on TiO_2 (d). The prominent absorption feature at 400 nm, absent in the pure catechol or TiO_2 cases, but present in the complex, was assigned to excitation of a catechol-TiO_2 charge transfer state. In Fig. 3.4, the recovery of the catechol-TiO_2 electron transfer bleach (at ~400 nm) and the optical absorption feature associated with the injected electron (at ~600 nm) are shown to mirror each other as a function of

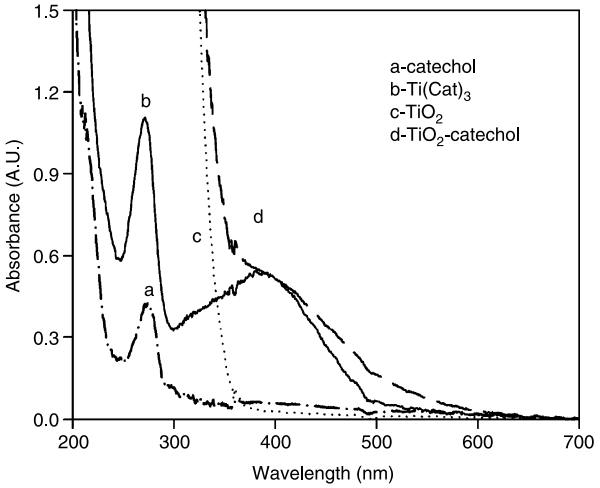

Fig. 3.3. UV–vis spectra for aqueous solutions of (a) catechol, (b) Ti(catechol)$_3^{2-}$, (c) suspended TiO_2 nanoparticles, and (d) catechol adsorbed on suspended TiO_2 nanoparticles.
Source: Reprinted with permission from Wang et al. [670].
© 2003, American Chemical Society.

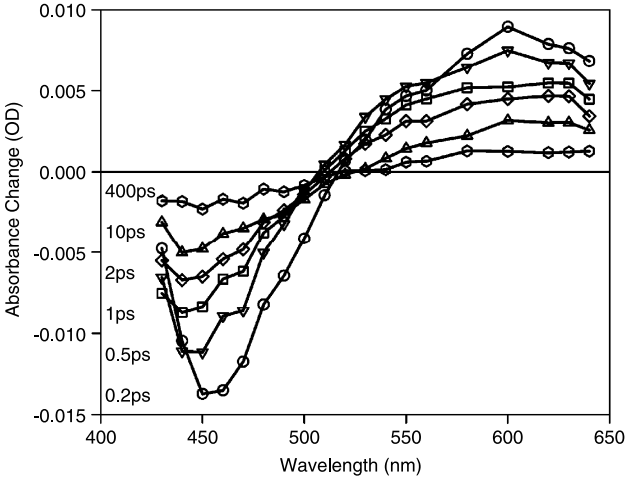

Fig. 3.4. Difference spectra from transient absorption of catechol adsorbed on suspended TiO_2 nanoparticles as a function of delay time after a 400 nm excitation.
Source: Reprinted with permission from Wang et al. [670].
© 2003, American Chemical Society.

time, illustrating both the timescale for electron injection (sub-picosecond) and that of the back-electron transfer process. The dynamics of excited charge transfer states from molecular systems on single crystal TiO_2 surfaces have yet to be explored.

Finally, Willig et al. [647,648,668] have shown that the coupling of electronic states between an excited dye and its cationic state can be as important in influencing electron transfer as the coupling between the dye and the TiO_2 CB states. These authors prepared vibrationally-hot and relatively long-lived (compared to the excited singlet lifetimes) wavepackets of anchored perylene chromophores attached to A nanoparticles. As shown in Fig. 3.5(C), the authors observed step function changes in the electron transfer probability over time from excitation of the 'wavepacket prepared' dye. These results suggest that the excited wavepacket moved in and out of optimal phase overlap with the electron transfer product state (the dye cation), an effect that was translated into the injection process. Memory of the wavepacket was also retained in subsequent excitation events of the ionized dye. The TiO_2 surface may have a role in this overlap, for example, by influencing the

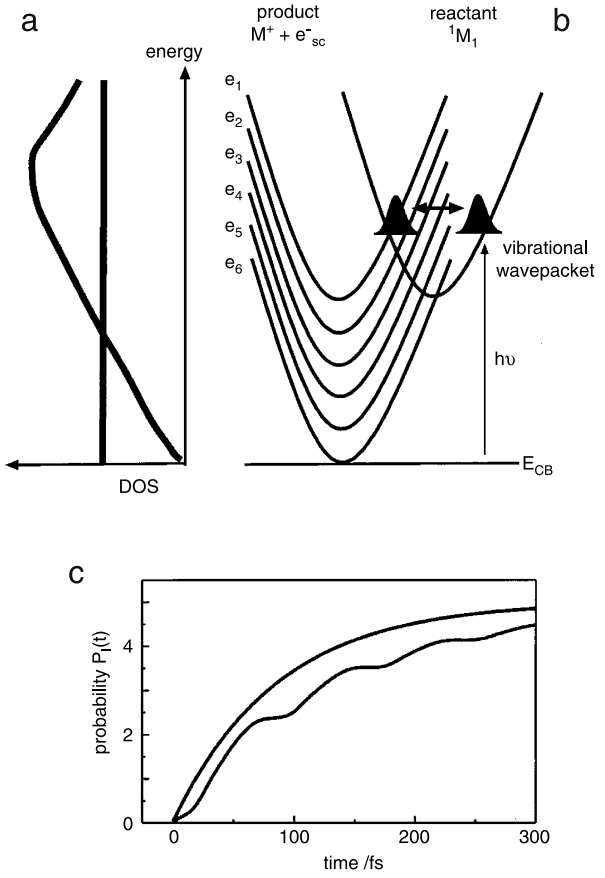

Fig. 3.5. Schematic illustration of electron transfer from an excited donor molecule into the continuum of empty electronic acceptor states in the CB of TiO_2. Two different DOS are shown in (A). Constant DOS gives a smooth rise in the formation of the product state (upper curve C), strongly energy-dependent DOS leads to a stepwise increase (lower curve in C) indicating pulsed electron transfer due to curve crossing effects during the periodic motion of the vibrational wavepacket in the donor state (B).
Source: Reprinted with permission from Zimmermann et al. [668].

potential energy surfaces of the excited and cationic states of the dye.

Dynamics studies on electron transfer processes in dye sensitized TiO_2 reveal that the coupling of electronic states between excited state molecules and the TiO_2 CB 'continuum' are strong and that transfer processes between the two are fast. In some cases, back-electron transfer processes (see Section 3.3 below) are also fast, but in almost all cases the 'continuum' takes over in thermalizing the transferred electron so that the process is not transient. While the transfer events associated with these systems are tailor-made for ultrafast dynamic studies (i.e., dye chromophores with well-known optical properties, strong adsorption energies and the ability to spectroscopically track the injected electron), results from studies on this type of electron transfer event on TiO_2 provide motivation for conducting similar detailed dynamics studies on other types of transfer events occurring on TiO_2.

3.2. Electron donor to TiO_2 valence band hole

Photooxidation on TiO_2 involves electron transfer from a fairly low DOS electronic state on an adsorbate to a more-or-less localized VB hole state generated in TiO_2 by a band-to-band excitation event. The properties of DSSC systems that make them so amenable for exploring electron transfer dynamics (Section 3.1) are largely absent in the other electron transfer categories explored in this review. Consider, for example, that with excitation of adsorbed dyes (which have fairly well-defined ground and excited states) one is dealing with light absorbers with fairly well-understood optical and electronic properties, that the photon energy is being absorbed exclusively in a fairly well-understood spatial region near the surface and that the electron transfer event can be followed dynamically both in terms of the transferred electron and the resulting dye cation. In contrast, both VB hole photooxidation (this section) and CB electron photoreduction (Section 3.3) stem from band-to-band transitions in TiO_2 resulting in carriers with a broad range of (carrier) energies, generated at ill-defined depths near or at the TiO_2 surface, and which are complicated to follow from either end of the event. As an example of such complications, several studies have questioned the accepted notion that charge carriers completely thermalize to the band edges before transfer (see Section 2.2). Thus, transfer can potentially involve a myriad of states at potential energies different from that of the band edges. Another requirement for being able to follow electron transfer dynamics in photooxidation is the ability to probe optically or chemically on the timescales of the transfer event. As will be seen below, there are not many photooxidation studies that have accomplished this task. Yet the electron transfer events of interest in this section (and the next) constitute the fundamental focus for much of the TiO_2 photocatalytic applications.

Thiocyanate (SCN^-) has been the most effective adsorbate for probing the dynamics of hole transfer events on TiO_2 [394,528,534,676,677], although no UHV studies of this system have been published to date. One of the early dynamical studies of SCN^- photooxidation on TiO_2 was done by Colombo and Bowman [528]. These authors utilized femtosecond diffuse reflectance spectroscopy to probe hole transfer from P-25 under both suspended and dry conditions. As shown in Fig. 3.6, they found that electron transfer from adsorbed SCN^- to a VB hole in TiO_2 occurred on the picosecond timescale, which in many cases was much faster than the timescale for charge recombination (see Section 2.5). Data in trace 'a' (no SCN^- present) provided a baseline for carrier recombination lifetimes. The decay curve under this condition was much slower than that when SCN^- was present ('b' and 'c'). This indicated that holes were able to readily diffuse to the nanoparticle surface without significant recombination and that the 'efficiency' of TiO_2 as a hole transfer photocatalyst had as much to do with the electron transfer process at the interface as it did with carrier transport issues. Similarly, Yang and Tamai [534] found that adsorbed SCN^- enhanced the transient absorption signal from trapped electrons on the picosecond timescale. As shown in Fig. 3.7, the transient signal from excited electrons rose sharply after excitation of TiO_2, but decayed slowly above ~0.5 ps due to recombination events. In contrast, when SCN^- was added to scavenge holes, the transient signal for excited electrons did not decay, indicating the hole transfer process occurred on a similar timescale. Other groups have reinforced this conclusion. Morishita et al. [394] observed that electron transfer from adsorbed SCN^- to non-thermalized VB holes in TiO_2 occurred on a 110–690 fs timescale, with the magnitude of the total transient reflectivity signal integrated over time being proportional to the loss of SCN^- concentration in solution. Similarly, Furube and coworkers [676] observed two timescales for hole transfer to adsorbed SCN^-, one that was sub-ps and another that was longer than 100 ps. The former was possibly due to transfer involving non-thermalized holes and the latter was assigned to holes trapped far from adsorbed SCN^- groups that presumably diffused to (or were otherwise brought into close proximity to) SCN^- groups at some later time. Although the chemistry occurring after electron transfer is not well-explored, it is likely that the electron transfer event in the SCN^- case is not reversible based on work by Morishita and coworkers, and that the immediate product of the reaction is likely

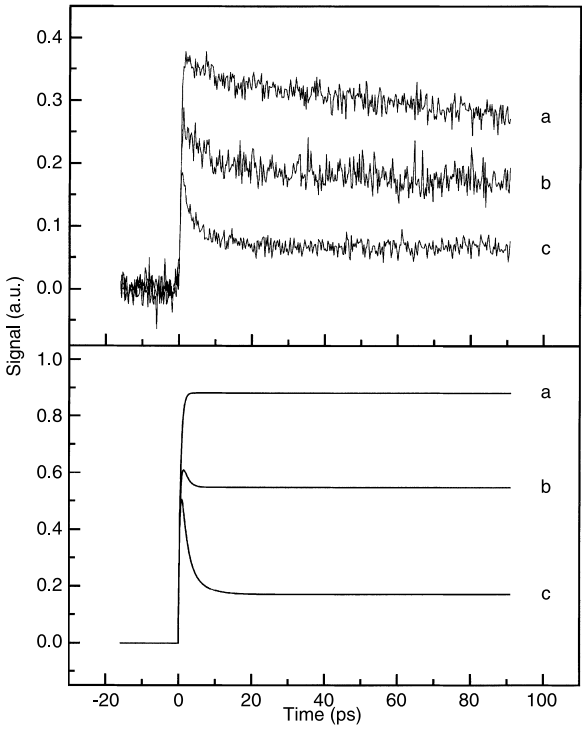

Fig. 3.6. Effect of SCN^- concentration ((a) 0 g/L, (b) 30 g/L and (c) 100 g/L) on e^-/h^+ pair recombination in TiO_2 probed by transient absorption (pump at 310 nm and probe at 620 nm). (Top: data, bottom: simulation of data.)
Source: Reprinted with permission from Colombo and Bowman [528].
© 1996, American Chemical Society.

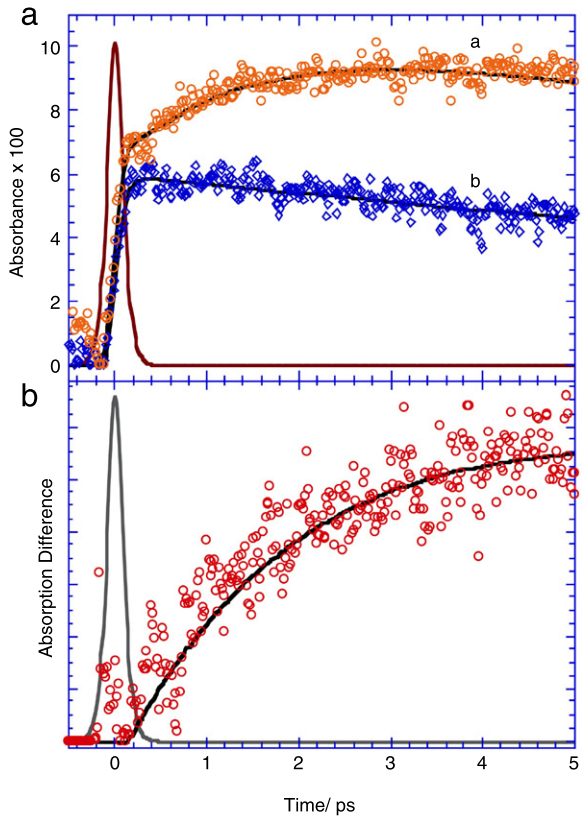

Fig. 3.7. (A) Transient absorption signals measured at 500 nm from 365 nm excitation of suspended A TiO_2 nanoparticles: (a) with and (b) without 0.3 M SCN^- present in solution. (B) difference spectra of 'a' minus 'b'. The sharp feature in both panels at time '0' is the instrumental response of the ~0.2 ps pump pulse.
Source: From Yang and Tamai [534]. Reproduced by permission of the PCCP Owner Societies.

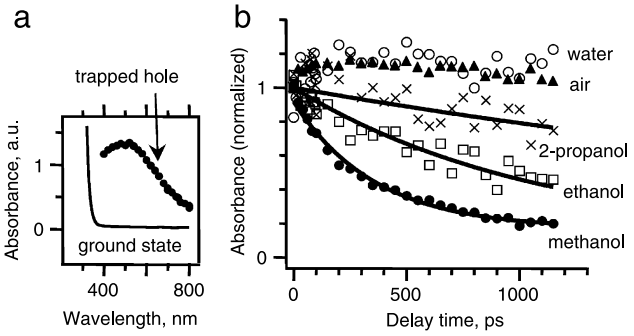

Fig. 3.8. (A) The transient absorption spectrum following 355 nm excitation of A TiO_2 nanocrystalline films. (B) Transient absorption signal at 400 nm following 355 nm excitation of TiO_2 nanocrystalline films exposed to air and to different air-saturated solutions.
Source: Reprinted with permission from Tamaki et al. [400].
© 2006, American Chemical Society.

the dimerized anion $(SCN)_2^-$, formed from reaction of a radical with an unreacted SCN^- [677].

These studies on hole transfer from TiO_2 to SCN^- set a benchmark of sorts for the dynamics of hole transfer reactions in TiO_2 photocatalysis. That is to say, when hole transfer times in adsorbate–nanoparticle TiO_2 systems are observed to be much longer than picoseconds, then the hole transfer dynamics are likely more responsible than are hole hopping dynamics in explaining the observed kinetics. The ability of an adsorbate to capture and retain a VB hole becomes the key factor. A few examples of this principle can be found in the TiO_2 literature. Rabani et al. [538] used transient visible light absorption to probe electron transfer dynamics on packed films of 5 nm TiO_2 particles. They observed that hole transfer to I^- (which converted to the dimerized anion as in the SCN^- case) occurred on the 10 ns timescale with little effect on the decay profiles of the excited electrons (probed at 600 nm) associated with electron trapping. In contrast, these authors observed that adsorbed alcohols (methanol or isopropanol) tended to trap holes for recombination rather than for electron transfer chemistry. Other groups have observed fast electron transfer to adsorbed alcohols. For example, Tamaki et al. [400] observed electron transfer from trapped holes in TiO_2 over a wide timescale depending on the alcohol (from ~100 ps for methanol to ~1 ns for ethanol and ~3 ns for isopropanol), as shown in Fig. 3.8. Similarly, Shkrob et al. [572] examined hole transfer to diols and carbohydrates bound to TiO_2 nanoparticle (~4.6 nm). These events occurred on the timescale of the 355 nm laser pulse width employed (3.3 ns), with up to 60% of the generated holes reacting rather than recombining. Shkrob and Sauer [539] also found that glycerol scavenged roughly half of the holes generated by 355 nm light within ~3 ps, with most of the rest either reacting over the next 200 ns or remaining unreacted. Finally, Tachikawa et al. [678] observed hole transfer to adsorbed 4-phenylbenzoic acid on TiO_2 (P-25) on a timescale below 100 ns, with decay of the resulting radical cation over ~5 μs by an unspecified pathway.

Based on these studies, it is fair to ask why UV photooxidation on TiO_2 is generally viewed as inefficient? The answer would appear to lie not in the ultimate limits of hole transfer rates, which the single electron transfer SCN^- examples show to be fast and efficient, but in the realization that in any overall reaction process requiring many transfer events, each to uniquely different species, that not all steps will be as fast and efficient as SCN^- photooxidation. In this sense, each electron transfer event in a photooxidation process will be governed by the properties of the

electron donor–VB hole relationship. A key challenge to the field will be identifying and improving the slow and inefficient steps.

As yet there are no examples of studies associated with electron transfer dynamics in photooxidation reactions on single crystal TiO_2 surfaces. However, recent work by Sporleder et al. [679] on photodesorption of O_2 from the R TiO_2(110) surface provide unique insights into a different aspect of photodynamics on TiO_2 not currently addressed by the studies discussed above, that being the issue of energy partitioning as a result of electron transfer. Sporleder et al. employed time of flight (TOF) techniques to explore the velocity distribution of photodesorbing O_2 molecules as a result of band-to-band excitation in TiO_2. O_2 molecules can be chemisorbed on R TiO_2(110) via a charge transfer reaction from Ti^{3+} sites to form (nominally) O_2^- surface species. Photodesorption is believed to proceed from a hole-mediated reaction that neutralizes these O_2^- species, resulting in O_2 molecules that find themselves on the repulsive section of the physisorbed potential energy surface, leading to prompt desorption. (More details on O_2 photodesorption from R TiO_2(110) are found in Section 5.) The extent to which these photodesorbing O_2 molecules retain this energy in departing from the surface reveals insights into the dynamics of the hole transfer event. Fig. 3.9 show TOF velocity (bottom *x*-scale) and energy (top *x*-scale) distributions resulting from O_2 photodesorption at various surface temperatures. The data show a large thermalized feature, reflective of the surface temperature, and two translationally 'hot' channels of O_2 photodesorption (centered at ~1750 and ~950 m/s). Oxygen molecules in these latter two channels depart from the surface with ~0.2–0.5 eV of kinetic energy and reflect two unique forms of adsorbed O_2 (nominally assigned to O_2 molecules in vacancy and non-vacancy sites). All three channels were shown to occur via substrate-mediated processes. Although these data do not address the internal energy of the desorbing O_2 molecules (i.e., their vibrational and rotational distributions), the data do show that energy partitioning after hole transfer can provide useful information into the types and number of different events occurring during hole transfer.

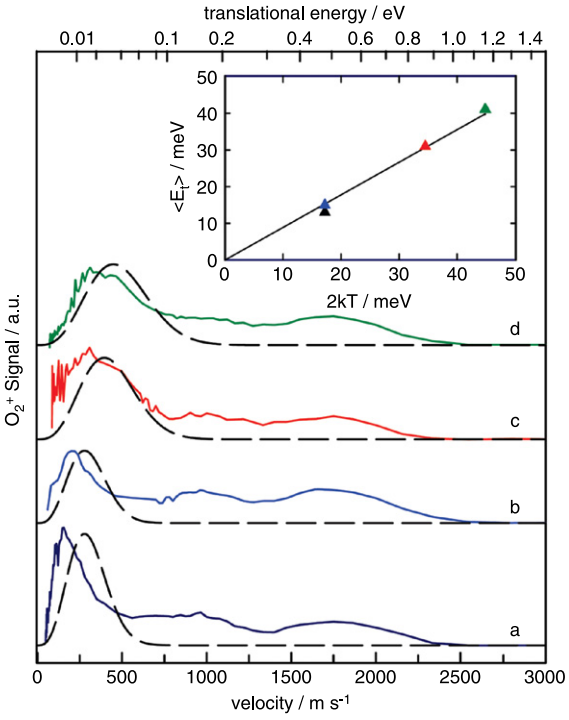

Fig. 3.9. Velocity distributions of O_2 PSD (using 298 nm light) from a reduced R TiO_2(110) surface pre-exposed to 80 L of O_2 at 100 K followed by different thermal treatments: (a) at 100 K, (b) heated to 260 K and recooled to 100 K, (c) heated to and held at 200 K, and (d) heated to and held at 260 K. Solid lines correspond to the flux and depletion corrected experimental data, and dashed lines are calculated Boltzmann distributions at the corresponding measurement temperature. Inset shows a plot of the mean translational energies of the "slow" velocity component as a function of the surface temperature.
Source: Reprinted with permission from Sporleder et al. [679].

3.3. TiO_2 conduction band to electron acceptor

The dynamics of photoreduction involve coupling of a CB electron to acceptor states on an adsorbed species. The coupling has to be strong (and energetically down-hill) in order to prevent back-electron transfer to the higher DOS in the TiO_2 CB. An example of this is seen in the photochemistry of alkyl halides on R TiO_2(110). Stair, Weitz and coworkers [680–683] have shown that bandgap excitation of TiO_2 leads to electron attachment to these adsorbed molecules, but does not result appreciable photodecomposition (as seen in the gas phase). Instead, rapid back-electron transfer to the surface occurs followed by photodesorption of the alkyl halide via the so-called Antoniewicz mechanism [684]. This process is illustrated in Fig. 3.10. Starting in the neutral state (and following the dashed lines), electron attachment causes a Franck–Condon-like transition to the (excited) ion state, whose potential energy minimum is situated closer to the surface. As the newly formed (metastable) ion relaxes toward the surface, it becomes neutralized by back-electron transfer. The neutral molecule then finds itself on a repulsive region of the potential energy surface for adsorption with sufficient energy to break the adsorption bond and desorb. The potential energy surfaces of the ion and the molecule, as well as the lifetimes of the ionized state, will influence the extent of energy retained after neutralization.

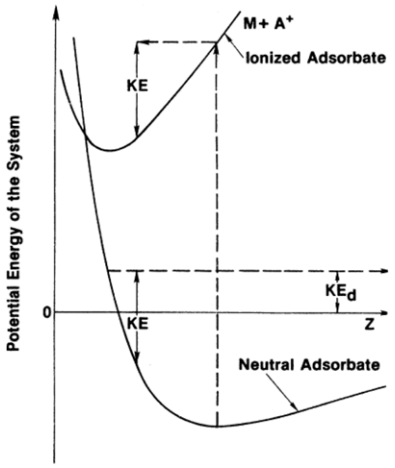

Fig. 3.10. Schematic model of the Antoniewicz model for excitation-induced desorption from surfaces. The vertical dashed arrow corresponds to the initial charge transfer event, placing the adsorbate on an "ionized adsorbate" potential energy surface. Prompt re-neutralization back to the "neutral" adsorbed potential energy surface results in the adsorbate retaining sufficient kinetic energy ('KE') for desorption.
Source: Reprinted with permission from Antoniewicz [684].

While there are many examples in the literature of studies that focus on the mechanistic details of photoreduction on TiO_2 (see Section 5), there are comparatively few photodynamics studies involving a photoreduction process. The difficulty lies in the unavailability of convenient molecular markers that are sensitive (on an ultrafast timescale) to electron attachment. One such

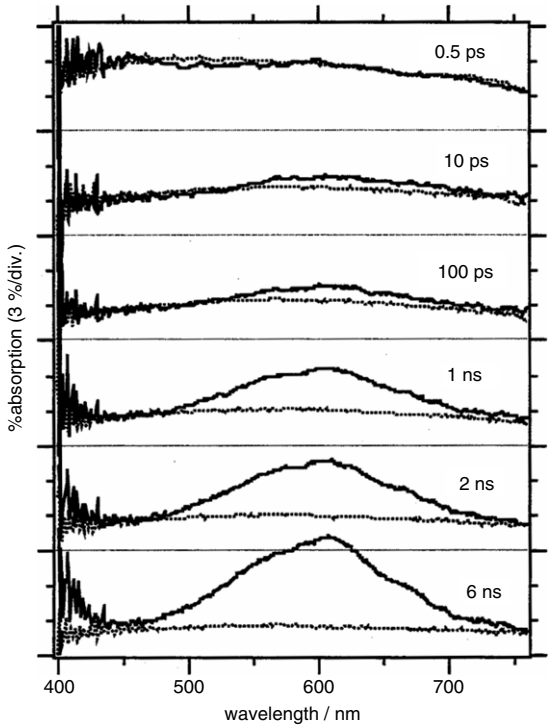

Fig. 3.11. Transient absorption spectra following various delay times after 390 nm excitation of suspended A nanoparticles in water at pH = 10 with (solid lines) and without (dotted lines) 0.7 M MV^{2+} present.
Source: From Asahi et al. [506].

molecule available to colloidal systems is the methyl viologen divalent cation (MV^{2+}) [506,685–687]. Asahi et al. [506] found that following bandgap excitation, electron transfer from TiO_2 to MV^{2+} adsorbed on colloidal A occurred on the picosecond to nanosecond time scales, as shown by appearance of the 605 nm absorption feature of MV^{+} in Fig. 3.11. These timescales are much longer than the electron trapping times in TiO_2 (see Section 2.4), suggesting that MV^{2+} reduction likely involved trapped electrons and not free CB electrons. In agreement with these conclusions, Martino et al. [558] used Fourier transformed EPR to track the kinetics of MV^{+} radical cation formation from electron transfer to the MV^{2+} dye. Their studies, utilizing either direct bandgap excitation or CB sensitization (with coadsorbed coumarin 343 dye), indicated that electron transfer to MV^{2+} was via trapped electron states on TiO_2. Assuming rates of photoreduction of MV^{2+} that are reflective of typical electron transfer processes from TiO_2 (in general), the dynamics of electron thermalization and trapping can be viewed as being much faster than electron transfer in this case. The question then is whether the photodynamics associated with MV^{2+} reduction is typical or anomalously slow compared to other photoreduction processes on TiO_2. In other words, how effectively does electron transfer compete with electron trapping? This is potentially a critical issue influencing the photoreducing power of TiO_2. The reduction potential is then defined not by the CB minimum energy but the energies of electron trapping states at TiO_2 surface [500].

A more detailed understanding of the dynamics of electron transfer from the TiO_2, potentially addressing the trap vs. CB issue, can be obtained from a wealth of information involving back-electron transfer events in molecular sensitization studies [163,164,433,493,494,496,497,507,532,545,601,608,609,618,621,624,650,662,667,670,675,688–696]. Typically, back-electron transfer in the DSSC setting is viewed as detrimental to solar light harvesting, but the dynamics of such events provide unique insights into the photoreduction aspects of TiO_2. It is generally held that the back-electron transfer process involves injected electrons that have thermalized and trapped in states located 'energetically' just below the TiO_2 CB edge and located 'physically' at surface or near-surface sites [493,494,496,497,507,532,545,662,670,689,693]. Many groups have observed non-exponential or multi-exponential kinetics for the back-electron transfer processes that have been ascribed to a distribution of trap energies [163,164,493,494,609,618,621,650,662,675,690,691] and/or trap locations [433,493,670,688,694]. (An exception to this is the work of Martini et al. [496,693] who observed single exponential recombination kinetics, reflective of a narrow trap energy distribution, for anthracene carboxylic acid dyes adsorbed on A nanoparticles.) Weng et al. [493] have shown that back-electron transfer rates following electron injection from adsorbed $Fe(CN)_6^{3-}$ were independent of TiO_2 particle size and preparation method, suggesting electron traps in the vicinity of the complex and the surface. Timescales for back-electron transfer processes span the picosecond to nanosecond ranges, which are considerably slower than the electron injection and thermalization times [163,164,493,494,496,497,532,609,618,667,675,691,693,695]. However, sub-picosecond back-electron transfer timescales have been observed [650,670,675], as have lifetimes in the microsecond and longer timescales [163,494,601,621,624,667]. In the DSSC setting, the lifetime of the trapped electron is a reflection on its ability to spatially separate from the ionized dye. The ability to electronically couple the trapped electron with the ionized dye is manifested in several ways. For example, Hilgendorff and Sundström [624] showed that back-electron transfer rates can depend on how fast the dye cation can 'cool' after the electron injection process. Generally, the injected electron will thermalize much faster than the newly generated dye cation, the latter finding itself in need of relaxing electronically and structurally after the injection process. Dye cations that retain memory of their non-thermalized state are more likely to experience back-electron transfer than those that have fully relaxed. Back-electron transfer rates are also dependent on the environment that the trapped electron finds itself. Haque et al. [689] have shown that back-electron transfer rates can strongly depend on both the local population of trapped electrons and the vicinity of adsorbed or solution phase cations/anions, both of which have an influence on the local electric field. (The local electric field can also be manipulated by changing the applied potential or electrolyte concentration.) By extension, one can see how these factors will come into play in more typical photoreduction (and photooxidation) dynamics.

An essential factor limiting back-electron transfer in the context of electron injection (or more generally in terms of electron transfer from TiO_2 to an adsorbate) is achieving good coupling between the electronic state of the trapped electron and that of the electron acceptor. Poor coupling between the electron trap state and acceptor contributes to long transfer lifetimes and high survival rates for the trapped electron, which is good for the DSSC applications, but not for photoreduction. Many groups have attempted to model the back-electron transfer process using the Marcus theory of electron transfer (see references in the *Journal of Physical Chemistry* issue dedicated to the career of Rudolph Marcus [697]). The degree of coupling has been expressed by observations of electron transfer falling in the Marcus inverted region [164,670,675,692,693,696], which implies that the rate of transfer should *decrease* as the thermodynamic driving force for transfer (i.e., the difference in zero-point energies between the donor and acceptor) is *increased*. Conceptually, this is derived from a decrease in coupling between the two states as they move farther apart in energy. For example, Ramakrishna et al. [164,675] examined electron transfer and back-electron transfer between a series of carboxylate-anchored xanthene dyes and TiO_2 using

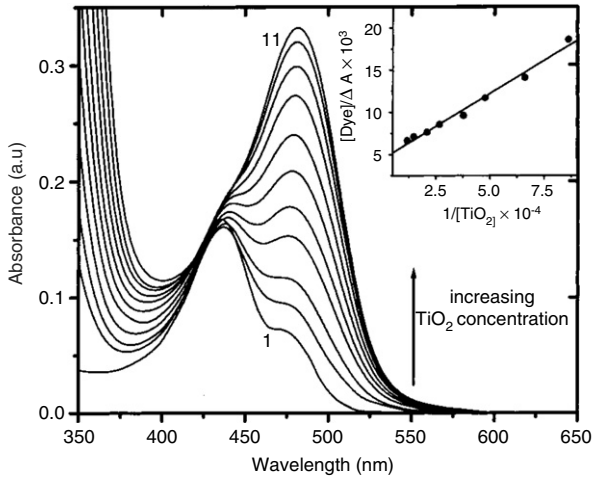

Fig. 3.12. UV–vis absorption spectra from increasing concentrations of TiO_2 nanoparticles in a fluorescein dye solution ($\sim 10^{-5}$ M) at pH = 2.8. Trace '1' is without TiO_2 present and trace '11' is for a 1.7 g/L concentration of TiO_2. (Inset shows Benesi–Hilderbrand plot for the charge transfer absorption feature.)
Source: Reprinted with permission from Ramakrishna and Ghosh [164].
© 2001, American Chemical Society.

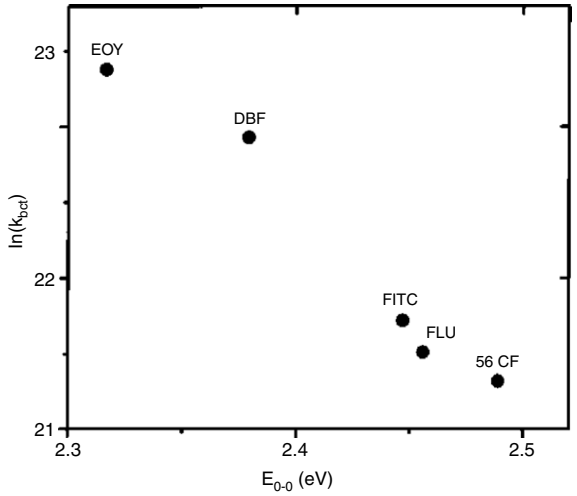

Fig. 3.13. Plot of the log of the back-electron transfer rate constant ('$\ln(k_{BET})$') for the ionized dye versus the transition energy of the dye- TiO_2 charge transfer complex (E_{00}) for several dyes (eosin yellowish (EOY), dibromo fluorescein (DBF), fluorescein isothiocyanate (FITC), fluorescein (FLU), and 5(6)-carboxyfluorescein (56CF)). (E_{00} is a linear function of the BET driving force.)
Source: Reprinted with permission from Ramakrishna and Ghosh [164].
© 2001, American Chemical Society.

picosecond transient absorption spectroscopy and fluorescence spectroscopy. Several of these xanthene dyes exhibited charge transfer adsorption states that redshifted their optical absorption features. Fig. 3.12 shows one such example with the appearance of a fluorescein dye — TiO_2 state that grew in at $\sim$485 nm with increasing TiO_2 concentration. Excitation of these charge transfer adsorption states for a series of functionalized xanthene dyes resulted, in each case, in electron transfer from the charge transfer state into the TiO_2 CB. By measuring the rates of subsequent back-electron transfer for this series of adsorbed dyes, the authors were able to show that the back-electron transfer process fell into the Marcus inverted region. As shown in Fig. 3.13, the back-electron transfer rates decreased as the driving force increased. Based on their analysis, Ramakrishna et al. proposed that the 'initial' state in the back-electron transfer process was a trapped electron. Assuming no significant variations in the electron coupling between the TiO_2 surface and the various 'ionized' dyes employed, these results demonstrate that the degree of coupling between electrons trapped on TiO_2 and an 'acceptor state' is important in influencing photoreduction rates on TiO_2. These authors proposed that the factors which resulted in a back-electron transfer event falling into the Marcus inverted region potentially could be exploited through surface modification to limit back-electron transfer (or conversely, to promote photoreduction).

In other examples of back-electron transfer on TiO_2, Zhang and coworkers [696] found that in the case of all-trans-retinoic acid sensitization of TiO_2, back-electron transfer occurred into both triplet and singlet states of the ionized dye. Because the singlet state was the ground state (and thus had a higher driving force for back-electron transfer), the authors observed that back-electron transfer to this state fell into the Marcus inverted region. However, back-electron transfer into the less stable triplet state was found to fall into the normal region, which accounted for it being observable. Yan and coworkers [695] observed normal Marcus back-electron transfer kinetics (faster electron transfer as the driving force increased) for a series of ligand-modified, phosphate-anchored Ru-based dyes. They also observed that these back-electron transfer processes were thermally activated, putting them in the normal regime. Although the overall driving force for each of these dyes should have placed the back-electron transfer process in the inverted region, these authors proposed that the rate limiting step had a smaller driving force and the overall relaxation to the ground state involved secondary processes, such as sequential electron and/or proton transfer events. The extent to which these observations are dependent on the TiO_2 surface structure and details of the dye adsorption state (e.g., structure, coverage, etc.) are not known.

Surprisingly, little dynamics work has been done on the important and widely utilized electron scavenger, the neutral O_2 molecule. At issue here are the dynamics of the reaction between a physisorbed O_2 molecule and an excited electron in TiO_2. One study, by Peiro et al. [509], has probed the O_2 scavenging process dynamically, but only on timescales longer than microseconds in which the issue of trapped versus 'free' CB electron transfer should be dominated by the former. An issue with O_2 is the unusually weak adsorption interaction with the (unreduced) TiO_2 surface making it difficult to the study its electron transfer dynamics. As will be discussed in Section 5, much is known about the chemistry between O_2 and Ti^{3+} sites on TiO_2 surfaces, but the dynamics of this reaction (in the context of electron transfer from a trapped electron and an O_2 molecule) are not well-understood.

3.4. TiO_2 valence band to acceptor hole

To this author's knowledge, there are no examples of dynamics studies involving hole injection into the TiO_2 VB (i.e., electron transfer from the TiO_2 VB to a 'hole' photochemically generated in an adsorbed species). In concept, one could imagine an 'inverse Grätzel cell' on TiO_2 in which an adsorbed dye's highest occupied molecular orbital (HOMO) resides in energy below the TiO_2 VB edge and the energy of an optically excited electron in the dye (its excited state) resided mid-gap, matching a suitable redox couple. Such a cell has been developed by Hagfeldt and coworkers [698, 699] using NiO (and other oxides), but a similar molecular system has not been identified for TiO_2.

Another potential arena for studying hole injection from TiO_2 would be the equivalent of back-electron transfer for photooxidation. In this case, a hole would be generated on TiO_2, transferred transiently to an adsorbate and then transferred back the TiO_2 VB. 'Back hole transfer', as odd as it may seem, may be very prevalent in photooxidation reactions on TiO_2 surfaces. However, identifying and studying such a process requires reliable photochemical 'markers' for both the oxidized adsorbate and the VB hole so that the dynamics of these can be followed.

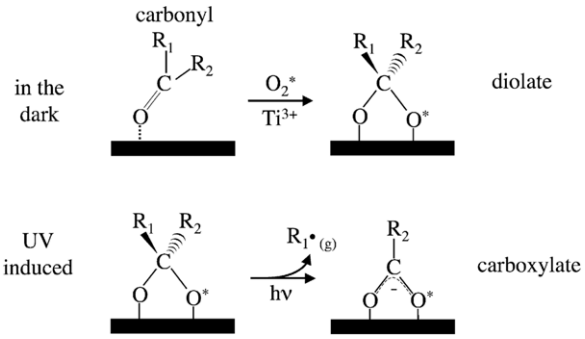

Fig. 4.1. Schematic model for the coupled chemical and photochemical reactions of adsorbed organic carbonyls with oxygen on the R TiO_2(110) surface.
Source: From Henderson [702].

4. Adsorption and the adsorbed state

The starting point for considering photoconversion of molecules on TiO_2 is the physical and electronic structures of the adsorbed state of the molecule. How a molecule binds on the TiO_2 surface influences its electronic structure and redox properties. Coverage, thermal stability and reactivity, adsorption structure and site, etc. are all important factors. The literature relating to the thermal chemistry of adsorbates on TiO_2 surfaces is too vast to review here, even in the (narrower) context of how it relates to photochemistry. Fortunately, a considerable amount of work has been done already on this subject by other review authors [175,566,700] in terms of single crystal TiO_2 surfaces. Instead, two examples of how these issues affect photocatalysis on TiO_2 will be briefly discussed in this section, these being 'structure sensitivity' and 'coverage dependence'. More details regarding the relationship between the adsorbed state and photochemistry will be touched on in Section 5 in the context of various photochemical reaction mechanistic studies on TiO_2 surfaces.

4.1. Structure sensitivity

Surface scientists generally refer to the relationship between how an adsorbate's structure at a particular surface site influences its surface chemistry as a 'structure sensitivity' or a 'structure–reactivity' relationship. While such associations are a common theme in many surface science studies, particularly in terms of heterogeneous catalysis, their relevance to heterogeneous photocatalysis has not been well-explored. There are a few examples emerging that show a correlation between adsorbate structure and photochemistry of TiO_2. For example, this author and collaborators [701–704] have shown that organic carbonyl molecules bound to the R TiO_2(110) surface in η^1 configurations (through the carbonyl oxygen lone pair to a surface Ti^{4+} site) are photochemically inactive to direct hole-mediated oxidation. However, when thermally 'activated' by coadsorbed oxygen, these species transform into photochemically active diolate species (see Fig. 4.1). In another example, Rusu and Yates. [705] showed that photocatalytic conversion of N_2O was slightly faster if the N-end of the molecule was bound to surface Ti^{4+} sites rather than if the O-end was utilized. Also, N_2 (the preferred product) was formed at low N_2O coverages with the N-end down species. Xu and coworkers [706] used DFT to show that the adsorption state of catechol on A TiO_2(101) influenced the optical absorption properties of the molecule. Similar findings have been reported for other dyes anchoring on TiO_2 surfaces [671,673,674,707–713]. For example, the issue of coordination of carboxylate anchors (mono versus bidentate) continues to be an important question in the efficiency of photoejection and stability of an adsorbed dye [707].

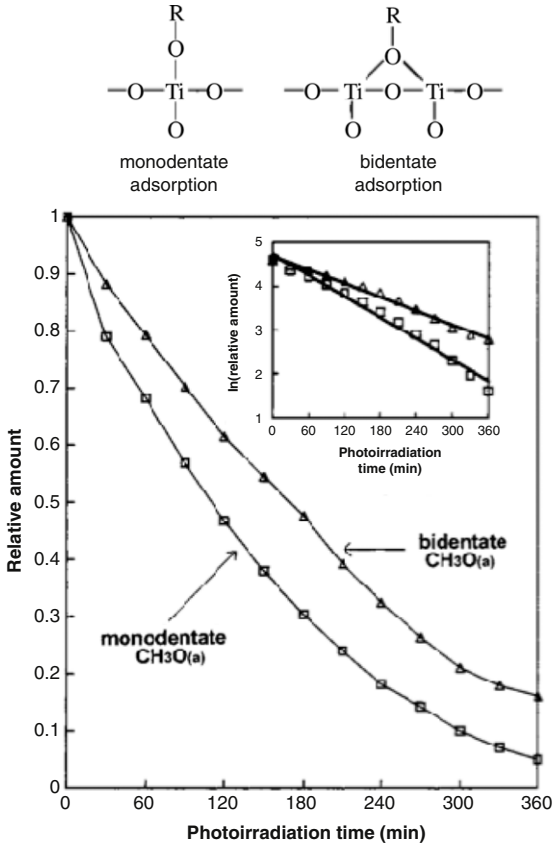

Fig. 4.2. Changes in the relative surface coverages of mono and bidentate ethoxy groups (see schematic model above) on P-25 estimated from the FTIR ν (C–O) feature as a function of UV irradiation time. The inset shows first order decay plots from these data.
Source: Reprinted and adapted with permission from Wu et al. [716].
© 2000, American Chemical Society.

One of the prevalent structure sensitivity issues in organic photooxidation is the relative photoreactivities of various molecularly and dissociatively adsorbed states of molecules containing O–H bonds [714]. For example, based on IR, Liao et al. [715] proposed that formic acid on P-25 was ~53 times more photoactive than formate. Similarly, Wu et al. [716] used FTIR to monitor the relative photoactivities of mono and bidentate-bonded alkoxy groups resulting from dissociative adsorption of methanol or ethanol on TiO_2. As shown in Fig. 4.2, these authors showed that the relative rate for disappearance of monodentate ethoxy groups was greater than that of the bidentate form (assuming no interconversion initiated by surface photochemistry). These data suggest that the monodentate form of an alkoxy on TiO_2 was ~1.5 times more reactive than the bidentate form, despite the fact that the authors found that the relative thermal stabilities of the two forms to be opposite. These data illustrate the potential importance that adsorbate–surface structure plays in photochemical reactions on TiO_2 surfaces.

4.2. Coverage dependence

Surface coverage has been shown to affect photocatalytic activity on TiO_2 surfaces in several examples [541,705,717–719]. This author and coworkers [541] have shown that the rate of trimethyl acetate (TMA) photodecomposition on R TiO_2(110) depended on the TMA surface coverage. As shown in Fig. 4.3, the extent of TMA photodecomposition during a 5 min UV irradiation period on R TiO_2(110) was nearly complete at low TMA coverage, decreased from 100% conversion (dotted line) at

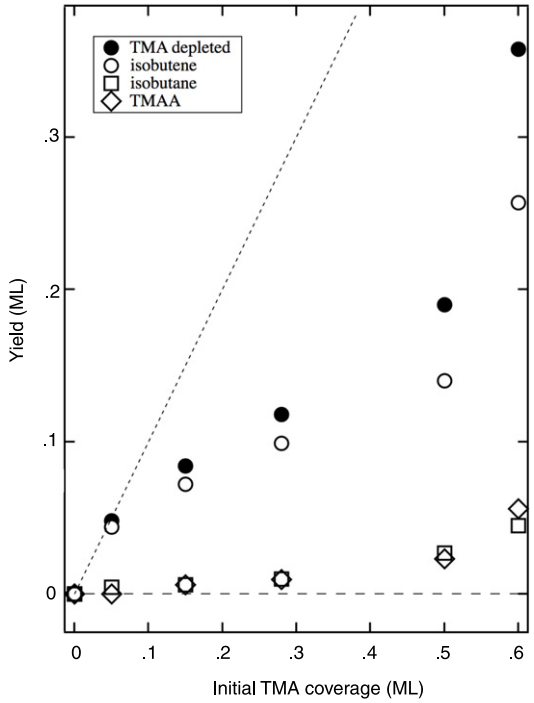

Fig. 4.3. Product yields during a 5 min UV irradiation period as a function of initial TMA coverage on R TiO_2(110). The total TMA photodecomposition yield was obtained from summation of the product yields. The dashed line represents 100% conversion of the initial TMA coverage to product.
Source: From Henderson et al. [541].

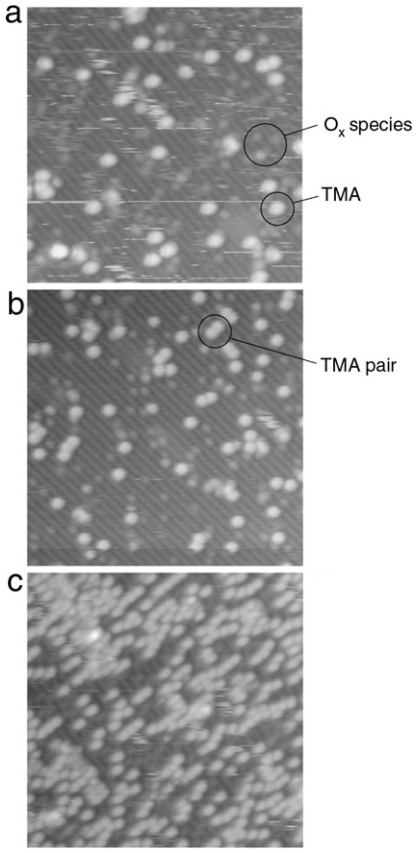

Fig. 4.4. STM images from various TMA coverages ((a) 0.014 ML, (b) 0.026 ML and (c) 0.13 ML) on R TiO_2(110). In each case, the surface was dosed with 200 L O_2 at 300 K prior to TMAA adsorption. Each image is nominally 21 × 21 nm, and obtained using a sample bias of +1.3 to +1.6 V and tunneling current of ~0.4 nA.
Source: From Henderson et al. [541].

intermediate coverage, and increased as the surface exceeded a 0.5 ML coverage. Because the yield at higher coverage approached values seen at the lowest coverages, the low (relative) yields at intermediate coverages could not be ascribed to insufficient photon exposure. Instead, STM results, shown in Fig. 4.4, suggest that the deviation from near 100% conversion at intermediate coverages was due to a local effect between neighboring TMA groups on the surface. At very low coverages (Fig. 4.4(a)), TMA groups were mostly isolated on the surface. As the coverage increased above ~0.03 ML (Fig. 4.4(b)), STM showed the formation of TMA–TMA line structures forming across bridging O rows. These structures appeared to be attractive in nature, as shown by comparison with higher coverage STM images (Fig. 4.4(c)). The attractive interactions are possibly mediated by surface OH groups (from the acid protons not observable by STM), because ample isolated adsorption sites were available at low coverages [720]. Onset of these line structures corresponded to the point at which the TMA photodecomposition yield decreased. In contrast, the rise in TMA photodecomposition yield above 0.5 ML was attributed to the instability of the densely packed surface. Because TMA photodecomposition was hole-mediated, O_2 was not essential to see photodecomposition and the decomposition products left the surface (see Section 5). Very different coverage dependence was observed for acetone photodecomposition on R TiO_2(110), where rates decreased by 10 fold as the surface became saturated with acetone [701]. In this case, O_2 was needed and a more stable photodecomposition product (acetate) accumulated on the surface which blocked access of O_2 to the surface. Similar observations have been made by Arsac et al. [721,722] for isopropyl alcohol (IPA) photooxidation on TiO_2, where complete conversion of IPA was limited by the ability of high coverages of the reactant to displace the intermediate (acetone) from the surface. In contrast, higher conversion of IPA was observed at low IPA coverage.

5. Mechanisms

The mechanistic aspects of photocatalytic reactions on TiO_2 are complex. This section will explore the mechanistic details associated with single electron transfer events for molecules with a wide variety of functional groups in both photooxidation and photoreduction reactions on TiO_2. Discussion in this section is organized into classes of molecules that allow identification of specific insights into single electron transfer steps. In most cases, mechanistic details are generally only available for stable surface species intermediates. The relationships between the 'non-thermal' processes associated with electron transfer and the thermal processes that follow as a consequence are also of importance. Studies on certain classes of reactants will not be included in this section because: (1) their inherent complexity negates opportunities for molecular insights (e.g., photooxidation of humic acids), (2) molecular insights are usually not the focus of such studies (e.g., colorimetric changes in dye photodegradation), or (3) the molecules represent special cases that will be discussed in Section 8 (e.g., CO_2 photoreduction or water splitting).

5.1. General issues

5.1.1. Direct versus indirect events

For every oxidation half reaction there must be a corresponding reduction half reaction (and vice versa). In a photoelectrochemical schemes, these may be separated spatially to different electrodes (surfaces), but they are still linked kinetically and thermodynamically. In the absence of an electrochemical circuit (e.g., reactions on

single TiO_2 nanoparticles), both reactions occur in a spatial region that allows for greater interdependence between oxidation and reduction steps.

One of the major mechanistic issues in photocatalytic reactions on TiO_2 is identification of the oxidant and reductant. In particular, there is frequent debate in the context of oxidation reactions about the relative roles of VB holes for direct oxidation versus hydroxyl radicals for so-called 'indirect' oxidation [13,397,678,717,723–737]. This debate often hinges on how OH radicals are formed, for example via direct hole oxidation of adsorbed H_2O and/or OH^- [731], or via electron scavenging reactions involving O_2 [730,732]. The involvement of OH• radicals can also depend on whether they are bound or free [738]. Not every reactant will necessarily be sensitive to only one of these processes, so identification of the primary process is important. For example, Minero et al. [739] indicated that the initial step in phenol photooxidation is hole-mediated, but OH•-initiated steps became more important in subsequent mechanistic steps. It is unclear whether this is because OH• does not readily react with adsorbed phenol, because the products do not react well with holes, or because OH• is not immediately generated. Reaction conditions can also play a role in deciding which oxidant is available and most useful. For example, Yu and Chuang [717] observed both OH• and holes as viable oxidizers of adsorbed ethanol, with coverage being a deciding factor. They proposed that OH• radicals are the key oxidizer at low ethanol coverage and the VB holes at high ethanol coverage. (The latter condition fits in with the inability of water or O_2 to gain access to the surface at high organic coverage [515,541].)

The key issue is not which oxidant is most important, but how can the roles of OH• radicals and holes be adequately characterized. Addressing this issue requires a detail understanding of the molecular-level details (electronic energy matching, spatial proximity, energy barriers, etc.) important in reactions of holes or radicals with particular reactants or intermediates. For example, the nature of the adsorbate being oxidized is of obvious importance in understanding how various oxidants perform [397,723,733,735,736]. Byrne et al. [723] compared photocurrent yields versus the extent of organic photooxidation on P-25 covered anodes under anaerobic conditions. Based on the photocurrent yield, they found that the efficiency of hole acceptors in four adsorbed organics followed the trend: oxalate > formate > acetate > methanol. This trend did not correlate with the relative reaction rates of these molecules with free OH• in solution.

An interesting indication that direct hole-mediated oxidation is not the only oxidation pathway in TiO_2 photocatalysis is found in observations of 'remote' oxidation [38,286,701,727,740–751]. In this phenomenon, oxidation events occur at regions of a TiO_2 sample not exposed to light or at non-TiO_2 surfaces that are line-of-sight from irradiated TiO_2 surfaces. Perhaps the first example of this phenomenon was by Kikuchi et al. [745] who observed the killing action of irradiated TiO_2 on *Escherichia coli* which were separated by distances of ~50 μm. A gas phase O_2-related species was suspected as the source of this remote photoactivity of TiO_2 [746], with H_2O_2 or OH• (generated from H_2O_2) being the major candidates [747,751]. Naito et al. [286] recently used molecular fluorescence markers to verify the emission of OH• from TiO_2 during UV irradiation. These authors found that the OH• yield was proportional to the gas phase concentration of O_2.

Ejection of non-oxygen related radicals may also play a role in 'remote' oxidation reactions. This author observed the ejection of methyl radicals from the surface of R TiO_2(110) during UHV photodecomposition of adsorbed acetone [701,752,753]. Similar observations have been made by Stair and coworkers for photodissociation of methyl iodide on this surface [680,754,755]. The methyl radicals emitted from adsorbed acetone were shown to further decompose on the chamber walls to yield formaldehyde. Recently, Shen and this author [756] have shown that methyl radicals ejected into ice overlayers (water or methanol) react to form a variety of products including CH_4 and C_2H_6. Organic radical ejection has also been observed under UHV conditions for several other adsorbates on R TiO_2(110) [543,702–704,757] suggesting that secondary reactions of these radicals may play important mechanistic roles in photocatalytic reactions on high surface area catalysts. Generation of organic radicals during photochemical processes on TiO_2 is not unexpected since, by definition, redox processes associated with e^-/h^+ pair generation on TiO_2 involve single electron transfer events (i.e., result in unpaired electrons). EPR has been used to observe formation of stable organic radicals during UV irradiation of TiO_2. For example, Murphy's group has detected a variety of R–OO• and R–C(O)–OO• radicals during low temperature photooxidation of carbonyls on TiO_2 [514,758,759]. Similar observations have been made by Coronado and Soria [760] for toluene, and by Nosaka et al. [734] for acetic acid. It remains a challenge to determine the fate of these radicals under reaction conditions as they spawn chain reactions or remain adsorbed awaiting additional direct or OH• radical mediated reactions.

5.1.2. Overall rates and quantum efficiencies

The issue of overall reaction rates and quantum efficiencies has attracted much attention in the TiO_2 photocatalytic literature. In general, one can view rates from two perspectives: that of individual electron transfer (or related thermal reaction) steps or from the overall process level. The former are complex in their molecular-level details and have greater significance in relationship to surface studies. In the latter case, evaluations of rates and quantum yields are complicated by many dependences at both the molecular and macromolecular levels. This review is focused on molecular-level details, and has dedicated Section 3 to illustrating some of the basic science knowledge that has been uncovered involving single electron transfer events. Considerable portions of this section are also concentrated on details of molecular-level mechanisms. Readers interested in better understanding process kinetics are directed to examples of work on the subject [7,78–80,761,762].

The subject of quantum efficiencies can also be viewed at the individual event level (photoabsorption and electron transfer) or at the process level, however determination of a quantum efficiency is not straightforward. As Serpone [36] pointed out, the concept of quantum efficiency is too frequently misused to mean the ratio of detected events per incident photon, but should actually be viewed as events per incident *absorbed* photon. The problem comes in measuring the optical absorption efficiency of a particular TiO_2 sample (because of complications associated with light scattering and penetration issues [763,764]), and making correlations between light absorption and a particular electron transfer event at a particular site on a surface. As mentioned previously, the interdependent fates of both charge carriers, as well as factors such as coverage, site heterogeneity, etc., make such correlations very difficult. Nevertheless, the literature contains useful examples of studies in which groups have used quantum efficiencies to characterize photocatalytic processes on TiO_2 [255,395,398,724,765–768]. For example, Cornu and coworkers [767] determined that the quantum yield for formate photooxidation on suspended TiO_2 was dictated primarily by charge carrier dynamics and not by mass transport (or related) effects.

5.1.3. Lattice oxygen

While molecular oxygen, water and surface hydroxyls are all clearly recognized sources of oxygen in photocatalytic reactions on TiO_2, the involvement of lattice oxygen in these reactions should also be considered in understanding photocatalysis on TiO_2. The issue here is not whether exchange or incorporation

reactions can occur during photocatalysis on TiO_2 surfaces (both are known to occur [175]), but whether lattice oxygen plays a direct mechanistic role (other than as a site) in photochemical reactions on TiO_2. Section 2.4 has reviewed literature on how holes can be trapped at under-coordinated O^{2-} sites on TiO_2 surfaces, but how bonds are formed and electrons are transferred between these sites and adsorbates is largely unknown. There have been suggestions in the literature that lattice oxygen plays a role in photooxidation reactions on TiO_2 [769–775] mainly because of its presence in products or intermediates (as determined through isotopic labeling studies). However, there have been other studies in which lattice oxygen was found not to be involved [776,777]. The challenge remains to provide spectroscopic evidence about the mechanistic role of lattice oxygen that can be distinguished from simple exchange processes.

5.1.4. Photoadsorption and photodesorption

The involvement of photoadsorption and photodesorption in photochemical processes on TiO_2 surface influences (in either a positive or negative manner) the coverages of adsorbed species. These phenomena can be viewed as the involvement of a charge carrier in generating (by photodesorption) or removing (by photoabsorption) an adsorption site on the surface. Perhaps the most extensively studied example of photodesorption from TiO_2 is that of O_2 [97,98,100,201,253,473,573,679,753,776,778–782]. Although discussed in detail below, O_2 photodesorption is believed to result from the interaction of a VB hole with an adsorbed $O_2^{\delta-}$ species, resulting in a neutral O_2 molecule that readily desorbs from the surface. Other examples of molecular photodesorption from TiO_2 surfaces include alkyl halides [680–682,754,755,757], CO [783], N_2O [705] and triethylamine [784]. The details of these events differ, but in each case the photodesorption event involves a charge carrier causing a charge change in the adsorbate–surface relationship that results in the adsorbate transitioning to a different potential energy surface (e.g., ion to neutral) that is more amenable to desorption. Conversely, trapping of a charge carrier at the surface (e.g., an electron at a surface Ti^{4+} site) can provide the setting for formation of a stronger chemisorption interaction between a molecule and the surface (i.e., photoadsorption). Literature examples of photoadsorption on TiO_2 include O_2, H_2, H_2O, NO, CH_4 and organic acids [9,387,388,556,778,785–790]. Research is needed into what charge carriers and what surface sites are involved in these photoabsorption and photodesorption events, and how these events promote, regulate or inhibit photocatalytic processes on TiO_2. For example, this author [753] has shown that O_2 photodesorption has little or no influence on the first photochemical step in acetone photooxidation on TiO_2(110) even though both processes are initiated by the same charge carrier (holes). As shown in Fig. 5.1, the yield of methyl radicals was unaffected by whether or not molecular O_2 was photodesorbed from the surface prior to acetone adsorption. The photodesorption dynamics for O_2 were found to be slower than those associated with methyl radical ejection (see inset). The scavenging of holes by adsorbed O_2^- was not seen to compete strongly with the same ability of acetone. (For more on O_2 photodesorption see Section 5.2.1.)

5.1.5. Surface defect formation

Aside from photoablation (rapid, local heating) or photoetching (photochemistry that initiates surface electrochemical damage), there is little evidence in the literature that UV light induces structural damage to TiO_2 surfaces. Under UHV conditions, Mezhenny et al. [791] found no evidence with STM for modification of the R TiO_2(110) surface as a result of UV photon irradiation. Their results suggest that this surface is not susceptible to UV photochemical effects such as photon-induced desorption of lattice oxygen or restructuring via band-to-band excitation processes. However, these authors did observe changes in the reduced (1×2) reconstructed TiO_2(110) surface as a result of photon irradiation.

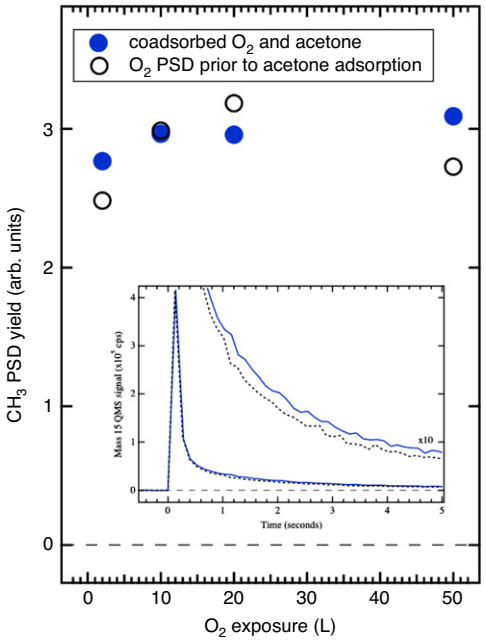

Fig. 5.1. Comparison of the CH_3 (mass 15) PSD yields in the initial 100 s of UV irradiation as a function of O_2 pre-exposure for acetone and oxygen coadsorbed on R TiO_2(110). Solid blue circles: O_2 pre-exposed at 100 K followed by flashing to 300 K and recooling to 100 K for adsorption of 0.18 ML acetone. Open black circles: O_2 pre-exposed at 100 K followed by flashing to 300 K and recooling to 250 K for 5-min UV exposure. The surface was then cooled to 100 K for adsorption of 0.18 ML acetone. The inset shows CH_3 PSD spectra for the 2 L O_2 cases. CH_3 PSD data taken during UV irradiation at 250 K.
Source: Adapted with permission from Henderson [753].

5.2. Photooxidation reactions

Photochemical processes can be categorized as photooxidation or photoreduction, but both half reactions must co-exist in close proximity in non-photoelectrochemical settings. In this section, the mechanistic details of photooxidation reactions on TiO_2 will be discussed, starting with discussion of the role of electron scavengers in photooxidation.

5.2.1. Electron scavengers: O_2

The roles of oxygen in photooxidation reactions over TiO_2 are sufficiently diverse and complex that they require concentrated attention. Fig. 5.2 shows a brief chronology of some unique insights resulting from fundamental studies of the interaction of oxygen with single crystal TiO_2 surfaces. This chronology illustrates how the field has progressed in terms of molecular-level descriptions of O_2 on TiO_2 surfaces in general. These insights relate to both surface chemistry and surface photochemistry.

O_2 surface chemistry: Perhaps the most logical place to start is with the thermal (non-photochemical) properties of O_2 on TiO_2 surfaces [792]. Considerable work has been invested in the study of oxygen surface chemistry on high surface area TiO_2 (not cited here). However, studies of O_2 on single crystal TiO_2 surfaces (particularly that of the R TiO_2(110) surface) have yielded the most detailed information on this subject from both experimental [98,192,199–202,473,515,526,541,566,573,679,780,

<1995: photoemission shows O_2 oxidizes oxygen vacancy defects (e.g., (803))
1995: two channels of O_2 photodesorption (781, 802)
1996: high temperature O_2-induced regrowth of TiO_2 with subsurface Ti^{3+} interstitials (808, 809, 845-847)
1998: O adatoms from O_2 dissociation at oxygen vacancies (799)
1999: theoretical models for spin-states of adsorbed O_2 (779)
1999: O_2 adsorption capacity greater than one molecule per vacancy; evidence for adsorbed $O_2^{\delta-}$ species; temperature dependence of O_2 dissociation (200)
2001: theoretical binding energies and charge states for adsorbed O_2 (818)
2003: reaction of O_2 with bridging OH groups (199)
2003: observation of O adatoms by STM (202)
2006: theoretical predictions of O_2 clusters (823)
2006: observation of physisorbed O_2 (798)
2008: O_2 dissociation at non-defect sites; role of subsurface defects in O_2 adsorption (526)
2008: O_2+OH reaction 'clears' the surface (526, 807)
2008: 'hot' O adatoms from O_2 dissociation at vacancies (796)
2009: STM evidence for HO_2 from reaction of O_2 with OH groups (797)
2009: photodesorption of hyperthermal O_2 (679)
2009: O_2 uptake proportional to electronic defects in surface (804, 811)
2010: Electron-mediated photodissociation of adsorbed O_2 (864)
2010: Angular dependence in CO_2 PSD during CO oxidation resulting from photodissociation of O_2 at vacancies (960)

Fig. 5.2. Brief chronology of various literature studies on the interaction of O_2 with the R TiO_2(110) surface.

781,793–799,780–813] and theoretical [779,782,812,814–832] points of view. Using the R TiO_2(110) surface as the prototype, it is clear from temperature programmed desorption (TPD) measurements at ~30 K that O_2 can only physisorb to TiO_2 surfaces if reduced cation sites are not present [798,800,804]. Similar conclusions can be drawn from many of the theoretical studies listed above. Studies of the O_2–TiO_2(110) system become most relevant to TiO_2 photochemistry when one considers the chemical interactions of O_2 with surface electronic defects (e.g., oxygen vacancies) on TiO_2(110). These sites mimic the electronic structure and reactivity of trapped electrons generated by photoexcitation events in TiO_2 (see Section 2). Studies of the interaction of O_2 with surface electronic defects on TiO_2 can therefore provide insights into electron scavenging reactions important in TiO_2 photooxidation. The activation energy for O_2 dissociative adsorption at vacancy sites on TiO_2(110) is high enough (in excess of ~0.7 eV) [815,828] that low temperature adsorption events do not result in dissociation. Fig. 5.3 shows O_2 TPD results from Kimmel and coworkers [800,804] illustrating both the physical and chemical interactions of O_2 with the reduced R TiO_2(110) surface. The lower right inset shows TPD of the coverage-dependent behavior of the interaction of physisorbed O_2 with the surface, while the upper right inset shows the amount of chemisorbed O_2 that evolves in TPD. Based on detailed TPD measurements using the physisorption component to calibrate O_2 coverage, these authors found that the 'irreversible' uptake of O_2 (i.e., not recoverable in TPD) by oxygen vacancy sites followed roughly a 2:1 ratio, with only a minority amount of chemisorbed O_2 recovered in TPD. These data provide a refinement of previous assessments by this author and coworkers [200] that proposed that each surface vacancy was responsible for binding up to three oxygen molecules. These findings imply that electrons associated with the oxygen vacancy sites on TiO_2(110) are not localized only at the defect, but have sufficient density at adjacent sites to allow charge transfer processes to occur there. This conclusion is consistent with theoretical and experimental findings for the delocalization of vacancy charge discussed in Section 2.4. The ability of O_2 to scavenge charge is not restricted to chemistry occurring at surface defect sites. Wendt and coworkers [526] used STM to characterize the reactivity of specific surface sites towards dissociative O_2 adsorption at room temperature. Fig. 5.4 shows STM images that indicate that O_2 dissociative adsorption occurs not only does at vacancies, resulting in filled vacancies and isolated O adatoms ('O_{ot}' in the figure) in agreement with previous work [202,799], but

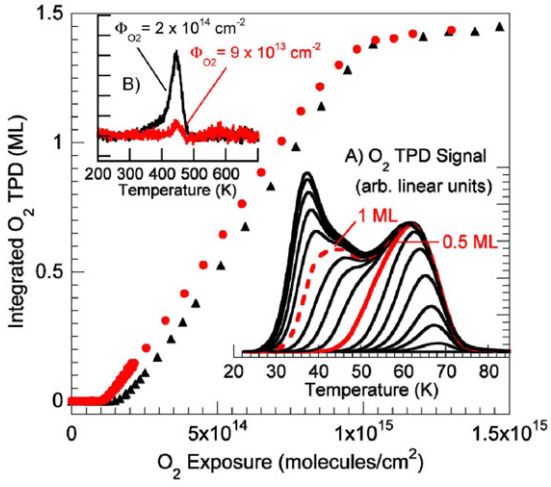

Fig. 5.3. Integrated O_2 TPD signals (for signal below 95 K) as a function of O_2 exposure from the reduced R TiO_2(110) surface possessing ~0.08 ML surface oxygen vacancy sites (circles) and from a slightly higher vacancy concentration generated by electron bombardment (triangles). (Insets A and B: O_2 TPD spectra from physisorbed and chemisorbed O_2, respectively.)
Source: Adapted with permission from Kimmel and Petrik [800].

also that O_2 dissociative adsorption occurs as pairs of O adatoms at non-vacancy sites. These authors attributed instances of non-vacancy O_2 dissociation to charge transfer chemistry involving subsurface Ti^{3+} interstitial sites. These results show that near-surface electronic defects with electronic signatures sufficiently strong at the surface can promote charge transfer to O_2 molecules transiently adsorbed in their vicinity. However, subsequent studies by other authors have linked non-vacancy dissociation of O_2 not to subsurface defects but to more extensive delocalization of charge associated with surface vacancies [804,811,812].

Evidence of electron transfer events to O_2 (not resulting in dissociation) is found both in removal of the signature Ti^{3+} electronic state features and in development of molecular forms of O_2 surface chemistry. For example, this author and collaborators [200,201] have shown that the EELS transition at 0.8 eV associated with surface Ti^{3+} sites was attenuated by O_2 adsorption on TiO_2(110) at 120 K, and completely disappeared after heating the surface to 200 K (see Fig. 1.8). EELS also showed generation of a new feature at 2.8

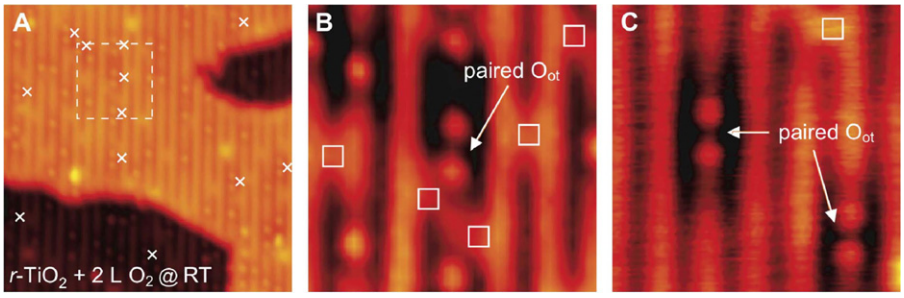

Fig. 5.4. STM images for the reaction of O_2 at 300 K with a R TiO_2(110) surface possessing ~0.017 ML of O_{br} sites. (A) After 2 L O_2 (155 × 155 Å); white crosses designate pairs of next-nearest O adatoms. (B) Expanded region indicated in 'A' (38 × 38 Å); unreacted O_{br} sites indicated with white squares. (C) Similar region after a 200 L O_2 exposure at 300 K. STM images acquired between 110 and 130 K. From Wendt et al. [526].
Source: Reprinted with permission from AAAS.

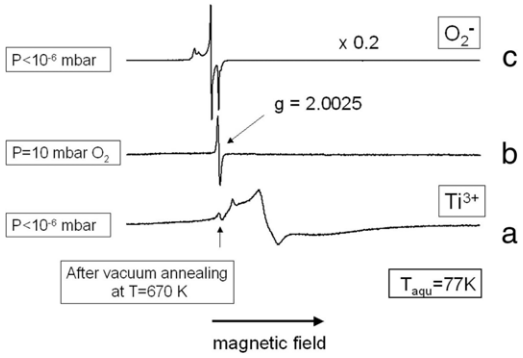

Fig. 5.5. EPR spectra resulting from TiO_2 nanoparticles: (a) exposed to water and then vacuum annealed at 670 K, (b) subsequently exposed to O_2, and (c) then evacuated.
Source: Reprinted with permission from Elser et al. [833].

eV which was assigned to an adsorbed $O_2^{\delta-}$ species based on comparisons with literature on organometallic Ti–O_2 complexes. Similar findings have been reached based on EPR measurements. Elser et al. [833] found that O_2 removed the EPR signatures of Ti^{3+} sites from vacuum reduced TiO_2 nanoparticles, replacing them with signals associated with O_2^- surface species (see Fig. 5.5). Also, a variety of O_2 structures and species resulting from electron transfer events have been proposed from various theoretical perspectives (see references above). These studies highlight briefly the evolving understanding of how O_2 interacts thermally with electronic defects on TiO_2 surfaces.

O_2 + H_2O/OH surface chemistry: The chemistry (and photochemistry) of O_2 on TiO_2 becomes much more diverse when water and/or OH are present on the surface. It is widely speculated that O_2 chemistry in the reductive channel of TiO_2 photooxidation reactions results in hydroxyl radicals that can participate in oxidative reactions (see Section 5.1.1). Spectroscopic observations of HO_2• [550,728,834–837] and H_2O_2 [730,838–840] (not to mention OH•) have been linked to reactions of O_2^- with water-related species on or near the TiO_2 surface. Exchange reactions between O_2 and other surface species initiated by light [841,842] also may involve reactions between O_2^- and water. In general, the literature points out two classes of mechanistic pathways for generation of HO_2• or H_2O_2 from O_2. One class involves reactions of O_2 with adsorbed species and the other involves O_2 reactions in the physisorbed or solution phase media (away from the TiO_2 surface) facilitated by liberation from the surface of charged or excited state O_2 species. For the purpose of this review, only pathways involving adsorbed species will be discussed.

Szczepankiewicz and coworkers [508,510,517] were perhaps the first to spectroscopically show the effects of O_2 exposure to

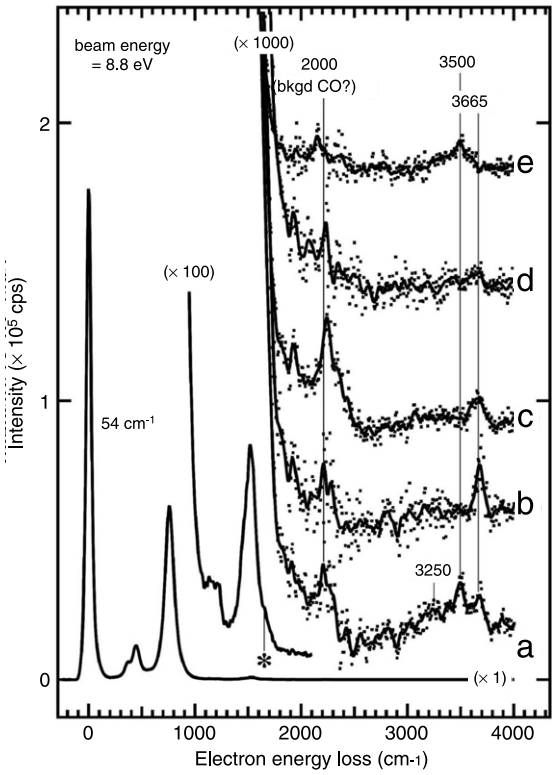

Fig. 5.6. Deconvoluted HREELS spectra from the reaction of O_2 with OH_{br} groups on R TiO_2(110) possessing ~0.14 ML O_{br} sites; (a) 1.2 ML of H_2O adsorbed at 120 K, (b) 'a' heated to 375 K, which removed adsorbed water leaving only the OH_{br} groups, (c) exposure of 'b' to 2 L O_2 at 120 K, and (d) 'c' heated to 230 K. In contrast, (e) shows ~1 ML of H_2O adsorbed *after* exposing the surface to 4 L O_2 at 120 K showing no OH_{br} group formation. Spectra recorded at 120 K.
Source: Reprinted with permission from Henderson et al. [199].

surface OH groups on TiO_2 surfaces at which excited electrons had been trapped (see Fig. 2.6). These authors found that the O–H groups associated with certain electron trap sites were altered by O_2 exposure, but that others were not. A similar effect was observed by this author [199] for the interaction of O_2 with bridging OH groups (OH_{br}) formed from the dissociation of water at oxygen vacancy sites on R TiO_2(110). As shown in Fig. 5.6, OH_{br} groups bound at Ti^{3+} sites on this surface give a strong ν (OH) feature at ~3665 cm^{-1}, which is close to the 3716 cm^{-1} feature ascribed by Szczepankiewicz et al. to similar surface sites on P-25. Exposure of these OH_{br} groups to O_2 at 120 K (Fig. 5.6(c)) resulted in weakening and widening of the vibrational feature, and subsequent heating to 200 K resulted in their disappearance (Fig. 5.6(d)). The reaction between O_2 and OH_{br} was also followed

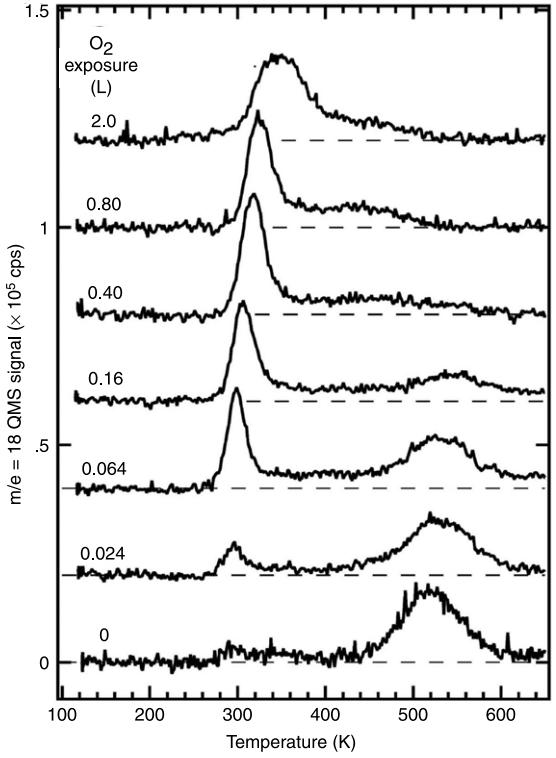

Fig. 5.7. H_2O TPD spectra obtained after exposure of OH_{br} groups (~0.28 ML) on R TiO_2(110) to various amounts of O_2 at 120 K. Surfaces with only OH_{br} groups were prepared by preheating a multilayer H_2O exposure to 370 K and recooling to 120 K prior to O_2 exposure.
Source: Reprinted with permission from Henderson et al. [199].
© 2003, American Chemical Society.

in TPD. As shown in Fig. 5.7, exposure of the R TiO_2(110) surface containing OH_{br} groups to O_2 resulted in 'titration' of the signature OH_{br} recombination TPD feature at ~500 K [843] and formation of a new H_2O TPD feature slightly above room temperature ascribed to recombination of terminal OH groups (OH_t) located at five-coordinate Ti^{4+} sites. The OH_t groups were presumably formed from a transiently adsorbed HO_2 surface species. The reaction probability per adsorbed O_2 molecule, taken from these data, was nearly unity suggesting the extraction of charge and a proton (i.e., a hydrogen atom) from the OH_{br} groups by O_2 was a highly favorable process.

Several STM studies have explored the interaction of O_2 with OH_{br} groups formed at defect sites on R TiO_2(110) [797,806,807,813,844]. Both Wendt et al. [806] and Zhang et al. [807] have shown that the reaction of O_2 with OH_{br} groups on this surface is mechanistically complex. Fig. 5.8, from the latter group's work, illustrates this point. Image (a) shows a surface containing ~0.13 ML of OH_{br} groups. Exposure of this surface to O_2 at room temperature resulted in disappearance of OH_{br} groups (images (b) and (c)), but little or no appearance of new surface features. At an optimal O_2 exposure (image (c)), the surface appeared 'clean', although the STM shows signs of the presence of some mobile species (water?). Surprisingly, continued exposure of O_2 resulted in appearance of features that could be ascribed to OH_t groups, as well as O adatoms (not labeled, but as faint features on the Ti rows) and several unidentified features. As shown in Fig. 5.9, Zhang et al. [807] observed that the changes in populations of OH_{br} and OH_t did not track each other. These authors found that water molecules, generated from the reaction of O_2 with OH_{br} groups, were responsible for the 'lost' mass in STM. There presence was evident in STM not only by the transient features discussed above, but also by the motions of OH_{br} groups (lower panel of Fig. 5.9), in agreement with previous STM studies [806]. Du and coworkers [797] used STM to identify intermediates in the reaction of O_2 with OH_{br} groups on R TiO_2(110). Fig. 5.10 shows 'before' and 'after' STM images from the dissociative adsorption of O_2 at a vacancy site (top images and cartoon), but also images associated with O_2 reacting with a single OH_{br} group (middle) and a pair of OH_{br} groups (bottom). The STM contrast of the resulting species on the Ti rows in the bottom two cases was shown to be distinctly different from that of the O adatom (top) or the OH_t group (see Fig. 5.8), leading these authors to propose the formation of an adsorbed HO_2 intermediate. Based on DFT calculations, these authors proposed that the resulting terminal HO_2 species was bound to the surface through the O-end with the OH-end hydrogen-bonded to a bridging O site. They calculated that in this configuration (Fig. 5.11) the binding energy was sufficient (~0.7 eV) to allow stabilization of the HO_2 species on the surface at room temperature. These calculations are consistent with QMMD simulations by Tilocca et al. [826] that predict formation of stable (on the MD simulation timescale) HO_2 and H_2O_2 species from reaction of O_2 with OH_{br} groups on R TiO_2(110). These authors also pointed out that the electronic defect is essential for the $O_2 + OH_{br}$ reaction to proceed as no reaction was observed for the interaction of O_2 with Ti^{4+}-OH groups. Although these reactions have not been experimentally examined on single crystal A surfaces, Filippone et al. [820] used ab initio DFT and MD simulations to show that the stability of O_2^- on A surfaces was enhanced by capturing protons from nearby water molecules to form adsorbed HO_2 species. The 'concentration' of near-surface electron density has been shown to have an impact on the reaction channel for the interaction of O_2 with surface OH^- groups [832].

Dissociated O_2: As mentioned above, one of the results of O_2 adsorption on reduced TiO_2(110) surfaces is electron attachment followed by dissociation to O adatoms [175,566,795–797,799,807,812,824,830]. The dissociation of O_2 at vacancies does not follow a 1-to-2 ratio (i.e., one O_2 molecule fills two vacancies), but a 1-to-1 ratio as shown in Reaction 1:

$$O_2\ (g) + O_{vac} \Rightarrow O_{br} + O\ (a). \quad (1)$$

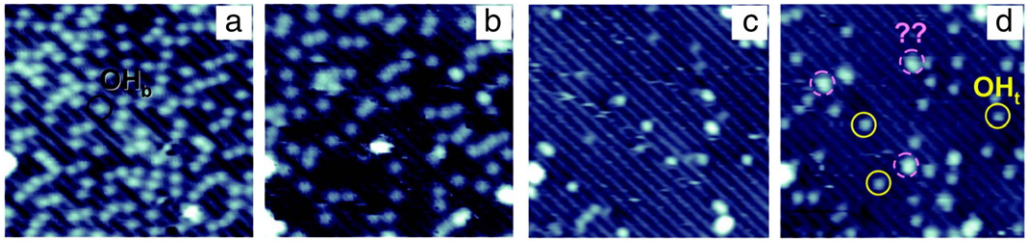

Fig. 5.8. STM images of the same area (15 × 15 nm) on the hydroxylated R TiO_2(110) surface (with OH_{br} coverage of ~0.126 ML) from: (a) before O_2 exposure, and (b–d) after sequential (cumulative) O_2 exposures of 2.4×10^{15}, 9.6×10^{15}, and 3.4×10^{16} O_2/cm^2, respectively.
Source: Reprinted with permission from Zhang et al. [807].
© 2009, American Chemical Society.

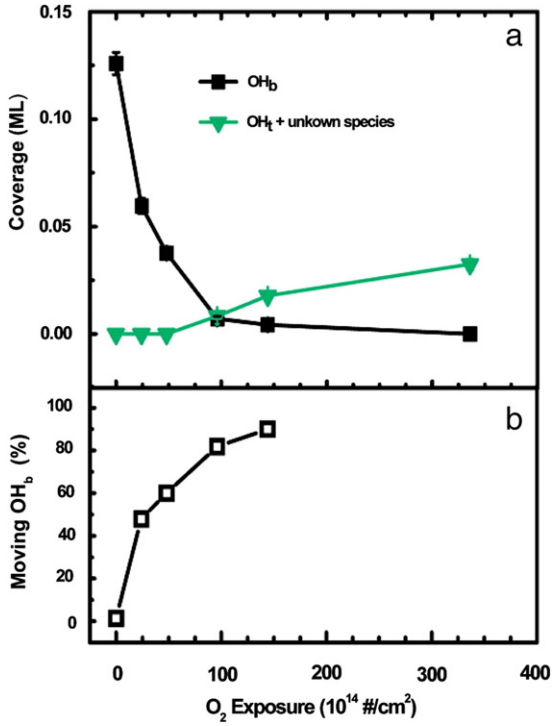

Fig. 5.9. (a) Changes in surface coverages from STM on a fully hydroxylated R TiO_2(110) surface, and (b) percentage of OH_{br} groups that moved between subsequent STM images (~2 min/image), both as a function of increasing O_2 exposure.
Source: Reprinted with permission from Zhang et al. [807].

The O adatom results from O_2 dissociation at vacancy (one adatom) and non-vacancy (two adatoms) sites, and in each case is structurally represented by an atop O atom residing at non-defect five-coordinated Ti^{4+} sites on the R TiO_2(110) surface. Because of a high diffusion barrier [812,824], O adatoms have not been observed to combine to generate O_2, but instead react with subsurface Ti interstitials diffusing from the bulk [526,808,809,845–849] to generate TiO_x surface species at temperatures >400 K. However, excess energy resulting from the exothermic nature of the dissociation process has been shown to generate 'hot' O adatoms that diffuse several lattice spacings before thermalizing [796]. The charge state and electronic structure of the adatom are not well-understood, although DFT calculations by Zhang and Lindan [830] suggest the adatom is not 2- (i.e., it possesses spin character).

Oxygen adatoms on R TiO_2(110) are known to promote thermal chemistry associated with O–H and N–H bond cleavage [799, 850] or organic carbonyl activation [702–704,851]. In particular, O adatoms have been shown to promote water dissociation on R TiO_2(110) [799,852,853], as shown in Reaction 2:

$$H_2O\ (a) + O\ (a) \Leftrightarrow 2OH_t\ (a). \quad (2)$$

This process was previously thought to occur exclusively through O adatom–water interactions at adjacent Ti^{4+} sites [799]. While this is probably the main pathway for Reaction 2, Du and coworkers [795] discovered that O adatoms *across* the O_{br} row also assisted in stabilizing water dissociation on R TiO_2(110), as shown in Fig. 5.12. Image (a) shows the TiO_2(110) surface with several O_{vac} sites (empty circle) and O adatoms (filled circle). A water molecule (moving too fast at room temperature to image) passing on the adjacent row transiently dissociated by donating a proton to a O_{br} site (many such events likely occurred as water diffused on the surface, but back transfer followed because the molecular state was more favorable). However, the O adatom captured this proton, resulting in formation of two *isolated* OH_t groups, one from the original water molecule and one from the proton transfer to the O adatom (in the box of the middle image). DFT calculations (bottom of Fig. 5.12) illustrated the mechanism and favorable energetics for this process. The STM image in Fig. 5.12(c) followed the future of this particular OH_t pair: transfer of the other proton

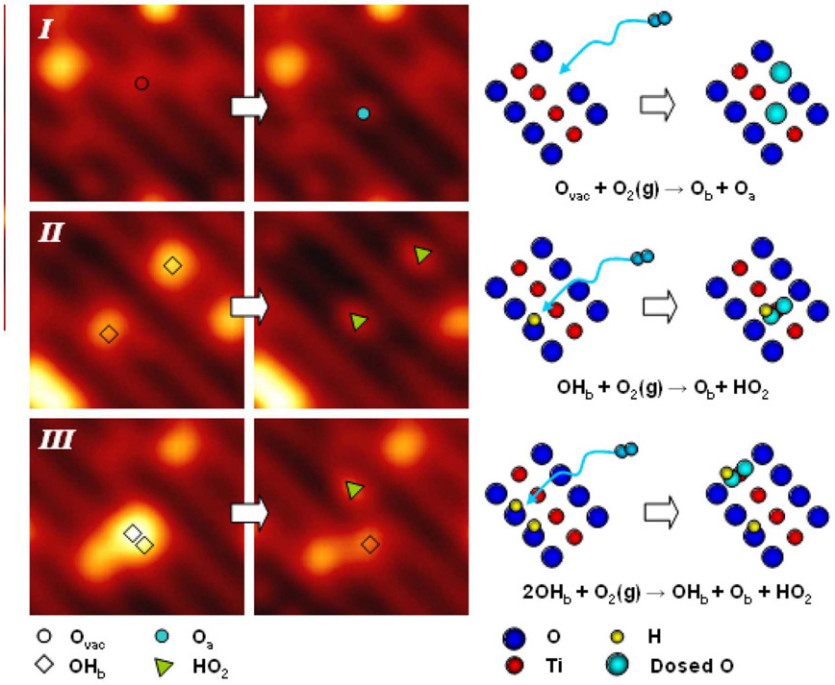

Fig. 5.10. (Left) STM images from three different regions (labeled I, II and III) of a partially hydroxylated R TiO_2(110) surface before and after O_2 exposure, and (right) cartoon models and reaction equations for the O_2 surface chemistry seen in the three cases.
Source: Adapted with permission from Du et al. [797].

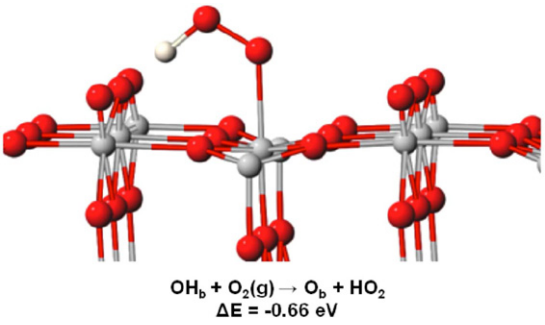

Fig. 5.11. Optimized structures obtained from DFT for terminally-bound HO_2 on the R TiO_2(110) surface. (Red, white and gray spheres represent O, H and Ti, respectively.) The associated formation reaction equation and energy are shown below.
Source: Adapted with permission from Du et al. [797].

reformed water, but now with the O adatom. The resulting water diffused to a vacancy site (bottom of image (c)) where it entered and dissociated to form two OH_{br} groups. These STM results, and others in the literature [526,792,797,807], illustrate the interesting interplay between O adatoms and other species on the R TiO_2(110) surface. The role of O adatoms on other TiO_2 single crystal surfaces (or on particulate TiO_2) has not been established. It is conceivable that the O adatom is a R TiO_2(110) phenomenon. However, given that charge transfer to O_2 readily facilitates its dissociation into O adatoms on the R TiO_2(110) surface it is not unreasonable to expect that this species will be present on other TiO_2 surfaces.

O_2 photochemistry: As studies on the interaction of O_2 with thermally generated Ti^{3+} sites on R TiO_2(110) have shown (see above), a molecularly adsorbed state of O_2 can be formed on TiO_2 surface resulting from electron transfer. This chemisorbed form of O_2 is adequately described as an $O_2^{\delta-}$ ('superoxo-like') species, although the extent of electron transfer needed to stabilize O_2 on a typical TiO_2 surface is not well-understood. There have been numerous observations of this species being formed as a result of electron attachment arising from band-to-band excitation of TiO_2 [387,503,509,548,550,559,730,744,760,835,836,838–840,854–859]. An example of this (mentioned above) is O_2 photoadsorption where UV irradiation of TiO_2 generates adsorption sites for O_2 [387,556,778,787,789,860]. Based on their studies on A nanoparticles, Berger et al. [387] speculated that two types of O_2 photoadsorption may occur. Using EPR results and simulations (shown in Fig. 5.13), these authors observed signals resulting from O_2 exposure to irradiated TiO_2 that could be attributed to reaction of O_2 with a trapped electron to form O_2^- and to reaction of O_2 with a trapped hole at a surface O^{2-} site to form an O_3^- species. As the work of Berger and coworkers illustrates, EPR has been useful in characterizing the electron scavenging role of O_2 [387,550,559,760,836,858]. EPR studies show that formation of O_2^- readily resulted from reaction of O_2 with trapped electrons at low temperature (<150 K). The observed O_2^- species rapidly degraded on warming to room temperature, indicative of the instability/reactivity of this species. The presence of organics also resulted in reactive removal of O_2^-, even at low temperature. The O_2^- species appeared to be the intermediate through which a variety of potentially important reactive O-containing species, such as O_3^- [387,571,760,836], O_2^{2-} [857] and H_2O_2/HO_2 species (see below) were photochemically formed. Studies on the reactivity of O_2 with injected electrons from excited sensitizers [834,861,862] showed similar observations to what was seen in the case of O_2 thermal reactions with surface Ti^{3+} defects. An interesting contrasting point was made by Yu et al. [862] who observed that O_2^- EPR signals persisted to room temperature when TiO_2 was sensitized, which was not the case in direct excitation of TiO_2. These authors proposed that in the absence of suitable hole scavengers, VB holes (which are not present when sensitizing TiO_2) eventually neutralized adsorbed O_2^- surface species on TiO_2.

Bahnemann et al. [503] have shown that the relative rate of O_2^- formation from the reaction of O_2 with trapped electrons was roughly 100 times slower than for the reaction of O_2 with solvated electrons in solution. This observation is consistent with conclusions of Perio and coworkers [509] who showed that electron trapping and detrapping rates in TiO_2 were much faster than the electron transfer rate to O_2. Important issues here are the rate of approach of gas phase or solvated O_2 to the TiO_2 surface and the residence time of O_2 in the vicinity of surface trapped electrons. The sticking probability of O_2 on R TiO_2(110) at ~20–30 K is high (~0.7) but not unity [798,800,804]. The effective sticking probability of O_2 on fully oxidized TiO_2(110) at room temperature is essentially zero [200]. Even on surfaces with oxygen vacancy defects, the initial sticking of O_2 above 200 K is essentially governed by Langmuirian kinetics [200]. These results suggest that the reaction probability of O_2 with trapped electrons on TiO_2 surfaces is considerably less than unity even under idealized conditions. The inability of O_2 to gain access to trapped charges on TiO_2 surfaces under less-than idealized conditions (e.g., with physisorbed water layers or with strongly bound organics) represents a major regulating influence on photooxidation reactions.

Oxygen photodesorption represents a unique photochemical pathway that occurs during photooxidation reactions on TiO_2. On one hand, it may be viewed as a detrimental process since it deprives the surface of chemisorbed O_2 and utilizes charge carriers in seemingly non-productive ways. On the other hand, the event itself can be used to understand both charge carrier dynamics and surface electron transfer processes, as well as a means of gauging the relative efficiencies of other photochemical processes. Additionally, retention of non-thermal kinetic and internal energy in the ejected O_2 molecule [679] might facilitate unexpected chemical processes in the media above the surface.

The most extensive work on the subject of O_2 photodesorption from a TiO_2 surface has been done from the R TiO_2(110) surface by the Yates' group [473,573,776,780,781,802]. Essential details from these studies are covered in review articles published by this group [97–100]. The process is generally believed to occur through a hole-mediated reaction, shown in Reaction 3:

$$O_2^- (a) + h^+ \Rightarrow O_2 (g). \quad (3)$$

Direct excitation of a charge transfer complex band has also been offered by other authors as a possible mechanism for O_2 photodesorption [782]. The Yates group has shown that at least two adsorbed states of O_2 contribute to their observed PSD profiles. They found that an 'α' state, formed on adsorption at 105 K, photodesorbed with a cross section of $\sim 8 \times 10^{-17}$ cm^2. This 'α' state thermally converted to a 'β' form above 250 K which exhibited faster PSD kinetics ($\sim 1.5 \times 10^{-15}$ cm^2). The dynamics of O_2 photodesorption from R TiO_2(110) have been explored by Sporleder et al. [679] using TOF methods. These results are discussed in Section 3.2 in the context of electron transfer dynamics. These authors confirmed the essential observations of the Yates group regarding two types for O_2 photodesorption. No photodesorption signal was observed above >400 K, which the authors attributed to O_2 dissociation (see above). The Yates groups also determined a photon energy threshold of ~3.1 eV that indicated that the photodesorption processes were substrate-mediated. The photon flux dependence of the initial O_2 PSD rate,

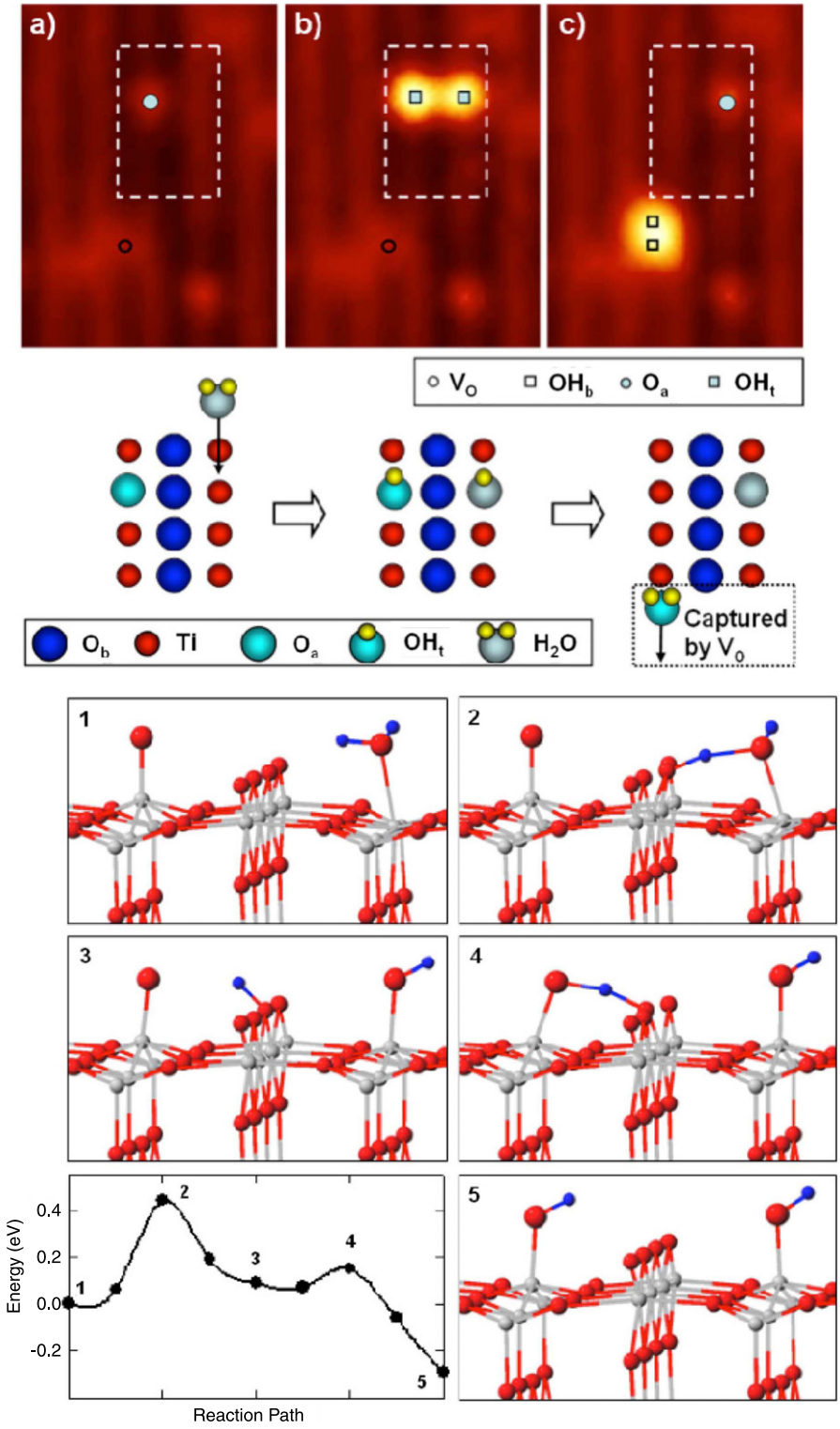

Fig. 5.12. (Top) Consecutive STM images showing the *apparent* motion of an O adatom across an O_{br} row as a result of its reaction with H_2O. The circles and squares indicate O adatoms and terminal OH groups (OH_t), respectively. (Middle) Ball models illustrating the processes observed in STM (above). (Bottom) Reaction energy profile and selected intermediate states from DFT for the process shown between the STM images labeled 'a' and 'b' above.
Source: Reprinted with permission from Du et al. [795].

shown in Fig. 5.14 [473], followed half-order kinetics consistent with an e^-/h^+ pair model. However, the observed PSD signal over time generally exhibited a multi-exponential form. Thompson and Yates [473] attributed the multi-exponential behavior of O_2 photodesorption to fractal-like kinetics arising from varying rates of e^-/h^+ pair recombination stemming from anisotropic electron diffusion across the surface.

Perkins and this author [201] examined the effect of water overlayers on the photodesorption of O_2 from TiO_2(110). They found that photodesorbed O_2 could be trapped below a thick

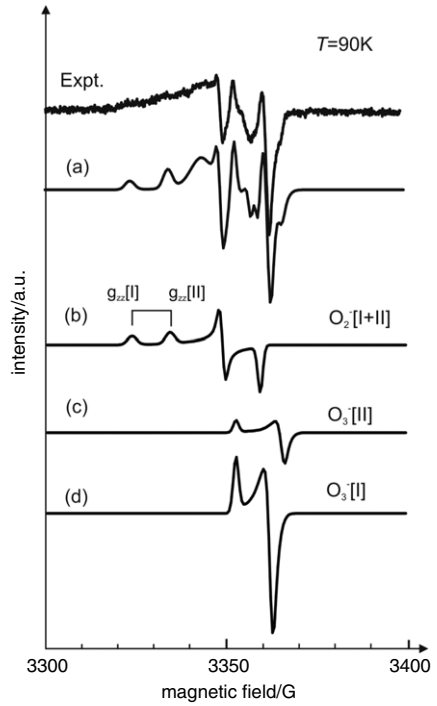

Fig. 5.13. EPR spectrum (labeled 'Expt.') resulting from exposure of O_2 to trapped charges on TiO_2 nanoparticles generated by UV irradiation at 90 K. Traces 'b-d' are simulated, single-component EPR spectra for various O_2^- species, and trace 'a' is the summation of traces 'b-d' generating the best fit to the experimental trace. © 2005 Wiley–VCH Verlag GmbH and Co. KGaA. Reproduced with permission.
Source: From Berger, et al. [387].

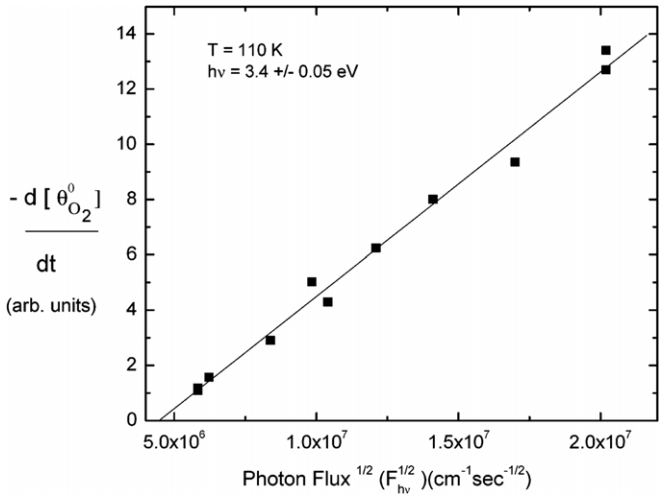

Fig. 5.14. Plot of the initial O_2 photodesorption rate as a function of the square root of the UV photon flux for PSD of O_2 from the R TiO_2(110) surface.
Source: Reprinted with permission from Thompson and Yates [473].
© 2006, American Chemical Society.

H_2O ice, which was able to desorb during the water phase transformation from amorphous to crystalline ice at ~145–160 K ([863] and references therein). The photodesorbed O_2 but was not recaptured by the surface. This observation suggests that either H_2O molecules from the ice occupied vacated O_2 binding sites during the photodesorption process or that charge recombination removed surface trapped electrons needed for electron transfer re-adsorption of O_2. These authors also observed a correlation between the depletion of the 410 K TPD O_2 feature and the photodesorption signal. Recently, Petrik and Kimmel [864,865] reported on the extent of photodissociation of adsorbed O_2 resulting from UV irradiation at 100 K. Using TPD of physisorbed O_2 as a diagnostic, these authors found that less than 50% of the adsorbed O_2 from a saturation exposure photodesorbed during UV irradiation, but roughly 20%–40% photodissociated. These authors proposed that the mechanism for photodissociation likely involved electron attachment, whereas photodesorption occurred through hole attachment.

Perhaps one of the most unusual observations of a photochemical event involving O_2 is the conversion of (ground state) triplet oxygen ($^3O_2$) to singlet oxygen ($^1O_2$) as a result of UV irradiation of O_2 adsorbed on TiO_2. Munuera and coworkers [866] first observed $^1O_2$ photodesorption from TiO_2 and correlated its appearance with the influence of surface Cl. Numerous groups have subsequently explored the formation and chemistry of this species on TiO_2 [286,728,834,867–875], with two groups examining this phenomenon in detail. Nosaka's group [872–874] used transient spectroscopy and phosphorescent markers to follow $^1O_2$ formation over a variety of TiO_2 samples. These authors proposed that $^1O_2$ was formed during back-electron transfer from O_2^- to the TiO_2 surface (most likely at a VB hole). The $^1O_2$ yield did not vary significantly on A and R, but increased with decreasing particle size and was highest between pH 5 and 11 indicating a link to surface OH populations. Naito et al. [286] used molecular fluorescence markers to verify the emission of singlet O_2 during UV irradiation of TiO_2. These authors also proposed that $^1O_2$ formed through electron attachment to $^3O_2$ (resulting in a chemisorbed species) followed by hole-mediated oxidation to the singlet or back to the triplet. To date, there have been no studies on the formation of singlet oxygen on a single crystal TiO_2 surface.

5.2.2. Electron scavengers: others

Although molecular oxygen is clearly the most commonly studied electron scavenger for photooxidation reactions, in principle any species with an electron affinity greater than that of a electron trap site on TiO_2 is a potential candidate. Two examples of alternate electron scavengers are Fe^{3+} (usually under aqueous conditions) [577,876–880] and NO gas [788,881–884]. The surface chemistry and photochemistry of these species have not been extensively studied, particularly not on a single crystal TiO_2 surface. Study of the electron scavenging role of Fe^{3+} seemingly requires aqueous conditions, but discussion in Section 6 will show that the electron scavenging role of adsorbed Fe^{3+} (as well as other cationic species) can be studied on TiO_2 under 'dry' conditions. Correlations between the reduction of these species with the oxidation of some other species are not common in the literature. The same can be said of NO, although in this case one might expect greater interchangeability between gaseous O_2 and NO in photooxidation reactions. For example, Jacobson et al. [884] proposed that NO was a more effective electron scavenger than O_2 in promoting of UV photodecomposition of catechol on R TiO_2(110).

5.2.3. Photooxidation reactants

Discussion now shifts to insights into the mechanisms of photooxidation reactions over TiO_2. The variety of reactants that have been explored in the literature is immense. The discussion will focus on systems in which molecular-level insights have been (or can be) achieved. As mentioned above, the emphasis is not on the complete mechanisms for photooxidation of reactants (i.e., all the way to CO_2 and H_2O), but on the mechanistic details associated with single electron transfer reactions. From understanding individual events, it is possible to gain insights into how charge carriers, secondary reactants (e.g., OH•) and thermal effects meld together to influence photocatalytic reactions on TiO_2. Readers interested in the entirety of a reactant's mechanistic

pathway can, to some extent, piece together a more extensive mechanistic picture through what is presented here for individual reactants. (For example, isopropanol photooxidizes to acetone which photooxidizes to acetate, etc.)

Alcohols

One of the most extensively studied classes of reactants in organic photooxidation over TiO_2 has been that of alcohols. Aside from the standard issue of holes versus OH• radicals, a common issue in alcohol photooxidation is the importance of molecular versus dissociative adsorption on the photoreactivities of adsorbed alcohols (see Section 4). Experimentally distinguishing between which form is more reactive is not straightforward, particularly since interconversions between these two species can be initiated by secondary reactions. Another point of interest is the effect of branching at the alpha-position in the alcohol as this affects the relative electronic properties of nearest and next-nearest neighbor C–C and C–H bonds.

Methanol: Mechanistic studies on the photooxidation of methanol suggest that both direct [553,716,885,886] and indirect [553,716, 733,765,886,887] oxidation processes occur, depending on the presence of water and the concentration of O_2. Formate and formaldehyde intermediates are viewed by some groups [765,885, 887] as the primary products of direct and indirect oxidation reactions, respectively, but the opposite way by others [716,886]. For example, Arana and coworkers [885] observed formate accumulation and surface poisoning during methanol photooxidation on dry TiO_2 which they assigned to a hole-mediated oxidative preference for the formate channel. However, the Lin group [716,886] observed with FTIR that formaldehyde was the main surface product in the absence of O_2 and formate in the presence of O_2, leading them to conclude that formate was formed via direct oxidation of adsorbed methoxy. This group also found evidence for preferential pathways in the photooxidation of methoxy (as mono and bidentate species) and methanol. More intermediates to these products have also been detected. Micic et al. [553] employed EPR at 1.9 K to follow hole transfer events after UV irradiation of methanol-covered TiO_2. In this setting, the involvement of other oxidative pathways (such as OH• production) was excluded. These authors detected CH_2OH• and CHO• radicals that were the result of hole transfer from Ti-O^- surface sites followed by H^+ transfer, as shown in Reactions 4 and 5:

$$Ti^{4+}\text{–}O^- + CH_3OH\ (a) \Rightarrow Ti^{4+}\text{–}O^{2-} + [CH_3OH]^+\ (a) \quad (4)$$

$$Ti^{4+}\text{–}O^{2-} + [CH_3OH]^+\ (a) \Rightarrow Ti^{4+}\text{–}OH^- + CH_2OH\bullet\ (a). \quad (5)$$

Whether these reactions occurred in a concerted or sequential process, as suggested above, is unclear. The authors also detected CH_3• radicals, but the source of these was assigned to trapped electron transfer events. To this author's knowledge, the only mechanistic study of methanol photochemistry on a TiO_2 single crystal was that performed by Zhou et al. [888] who observed UV light induced cleavage of the CH_3O –H bond for methanol on R TiO_2(110).

Ethanol: Commonly observed surface and/or liberated intermediates in photooxidation of ethanol include acetaldehyde [715, 889–896] and carboxylates (acetate, formate or their corresponding acids) [715–717,793,891–897], with one group detecting 1,1-diethoxyethane [897]. The observation of this latter species, by the Raftery group using solid state nuclear magnetic resonance (NMR), came from photooxidation of ethanol on three different TiO_2 catalysts. This group also indicated that the ethoxy species appeared to photooxidize faster than molecularly adsorbed ethanol [891]. Muggli et al. [893–895] examined the photooxidation of ethanol on P-25. Using isotopically labeling, they determined that CO_2 evolved in the gas phase first from conversion of the α-carbon.

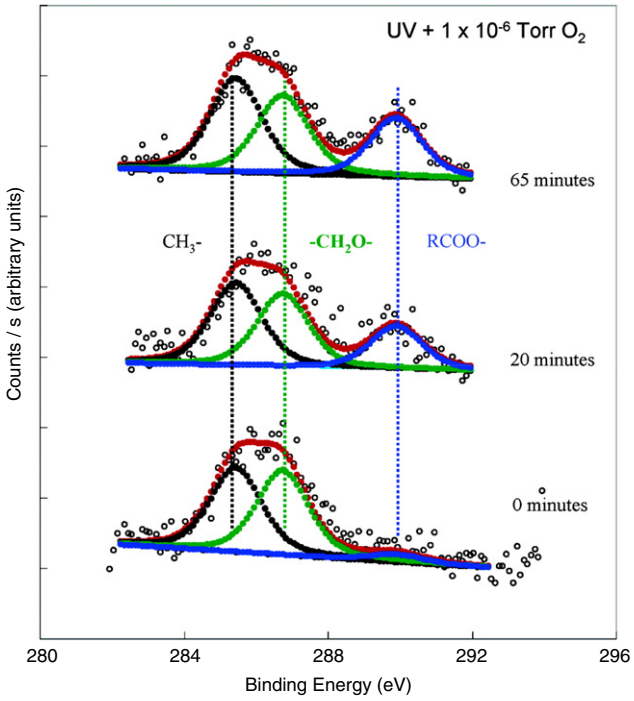

Fig. 5.15. C 1s XPS spectra from saturation ethanol on R TiO_2(110) at 300 K (lower trace), followed by UV irradiation in 1×10^{-6} Torr O_2 for two time periods (middle and upper traces).
Source: Reprinted with permission from Jayaweera et al. [793].
© 2007, American Chemical Society.

The same was observed for acetaldehyde and acetic acid, suggesting a common surface intermediate before cleavage of the C–C bond. Yu and Chuang. [717] also examined the photooxidation of ethanol on P-25 and observed strong coverage dependence in the rate, with high coverage situations resulting in the surface becoming populated with carboxylates that blocked access of O_2 to the surface. Jayaweera et al. [793] utilized XPS to track the changes in coverage and adsorbate nature during UV irradiation of ethanol on R TiO_2(110). Their C 1s XPS spectral results as a function of UV irradiation, shown in Fig. 5.15, clearly indicate a conversion of ethanol/ethoxy species into carboxylates without any other detectable product being formed. Based on oxygen pressure dependent studies, these authors proposed that the initial step in ethanol photooxidation involved attack of an O_2^- species. As shown in Fig. 5.16, the attenuation of C1s features ascribed to ethanol showed a strong O_2 pressure dependence.

Isopropyl alcohol: Photooxidation of 2-propanol (isopropanol) presents an interesting case because the reaction exhibits near 100% selectivity toward acetone [721,722,898–904]. Conversion of 2-propanol to acetone requires two oxidative steps, and the intermediate associated with the first step has not that been identified. Involvement of thermal chemistry, particularly in forming adsorbed isoproxy groups, has been shown to be important [900]. Using solid state NMR, Xu et al. [898,899] observed two reaction pathways for 2-propanol over P-25: one involving weakly bound 2-propanol molecules that slowly converted to acetone and another that involved rapid conversion of isopropyl groups directly to CO_2. In contrast, Arsac et al. [721,722], using FTIR, tracked conversion of both molecular and dissociative 2-propanol through acetone.

Several studies have shown the importance of gas phase O_2 in the conversion of 2-propanol to acetone [721,722,898–904]. In particular, Brinkley and Engel [900–902] examined the photooxidation of 2-propanol on R TiO_2(110) and (100) surfaces in UHV, and concluded that O_2 was necessary for photooxidation.

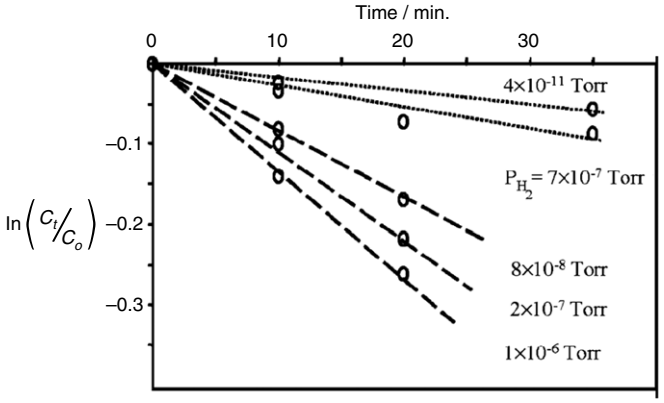

Fig. 5.16. First order decay plots from changes in the C 1s integrated areas during photooxidation of ethanol on R TiO_2(110) at room temperature as a function of several O_2 pressures. Included are data from a background of H_2 (7×10^{-7} Torr) for comparison with that of the lowest O_2 pressure.
Source: Adapted with permission from Jayaweera et al. [793].
© 2007, American Chemical Society.

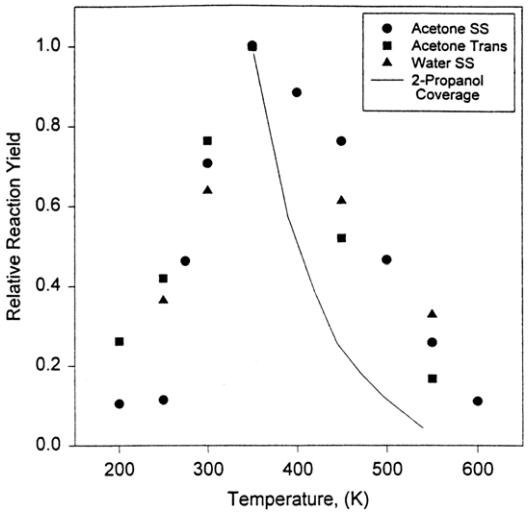

Fig. 5.17. Steady-state ('SS') and transient ('Trans') yields of acetone and water from UV photooxidation of 2-propanol impinging on R TiO_2(110) in a 7:1 molecular beam mixture of O_2 + isopropanol (latter flux of ~0.1 ML/s) as a function of the surface temperature. The solid line represents the approximate surface coverage of 2-propanol as a function of surface temperature.
Source: Reprinted with permission from Brinkley and Engel [901].
© 1998, American Chemical Society.

In agreement with others [721,722], Brinkley and Engel found that acetone poisoned the surface by site blocking. They showed that the reaction rate was maximized by increasing the surface temperature (as shown in Fig. 5.17) through which a balance was achieved between removal of acetone from the surface (which desorbs above room temperature) and retention of 2-propanol on the surface (which desorbs at ~400 K). As shown in Fig. 5.17, the optimal temperature under the authors' conditions was ~350 K.

Other alcohols: Mechanistic studies on the photooxidation of other alcohols on TiO_2 include: 1-propanol [885], 1-butanol [885,905,906], t-butanol [907–909], phenol [467,910–912], and poly-ols and carbohydrates [572]. Of these, the photooxidation of phenol represents an unusual example of photooxidation over TiO_2. Although phenol is an important organic molecule in TiO_2 photooxidation studies (over eighty studies have utilized this molecule in the last 10+ years), there are surprisingly few studies on the mechanistic details of its photooxidation (and none involving single crystal TiO_2 surfaces). The major intermediates in phenol photooxidation

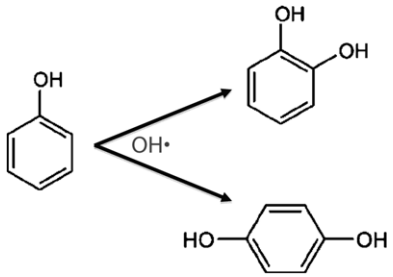

Fig. 5.18. OH• addition reactions to the ring of phenol.
Source: Images from Wikipedia.

appear to be catechol (1,2-dihydroxybenzene) and hydroquinone (1,4-dihydroxybenzene) [467,910–913] (Fig. 5.18). Hydroxylation at the ortho and para positions is consistent with the electron donating influence of the phenol's OH group on the aromatic ring (see [914] for a review Hammett constants and substituent effects relating to phenyl ring reactions). Researchers have therefore proposed that phenol oxidation on TiO_2 involves OH• attack rather than direct hole-mediated oxidation. However, there are no mechanistic details available on whether this reaction exhibits a preference for molecularly or dissociatively adsorbed phenol, and how hole-mediated oxidation might proceed (e.g., in the absence of OH groups).

Aldehydes

A few studies on acetaldehyde photooxidation over high surface area TiO_2 point to acetate as the immediate reaction product [915–917], although details of what becomes of the aldehydic hydrogen are sketchy. Jenkins and Murphy [514] have examined acetaldehyde photooxidation on TiO_2 with EPR and found evidence for $CH_3C(O)OO$• radicals, suggestive of O_2^- attack on either adsorbed acetaldehyde or an acetyl intermediate. In a separate study, this group also detected evidence for liberation of acetyl radicals during room temperature irradiation experiments [918]. In a UHV study on R TiO_2(110), Zehr and this author [704] examined the photodecomposition of acetaldehyde using TPD and PSD. Acetaldehyde exhibited no photoactivity in the absence of coadsorbed oxygen, but followed the same mechanistic pathway exhibited for acetone on this surface (see below), namely formation of a diolate from a thermal reaction between oxygen adatoms and acetaldehyde followed by photoactivation of the C–C bond leading to ejection of a methyl radical into vacuum and formation of a formate group on the surface. Acetate was only detected as a minor thermal product of acetaldehyde, presumably at surface defect sites. Mechanistic studies on higher molecular weight aldehydes [514,915] and on formaldehyde [514,917] are few. Photoreactions of formaldehyde are difficult to follow mechanistically because the immediate reaction products are rapidly converted to gaseous C_1 products (i.e., CO_2) during most studies.

Alkanes and alkenes

The key issue with photooxidation reactions of alkanes and alkenes on TiO_2 is that these molecules do not bind strongly to oxide surfaces. As a consequence, the first oxidation step is likely to generate an intermediate that binds more strongly to the surface than does the parent reactant. This situation exposes the parent molecule to site blocking by its more strongly bound reaction intermediates. The most extensively examined alkane on TiO_2 from a mechanistic perspective is cyclohexane [778,919–923]. Photooxidation of cyclohexane leads initially to cyclohexanol and cyclohexanone, but not to cyclohexene or ring-opening products. It appears that the former products result from not one but multiple mechanistic steps [920,922,923]. For example, Brusa and Grela [920] examined the photooxidation of cyclohexane

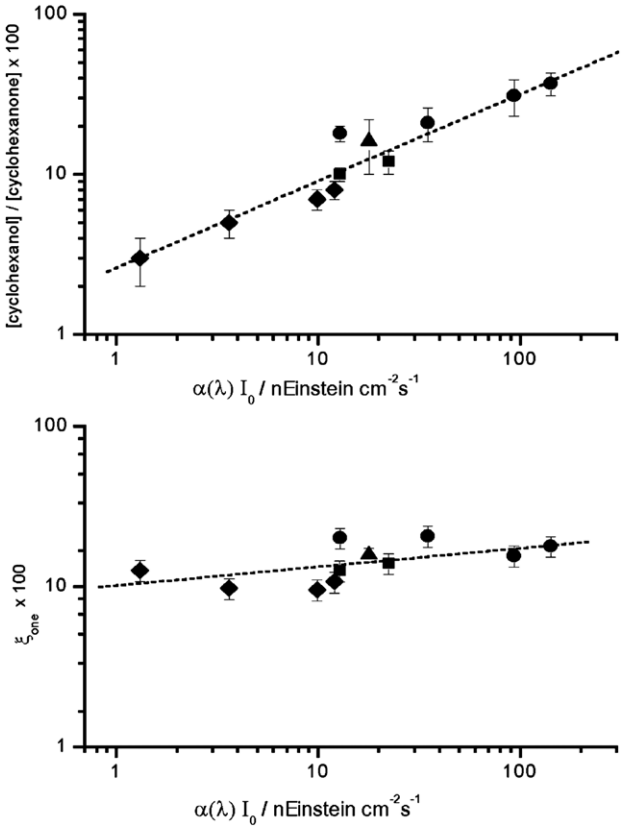

Fig. 5.19. (Top) Ratio of cyclohexanol to cyclohexanone produced during photooxidation of cyclohexane over TiO_2 using 254 (triangles), 303 (circles), 330 (squares) and 366 (diamonds) nm light as a function of photon flux. (Bottom) Photonic efficiencies for generating cyclohexanone from the data shown above.
Source: Reprinted with permission from Brusa and Grela [920].

on P-25 as a function of light intensity and wavelength. These authors observed that the ratio of cyclohexanol to cyclohexanone increased with increasing photon flux at several wavelengths in the UV, as shown in the upper portion of Fig. 5.19. Brusa and Grela proposed that higher carrier concentrations (resulting from higher photon fluxes) favored cyclohexanol formation, and that the mechanistic link was in the increased population of trap states needed to generate species important in formation of the alcohol. The effect was not due to the energy of the carriers (which literature in Section 2 would suggest rapidly thermalize to the band edges) as no wavelength dependence was observed in either the cyclohexanol to cyclohexanone yield ratio or in the photonic efficiencies (shown for cyclohexanone in the bottom portion of Fig. 5.19). Boarini et al. [922] also proposed that cyclohexanol and cyclohexanone resulted from separate reaction processes. These authors used an OH radical scavenging agent to preferentially eliminate OH during the reaction. They observed a decline in cyclohexanol formation but little change in cyclohexanone. They proposed that cyclohexanol was formed from reaction of a cyclohexyl radical (generated by a hole-mediated process) with OH, while cyclohexanone was formed from a reaction with an O_2-related species.

Mechanistic photooxidation studies on other alkanes and alkenes include: methane [924–926], ethylene [738], propane [927,928], propylene [929–931], isobutene [929] and heptane [932]. Studies on methane illustrate the interesting diversity of alkane photooxidation, where groups have observed selective oxidation to methanol [924], methyl coupling to ethane [925,926] and carboxylation reactions [926].

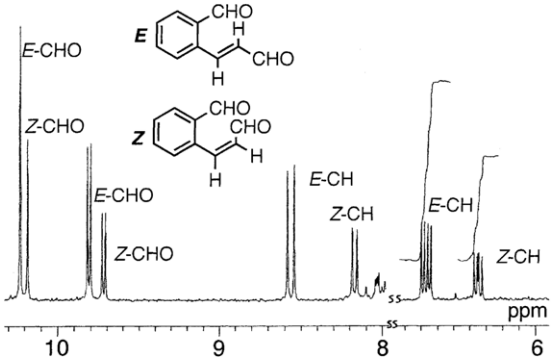

Fig. 5.20. ^{1}H NMR spectrum from an E (trans) and Z (cis) isomeric mixture of 2-formylcinnamaldehdye generated via photooxidation of naphthalene over TiO_2. (Solvent: $CDCl_3$).
Source: From Ohno et al. [949].

Aromatics

Three main types of simple aromatics (i.e., those without functional groups) have been examined in photooxidation studies on TiO_2: benzene, toluene and polycyclics. There have been several mechanistic studies on benzene [912,933–939], although this molecule's weak binding to oxide surfaces makes molecular studies difficult. Phenol and surface-bound phenoxy are the immediate reaction products [933,935–938], as well as there being evidence for hole-mediated oxidation pathways that do not pass through phenol/phenoxy [912]. There are few details on the mechanism of phenol formation from benzene other than suggestions that it involves OH radical attack [936,938].

The initial action on toluene is at the methyl group, not the aromatic ring, resulting in benzaldehyde as the first prominent intermediate in the reaction [571,940–945]. A few groups [941,943,946,947] have also detected small amounts of benzyl alcohol, suggesting this species is a reaction intermediate between toluene and benzaldehyde, as shown in Reaction 6:

$$C_6H_5\text{–}CH_3 \Rightarrow\Rightarrow C_6H_5\text{–}CH_2OH \Rightarrow\Rightarrow C_6H_5\text{–}CHO. \quad (6)$$

Transitions between these species require multiple steps and/or concerted processes involving either C–H bond cleavage plus C–O bond formation (first step) or multiple C–H bond cleavages (second step). The preference for oxidation at the methyl group (as opposed to the ring) was examined by Coronado and Soria [760], who detected in EPR at 77 K a $C_6H_5\text{–}CH_2\text{–}OO$ radical resulting from O_2^- attack. The only observation of immediate action on the ring was by Marcì et al. [946] who detected trace amounts of p-cresol ($HO\text{–}C_6H_4\text{–}CH_3$). Other groups have proposed that the photooxidation of toluene requires surface OH groups [942,944,945], most likely as binding sites for the parent, although involvement of these sites in electron transfer cannot be excluded. There is also some debate regarding whether or not benzoate, formed from additional oxidation of benzaldehyde, acts as a poison in the reaction [940,941,947].

Mechanistic studies of polycyclic aromatics, such as biphenyl [948], naphthalene [949–952], anthracene [951] and pryene [953], show similar trends as seen with benzene. Taking naphthalene as an example, OH• attack to generate naphthols appears to be the immediate mechanistic step in photooxidation of these polycyclics [950]. Subsequent mechanistic steps result in additional hydroxylation or in ring-opening events [949,950,952]. An excellent example of this is from the work of Ohno et al. [949] who used NMR to show that an immediate C–C bond cleavage product of naphthalene photooxidation was 2-formylcinnamaldehyde in both cis and trans, with the latter favored as shown by ^{1}H NMR (Fig. 5.20).

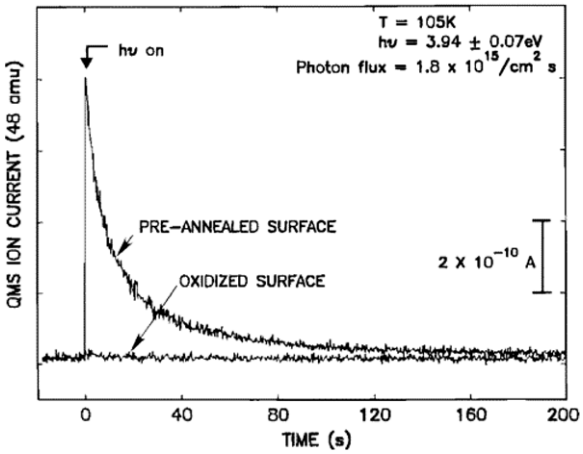

Fig. 5.21. Comparison of the CO_2 PSD spectra resulting from CO photooxidation (using UV light) at 105 K on reduced ('pre-annealed') and oxidized R TiO_2(110) surfaces.
Source: Reprinted with permission from Linsebigler et al. [776].

Carbon monoxide

Photooxidation of CO to CO_2 is a process that likely involves electron transfer chemistry with an adsorbed O_2 molecule rather than with an adsorbed CO molecule. Mechanistic insights from studies of CO photooxidation on high surface area TiO_2 [783, 954–956] are complicated by both the weak binding of the reactants (CO and O_2) and product, and the apparent absence of stable surface intermediates in the reaction. However, CO photooxidation provides an ideal setting for examining the role of various oxygen species in photooxidation reactions on TiO_2, and for exploring molecular dynamics and energy transfer during heterogeneous photochemical reactions. Regarding the former point, the Yates group [776,780,802,957] has invested considerable effort in examining the role of oxygen in CO photooxidation on the R TiO_2(110) surface. Using knowledge obtained from detailed studies on O_2 photodesorption (see above), they performed CO_2 photodesorption studies on various adlayers of CO and oxygen. One of their key findings, shown in Fig. 5.21, was that CO_2 was only generated on the vacuum annealed (reduced) surface. These authors also observed that only one form of molecularly adsorbed O_2 (the so-called 'α' form) was involved in CO photooxidation and that neither dissociatively adsorbed O_2 or lattice oxygen had a direct role. The Yates group also observed that the effective cross section for CO oxidation was approximately the same as that for O_2 PSD of the α-O_2 species, suggesting that photoactivation of this O_2 species was the important step in CO photooxidation. Based on wavelength specific studies, these authors indicated that activation of α-O_2 was via substrate excitation. Also, the absence of CO oxidation on a fully oxidized TiO_2(110) surface indicated that surface electron density (i.e., trapped electrons or oxygen vacancies) was needed to chemisorb the α form of O_2. More recently, the Wöll group [958,959] examined CO photooxidation on TiO_2(110) at 110 K using high resolution EELS (HREELS) and FTIR. Their results largely concurred with those of the Yates group. Wöll and coworkers estimated an effective cross section of $\sim 1 \times 10^{-18}$ cm^2 by monitoring depletion of the ν (CO) feature at 2190 cm^{-1} in a background of O_2 while irradiating with 3.2 eV light. They also detected adsorbed CO_2 at 2345 cm^{-1} indicating that not all product escaped the surface as a result of the reaction at 110 K.

Recently, Petrik and Kimmel [960] examined CO photooxidation on TiO_2(110) using angle-resolved PSD and TPD. These authors observed that CO_2 generated photochemically desorbed in two angular distributions peaked at $\pm 40°$ from the surface normal toward the surface $\langle 1\bar{1}0 \rangle$ directions (i.e., perpendicular to the bridging oxygen row direction). Absence of strong CO_2 photodesorption signal along the surface normal suggests that the product did not thermalize with the surface during formation but retained some degree of the characteristics of the key reaction coordinate, which the authors (and others (957b) proposed involved O–O dissociation as the key step. A similar CO PSD angular distribution was observed by Petrik and Kimmel, suggestive of unsuccessful oxidation attempts that imparted energy sufficient for desorption along the reaction coordinate.

Carboxylic acids

Surface carboxylates, formed from thermal decomposition of carboxylic acids or as intermediates in reactions of other organics, are both very stable on oxide surfaces and represent one of the more interesting classes of molecules for photocatalysis studies on TiO_2. These adsorbates are also interesting probes in studies of surface chemistry on single crystal TiO_2 surfaces [566,700]. The large volume of work on the photochemistry of these adsorbates is sorted into the following categories: formic acid (formate), acetic acid (acetate), trimethyl acetic acid (TMAA) and miscellaneous organic acids.

Formic acid: The photooxidation of formate (from formic acid) on TiO_2 surface does not appear to pass through any detectable surface intermediates before resulting in CO_2 (or CO_2^- in some cases) [715,733,769,790,961–963]. There is disagreement in the literature regarding whether formate photodecomposes directly by a hole-mediated pathway (Reaction 7),

$$HCOO^- \text{ (a)} + h^+ \Rightarrow CO_2 \text{ (g)} + H \text{ (a)} \quad (7)$$

or via indirect pathways such as OH radical attack (Reaction 8):

$$HCOO^- \text{ (a)} + OH\bullet \Rightarrow CO_2^- \text{ (a)} + H_2O \text{ (a)}. \quad (8)$$

Reaction 7 is also known as the photo-Kolbe reaction [964,965]. Differentiating between these two mechanisms is difficult in gas–surface photooxidation studies, but in suspended systems evolution of the CO_2^- anion can provide insights into the mechanism. Perissinotti et al. [963] used spin traps to capture and quantify the amount of CO_2^- formed from formate photodecomposition on TiO_2 suspensions. They estimated that ~30% of the measured formate photodecomposition resulted in CO_2^-, which the authors assumed was formed from H atom abstraction by OH radical. The remaining formate photodecomposition presumably evolved as CO_2 gas via direct hole-mediated reactions.

The influence of water on formate photodecomposition was assessed by Liao et al. [715], who detected an enhanced rate of formic acid photodecomposition (by roughly a factor of 2) when water was present. They also observed that the per-molecule rate of formic acid photodecomposition in O_2 was roughly 53 times greater when their TiO_2 surface was saturated with the molecule as compared to when only formate groups were present on the surface (under dry conditions with no OH groups retained on the surface). These results suggest that a pure hole-mediated reaction in the formate case may not be as favorable as when hydrogen-bonding interactions are available (either from water or a hydrogen-bonded overlayer of formic acid). (Interestingly, no such distinction between the carboxylate and the parent acid was observed in the acetic acid case [966].) Muggli and Backes [962] found that water did not displace adsorbed formate from the surface to the extent that it hindered photooxidation (as seen for other organics, see below). Regarding the involvement of O_2, most groups have found that O_2 improved formic acid photodecomposition rates, but Lee and Falconer [769] proposed that formic acid could be photodecomposed on TiO_2 in the absence of O_2 using lattice oxygen. From a charge balance perspective, this

would require reduction of the surface since O_2 was not present as an electron scavenger. These authors showed that O_2 could be adsorbed subsequently in the dark, indicating the generation of reduced surface sites.

Acetic acid: Fundamental study of acetic acid (or adsorbed acetate) photodecomposition on TiO_2 is considerably more straightforward than the case of formic acid (formate). Groups have undertaken mechanistic studies of this adsorbate on both single crystal [701,777,967–969] and high surface area [734,790,966, 970–973] TiO_2. Starting with the latter case, Nosaka et al. [734] have proposed both hole-mediated and OH•-mediated photodecomposition mechanisms for adsorbed acetate. Using EPR, these authors observed CH_3 radical production from a photo-Kolbe reaction involving hole-mediated oxidation of acetate. They also detected CH_2COOH• radicals resulting from OH• attack on the methyl C–H bonds. Support for the former reaction was obtained from observations of small amounts of CH_4 and C_2H_6 as products [966, 970,972], although formation of oxygenates as well may point to the latter reaction [970,971]. Isotopic labeling studies by Muggli, Falconer and colleagues [966,971,973] have provided additional insights into the photooxidation reaction. These authors observed that the evolution of CO_2 containing the carboxylate carbon was prompt. In contrast, CO_2 evolution from the methyl carbon was delayed, and proceeding through surface intermediates (such as methoxy, formaldehyde and formate) that lead to CO_2 only when O_2 was present.

The Idriss group has examined the photooxidation of acetic acid over the R TiO_2(110) [777], TiO_2(011) [969] and TiO_2(001) [967, 968] surfaces under UHV conditions. The latter surface, which exhibits two reconstructed terminations (see Section 7.2.3), was shown to photodecompose acetate via a photo-Kolbe reaction that yielded H_2O, CO_2, CH_4 and C_2H_6 as products. Increasing the O_2 pressure favored ethane and significantly inhibited CH_4 formation, in agreement to what was seen on high surface area TiO_2 [966, 970,972]. This trend suggests that maintaining an oxidized surface favors CH_3 radical combination, while a reduced surface favors reaction of CH_3 radicals with surface OH groups to form CH_4. On the TiO_2(110) surface, Idriss et al. [777] observed significant attenuation of surface acetates in XPS from UV irradiation in 10^{-6} to 10^{-7} Torr O_2, however no attenuation was observed in the absence of O_2. A similar result was noted by this author [701] for compressed overlayers of acetate and acetone in the presence of 5×10^{-7} Torr O_2, a situation in which O_2 was unable to gain access to the surface. While an effective photodecomposition cross section of $6–8 \times 10^{-18}$ cm^2 for acetate was measured by Idriss et al. in background O_2 [777], the effective cross section observed by this author was $<10^{-24}$ cm^2 in UHV [974]. Based on studies described below for trimethyl acetate photodecomposition, the role of O_2 in the acetate case is likely to be more than just electron scavenging, which points to the possibility of indirect processes.

Trimethylacetic acid: Fundamental studies on the photodecomposition of trimethyl acetic acid (TMAA) on TiO_2 single crystal surfaces have provided unique insights into single electron transfer photooxidation events. This author, Onishi and colleagues [202,515, 541,543,700,720,975,976] have extensively examined the chemistry and photochemistry of trimethyl acetate on R TiO_2(110) using PSD, TPD, EELS and STM, and more recently on A TiO_2(001) by Ohsawa et al. [290,542] using PSD and STM. As with other organic carboxylic acids, TMAA thermally decomposes on R TiO_2(110) to generate trimethyl acetate (TMA) groups and an acid proton deposited on a O_{br} site. The TMA group is an attractive probe for surface photochemistry on TiO_2 surfaces for several reasons. First, it binds strongly to TiO_2 surfaces at room temperature, thermally decomposing at temperatures above 550 K to mainly isobutene, water and CO. Second, it forms a well-ordered (2×1) overlayer on

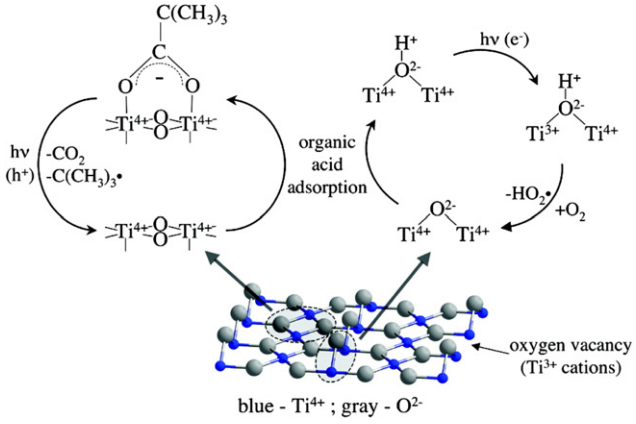

Fig. 5.22. Reaction scheme for both redox processes associated with photodecomposition of trimethyl acetic acid (TMAA) on the R TiO_2(110) surface.
Source: Reprinted with permission from Henderson et al. [202].
© 2003, American Chemical Society.

R TiO_2(110) in which each carboxylate bridges two surface Ti^{4+} sites. The carboxylate does not diffuse across the surface at room temperature [700], which facilitates use of STM for probing its structure, surface chemistry and surface photochemistry. Finally, and perhaps most importantly, its surface photochemistry is believed to occur via a single electron transfer event, as shown in Fig. 5.22 [202]. A hole reacts with the carboxylate via the photo-Kolbe mechanism [964,965] and the excited electron is trapped at a surface OH group in the absence of gas phase O_2 (see below). The kinetics were fast under UHV conditions (cross section of $\sim 10^{-18}$ cm^2), but not too fast for convenient study. At room temperature, the products of the single electron transfer photodecomposition of TMA were gaseous (CO_2, isobutene and isobutane), leaving no surface products (other than the acid proton). This latter trait allows real-time analysis of specific photodecomposition events using STM, as well as monitoring of global kinetics using PSD. (Conversely, if photolysis is performed at 100 K, the surface becomes populated with t-butyl groups and CO_2, both of which desorb at higher temperature, the former after disproportionating to isobutene and isobutene.)

Hole-mediated photodecomposition of TMA results from electron transfer from the carboxylate's π system to a VB hole, resulting in opening of the O–C–O bond angle and cleavage of the $(CH_3)_3C$–C bond. This process does not require gas phase oxygen as the photoexcited electrons are trapped by the surface, as shown by EELS measurements of Fig. 5.23 [202]. Trace (a) shows the spectrum for a TMA saturated overlayer on the oxidized TiO_2(110) surface in which there was no evidence for Ti^{3+} surface sites. As the surface was irradiated with UV light, the signature of surface Ti^{3+} (at 0.8 eV) grew in. The intensity of this signal (calibrated from the vacuum annealed surface signal) was linear with respect to the PSD yields of CO_2 and isobutene, although not 1:1, indicating a correlation between the two half reactions (excited electron and VB hole). Subsequent exposure to O_2 diminished the signal from trapped electrons, as expected.

The presence of gas phase O_2 accelerated the reaction by rapidly titrating off trapped electrons [202,515,541], but also altered the direction of the reaction. The rate acceleration effect was seen both in STM (Fig. 5.24) and in PSD (Fig. 5.25). Starting with a near-saturated surface, STM showed that the initial rate at which TMA molecules 'disappeared' (were photodecomposed) was slow, as shown by (a) and (b) in Fig. 5.24. After sufficient decomposition occurred allowing O_2 access to the surface, voids opened in the TMA adlayer and rapidly expanded to deplete the terraces of TMA (images (c) through (e)). During this process, new features

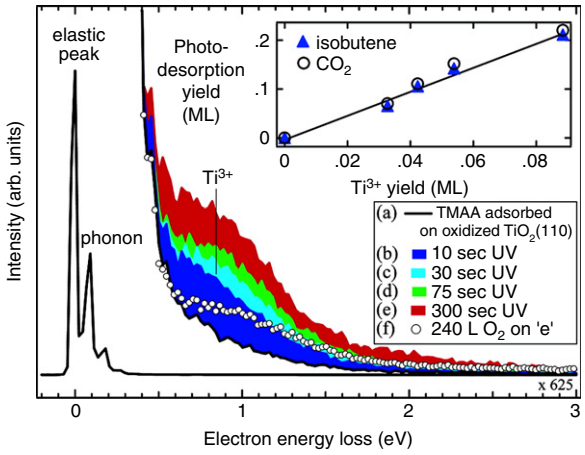

Fig. 5.23. EELS spectra from saturation trimethyl acetic acid (TMAA) on the oxidized R TiO_2(110) surface at 300 K. (a) The TMAA-covered surface prior to UV; (b–e) after UV irradiation for various time periods; (f) exposure of 'e' to 240 L of O_2. Inset: correlation between the isobutene and CO_2 photodesorption yields and the approximate Ti^{3+} yield generated during photolysis.
Source: Reprinted with permission from Henderson et al. [202].
© 2003, American Chemical Society.

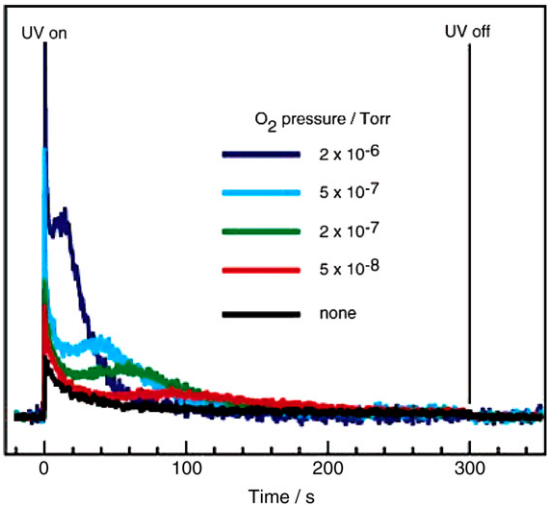

Fig. 5.25. Isobutene photodesorption signals during TMA photodecomposition on R TiO_2(110) as a function of O_2 background pressure.
Source: Adapted with permission from Uetsuka et al. [515].
© 2004, American Chemical Society.

were detected by STM (see expanded region of image (d)) that were assigned to water- and oxygen-related species formed from reactions of O_2 with surface Ti^{3+}–OH^- groups (see Section 5.2.1). The O_2-induced acceleration effect was also apparent in the 'global' reaction kinetics shown by isobutene PSD in Fig. 5.25. In the absence of O_2, the rate resembled first order decay kinetics (black trace), and STM showed a more-or-less random removal of TMA groups (see image labeled 'hydrophobic' in Fig. 5.26). As oxygen was emitted, the initial rate increased and a 'hump' developed at latter times which became more prominent and moved to shorter times as the O_2 pressure was increased. The 'hump' corresponded to the rate acceleration observed in STM at the point that O_2 gained access to the surface.

Fig. 5.26 [541] shows that a selectivity change occurred in TMA photodecomposition commensurate with the acceleration effect seen in STM and PSD. The plots to the right in Fig. 5.26 show the isobutene fractional yield (obtained from tracking the isobutene and isobutene PSD signals) as a function of irradiation time for identically prepared saturation TMA overlayers, but with different gas phase pressures of O_2 during irradiation. As indicated to the left of the plots, the *y*-axis value of '1' corresponded to 100% isobutene expressed by Reaction 9:

$$(CH_3)_3CCOO^- \text{ (a)} + 1/2\ O_2 \text{ (g)} + h^+ \Rightarrow (CH_3)_2CCH_2 \text{ (g)} + CO_2 \text{ (g)} + OH \text{ (a)}. \quad (9)$$

In contrast, the *y*-axis value of '0.5' corresponded to a 50:50 mixture of isobutene ('ene') and isobutene ('ane') according to Reaction 10:

$$2(CH_3)_3CCOO^- \text{ (a)} + 2h^+ \Rightarrow (CH_3)_2CCH_2 \text{ (g)} + (CH_3)_3CH \text{ (g)} + 2CO_2 \text{ (g)}. \quad (10)$$

In the absence of O_2, the reaction selectivity settled in with stoichiometry reflective of Reaction 10. Under these conditions,

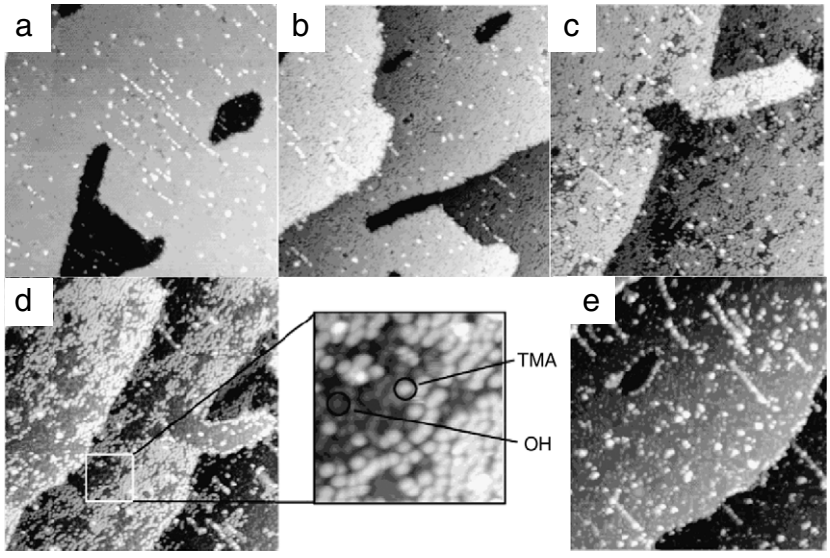

Fig. 5.24. STM images (88 × 88 nm) from UV irradiation of a saturated TMA-covered R TiO_2(110) surface in 1 × 10^{-7} Torr O_2 at 280 K. (a) TMA prior to UV, and after UV irradiation for: (b) 10, (c) 15, (d) 20 and (e) 30 min. Expanded image of 'd' shows unreacted TMA groups and OH species. Images were recorded in the dark. (Sample bias voltage: +1.5 to +2.0 V; tunnel current: 0.4 nA.)
Source: Adapted with permission from Uetsuka et al. [515].
© 2004, American Chemical Society.

STM showed random decomposition of TMA. With O_2 present, the 'ene' to 'ane' selectivity initially tracked that of the anaerobic case, but abruptly shifted toward 'ene' at the points at which the rate acceleration was observed, that is, when the voids opened in the (hydrophobic) TMA adlayer. Taken together, these data suggest that establishment of hydrophilic domains which permit access of O_2 to the surface can facilitate both rate acceleration and selectivity changes during organic photooxidation reactions on TiO_2 surfaces. Based on the TMA case, it is likely that establishment of similar hydrophobic–hydrophilic domains could govern the kinetics and reaction pathways in other organic photooxidation reactions, with the overall kinetics having a complicated dependence on the rates of O_2 and organic arriving at the surface, and the surface coverages of hydrophilic (e.g., water) and hydrophobic (e.g., organic fragments) products and intermediates.

TMA has also been used as a probe molecule for gauging photochemistry on the A TiO_2(001) surface. Ohsawa et al. [290,542] examined the role of N-doping in initiating visible light activity on TiO_2 surfaces (discussed in Section 1). The A TiO_2(001) surface is known to reconstruct into a $(4 \times 1)/(1 \times 4)$ 'ridge-and-trough' structure [977–979], which limits the ability of STM to imaging adsorbates bound in the troughs [980]. Fig. 5.27 shows STM images from TMA bound to ridge sites on the A TiO_2(001) surface, followed by depletion of the TMA surface coverage during anaerobic UV irradiation, similarly to what was seen on the R TiO_2(110) surface. The convenience of following TMA photodecomposition processes in STM or PSD has allowed for a direct comparison of the photoactivities of A and R on a per-molecule basis (see Section 7.1.2 below). From these data, the authors were able to show that the hole-mediated decomposition of TMA proceeded with greater than or equivalent per-molecule rates on R TiO_2(110) compared to A TiO_2(001).

Miscellaneous carboxylic acids: An interesting class of organic acids in photocatalysis reactions on TiO_2 are the dicarboxylic acids which, as the name indicates, have two carboxylate groups available for simultaneous interactions with the surface. Studies of the photodecomposition of these species are generally restricted to non-vacuum deposition methods because of their very low vapor pressures. Photodecomposition of oxalic acid, the smallest dicarboxylic acid, is widely employed in TiO_2 photocatalysis studies. Mendive and coworkers [981–983] examined the structure and photodecomposition of oxalate and oxalic acid on TiO_2 both experimentally and theoretically. They observed multiple adsorption states of the molecule depending on the degree of O–H bond cleavage, and interconversion of the various forms during photon exposure.

Mechanistic photochemistry studies exist on several higher molecular weight dicarboxylic acids, in particular C_3 malonic acid [984,985], C_4 succinic acid [985], and the two C_4 alkene isomers (maleic and fumaric acids) [986] which can be photochemically interconverted. As an example, Dolamic and Bürgi [985] examined photodecomposition of malonic and succinic acids on colloidal P-25 using attenuated total reflectance IR (ATR-IR). They concluded that photodecomposition proceeded through a photo-Kolbe reaction that shortened the chains by one C unit to the next smallest dicarboxylate. The reactions occurred at a slower rate in the absence of dissolved O_2.

Other interesting carboxylic acids for which mechanistic photochemistry studies have been conducted on TiO_2 include C_3–C_5 straight chain [790,987] and branched [988] alkyl acids, stearic acid [989,990], benzoic acid [991], and multifunctional carboxylic acids such as glyoxylic acid [992] and salicylic acid [993]. In a study of benzoate photodecomposition on TiO_2, Ajmera et al. [991] found that this molecule did not decarboxylate via a hole-mediated (photo-Kolbe) mechanism, but displayed ortho and para addition of OH to the phenyl ring in the same manner as seen for photooxidation of phenol (see above). This points both to the inherent stability of the phenyl-COO^- bond resisting electron extraction from the carboxylate's π system and to the involvement of an indirect (OH•-driven) mechanism. In the alkyl systems, Serpone and coworkers [790,988] have shown that one can use chain length or branching to predict how rapid an alkyl carboxylate will decompose and what the reaction intermediates might be. Also, packing of alkyl carboxylates on a TiO_2 surface has been shown to influence the photodecomposition of both short and long chain carboxylates [989,990].

Halocarbons

Halocarbons are a diverse and widely-considered class of photooxidation molecules examined on TiO_2. The photodecomposition mechanisms of these molecules are complicated and (in some cases) controversial because free radical reactions appear to play important roles along side those of direct reactions with charge carriers. Contributions from water, spanning the conditions of gas phase to aqueous, also complicate determinations of reaction mechanisms.

C_1 halocarbons: Despite having only one carbon center, the photooxidation reactions of CCl_4, $CHCl_3$, CH_2Cl_2 and CH_3Cl over TiO_2 are complex. A wide variety of reaction products and intermediates have been observed, including phosgene, formyl chloride, CO, CO_2, more-chlorinated C_1 species, non-chlorinated C_1 fragments (e.g., formaldehyde, methoxy) and chlorinated C_2 species [994–999]. Formation of more-chlorinated species (e.g., CH_2Cl_2 from CH_3Cl photooxidation [994]) suggests a radical propagation mechanism [994,995,1000]. Stark and Rabani [1000] showed that the quantum yields of chloride formation for CCl_4 photodegradation in both aerated and deaerated conditions exceeded unity, indicating extensive radical chain reactions. Evidence for C_1 radicals was obtained by Choi and Hoffmann [1001] using radical trapping techniques. These authors showed that dichlorocarbene and trichloromethyl radical were intermediates in the photodecomposition of CCl_4 over suspended TiO_2. The authors' kinetic analysis suggested that a two-electron transfer process was key to formation of the dichlorocarbene intermediate.

O_2 significantly enhances C_1 halocarbon photodecomposition reactions [994,998]. Water/OH may not be necessary in some cases [994], although build-up of surface chloride was detected in non-aqueous conditions [1002]. Calza et al. [996,997] found that the rate limiting half reaction step depended on the C_1 halocarbon. They observed that CCl_4 degradation proceeded mainly via a reductive pathway (O_2 not needed), whereas CH_2Cl_2 degradation was mainly via oxidative channels. Both oxidative and reductive pathways were observed for $CHCl_3$. The reactivity trend was $CCl_4 > CHCl_3 > CH_2Cl_2$.

Trichloroethylene: This molecule is perhaps the most extensively studied halocarbon in the TiO_2 photocatalysis literature. As in the case of C_1 halocarbons, the possibility of radical chain reactions results in complex redox chemistry for trichloroethylene (TCE). A wide variety of chlorinated C_1 and C_2 products have been detected [718,1003–1012], with dichloroacetyl chloride being the most frequently observed 'direct' immediate product of TCE photochemistry [718,1003–1005,1007,1009–1011]. However, the mechanism for formation of this intermediate is not clear. Fan and Yates [718] studied the photooxidation of TCE on P-25 using FTIR with emphasis on the role of water. As shown in Fig. 5.28, they observed isotopic shifts in the various O-containing products based on the O_2 isotope used. However, when $^{18}O_2$ and $H_2^{16}O$ were employed together these authors did not detect an isotopic contribution to the products from $H_2^{16}O$. For example, the phosgene ν (C=O) stretching region ($\sim$1800–1850 cm^{-1}) only possessed signal for the $^{18}O{=}CCl_2$ species when the $^{18}O_2 + H_2^{16}O$ gas mixture

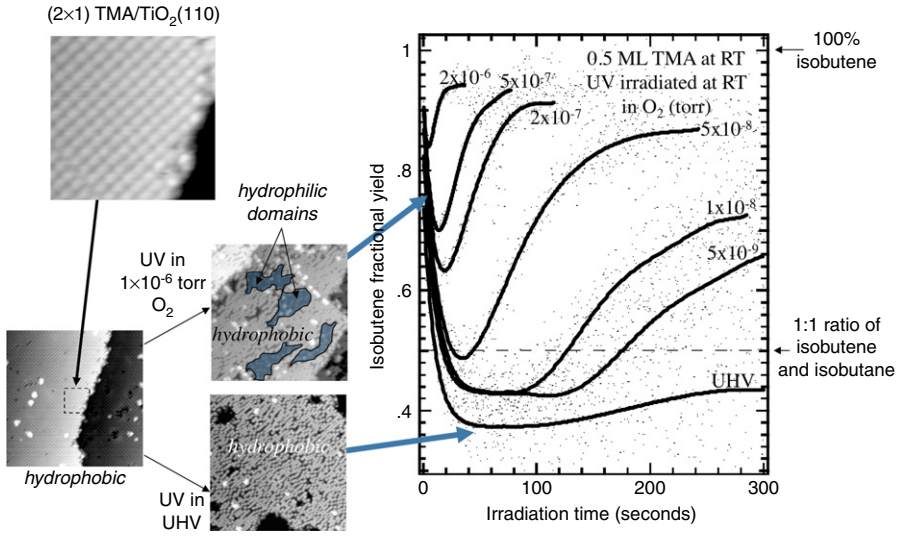

Fig. 5.26. Correlations between STM images (left) and isobutene fractional PSD yields (isobutene/(isobutene + isobutene)) evolving during photodecomposition of TMA on R TiO_2(110) in various O_2 pressures (right). Blue arrows indicate that approximate points at which the STM images were recorded. (For interpretation of the references to color in this figure legend, the reader is referred to the web version of this article.)
Source: Adapted from Henderson et al. [541].

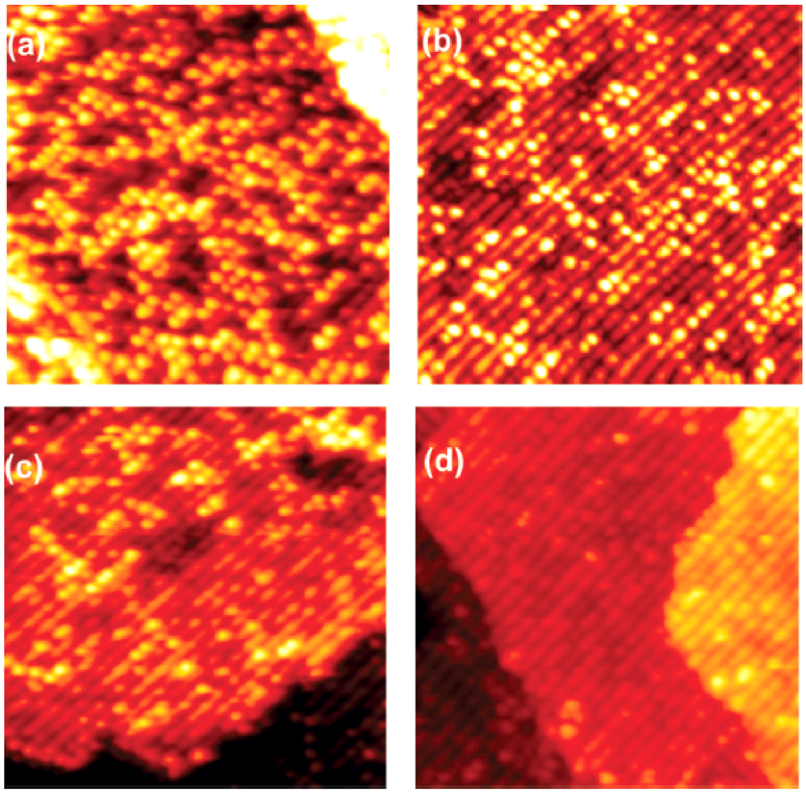

Fig. 5.27. STM images for the TMA-covered A TiO_2(001) surface: (a) prior to UV irradiation, and (b–d) after 0.7, 1.0 and 2.0 hr UV exposures in UHV, respectively. (Images are 40 × 40 nm.)
Source: Reprinted with permission from Ohsawa et al. [542].

was employed. Based on these results, Fan and Yates proposed that photooxidation occurred through a hole-mediated pathway and that molecular oxygen was involved in oxidation steps. In agreement with these results, other groups have shown that O_2 is essential in TCE photooxidation [1003,1004,1009]. Whether O_2 is needed to scavenge electrons or to participate directly in reactions with TCE is unclear. Recent work by Chatterjee et al. [1013] suggests that TCE photodegradation can proceed in the absence of VB holes by means of radicals generated from electrons injected by excitation of dye sensitized TiO_2.

Other groups have proposed that water is an important ingredient in TCE photooxidation [1006,1014], perhaps not necessarily in the first step of photooxidation but in assisting in the removal of strongly bound surface species that might interfere in the reaction [718,1008,1009]. For example, chloride not only blocks surface sites, but it also shifts the reaction selectivity away

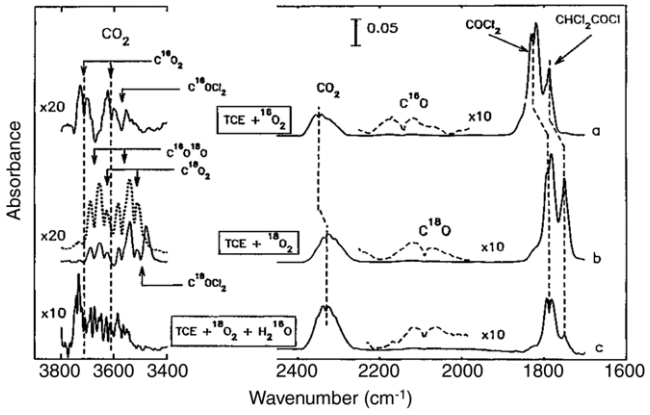

Fig. 5.28. Oxygen isotopic shifts in FTIR for various oxygen-containing species liberated during UV photodecomposition of trichloroethylene (TCE) over TiO_2 in: (a) $^{16}O_2$, (b) $^{18}O_2$, and (c) $^{18}O_2 + H_2^{16}O$.
Source: Reprinted with permission from Fan and Yates [718].
© 1996, American Chemical Society.

from full mineralization toward formation of more-chlorinated reaction products. Hung and Marinas [1006] have shown that higher chlorinated products (such as hexachloroethane, pentachloroethane and tetrachloroethylene) were formed preferentially to chlorinated C_1 products when the O_2 partial pressure was decreased. The total TCE conversion also rapidly dropped at low O_2 concentrations. Prechlorination of TiO_2 surface has also been shown to increase yields of chlorinated fragments in TCE photooxidation [1012]. Yamazaki et al. [1015] considered the impact of residual surface Cl on the conversion of TCE to final products. They observed that surface Cl was able to chlorinate ethylene, an observation that points to the need to remove it from the surface. They also showed that the reaction between TCE and OH radicals was the thermodynamically preferred pathway over that of Cl radical attack.

Fluoro-, bromo- and iodo-hydrocarbons: The photoreactions of brominated or iodinated hydrocarbons over TiO_2 differ from those of chlorocarbons in two noteworthy ways. First, these molecules are open to both substrate-mediated electron transfer processes *and* intramolecular UV photoabsorption events (whereas chlorocarbons only experience the former with typical UV sources). Second, the radical chain reactions seen for chlorinated hydrocarbons do not appear to occur for brominated or iodinated hydrocarbons. However, similarities with the chlorocarbons do exist. For example, Calza and coworkers [1016] found that photodegradation of CBr_4, $CHBr_3$ and CH_2Br_2 over TiO_2 exhibited the same reductive/oxidative preferences as seen for their chlorinated counterparts (see above). Namely, that both brominated and non-brominated intermediates were observed, and the preference for reductive degradation decreased in the series CBr_4 to $CHBr_3$ to CH_2Br_2. Gas phase O_2 was shown to be essential in the photodecomposition reactions of CH_2I_2 and C_2H_5I over TiO_2, with various oxygenates detected by FTIR [1017,1018].

The most extensive work involving photochemical processes of brominated or iodinated hydrocarbons on a single crystal TiO_2 surface was done by the Stair, Weitz and coworkers [680–683,754,755]. These authors examined the photochemistry of methyl iodide and methyl bromide on R TiO_2(110) using 257 and 320 nm laser light. Direct, intramolecular excitations (typically involving transitions between non-bonding to antibonding σ^* states) did not result in surface photochemistry, with all yields and photodesorption profiles pointing to substrate-mediated processes. This observation indicated that direct excitation of these adsorbates was rapidly quenched by electronic coupling with the TiO_2 surface. However, these authors detected photodesorption of parent molecules occurring through an Antoniewicz-like desorption process (see Fig. 3.10) in which transient electron attachment electrostatically drew the resulting CH_3X^- species toward the surface and back-electron transfer then put the neutralized CH_3X molecule high on the repulsive region of its potential energy surface leading to desorption. Little or no C–Br cleavage was detected and the extent of C–I bond cleavage was severely limited in the methyl iodide case by rapid back-electron transfer. White and this author [757] extended this approach to the study of t-butyl iodide photochemistry on R TiO_2(110), with much the same results. The main pathway observed was photodesorption of the parent, most likely via a substrate-mediated Antoniewicz-like process. A secondary pathway of C-I bond cleavage to t-butyl and I was also detected, with the former decomposing to isobutene at 100 K. These R TiO_2(110) results suggest that photodesorption events involving parent halocarbons (occurring via rapid electron attachment–detachment processes) may have a role in regulating and limiting coverages of halocarbons on TiO_2 surfaces. Finally, Zehr and coworkers [703,1019] found that fluorine-substituted acetones undergo significant variations in the photodecomposition pathway of acetone on R TiO_2(110) (which is discussed in detail below) presumably due to changes in the C–C bond strengths and electronic structure of acetone as a result of fluorination.

Ketones

Mechanistic studies of ketones on high surface area TiO_2 have primarily involved acetone [228,701,753,758,759,775,892,899,1020–1022], with fewer studies on butanone or higher molecular weight ketones [744,758,1023–1026]. Acetone is a useful probe molecule because it binds to most oxide surfaces in mainly one adsorbed structure, an 'η^1' configuration involving coordination to a surface cation through a lone pair on the oxygen. Acetone also exhibits minor adsorption pathways via surface condensation reactions that are potentially important in photocatalysis on TiO_2 [775,899,1020,1021]. For example, two acetone molecules have been shown to react according to Reaction 11 to form mesityl oxide.

$$2(CH_3)_2CO \Rightarrow CH_3C(O)CH{=}C(CH_3)_2 + H_2O. \quad (11)$$

While some groups [775,899,1021] proposed that condensates constitute the major pathway in acetone photodecomposition on TiO_2, Luo and Falconer [1020] proposed that acetone condensates contributed to catalyst deactivation because these species are not as photochemically reactive as molecular acetone.

The mechanistic complexities of acetone photooxidation have received much attention. The initial step in acetone photooxidation on P-25 has been probed by the Murphy group [758,759] using EPR at low temperatures. At 100 K, they detected a $CH_3C(O)CH_2OO\bullet$ species that decomposed to EPR-silent products above 150 K. These authors proposed that hole-mediated reactions generated the $CH_3C(O)CH_2\bullet$ radical (with H^+ transfer to the surface) followed by subsequent reaction of the radical with O_2. The authors also proposed that electron-mediated processes might be responsible for formation of the $CH_3C(O)CH_2OO\bullet$ radical. For example, Lv et al. [1022] modeled acetone photooxidation on the (1 × 1) structure of A TiO_2(001) (unreconstructed) using QMMD in the tight-binding approximation. These authors found that the reaction of 'free' OH with adsorbed acetone led to H atom abstraction and formation of a $CH_3C(O)CH_2\bullet$ species. Product variations as a function of time were monitored using FTIR by Coronado et al. [892]. They observed four major intermediates from acetone photodecomposition on TiO_2: acetate, formate, acetaldehyde and formic acid that increased in yield at roughly similar rates, accompanied by a mirrored decrease in the acetone and surface OH signals. These authors suggested that "*…acetone molecules break after the attack of the photogenerated charge carriers to yield a two-carbon molecule and a single carbon one*". In other

words, the first mechanistic step is aimed at a C–C bond. Similar distributions of C_1 and C_2 species have been detected by other groups [228,1021].

This author [701,753,851] examined the photodecomposition of acetone on the R TiO_2(110) surface under UHV conditions using TPD, PSD and HREELS. The most stable form of adsorbed acetone (the η^1 species) was found to be photo-inactive under UHV conditions, possessing a photodecomposition cross section of $< 10^{-24}$ cm^2 (the experimental limit of those studies). In contrast, the gas phase photochemical fragmentation cross section of acetone in the UV has been estimated at $\sim 10^{-22}$ cm^2 [1027]. Based on this observation, this author concluded that the TiO_2 surface quenched internal excitations of adsorbed acetone, as was the case for halocarbons on this surface (see above). However, photoactivity was observed when η^1-acetone was thermally converted (in the dark) to an acetone diolate via reaction with a coadsorbed oxygen species (likely the O adatom). The acetone diolate species was more stable on the R TiO_2(110) surface than acetone, and required only a $\sim$10 kJ/mol barrier for formation from the parent. In the absence of UV light, the diolate thermally decomposed back to acetone (and an adsorbed O atom) with no 'memory' of which O the acetone molecule came to the surface. Exposure of adsorbed acetone diolate on R TiO_2(110) to UV light resulted in photodecomposition via a substrate-mediated process (likely hole-mediated) that ejected methyl radicals into the gas phase and left acetate groups on the surface. Fig. 5.29 [753] shows CH_3• PSD profiles for a set coverage of acetone (0.18 ML) adsorbed on R TiO_2(110) with various pre-exposures of O_2. No photodesorption (or photochemistry) was observed without O_2, but the CH_3• yield increased in a sharp PSD feature with small pre-exposures of O_2. A comparison between the photochemistry of acetone on TiO_2 powders and on the TiO_2(110) surface suggests that ejected C_1 radicals seen in the latter may be (partially) responsible for the C_1 surface fragments seen in the former. For example, ejected CH_3 could react on the pore walls to form formate or formaldehyde. Shen and this author [756] have shown that these CH_3 radicals react with ice overlayers to form methane and ethane.

The combined thermal and photochemical pathway of acetone photodecomposition on R TiO_2(110) is illustrated in Fig. 4.1 for a generalized organic carbonyl molecule (with CH_3 groups replaced by R_1 and R_2 groups). This mechanism was the only photochemical process observed for acetone and for various other organic carbonyls on the R TiO_2(110) surface under UHV conditions. For example, butanone photodecomposed through ethyl radical ejection from a butanone diolate, leaving acetate on the surface [702]. Similarly, irradiation of adsorbed acetaldehyde diolate lead to methyl radical ejection and formate left on the surface [704]. (In neither case was photochemistry observed without formation of the respective diolate.) In these cases, the weaker bond was broken leaving the more stable carboxylate species on the surface. This trend suggests a thermodynamic driving force [1028]. However, the case of trifluoroacetone [703], where a partitioning existed between cleavage of the stronger C–CH_3 in some cases and cleavage of the weaker C–CF_3 bond in others, suggests that dynamics in the excited (neutralized) diolate also plays a role.

Nitrogen-containing molecules

While many of the most commonly studied N-containing molecules are also multifunctional, possessing more than one functional group that comes into play during electron transfer processes (e.g., nitrophenols and amino acids), there are several N-containing molecules in which N serves as the focal point for the photooxidation process. Calza and coworkers [32] provided a valuable overview of the photochemistry of N-containing organics on TiO_2 surfaces that shows that the mechanistic fate of N

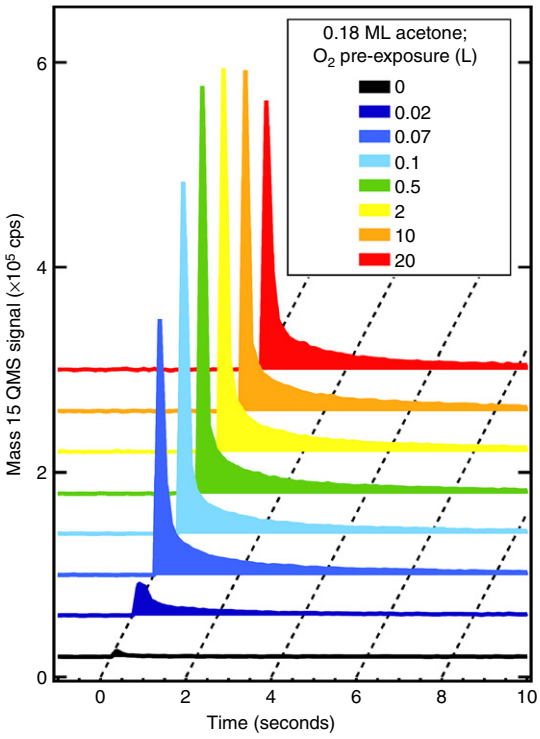

Fig. 5.29. CH_3 PSD traces resulting from UV irradiation (at 250 K) of 0.18 ML acetone adsorbed on various pre-exposures of O_2 on R TiO_2(110) at 100 K. (For interpretation of the references to color in this figure legend, the reader is referred to the web version of this article.)
Source: Reprinted with permission from Henderson [753].

is often diverse. For many N-containing molecules, there is potential for both photoreduction and photooxidation to occur under the same reaction conditions. This interesting aspect of N-containing molecules is briefly touched on below in a section on multifunctional molecules, but can also be seen by comparing the photooxidative behaviors discussed in this section with the photoreduction events discussed in Section 5.3.

Nitric oxide: NO is the simplest N-containing molecule studied in TiO_2 photocatalysis. Although it is generally considered as a reactant in photoreduction reactions (see Section 5.3) or in selective oxidation of ammonia (see below) and organics [1029], there have been reports of its photooxidation to adsorbed nitrates [1030–1034].

Ammonia: The photochemistry of NH_3 (or NH_4^+) on TiO_2 is potentially important in the selective reduction of NO_x species (to N_2), but surprisingly has not been widely studied from a mechanistic viewpoint. Yamazoe et al. [557,1035,1036] have published several papers on NH_3 photooxidation on TiO_2 from the perspective of promoting selective NO reduction. These authors found that NH_3 binds strongly to Lewis acid sites (Ti^{4+}) on TiO_2 surfaces, and that UV irradiation resulted in NH_2• signals in EPR. These observations are supported by previous work from Chuang et al. [1037]. Yamazoe and coworkers proposed that NH_2• radicals were formed from direct hole transfer to adsorbed NH_3. Production of N_2 resulted from a series of thermal reactions between adsorbed NO_x species (formed from NO adsorption) with NH_2•. The NH_3 + NO reaction also could be stimulated using visible light based on data from action spectroscopy. Using DFT calculations of NH_3 adsorbed on A TiO_2(101), these authors proposed that the visible light activity resulted from exciting an electron from a N 2p state on NH_3 to a Ti 3d CB state, similar to what is proposed for N-doped TiO_2 (see Section 1).

Zhu et al. [1038,1039] have examined the photooxidation of NH_3/NH_4^+ over suspended TiO_2. These authors concluded that the

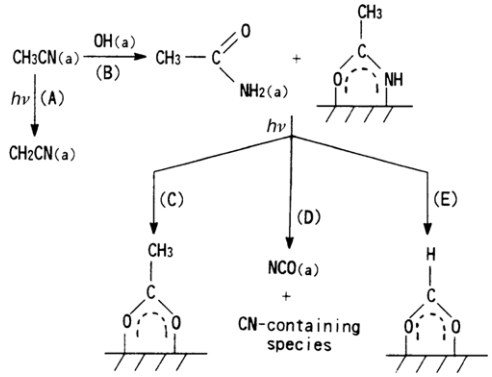

Fig. 5.30. Reaction scheme for the thermal and photochemical reactions of acetonitrile on TiO_2 surfaces.
Source: From Chuang et al. [1046]. Reproduced by permission of the PCCP Owner Societies.

rate limiting step was photooxidation to nitrite and not that of nitrite to nitrate. They also concluded that pH dependence in this reaction was due to natural solution phase equilibrium between aqueous NH_3 and NH_4^+, and not due to any electrostatic repulsions at low pH between NH_4^+ and the positively charged TiO_2 surface. This conclusion led the authors to propose that adsorbed NH_3, and not adsorbed ammonium ion, was the key reactant. These findings were similar to those by Kim and Choi [1040] who examined photooxidation of a series of protonated and neutral methylamines (see below).

Cyanide: Photooxidation of cyanide ion over TiO_2 surfaces appears to follow a mechanistic pathway through cyanate (OCN^-), most likely via a direct hole-mediated mechanism that generates cyanide radicals [1041–1045]. The mechanism by which the cyanide radical bonds to an oxygen-containing species is not known, although several groups have speculated on the role of hydroxyls in this process.

Acetonitrile: Both molecular and dissociative forms of acetonitrile (CH_3CN) result from its exposure to TiO_2 surfaces. Both forms appear to play a role in photooxidation of this molecule. Several groups have used vibrational spectroscopy to show that CH_3CN binds molecularly to Ti^{4+} sites and dissociatively through the influence of surface OH groups [772,1046–1049]. Chuang et al. [1046] have shown that the latter adsorption process results in $CH_3C(O)NH_2$ and $CH_3C(O)NH$ surface species, most likely with the N coordinated to a surface Ti^{4+} sites and a surface OH having attacked the cyanide C atom. As shown in Fig. 5.30, Chuang et al. proposed that these species photodecompose on the surface to adsorbed CH_3COO^-, $HCOO^-$, NCO and CN-containing species. In contrast, both Chuang et al. [1046] and Zhuang et al. [772] have shown that photochemical attack on *molecularly* adsorbed CH_3CN occurred at the methyl group and not at the cyanide end of the molecule. The latter research group has also shown that O_2 was necessary, but that water was not involved.

Alkylamines: A few groups have examined the mechanisms for the photooxidation of alkylamines on TiO_2, including those for various methylamines [1040,1050,1051], for triethylamine [784, 1052] and for 1-butylamine [906]. Kim and Choi [1040] examined the photooxidation of a series of methylamines from monomethylamine to tetramethyl ammonium ion. By varying pH, they found that the neutral amines reacted more readily than the protonated amines, leading this authors to propose that OH• attack on the N lone pair was the initial reaction step. The 'odd-man-out' in this series was tetramethyl ammonium ion, which does not have a N lone pair to protonate. In this case, OH• attack involved H abstraction from a methyl, leading to de-methylation.

Phosphorous- and sulfur-containing molecules

One of the general conclusions from studies on the photooxidation of organophosphorus compounds on TiO_2 is that the oxidized phosphorus product (usually a phosphate) tends to poison the surface during gas phase reactions [719,1053–1056], but does not in buffered solution phase settings [1057–1059]. This simple observation suggests that adsorbed phosphates can be hydrated and removed from the surface into solution. In fact, TiO_2 photoactivity lost in gas phase applications due to phosphate build-up can be recovered by washing the catalyst [1054]. The mechanism(s) by which this happens is not clear. In terms of organophosphate photooxidation, studies seem to indicate that phosphonate (P–C) linkages are more stable against photooxidation than are phosphoester (P–O–C) linkages [1053,1054,1056,1058,1059]. This suggests that organic ligands on P-containing molecules are the main points of photooxidation activity and not the P atom itself [1060]. P–F bonds appear to be more susceptible to hydration than to photooxidation [1055,1056]. As with many organic molecules on TiO_2, high surface coverages of organophosphates also appeared to block access of O_2 to the surface, thus limiting photooxidation rates [719,1060].

In photoreactions of organosulfides on TiO_2, charge carrier or OH• attack on the organic substituents leading to cleavage of the C–S bond appears to be key. This has been shown in studies on a variety of simple organosulfides, including: CH_3SH [1061], $(CH_3)_2S$ [1062–1065], $(CH_3CH_2)_2S$ [1066,1067], and thiophenes [1064,1068], as well as more complex organosulfides such as chemical warfare simulants (like 2-chloroethyl ethyl sulfide) [771,1069–1075]. As in the case of P-containing molecules, there is concern about the TiO_2 surface becoming contaminated with S-containing products (namely sulfate) [1063,1067,1076–1080]. Studies on the photooxidation of SO_2 [1077,1078,1080] or H_2S [1076,1081,1082] have also shown a tendency for the TiO_2 surface to accumulate surface sulfate. However, in contrast to the case of P-containing molecules, absorbed sulfate has been shown to evolve from the surface as SO_2 without requiring reprocessing of the photocatalyst with solution [1062,1064].

Multifunctional molecules

Probe molecules for surface studies are often chosen based on their simplicity and ability to mimic the chemical properties of more complex molecules. Typically, an ideal probe molecule might possess a single functional group, such as a carboxylic acid or halogen, through which binding to a surface and charge transfer chemistry takes place. Probe molecules with multiple functionalities can lead to multiple binding configurations and multiple electron transfer pathways, but they can also reveal mechanistic preferences. The photooxidation reactions of several multifunctional molecules are examined below to provide a sense of how photochemical mechanisms are affected when two or more functional groups are present.

Substituted phenols: As discussed above in the section on alcohols, phenol is a commonly examined probe molecule for photooxidation reactions on TiO_2. Substituted phenols (e.g., chlorophenols) have been widely studied. Phenol tends to photodecompose on TiO_2 via OH• attack on the ortho and para positions to form dihydroxybenzenes. The charge donating/withdrawing balance at each (remaining) position is significantly altered if another substituent is added to the ring. For example, Palmisano et al. [913] examined the mechanisms of photodecomposition for several *mono-substituted* benzenes over colloidal A. They observed that electron donating substituents (e.g., OH, NH_2, $NHC(O)CH_3$) resulted in mainly ortho- and para-monohydroxy derivatives of these molecules in first reaction step. Electron-withdrawing substituents (e.g., NO_2, CN, $C(O)CH_3$) resulted in monohydroxy derivatives at all three positions. The authors ascribed these behaviors

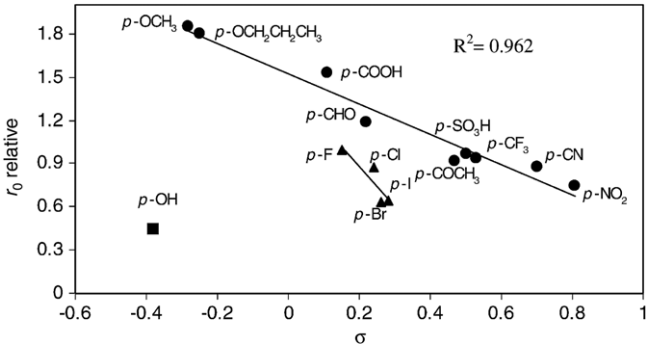

Fig. 5.31. Relationship between the initial degradation rate (r_o) and the Hammett constants (σ) of *p*-substituted phenols. Circle, triangle, and square symbols represent non-halogens, halogens, and hydroxy substituents, respectively.
Source: From Parra et al. [1083].

to the expected stabilities of resonance structures arising from OH• attack at each position. However, the next step in the photooxidation of the resulting hydroxy derivatives was more difficult to predict. Parra et al. [1083] have examined the photodecomposition of dihydroxybenzenes, as well as various para-substituted phenols, on TiO_2, correlating the observed photoactivity with the electronic structures obtained from *ab initio* calculations. For the dihydroxys, they found that the initial photodegradation activity followed the series: meta- (resorcinol) > para- (hydroquinone) > ortho- (catechol) dihydroxybenzene configurations, consistent with what the authors expected based on the ability of a VB hole to interact with the HOMO of each molecule. Similarly, Fig. 5.31 shows that the initial photodegradation rates for para-substituted phenol more-or-less followed what was expected from Hammett constants [914], with the activity increasing proportional to the degree of electron donating ability of the para-substituent. The calculations of Parra et al. also showed that more detailed correlations between reactivity and electronic structure could be obtained by considering the molecule's zero-point energy change with substitution and its quadrupole moment in the *x*–*y* plane, as both of these factors influenced orbital energies and symmetries.

Nitrophenols and aminophenols, in particular, are interesting molecules in photodecomposition reactions on TiO_2 because of a reductive process in one sets up photooxidation in the other. Maurino et al. [1084] have shown that both classes of molecules exhibited variations in their photooxidation mechanisms, with the nitrophenols open to both oxidative (OH• addition to the ring) and reductive (nitro to amine conversion) reactions. Once formed, aminophenols experienced either amine oxidation or OH• induced ring addition. Hydroxyl addition has also been observed by other authors [1085,1086] for nitrophenols.

Photooxidation of chlorophenols on TiO_2 has been examined mechanistically by several groups [168–172,467,1087–1092]. These molecules are generally believed to bind to the surface via the molecule's OH group, either molecularly or dissociatively. The main mechanistic questions continue to be whether the photoreactivity of these molecules are via direct or indirect processes. For example, Axelsson and Dunne [1092] examined the photooxidation of 3,4-dichlorophenol over TiO_2 and observed two initial reaction steps: chloride abstraction and OH addition. The presence of O_2 inhibited the former reaction and promoted the latter, leading the authors to conclude that electron attachment was key in describing the first step in chlorophenol degradation. Emeline and Serpone [467] also observed these two independent reaction processes, but found them to exhibit different spectral dependences in the UV. While the mechanism of phenol degradation was wavelength independent, these authors observed that variations in the selectivity of chlorophenol photoreactivity with wavelength were observed between pathways leading to chlorocatechol (OH addition) and those leading to hydroquinone and benzoquinone (Cl^- abstraction). The authors attributed this to one mechanistic pathway involving one carrier in the phenol case (assigned to OH), but multiple pathways in the chlorophenol case involving both OH• and CB electrons. Based on these observations, Emeline and Serpone proposed that excitations with different photon energies led to different arrival rates of carriers to the surface.

Interestingly, the UV wavelength dependent behavior observed by Emeline and Serpone for chlorophenol has been shown to extend into the visible. Chlorinated phenols form charge transfer complexes at TiO_2 surfaces that exhibit photoresponses distinctly different from those of the 'free' parent molecule or of the bare TiO_2 photocatalyst [168–172]. In this case, there is the possibility for photochemistry resulting from excitation of the charge transfer complex as well as from charge carriers arising from band-to-band excitations. For example, Gray and coworkers [169,170,172] used EPR to demonstrate visible light

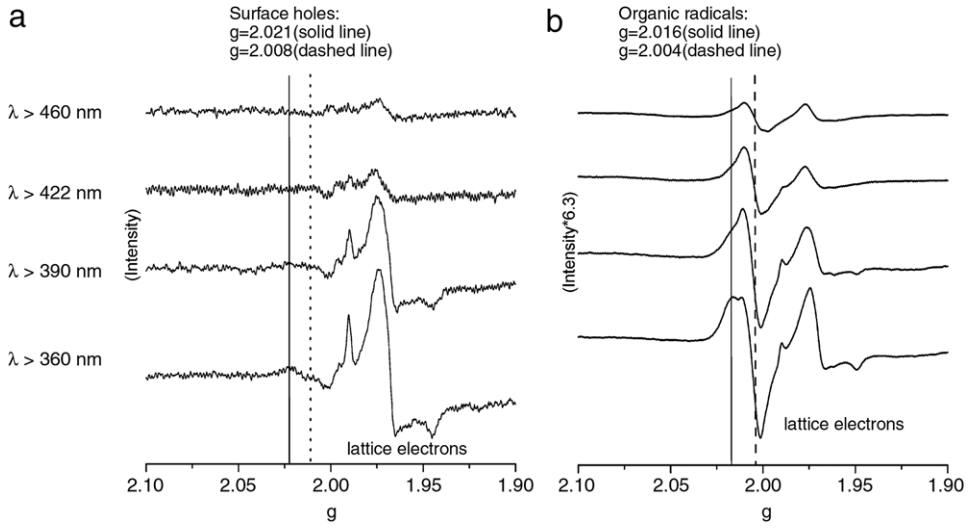

Fig. 5.32. EPR spectra of irradiated: (a) P-25 in water, and (b) 2,4,6-trichlorophenol (TCP) on P-25, both as a function of increasing light wavelengths. (Spectra obtained from 2,4,6-TCP on P-25 were ~6 times more intense than those from P-25 in water.)
Source: Reprinted with permission from Hurum et al. [169].

activity for various chlorophenols on TiO_2 (see Fig. 5.32 for results from 2,4,5-trichlorophenol). They ascribed this activity to excitation of a chlorophenoxy — TiO_2 complex followed by transfer of the excited electron into the TiO_2 CB and formation of a chlorophenoxy radical. Trapping of the transferred electron from visible light excitation of the charge transfer complex (right side of Fig. 5.32) was apparent from a direct comparison of the 'lattice electron' signals obtained from irradiation of bare TiO_2 with UV light (left side). These authors verified the existence of the resulting organic radicals using EPR and detected radical-initiated polymerization reactions that were not initiated by band-to-band excitation events. Based on these results, Gray et al. proposed that excitation of charge transfer complexes may be more selective in promoting photochemistry different from that in conventional TiO_2 photocatalysis. In agreement with these results, Kim and Choi [168] observed visible light photodecomposition of 4-chlorophenol over TiO_2. The existence of the CB electron from visible light excitation of the 4-chlorophenol charge transfer complex was confirmed with photoconductivity measurements. Decomposition of the ionized charge transfer complex resulted in immediate Cl^- formation and 4-CP degradation, with slow evolution of CO_2 occurring through an as-yet unknown series of steps. Complete mineralization was only achieved with UV. This is because the charge transfer complex was destroyed in the first transfer step and no visible light activity was possible thereafter.

Amine versus carboxylate: There are two good examples of molecules that combine amino and carboxylate groups: amino acids and ethylenediaminetetraacetic acid (EDTA) ligated complexes. Mechanistic details from studies on EDTA complex photodegradation are complicated by the involvement of metal cations to which EDTA is typically coordinated. In contrast, studies on the photodegradation of amino acids on TiO_2 are generally free of ligation effects. Based on simple studies of molecules possessing either amino or carboxylate groups (e.g., see [175]), both functional groups could potentially be involved in binding an amino acid to TiO_2. In other cases, additional functionalities of an amino acid could come into play (e.g., the –OH group of serine). The binding mode of an amino acid to a TiO_2 surface will be important in influencing how charge carriers and other reactive species respond to these adsorbates. Photodecomposition reactions of this class of multifunctional molecules on TiO_2 are extremely complex and difficult to fully characterize. The adsorption configurations of several amino acids on single crystal TiO_2 surface have been examined theoretically or experimentally [1093–1097], but correlations between their adsorption structures and photochemistry do not yet exist in the literature. Nevertheless, several research groups have examined these systems because of their importance in biomolecule–oxide interactions (see Section 8). Matsushita et al. [1098] examined the photooxidation of alanine ($NH_2CH(CH_3)COOH$) on several TiO_2 samples and found acetic acid (acetate) as a common intermediate in each case suggesting C–C and C–N bond cleavage as key reaction steps. Hidaka et al. [1099] examined the 'fate' of N in the photodecomposition of a variety of amino acids on TiO_2. They found that the preferred product tended to be ammonium ion, but that the ratio of ammonium to nitrate depended on the amino acid's structure. The fate of the N-containing product may also be linked to variations in the conditions that resulted from decomposition of the amino acid itself. For example, Tran and coworkers [1100] observed that the isoelectric point of TiO_2 shifted to lower values during photodecomposition of the most reactive amino acids on TiO_2. They also observed that the most reactive amino acids possessed additional OH or NH groups.

Halogen vs. sulfide: Panayotov et al. [771,1073] and Thompson et al. [771,1073] both found that Cl substitution at the beta position of an ethyl group in diethyl sulfide did not significantly alter the photodecomposition mechanism of this molecule on a TiO_2–SiO_2 catalyst. However, two different decomposition rates were observed on the R TiO_2(110) surface suggesting that variations in adsorption structure may influence the photodecomposition rate.

Halogenated acids: Irrespective of the degree of halogenation, halogenated organic acids still bind to TiO_2 via the carboxylate linkage. This preferred adsorption geometry may lead these adsorbates to photodecompose via hole-mediated decarboxylation (the photo-Kolbe reaction) [1101,1102], although other authors have proposed that dehalogenation should compete with decarboxylation [1103,1104].

5.3. Photoreduction reactions

5.3.1. Hole scavengers

In concept, the nature of the hole scavenger is as important to successfully accomplishing a photoreduction reaction over TiO_2 as is the role of O_2 (or some other such electron scavenger) is to successful photooxidation. There are published examples in which the choice of the hole scavenger can make the difference between no photoactivity and sustained photoreduction rates (see below). However, in general, there has not been sufficient research aimed at understanding the interplay between the mechanistic aspects of photoreduction and the choice of hole scavenger. As Section 6 will attempt to shown, choice of the wrong hole scavenger can result in unanticipated competition for surface sites. At present, the literature does not point to a 'hole-scavenger-of-choice', at least not to the degree that O_2 is recognized as the electron scavenger of choice. Ideally, it would be preferable to have water operate as a hole scavenger, but as Section 8 will highlight, there are difficulties associating with performing water photooxidation on TiO_2.

5.3.2. Photoreduction reactants

This section briefly examines some of the main photoreduction reactions studied mechanistically over TiO_2. Very notable exceptions not covered in this section are the photoreduction reactants H_2O and CO_2. Because these molecules represent unique challenges to photochemistry on TiO_2, their photoreduction will be discussed separately in Section 8. Aside from H_2O and CO_2, the most intensely studied photoreduction systems are those of metal cations photodeposited on TiO_2 from solution.

Metal cations: Photoreduction studies involving deposition of metal from solution on TiO_2 surface have been a very popular topic of study. Examples of metal cation systems examined in the literature include: Ag^+ [524,525,1105–1118]; Au^{3+} [1117, 1119–1121]; Cd^{2+} [1122–1124]; Cr^{6+} [233,1119,1125–1140]; Cu^{2+} [1119,1125,1128,1130,1135,1141–1151]; Fe^{3+} [1134,1145]; Hg^{2+} [1119,1131,1149,1152,1153]; Ni^{2+} [1125,1141,1142,1154, 1155]; Pb^{2+} [555,1142,1156]; Pt^{4+} [1157]; Rh^{3+} [1141,1158]; Tl^+ [1122]; U^{6+} [1159–1161]; and Zn^{2+} [1125,1141,1142]. As Rajeshwar et al. [1119] have shown, trends in the metal cation photoreducing ability of TiO_2 can be made from correlations of metal cation redox potentials relative to the TiO_2 CB edge, as shown in Fig. 5.33 for a few examples. Numerous groups have also shown that these potentials can be shifted (to increase or decrease activity) by pH, by electrolyte concentration or by coadsorbates. Kabra and coworkers [1125,1141,1142] provided several examples of these effects with regard to metal photoreduction on TiO_2. In fact, virtually all examples of metal cation photoreduction on TiO_2 involve studies under aqueous conditions, so factors such as pH, electrolyte concentration, counter ion selection, degree of catalyst suspension and cation complexation are routinely considered as potentially important.

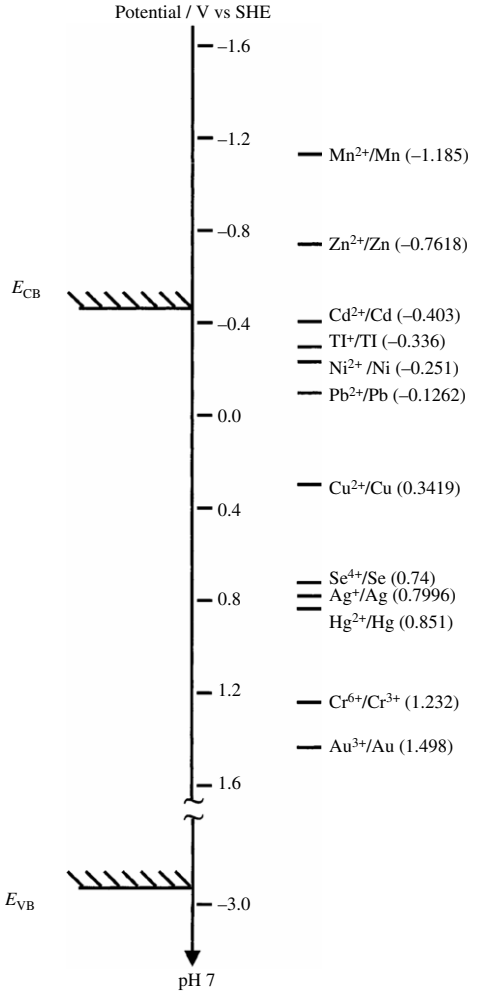

Fig. 5.33. Relative positions of the CB and VB edges of TiO_2 and the redox potentials (versus SHE) of various metal cations.
Source: From Rajeshwar et al. [1119].

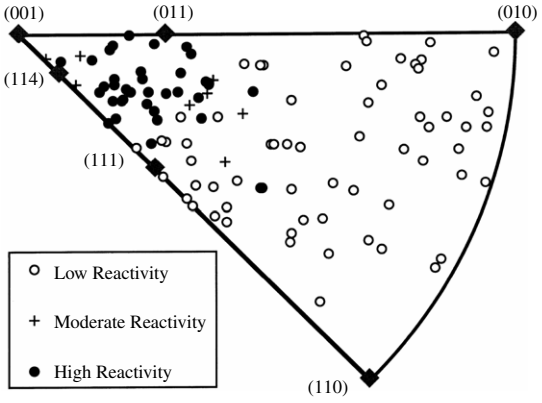

Fig. 5.34. Relative reactivities of various surface orientations of R TiO_2 for photoreduction of Ag^{+}. Each point in the stereographic projection represents an observed grain orientation. High, moderate and low reactivity grains are indicated by solid circles, crosses and empty circles, respectively. Diamonds represent the locations of the common low-index planes of R.
Source: Reprinted with permission from Lowekamp et al. [1108].

The boundary region between active and inactive metal cations in the assessment of Rajeshwar et al. [1119] is the TiO_2 CB minimum position. However, potential energy can be lost due to electron trapping (see Section 2.4), which places an additional limitation on the reductive power of TiO_2. For example, these authors found little activity for Tl^{+}, Ni^{2+}, Cd^{2+} and Pb^{2+} photoreduction on TiO_2 despite the fact that the reduction potentials of these metal cations were all accessible from the TiO_2 CB minimum at flat-band potentials (see Fig. 5.33). In contrast, if photoexcited electrons lose ~0.5–1 eV in reductive power due to trapping, it is not surprising that these metals would become inactive to electron transfer due to electron trapping.

A few groups [525,555,1110] have shown that metal cation photoreduction on TiO_2 occurred at trapped electron sites (Ti^{3+}). Grain boundaries and surface defects have also been shown to be surface regions at which Ag^{+} reduction and/or Ag metal nucleation occurs [524,525,1109,1117]. In a similar sense, specific facets of TiO_2 have be shown to be more active for photoreduction. Rohrer et al. [1107,1108] and Yamamoto et al. [1111] have both shown a strong orientational preference in the Ag photodeposition on R surfaces, occurring preferentially on smooth (100) and (101) surfaces relative to (110), (001) or (111) surfaces. For example, the former group [1108] reached this conclusion by mapping out Ag^{+} photoreduction activity across a polycrystalline TiO_2 sample using AFM (see Fig. 5.34). However, surface roughness tended to negate an orientational preference, suggesting that *local* structure at specific sites (defect or not) was also a key issue in ascribing active sites for Ag photodeposition. Nevertheless, these results suggest that specific facets on a TiO_2 nanoparticle will exhibit higher photoreduction activity for metal cations than will others.

A key issue unresolved in these site-dependent studies of metal photodeposition on TiO_2 is whether the sites for electron transfer (e.g., electron trap sites) are also the same sites at which the reduced metal ends up nucleating. Assigning where a metal ends up (nucleates) on TiO_2 to where it was reduced can be problematic because clear distinctions do not exist in the metal photoreduction literature between electron transfer sites and metal nucleation sites. An additional complication is whether electron transfer sites become more act as self-poisoned if they also act as preferred nucleation sites. There are indications, based on the Ag^{+} photoreduction work of Szabo-Bardos et al. [1113], that the preferred photoreduction site ended up being wherever Ag became nucleated. In other words, the resulting Ag nanoparticles acted as electron traps (see Section 6.1) facilitating additional Ag^{+} reduction. Similar 'cooperative' effects may be responsible for enhanced photoreduction rates in mixed metal cation systems (e.g., Cu^{2+} and Cr^{6+} [1130], and Fe^{3+} and Cr^{6+} [1134]). Finally, Wang and Wan [1148] have shown that dissolution processes can complicate the issue of identifying reduction and nucleation sites. These authors have shown that Cu^{2+} can be reduced to surface Cu^{+} species (e.g., suboxides), which under certain conditions are dissolved back into solution and further reduced to Cu metal, potentially at different surface sites on the photocatalyst.

As mentioned above, for every reduction reaction there needs to be a balancing oxidation reaction. In the absence of an electrochemical setting, this oxidation process must take place on the same photocatalyst in which reductive deposition of the metal is occurring. Research from several groups [233,555,1113,1118,1124,1132,1135,1136,1138,1149–1151,1156,1158] has shown that choice of the sacrificial electron donor (usually an organic) is key to efficient metal photoreduction. This is not simply an issue of balancing redox potentials (although that is important), but also selecting an electron donor that does not compete for surface sites or otherwise interfere with the metal reduction process. (This also applies to the byproducts of the oxidation process.) Another issue is one of complexation. Several groups [1123,1144,1145,1149,1151,1161] have shown that the presence of coordinated ligands to a metal cation can affect its photoreduction on TiO_2, either by blocking access of the complexed metal to the surface or by altering its redox potential. For example,

Chen et al. [1149] have shown that ligands may become detached from metal complexes and bind strongly to TiO_2 surfaces.

The mechanisms of metal cation photoreduction on TiO_2 surfaces have not been well-studied. The question of single, sequential electron transfer events versus multiple, simultaneous electron transfers is an issue when metal cation valence changes are greater than one. In the case of Cr^{6+} photoreduction to Cr^{3+}, Testa et al. [1126,1127] used EPR to show that the photoreduction mechanism involved single electron transfer steps, passing through a metastable Cr^{5+} species, even though the Cr^{5+} state is not typically deemed to be stable. (Disproportionation of two Cr^{4+} cations was excluded as the source of Cr^{5+} in EPR.) Testa and coworkers also found that oxalate in solution exerted a stabilizing influence on the Cr^{5+} intermediate. While most groups envision metal cation photoreduction in terms of direct electron transfer from TiO_2, three groups [1122,1154,1155] have shown that indirect reduction processes are also possible. These groups proposed that species such as CO_2^- (generated, for example, via photooxidation of oxalate) can be active for reduction of certain metal cations on TiO_2.

Nitrogen-containing molecules: Photoreduction studies of nitrogen-containing molecules on TiO_2 have been diverse, including those involving NO [557,788,881–883,1162–1165], N_2O [705,1166], NO_2 [1167], nitrate or nitrite [1168–1170], and a variety of nitro-substituted aromatics [685,1171–1175]. As mentioned in Section 5.2, studies on NO have been approached mainly from the perspective of using ammonia or CO to perform selective catalytic reduction [557,788,881–883]. The Tanaka group [557,882, 883] has shown that photoreduction of NO by NH_3 occurs through an indirect process in which the NH_2 radical was generated and reacted directly with NO. Their studies also showed that O_2 was necessary to scavenge electrons, otherwise N_2 was not formed. In the absence of NH_3 or CO, Rusu and Yates [1162], and the Anpo group [1163–1165] have both shown that N–N bond formation resulted in production of gaseous N_2O.

Miscellaneous molecules: Several groups have examined the photoreduction of selenate (SeO_4^{2-}) over TiO_2 [1176–1182]. The photochemistry of this species is interesting because of the variety of Se oxidation states that result from reduction. Final products tend to be elemental Se and H_2Se, both passing through a selenite intermediate (SeO_3^{2-}). Tan et al. [1179–1182] have shown that the nature of the sacrificial electron donor is important, with formate showing the most promise. Other photoreduction systems of interest include iodine/triiodide [422,495] and a variety of halocarbons photoreduced through radical chain reactions [1001,1183–1185].

6. Poisons and promoters

A wide variety of chemical species are known to impact thermal heterogeneous catalytic processes through poisoning or promoting influences. Typically, the influences of poisons and promoters in catalysis are thought to occur through the altering of energetics, the shifting of reaction pathways, blocking of sites, or some similar 'molecular-level' influence on the catalyst or the catalytic reaction. Poisons and promoters are also important in heterogeneous photocatalysis, although their influence is usually not viewed from the same perspective as in thermal catalysis. In heterogeneous photocatalysis, the influence of poisons or promoters is not restricted to interactions on the 'ground state' potential energy surface (which is typically the arena of influence in thermal catalysis), but also on the 'excited state', which includes the electron transfer potential energy surfaces associated with photoabsorption and electron transfer events. For example, photocatalysis researchers use of promoters to influence photoabsorption is often referred to as 'doping' (Section 1), where modifications of a photocatalyst's photoabsorptivity is correlated with observed photocatalytic activity. Often, it is difficult to evaluate the influence of an additive on photocatalytic behavior from a fundamental, molecular-level perspective because of the complex natures of most TiO_2 samples and preparation methods. In this section, discussion will focus on molecular-level phenomena ascribable to poisoning or promoting of TiO_2 photocatalysts. The objective will be to provide insights into how additives influence both ground state (e.g., site blocking) and excited state phenomena (e.g., charge carrier trapping). For convenience, discussion is organized into the types of additives.

6.1. Noble metals

As in thermal heterogeneous catalysis, supported noble metal particles are one of the most common promoters (or co-catalyst) in TiO_2 photocatalysis. Aside from promoting thermal chemistry, these 'additives' assist in charge carrier separation and trapping. Key factors in understanding the influence of a supported noble metal particle on TiO_2 photocatalysis include: the noble metal particle properties (e.g., size, shape, coverage and nucleation site), the influence of the noble metal on TiO_2 itself (e.g., creation of interfacial states), thermal versus non-thermal processes on the noble metal (i.e., its chemistry), and mass transport between the noble metal particle and TiO_2 (i.e., 'spillover'). Many of these themes are common irrespective of the noble metal, but because results for some metals on TiO_2 highlight unique properties, discussion is subdivided according to the metal (as oppose to the 'effect').

Platinum: The most extensively studied noble metal co-catalyst for promoting photocatalysis on TiO_2 is platinum [30,33,51,161,533, 551,562,599,774,783,907,943,955,957,1088,1104,1186–1231]. The most commonly ascribed effect of Pt (or most other supported noble metal on TiO_2) is its ability to promote charge carrier separation (e.g. via formation a Schottky barrier at the metal-TiO_2 interface) with electrons being accumulating on the metal and holes remaining on TiO_2 [33,51,161,533,551,562,975,1186,1189,1192, 1193,1195,1198,1199,1209,1210,1221,1222,1225–1227,1230]. Enhancement from supported Pt particles has also been attributed to the shifting of band edges that makes certain electron transfer processes more favorable in the vicinity of the supported metal particle [1198,1216,1220]. Other sources of enhancement in photocatalytic reactions on TiO_2 due to supported Pt include: a greater electron scavenging capability for O_2 [161,1193,1222,1230], enhanced surface chemistry that redirects mechanisms and assists in removing strongly bound intermediates that might impede activity [774,943,1104,1193,1194,1206,1229], promotion of OH• formation [1188], de-aggregation TiO_2 particles in suspensions [30], and promotion of proton reduction to adsorbed H atoms [774, 1187,1189,1218,1228]. As an example of the latter effect, Blount et al. [774] found that Pt supported on TiO_2 P-25 enabled generation of H_2 from photodecomposition of simple organics under anaerobic conditions, presumably via spillover of H^+ from TiO_2 to the metal. In this application, Pt might not be the most active noble metal on TiO_2. For a series of noble metal co-catalysts (M) supported on TiO_2, Ranjit et al. [1214] observed that the rate of N_2 photoreduction to NH_3 varied with the M–H bond strength for that metal. The highest M–H strengths resulted in the higher rates of NH_3 formation, as shown in Fig. 6.1 (no NH_3 was formed without the co-catalyst present). The metal trend observed was Ru > Rh > Pd > Pt. Their results suggest that the ability of noble metal supported TiO_2 to photoreduced N_2 to NH_3 directly related to the stability of H on the noble metal co-catalyst. Interestingly, however, Pt was more suited for the opposite reaction (selective ammonia photooxidation). Lee et al. [1205] observed that Pt supported on

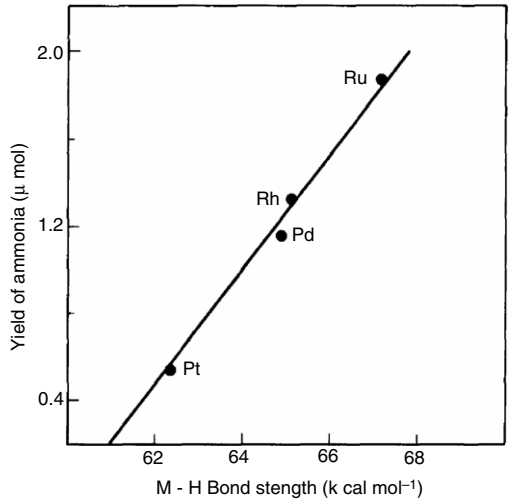

Fig. 6.1. Plot of metal–hydrogen (M–H) bond strengths versus observed yields of NH_3 from photoreduction of N_2 over TiO_2-supported noble metal photocatalysts. *Source:* From Ranjit et al. [1214].

TiO_2 promoted N_2 formation from NH_3 as opposed to NH_3 being oxidized to undesirable NO_x products. The latter was seen on bare TiO_2 or TiO_2-supported Au photocatalysts. These authors proposed that the ability of Pt to selectively form N_2 was due to the stability of NH_x species on Pt and the ability of Pt to reverse undesirable oxidation events (e.g., N_2O formation). In this sense, Pt should perform better than other noble metals co-catalysts in solar fuel cell applications that employ ammonia as a sacrificial electron donor.

Scanning probe techniques have enabled researchers to study the influence of noble metals (such as Pt) on TiO_2 at the local scale. Onishi's group [975,1198] has used STM and scanning Kelvin probe techniques to study the influence of Pt nanoparticles on R TiO_2(110) photochemistry. Using trimethyl acetate (TMA) as a probe molecule, these authors found no spatial preference in photodecomposition activity relating to the distance between the photodecomposing molecule and the nearest Pt particle, as shown in the left two images of Fig. 6.2. This observation suggested that local field effects in the vicinity of Pt particles do not significantly inhibit or promote hole-mediated TMA photochemistry on TiO_2. However, these authors did observe an overall (global) enhancement in TMA photodecomposition due to Pt, based on similar measurements without Pt present (right two images). This was tentatively attributed to Pt trapping CB electrons. Based on the enhancement seen relative to the 'clean' surface, these authors estimated the electron trapping capacity of an average Pt particle on their R TiO_2(110) surface was ~0.06 electrons per Pt atom. Onishi's group [1198] also used scanning Kelvin probe force microscopy to show that the local work function of a Pt particle on R TiO_2(110) was 0.1–0.3 eV less than that of the surrounding oxide surface. This was opposite from what these authors expected based on work function values for the separate materials (which would suggest electron transfer from Pt to TiO_2). However, photolysis leading to hole-mediated photodecomposition of TMA (adsorbed on the TiO_2 regions) resulted in a positive shift in the Pt work function which the authors ascribed to electron trapping on Pt. The largest shifts occurred preferentially on the smallest Pt clusters. In separate work, this group [533] used transient IR absorption spectroscopy to follow trapping, detrapping and lifetimes of electrons excited in high surface area TiO_2 with supported Pt. They found that relaxation and trapping timescales were about the same for Pt/TiO_2 as for TiO_2, but the recombination timescale was much longer for the Pt/TiO_2 system. This suggests that long-lived electron trap states resulted from electron transfer to the Pt particles.

The influence of Pt on TiO_2 photocatalysis is not always positive. Several groups have observed either negative effects or no significant impact from nanoparticles of Pt on TiO_2 [159,943,1192,1196,1200,1201]. For example, Emilio et al. [1192] showed that Pt particles on TiO_2 could act as charge recombination centers. In other cases, authors proposed that Pt blocked active sites on TiO_2 [159]. The amount of Pt can play a major role in deciding whether a positive, negative or null effect is observed. Several authors have observed that an optimal loading of Pt existed for promoting photocatalytic rates on TiO_2 surfaces [1088,1189,1203,1209,1212,1214,1219,1221,1224]. Typical optimal Pt loadings were ~1 wt%, with loadings above the optimal amount resulting in attenuation of photochemical rates as a result of blocking of the TiO_2 surface. For example, Chen et al. [1189] showed that the *adsorption* capacity of TiO_2 decreased as the Pt loading was increased.

A detailed study of the effect of Pt on CO photooxidation was carried out by Linsebigler et al. [957] using the R TiO_2(110) surface as a model. These authors observed no enhancement in the rate of CO photooxidation on TiO_2(110) when Pt clusters were present. Instead, as shown in Fig. 6.3, they found that as little as ~0.02 ML of Pt had a noticeable effect in attenuating the photochemical yield of CO_2, presumably through blocking of the CO oxidation active sites (surface oxygen vacancies). Virtually no CO_2 was observed with ~0.15 ML of Pt. Their results did not provide evidence that Pt clusters were important in electron trapping, causing these authors to question schemes proposed in the literature in which Schottky barrier formation promotes charge separation. In contrast, several groups have shown that Pt enhanced CO photooxidation on high surface area TiO_2 [783,955,956,1191,1197,1208,1231,1232]. For example, Einaga and coworkers [783,1191,1197] observed significant enhancements in CO photooxidation when Pt nanoparticles were supported on TiO_2, and proposed that the Pt particles acted as reservoirs of

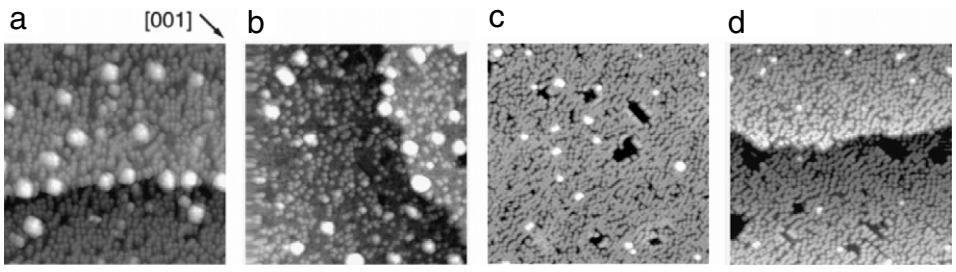

Fig. 6.2. STM images following UV irradiation of TMA on the Pt-modified R TiO_2(110) surface for (a) 1 and (b) 3 h. Images from similar irradiation periods of TMA on the 'Pt-free' surface are shown in (c) and (d), respectively. (Brighter 'bumps' in (c) and (d) are TiO_x islands, not Pt particles.) (Image conditions: 40 × 40 nm, +1.6 V bias, 0.4 nA tunneling current).
Source: Reprinted with permission from Uetsuka et al. [975].

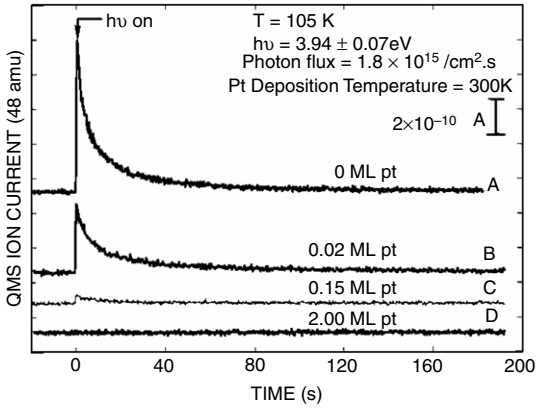

Fig. 6.3. Photodesorption of CO_2 resulting from reaction of CO and O_2 on R TiO_2(110) with various Pt surface coverages.
Source: Reprinted with permission from Linsebigler et al. [957].
© 1996, American Chemical Society.

CO (since TiO_2 only weakly binds CO at room temperature). This contradiction between work on the R TiO_2(110) surface (where oxygen vacancies are needed for CO photooxidation) versus high surface area TiO_2 (where the active sites are not well-understood) suggests that more information is needed not only about the CO photooxidation reaction, but also about how noble metals like Pt reside on TiO_2 surfaces. It is not unreasonable to assume that the structure of the TiO_2 surface should influence the role of supported noble metal particles in photochemistry on TiO_2. Several groups have shown that the method of preparing Pt nanoparticles on TiO_2 (e.g., photodeposition versus thermal or chemical reduction) affects photocatalytic performance [1201,1202,1223,1231]. For example, Kennedy et al. [1202] suggested that the method of preparing Pt nanoparticles on TiO_2 had a greater potential impact on the properties of the TiO_2 surface than on the properties of the resulting Pt nanoparticles. In cases where Pt was prepared from reduction of salt precursors, Lee and Choi [1204] have shown that residual unreduced Pt (ions or oxide) acted as charge recombination centers inhibiting the photodecomposition activity of TiO_2 for chlorinated organics.

Silver: TiO_2-supported silver has received attention not only for its use as a photocatalyst [148,149,551,659,1088,1114,1166,1215,1233–1255] but also because the main particle preparation method itself (photoreduction of silver salts) provides insights into photoreductive processes on TiO_2 (see Section 5.3). As with other noble metals, supported Ag nanoparticles are believed to promote charge separation and electron trapping [150–152,551,659,1233,1236,1238,1241–1246,1251,1253–1255], and to facilitate surface chemistry not seen on bare TiO_2 surfaces [1088,1114,1166,1215,1233,1234,1237–1239,1241,1248]. As an example, Kominami et al. [1233] found that among TiO_2-supported noble metals, Ag and Cu were best at assisting nitrate photoreduction to ammonia because these metals displayed the best activity for H^+ reduction by photoexcited electrons trapped at the noble metal particles. There is also evidence that supported Ag assists in maintaining high

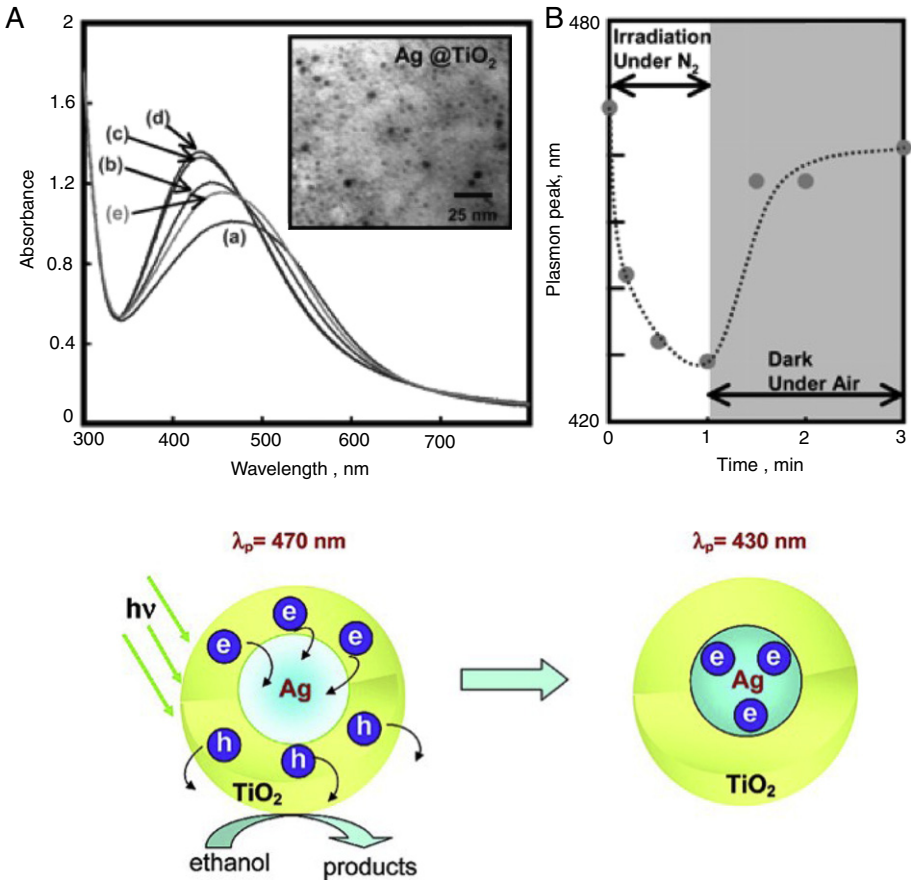

Fig. 6.4. (Above) (A) UV–vis absorption spectra of Ag–TiO_2 core–shell colloids suspended in ethanol: (a) before UV irradiation, (b–d) after exposure to UV light (>300 nm) for 10, 30 and 60 s, respectively, and (e) after exposure of the UV-irradiated suspension to air. (Inset shows TEM of the (dried) core–shell material.) (B) Shift in the Ag plasmon absorption peak during UV irradiation and during subsequent exposure to air. (Below) Schematic model for electron–hole pair separation and electron transfer processes occurring on Ag–TiO_2 core–shell materials.
Source: Reprinted with permission from Hirakawa and Kamat [149].
© 2004, American Chemical Society.

surface area photocatalysts by separating TiO_2 particles from each other [1243,1245]. In general, these effects are dependent on the optimal loading of silver, which is generally found to be below ~1 wt% [1088,1114,1235,1238,1243,1249,1250,1254].

The well-known plasmon feature of Ag (see Section 1.3.2) was used by Hirakawa and Kamat [149,1240] to gauge the electron trapping ability of Ag–TiO_2 core–shell clusters. These authors found that the Ag plasmon feature shifted from 460 nm to 430 nm during UV photooxidation of ethanol, as shown in Fig. 6.4. The magnitude of the shift reflected the extent of electron trapping in the Ag core. These authors estimated that each core in their samples on average trapped up to 42 electrons while still maintaining ethanol photooxidation activity (illustrated schematically in the bottom of Fig. 6.4). Assuming Ag core sizes between 2 and 4 nm, the typical charge density trapped per Ag atom would be ~0.01–0.09 electrons per metal atom, which is comparable to the value of 0.06 electrons per Pt observed by Uetsuka et al. [975] for electron trapping by Pt nanoparticles on R TiO_2(110) (see above). Hirakawa and Kamat also found that the charge build-up on the Ag core could be released through the TiO_2 shell by exposure to air (right side of Fig. 6.4), indicating a significant degree of charge delocalization and/or transfer across the Ag–TiO_2 interface.

Gold: The properties of Au nanoparticles have received considerable attention in thermal heterogeneous catalysis research [1256–1262], and additional attention is being paid to the photocatalytic properties of nanoscale Au particles on TiO_2. Several groups have seen enhancements in photocatalysis over TiO_2 from the addition of Au as a co-catalyst [156,1089,1187,1196,1236,1242,1263–1272]. As with other noble metals on TiO_2, there is an optimal loading for this enhancement [1089,1263,1265–1269], but unlike with other metals the optimal loading may relate more to the size of the Au nanoparticles [1089,1265,1267–1269] than with the amount of surface area they occupy [156,1089,1196]. While the source of the unusual catalytic properties of nanoscale Au remains a subject of intense debate, it is clear that the physical and/or electronic structures of small ($\leq$2 nm) Au particles differ considerably from those of larger Au particles or extended Au surfaces. Enhancement of photocatalysis due to Au on TiO_2 is linked (at least in part) to the unique properties that result from nanoscaling Au. For example, Subramanian et al. [1267] found that smaller Au particles supported on TiO_2 were more effective as electron transfer centers in photoreduction of C_{60} because the smaller particles shifted the Fermi level to more negative values. Orlov and coworkers [1089] also observed a size dependence in the enhancement of Au on TiO_2 for 4-chlorophenol photooxidation, with particles below 3 nm being most active. In contrast, larger Au loadings (which resulted in larger Au particles) suppressed reactivity. The authors attributed this to elimination of surface OH groups. In another example of Au particle size dependence, Wu et al. [1268] found that the relative rate of H_2 production from methanol, formaldehyde and formic acid photodecomposition on TiO_2 (under anaerobic conditions) increased as the size of supported Au particles decreased from 10 nm to less than 3 nm (see Fig. 6.5). They attributed this behavior to the influence of small Au particles in altering the photodecomposition products of formate (the common surface intermediate in each case) from $CO + H_2O$ to $CO_2 + H_2$. Curiously, the amount of H_2 produced from methanol was considerably less than that from formic acid or formaldehyde, despite the greater number of C–H bonds available. This suggests that the conversion of methanol to formate was somehow inhibited (even with Au present). Nevertheless, the shift in product formation toward H_2 when Au was present suggested that even in the methanol case Au nanoparticles played an important role in promoting a photocatalytic water–gas shift reaction on TiO_2.

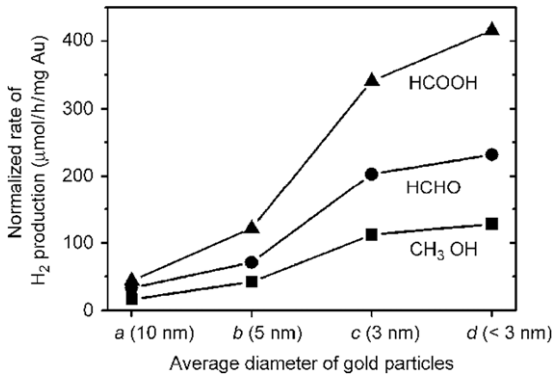

Fig. 6.5. Normalized rates of H_2 production during photocatalytic reforming of CH_3OH, CH_2O and HCOOH over Au/TiO_2 photocatalysts for four particle size distributions of supported Au. Rates normalized to amount of Au present.
Source: From Wu et al. [1268].

As with other noble metals supported on TiO_2, studies propose that supported Au nanoparticles on TiO_2 assisted in: charge carrier separation and electron trapping [1236,1242,1265,1267,1269,1270], interfacial electron transfer processes [1271], and H_2 formation [1187,1268]. As with Pt (see above), the photochemical properties of supported Au also depended on the preparation method [1272]. One of the interesting aspects of Au supported on TiO_2 is the issue of metallic versus ionic Au [156,1270]. Subramanian et al. [156] have shown that both Au^0 and Au^{3+} enhanced SCN^- photooxidation on TiO_2, but that the enhancement significantly attenuated as the Au coverage increased. The promotion effect of the ionic species resulted from enhanced electron scavenging, but at high surface coverages the gold ions could also cause charge recombination. In contrast, the benefits of the metallic state became overshadowed at high metal coverages by the tendency of the metal to block sites on the TiO_2 surface.

Palladium: As a co-catalyst on TiO_2, Pd contributes many of the same benefits seen for other noble metal particles [1187,1214,1228,1233,1273–1279]. For example, Sano and coworkers [1215,1278] have shown that addition of Pd nanoparticles to TiO_2 resulted in more complete mineralization of vinyl chloride through surface reactions that minimized emission of gaseous chlorocarbon intermediates. Deactivation of TiO_2 as a result of strongly bound organic intermediates was also minimized with Pd present [1279]. Hydrogen production was enhanced for Pd/TiO_2 relative to TiO_2 alone [1228,1276,1277]. On the latter point, Bowker et al. [1276,1277] examined the Pd loading dependence on the anaerobic photochemical conversion of methanol and water on P-25 to CO_2 and H_2. As shown in Fig. 6.6, they found that the rate of H_2 production increased with Pd loading up to ~1%, then sharply dropped for Pd loadings above 1%. The 1% loading appears to be a limit that is similar for Pt, Ag, Au and Pd, and likely relates to an optimal particle size. Bowker et al. proposed that at the 1% loading level provided particles with optimal periphery on TiO_2 to act as active sites, in this case for conversion of CH_3OH to H_2. The slow step in the overall reaction involved oxidation of CO (which unfortunately tended to cover the Pd particles).

Rhodium: Rhodium has not been extensively examined for its co-catalytic properties in TiO_2 photocatalysis in comparison to other noble metals. While as a supported nanoparticle it has been shown to exhibit many of the benefits of other noble metals (e.g., in promoting certain photooxidation [1280,1281] or photoreduction [1214,1228] processes), it (like Au) has been shown to exhibit the unique capability of existing on the TiO_2 surface as stable isolated cations at low loadings and mildly reductive conditions. Rasko and coworkers [1282,1283] have shown that isolated Rh^+ species on TiO_2 act as catalytic centers for

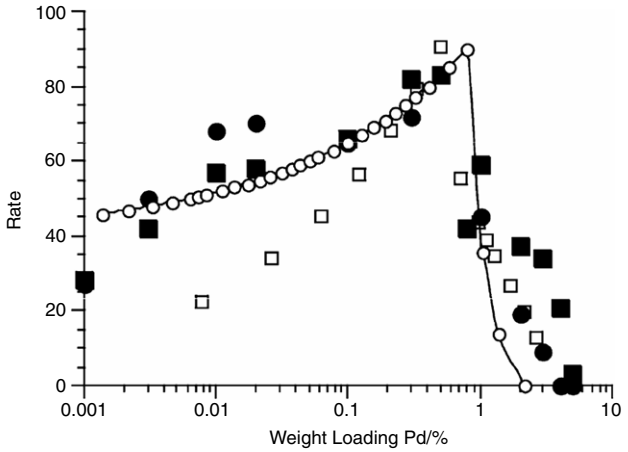

Fig. 6.6. Dependence of the H_2 production rate on the weight loading of Pd during photocatalytic reforming of methanol over TiO_2. Solid symbols: data from different sets of photocatalysts; open symbols: mathematical descriptions of the rate based on a simple Pd surface area model (squares) and on a Pd particle perimeter model (circles).
Source: From Bowker et al. [1276].

photoactivation of CO_2 and NO. Similarly, Kohno et al. [1284] found that a Rh^+ species on TiO_2 played a role in the photoreduction of CO_2.

Copper (and nickel): Uses of copper as a co-catalyst in assisting photochemistry on TiO_2 present anomalous cases because Cu can be present on TiO_2 in metallic, ionic and/or oxidic states depending on the circumstances. (Although not a noble metal, Ni also shows similar properties as Cu in this setting and will thus be included in this discussion.) Two or more of these states of Cu or Ni can co-exist on TiO_2 during a photochemical reaction making it difficult to identify which is more active. Varying redox conditions during a reaction can also swing the valence state of those metals back and forth from metallic to ionic. In concept, one might assume that these metals could perform the same charge separation functions for which metals such as Ag and Pt are well-known. In fact, Tsuji and coworkers [1285] have proposed that Cu metal implanted in R TiO_2 exhibited such a promotion effect for methylene blue photodegradation. However, the problem arises in maintaining the metallic state when supported Cu or Ni particles are exposed to oxidative conditions. For example, Zhou et al. [1286] have shown that both Cu and Ni nanoparticles supported on R TiO_2(110) were dispersed (and presumably oxidized) by O_2 exposure at room temperature under UHV conditions. Because of the ease with which these metals, as nanoparticles supported on TiO_2, can be oxidized, it is unclear whether the promotion properties of these metals in their metallic states has been (or even can be) adequately explored. Even for photoreduction reactions, where the metallic state of Cu might be more likely retained, groups have shown that metallic Cu particles were not the most active form of Cu on TiO_2 for the photoconversion of CO_2 [1287,1288]. Wu and Lee [1289] found that Cu nanoparticles on TiO_2 promoted H_2 photoproduction from aqueous CH_3OH solutions, but that the photoreaction eventually oxidized the Cu particles resulting in decreased performance. The issue then becomes the interplay between the various states of Cu (or Ni) on TiO_2, and the relative influence of their ionic and oxidic states.

6.2. Acidic and basic conditions

While not typically considered from the view point of poisoning or promoting, manipulation of pH has been shown to have a significant impact on the rates of photochemical reactions on TiO_2 in solution. Numerous groups have shown that optimal pH ranges exist for various photoreactions on TiO_2. Loosely dividing the pH range into 'high' and 'low', literature reports indicate that high pH favors photooxidation of chlorinated anilines [1290], 2-chlorophenol [1291], 1,4-dihydoxybenzene [1292], TNT [1293], and ammonia [1038], while low pH favors photooxidation of alcohols [1294], organic acids [1294–1297], chlorocarbons [1294], and nitro/aminophenols [1084]. For example, in the solution phase photooxidation of ammonia, Zhu and coworkers [1038] found that the rate was proportional to the ammonia concentration in solution and not the ammonium ion concentration based on pH-dependent measurements. While electrostatics between ammonium ion and the surface did not appear to play a major role in the observed pH dependence, it did play a role in the photooxidation of nitrite to nitrate. Dependences on pH have also been observed in various photoreduction reactions [1001,1142, 1298–1300]. In many cases, the influence of pH on photochemical reactions relates to adsorbate stabilities and not necessarily to electron transfer events [993,1290,1298,1299,1301–1305]. In this sense, surface coverages can be manipulated with pH, resulting in either favorable or unfavorable conditions. It is also to be expected that photochemical reactions themselves can result in pH changes that impact rates [878,1100,1295,1304] or change selectivities [1291,1305].

Aside from chemical effects, it is well-known in the photoelectrochemical literature that pH can be varied to shift band positions and surface electrostatics that influence charge carrier dynamics [125,569,580,660,878,1306–1308]. In non-aqueous systems, the degree of band edge shifting in a particular solvent system has been shown to scale with the proton donor ability of the solvent [1308]. As shown in Fig. 6.7, Lyon and Hupp [1309] found that the TiO_2 CB edge exhibited Nernstian dependence with pH, shifting by −64 mV per pH unit in the range of −8 to +23 pH. (See the Fujishima review [2] for more details on this effect.) In concept, shifts in band edges brought about by changing pH can be used to control some electron transfer process, or possibly shift conditions from oxidative to reductive. For example, Cornu et al. [1306] used transient techniques to track methyl orange photodecomposition on suspended P-25 as a function of pH. These authors detected a crossover at pH ∼8 between the rate limiting step in the photodecomposition of methyl orange from it being oxidative to reductive. Above a pH of 8, the rate limiting step was oxidation and O_2 reduction was rate limiting at lower pH values. These authors proposed that the surface potential resulting from pH influenced the charge carrier transfer rates. In a single electron transfer example, Qu and Meyer [1310] examined how pH affected charge injection from Ru-based dyes into TiO_2. They found that surface proton coverage (in a non-aqueous solvent) impacted the charge injection efficiencies, surface coverage of the dye, the lifetime of the excited dye and the adsorbed structure of the dye. Injection rates tended to be higher a low pH and (conversely) the excited dye's lifetime was longer at low pH.

6.3. Water

Water has long been viewed as an important molecule in photocatalysis on TiO_2. In a cursory sense, the importance of water in oxide surface chemistry [853] is not unlike that of the importance that CO has as a probe molecule and a reactant/product in many thermal catalytic processes on metal surfaces. Water is pervasive in almost all applications of TiO_2 as a photocatalyst either as a solvent, a reactant or a product. Fu et al. [93] summed up the two major influences of water in photocatalysis on TiO_2 as the provider of raw material for OH• production and the blocker of surface sites needed for reactants. These opposite effects can manifest themselves in any particular reaction as a function relative humidity (RH), as illustrated in Fig. 6.8. Using organic

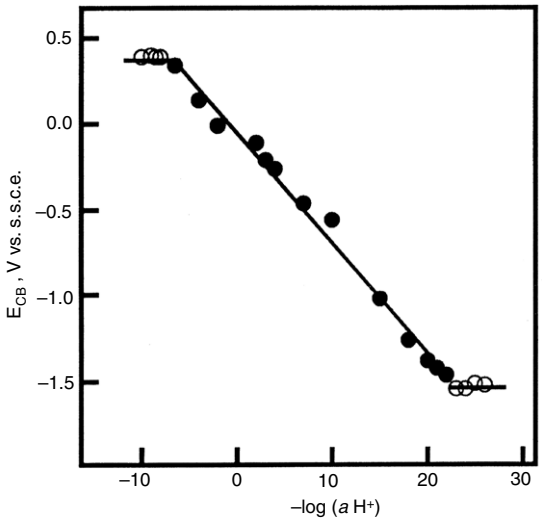

Fig. 6.7. Dependence of the TiO_2 CB edge potential on solution pH. *Source:* Reprinted with permission from Lyon and Hupp [1309]. © 1999, American Chemical Society.

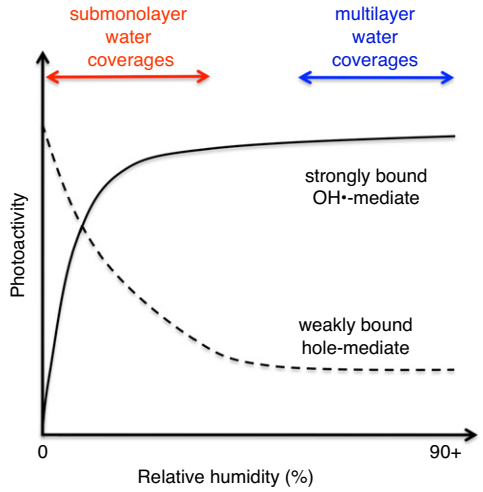

Fig. 6.8. Schematic illustration of the opposing influences of water on organic photooxidation reactions over TiO_2.

photooxidation as an example, Fu and coworkers proposed that the interplay between these two roles of water, as promoter and inhibitor, depends on the relative concentrations of water and organic present, the relative binding of water versus organic to the surface, and the mechanism(s) by which the organic is photochemically activated (e.g., OH● versus direct hole oxidation). If the organic binds weakly and prefers oxidation by holes, the rate of its initial photooxidation step will decrease with small increases in RH, reaching a minimum at higher RH values where water dominates the chemisorbed layer (dashed line of Fig. 6.8). In contrast, a strongly bound organic that oxidizes by OH● will have a low rate of photooxidation at very low RH, and will see a rate increase with increasing RH (solid line of Fig. 6.8). Formation of a water multilayer (or a physisorbed/solvation layer) may further promote or (conversely) hinder rates depending on the details of OH● formation and it reaction with the organic. In some cases (e.g., those most active for OH●), solution phase chemistry enhances rates.

Probing the interplay between water poisoning and promoting is probably best explored in gas phase studies because reactions under aqueous conditions are already dominated (for better or worse) by water as a solvent. The aqueous condition can, to some extent, be used as a benchmark for understanding the effects of high RH. Numerous gas phase studies support the conclusions of Fu and coworkers in attributing the influence of water in photocatalysis on TiO_2 to the roles of promoter or inhibitor. Examples include the photooxidation reactions of propane [927], toluene [1311,1312], 1-butene [1313,1314], methanol [1312], 2-propanol [903], trichloroethylene [1006,1014, 1315], triethylamine [1052], formaldehyde [1311,1316], formic acid [1316], stearic acids [743], and diethyl sulfide [1066]. In terms of RH, the point at which the conflicting influences of water transition depends on many factors (including those mentioned above). For 1-butene, Cao et al. [1313,1314] found that trace amounts of water enhanced photooxidation rates, but amounts above the trace level inhibited rates. In contrast, Hagglund and coworkers [927] observed a promoting influence of water on propane photooxidation up to RH values in which a full water monolayer was established. Above this point, an additional physisorbed layer of water (on top of the chemisorbed layer) inhibited propane photooxidation presumably by blocking access of propane to the surface.

Before going into more detail on the promoting and inhibiting roles of water, it is worth noting that there are instances in the literature in which water appeared to play little or no role in photocatalysis on TiO_2, or in which its beneficial and detrimental influences canceled each other out. These include photooxidation of acetonitrile [1317,1318], butanone [1026], acetone and methyl isobutyl ketone. [1025], methanol [1166], ethanol [893], various aromatics [1319], trichloroethylene [718], CH_3Cl [994,1320] and acetic acid [970,1047]. For example, as mentioned in Section 5.2.3, Fan and Yates [718] excluded direct involvement of water in trichloroethylene photooxidation over TiO_2 because oxygen incorporation from isotopically-labeled water into the oxygenated intermediates (dichloroacetyl chloride, phosgene or CO) did not occur. Comparison of this list with the one in the previous paragraph (of molecules promoted by water) reveals conflicts, suggesting that the reaction conditions and/or the catalyst may be factors in how water influences a particular photocatalytic reaction. The comparison also suggests that deciphering the role of water in TiO_2 photocatalysis is not straightforward. During mineralization of a reactant, water may promote one oxidation step, inhibit another and have no influence on others. In this sense, unraveling the influence of water requires examination of its influence on each mechanistic step, whether they be electron transfer processes or thermally initiated steps.

6.3.1. Inhibitor

The inhibiting role of water in photocatalysis on TiO_2 is generally viewed as one of a site blocker. Two types of site blocking can be imagined, one in which water occupies key adsorption and/or reaction sites on the surface, and one in which water, acting as a solvent, inhibits access of reactants to the oxide–solution interface. Differentiating between these two types of site blocking processes requires control of water coverage, for example through manipulation of the RH. This is illustrated in the several of the references discussed above, with inhibition increasing at RH levels at which either a fully chemisorbed layer of water is established or at which physisorbed layers become stable. Examples of photooxidation studies on TiO_2 in which authors observed chemisorbed water acting as a site blocker include: CO [783], formaldehyde [1316], methanol [714], ethanol [890, 897], acetaldehyde [1321], acetone [752,1026], ethylene [738, 1322], 1-butene [1313,1314], butadiene [1311], toluene [941,943], and trichloroethylene [1006,1315]. As an example, Fig. 6.9 from this author's work [752,1323] shows that water inhibited acetone

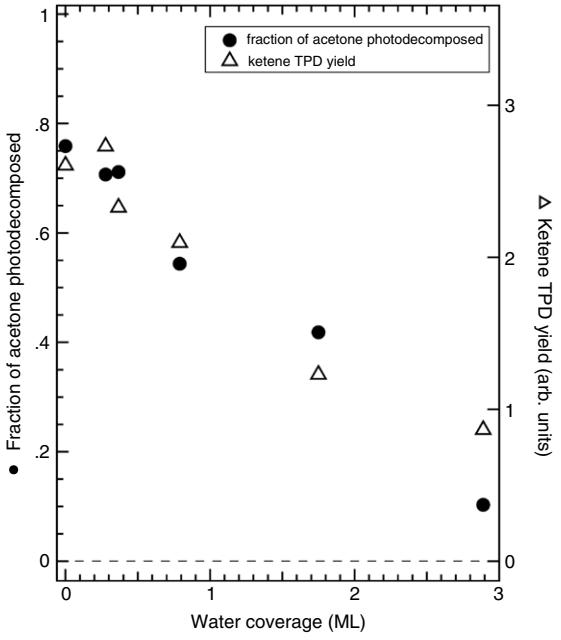

Fig. 6.9. Effect of the coadsorbed water coverage on the conversion and product formation during UV photodecomposition of 0.25 ML acetone on R TiO_2(110). *Source:* From Henderson [752].

photodecomposition to acetate (gauged in post-irradiation TPD by ketene formation) on R TiO_2(110) at 100 K by displacing acetone from the first layer to the physisorbed layer. Acetone was able to compete for surface sites sufficiently to allow for some activity even with 3 ML of water coadsorbed. The inhibition of acetone photochemistry on R TiO_2(110) by water likely lies in the ability of adsorbed water molecules to adapt to intermolecular (dipole–dipole) repulsions at high coverage through formation of hydrogen-bonding interactions with the surface and with neighboring water molecules. In contrast, acetone, which binds to oxides predominately through the lone pair electrons on the oxygen atom with opposing molecular dipoles, could not adapt to high coverages without destabilization. Acetone, in isolation, is bound more strongly to TiO_2 than water, but at high coverage acetone is susceptible to displacement from chemisorption sites due to repulsive intermolecular interactions. Another example of the inhibiting influence of water is found in the work of Hung and Marinas [1006]. These authors showed that increasing the RH both decreased the total TCE conversion and shifted the product distribution toward *more* chlorinated degradation products. This effectively decreased the efficiency of chlorocarbon degradation over TiO_2 by requiring additional redox processes for full mineralization.

Water layers located above TiO_2 surfaces can, by forming hydrogen-bonded networks in physisorbed situations, limit access of a reactant (such as O_2 [199]) to the TiO_2 surface. Fu and coworkers [1322] suggested that the tendency of water to form stable overlayers on TiO_2 at room temperature resulted in destabilization of many other adsorbates or limited their access to the surface. These influences could be partially alleviated by increasing the reaction temperature (to ~50–100 °C), which lowers the water coverage on the surface. (The opposite may be the case when water is a promoter [1312].)

6.3.2. Promoter

While the inhibiting role of water in TiO_2 photochemistry takes on one dimension (that of site blocking) [93], the promoting role of water is multidimensional [93,192–196,201,328,526,637,658,714,715,717,775,784,795,797,806,807,820,841,907,908,927,929,932,937,941, 942, 944–947, 962, 966, 971, 1004–1006, 1009, 1056, 1100, 1101, 1201,1312,1314,1315,1318,1324–1335]. For example, low coverages of water on TiO_2 have been shown to promote electron injection from excited dyes and sensitizers [637,658,1324], presumably by favorably modifying the electrostatics at the injection site. Water, as a solvent, can provide hydrogen-bonding networks that assist in: stabilizing surface species important in O_2 photoreduction [820], minimizing depletion of important surface species (such as O_2) that result from photodesorption [201], or stabilizing excited electrons in surface states [192–196]. Water has also been shown to promote selectivity changes in photooxidation of several organics on TiO_2, including trichloroethylene [1004,1006, 1315], toluene [947,1325], acetic acid [966], ethanol [717], triethylamine [784], and organophosphates and phosphonates [1056]. Many strongly bound reaction intermediates that tend to 'deactivate' photocatalytic reactions on TiO_2 surfaces (e.g., organic carboxylates) can be displaced or better chemically/photochemically processed with water present [93,717,941,1009,1056,1201,1326, 1327,1333]. For example, Fu and coworkers [93] proposed that water assisted in removing strongly bound Cl^- (as HCl) that accumulated on TiO_2 surfaces during photodegradation of chlorocarbons. High photooxidation rates can be sustained over longer periods of time with small partial pressures of water [932,946,1318]. Water can also assist in moderating and redistributing surface coverages of reactants, intermediates and products [714,962,971,1101].

Perhaps the most commonly attributed benefit of water to photochemical processes on TiO_2 is generating surface OH groups that can act as adsorption or reaction centers, or generating reactive radicals (such as OH• or OOH•) that open up indirect reaction pathways [328,775,932,937,942,944,945,1100,1311, 1313,1314,1325,1326,1328–1333]. The latter promoting attribute of water is well-known in the TiO_2 literature (see Fujishima, et al. [2]), but difficult to follow at the molecular-level. There is still much confusion as to whether OH• radicals are generated in reductive O_2 electron attachment processes (see Section 5.2.1) or via water/OH^- oxidative processes (see Section 8). The role of water/OH^- in providing surface binding sites has been more easily examined. For example, Ding and coworkers [1332] have shown that the photoactivity losses observed during transformation of high surface area A to low surface R have more to do with decreases in the availability of surface OH groups (i.e., surface area for OH groups) than in changes from one polymorph to another.

Finally, while much work has focused on the role of water as a reactant in chemical and photochemical reactions on TiO_2, researchers are also considering the role of water as a co-catalyst in processes on TiO_2. As a co-catalyst, water might participate directly in reactions, being consumed and reformed, or it might participate indirectly, for example through hydrogen-bonding interactions. It is clear from isotopic labeling studies on high surface area TiO_2 (such as that by Muggli and Falconer [841]) that the oxygen atom in water can be incorporated into the products and intermediates of a typical photooxidation reaction. However, the ability to differentiate between water as a reactant and as a co-catalyst is difficult on high surface area materials. Robbins and this author [929] showed that partial oxidation of propylene and isobutene on R TiO_2(110) required trace amounts of water on the surface in order for molecular oxygen to activate these molecules. Similarly, Wahab et al. [1335] proposed that water assisted O_2 in ring-opening reactions during the photooxidation of chlorobenzene on the A TiO_2(001), TiO_2(100) and TiO_2(010) surfaces. As discussed in Section 5.2.1, several scanning probe studies on the R TiO_2(110) surface have shown that water assists in moving protons and oxygen atoms along and across bridging oxygen rows, and aides in activating O_2 on the surface [526,795,797,806,807]. These studies all point to the need for

a deeper understanding of the roles of water in chemistry and photochemistry on TiO_2.

6.4. Oxide additives

TiO_2-containing mixed oxide and oxide–oxide interfacial systems have been extensively explored for their potential utility in promoting photocatalysis, particularly with visible light. An exhaustive list of oxides studied in conjunction with TiO_2 is not compiled here, but examples of the most popular systems are highlighted. The discussion in this section is organized according to the various common (surface) effects that oxides have in promoting/inhibiting photocatalysis on TiO_2. Often the influence of an oxide on TiO_2 photocatalysis is a combination of several effects [1336].

6.4.1. Physical effects

Thermal stability: Addition of an oxide to TiO_2 or preparation of TiO_2 particles supported on an oxide (for example, a mesoporous support) have been used to provide thermal stability to TiO_2. While photochemical reactions are not usually run at temperatures at which thermal instabilities in TiO_2 occur, preparation procedures for TiO_2 photocatalysts routinely require thermal treatments to crystallize or dehydrate the material. Two undesirable outcomes typically observed from thermal treatment are phase transformation and surface area loss (the latter also occurring during the former). Studies have shown that the A-to-R phase transformation can be inhibited by addition of SiO_2 [1337–1341], La_2O_3 [1342], ZrO_2 [1343–1347], ZnO [1348], WO_3 [142,1349], CeO_2 [1350] or SnO_2 [1351,1352]. Similarly, TiO_2 particle sintering can be limited by inclusion of SiO_2 [1339–1341], ZrO_2 [1343,1344,1353], CeO_2 [1350] or SnO_2 [1351,1352]. Both of these effects are linked to the ability of the supported oxides to inhibit formation of interfaces between TiO_2 particles that lead to surface area loss and sintering.

Oxide supports: Supporting TiO_2 on another oxide material provides opportunities for better TiO_2 dispersion, higher effective surface area and more uniform particle sizes. In most cases, enhanced dispersion is achieved by preparing TiO_2 supported on another oxide, but in some cases small amounts of an oxide added to (larger) TiO_2 particles can assist in minimizing TiO_2–TiO_2 interactions that lead to sintering [594,1354]. Typical oxide supports that promote TiO_2 particle dispersion include SiO_2 [594,1041,1332,1355–1362], ZrO_2 [1346,1347], Al_2O_3 [1355,1363–1365], ZnO [1366] and various zeolite supports [26,1367–1372]. Zeolites (for example) provide uniform pore structures that limit TiO_2 particle sizes. Similar confinement effects are achieved with mesoporous oxide supports. The chemical and structural interactions that promote TiO_2-support interactions are largely unexplored in the literature.

Site blocking: Oxides residing on a TiO_2 surface can block adsorption or reaction sites, effects generally thought of as detrimental to catalysis. Examples include inhibition of toluene photooxidation on TiO_2 by supported CeO_2 [571], and attenuation of N_2 and 2-propanol adsorption by supported Al_2O_3 or SiO_2 during photoreactions on TiO_2 [1373–1375]. In other cases, supported oxides have been reported to block sites on TiO_2 surfaces that are important in electron transfer processes [230,1376,1377].

6.4.2. Chemical effects

Oxide-on-oxide systems offer the potential for new reaction sites at the interfaces where the oxides meet. In heterogeneous photocatalysis, there is also the possibility that these interfacial sites could act as unique electron transfer sites. Numerous studies have shown that enhanced photocatalytic properties of TiO_2-supported oxides or oxide-supported TiO_2 can be linked to the creation of new adsorption and/or reactions sites not found on TiO_2 alone. This has been seen for a number of oxides supported on TiO_2, including: CuO for photoreduction of CO_2 [1287]; Al_2O_3 for benzophenone photooxidation [1378]; CaO for photocatalytic NO_x abatement [1379]; MgO for photooxidation of surfactants [1380,1381]; NiO for CO photooxidation [1382]; SiO_2 for dye photodegradation [1383], TCE photodecomposition [1384], toluene photooxidation [947], and 2-chloroethyl ethyl sulfide photodecomposition [1073]; and WO_3 for photooxidation of 2-propanol [1385], nitrophenol [1386] and ammonia [1387]. In many cases, the oxide- TiO_2 interface offers unique environments for the generation of OH groups that are more easily photooxidized (to radicals) [1388,1389]. In other cases, the presence of the supported oxide alters the acid–base properties of TiO_2 in the vicinity of the supported oxide [1298,1385,1390,1391]. For example, Noguchi et al. [1298] showed that alumina supported on TiO_2 resulted in a shift in the isoelectric point of TiO_2 to higher pH, which in turn altered the adsorption properties of different species from solution. These authors proposed that a judicious selection of an inert oxide on TiO_2 could provide a means of tuning surface charges without altering solution conditions.

Supported oxides that are more 'reducible' than TiO_2 can act as electron scavenging and storage sites, allowing photooxidation reactions to occur under conditions in which the electron scavenging half reaction is limited (e.g., by periodic changes in O_2 partial pressure or by site blocking). In this case, the supported oxide does not necessarily act as a co-catalyst (unless a mechanism is included for its regeneration) but more as a reactant. Examples included supported CuO [1392], WO_3 [1393–1397] and MoO_3 [1396]. In other cases, supported oxides can become dissolved into TiO_2 during heating, resulting in altered photocatalytic activities [1398–1403]. Beydoun and Amal [1398] found that heating TiO_2–Fe_3O_4 core–shell assemblies resulted in loss of TiO_2 surface area by sintering and diffusion of Fe into TiO_2, both of which diminished the photoactivity. Photochemical dissolution of the magnetite phase and e^-/h^+ pair recombination at the interface were also found to decrease photoactivity [1399,1400]. Fe_2O_3 on TiO_2 also exhibits interdiffusion of Fe into TiO_2 during heating which results in photochemical deactivation [1403].

6.4.3. Electronic effects

Heterojunctions: Supporting an oxide on TiO_2 (or *vice versa*) can also alter the electronic properties that influence charge carrier generation (see Section 1), separation and transfer. If the supported oxide is a semiconductor, then there is the potential for generation of a heterojunction at the oxide–oxide interface resulting in a band offset that promotes charge separation across the interface. This situation has been proposed for a variety of oxides on TiO_2, including: Cu_2O [1404–1408], CuO [1409–1411], ZnO [1412], WO_3 [143,1413–1418], SnO_2 [1351,1419–1427], RuO_2 [1428], CeO_2 [1429], and $SrTiO_3$ [1430]. Oxides with CB edges that are at lower potential than the electron trapping potential of TiO_2 can accept charge from TiO_2. As an example, Wang et al. [1413] used Kelvin probe force microscopy to show electron transfer between TiO_2 and WO_3. Fig. 6.10 shows topographical ('(a)') and potential ('(b)–(d)') images for a composite film mixture of WO_3 nanoparticles supported on a TiO_2 particle film. (The circle in each images provides the common reference point.) In the latter case, the contrast represents the variation in the surface contact potential, with dark features representing WO_3 particles at lower contact potential (greater local work function). Images in Fig. 6.10(b)–(d) represent a 'dark'–'light'–'dark' cycle showing a nearly uniform change in the overall surface potential resulting

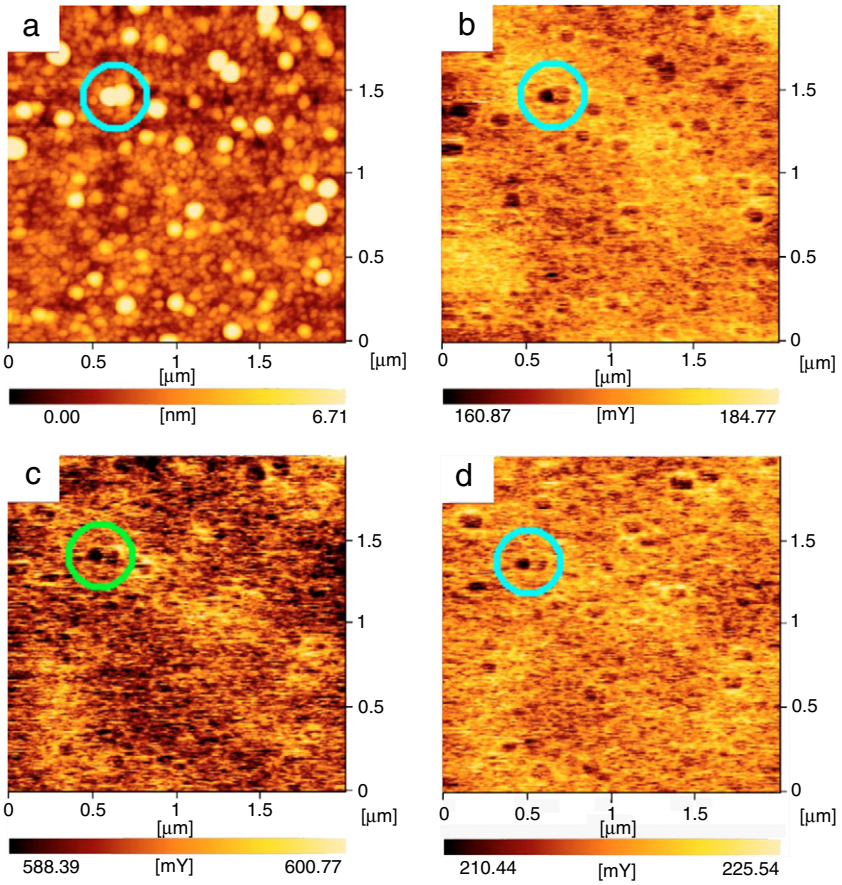

Fig. 6.10. Morphology (a) and surface potential (b–d) images of WO_3–TiO_2 nanocomposite films. (See text for image descriptions.)
Source: Reprinted with permission from Wang et al. [1413].

from UV irradiation (image 'c'). The magnitude of the change in a given region was ~0.4 eV, and represented electron accumulation on WO_3 particles and hole accumulation on TiO_2 regions. These data show evidence of UV-induced charge transfer between TiO_2 and WO_3. The charge transfer could be from either electron transfer from the TiO_2 CB to the WO_3 CB, or hole transfer from the WO_3 VB to the TiO_2 VB. Image 'd' shows that in the dark, the particle surfaces regain some, but not all, of their previous contrast pattern suggesting that long-lived charge traps were retained. Tuan et al. [1430] proposed a similar situation for epitaxial films of A TiO_2(001) grown on $SrTiO_3$(100). In contrast, other heterojunctions (such as the Cu_2O/TiO_2 system [1408]) promote hole accumulation on the supported oxide and electron accumulation on TiO_2. The CuO/TiO_2 system is an interesting case in which the flat-band potentials of each oxide would suggest that a heterojunction should not exist. However, Jin et al. [1409] proposed that electron transfer from TiO_2 to CuO occurred during photocatalytic water reduction due to charge build-up on CuO that shifted its CB edge to lower potentials. Similar effects might be expect in other oxide/TiO_2 systems where the band edge positions can be manipulated by controlling the interfacial structure and/or surface chemistry.

Interfacial states: Interfaces between oxides and TiO_2 provide situations for enhanced photocatalytic activity. For example, Hernandez-Alonso et al. [1431] found that binary mixtures of TiO_2 and ZrO_2 particles exhibited greater photocatalytic activity for photooxidation of acetone and methylcyclohexane than did solid solutions of similar amounts of the two oxides. This points to the interfaces between the oxide particles having a promoting influence not seen in a mixed suspensions of ZrO_2 and TiO_2. Similarly, Mn_2O_3 clusters on TiO_2 showed greater activity for dye photodegradation than did Mn^{4+}-doped TiO_2 [1432]. Oxide–TiO_2 interfaces also generate electronic states that pin the system's Fermi level [1433], or act as charge trapping and/or charge recombination sites [592,594,1350,1375,1434–1437]. For example, Li and coworkers [1435] found that low coverages of supported CuO on R TiO_2 nanoparticles promoted methylene blue photodecomposition but that larger loadings resulted in diminished activity (see Fig. 6.11). Based on EPR and XPS results, Li et al. attributed this behavior to trapping of electrons at interfacial TiO_2–CuO states associated with non-bulk-like CuO clusters. At higher loadings, these authors found that larger CuO particles blocked sites and contributed to charge recombination. Gesenhues [1375] found that Al_2O_3 particles embedded in the bulk of R particles had a more significant influence in hindering photodegradation of paint pigments than did the same amount of Al_2O_3 residing on the TiO_2 surface. Gesenhues proposed that Al_2O_3–TiO_2 interfaces acted as trapping and recombination sites, inhibiting the (undesirable) photochemistry in applications of TiO_2 as a white pigment. The structural origin of these interfacial traps and recombination centers in the Al_2O_3–TiO_2 system is unclear, however Sanchez-Agudo and coworkers [1438–1440] have shown that Ti–O bonds at the TiO_2–Al_2O_3 interface lose some of their covalence (i.e., the VB states at the interface lose some of their Ti 3d character) which likely influences the electronic character and stability of holes at those sites. Similar observations where seen for the TiO_2–MgO interface [1440], suggesting that the degree of ionic versus covalent character in TiO_2 can be manipulated in this way.

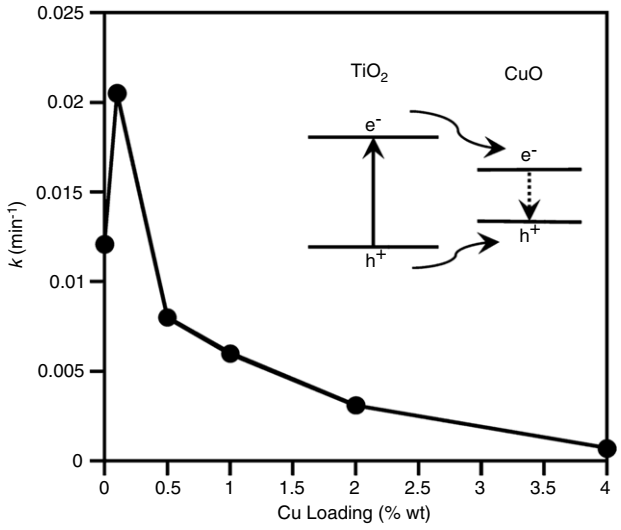

Fig. 6.11. Dependence on the first order rate constants (k) for methylene blue photodegradation over CuO–TiO_2 nanocomposites on the Cu loading. Inset: a schematic diagram showing the photoinduced charge separation between TiO_2 and CuO.
Source: Reprinted with permission from Li et al. [1435].
© 2008, American Chemical Society.

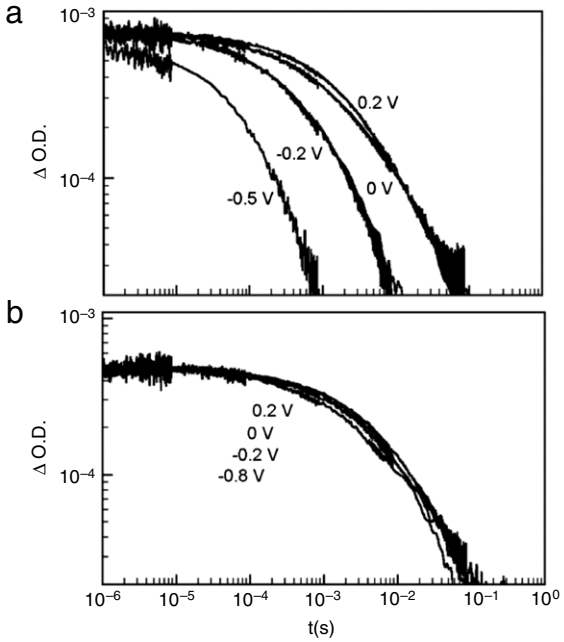

Fig. 6.12. Transient absorption signals for the $RyL_2(NCS)_2$ dye cation as a function of bias voltage after electron injection into nanocrystalline TiO_2 films (a) without and (b) with Al_2O_3 coatings.
Source: Reprinted with permission from Fabregat-Santiago et al. [1441].
© 2004, American Institute of Physics.

Oxide overlayers on TiO_2 have been shown to promote electron injection yields in DSSC applications by removing surface trap sites that confine the injected electron in the vicinity of the ionized dye and/or by providing an electronic barrier to back-electron transfer. This condition has been achieved with thin films of Al_2O_3 [1441–1445], SiO_2 [1445], NiO [698,1446,1447], ZrO_2 [1445] and ZnO [1448–1450] on TiO_2. Fabregat-Santiago et al. [1441] found that a thin coating of Al_2O_3 on TiO_2 increased the photocurrent yield in DSSC by decreasing the back-electron transfer rates by a factor of 3–4. The upper panel of Fig. 6.12 shows that reduction of the ionized dye on a TiO_2 film was accelerated at negative potentials (as revealed by the rapid decay of the dye cation's transient absorption signal), whereas no applied potential dependence was observed in the Al_2O_3-coated reflective of the absence of back-electron transfer. In contrast, while other groups have found that ZnO films promote charge transport in TiO_2 [1448, 1449], Park et al. [1450] found that a thin ZnO shell on a TiO_2 core significantly inhibited particle-to-particle electron transfer, thus limiting the DSSC photocurrent.

6.5. Metal cations

Metal cation doping of TiO_2 for photocatalytic applications has been extensively explored in the literature. Many papers that deal with metal cation doping focus on manipulating the optical absorption behavior of TiO_2 instead of on altering the surface properties of TiO_2. While issues associated with the former mostly involve studies of bulk doping (see Section 1), this section examines how metal cations adsorbed on the TiO_2 surface alter its photocatalytic properties. Significant challenges associated with surface modification of TiO_2 by metal cations are in determining where the metal cation resides on the surface, what are its possible oxidation states and coordination environments, and how do these properties influence (enhance or diminish) the photocatalytic properties of TiO_2. In many 'doping' studies, the metal cation is incorporated in the TiO_2 lattice during a sol–gel (or similar preparatory) stage. Because such preparation methods typically result in both surface and bulk modifications of TiO_2, it can be difficult to distinguish between bulk and surface effects. For simplicity, discussion here will focus on metal cation additives that reside, because of the preparation method, preferentially on the surface of TiO_2. The aim of this distinction is to attempt to draw a correlation between the physical and chemical properties of 'surface-doped' TiO_2 and their photocatalytic activities. Instead of focusing on various metal-doped systems (such as was done in Section 6.1 for noble metals), this section identifies various phenomena associated with the influence of surface cations on TiO_2.

New active sites: An obvious effect of metal cations added to the surface of TiO_2 is the generation of new active sites. Examples include TiO_2 surfaces modified with: Cu^+/Cu^{2+} [1031,1145,1451–1454]; Fe^{3+} [1455]; Zn^{2+} [1456]; V^{5+} [1031]; and Cr^{3+} [1031]. Yamashita and coworkers [1454] suggested that isolated surface Cu^+ sites on TiO_2 assisted in methanol formation during CO_2 photoreduction. Surface Fe^{3+} cations enhanced maleic acid photooxidation [1455] by generating new adsorption sites. Wu and Cheng [1031] observed that adsorbed metal cations (Cu, V or Cr) acted as adsorption sites for NO and promoted NO photooxidation over TiO_2. In general, these examples do not show clear distinctions between the metal cations acting as typical catalytic enhancers versus acting as surfaces sites that promote electron transfer.

Site blocking: In contrast to metal cations acting as adsorption sites, other studies show examples of site blocking by adsorbed metal cations. For example, Mu et al. [1457] observed that adsorbed Mn^{2+} cations on TiO_2 blocked adsorption sites needed for dye photodegradation. Similarly, surface Fe^{3+} cations inhibited ethanol photooxidation on TiO_2 by blocking adsorption sites [1458]. Adsorbed Al^{3+} cations diminished the build-up of strongly bound surface intermediates that inhibited salicylic acid photodecomposition on TiO_2 [1459]. In a slightly different sense, addition of Fe^{3+} to the surface of A was shown to inhibit formation of surface sites that can initiating the A-to-R phase transformation [1458].

Charge separation, recombination and/or transfer: Metal cations adsorbed on a TiO_2 surface can act as sites at which charge carriers are separated and/or trapped, as sites where charges recombine, or as sites where electron transfer is enhanced. For example, Murakami

et al. [1460] found that certain transition metal cations (Fe^{3+}, Cu^{2+}, Ni^{2+} and Cr^{3+}) on TiO_2 acted as electron acceptors from the TiO_2 CB, promoting charge carrier separation and efficient photooxidation. In some cases, the ability of adsorbed metal cations to scavenge CB electrons had a negative effect on O_2 photoreduction, particularly when the reaction products of O_2 photoreduction were needed to promote indirect oxidation processes [230,1288,1461]. Adsorbed cations have been shown to inhibit back-electron transfer in DSSC situations [1324,1462,1463]. The presence of cationic species (e.g., Mg^{2+}, Li^+, Na^+ and K^+) at the surface of TiO_2 stabilized I^- at or near the surface, enhancing its rate of oxidation (by a photoionized dye) in DSSC applications [1463]. In other cases, adsorbed surface cations enhanced charge recombination [1464].

Modified surface electrostatics and potentials: Adsorbed metal cations can also alter the electrostatics at the surface that promote or inhibit electron transfer processes. For example, Pelet et al. [1463] showed that oxidation of I^- (and formation of I_2^-) were facilitated on the TiO_2 surface with alkali promoters that reversed the surface charge from negative to positive. This change allowed I^- adsorption and oxidation (in this case by a dye cation). Similarly, Nakade et al. [694] used adsorbed Li^+ to enhance the I^-/I_3^- redox couple reaction through modification of the surface potential. Sakaguchi and coworkers [904] found that the degree of enhancement in acetone photooxidation on TiO_2 by 3+ lanthanides (Yb^{3+}, Eu^{3+}, Sm^{3+} and Ce^{3+}) tracked the ionic radius of the metal ion, suggesting their role was electrostatic in nature.

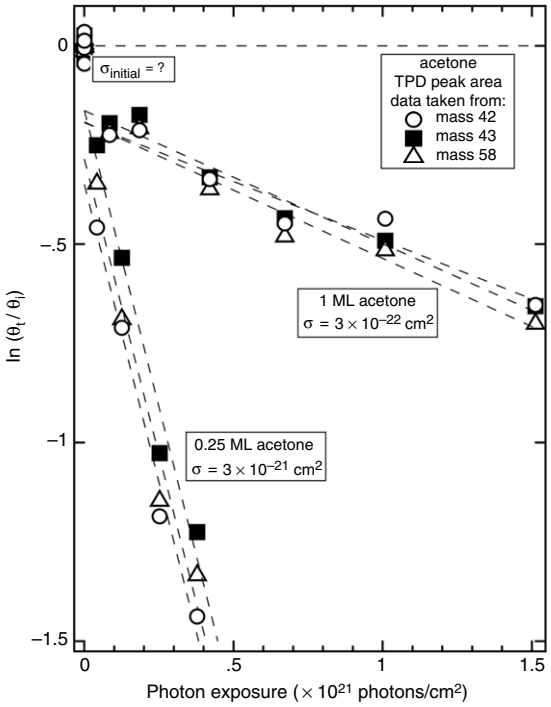

Fig. 6.13. Acetone photodecomposition cross section measurements for UV photodecomposition of two initial acetone coverages on R TiO_2(110).
Source: Reprinted with permission from Henderson [701].
© 2005, American Chemical Society.

6.6. Miscellaneous poisons and promoters

6.6.1. Self-poisoning

In many heterogeneous photocatalysis applications, both redox processes are required to occur on the same catalyst, necessitating establishment of a balance between the various oxidation and reduction reactions in order for the overall process to occur. However, if one reactant (e.g., an organic) binds strongly and covers the TiO_2 surface, access of another reactant (e.g., oxygen) to the surface may be limited. In this sense, some reactants may 'self-poison' their own photocatalytic degradation. This has been seen for numerous reactants, such as: acetone [701], trimethyl acetate [515,543], trichloroethylene [718], ethanol [841], acetaldehyde [841], various phosphates and organophosphorus compounds [719,1053,1056], styrene [1465], and N_2O [705]. This author [701] observed a 10 fold decrease in the rate of acetone photodecomposition to acetate on R TiO_2(110) when the initial acetone coverage was increased from 0.25 ML to a full 1 ML coverage (Fig. 6.13). This self-inhibition in the rate of acetone photodecomposition was due to the inability of O_2 to gain access to the acetone-covered surface.

6.6.2. Reaction product/intermediate poisoning

Because each electron transfer step in an overall, multi-electron electron transfer photocatalytic reaction is unique, the intermediate products of one step might act to inhibit the kinetics of another (for example, by site blocking). Water, as a photoproduct of many oxidation and reduction reactions, may have such an influence based on discussion in Section 6.3. Reaction conditions targeted to enhance a particular electron transfer process (e.g., one requiring direct hole transfer) in an overall reaction might backfire when it comes to a subsequent step that required a different reaction process, resulting in build-up of a more strongly bound, less reactive surface intermediate. Insights into photochemical competition between reactants and intermediates can be obtain by comparing relative reactivities of binary reactant mixtures, such as has been done by Lichtin and coworkers [1466]. Conversely, one can identify the various key reaction steps and the inhibiting intermediates/products for a particular reactant and then 'redesign' conditions for overall efficiency. More common are cases in which an intermediate from a particular reactant acts as an inhibitor. Examples including: acetate or condensation products from acetone: [701,1020], acetaldehyde from ethanol [890,893], benzaldehyde, benzoate and other aromatics from toluene [941–943,946,947,1318], acetone from isopropanol or propane [903,927], acetate from catechol or resorcinol [1467], sulfates/sulfites from sulfides or organosulfides [1067,1074,1082], and halides or halocarbon fragments from halocarbons [718,1006,1008,1009,1015]. Similarly, in systems in which a co-catalyst is employed, build-up of a strongly bound intermediate on the co-catalyst might have adverse effects on the overall reaction process. Perhaps a classic example of this effect is the saturation of a noble metal co-catalyst surface with CO [955,1276,1277,1284,1468]. As an example, Bowker's group [1276,1277] has shown that CO build-up on Pd particles on TiO_2 can inhibit photocatalytic rates of methanol reforming to H_2.

6.6.3. Oxyanions

Oxyanions such as sulfate, phosphate, nitrate and carbonate can bind strongly to TiO_2 surfaces, initiating a variety of effects that include site blocking, modification of surface electrostatics, stabilization of high surface areas, and formation of new adsorption sites or charge trapping sites. These effects can conflict with each other rendering net promotion in some cases and inhibition in others. Numerous studies have shown inhibited photocatalytic performance on TiO_2 with surface oxyanions, such as nitrate [1469–1472], carbonate [1067,1313,1314,1470,1473], sulfate [1067,1078,1316,1470–1472,1474], and phosphate [1291,1470–1472]. For example, Chen and coworkers [1470] found that surface oxyanions competed with dichloroethane for adsorption sites during photooxidation of this molecule on TiO_2. Cao et al. [1473] found that strongly bound carbonates reduced the photoactivity of TiO_2 for phenol photooxidation, especially when the TiO_2 photo-

catalyst was prepared from sol gels under basic conditions where more OH groups were present. In some cases, the inhibiting effect of surface oxyanions can be reduced by washing the photocatalyst [1078,1472], which shows that these species are easily hydrated and removed from the surface.

In contrast, other groups have shown that under certain conditions surface phosphate [1475–1477] or sulfate [1474,1475, 1478–1485] can promote photocatalytic reactions. Nakajima and coworkers [1480] proposed that adsorbed sulfate diminished the binding strength of certain adsorbates on TiO_2, amounting to a promotion effect when strongly bound intermediates (such as seen in the toluene photooxidation process) were destabilized. Similarly, Wu et al. [1475] found that adsorbed phosphate and sulfate on TiO_2 surfaces with supported Pt nanoparticles decreased the formation of CO (which poisons Pt) during methanol photocatalytic reforming without diminishing the amount of H_2 formed. Muggli and coworkers [1481] suggested that the promoting role of sulfating TiO_2 was mostly due to preservation of high surface area TiO_2 during thermal pretreatment. A similar feat was ascribed to surface phosphates [1476,1477]. Colon et al. [1482, 1483] suggested that sulfating TiO_2 chemically generated reactive centers on the surface not present without sulfating, but that sulfate did not remain on the surface. Similarly, Wang et al. [1485] proposed that sulfate treatment increased the concentration of highly acidic surface sites. Other groups have proposed that surface sulfate acts as an electron trap, facilitating charge separation [1479, 1484].

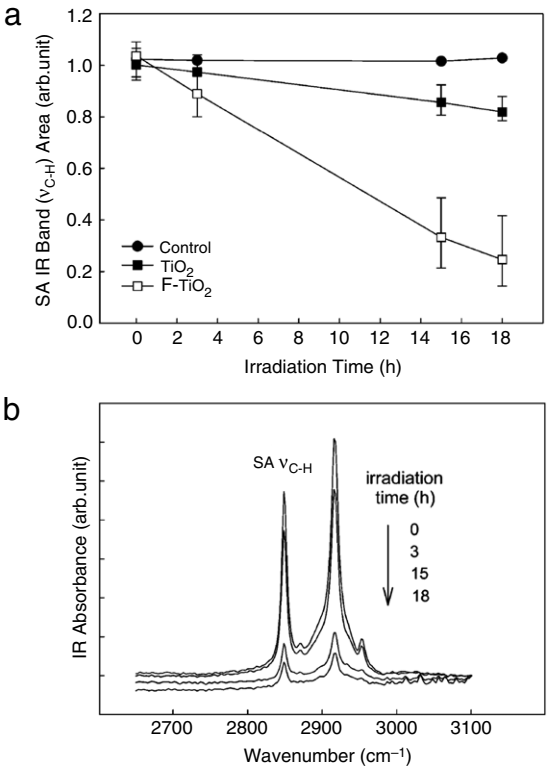

Fig. 6.14. 'Remote' photooxidation of stearic acid (adsorbed on a glass slide) from UV irradiation of TiO_2 and fluorinated TiO_2 films. Bottom: changes in the ν (C–H) region from FTIR for the stearic acid film during irradiation of F-doped TiO_2 remotely located (see text). Top: Comparison of the rate of ν (C–H) intensity for three different irradiation samples.
Source: Reprinted with permission from Park and Choi [743].

6.6.4. Halides

Despite the large volume of work in the literature on the photodegradation of chlorinated hydrocarbons, the most intensely studied halogen in terms of its modifying effects on TiO_2 photochemistry is that of fluorine. Fluorination of TiO_2 surfaces is generally believed to substitute surface OH groups with F [725,739, 1486–1488]. In agreement with this assertion, Tang et al. [1489] have shown that surface fluorination did not significantly alter the bulk structure or optical properties of TiO_2, but increased its surface acidity, which in turn enhanced the binding of polar molecules to the surface. Other groups have also shown that surface fluorination strongly affects adsorption processes [1490, 1491]. However, the main influence of surface fluorination may be in how it influences OH• production. Park and Choi [353] suggested that surface fluorination enhanced photochemical processes that rely on OH• attack, but inhibited those that rely solely on direct hole-mediated electron transfer chemistry. This conclusion is also held by other groups [739,1487,1488]. Park and Choi [743] showed that the 'remote' photooxidation (see Section 5.1.1) of stearic acids was enhanced by surface fluorination of TiO_2. Fig. 6.14(a) and (b) shows changes in the FTIR of stearic acid adsorbed on a glass slide spatially separated by ~30 μm from an irradiated TiO_2 sample. Little change was observed for undoped TiO_2, but significant stearic acid decomposition was observed when the TiO_2 sample was surface-doped with fluoride. This observation supports the notion that surface fluorination lowers the barrier to formation and/or emission of reactive radicals from TiO_2 surfaces. Many groups suspect that hydrogen peroxide is a key species in remote photooxidation on TiO_2. This species is formed in the electron-mediated half reactions of O_2. Maurino et al. [1486] have shown that surface fluorination of TiO_2 promoted photochemical production of hydrogen peroxide, the production rate of which was proportional to the surface Ti–F coverage. Mrowetz and Selli [1492] also observed enhanced hydrogen peroxide photoyields on fluorinated TiO_2.

Studies on the surface modification of TiO_2 by other halides are less abundant. There are inconclusive results on the effect of surface Cl on photooxidation reactions, exhibiting either an inhibiting influence on surface photooxidation reactions or no influence at all [1296,1302,1472,1493–1495]. d'Hennezel and Ollis [1494] have shown that surface chlorination enhanced the overall photooxidation of toluene and hexane, had no effect on 1-butanol, and inhibited acetone photooxidation. This diverse behavior points to selective effects by adsorbed Cl^- on specific reactants and intermediates. Horikoshi et al. [1495] pointed out that of the halides, only surface bromide had an effect on the photooxidation of phenol, diminishing the reaction rated by a factor of three. These authors attributed to influence of Br^- to either site blocking or charge scavenging. Surface Br^- and I^- have also been shown to inhibit surfactant photodegradation on TiO_2 [1496]. The source of this effect in the I^- case may be its ability to readily scavenge VB holes [725].

6.6.5. Sensitizers

Molecular or semiconductor sensitizers are generally used with TiO_2 in photovoltaic applications or in photoelectrochemical situations in which electrons are shuttled through TiO_2 to a counter electrode where desired chemical conversions take place (i.e., away from the TiO_2 surface). (As an example, see work of Treadway et al. [1497] who used Ru(II)-based chromophores anchored to a TiO_2-coated anode to promote 2-propanol conversion to acetone at the photooxidized Ru center and water reduction at a Pt counter electrode.) There are instances in which sensitizers have been used to promote photocatalysis on TiO_2. Examples include use of metal sulfide heterojunctions [341, 926,1498–1511] and molecular dyes [1013,1512,1513] that, on

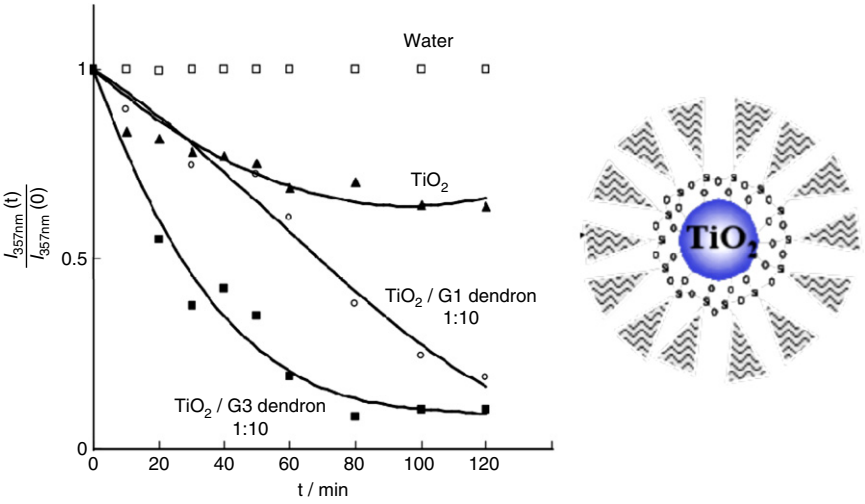

Fig. 6.15. Left: comparison of the photodegradation rates of 2,4-dichlorophenoxyacetic acid (2,4-DPA) on bare TiO_2 nanoparticles (triangles) and those protected by poly(amido amine) dendrimers (open circles and filled squares). Right: illustration of a dendrimer-covered TiO_2 nanoparticle.
Source: Adapted from Nakanishi and Imae [1514].

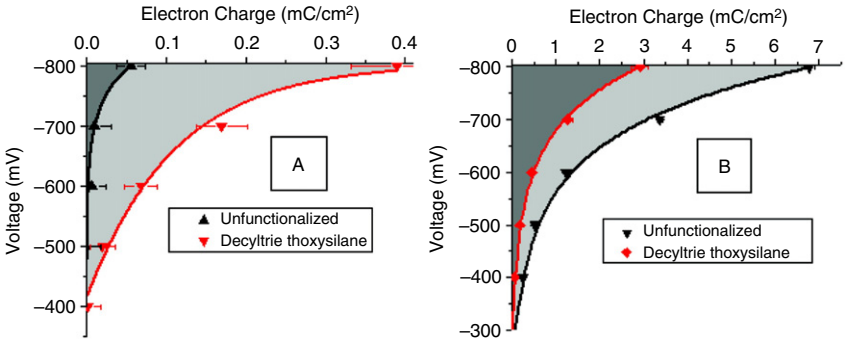

Fig. 6.16. Shifts in the unoccupied CB DOS (expressed as electron charge versus potential) for nanocrystalline A TiO_2 resulting from surface functionalization with decyltriethoxysilane in (A) 0.1 M $TBAClO_4$ acetonitrile electrolyte, and (B) 0.1 M $LiClO_4$ acetonitrile electrolyte.
Source: Reprinted with permission from Morris and Meyer [1515].

excitation, inject electrons into the TiO_2 CB for photoreduction reactions.

6.6.6. Surface functionalizers

Generating TiO_2 nanoparticles with well-defined particles sizes, and keeping suspensions of these from agglomerating, can be challenging. Several groups have discovered that surface functionalization can assist in this effort. For example, Nakanishi and Imae [1514] discovered that siloxyl-terminated dendrons, when adsorbed on TiO_2, prevented nanoparticles from agglomerating by forming a protective sphere around the particle that limited approach of other particles (see cartoon in Fig. 6.15). The degree of agglomeration inversely varied with the degree of branching in the dendron, but no inhibition of reactant molecules access to the TiO_2 surface was detected. This is shown in Fig. 6.15 for the photooxidation of 2,4-dichlorophenoxyacetic acid on bare TiO_2 and on TiO_2 modified with single-branched (G1) and triple-branched (G3) dendrons. Greater activity, as a result of more limited particle agglomeration, was observed with more branched dendrons. Also, dendron photooxidation was not observed, which might be linked to the stability of the TiO_2–siloxyl linkage. Similar results were achieved by Satoh et al. [124] for TiO_2 nanoparticles below 2 nm in size. In contrast, Egerton et al. [1374] found that while adsorbed stearate was used to stabilize TiO_2 in suspension, it also inhibited the photodecomposition of 2-propanol, presumably because it blocked access of molecules to the surface. Surface functionalization can also be used to tune the potential and DOS of electron acceptor states in DSSC applications, as shown by changes in the charge injection yields for the cases of decyltriethoxysilane-modified TiO_2 films in two different electrolyte solutions from the work of Morris and Meyer [1515] (Fig. 6.16). These authors proposed that functionalization of the TiO_2 surface could be used to shift the CB DOS and thus influencing electron injection yields.

6.6.7. Carbon nanotubes

Carbon nanotubes, nanofibers and composites have been used by groups as supports to promote dispersion of TiO_2. For example, see work of Fu et al. [1516] who used carbon fibers to minimize TiO_2 nanoparticle agglomeration. Carbon nanotubes, in particular, offer high surface areas, structurally uniform surfaces and high thermal stabilities in comparison with other forms of carbon. While the attachment chemistry is not well-understood, several groups have shown that carbon nanotubes can be used to effectively disperse TiO_2 nanoparticles [1517–1521].

7. Phase and form

The terms ‘phase’ and ‘form’ were chosen for this section to illustrate the diverse ways in which surface structure can influence TiO_2 photocatalysis. The terms ‘phase’ and ‘form’ tend to have large scale connotations, but they both have significant implications for

the local (atomic) physical and electronic structures that are the 'standard' ways in which surface scientists think about surface structure. Phase refers to the crystallographic uniqueness of the TiO_2 surface, spanning a spectrum from amorphous to highly crystalline A and R. Form refers to the state a particular phase might be in (e.g., a nanoparticle, a structural domain in a thin film or a macroscopically large single crystal). TiO_2 surfaces are rich in structural variations that directly impact chemistry and photochemistry. The richness in structure is seen both in the arrangement of atoms ('physical' structure) and the distribution of states ('electronic' structure). Emerging expertise in the design of TiO_2 surface structures aims at optimizing the physical and electronic structures for optimal photocatalytic performance.

7.1. Phase

7.1.1. Crystalline versus amorphous

The degree of surface crystallinity has a significant influence on TiO_2 photocatalytic activity in materials such as nanoparticles, thin films, mesoporous networks, nanotubes and rods, and sol gels [112,369,398,595,600,693,1522–1542]. The correlation between photoactivity and crystallinity is particularly relevant in A nanoparticles because this is the low temperature phase of TiO_2. Poorly crystallized A materials are routinely annealed to improve crystallinity (and hence photocatalytic performance). Angelomé et al. [1523] observed that the extent of salicylic acid photodegradation on mesoporous A varied with crystallinity based on Ti K-edge X-ray absorption near-edge structure (XANES) measurements. Fig. 7.1 shows changes in the Ti K-edge XANES leading edge for 150 nm thick films of A grown on ITO (a) and Si (b) substrates. As the films were annealed to higher temperatures, the A XANES profile sharpened. Intensity at the leading edge feature (at ~4968 eV), which is most reflective of Ti in an octahedral field, was used to gauge crystallinity. In Fig. 7.2, Angelome and coworkers [1523] showed that the extent of salicylate photodecomposition ("PD%") scaled with the fraction of crystallized A present. (Their data also show that "crystallized" A on silicon performed better than that on indium tin oxide.) Similar conclusions about the importance of surface crystallinity have been reached by others. Grela and Colussi [398] observed a 10 fold increase in the quantum yield of the first step of nitrophenol photodegradation with highly crystallized TiO_2 over that of poorly crystallized sols. Colbeau-Justin et al. [112] observed longer carrier lifetimes with improved crystallinity of A. In the context of dye sensitized TiO_2, Martini et al. [693] observed that the forward/reverse electron transfer rates from/to anthracene carboxylic acid dyes on TiO_2 nanoparticles were faster in crystalline A than in amorphous TiO_2. These authors attributed the fast rates to the greater efficiency of electronic coupling between the dye's excited state or ionic state and acceptor/donor states in TiO_2.

The improvement of photocatalytic performance with increased crystallinity is generally attributed to the removal of dangling bonds and distorted lattice structures that act as charge trapping and/or recombination sites. The role of surface versus bulk crystallinity has not been explored primarily because it is difficult to differentiate between the two in typical TiO_2 materials. Because surfaces possess dangling bonds and readily restructure relative to the ideal bulk structures, it is not unreasonable to expect that the structural quality of a TiO_2 surface should play a major role in influencing surface charge carrier stabilities. Determining the impact of surface crystallinity on photoactivity is also complicated by other phenomena. For example, Vorontsov et al. [1538] have shown that increased crystallinity can also be accompanied by the adverse effects of the losses of surface OH coverage and total surface area. Purely amorphous TiO_2 is photo-inactive irrespective of its surface OH population or surface area [600]. In mixed polymorph systems (see below), the ratio of phases and how they interact can also offset the positive influences of improved crystallinity. The risks associated with achieving higher crystallinity in TiO_2 nanoparticles are the loss of surface area (due to sintering) and (in the A case) phase transition.

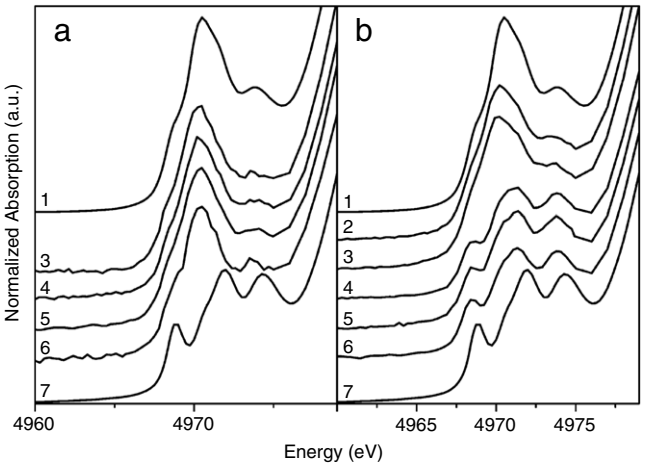

Fig. 7.1. Ti K-edge XANES spectra from mesoporous TiO_2 films deposited on (a) ITO and (b) Si substrates. Spectra labeled '1' and '7' are for amorphous-like and crystalline A TiO_2, respectively, and those labeled '2–6' correspond to thermal transitions between the two end points resulting from annealing in air at 250, 300, 350, 400 and 450 °C, respectively.
Source: Reprinted with permission from Angelome et al. [1523].

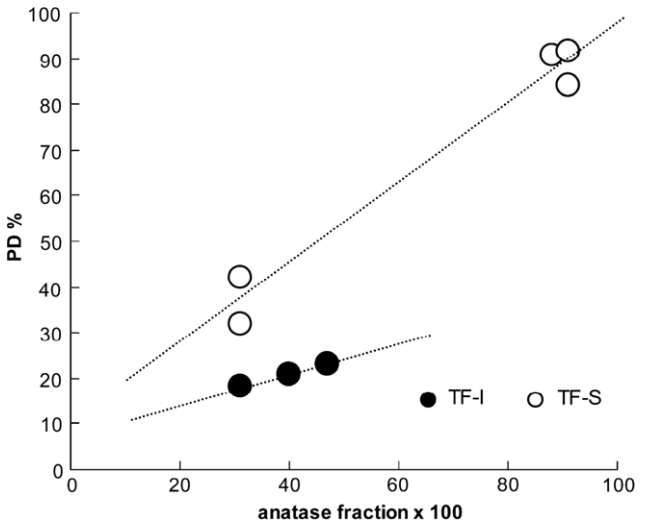

Fig. 7.2. Correlation between the extent of salicylate photodegradation ('PD%') and the crystallinity of mesoporous A TiO_2 films (expressed as a fraction relative to the content of amorphous TiO_2 present) deposited on ITO (filled circles) and Si (open circles) substrates.
Source: Reprinted with permission from Angelome et al. [1523].

7.1.2. Anatase versus rutile

A common perception in the TiO_2 photocatalysis literature is that the A phase is inherently more photoactive than the R phase. There are three issues to consider in such comparisons: (1) how the respective bulks of A and R respond to light absorption and charge transport, (2) how the surfaces of A and R respond to charge trapping and transfer, and (3) how the surfaces of A and R respond

chemically to the adsorbates involved (directly or indirectly) in electron transfer reactions. The first of these issues relates to the differences in the solid state properties of the two polymorphs, and the latter two have more to do with the surface properties of the many different facets of A and R. While this review focuses on the surfaces of TiO_2, it is important to consider how the bulk properties of these two polymorphs may influence heterogeneous photocatalysis. (As discussions in Sections 1 and 2 show, the photoabsorption properties and charge carrier dynamics of A and R differ from each other.) Aside from the bulk structure (which impacts surface structure), the most common difference between A and R is their optical bandgap. Kavan et al. [116] point out that the difference between the 3.2 eV bandgap of A and the 3.0 eV bandgap of R lies mainly in the position of the CB edge, the edge for A being ~0.2 eV higher than that of R.

One area in which the surfaces of A and R significantly differ from each other is in terms of their relative surface reducibilities. While this quality may not seem directly relevant to photocatalysis, the ability of a TiO_2 surface to stabilize a redox change impacts how it responds to charge carriers that arrive there during photocatalysis. The reducibilities of A, R and P-25 were explored by Komaguchi et al. [186] using vacuum annealing and reaction with H_2 at 773 K, followed by quantification and characterization of the resulting surface Ti^{3+} profiles at 77 K with EPR. The authors' EPR data showed that R was more easily reduced (with H_2 or vacuum annealing) than A, irrespective of whether it existed as separate phase or in the mixed-phase P-25. For example, the authors observed Ti^{3+} signals for R heated in vacuum at 673 K whereas no evidence for surface or bulk reduction was detected for A with similar treatments. (As will be discussed below, the R component in P-25 is believed to accommodate excited electrons more readily than the A component.) Exposure of reduced P-25 to air resulted in preferential oxidation of Ti^{3+} groups in R, presumably located at the surface, whereas Ti^{3+} groups in A, when formed, were not removed by air exposure suggesting subsurface reduction centers. The relative ease with which A and R single crystal surfaces are reduced (see [175, 1543]) provides additional insights into how specific surface orientations of each polymorph respond to the effective 'reductive' or 'oxidative' conditions associated with charge carrier trapping and transfer at their surfaces. Although considerably more work exists in the literature on single crystal surfaces of R than A, the available studies on both suggest that R surfaces are considerably easier to vacuum reduce than are A surfaces [175].

The perception that A is the more photocatalytically active polymorph of TiO_2 often results from the greater stability of A as high surface area nanoparticles. As Addamo et al. [1544] have pointed out, it is difficult to accurately compare different polymorphs of TiO_2 due to surface area differences and lack of knowledge regarding what fraction of a nanoparticle's surface is active. Recently, new preparation methods that generate R nanoparticles with sizes less than 10 nm have allowed direct comparisons of A and R nanoparticles with comparable surface areas. Numerous studies show that R nanoparticles with sizes similar to those of A nanoparticles have comparable or even greater photoactivities [1157,1330,1478,1542,1545–1552]. For example, Sun and coworkers [1330] showed that the activity of 7 nm sized R nanoparticles was greater than that of comparable A nanoparticles for phenol photodegradation, an observation they linked to a greater population of OH groups on the former. Ohno and coworkers [1157] showed that similar photoactivities for A and R held for large particles. They found that R particles of micron size were more efficient at separating charge between crystal faces than was seen with comparably sized A particles. This was attributed to the emerging contribution of the (110) faces for larger R particles. Other authors [1542] have shown that the normalized photoactivities of R nanoparticles depends on the particle size, increasing with decreasing size.

Table 7.1
Calculated surface free energies γ and surface tensions σ (J/m^2) of prominent facets on clean, partially hydrogenated and fully hydrogenated TiO_2 nanoparticles. Top: anatase; bottom: rutile. © 2004, by the American Physical Society.
Source: Reprinted with permission from Barnard and Zapol [1553].

Surface	Clean		Partial		Full	
	γ	σ	γ	σ	γ	σ
(001)	0.51	2.07	0.86	0.50	0.84	0.91
(100)	0.39	0.60	0.55	0.23	0.65	−0.19
(101)	0.35	0.51	0.51	0.71	0.63	0.09
(100)	0.60	0.95	0.71	0.66	1.82	0.80
(110)	0.47	1.25	0.56	1.96	0.84	1.27
(011)	0.95	1.50	1.02	0.39	1.19	1.38

The interplay between the degree of hydration or hydroxylation and particle size is important in influencing what crystal faces of A and R are available. Barnard and Zapol [1553] examined the phase stability of A and R as a function of particle size and degree of hydroxylation using DFT. These authors calculated the total surface free energies and surface tensions of A and R nanoparticles as a function of size and shape for "clean", and for partially and fully "hydrogenated" facets. The partial case pertained to all under-coordinated O sites capped with H atoms, while the fully hydrogenated case also had all under-coordinated Ti sites capped with H atoms. (These conditions, in effect, provide a coarse assessment of the surface stability as a function of H atom reduction.) As shown in Table 7.1, the surface free energies of the major facets of A and R revealed that the A TiO_2(101) and R TiO_2(110) facets were the most stable. However, the relative stabilities changed as the extent of hydrogenation increased, resulting in the illustrative particle shape changes shown by the Wulff constructions in Fig. 7.3. Barnard and Zapol also found that extensive hydrogenation induced shape changes in R nanoparticles that decreased the {110} facet contributions relative to that of the {101} facets. Virtually no such change was seen in A. The crossover points in relative stabilities of partially and fully hydrogenated A and R are shown in Fig. 7.4. Clean (not shown) and partially hydrogenated (top) A particles were more stable than comparably sized R particles below ~9 nm, but the crossover point for fully hydrogenated A and R was at a much larger size (23 nm). These data suggest that large R particles (>10 nm) are better suited for stabilizing reduction than are A particles of comparable size.

Observations of comparable reactivities on A and R nanoparticles point to a greater need for understanding how issues such as morphology [1525,1554], surface structure and surface chemistry [290,542], the properties of the target molecule [1555] and the overall mechanistic details of a photocatalytic reaction [928, 1545,1552] come into play when comparing the inherent photoreactivities of A and R. Along this line, Andersson et al. [1545] found that the initial rate of phenol photodegradation was greater on suspended R nanoparticles than on equivalently sized A nanoparticles, but sustained rates were greater for A because strongly bound intermediates tended to diminish the photoactivity of R nanoparticles.

Much of the difficulty encountered in comparing the photoactivities of A and R nanoparticles lies in not being able to perform direct site-to-site comparisons. Single crystal A surfaces are not (currently) commercially available, which make direct comparisons with data from R single crystals difficult. In the first direct comparison of photoactivity on A and R single crystal surfaces under UHV conditions, Ohsawa et al. [290,542] observed comparable photodecomposition rates of TMA on a per-molecule basis for A TiO_2(001) and R TiO_2(110). Fig. 7.5 shows the evolution of CO_2 from hole-mediated photodecomposition of TMA on a 30 nm thick

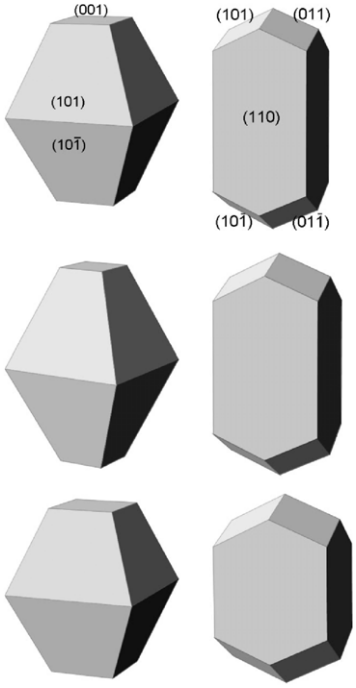

Fig. 7.3. Wulff constructions for clean (top), partially hydrogenated (center), and fully hydrogenated (bottom) anatase (left) and rutile (right) calculated using the surface free energies listed in Table 7.1.
Source: Reprinted with permission from Barnard and Zapol [1553].
© 2004, by the American Physical Society.

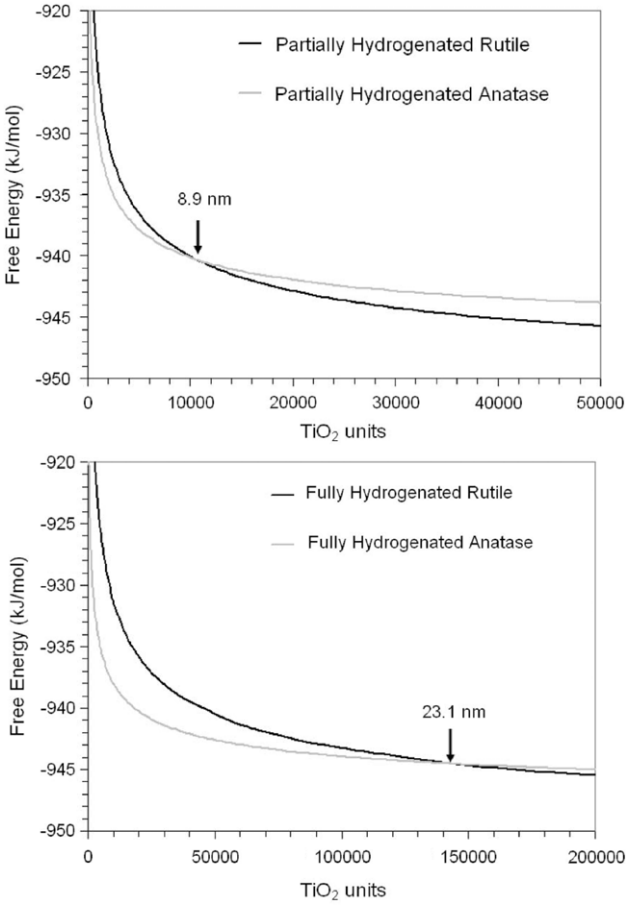

Fig. 7.4. Free energy as a function of the number of TiO_2 units for anatase and rutile (calculated using the shapes in Fig. 7.3, and the γ and σ values from Table 7.1) for partially hydrogenated (top) and fully hydrogenated surfaces (bottom). Intersections indicate the particle sizes (expressed as particle diameter for A) at which the phase transition is expected.
Source: Reprinted with permission from Barnard and Zapol [1553].
© 2004, by the American Physical Society.

film of epitaxial A TiO_2(001) grown on Nb-doped $SrTiO_3$(100) and a comparable homoepitaxial R TiO_2(110) film grown on R TiO_2(110). (The A film thickness precluded significant contribution from light absorption by the $SrTiO_3$ substrate.) The initial rates of CO_2 evolution were comparable, as demonstrated by the first order rate analysis shown in the inset (both ~0.2 s^{-1}) but the rate of TMA photodecomposition attenuated faster for A TiO_2(001) than for R TiO_2(110). Those experiments were performed under anaerobic conditions, so the role of surface electron trapping likely was a factor in the higher sustained rates on R TiO_2(110) compared to A TiO_2(001).

7.1.3. Mixed-phase

Irrespective of the debate over the relative photocatalytic performance of A and R, it is becoming apparent that mixed-phase TiO_2 photocatalysts show interesting photocatalytic properties not seen in either single phase [42,499,524,583,882,928,949,1338,1474,1539,1556–1566]. This is particularly true of Degussa P-25, the 'gold-standard' by which other TiO_2 photocatalysts are frequently evaluated. The widely acknowledged exceptional photoactivity of P-25 [140,170,186,518,556,778,880,1328,1532,1567–1572] is frequently attributed to a cooperative effect between its composite mixture of ~75% A and ~25% R. Much work has been dedicated toward understanding this material's photocatalytic capabilities. One of the continuing challenges has been the difficulty of characterizing this material. It is still unclear how A and R are distributed in powders of mixed-phase TiO_2 like P-25. Recently, Asarai and coworkers [1573] performed STM on P-25, and (in some cases) these authors could distinguish between A and R based on atomic-level structural details.

The enhanced activity of P-25 and other A + R mixtures is generally thought to lie in the interfacial properties between A and R [42,140,170,186,499,524,583,949,1474,1557–1560,1564,1571,1574–1576] and not due to some cooperative effect of their individual photochemical properties (although there is debate on this point; see below). Chemical contact between particles of these phases has been shown to be necessary to obtain an enhancement from mixed-phase TiO_2 [1474,1568,1575]. (Surprisingly, the same thing has been shown for A alone, where particle–particle contact provides better charge trapping than seen in isolated A particles [833].) A widely held explanation of the need for A–R contact relates to their relative band edge positions. Because the bandgaps of the two polymorphs are slightly different (3.0 eV for R and 3.2 eV for A), there exists the possibility for formation of a heterojunction between the two in which electron transfer can occur [140,186,583,949,1557,1559,1560,1564,1574]. In this sense, A–R interfaces can potentially facilitate charge separation. Many groups have proposed that after Fermi level alignment, the CB edge of R should be lower than that of A, resulting in favorable conditions for electron transfer from A to R [186,583,1557,1559,1560,1574]. This is consistent with observations of reduction processes, such as Ag^+ photodeposition [524,1559], occurring preferentially on R domains in mixed-phase TiO_2 photocatalysts. For example, Kawahara et al. [1559] show in Fig. 7.6 a scanning electron microscopy (SEM) image (top) for a patterned A–R interface after Ag photodeposition. The accompanying X-ray emission (XES) spectrum (bottom) shows that Ag was preferentially deposited on the R half of the interface (the oxidation half reaction was not specified, but presumably occurred on the A portion.) In contrast, other groups have proposed

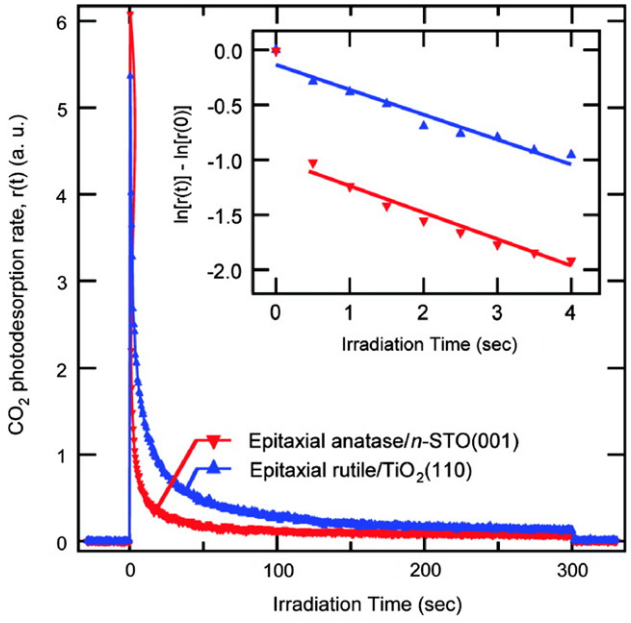

Fig. 7.5. Comparison of the CO_2 PSD rates from UV photodecomposition of TMA on epitaxial films of A TiO_2(001) (red, inverted triangles) and R TiO_2(110) (blue, triangles) normalized to TMA coverage. Inset shows rate plots from the PSD data.
Source: Reprinted with permission from Ohsawa et al. [542].
© 2008, American Chemical Society.

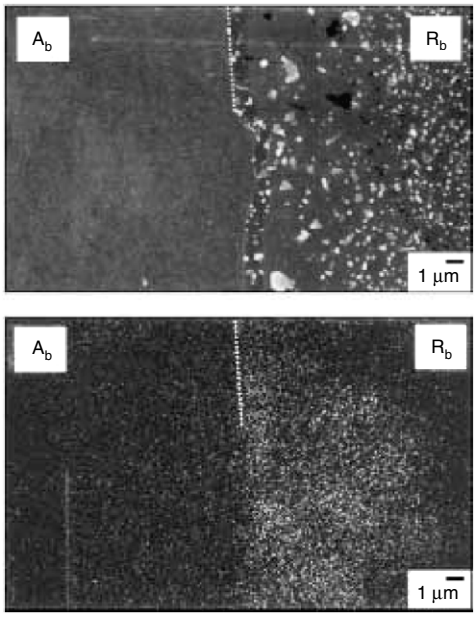

Fig. 7.6. (Top) SEM micrograph and (bottom) X-ray emission image for Ag from the same boundary region between anatase and rutile after photoreductive deposition of Ag. The dashed line marks the boundary. © 2002 Wiley–VCH Verlag GmbH & Co. KGa.
Source: Reproduced with permission from Kawahara et al. [1559].

that electrons in the CB of R are transferred to A [140,949]. Hurum et al. proposed that the key issue is the energy of electron trap sites and not the positions of the band edges. These authors proposed that electron trap sites can be more stable on A, resulting in greater stabilization of electron transfer from R to A. The interfacial region between A and R can also act as charge trapping sites, facilitating charge separation [42,499]. Other groups have proposed that the A–R interfacial region has slightly modified optical properties compared to those of the pure phases, enabling photoactivity with sub-bandgap light [113,170].

The nature of the atomic-level contact between A and R that facilitates enhanced charge separation is not well-understood. Knowledge of the interfacial structure may lead to better synthetic optimization of the interface [1562]. Recently, Shao et al. [1577] grew single phase A and mixed-phase A + R films on lattice-matched substrates of $SrTiO_3$(100) and $LaAlO_3$(100) using molecular beam epitaxy (MBE) methods. By temporarily increasing the deposition flux of Ti beyond the ideal rate for A growth, these authors found that R inclusions formed within the A lattice (see Fig. 7.7). After many such growths, Shao and coworkers observed with high resolution transmission electron microscopy (HRTEM) that certain A–R interfaces were preferentially seen between A and R. In particular, A TiO_2(110) planes tended to match up with R TiO_2(101) crystallite faces, as did A TiO_2(001) and R TiO_2(100) interfaces. Based on these results, Deskins et al. [1578] used near-coincidence site lattice theory to construct energy minimized interfaces between these (and other pairs) of A and R crystal planes. Fig. 7.8 shows energy minimized interfacial structures between the R TiO_2(110) face and the (101), (100) and (001) faces of A. Deskins and coworkers found that, in each case, A–R interfaces were stabilized by maximizing the formation of 6-coordinate Ti (thus minimizing the number of Ti dangling bonds). Their calculations showed that although the A–R interfaces were disordered (as one might expect), the distortions were limited to regions of only about 4 Å about the plane of contact, with the R side attaining rutile-like octahedral and the A side shouldering the majority of the disorder. This finding is consistent with the preference for A to transform into R (i.e., to accommodate itself to the R structure). These results also suggest that dangling bonds at the interface are located more on the A side than on the R side. Energy minimization relative to the pre-united cases was seen for all the cases studied, but some interfaces (such as the A TiO_2(101)–R TiO_2(110) pair and the A TiO_2(100)–R TiO_2(100) pair) showed significantly greater degrees of stabilization suggesting that these might be preferred contact points between A and R in mixed-phase TiO_2.

Despite arguments in favor of the interface being the key issue, other groups have proposed that achieving photocatalytic enhancement with A + R mixtures depends on the photocatalytic reaction being examined [880,1112,1579]. For example, Ohno et al. [880] proposed that R is uniquely suited for the electron scavenging chemistry of O_2 because no enhancement of A + R mixtures was seen when Fe^{3+} was used as an electron scavenger. Tseng et al. [1580] have suggested that surface area is the main issue. In particular, the influence of particle agglomeration can be optimized by adjusting the A-to-R ratio.

Manipulation of the A-to-R ratio has been shown to vary the degree of enhancement in mixed-phase TiO_2. The 'optimal' R content seen for mixed-phase TiO_2 has varied over a wide range, from <10% up to >70% depending on the preparation method and the photocatalytic reaction of interest [949,1474,1556,1558,1561,1565,1566]. Methods for varying the ratio differ, including use of mechanical mixtures, controlled sol–gel growth [1565], etching of one phase relative to the other [880,1560] or (the most common) thermal processing through the A-to-R phase transformation [949,1558,1566,1581–1583]. The A-to-R phase transition starts at the surfaces of A particles [1458,1584], or at A–A interfaces [1342,1576] at temperatures above ~850 K [1342,1580,1585,1586]. Thermal processes other than the phase transformation (such as dehydration, sintering or particle restructuring) can also occur during heating. The activity of P-25 (and presumably other mixed-phase TiO_2 photocatalysts) can be improved by hydrotreatment [1328] or mild calcination [1532], and more active mixtures of A and R have been prepared by varying the content or physical properties of the phases.

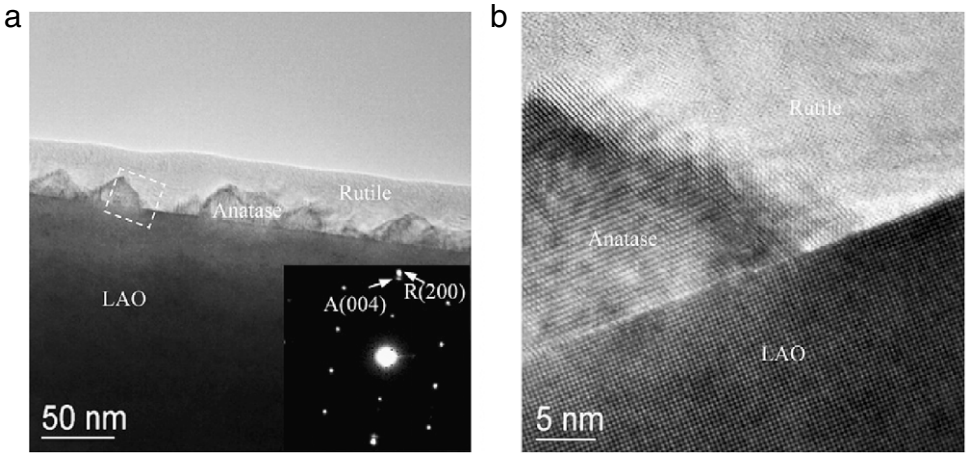

Fig. 7.7. (a) Bright field TEM image (inset: selected area diffraction pattern for the film), and (b) high resolution lattice image, both showing that the rutile/anatase/$LaAlO_3$ (LAO) interface (box in 'a') resulting from extreme growth conditions for MBE growth of TiO_2 on LAO.
Source: From Shao et al. [1577].

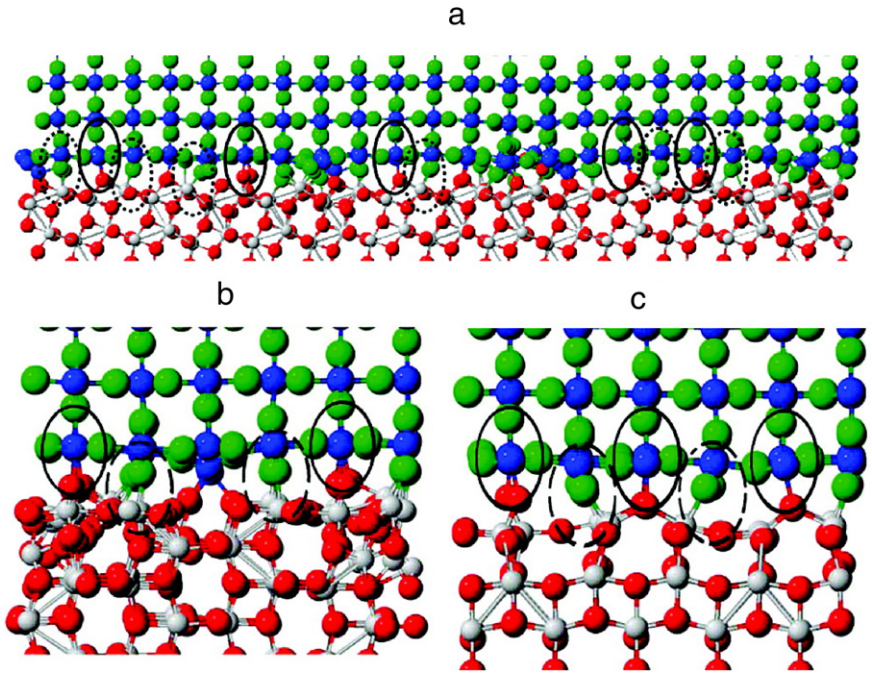

Fig. 7.8. Most stable interfaces between R TiO_2(110) and various A terminations: (a) TiO_2(101), (b) TiO_2(100), and (c) TiO_2(001). Red and green spheres represent O atoms from A and R, respectively, and gray and blue spheres represent Ti atoms from A and R, respectively. The solid circled regions show the lifting of A surface O atoms to form six-coordinated R-like Ti coordinations, whereas dashed circled region show O_b sites on R TiO_2(110) bonding to A Ti atoms. (For interpretation of the references to color in this figure legend, the reader is referred to the web version of this article.)
Source: Reprinted with permission from Deskins et al. [1578].

7.1.4. Brookite

There are examples in the literature of photocatalytic studies on pure-phase brookite (B) [1544,1587–1594], as well as mixed-phase photocatalysts containing B (not cited). As an example, Addamo et al. [1544] compared the photodecomposition rates of 2-propanol on A, R and B, and found that B had an activity comparable to that of A for similar particle sizes. However, surface science studies on this polymorph are few (if any). Detailed understanding of the surface structure, chemistry and photochemistry must await the availability of single crystal samples or high quality epitaxial films.

7.1.5. Tetrahedral TiO_2

The characteristic structural feature of the common TiO_2 phases is that of Ti^{4+} in an octahedral field of O^{2-} anions. However, the low energy structures of small gas phase TiO_2 clusters have Ti^{4+} cations in tetrahedral geometries [123,1595–1597], with octahedral character only developing for cluster sizes greater than ~5 TiO_2 units. These studies suggest that very small TiO_2 clusters or isolated Ti^{4+} cations on supports or embedded into the surfaces of suitable hosts should have structural and chemical properties that are different from those of the common TiO_2 polymorphs. While isolated Ti^{4+} cations or small TiO_2 clusters cannot rightly

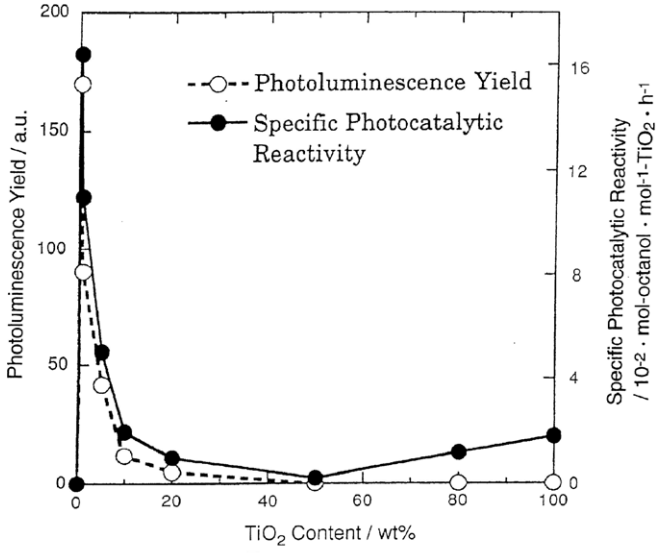

Fig. 7.9. Correlation between the photoluminescence yield and the photoactivity for liquid-phase oxidation of 1-octanol to 1-octanal from binary mixtures of TiO_2 and SiO_2.
Source: Reprinted with permission from Yamashita et al. [1603].

be consider as a 'phase' of TiO_2, discussion of their properties here may inspire more work into unique and innovative phases of TiO_2. Two examples of studies on tetrahedral TiO_2 will be considered. A challenge for surface scientists will be to find models of these types of sites that can be studied under controlled conditions.

Tetrahedral Ti^{4+} on silica: In concept, a TiO_2 unit supported on an oxide surface possessing tetrahedral structure might adopt a similar structure based on a templating interaction. Such has been shown to be the case for isolated tetrahedral Ti^{4+} sites supported on SiO_2 surfaces [134,930,931,1598–1606]. Liu and Davis [134] examined mixed TiO_2–SiO_2 materials using X-ray absorption spectroscopy (XAS), XANES and UV–vis as the TiO_2 content was decreased. They observed that the optical absorption threshold was blueshifted and the Ti coordination developed more tetrahedral character as the TiO_2 content was decreased. TiO_2 clusters of less than 1 nm in diameter were still observed even with an isolated-to-cluster site ratio of 8 to 1. Based on a correlations between the photocatalytic activity (for oxidation of 1-octanol to 1-octanal) and the photoluminescence (at ~480 nm) as a function of TiO_2 content (see Fig. 7.9), Yamashita et al. [1603] proposed that the high activity of isolated tetrahedral Ti^{4+} on silica was attributable to excitation of a long-lived electron transfer state. They proposed a localized excitation, with a final state resembling Ti^{3+}–O^-, where a 2p electron on oxygen was excited to a 3d orbital on titanium.

The impact of isolated Ti^{4+} sites on photocatalysis has also been seen in the selective photooxidation of propylene to propylene oxide [930,931,1598,1599]. Murata and coworkers. [931] observed that the activity for propylene photooxidation to propylene oxide decreased when the population of TiO_2 clusters increased relative to that of isolated tetrahedral Ti^{4+} sites. Similarly, Amano et al. [1599] observed different reactivities of propylene toward oxygen depending on whether the 4th coordination site of tetrahedral Ti^{4+} was occupied by OH^-, which was active toward O_2, or by an oxo group (Ti=O), which (like in other supported metals such as V^{5+} or Cr^{5+}) was not active.

Tetrahedral Ti^{4+} in frameworks: In contrast to supported tetrahedral Ti^{4+}, there are several examples of tetrahedral Ti^{4+} sites that have been built into supporting frameworks of zeolites [1607,1608] or of mesoporous/nanoporous systems [1476,1609–1614]. The Anpo group [33,1615] is a leader in exploration of the photocatalytic activity of tetrahedral Ti^{4+} in zeolite systems, particularly in the settings of CO_2 photoreduction [1186,1616–1622] and NO photoreduction [1164,1165,1372,1623–1625]. In an example of work from this group, Zhang et al. [1372] incorporated Ti^{4+} into various zeolites with differing Si:Al ratios using ion exchange. The Ti^{4+} geometry was shown to be tetrahedral based on extended X-ray absorption fine structure (EXAFS) measurements, diffuse reflectance absorption and photoluminescence. These authors observed that the tetrahedral Ti^{4+} sites photocatalyzed conversion of NO to $N_2 + O_2$, but that N_2O was formed instead at octahedral Ti^{4+} sites associated with clusters of TiO_2 impregnated into the zeolite pores.

7.2. Form

Considerable effort has been invested in preparing new forms of TiO_2 materials that possess new properties relevant to heterogeneous photocatalysis (e.g., nanoscaled features with altered optical or chemical properties) or utilized existing properties tailored for new applications of photocatalysis (e.g., mesoporous films for size-selected molecular photoconversion). Chen and Mao [14] recently reviewed many of the novel material synthetic approaches relevant to TiO_2. In this section, the relationships between various forms of TiO_2 and their surface photocatalytic properties will be discussed.

7.2.1. Particle surfaces

By far the most commonly studied form of TiO_2 is that of a particulate. However, the surfaces of particles are inherently difficult to characterize because the degree of heterogeneity is too extensive to permit the development of site-specific correlations with activity. Progress has been made in understanding how the nature of TiO_2 particle surfaces affects surface chemistry and photochemistry. In this section, the impact of a few common variables in particle design on TiO_2 photocatalysis are considered. While the majority of the discussion here focuses on experimental studies, it should be pointed out that advancements in theoretical modeling of large systems are beginning to provide unique insights into the properties of TiO_2 nanoparticles [1553,1626].

Particle shape: It should come as no surprise that the shape of a TiO_2 nanoparticle influences its surface chemistry and photochemistry, but translating shape-dependences into site-specific information is difficult. The issue here is not how TiO_2 can be made to adopt many different particle shapes, but how shape influences photoactivity. The shapes of nanoparticles are often difficult to control and difficult to characterize. TiO_2 particles have been grown in a wide variety of shapes, including spheres, tubes, rods, cubes, sheets, polyhedrals and more. Recent examples are found in the works of Yang et al. [1627], and of Alivov and Fan [1628] who both showed that the shape of A nanoparticles could be engineered by controlling surface termination agents during growth. In both cases, the relative areas of {001} facets were maximized by limiting the growth rate at these surfaces relative to those of the typically larger, but slower growing {011} facets. A number of groups have conducted studies in which detailed particle shape characterization has been coupled with estimations of photoactivity [521,1564,1575,1629–1633]. From these studies, it becomes evident that an activity–shape relationship actually translates into an activity–facet relationship. For example, Cho et al. [1633] followed the morphological changes (from a pre-crystalline sol–gel state to fully crystallized bipyramidal particles) occurring in large A particles in correlation with their photoactivity for chloroform photodegradation in solution. These authors

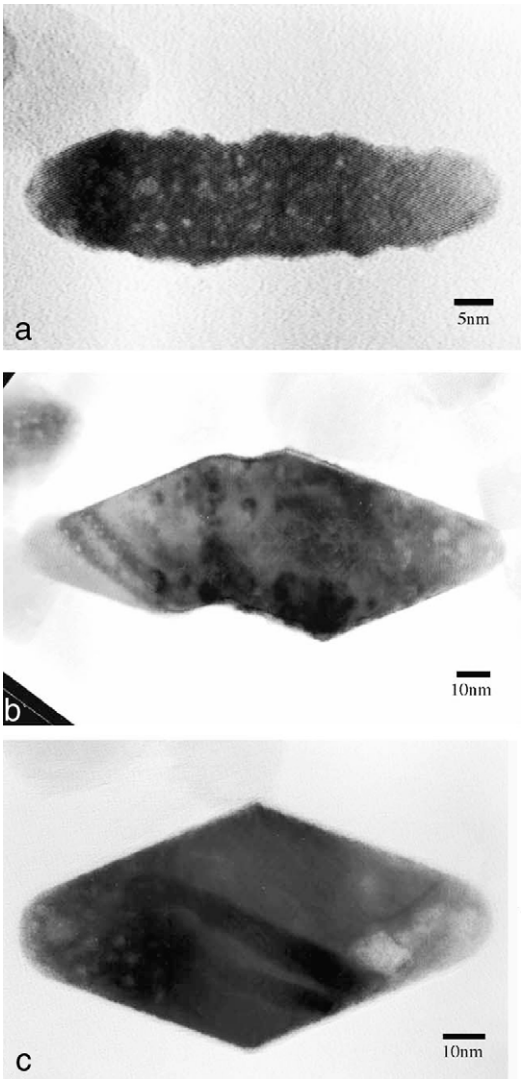

Fig. 7.10. HRTEM images of anatase nanocrystals during different stages of growth. (See text for details.)
Source: Adapted from Cho et al. [1633].

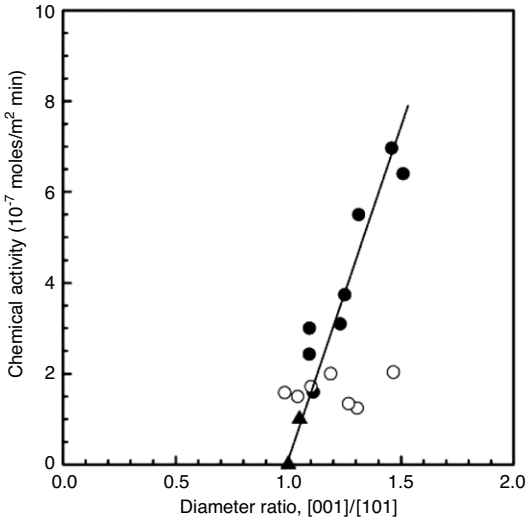

Fig. 7.11. Activity for chloroform photodegradation on anatase nanoparticles at various stages of crystallization (see text) as a function of the diameter ratio of the nanoparticles (⟨001⟩ to ⟨101⟩ directions). The diameter ratio is directly proportional to the area fraction of the {101} facets in highly crystalline A.
Source: From Cho et al. [1633].

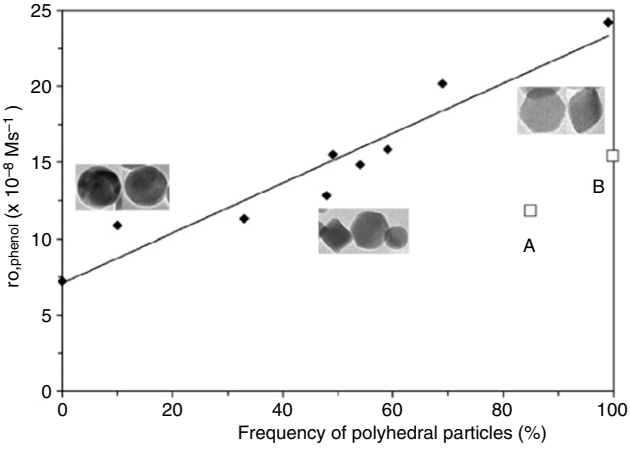

Fig. 7.12. Initial rate of phenol photodecomposition as a function of the frequency of particles with polyhedral shapes. Insets shows SEM images of typical particle shapes at the approximate *x*-axis regions of the plot. (Points 'A' and 'B' are for Degussa P-25.)
Source: Adapted from Balázs et al. [1632].

observed four key stages in the shape evolution of A: (1) formation of A nuclei; (2) rapid growth of A particles along their ⟨001⟩ directions through oriented attachments between semicrystalline particles; (3) a flattening of the zigzag {101} pyramidal facets; and (4) rapid growth along the ⟨001⟩ directions that increased the relative sizes of the {101} facets. Examples of A particles in the third stage are shown in Fig. 7.10(a) and (b), and in the fourth stage in Fig. 7.10(c). Chloroform photoactivity significantly increased during the last stages of crystallization (stage 3 to 4), as shown in Fig. 7.11. The authors ascribed this behavior not so much to refinement of bulk crystallinity but to development of well-ordered {101} facets which the authors proposed were more active for OH• radical formation. The development of {101} facets was apparent in the physical size changes of the particle, as expressed by the ratio of the diameters along the ⟨001⟩/⟨101⟩ directions (Fig. 7.11). (The absence of change in photoactivity during stage 3 was associated with 'flattening' of {101} facets since these facets did not increase in area during this stage.) These data show a strong preference in the photodecomposition of chloroform for {101} facets over that of {001} facets in A nanoparticles.

Other groups have shown that A nanoparticles that were grown with polyhedral-like particles shapes were more photoactive than those with rounded or spherically shapes. For example, Balazs et al. [1632] showed that phenol photodecomposition activity increased with the degree of polyhedral character in their A nanoparticles (see Fig. 7.12). These data are consistent with the interdependent properties of order (crystallinity) and development of specific surface facets with high photoactivity. Similarly, Liao et al. [1630] found that TiO_2 nanoparticle photoactivity could be optimized by engineering particle shapes using surfactant agents. Fig. 7.13 shows that these authors optimized the rate of methyl orange photodecomposition by generating particles with cubic-like shapes, as opposed to elliptical or nanorod shapes. There have also been suggestions that particles with 'rounded' edges and corners should be more photoactive [1631], and that particle distributions that include a mixture of particle shapes should be more photoactive [1629].

Particle size: Changes in particle size influence photoactivity through changes in surface area, light scattering and light absorptivity. The latter includes quantum size effects discussed in Section 1. Particle size effects on photocatalysis can work in cooperation or conflict with each other [1634,1635]. The nature of particle–particle interactions and particle aggregate sizes also

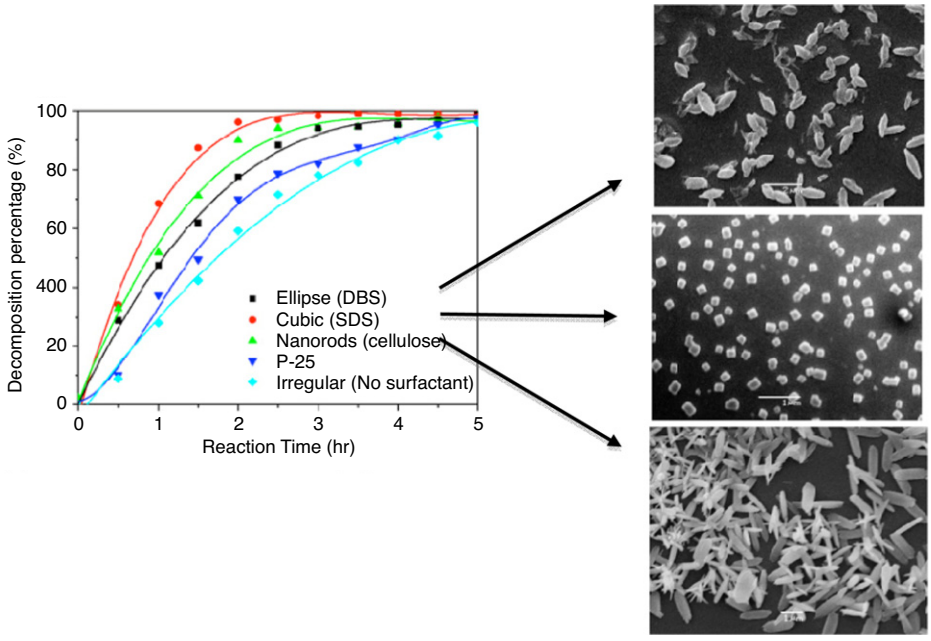

Fig. 7.13. (Left) Comparison of the methyl orange photodegradation activities from different shape-controlled TiO_2 nanoparticles prepared from $TiCl_4$. (Right) SEM images from the indicated particle preparation methods. (See paper for preparation details.)
Source: Adapted from Liao et al. [1630].

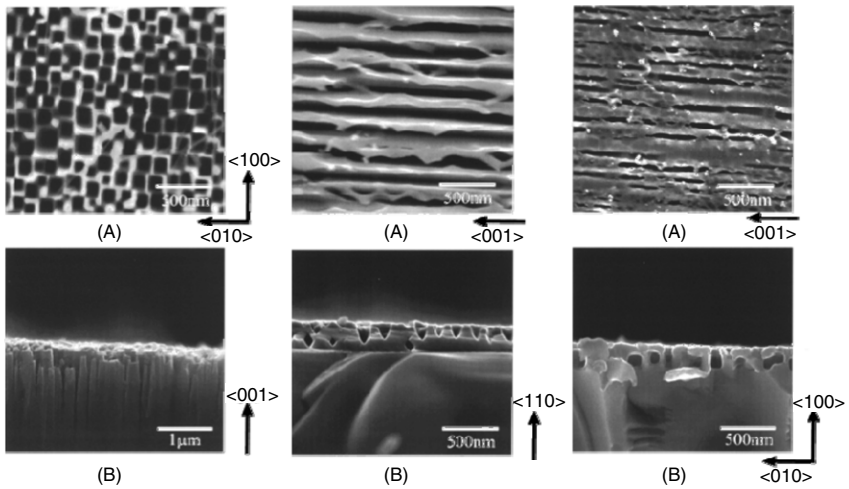

Fig. 7.14. SEM images for the R TiO_2(001), TiO_2(110) and TiO_2(100) electrode surfaces (left to right) photoetched in 0.05 M H_2SO_4 under potential scans for 180 min. (A) Along the surface normal, and (B) cross section.
Source: Reprinted with permission from Tsujiko et al. [1653].

correlates to some degree with individual particle sizes, feeding back into the influence on surface area, light scattering and light absorptivity. (For example, see the work of Maira et al. [130].) These phenomena have been well-documented in the literature. The issue of how TiO_2 surfaces are affected (in terms of the chemical and photochemical properties) by changes in particle size has received less attention. The surface properties of TiO_2 should change with decreasing size as a 'particle' (with recognizable bulk or bulk-like region) becomes a 'cluster' (with no recognizable bulk). As mentioned in Section 7.1.5, one of the attributes of TiO_2 clusters is the presence of tetrahedral Ti^{4+} cations. Transitions from micron-sized particles to nanoparticles to clusters should also result in increases in surface energy [1553,1636], lattice distortion/strain [1149,1533,1595,1637], and changing surface dangling bond populations [1595,1636], all of which will affect how adsorbates interact with the surface and how charge carriers are stabilized at the surface. Several studies [496,1356,1522,1638] proposed that charge carrier injection and/or trapping at particle surface sites depends on the particle's size, with larger particles exhibiting more stable surface sites for electron trapping. For example, Ahn et al. [1356] varied the TiO_2 particle size range using porous silica templates with varying pore sizes. They observed that the yields of EPR signals associated with trapped holes and electrons were larger for TiO_2 particles formed in smaller silica pores, but the stabilities of both trapped carriers were greater (i.e., longer lived) for particles formed in larger pores. The interplay between particle surface area, which provides high relative OH^- coverages for OH formation, and particle volume 'integrity' (which maximizes hole stability) involves optimal particle size engineering, as discussed by Carneiro et al. [737].

Particle suspensions: A particle in suspension is essentially separated from the influence of neighboring particles by a solvent.

In concept, one could remove the role of particle–particle interfaces, grain boundary charge trapping and recombination, and surface area loss through agglomeration by utilizing suspended TiO_2 photocatalysts (although site blocking due to the solvent would be unavoidable). Numerous groups have shown that TiO_2 suspensions behave differently, often with greater photoactivity, than supported or immobilized systems [1639–1643]. Two examples of this are in the works of Cohen-Yaniv et al. [1639] and Gumy et al. [1641], both of which showed that suspended systems offered better contact between microbial targets and TiO_2 particles than did immobilized TiO_2. In contrast, certain photoreactions show little or no difference between suspended and supported/immobilized systems [602,1641,1644,1645]. While suspended systems are not always practical, Geissen and coworkers [1647] pointed out that while fixed or immobilized systems are often viewed as more desirable for catalyst retrieval, reprocessing, etc., the benefits of higher activity in suspended system can overcome separation costs. The key surface issues associated with suspended TiO_2 relate to the high level of hydroxylation/hydration that is encountered in solution compared to immobilized TiO_2. While much is known about the surfaces of TiO_2 exposed to controlled sub-monolayer amounts of water [853], much less is known at the molecular-level about solvent-covered TiO_2 surfaces.

As in immobilized systems, agglomeration in a suspension can affect photoactivity. For example, Egerton and Tooley [1646] observed a decrease in the 2-propanol photodecomposition activity for finely dispersed TiO_2 colloids relative to more coarsely dispersed (agglomerated) TiO_2 colloids. They ascribed this to attenuation of light in the colloid and not to chemical effects occurring between particles. They found that a greater amount of light was being absorbed by fewer particles when TiO_2 was highly dispersed. Despite the higher absorptivity on these, the expected additional reactivity was negated by a lack of absorption deeper into the colloid. UV–vis measurements showed that more light penetrated coarsely dispersed colloid than finely dispersed (for the same amount of TiO_2).

7.2.2. Surfaces of novel TiO_2 materials

Mesoporous TiO_2: The correlations discussed above between photocatalytic performance and TiO_2 nanoparticle surface properties also hold true for other 'high surface area' forms of TiO_2 that are not particulate in nature. For example, the use of mesoporous TiO_2 materials in photocatalytic studies is extensive. While the majority of the literature on this subject appears to focus on correlations of the preparation conditions (e.g., pore size, surface area and degree of crystallization [1648,1649]) with observed photocatalytic activity, some studies have considered the mesoporosity itself affects surface properties important in photocatalysis. Just as the shape and size of a nanoparticle can affect its surface properties (see Section 7.2.1), the shapes and sizes of pores within a mesoporous and nanoporous network can affect the properties of the pore walls (i.e., their surfaces). For example, Zhang et al. [1537] and Angelome et al. [1523] both found that the pore structure and degree of crystallinity in mesoporous TiO_2 films affected their photocatalytic properties. Optimizing the templating influence of the substrates on which the mesoporous films were grown assisted in maximizing the crystallinity of films with well-defined pore structures. Similarly, Carreon and workers [1650] found that pore architecture played an important role in the photocatalytic activity of mesoporous TiO_2.

Nanotubes and nanorods: Research on TiO_2 nanotubes or nanorods is not found much in the literature prior to the year 2000, but has grown in interest since because of the potential application of these materials in electrochemistry and photoelectrochemistry [68,1651]. The surfaces of these materials have not received much attention, although literature has emerged on correlations between the orientations of these materials and their photocatalytic activities. For example, Joo et al. [128] found that (001)-oriented A nanorods outperformed P-25 in photokilling of *E. coli*. There are conflicting conclusions with regard to the possibility of charge confinement in TiO_2 nanotubes with narrow walls [407, 1526]. Paulose et al. [1652] observed high photoconversion efficiencies for dye sensitized TiO_2 nanotubes which they attributed to the absence of charge trapping sites common to nanoparticulate films.

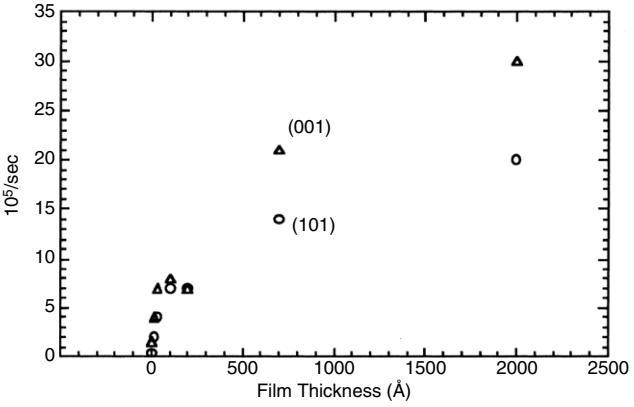

Fig. 7.15. Rates for Ag^+ photoreduction on R TiO_2(001) and TiO_2(101) films grown on different sapphire substrates as a function of film thickness.
Source: Reprinted with permission from Hotsenpiller et al. [1107].
© 1998, American Chemical Society.

Etched surfaces: Nakato et al. [1653,1654] have photoetched R TiO_2(100), (110) and (001) single crystal surfaces in dilute H_2SO_4 under anodic conditions to see how etch pit structures evolved and how these structures influenced photocatalytic processes (such as water photooxidation). As shown in Fig. 7.14, they found that photoetching preferentially occurred along ⟨001⟩ directions in these R crystal faces. The etched R TiO_2(001) surface possessed square pits and channels with walls aligned on ⟨100⟩ directions. Photoetching of the (110) and (100) surfaces resulted in grooves running along the ⟨001⟩ directions but with different groove profiles (triangular on (110) with exposed {100} facets and square-walled grooves on the (100) surface with expose {010} facets). Based on these results, the authors proposed that photoetching under their conditions was slower than the rate of water photooxidation on the R TiO_2(100) faces but faster on other faces of R.

Nanoscaled film thickness: Nanoscaled TiO_2 is generally thought of in 3 dimensions, but it is possible to vary only one dimension in exploring the thickness dependence of ordered TiO_2 films on photocatalytic activity. Hotsenpiller and coworkers [1107] have examined the photoreduction of Ag^+ on TiO_2 thin films grown by vapor deposition on various single crystal sapphire surfaces. The films exhibit preferential orientations due to the underlying sapphire surface structure, but were not highly ordered due to lattice mismatch effects. Nevertheless, the authors' data showed a clear distinction in Ag^+ photoreductive activity with film thickness (see Fig. 7.15). Two thickness regimes were observed, roughly above and below a ∼10 nm thickness. Changes in photoactivity as a function of film thickness were attributed to a combination of factors that changed with thickness, including increased absorptivity with increasing thickness, development of long-range surface order with increasing thickness (and with sapphire orientation), and nanostructural clustering of TiO_2 with decreasing thickness. Systematic variations in these effects can, in

concept, be used to tune photocatalytic activity in TiO_2 thin film systems.

7.2.3. Single crystal surfaces

Single crystal TiO_2 surfaces are proving to be ideal settings in which to study heterogeneous photocatalysis at the molecular-level. The attractiveness of these surfaces is that they offer an ideal interfacial setting in which to understand the interplay between surface structure (physical and electronic) and surface (photo)chemical reactivity. Given that crystalline nanoparticles are comprised of facets with the common TiO_2 terminations (e.g., in A: {101} or {001}; in R: {110} or {101}), insights into important surface processes can be obtained using model surfaces with these orientations. This section highlights some of the insights obtained from single crystal A and R surfaces that are relevant to photocatalytic studies on TiO_2 materials. Many examples emerging in the literature of mechanistic studies involving photochemical reactions on TiO_2 single crystal surfaces are discussed in Section 5. Several articles reviewing surface photochemistry from the Yates group [97–100] also illustrate the breadth of insights that can be obtained from studying photochemistry on single crystal TiO_2. Additionally, recent review articles by Diebold [175], by Pang et al. [566], and by Dohnálek et al. [792] have delved deeply into the properties of TiO_2 single crystal surfaces (particularly that of the R TiO_2(110) surface). This section will focus on new insights into TiO_2 surface photocatalysis obtained from studies on the physical and electronic properties of TiO_2 single crystal surfaces.

TiO_2 surfaces are generally thought of as possessing amphoteric Brönsted acid/base properties and strong Lewis acid character due to under-coordinated Ti^{4+} cation sites. Because TiO_2 is a reducible oxide, it is also possible to have redox behavior at the surface. Oxygen vacancy sites on R TiO_2(110) are a well-known example of TiO_2 surface sites capable of redox behavior [175,566,792]. Specific sites with similar behavior have not been well-documented on other TiO_2 surface. It is also generally held that the VB region of TiO_2 is dominated by states with O 2p character and the CB by states with Ti 3d character. Both theory [232,706,1655–1660] and experiment [1543,1656,1661–1666] show that the degree of covalent character in TiO_2 is not insignificant. The degree of mixing between O 2p and Ti 3d/4s states in the TiO_2 VB and CB states may therefore have an impact on TiO_2 photochemistry. The degree to which a surface of TiO_2 alters the bulk electronic structure properties of TiO_2 (e.g., by changing the degree of orbital mixing in the VB or CB) is of importance in this section. Also, the issue of how a surface alters the VB/CB DOS, their energies and state mixing in TiO_2 is important, as well as how these change from surface to surface.

7.2.3.1. Rutile surfaces. The most commonly studied TiO_2 single crystal surface is the R TiO_2(110) surface. There is general agreement that the (110) surface is the thermodynamically most stable termination of R [175,566,1667,1668]. Therefore, focusing discussion on how the electronic structure of this particular surface impacts TiO_2 photocatalysis seems a reasonable place to start. The VB structure of the R TiO_2(110) surface is well-studied and fairly well-understood (see [175,566]). UPS spectra provide a reasonable representation of not only the surface DOS from which a band-to-band excitation would originate but also the manifold of states through which a VB hole would thermalized to the VB edge. The character of these states (as mentioned above) is primarily, but not exclusively, O 2p. Zhang et al. [1665] and Heise et al. [1664] employed resonant photoemission (using the Ti 3p to 3d resonance) to show that the VB of R TiO_2(110) possessed significant Ti 3d character. Interestingly, however, the latter group found that the character of the VB maximum (presumably where holes would thermalized to) at the surface was predominately of

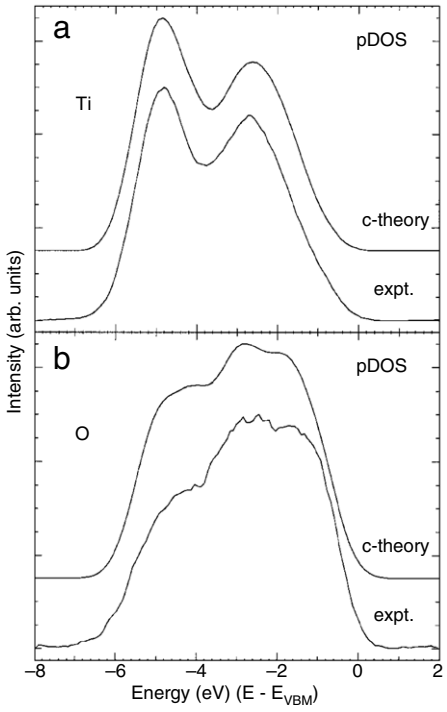

Fig. 7.16. Comparison of the calculated (with an *ab initio* LDA plane approximation) and experimental (from photoemission) VB density of states (DOS) for Ti (top) and O (bottom) in rutile TiO_2.
Source: Reprinted with permission from Woicik et al. [1656].

O 2p character, possessing less Ti 3d character than the rest of the VB. More recent studies by Prince et al. [1663] concurred with this finding by pointing out that the degree of mixing increased as one moved deeper into the VB. The existence of some Ti 3d character at the VB edge for the electronic states at the surface of TiO_2(110) suggests that holes arriving at this surface will possess mostly O 2p character (i.e., reside mostly at surface O sites), but will also possess contributions from neighboring or underlying Ti cation sites. In a different approach, Woicik et al. [1656] examined the Ti and O VB components of the R TiO_2(110), obtaining "site-specific" information from XPS by using photon energies selected based on the Bragg scattering conditions for specific atoms/layers in the surface (i.e., O only or O + Ti). These data, shown in Fig. 7.16, were then compared with the O and Ti DOS obtained by *ab initio* LDA calculations. While the general shapes obtained from theory and experiment matched, these authors found that the thresholds and relative contributions from O and Ti differed somewhat. Nevertheless, both approaches showed that the contribution of Ti 3d character in the VB was not insignificant and increased deeper into the VB. By extension, a VB hole should lose Ti 3d character and gain O 2p character as it thermalizes to the top of the VB. Another implication of these VB electronic structure assessments for photochemistry on R TiO_2(110) is that holes in the R TiO_2 VB (and presumably also electrons in the CB) cannot be thought of as having purely O 2p character (Ti 3d in the case of the CB). A hole arriving at the surface will possess orbital character associated with both Ti^{4+} and O^{2-} atoms. Adsorbates electrostatically bound at cation sites should not be considered as unable to have direct electronic interactions with holes simply because the VB is predominately considered O 2p in character.

The picture of the electronic structure of the R TiO_2(110) CB is less clear because of the greater challenge associated with experimentally or theoretically characterizing unoccupied states. The unoccupied surface states in TiO_2 are predominately

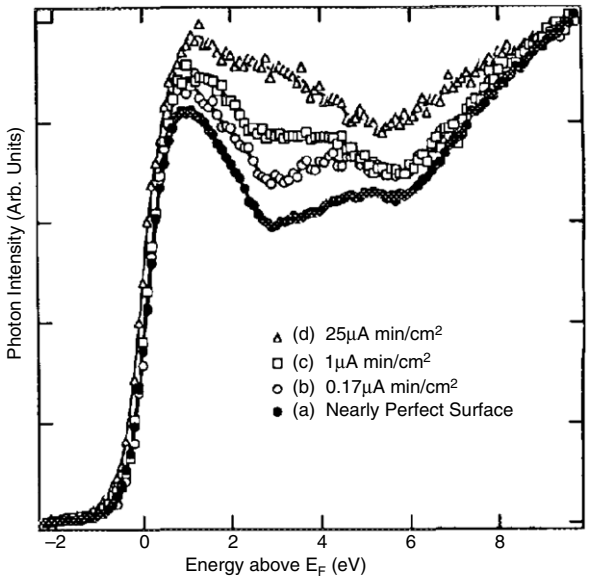

Fig. 7.17. Inverse photoemission spectra from 'nearly perfect' and ion bombarded R TiO_2(110) surfaces.
Source: Reprinted with permission from See and Bartynski [1671].
© 1992, American Vacuum Society.

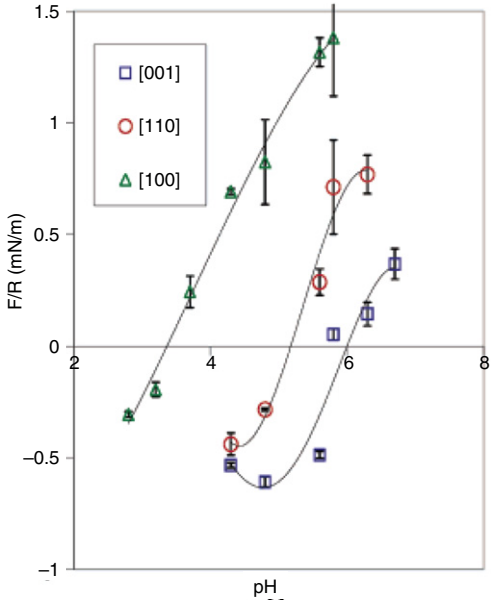

Fig. 7.18. Maximum interaction forces (determined with AFM) on the indicated rutile TiO_2 surfaces in 0.001 M KCl as a function of the solution pH. The *x*-intercepts correspond to the isoelectric points for each surface.
Source: Reprinted with permission from Bullard and Cima [1673].
© 2006, American Chemical Society.

Ti 3d derived. (Unoccupied states that can be categorized as 'predominately' O-derived lie >10 eV above the Fermi level [1669].) Core-level techniques such as near-edge X-ray absorption fine structure (NEXAFS, see [1666] and references therein) or TEM-EELS (see [1670]) have been used successfully to probe core-to-CB level transitions in TiO_2. Well-defined core levels allow one to associate observed structure from these techniques to the DOS in the TiO_2 CB. In contrast, techniques such as UV–vis and EELS, which both probe VB-to-CB transitions, must deal with the convolution of DOS in the VB and the CB. Another technique that provides a picture of unoccupied states at surfaces is inverse photoemission spectroscopy (IPS). See and coworkers used this technique to characterize the unoccupied states of R TiO_2(110) [1671,1672]. As shown in Fig. 7.17, IPS of R the TiO_2(110) surface shows the first (and most prominent) maximum in the CB to be at ~1.0 eV above Fermi level. Ion beam sputtering, which preferentially removes oxygen leaving a reduced (albeit damaged) surface, did not alter the position of this lowest energy maximum, but did increase the DOS at higher energies. One might expect, based on these results, that the relative DOS in the CB would shift to higher energy for surfaces that were reduced or that possessed high concentrations of trapped electrons. See et al. extended use of this technique by employing angle-resolved measurements to map out dispersion of the ~1 eV unoccupied state. They found that the majority of states showed only small amounts of dispersion in $k_{\|}$, indicating general localization of these states.

While the R TiO_2(110) surface is the most widely utilized single crystal surface in chemical or photochemical studies (see Section 5), it does not necessarily mean that this surface termination is the most important one to photocatalytic processes on nanocrystalline R. Several studies have emerged that compare the photochemical and electronic structure properties of various R (and A) surfaces. For example, Bullard and Cima [1673] utilized AFM to determined isoelectric points (IEP) of three R single crystal surfaces. They found that the IEP varied considerably with the crystal face structure, from pH values of 3.2–3.7 for R TiO_2(100) to 4.8–5.5 for R TiO_2(110) to 5.5–5.8 for R TiO_2(001) (see Fig. 7.18). These authors proposed that the trend in these ranges matched the relative acid/base site densities, taking into account cation coordination numbers, for sites on each ideal surface. While factors such as the nature and concentration of electrolyte require additional study, these data suggest that in aqueous solution the R TiO_2(100) surface should be more basic and the R TiO_2(001) surface should be more acidic. This comparison was made with the realization at the R TiO_2(001) surface reconstructs under vacuum conditions [175] and that its structural properties under aqueous conditions are not known. Nevertheless, the comparison shows that at a given pH R nanoparticles will likely have variations in the electrostatic environment from facet to facet. In other work, Nakamura et al. [1674] found that a ~0.1 eV difference existed between the flat-band potentials of the R TiO_2(100) and TiO_2(110) surfaces (as determined from Mott–Schottky plots for the onset of photocurrent during water photooxidation), with the former surface's flat-band potential being at more negative potential. This implies that the band edges for the (100) surface were slightly more positive in potential relative to those of the R TiO_2(110) surface. Consistent with these data, the same group [1675] utilized a scanning Auger microprobe to investigate the local work function of atomically flat terrace regions on the R TiO_2(110) and R TiO_2(100) surfaces. They found that the work functions for these surfaces, revealed by the onset of secondary electron emission, were 4.13 and 4.20 eV, respectively, which the authors pointed out was consistent with the flat-band measurements. (The one caveat to these measurements is that the Auger microprobe utilizes a 10 keV electron beam with ~1 nA being deposited in a 50 μm diameter spot (corresponding to ~50 μ A/cm^2) which can cause substantial surface damage via electron-stimulated desorption of lattice oxygen.)

Relative differences in band edges across R surface terminations can also be seen in studies of the photoreduction of Ag^+. Rohrer and coworkers [1107,1108] examined the relative activity Ag metal photodesorption as a function of R crystal face structure. On microcrystalline R, they found that the activities of the {011}, {111} and {001} family of facets was the greatest, but those with {100}/{010} or {110} character were less active for Ag^+ photoreduction (see Fig. 5.34). These observations on microfacetted films also matched the relative Ag^+ photoreduction

activity observed on extended R surfaces (single crystal and highly oriented thin film surfaces). In this case, the most active surfaces for Ag^+ photodeposition were the (101), (111) and (001) terminations and the least active were the (100) and (110). Although the relative surface roughness for the various surfaces (ideal and polycrystalline) were not known, these authors proposed that charge separation/transport (which relates to the relative band edge positions) and surface chemistry (which relates to site-specificity and surface atomic structure) were the key issues. (Because these studies were not photoelectrochemical, the surface structural dependence of the oxidation half reaction must also come into play.) Consistent with the results of Rohrer et al., Yamamoto et al. [1111] also showed that the rate of Ag^+ photoreduction followed a similar trend for various R single crystal surfaces, namely the activity following this progression: (101) > (100) > (001) > (111) > (110). These studies suggest that if point charges emerging from the bulk of a nanoparticle to the surface can sense the electrostatic and electronic structure variations between facets, then photocatalysts can be optimized by designing shapes to maximize particular active facets.

In other surface structure-sensitivity studies on single crystal R surfaces, Imanishi and coworkers examined the influence of R surface structure on dye sensitization [672,673]. On pristine surfaces, they found no significant difference in the per-molecule injection photocurrent from excitation of a benzothiazole merocyanine dye into the surfaces of R TiO_2(100) and TiO_2(110) despite the fact that NEXAFS data suggests the dye binds more strongly to the (110) surface [673]. Similar conclusions were reached by Lu et al. in comparison of charge injection from the N3 dye into the R TiO_2(001), R TiO_2(100), A TiO_2(101) and A TiO_2(001) surfaces [633]. Aside from the relative amount of adsorbed dye (which was higher on the R TiO_2(110) surface due to more favorable packing), absence of a difference in the incident photon conversion efficiencies was attributed to the orbital energy of the excited dye's electron lying higher in the CB where the DOS was essentially independent of surface structure. Small differences in the coupling of the ground state molecule to these surfaces were deemed less significant compared to the magnitude of the coupling of the excited electron with Ti 3d states in the surfaces. On surfaces pretreated in a H_2 atmosphere at 550 °C prior to sensitization in solution, these authors found that the photocurrent generated on R TiO_2(110) was over a factor of 10 greater than that on other surfaces [672]. They attributed this to generation of inactive (defective) regions on other surfaces as a result of surface reduction. These studies suggest that the structure of R TiO_2 surfaces plays more of a role in how sensitizers are adsorbed than in influencing their photoinjection properties.

Two groups have examined the relative activities of various R surface terminations using UHV-based studies of organic photooxidation. Brinkley and Engel [900] observed that the (110) surface of R was more photoactive for 2-propanol photodecomposition than the (100) surface. They attributed this partially to differences in the thermal chemistry of 2-propanol on the two surfaces. Wilson and Idriss [967,968] examined the activity of acetic acid (acetate) photodecomposition on two different surface reconstructions of the R TiO_2(001) surface. (See references in [967,968,175] for more information on the atomic-level structures of the R TiO_2(001) reconstructions.) They found that the rate of acetate photodecomposition (as measured by depletion of the C 1s features in XPS) was ~10 times greater on the {011}-faceted termination than on the {114}-faceted termination. This difference was also evident in the relative rates for evolution of gaseous products (as detected by mass spectrometry), as illustrated in Fig. 7.19 for the generation of ethane. Because both surface reconstructions resided on the same bulk material, changes in the photochemistry of acetic acid could be directly tied to the surface termination structures. The authors attributed the differences in photoactivity to differences in

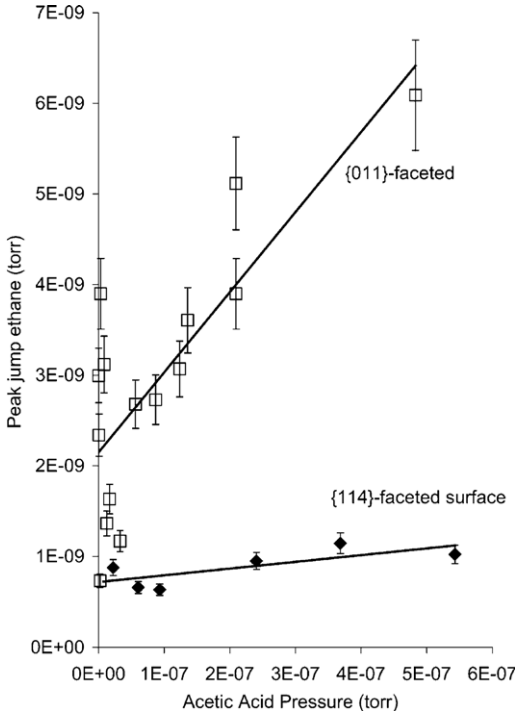

Fig. 7.19. Ethane production from photodecomposition of adsorbed acetate on two terminations of the R TiO_2(001) surface as a function of acetic acid chamber pressure (in ~5 × 10^{-10} Torr O_2) at 300 K.
Source: From Wilson and Idriss [967].

the electrostatics encountered by holes as the diffused from the bulk to the surface. There are also differences in the surface populations of dangling bonds and surface long-range order between the two reconstructions that might come into play in influencing charge carrier lifetimes at the surface. In other words, the specific arrangements of cation and anion surface sites on TiO_2 is important in influencing both adsorbate properties and those of charge carriers

Finally, studies discussed above illustrate the influence that surface structure plays in influencing photochemistry on R single crystal surfaces, but the effect that surface photochemical processes play in influencing surface structure is not well-understood. As mentioned above, Nakato's group [672,1653,1654,1675] has shown that R surfaces can be photoetched, but in the context of somewhat harsh electrochemical conditions. There are also examples in the literature of the electronic or electron paramagnetic signatures of photoinduced charge accumulation in R powders. There do not appear to be any indications in the literature that UV irradiation of R single crystal surfaces in vacuum induces surface reconstructions or surface damage. For example, Mezhenny et al. [791] used STM to show that the (1 × 1) surface R TiO_2(110) was unaffected by extensive UV irradiation. These authors did observe, however, that areas of the (1 × 2) reconstructed surface, which is Ti_2O_3-like, were susceptible to UV-induced surface oxygen removal. This suggests that once a R surface is 'damaged' it might be more susceptible to additional 'structural' changes as a result of surface photochemical effects.

7.2.3.2. Anatase surfaces. Photochemical and chemical surface studies on A single crystal surfaces are not nearly as abundant in the literature as are those on R surfaces. Of the two prominent surface terminations of A (the (101) and (001) faces), the A TiO_2(101) surfaces has been shown to be stable as in an ideal, (1 × 1) structure [1676,1677]. In contrast, the A TiO_2(001) surface reconstructs into a (4 × 1)/(1 × 4) structure consisting of a ridge-

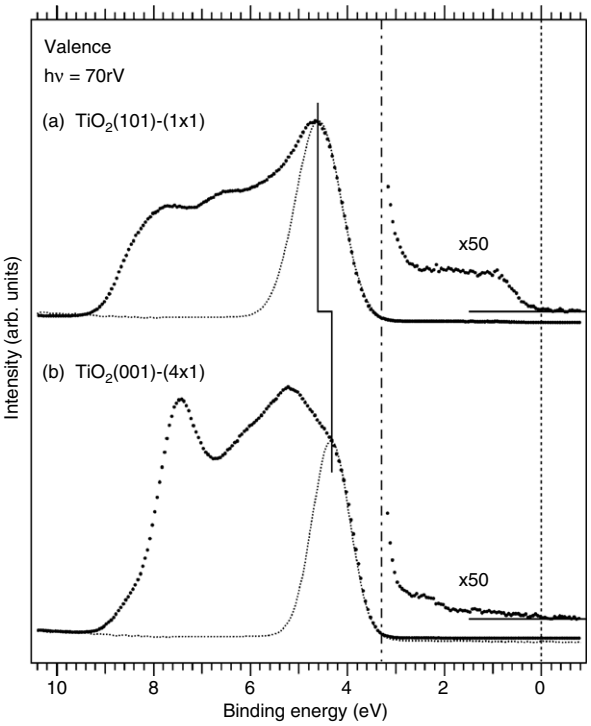

Fig. 7.20. Valence band photoemission spectra from the A TiO_2(101) and TiO_2(001) surfaces. The energy scale is relative to the sample holder's Fermi level (dashed vertical line). The Gaussian peaks (dotted curves) represent fits to VB maximum edge. The vertical dash–dot line marks the VB maximum (assuming alignment of the CB minimum and the Fermi level).
Source: Reprinted with permission from Sandell et al. [1679].

and-trough type structure without a significant amount of surface reduction [977,979,980,1678]. (The (4 × 1)/(1 × 4) designation is used because the rough-and-trough directions flips 90° for each terrace-to-terrace transition on the A TiO_2(001) surface.) This reconstruction appears to be more thermodynamically stable than the ideal (1 × 1) surface under UHV conditions. It remains to be seen whether the A TiO_2(001) surface, can be stabilized in a (1 × 1) structure in other environments (i.e., high pressures or aqueous conditions).

In terms of the electronic structure of A single crystal surfaces, Sandell et al. [1679] conducted XAS and photoemission measurements, coupled with DFT calculations, on the occupied and unoccupied electronic structures of the A TiO_2(101) and A TiO_2(001) surfaces. These authors found very little surface reduction for annealed A TiO_2(101) or A TiO_2(001) based on VB photoemission (as shown in Fig. 7.20), although the latter showed more indications of surface reduction based on the signal intensity near the Fermi level ('0' eV BE). States at the bottom of the CB possessed mostly Ti 3d (d_{xy}) in character for stoichiometric TiO_2, but surface Ti atoms with ~4% of an electron charge (i.e., slightly reduced) resulted in their lowest lying states developing more O 2p character. Based on this observation, electron trapping at A surfaces will cause the Ti 3d states associated with the trap sites to change their character from mostly Ti 3d to a mixture of Ti 3d and O 2p.

Thomas et al. [1661] examined the degree of Ti–O orbital mixing in the VB of A TiO_2(101) and A TiO_2(001) (bulk and surface) using resonant photoemission. They found that the degrees of mixing in the bulk and surface of A TiO_2(101) were similar, but that the A TiO_2(001) surface showed more mixing at the VB edge than did the A TiO_2(101) surface. These authors suggested that the (4 × 1)/(1 × 4) reconstruction of the A TiO_2(001) surface was 'non-anatase-like'. That is, it exhibited a significant reconstruction that altered its bulk VB contributions of Ti and O at the band edge. Thomas et al. [1543] also used resonant photoemission and XAS to study the electronic structures of the A TiO_2(101), A TiO_2(001) and R TiO_2(110) surfaces. Fig. 7.21 shows VB photoemission spectra for the three surfaces as the photon energy was swept through the Ti 3p to Ti 3d resonance transition energy (see photon energies in ascending traces). Emission processes on resonance with this transition were enhanced when their Ti 3d contributions were high. The authors selected four spectral features for analysis: the two main VB peaks (labeled 'A' and 'B' at BE = 8.2 and 5.8 eV, respectively), the VB maximum edge (labeled 'C' at BE = 4.4 eV), and the surface defect state, typically attributed to oxygen vacancy sites (labeled 'D' at BE = 1.1 eV). (A fifth feature, at 6.7 eV was also monitored for R TiO_2(110).) Examination of the intensities at these various points as the photon energy was swept through the Ti 3p to 3d resonance showed that the greatest contribution of Ti 3d states in the VB was typically in the 8.2 eV peak (see Fig. 7.22). Total Ti 3d contributions in the VB of A TiO_2(001) and R TiO_2(110) were comparable, but much less was seen for A TiO_2(101). In particular, Thomas and coworkers found that the contribution of Ti 3d states at the VB maximum in A TiO_2(101) was negligible. This suggests that a hole thermalized to the VB maximum and diffused to the A TiO_2(101) surface will be localized on O 2p states, but will have a mixture of Ti 3d and O 1s character at the surfaces of R TiO_2(110) and A TiO_2(001). Conversely, electrons at the bottom of the A TiO_2(101) CB should have little O 2p character compared to R TiO_2(110) or A TiO_2(001). The authors also noted that the presence of surface defects assisted mixing, but that the A TiO_2(001) surface, despite its reconstruction, possessed little electronic defect character (i.e., surface reduction) in photoemission. The authors speculated that the degree of mixing should influence photochemical processes, for example, by varying the charge transfer dynamics for adsorbates as a function of on what surfaces they are adsorbed. For example, one might expect that surfaces with less Ti 3d–O 2p mixing should be more suitable for charge carrier trapping and less likely to permit charge recombination.

Comparisons of the photocatalytic activities of different A single crystals are few. Hengerer et al. [1680] compared photoelectrochemical oxidation of water on A TiO_2(101) and TiO_2(001). They observed that this reaction occurred at more negative potentials for A TiO_2(001). This was linked to a more negative flat-band potential for A TiO_2(001) (by 0.06 V) that the authors attributed to a greater ability of this surface to thermally dissociate water in comparison with the A TiO_2(101) surface [1681–1684]. As mentioned above, the (001) surface is a rough-and-trough reconstructed structure possessing (4 × 1)/(1 × 4) order. In contrast, the (101) surface appears to be bulk-terminated in its structure. Ohsawa et al. [542] used STM and PSD to show that the probability of a hole-mediated photodecomposition event (in this case, of TMA) on the ridges of the (4 × 1)/(1 × 4) reconstruction of A TiO_2(001) was not significantly different from that in the troughs. This suggests that the atomically rough surface characteristic of the A TiO_2(001) surface does not tend to localize holes at any specific structural locale (ridge or trough) on this surface.

7.2.3.3. Surface defects. Structural defects play an important role in influencing the chemical and electronic properties of TiO_2 surfaces [175,566,792]. It is expected that defect sites will also influence surface photochemistry on TiO_2, although the field has not yet extensively reported such correlations. For example, while much is known about the properties of oxygen vacancy sites on the R TiO_2(110) surface, the influence of these sites on surface photochemistry is poorly understood. For the purposes of this review, two types of surface defects will be considered as

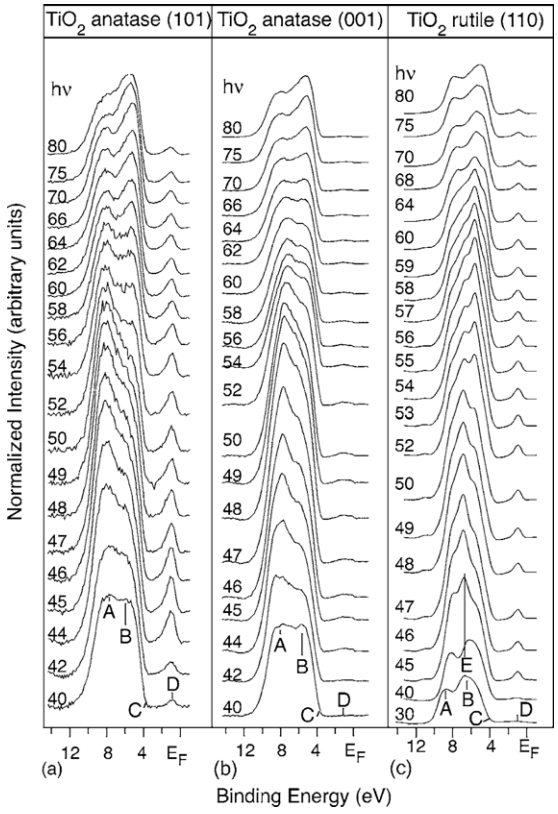

Fig. 7.21. Resonant photoemission spectra from TiO_2 surfaces: (a) A TiO_2(101), (b) A TiO_2(001), and (c) R TiO_2(110) as a function of photon energy. (See text for explanations of points A–E.)
Source: Reprinted with permission from Thomas et al. [1543].

to how they might influence surface photochemistry. These are point defects (such as oxygen vacancies) and extended defects (such as steps or reconstructions). Relaxations of ideal (1 × 1) surface structures away from that expected bulk termination structures [1685–1691] might be considered as a type of defect surface structure (in relation to the ideal bulk structure), but their influence on surface photochemistry should be subtle relative to the influence of other types of surface defects.

Point defects: As mentioned above, the most widely studied defect on a TiO_2 surface is that of the oxygen vacancy site on the R TiO_2(110) surface [175,566,792]. Studies on the chemical, electronic and structural properties of these defects are numerous. It is believed that oxygen vacancies form on R TiO_2(110) in response to surface reduction (usually initiated thermally). The vacancy, as a structural entity, appears to be the lowest energy response (in vacuum) to low levels of surface or bulk reduction, whereas Ti_2O_3-like line defects appear on this surface as a result of more extensive levels of reduction. Each vacancy nominally possesses two Ti^{3+} cations, with the overall spin state of the vacancy likely that of a triplet configuration. This results in a 'donor' surface state located in energy roughly 1 eV below the CB edge. Purton et al. [1667] have shown that this electronic feature possesses mostly Ti 3d character. Interestingly, while the bulk donor density of 'mildly' reduced R is typically 1 center per $\sim 10^4$ unit cells [575], the reduced cation concentration associated with vacancy defects on the R TiO_2(110) surface is typically ~5%–10% [175,566,792]. This illustrates that energetically the R TiO_2(110) surface can stabilize considering more 'reduction' than can the bulk, which in turn suggests that this surface can stabilize a higher relative percentages of trapped electrons compared to the bulk. This author and coworkers [202,515,543] have shown that R TiO_2(110) surface possessing ~0.1 ML of oxygen vacancy sites can still facilitate hole-mediated decomposition of adsorbed organics in the absence of O_2 and still accommodate the additional electron density of the excited electrons at the surface.

Direct involvement of oxygen vacancies in photochemical processes on R TiO_2(110), as both electronic defects and structural entities, has been observed in the photooxidation reactions of CO [776], 2-propanol [901] and CH_3Cl [1320]. It perhaps goes without saying that the oxygen vacancy, as a structural entity, exists only under UHV conditions given the high reactivity of these sites to water and O_2 [175,566,792]. Nevertheless, as an electronic entity, much can be learned about electron transfer processes on TiO_2 surfaces from studies of these sites. The extent to which oxygen vacancy sites on R TiO_2(110) can provide insights into TiO_2 photocatalysis is currently a topic of growing interest in the literature. The Petek group [192–197] has explored how excitations of the electronic states associated with these defects might be involved in electron transfer processes at TiO_2 interfaces with hydrogen-bonding adlayers. As discussed in Section 3, they observed short-lived excited states associated with defect electrons and solvent molecules (water or methanol). However, this author is unaware of examples in which excitations of defect electrons resulted in bond-forming or bond-breaking events on R TiO_2(110). Instead, oxygen vacancies on TiO_2(110) have emerged as excellent models for reactions between adsorbates and excited/trapped electrons on TiO_2 surfaces. For example, much has been learned about the electron scavenging behavior of O_2 in photooxidation reactions based on studies of the interaction of O_2 with vacancies on R TiO_2(110) (see Section 5).

One of the key issues associated with the oxygen vacancy site on R TiO_2(110) has been determining the degree to which charge delocalization occurs and how delocalization may affect electron transfer reactions at the surface. A variety of theoretical assessments have examined this issue [487,526,527,806,827,829,831,844,1655,1658,1660,1667,1692–1702]. Experimentally, techniques such as angle-resolved photoemission [1703] and STM [527] have attempted to address the degree of localization of electronic defect states on the surface of R TiO_2(110). The former study found little evidence for dispersion in the defect state, whereas results from the latter study showed a significant degree of delocalization within the surface (see Section 2 for more details). Recently, Krüger et al. [1704] examined the degree of delocalization of the electronic state associated with surface vacancies on R TiO_2(110) using resonant photoelectron diffraction. By generating 2D maps of the electron emission patterns from ionization of the defect state (located at ~1 eV below the CB minimum) and fitting these patterns to reasonable structural models, these authors concluded that electron density associated with the O vacancy state was distributed over several cations in the surface and subsurface. Fig. 7.23 shows a ball-and-stick model of the R TiO_2(110) surface with a single oxygen vacancy site (labeled 'V') and designations of six unique Ti cation sites in the vicinity of the vacancy. The authors' photoelectron diffraction pattern for electron emission from the Ti 2p core state, reflective of all cation sites in the near-surface region, is shown in the left of Fig. 7.24, whereas the emission pattern from the defect state is shown to the right. Diffraction features were designated based on the emitter and scatterer. For example, feature 'Ti1–O1' corresponded to emission from the Ti cation labeled '1' (under the bridging oxygens) scattered by O1 (the bridging oxygens). At first inspection, it is clear that the defect state has several features in common with the Ti 2p pattern, but not all features map onto each other. Comparison of the two diffraction patterns suggests that a significant signal from the defect came from Ti sites in the subsurface region. Signal was detected from the vacancy cations themselves (i.e., from Ti1), but it was difficult to determine how much signal was associated with the surface five-coordinate Ti cations

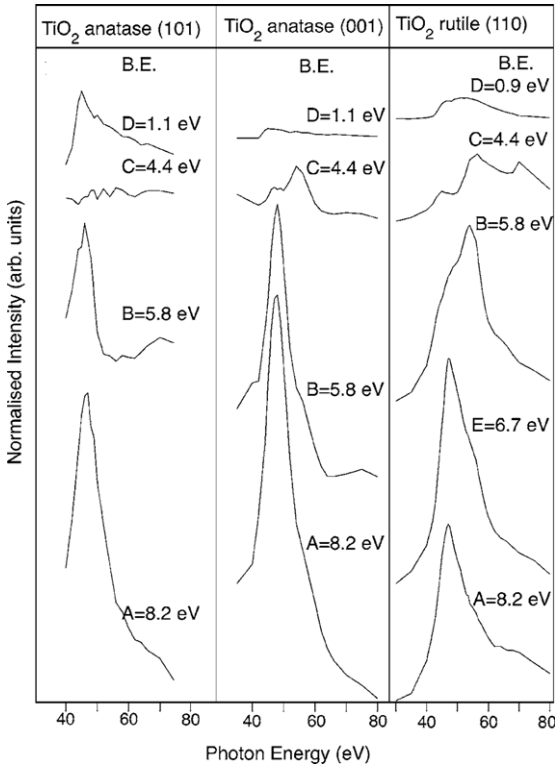

Fig. 7.22. Resonant photoemission signals as a function of photon energy measured at points A–E in Fig. 7.21 for A TiO_2(101), A TiO_2(001) and R TiO_2(110).
Source: Reprinted with permission from Thomas et al. [1543].
© 2007, by the American Physical Society.

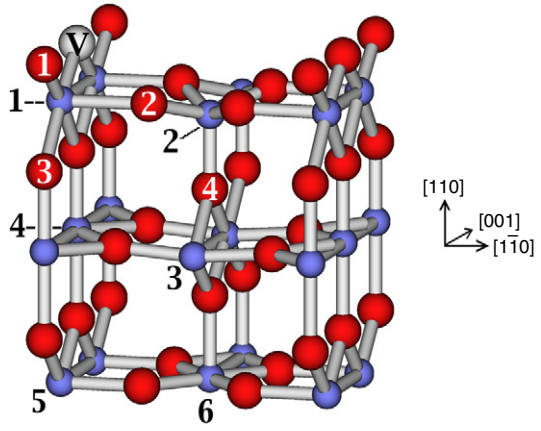

Fig. 7.23. Ball-and-stick model of the R TiO_2(110) surface and near-surface. Red (big) and blue (small) balls are O and Ti, respectively. 'V' indicates an O_{br} vacancy site. Numbers correspond to specific sites discussed in the text. (For interpretation of the references to color in this figure legend, the reader is referred to the web version of this article.)
Source: Reprinted with permission from Kruger et al. [1704].
© 2008, by the American Physical Society.

(labeled as Ti2 in Fig. 7.23) because their diffraction signal had no scatterers except in the in-plane directions (e.g., Ti2–O2). Nevertheless, these data suggest that the defect state on R TiO_2(110) is significantly delocalized in nature.

There have been few studies exploring the properties of point defects on TiO_2 surfaces other than that of the R TiO_2(110) surface. The groups of Diebold and Selloni [1705–1707] have examined oxygen vacancy defects on the R TiO_2(101) surface using STM and DFT approaches. These same authors have also looked at oxygen vacancies and subsurface point defects on the A TiO_2(101) surface [1676,1677,1708,1709]. They found that surface point

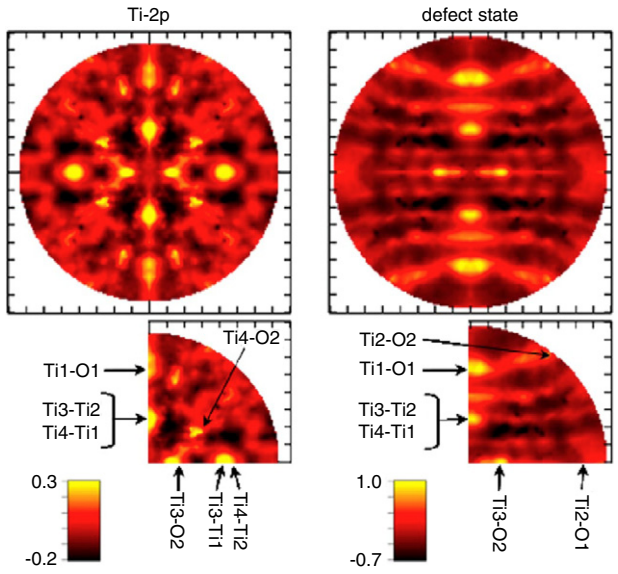

Fig. 7.24. (Top) Symmetrized photoelectron diffraction (PED) patterns from measurements in one quadrant (bottom) as a function of incident (θ) and azimuthal (ϕ) angles. Left: Standard PED from the Ti-2p3/2 core level. Right: Resonant PED from the bandgap defect state. The projection is linear in θ with the surface normal ($\theta = 0$) in the center. $\phi = 0$ ($\phi = 90$) is found at 3 o'clock (12 o'clock) and corresponds to the [−110] ((001)) direction. Number pairs in bottom indicate emitter–scatterer pairs (see Fig. 7.23).
Source: Reprinted with permission from Kruger et al. [1704].
© 2008, by the American Physical Society.

defects were less common on these surfaces compared to the R TiO_2(110) surface, but that shallow donor defects (such as Ti^{3+} sites) appeared to prefer subsurface sites rather than surface sites. By extension, this would suggest that excited electrons would not prefer trap sites on the A TiO_2(101) surface.

Extended defects: Two main types of extended defects are seen on TiO_2 surfaces: steps and reconstructions. Steps are prevalent irrespective of the level of surface reduction, but little is known about how these extended defects respond to shallow donor electrons. The R TiO_2(110) surface appears to be an exception in terms of how it responds to low levels of surface reduction. In contrast, the R TiO_2(100) and TiO_2(001) surfaces respond to low levels of reduction by reconstructing instead of stabilizing reduction as point defects [175,566]. However, even the R TiO_2(110) surface is known to reconstruct in order to accommodate high levels of surface reduction. Unfortunately, little is known about how these structural features respond to light or how adsorbates located in their vicinity respond to point charges generated by light. Komiyama and Li [203,204] used STM with modulated light sources (3 kHz) to observe changes in the tunneling current associated with charge carriers trapped at R TiO_2(110) surface sites. At photon energies above the R TiO_2 bandgap, these authors observed bright spots distributed over the surface. Some of these features could be linked to Ti^{3+}-related defects, such as the Ti_2O_3-like strands protruding from step edges. Irradiation with photon energies below the TiO_2 bandgap also resulted in new contrast features at these (and other) defects, suggesting that these excitations were localized and long-lived (on the STM imaging timescale). While it is unclear how to interpret the modulated change in the STM tunneling current in terms of which carriers were being observed, these data suggest that STM is responsive to photoexcitation events at TiO_2 surfaces and (in general) can detect such changes occurring at defects on the surface. Refinement of the scanning tunneling spectroscopy approach to STM [1710] also holds promise for interrogating variations in electronic structure associated with

local phenomena such as band bending or adsorbate-induced electrostatic potentials.

Step edges present unique physical and electronic structure environments on oxide surfaces that alter the reactivities of water and other typical adsorbates (e.g., see work of Gong et al. for the influence of steps on small molecule reactivity on A TiO_2(101) [1682,1711]). Uetsuka and coworkers [515] observed that the least reactive surface sites for hole-mediated photodecomposition of TMA on R TiO_2(110) were the step edges. This observation suggests that the electrostatics at step edges on this surface may repel holes but attract electrons. In contrast, Nakamura, et al. [584] proposed that kinks and other low coordination sites are the active sites on R TiO_2(110) and TiO_2(100) for water photooxidation (see below).

8. Special situations

There are several 'special situations' in which TiO_2 has contributed to fundamental research into heterogeneous photocatalysis. These include dye sensitized solar cells (DSSC), water splitting, CO_2 photoreduction, bactericide, photoinduced hydrophilicity and 'synthesis by photons'. With the exception of DSSC studies (discussion of which is sprinkled throughout this review), this section attempts to highlight some of the literature findings and research opportunities in these various areas, particularly when TiO_2 single crystal surfaces were used as models.

8.1. Water splitting

Water splitting is often termed 'the holy grail' of heterogeneous photocatalysis, and much has already been written about the use of TiO_2 in promoting photocatalytic processes associated with either the oxidative or reductive aspects of this reaction [3,10,43–59]. Fundamental studies of the chemistry of water (and hydroxyls) on single crystal TiO_2 surfaces provide a starting point for understanding the photochemical properties of this process [853]. Extensive experimental [138,192,194,195,199,527,566,580,792,795,797,799,803,804,807,810,843,852,1681,1683,1712–1717] and theoretical [193,522,527,792,810,824,826,830,831,1660,1682,1684,1711,1712,1717–1719] work has been invested in understanding the molecular-level interactions of water with single crystal TiO_2 surfaces. This author is unaware of any reports to date in which photochemical water splitting (in either half reaction) was performed on a single crystal TiO_2 surface under UHV conditions. This is despite the fact that the flat-band positions of either polymorph should (in concept) support these reactions [2].

8.1.1. Water oxidation

In concept, water photooxidation should be accessible on single crystal TiO_2 surfaces because the single electron oxidation potential of OH^- is above the VB maximum of either TiO_2 polymorph at flat-band potentials (see discussion and references in [2]). Fig. 8.1, from the work of Imanishi et al. [580] illustrates the band positions and redox potentials in relationship to various solution and adsorbed phase orbital positions for water and OH^-. The overall objective in water photooxidation is to convert water to oxygen using VB holes, according to Reaction 12:

$$H_2O + 2h^+ \Rightarrow 1/2\ O_2\ (g) + 2H^+. \quad (12)$$

Perhaps an equally significant objective of water photooxidation is to find ways that water (or OH^-) can act as a sacrificial electron donor. In this sense, O_2 formation would not be essential, and the key water oxidation reaction would be a single electron transfer step (Reaction 13):

$$H_2O + h^+ \Rightarrow OH\bullet + H^+. \quad (13)$$

As simple as Reaction 13 seems, it does not readily occur on TiO_2 surfaces. Salvador [732] has argued that thermalized VB holes on TiO_2 surfaces do not have the potential energy needed to oxidize either adsorbed H_2O or OH^- groups. That author states "…*from a thermodynamic point of view* (H_2O photooxidation is) *only possible if the energy of filled surface states associated with adsorbed water species is equal or lower than the energy of filled surface states associated with terminal oxygen ions, which constitute the top of the VB at the* TiO_2 *surface*". (See Fig. 8.1 for schematic view of these relationships.) This statement is made with the realization that on a local scale, the electron structures of species (adsorbed water/OH^-) in the vicinity of a surface trapped hole (e.g., at a terminal O anion site) will be modified, but likely not to the extent needed to make hole transfer to these species favorable, even though mixing between VB hole states and O 2p states of adsorbed water/OH^- should not be negligible [522]. Consistent with Salvador's premise, the Nakato group [580,584,1720] has proposed that the key step in water photooxidation involves a nucleophilic attack of water in the aqueous/physisorbed phase with a trapped surface hole on a surface 3-coordinate O anion site and not due to a hole reaction with an adsorbed H_2O/OH^- species. In this case, variations in dynamics at the solvent–surface interface may provide transient conditions in which energy matching between a VB hole and water/OH^- might be more favorable. A similar supposition has been made by Cheng and Selloni [1721] for OH^- oxidation by VB holes at the surface of A TiO_2(101).

In a different mechanistic approach, Valdés et al. [1718,1722] examined the energetics of the water photoelectrocatalytic oxidation reaction on R TiO_2(110) as a function of applied bias, pH and coverage using the potential of thermalized VB hole as a reference point. Based on their calculations, which were done in the absence of interactions typical to solution conditions, these authors proposed a 4 step mechanism for water oxidation involving single electron/proton transfer events, as shown in Reactions 14–17:

$$H_2O + {}^* \Rightarrow OH\bullet{}^* + H^+ + e^- \quad (14)$$

$$OH\bullet{}^* \Rightarrow O^* + H^+ + e^- \quad (15)$$

$$H_2O + O^* \Rightarrow HOO\bullet{}^* + H^+ + e^- \quad (16)$$

$$HOO\bullet{}^* \Rightarrow O_2 + H^+ + e^- \quad (17)$$

where '*' represents a 5-coordinate Ti^{4+} site on the R TiO_2(110) surface. Several adsorbate terminations of the R TiO_2(110) surface were used, with the most favorable being the fully O-terminated surface. The energetics for these reactions on this surface, as a function of potential at two pH extremes, are shown in Fig. 8.2. (Direct combination of O atoms (O^*) to form O_2 can be excluded from this reaction mechanism based on their high stability and high barrier to diffusion on the R TiO_2(110) surface [824].) As is known in the literature, the zero bias (flat-band) process (solid lines) is energetically unfavorable, with Reaction 14 being the rate limiting step. However, the authors showed that only modest biases were required in their calculations to make the overall reaction on this surface favorable. Valdés et al. proposed that the surface potential of the O-termination, under irradiation, was sufficient to permit water photooxidation at room temperature if cathodic processes were not the rate limiting step. The question arises then as to why water photooxidation has not been reported on R TiO_2(110) under UHV conditions. One explanation could be that cathodic processes (water reduction or some available electron scavenging reaction) are the rate limiting step. Kinetic limitations in UHV may also include the flux of holes, the lifetimes of key intermediates (such as adsorbed HOO•) or the stability of the O-terminated surface (which has not been observed experimentally). Alternatively, the dynamics of a solvation layer may be necessary, as suggested above.

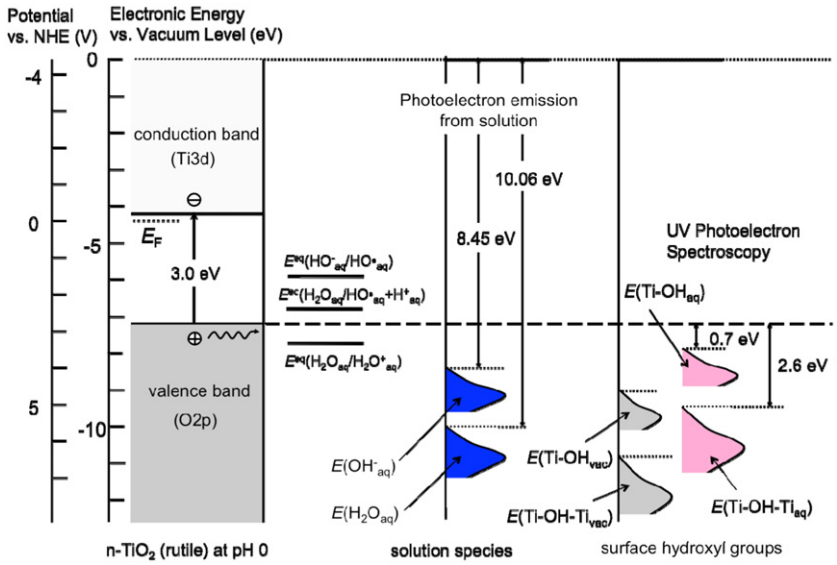

Fig. 8.1. Energy levels of O 2p states for various oxygen species at the surface of TiO_2 estimated from literature photoemission spectra, referenced to the CB and VB edges TiO_2 at pH 0. (See paper for details.)
Source: Reprinted with permission from Imanishi et al. [580].
© 2007, American Chemical Society.

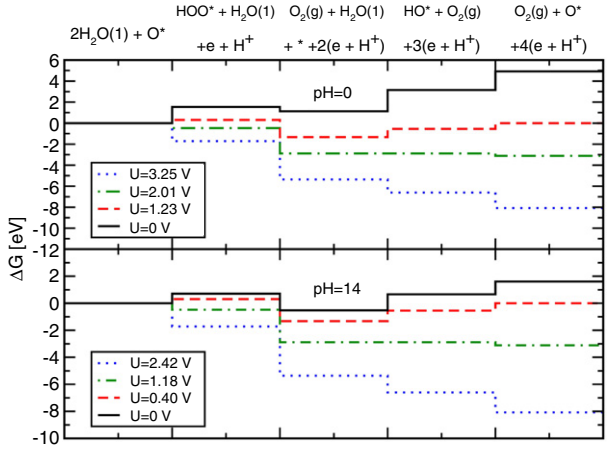

Fig. 8.2. Free energies of intermediates in the water photooxidation reaction on the O-termination surface of R TiO_2(110) at pH = 0 and 14 as a function of surface potential (U).
Source: Reprinted with permission from Valdes et al. [1718].
© 2008, American Chemical Society.

Studies detailed in Section 5.2 suggest that hole-mediated reactions on R TiO_2(110) are not limited by issues associated with creation, transport or surface stabilization of holes. As highlighted in the discussion on SCN^- photooxidation (Section 3.2), the survival rate of holes reaching the TiO_2 surface is sufficiently high that one can surmise that slow transfer rates in other adsorbate systems are likely due to the electron transfer process in question. The degree of surface oxidation, however, does have a significant influence on hole-mediated electron transfer rates on R TiO_2(110) [202]. At present, the approach of Valdés and coworkers involving a thermodynamic assessment to modeling water oxidation has not been extended to other R TiO_2 terminations or to A in attempt to better understand the relative importance of thermodynamic versus kinetic limitations of water oxidation on TiO_2. A next step might be the A TiO_2(101) surface, which Kavan et al. [116] found photooxidizes water at flat-band potential relative to the 0.2 eV bias required on R TiO_2(001).

8.1.2. Water reduction

A major limitation of water photoreduction on TiO_2 surfaces appears to be the H_2 formation step. Noble metal co-catalysts

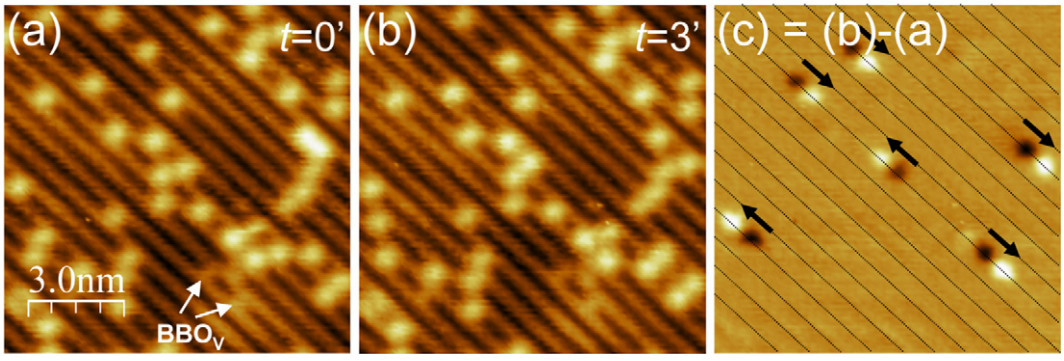

Fig. 8.3. STM images (a and b) on hydroxyl-covered R TiO_2(110) at 381 K acquired three minutes apart. (c) Difference image (b–a). The dark and bright spots represent the initial and final hydrogen positions, respectively. The black arrows show the hopping directions. Black lines mark positions of the O_{br} rows. (Image conditions: 1.5 V bias, 0.1 nA current.)
Source: Reprinted with permission from Li et al. [1716].
© 2008, American Chemical Society.

have been used to assist in lowering the H_2 formation barrier (see Section 6.1), but little is known about the molecular-level details of mass and charge transport between TiO_2 and supported metal particles. The impact of the choice of electron donor on the production of H_2 from water photoreduction on Pt/TiO_2 is a prime example [1723]. As in the photooxidation case, the flat-band CB position of TiO_2 (especially in A) appears to be sufficient to promote reduction of water, however potential energy loss from electron trapping remains an issue (see Sections 2.4 and 5.3). For example, it is well-known that oxygen vacancy sites on the R TiO_2(110) surface dissociate water [175,566,792,853], but that the thermodynamic preference is for recombination of the fragments to reform water instead of H_2 production, as shown in Reactions 18 and 19:

$$H_2O + \text{vac}(2Ti^{3+}) + O_{br}^{2-} \Rightarrow 2OH_{br}^{-}(2Ti^{3+}) \quad (18)$$

$$2OH_{br}^{-} \Rightarrow H_2O + \text{vac}(2Ti^{3+}) + O_{br}^{2-} \quad (19)$$

and not Reaction 20:

$$2OH_{br}^{-}(2Ti^{3+}) \Rightarrow H_2\,(g) + 2O_{br}^{2-}(2Ti^{4+}) \quad (20)$$

(where 'vac' signifies a bridging oxygen vacancy possessing nominally two Ti^{3+} sites). Absence of H_2 formation, when all the raw ingredients are present (two protons and two near-CB edge electrons) in close proximity suggests kinetic and/or thermodynamic barriers to H_2 formation on bare TiO_2. Insights in the diffusion of H atoms along the rows of bridging oxygen sites on R TiO_2(110) by Li and coworkers [1716] indicate the former at least. Using STM and DFT, these authors examined the hopping of H atoms along the O_{br}^{2-} rows on R TiO_2(110). As shown in Fig. 8.3, their data shows that STM was able to follow the motion of H along the O_{br}^{2-} rows. Analysis of many H hopping events as a function of temperature provided data for construction of Arrhenius plots for determination of the H and D hopping kinetic parameters, as shown in Fig. 8.4. The energy barriers for hopping were sufficiently high (~0.75 eV for H and ~0.85 eV for D) to preclude significant numbers of hopping events occurring at room temperature (at low H/D coverages). However, an unusual finding from their studies was the very low prefactors ($\sim 10^{7.5-8.5}$ s^{-1}) associated with hopping indicated a non-classical mechanism, such as tunneling (which would be consistent with the H/D differences). As an aside, Li and coworkers also showed that two OH_{br}^{-} groups formed from water dissociation in an oxygen vacancy sites on R TiO_2(110) were inequivalent based on STM observations that indicated that the deposited H atom was the first to move in the majority of cases (see Fig. 8.5). After the first hopping event, both H atoms exhibited the same hopping kinetics irrespective of their origin. These data indicate that the electronic structure of the vacancy sites on R TiO_2(110) retained some of its 'pre-water dissociation' character and only adopted a new electronic character after the H atoms moved away from each other. Both STM and DFT showed that the return of the two separated H atoms (or of any two H atoms for that matter) to a paired configuration seen when water first dissociated was highly unlikely at room temperature. So, to the extent that oxygen vacancy sites can mimic the properties of photoexcited/trapped electrons on TiO_2 surfaces, these results point to significant barriers in the approach of two H atoms to each other in order to form H_2.

The ability of water to be reduced by attachment of an excited electron (as opposed to trapped electrons that can be modeled with oxygen vacancy sites) has been explored by this author and colleagues [199]. Fig. 8.6 shows EELS data for the R TiO_2(110) surface with and without various water treatments. Trace 'a' corresponds to the clean surface (with a high surface concentration of oxygen vacancy sites) showing the ~0.9 eV optical excitation event associated with localized electrons at the defects, the band-to-band threshold at ~3 eV, and peak transitions in the band-to-band transition at ~4 eV (shoulder) and 5.2 eV (see

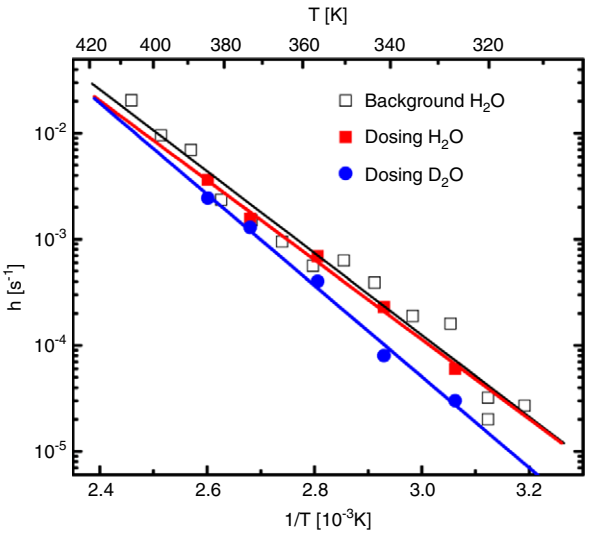

Fig. 8.4. Arrhenius plot for the along-row diffusion of H and D for separated hydroxyl groups on the R TiO_2(110) surface. Best fits to the data are shown with solid lines, yielding prefactors of $10^{7.6\pm0.6}$, $10^{7.3\pm0.4}$, and $10^{8.6\pm0.6}$ s^{-1} and diffusion barriers of 0.76 ± 0.06, 0.74 ± 0.03, and 0.85 ± 0.04 eV for background H_2O (black), dosed H_2O (red), and dosed D_2O (blue), respectively. (For interpretation of the references to color in this figure legend, the reader is referred to the web version of this article.)
Source: Reprinted with permission from Li et al. [1716].

Section 1). Deposition of a thick ice film on the surface facilitated measurement of the water 'bandgap' (~7.2 eV) and the peak HOMO–LUMO (lowest unoccupied molecular orbital) transition energy in water at ~8.3 eV (trace 'b'). (Notice that features from TiO_2 were absent indicating a thick ice.) At the monolayer H_2O coverage (trace 'c'), this latter transition was weak (if present at all), but two other findings were more noteworthy. First, the defect feature was relatively unaffected by water, in agreement with previous photoemission studies [803], indicating little if any charge transfer from Ti^{3+} to adsorbed water. Second, the band-to-band region was overshadowed by a strong feature at 6.2 eV that disappeared after thermal removal of chemisorbed water (traces 'd' and 'e'). Using photoemission data in the literature for the VB region of R TiO_2(110), these authors assigned the 6.2 eV feature to excitation of a VB electron (at ~5–5.5 eV below the Fermi level) to the LUMO of adsorbed H_2O ($4a_1$ state). This assignment places the LUMO of an adsorbed water molecule at ~1.2 eV above Fermi level, commensurate with a point of high DOS in the TiO_2 CB (see Section 1), but perhaps too high in energy for an electron at the CB minimum to couple. Attempts to photochemically access such transitions with UV light for water on R TiO_2(110) have not resulted in spectral or chemical evidence for dissociated water [1724,1725]. These data suggest that water photoreduction on R TiO_2(110) does not readily proceed via electron attachment to adsorbed water molecules, particularly in the absence of a suitable co-catalyst.

8.2. CO_2 *photoreduction*

The subjects of CO_2 capture and conversion have grown in interest among heterogeneous photochemists, particularly as the world becomes increasingly 'CO_2-conscious'. Usubharatana and coworkers [1726] have reviewed the literature on CO_2 heterogeneous photocatalysis. While some groups have employed TiO_2-based catalysts, it is clear that the most viable materials are not TiO_2-based. Nevertheless, TiO_2 and TiO_2-based materials continue to provide unique settings for better understanding CO_2 surface chemistry and photochemistry [1186,1287,1288,1404,

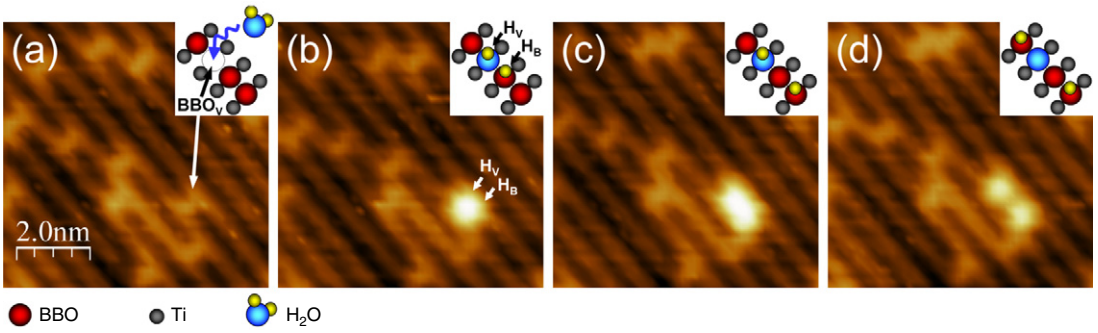

Fig. 8.5. STM images of the same area on R TiO_2(110) at 357 K during dissociative adsorption of water at an O_{br} vacancy site: (a) clean surface with several O_{br} vacancy sites (labeled 'BBO_v'); (b) after dissociation of a water molecule at the vacancy site labeled in 'a' generating a geminate hydroxyl pair (H_V marks the OH hydrogen at the previous vacancy location and 'H_B' the hydrogen that split off to a neighboring O_{br} site); (c) after a single hop of the H_B hydrogen; and (d) after subsequent hops of the H_V hydrogen. Insets show the ball models illustrating the corresponding processes. (Image conditions: 1.5 V bias, 0.1 nA current.)
Source: Reprinted with permission from Li et al. [1716].

1468,1518,1604,1619–1622,1727–1745]. In general, such studies suggest that either co-catalysts or thermal activation is required for CO_2 photoreduction on TiO_2. However, mechanistic details associated with single electron transfer events are few. CO_2^- is believed by some groups to be a key surface intermediate in photoreduction on TiO_2, implying direct electron attachment to an adsorbed CO_2-containing species [1727,1728,1746]. The transition from this species to those possessing C–H bonds is still unclear.

The only published results on the photoreduction of CO_2 on a TiO_2 single crystal surface were briefly reported by Anpo et al. [1730] for the R TiO_2(100) and TiO_2(110) surfaces. These authors examined these surfaces before and after exposure to CO_2 + H_2O gas mixtures (under non-UHV conditions), with and without UV irradiation. Analysis of the reactor background indicated methane and methanol formation (only the former from TiO_2(100)), and subsequent surface analysis in vacuum with HREELS showed evidence for surface species possessing C–H bonds (see Fig. 8.7). These features were not observed without UV irradiation indicating their source was not background reactions in the reactor. The nature of these C–H containing surface species, their formation pathways and their sensitivities to surface structure, coverage, water, co-catalysts, etc., await further study.

8.3. Bactericide

The ability of TiO_2 to kill bacteria, destroy viruses and perform chemical transformations on a wide range of biomolecules under UV irradiation is an intriguing and potentially commercially important attribute of this material's photocatalytic properties. Numerous studies have explored this phenomena with high surface area and thin film TiO_2 samples [128,339,745,1395,1563, 1639,1641,1747–1774]. This aspect of TiO_2 photocatalysis was recently reviewed by Fujishima and coworkers [2], and will only briefly be visited in this review.

The mechanism of bactericide (and other forms of bioorganism killing) is widely believed to involve destruction of cell walls [745, 1747,1748,1751,1753–1755], presumably through the chemical action of OH• (or related radical species). For example, Maness et al. [1747] examined the mechanism of *E. coli* K-12 cell death resulting from TiO_2 photolysis. They observed death only with TiO_2 present under illumination. The rate of cell death matched the rate of malondialdehyde production resulting from peroxidation of the cell membrane lipids. Loss of the cell's respiratory ability (as noted by a change in O_2 uptake and in electron donor concentration) matched the kill rate, leading these authors to conclude that degradation of polyunsaturated phospholipid portion of the cell's lipid membrane was the cause. Destruction of cell walls via

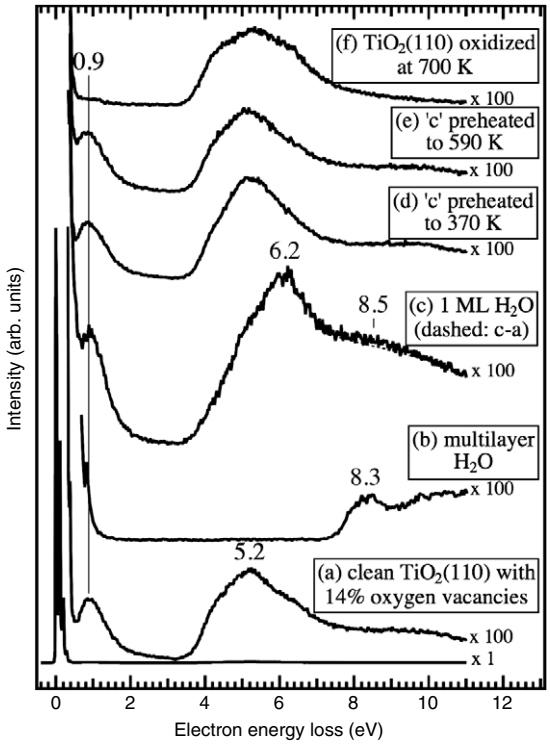

Fig. 8.6. EELS spectra from the interaction of water and oxygen on R TiO_2(110) with 0.14 ML oxygen vacancy sites: (a) clean surface; (b) multilayer H_2O; (c) 1 ML of H_2O; (d) 1 ML of H_2O after heating to 370 K; (e) 1 ML of H_2O after preheating to 590 K; (f) 1 ML of H_2O after exposure to O_2 at 700 K. All spectra recorded at 120 K.
Source: Reprinted with permission from Henderson et al. [199].

TiO_2 photochemistry can also be observed with scanning probe techniques, as shown in Fig. 8.8 from the work of Nadtochenko et al. [1775–1778]. Cell destruction was apparent in the case of *E. coli* and TiO_2 irradiated with UV (second image from top), but not in the absence of irradiation (first image) or when cells were irradiated in the absence of TiO_2 (bottom images). Commensurate with scanning probe evidence for cell wall failure, Nadtochenko and coworkers observed formation of peroxidation products that signaled oncoming of bacterial lyses and spectral evidence for cell wall degradation.

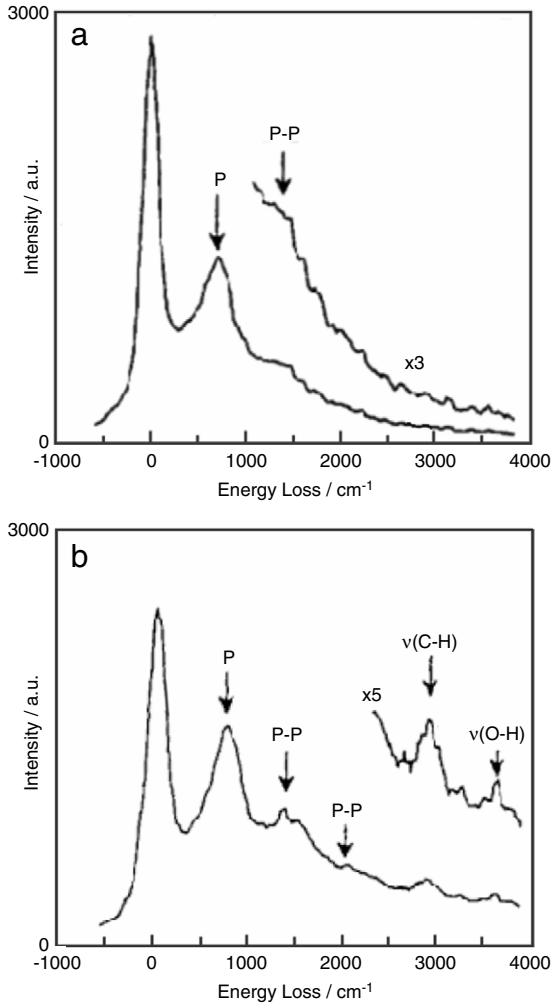

Fig. 8.7. HREELS spectra of the R TiO_2(100) surface before (a) and after (b) exposure to 1:3 gas mixture of CO_2 and H_2O (4 Torr total) and irradiated with UV light. ('P' corresponds to a phonon feature and 'P–P' to a multiple phonon feature.)
Source: From Anpo et al. [1730].

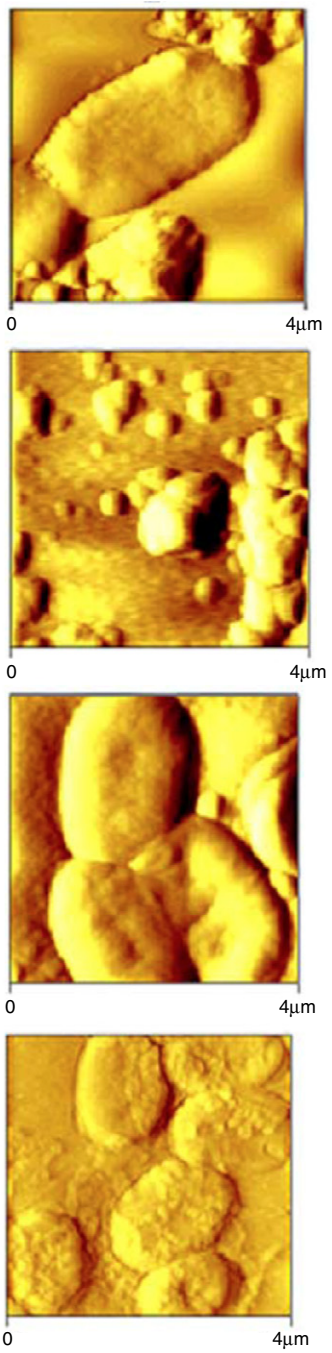

Fig. 8.8. AFM images of *E. coli* and P-25: *E. coli* alone (top); *E. coli* in a P-25 slurry after 1 h UV irradiation (second down); *E. coli* without Degussa P-25 (third down); *E. coli* without P-25 after 1 h UV irradiation (bottom).
Source: Adapted from Nadtochenko et al. [1775].

8.4. Photoinduced hydrophilicity

Fujishima and coworkers [2] highlighted one of the interesting applications of TiO_2 as a photocatalyst — that of coatings on glass surfaces that promote self-cleaning, antifogging and similar other functions. In particular, the so-called 'photoinduced hydrophilicity' effect has received considerable attention in the literature [265,266,740,1779–1814]. It can be shown that UV irradiation of a wide variety of TiO_2 surfaces under ambient conditions causes water droplets to smooth out and fog to clear. These effects are reversed if the light is turned off or if O_2 is removed from the ambient. As can be glean from the Fujishima et al. review [2], there is considerable controversy as to the *main* source of this effect, with groups falling into two camps: (1) those attributing the effect to UV light induced modifications of the TiO_2 surface that facilitate better wetting [1783–1791]; and (2) those attributing the effect to the well-known photooxidation properties of TiO_2 in removing hydrophobic organic adlayers from the TiO_2 surface [740,1779–1782]. Both sides of this issue have been presented in the Fujishima et al. review [2], and need not be repeated here. However, this review will make three comments on this subject from a surface science perspective. The first is that clean TiO_2 single crystal surfaces are inherently hydrophilic in nature based on numerous UHV studies on water adsorption (see Section 8.1 above). This assertion is intended to correct a mistaken impression to the contrary made in the Fujishima et al. review (on p. 562), which stated that one of the conclusions of White et al. [1782] was that "*…the original* TiO_2 *surface is highly hydrophobic, without UV illumination, because it is clean…*". The work by White et al. shows that TiO_2 surfaces are inherently hydrophilic and do not require surface defects for water 'wetting' to occur. The second point is that there is no evidence in the surface science literature (as yet) for UV irradiation generating structural defects on the local or extended scales. Nakato's group [672,1653,1654,1675] has shown that TiO_2 surfaces can be roughened and etched under photoelectrochemical conditions with an etchant present (such as hypochlorite), but these conditions are unlike those reported in

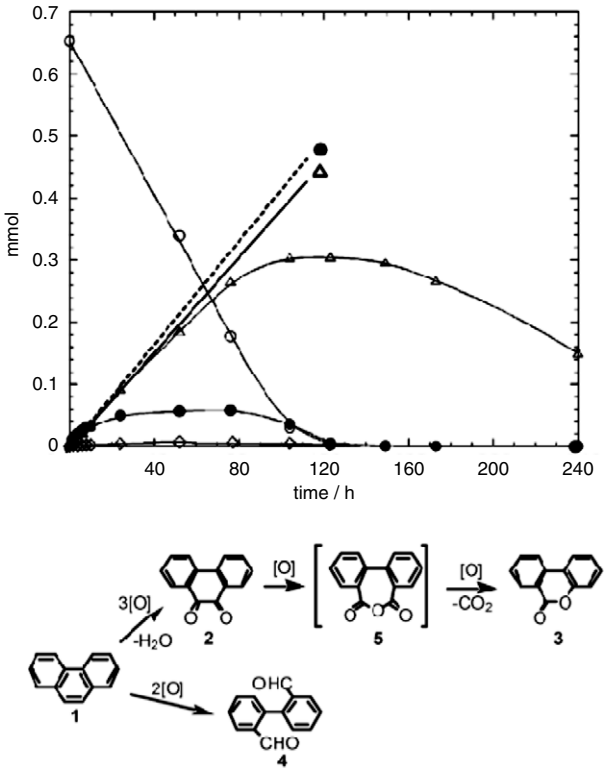

Fig. 8.9. (Top) Time-dependent changes in the amounts (based on HPLC) of 1 (open circles), 2 (diamonds), 3 (triangles), and 4 (filled circles) resulting from partial photooxidation of phenanthrene (1) on TiO_2. Solid and dashed lines are extrapolations of initial rates of the indicated species. (Bottom) Proposed reaction mechanism.
Source: From Higashida et al. [1825]. Reproduced by permission of the Royal Society of Chemistry.

typical studies. Also, the etched surface structures generated by Nakato and coworkers have not been shown to increase surface wetting. Finally, UHV scientists know that even brief exposure of surfaces to atmospheres of 10^{-6} Torr or higher pressure result in rapid surface contamination by a variety of strongly bound species that include organics. Even in a glove box with part-per-billion atmospheric control, the flux of 'background gases' at a surface will be at the monolayers-per-second level. Under these conditions, it is not possible for researchers to control surface contamination to a level needed in order to adequately differentiate between the two mechanisms ascribed to the photohydrophilicity effect. Clearly, more studies are required under conditions in which the effects of background hydrocarbon contamination can be better controlled (e.g., see work by Zubkov and coworkers [1780]).

8.5. Synthesis by photons

There may come a time when photochemical processes at heterogeneous surfaces are used for applications other than generation of electricity (i.e., DSSC), production of energy storage molecules (i.e., H_2 from H_2O or hydrocarbons from CO_2), or for environmental remediation through photochemical mineralization of contaminants. Papers are emerging in the field which have examined specialized synthetic processes using TiO_2 as a photocatalyst. Examples include selective formation of certain biomolecules [1815–1817], carbemide formation [1818], Cl_2 production [1819], cross-linking in fibers [1820,1821], epoxidation and selective oxidation reactions [926,929,1021,1598,1822–1827], ozone formation [1828], hydrogen peroxide production [1486, 1829,1830], selective isomerization reactions [986], nitro group addition [1831,1832], polymerization processes [1833–1836], urea formation [1837,1838] and a variety of other miscellaneous processes [925,1368,1839–1846]. The photooxidation of alkenes to generate epoxides has been explored in the cases of several molecules, including 1-hexene [1823], 1-decene: [1823,1847], various cyclic olefins [1598], propene [1822], and styrene [1824]. In these examples, careful control of the oxidative conditions is needed to promote the desired product but prevent additional oxidation. By controlling the extent of photooxidation, Higashida and coworkers [1825] were able to perform partial oxidation reactions on phenanthrene over P-25, as shown in Fig. 8.9. In other cases, the absence of O_2 is required. For example, Senanayake and Idriss [1817] followed photoreactions of formamide (NH_2CHO) on the reconstructed surface of R TiO_2(001) under UHV conditions (i.e., extremely low O_2 partial pressure). They found that UV irradiation of this adsorbed molecule lead to C–C and C–N bond formation reactions as opposed to the oxidation reactions expected with O_2 present. These bond formation processes yielded trace amounts of several important biomolecules (e.g., DNA bases) adsorbed on the surface. The authors speculated that such heterogeneous photoreactions (not necessarily on TiO_2) may have played important roles in synthesis of biomolecules needed in emergence of biological systems during early evolution.

9. Conclusions

This review highlights some of the significant insights obtained from molecular-level studies of TiO_2 photocatalysis, in particular those obtained using a surface science perspective. Examples include:

- the ability to prepare well-defined surfaces, in some cases doped with high certainty, and characterize experimentally and theoretically correlations between TiO_2 surface properties and photocatalytic behavior;
- the ability to mechanistically and dynamically follow single electron transfer events at TiO_2 surfaces;
- the ability to correlate bulk phenomena (such as photon absorption or carrier hopping) with surface events;
- the ability to relate adsorbate chemistry and structure on a site-by-site basis with molecular charge transfer reactivity;
- the ability to decipher the complex, interdependent thermal and non-thermal chemistries associated with redox processes involving many concurring electron transfer events;
- the ability to define surface structures of complex TiO_2 photocatalytic materials with specific properties that optimize activity.

Numerous opportunities and challenges still remain. The R TiO_2 (110) surface has proved indispensable in providing researchers with a setting for studying fundamental processes important to TiO_2 photocatalysis under well-controlled conditions. Work on other well-defined TiO_2 surfaces (e.g., other important orientations of R or A) is moving forward. The ability of researchers to utilize single crystal surfaces to model *indirect* processes (such as OH• formation and reaction) remains to be seen. While many studies point to the influences that additives (e.g., dopants, co-catalysts, etc.) have on TiO_2 photocatalysis, much work is still needed on the molecular-level in order to understand how these additives influence such phenomena as photon absorption, electron transfer and thermal/non-thermal chemistry at TiO_2 surfaces. Work is needed that probes spin states, trap states and electron transfer events. More detailed knowledge is needed about the dynamics of electron transfer in order to design surfaces/interfaces that promote (or inhibit as the case may be) particular events. Many fundamental insights have been obtained from studying thermodynamically 'down-hill' photoreactions such

as organic photooxidation, but little is known at the molecular-level about the electron transfer dynamics and mechanistic aspects of important 'up-hill' reactions such as water photooxidation or C–H bond formation reactions. This review has illustrated how a surface science perspective on TiO_2 photocatalysis can provide unique insights and motivate more fundamental research in heterogeneous photocatalysis.

Acknowledgments

This work was supported by the US Department of Energy, Office of Basic Energy Sciences, Division of Chemical Sciences. Pacific Northwest National Laboratory is a multiprogram national laboratory operated for the US Department of Energy by the Battelle Memorial Institute under contract DEAC06-76RLO1830.

References

[1] A. Fujishima, K. Honda, Nature 238 (1972) 37.
[2] A. Fujishima, X. Zhang, D.A. Tryk, Surface Science Reports 63 (2008) 515.
[3] M. Grätzel, Modern Aspects of Electrochemistry 15 (1983) 83.
[4] P.V. Kamat, Chemical Reviews 93 (1993) 267.
[5] A. Emeline, A. Salinaro, V.K. Ryabchuk, N. Serpone, International Journal of Photoenergy 3 (2001) 1.
[6] A.V. Emeline, V.K. Ryabchuk, N. Serpone, Catalysis Today 122 (2007) 91.
[7] A.V. Emeline, V.K. Ryabchuk, N. Serpone, Journal of Physical Chemistry B 109 (2005) 18515.
[8] K. Rajeshwar, Journal of Applied Electrochemistry 15 (1985) 1.
[9] V. Ryabchuk, International Journal of Photoenergy 6 (2004) 95.
[10] K. Rajeshwar, Journal of Applied Electrochemistry 37 (2007) 765.
[11] Y. Xu, M.A.A. Schoonen, American Mineralogist 85 (2000) 543.
[12] Y. Matsumoto, Journal of Solid State Chemistry 126 (1996) 227.
[13] N. Serpone, R.F. Khairutdinov, Studies in Surface Science and Catalysis 103 (1996) 417.
[14] X. Chen, S.S. Mao, Chemical Reviews 107 (2007) 2891.
[15] R.L. Pozzo, M.A. Baltanas, A.E. Cassano, Catalysis Today 39 (1997) 219.
[16] J.M. Herrmann, Catalysis Today 53 (1999) 115.
[17] L. Jing, Y. Qu, B. Wang, S. Li, B. Jiang, L. Yang, F. Wei, H. Fu, J. Sun, Solar Energy Materials and Solar Cells 90 (2006) 1773.
[18] A. Fujishima, T.N. Rao, Pure and Applied Chemistry 70 (1998) 2177.
[19] A. Fujishima, T.N. Rao, D.A. Tryk, Journal of Photochemistry and Photobiology C 1 (2000) 1.
[20] A. Mills, R.H. Davies, D. Worsley, Chemical Society Reviews 22 (1993) 417.
[21] A. Mills, M. Mcfarlane, Catalysis Today 129 (2007) 22.
[22] A. Mills, S. Lehunte, Journal of Photochemistry and Photobiology A 108 (1997) 1.
[23] D.F. Ollis, CatTech 2 (1998) 149.
[24] M. Kitano, M. Matsuoka, M. Ueshima, M. Anpo, Applied Catalysis A 325 (2007) 1.
[25] O. Carp, C.L. Huisman, A. Reller, Progress in Solid State Chemistry 32 (2004) 33.
[26] S. Anandan, M. Yoon, Journal of Photochemistry and Photobiology C 4 (2003) 5.
[27] M.R. Hoffmann, S.T. Martin, W.Y. Choi, D.W. Bahnemann, Chemical Reviews 95 (1995) 69.
[28] T. Rajh, O.V. Makarova, M.C. Thurnauer, D. Cropek, in: M.-I. Baraton (Ed.),Synthesis, Functionalization and Surface Treatment of Nanoparticles, Los Angeles, CA, 2003.
[29] M.A. Fox, M.T. Dulay, Chemical Reviews 93 (1993) 341.
[30] C.Y. Wang, R. Pagel, J.K. Dohrmann, D.W. Bahnemann, Comptes Rendus Chimie 9 (2006) 761.
[31] A. Fujishima, X.T. Zhang, Comptes Rendus Chimie 9 (2006) 750.
[32] P. Calza, E. Pelizzetti, C. Minero, Journal of Applied Electrochemistry 35 (2005) 665.
[33] M. Anpo, M. Takeuchi, Journal of Catalysis 216 (2003) 505.
[34] K. Hashimoto, H. Irie, A. Fujishima, Japanese Journal of Applied Physics 1 44 (2005) 8269.
[35] T. Tachikawa, M. Fujitsuka, T. Majima, Journal of Physical Chemistry C 111 (2007) 5259.
[36] N. Serpone, Journal of Photochemistry and Photobiology A 104 (1997) 1.
[37] U.I. Gaya, A.H. Abdullah, Journal of Photochemistry and Photobiology C 9 (2008) 1.
[38] A. Mills, S. Hodgen, S.K. Lee, Research on Chemical Intermediates 31 (2005) 295.
[39] N. Serpone, Solar Energy Materials and Solar Cells 38 (1995) 369.
[40] E. Pelizzetti, Solar Energy Materials and Solar Cells 38 (1995) 453.
[41] K. Iino, M. Kitano, M. Takeuchi, M. Matsuoka, M. Anpo, Current Applied Physics 6 (2006) 982.
[42] G.H. Li., K.A. Gray, Chemical Physics 339 (2007) 173.
[43] (a) J. Nowotny, C.C. Sorrell, T. Bak, L.R. Sheppard, Solar Energy 78 (2005) 593;
(b) T. Bak, J. Nowotny, M. Rekas, C.C. Sorrell, International Journal of Hydrogen Energy 27 (2002) 991.
[44] J. Nowotny, T. Bak, M.K. Nowotny, L.R. Sheppard, Journal of Physical Chemistry B 110 (2006) 18492.
[45] M. Ashokkumar, International Journal of Hydrogen Energy 23 (1998) 427.
[46] N. Serpone, E. Pelizzetti, M. Grätzel, Coordination Chemistry Reviews 64 (1985) 225.
[47] M. Grätzel, Accounts of Chemical Research 14 (1981) 376.
[48] N. Serpone, J.R. Norris Jr., Dan Miesel (Eds.), Photochemical Energy Conversion, New York, 1989.
[49] T. Ohta, International Journal of Hydrogen Energy 13 (1988) 333.
[50] A.J. Bard, M.A. Fox, Accounts of Chemical Research 28 (1995) 141.
[51] A. Yamakata, T. Ishibashi, H. Onishi, Journal of Molecular Catalysis A 199 (2003) 85.
[52] V.N. Parmon, Advances in Hydrogen Energy 9 (1990) 801.
[53] N. Getoff, International Journal of Hydrogen Energy 9 (1984) 997.
[54] M. Kitano, K. Tsujimaru, M. Anpo, Topics in Catalysis 49 (2008) 4.
[55] M. Ni, M.K.H. Leung, D.Y.C. Leung, K. Sumathy, Renewable and Sustainable Energy Reviews 11 (2007) 401.
[56] T. Takata, A. Tanaka, M. Hara, J.N. Kondo, K. Domen, Catalysis Today 44 (1998) 17.
[57] P.R. Ryason, Energy Sources 4 (1978) 1.
[58] D.E. Scaife, Solar Energy 25 (1980) 41.
[59] M. Matsuoka, M. Kitano, M. Takeuchi, K. Tsujimaru, M. Anpo, J.M. Thomas, Catalysis Today 122 (2007) 51.
[60] M.G. Walter, E.L. Warren, J.R. Mckone, S.W. Boettcher, Q.X. Mi, E.A. Santori, N.S. Lewis, Chemical Reviews 110 (2010) 6446.
[61] A. Hagfeldt, M. Grätzel, Chemical Reviews 95 (1995) 49.
[62] D.A. Tryk, A. Fujishima, K. Honda, Electrochimica Acta 45 (2000) 2363.
[63] G.A. Shreve, N.S. Lewis, Journal of the Electrochemical Society 142 (1995) 112.
[64] H. Tributsch, F. Willig, Solar Energy Materials and Solar Cells 38 (1995) 355.
[65] W.R. Duncan, O.V. Prezhdo, Annual Review of Physical Chemistry 58 (2007) 143.
[66] P.V. Kamat, Journal of Physical Chemistry C 111 (2007) 2834.
[67] L. Gundlach, R. Ernstorfer, F. Willig, Progress in Surface Science 82 (2007) 355.
[68] G.K. Mor, O.K. Varghese, M. Paulose, K. Shankar, C.A. Grimes, Solar Energy Materials and Solar Cells 90 (2006) 2011.
[69] M. Grätzel, Journal of Photochemistry and Photobiology A 164 (2004) 3.
[70] M. Grätzel, Inorganic Chemistry 44 (2005) 6841.
[71] J.R. Durrant, Journal of Photochemistry and Photobiology A 148 (2002) 5.
[72] O.V. Prezhdo, W.R. Duncan, V.V. Prezhdo, Accounts of Chemical Research 41 (2008) 339.
[73] G.J. Meyer, Journal of Photochemistry and Photobiology A 158 (2003) 119.
[74] J.Z. Zhang, Journal of Physical Chemistry B 104 (2000) 7239.
[75] K.M.P. Bandaranayake, M.K. Indika Senevirathna, P.M.G.M. Prasad Weligamuwa, K. Tennakone, Coordination Chemistry Reviews 248 (2004) 1277.
[76] M.T. Spitler, B.A. Parkinson, Accounts of Chemical Research 42 (2009) 2017.
[77] A. Hagfeldt, G. Boschloo, L.C. Sun, L. Kloo, H. Pettersson, Chemical Reviews 110 (2010) 6595.
[78] D.F. Ollis, Topics in Catalysis 35 (2005) 217.
[79] R.K. Herz, Chemical Engineering Journal 99 (2004) 237.
[80] P.R. Gogate, A.B. Pandit, AIChE Journal 50 (2004) 1051.
[81] A. Wold, Chemistry of Materials 5 (1993) 280.
[82] D. Ljubas, Energy 30 (2005) 1699.
[83] O.M. Alfano, D. Bahnemann, A.E. Cassano, R. Dillert, R. Goslich, Catalysis Today 58 (2000) 199.
[84] D.S. Bhatkhande, V.G. Pangarkar, A. Beenackers, Journal of Chemical Technology and Biotechnology 77 (2002) 102.
[85] D. Hufschmidt, L. Liu, V. Selzer, D. Bahnemann, Water Science and Technology 49 (2004) 135.
[86] M. Romero, J. Blanco, B. Sanchez, A. Vidal, S. Malato, A.I. Cardona, E. Garcia, Solar Energy 66 (1999) 169.
[87] J.C. Zhao, C.C. Chen, W.H. Ma, Topics in Catalysis 35 (2005) 269.
[88] J.M. Herrmann, C. Guillard, P. Pichat, Catalysis Today 17 (1993) 7.
[89] K. Kabra, R. Chaudhary, R.L. Sawhney, Industrial & Engineering Chemistry Research 43 (2004) 7683.
[90] I.K. Konstantinou, T.A. Albanis, Applied Catalysis B 49 (2004) 1.
[91] J. Peral, X. Domenech, D.F. Ollis, Journal of Chemical Technology and Biotechnology 70 (1997) 117.
[92] Y. Paz, Comptes Rendus Chimie 9 (2006) 774.
[93] X. Fu, W.A. Zeltner, M.A. Anderson, Studies in Surface Science and Catalysis 103 (1996) 445.
[94] O. Legrini, E. Oliveros, A.M. Braun, Chemical Reviews 93 (1993) 671.
[95] K. Pirkanniemi, M. Sillanpaa, Chemosphere 48 (2002) 1047.
[96] J. Zhao, X.D. Yang, Building and Environment 38 (2003) 645.
[97] T.L. Thompson, J.T. Yates Jr., Chemical Reviews 106 (2006) 4428.
[98] T.L. Thompson, J.T. Yates Jr., Topics in Catalysis 35 (2005) 197.
[99] A.L. Linsebigler, G. Lu, J.T. Yates Jr., Chemical Reviews 95 (1995) 735.
[100] J.T. Yates Jr., Surface Science 603 (2009) 1605.
[101] M. Murakami, Y. Matsumoto, K. Nakajima, T. Makino, Y. Segawa, T. Chikyow, P. Ahmet, M. Kawasaki, H. Koinuma, Applied Physics Letters 78 (2001) 2664.
[102] T. Sekiya, M. Igarashi, S. Kurita, S. Takekawa, M. Fujisawa, Journal of Electron Spectroscopy and Related Phenomena 92 (1998) 247.
[103] K.M. Glassford, J.R. Chelikowsky, Physical Review B 45 (1992) 3874.

[104] O.V. Krasovska, E.E. Krasovskii, V.V. Nemoshkalenko, V.N. Antonov, Journal of Electron Spectroscopy and Related Phenomena 76 (1995) 753.
[105] S.-D. Mo, W.Y. Ching, Physical Review B 51 (1995) 13023.
[106] N. Hosaka, T. Sekiya, M. Fujisawa, S. Kurita, Journal of Electron Spectroscopy and Related Phenomena 78 (1996) 75.
[107] D. Kurita, S. Ohta, K. Sugiura, H. Ohta, K. Koumoto, Journal of Applied Physics 100 (2006) 096105.
[108] T. Sumita, T. Yamaki, S. Yamamoto, A. Miyashita, Applied Surface Science 200 (2002) 21.
[109] C. Itoh, K. Iwahashi, K. Kan'no, Nuclear Instruments & Methods in Physics Research B 191 (2002) 271.
[110] H. Tang, K. Prasad, R. Sanjines, P.E. Schmid, F. Levy, Journal of Applied Physics 75 (1994) 2042.
[111] S. Leytner, J.T. Hupp, Chemical Physics Letters 330 (2000) 231.
[112] C. Colbeau-Justin, M. Kunst, D. Huguenin, Journal of Materials Science 38 (2003) 2429.
[113] T. Toyoda, I. Tsuboya, Review of Scientific Instruments 74 (2003) 782.
[114] H. Tang, H. Berger, P.E. Schmid, F. Levy, Solid State Communications 92 (1994) 267.
[115] Z.C. Wang, U. Helmersson, P.O. Kall, Thin Solid Films 405 (2002) 50.
[116] L. Kavan, M. Grätzel, S.E. Gilbert, C. Klemenz, H.J. Scheel, Journal of the American Chemical Society 118 (1996) 6716.
[117] A. Amtout, R. Leonelli, Physical Review B 51 (1995) 6842.
[118] H. Tang, F. Levy, H. Berger, P.E. Schmid, Physical Review B 52 (1995) 7771.
[119] H. Tang, H. Berger, P.E. Schmid, F. Levy, G. Burri, Solid State Communications 87 (1993) 847.
[120] R. Asahi, Y. Taga, W. Mannstadt, A.J. Freeman, Physical Review B 61 (2000) 7459.
[121] R. Zallen, M.P. Moret, Solid State Communications 137 (2006) 154.
[122] M. Koelsch, S. Cassaignon, J.F. Guillemoles, J.R. Jolivet, Thin Solid Films 403 (2002) 312.
[123] Z.W. Qu, G.J. Kroes, Journal of Physical Chemistry B 110 (2006) 8998.
[124] N. Satoh, T. Nakashima, K. Kamikura, K. Yamamoto, Nature Nanotechnology 3 (2008) 106.
[125] C. Kormann, D.W. Bahnemann, M.R. Hoffmann, Journal of Physical Chemistry 92 (1988) 5196.
[126] H.S. Lee, C.S. Woo, B.K. Youn, S.Y. Kim, S.T. Oh, Y.E. Sung, H.I. Lee, Topics in Catalysis 35 (2005) 255.
[127] B. Enright, D. Fitzmaurice, Journal of Physical Chemistry 100 (1996) 1027.
[128] J. Joo, S.G. Kwon, T. Yu, M. Cho, J. Lee, J. Yoon, T. Hyeon, Journal of Physical Chemistry B 109 (2005) 15297.
[129] Y. Li, T.J. White, S.H. Lim, Journal of Solid State Chemistry 177 (2004) 1372.
[130] A.J. Maira, K.L. Yeung, C.Y. Lee, P.L. Yue, C.K. Chan, Journal of Catalysis 192 (2000) 185.
[131] K.M. Reddy, S.V. Manorama, A.R. Reddy, Materials Chemistry and Physics 78 (2003) 239.
[132] Y.J. Liu, R.O. Claus, Journal of the American Chemical Society 119 (1997) 5273.
[133] S. Corrent, G. Cosa, J.C. Scaiano, M.S. Galletero, M. Alvaro, H. Garcia, Chemistry of Materials 13 (2001) 715.
[134] Z.F. Liu, R.J. Davis, Journal of Physical Chemistry 98 (1994) 1253.
[135] X.D. Zhang, W. He, Rare Metal Materials and Engineering 32 (2003) 812.
[136] N. Serpone, D. Lawless, R. Khairutdinov, Journal of Physical Chemistry 99 (1995) 16646.
[137] S. Monticone, R. Tufeu, A.V. Kanaev, E. Scolan, C. Sanchez, Applied Surface Science 162–163 (2000) 565.
[138] E. Kobayashi, K. Matsuda, G. Mizutani, S. Ushioda, Surface Science 427–428 (1999) 294.
[139] (a) E. Kobayashi, T. Wakasugi, G. Mizutani, S. Ushioda, Surface Science 402–404 (1998) 537;
(b) M. Omote, H. Kitaoka, E. Kobayashi, O. Suzuki, K. Aratake, H. Sano, G. Mizutani, W. Wolf, R. Podloucky, Journal of Physics: Condensed Matter 17 (2005) S175.
[140] D.C. Hurum, A.G. Agrios, K.A. Gray, T. Rajh, M.C. Thurnauer, Journal of Physical Chemistry B 107 (2003) 4545.
[141] J.H. Park, O.O. Park, S. Kim, Applied Physics Letters 89 (2006) 163106.
[142] H.Y. Song, H.F. Jiang, X.Q. Liu, G.Y. Meng, Journal of Photochemistry and Photobiology A 181 (2006) 421.
[143] X.Z. Li., F.B. Li., C.L. Yang, W.K. Ge, Journal of Photochemistry and Photobiology A 141 (2001) 209.
[144] T. Takahashi, H. Nakabayashi, N. Yamada, J. Tanabe, Journal of Vacuum Science & Technology A 21 (2003) 1409.
[145] M. Maeda, K. Hirota, Applied Catalysis A 302 (2006) 305.
[146] H.Y. Liu, L. Gao, Journal of the American Ceramic Society 89 (2006) 370.
[147] X.H. An, G.W. Meng, M.G. Zhang, Y.T. Tian, S.H. Sun, L.D. Zhang, Materials Letters 60 (2006) 2586.
[148] H. Zhang, G. Wang, D. Chen, X. Lv, J. Li, Chemistry of Materials 20 (2008) 6543.
[149] T. Hirakawa, P.V. Kamat, Langmuir 20 (2004) 5645.
[150] H. Tsuji, N. Sakai, H. Sugahara, Y. Gotoh, J. Ishikawa, Nuclear Instruments & Methods in Physics Research, Section B 237 (2005) 433.
[151] H. Tsuji, N. Sakai, Y. Gotoh, J. Ishikawa, Nuclear Instruments & Methods in Physics Research Section B 242 (2006) 129.
[152] H. Tsuji, H. Sugahara, Y. Gotoh, J. Ishikawa, Nuclear Instruments & Methods in Physics Research Section B 206 (2003) 249.
[153] A. Gorzkowska-Sobas, E. Kusior, M. Radecka, K. Zakrzewska, Surface Science 600 (2006) 3964.
[154] J.W. Yoon, T. Sasaki, N. Koshizaki, Thin Solid Films 483 (2005) 276.
[155] Y. Tian, T. Tatsuma, Journal of the American Chemical Society 127 (2005) 7632.
[156] V. Subramanian, E.E. Wolf, P.V. Kamat, Langmuir 19 (2003) 469.
[157] L.C. Du, A. Furube, K. Yamamoto, K. Hara, R. Katoh, M. Tachiya, Journal of Physical Chemistry C 113 (2009) 6454.
[158] X.G. Hou, X.N. Gu, Y. Hu, J.F. Zhang, A.D. Liu, Nuclear Instruments & Methods in Physics Research Section B 251 (2006) 429.
[159] M.D. Driessen, V.H. Grassian, Journal of Physical Chemistry B 102 (1998) 1418.
[160] S. Kim, S.-J. Hwang, W. Choi, Journal of Physical Chemistry B 109 (2005) 24260.
[161] B. Sun, P.G. Smirniotis, P. Boolchand, Langmuir 21 (2005) 11397.
[162] T. Sasaki, N. Koshizaki, J.W. Yoon, K.M. Beck, Journal of Photochemistry and Photobiology A 145 (2001) 11.
[163] T. Hannappel, B. Burfeindt, W. Storck, F. Willig, Journal of Physical Chemistry B 101 (1997) 6799.
[164] G. Ramakrishna, H.N. Ghosh, Journal of Physical Chemistry B 105 (2001) 7000.
[165] J.M. Szarko, A. Neubauer, A. Bartelt, L. Socaciu-Siebert, F. Birkner, K. Schwarzburg, T. Hannappel, R. Eichberger, Journal of Physical Chemistry C 112 (2008) 10542.
[166] K.A. Walters, D.A. Gaal, J.T. Hupp, Journal of Physical Chemistry B 106 (2002) 5139.
[167] B. Zou, L. Xiao, T. Li., J. Zhao, Z. Lai, S. Gu, Applied Physics Letters 59 (1991) 1826.
[168] S. Kim, W. Choi, Journal of Physical Chemistry B 109 (2005) 5143.
[169] D.C. Hurum, K.A. Gray, T. Rajh, M.C. Thurnauer, Journal of Physical Chemistry B 108 (2004) 16483.
[170] A.G. Agrios, K.A. Gray, E. Weitz, Langmuir 19 (2003) 1402.
[171] S. Usseglio, P. Calza, A. Damin, C. Minero, S. Bordiga, C. Lamberti, E. Pelizzetti, A. Zecchina, Chemistry of Materials 18 (2006) 3412.
[172] A.G. Agrios, K.A. Gray, E. Weitz, Langmuir 20 (2004) 5911.
[173] V.N. Kuznetsov, N. Serpone, Journal of Physical Chemistry B 110 (2006) 25203.
[174] N. Serpone, Journal of Physical Chemistry B 110 (2006) 24287.
[175] U. Diebold, Surface Science Reports 48 (2003) 53.
[176] M.G. Blanchin, Key Engineering Materials 155–156 (1999) 359.
[177] I. Dawson, P.D. Bristowe, J.A. White, M.C. Payne, Materials Research Society Symposium Proceedings 453 (1997) 203.
[178] M.A. Henderson, Surface Science 419 (1999) 174.
[179] J. Nowotny, M. Radecka, M. Rekas, Journal of Physics and Chemistry of Solids 58 (1997) 927.
[180] E. Cho, S. Han, H.S. Ahn, K.R. Lee, S.K. Kim, C.S. Hwang, Physical Review B 73 (2006) 193202.
[181] F.M. Hossain, G.E. Murch, L. Sheppard, J. Nowotny, Diffusion and Defect Data–Solid State Data, Pt. A 251–252 (2006) 1.
[182] D.K. Lee, J.I. Jeon, M.H. Kim, W. Choi, H.I. Yoo, Journal of Solid State Chemistry 178 (2005) 185.
[183] S. Na-Phattalung, M.F. Smith, K. Kim, M.-H. Du, S.-H. Wei, S.B. Zhang, S. Limpijumnong, Physical Review B 73 (2006) 125205.
[184] Z.S. Lin, A. Orlov, R.M. Lambert, M.C. Payne, Journal of Physical Chemistry B 109 (2005) 20948.
[185] V.M. Khomenko, K. Langer, H. Rager, A. Fett, Physics and Chemistry of Minerals 25 (1998) 338.
[186] (a) K. Komaguchi, H. Nakano, A. Araki, Y. Harima, Chemical Physics Letters 428 (2006) 338;
(b) K. Komaguchi, T. Maruoka, H. Nakano, I. Imae, Y. Ooyama, Y. Harima, Journal of Physical Chemistry C 114 (2010) 1240.
[187] H.M. Liu, W.S. Yang, Y. Ma, J.N. Yao, Applied Catalysis A 299 (2006) 218.
[188] I. Justicia, G. Garcia, G.A. Battiston, R. Gerbasi, F. Ager, M. Guerra, J. Caixach, J.A. Pardo, J. Rivera, A. Figueras, Electrochimica Acta 50 (2005) 4605.
[189] I. Justicia, G. Garcia, L. Vazquez, J. Santiso, P. Ordejon, G. Battiston, R. Gerbasi, A. Figueras, Sensors and Actuators B B109 (2005) 52.
[190] I. Justicia, P. Ordejon, G. Canto, J.L. Mozos, J. Fraxedas, G.A. Battiston, R. Gerbasi, A. Figueras, Advanced Materials 14 (2002) 1399.
[191] I.N. Martyanov, S. Uma, S. Rodrigues, K.J. Klabunde, Chemical Communications (2004) 2476.
[192] K. Onda, B. Li., H. Petek, Physical Review B 70 (2004) 045415.
[193] J. Zhao, B. Li, K.D. Jordan, J.L. Yang, H. Petek, Physical Review B 73 (2006) 195309.
[194] K. Onda, B. Li, J. Zhao, K.D. Jordan, J.L. Yang, H. Petek, Science 308 (2005) 1154.
[195] B. Li., J. Zhao, K. Onda, K.D. Jordan, J.L. Yang, H. Petek, Science 311 (2006) 1436.
[196] (a) K. Onda, B. Li., J. Zhao, H. Petek, Surface Science 593 (2005) 32;
(b) J. Zhao, J.L. Yang, H. Petek, Physical Review B 80 (2009) 235416.
[197] H. Petek, J. Zhao, Chemical Reviews 110 (2010) 7082.
[198] D. Ino, K. Watanabe, N. Takagi, Y. Matsumoto, Journal of Physical Chemistry B 109 (2005) 18018.
[199] M.A. Henderson, W.S. Epling, C.H.F. Peden, C.L. Perkins, Journal of Physical Chemistry B 107 (2003) 534.
[200] M.A. Henderson, W.S. Epling, C.L. Perkins, C.H.F. Peden, U. Diebold, Journal of Physical Chemistry B 103 (1999) 5328.
[201] C.L. Perkins, M.A. Henderson, Journal of Physical Chemistry B 105 (2001) 3856.

[202] M.A. Henderson, J.M. White, H. Uetsuka, H. Onishi, Journal of the American Chemical Society 125 (2003) 14974.
[203] M. Komiyama, Y.-J. Li, Applied Surface Science 244 (2005) 550.
[204] M. Komiyama, Y.-J. Li, Japanese Journal of Applied Physics 1 43 (2004) 4584.
[205] R. Bechstein, M. Kitta, J. Schuette, H. Onishi, A. Kuehnle, Nanotechnology 20 (2009) 264003.
[206] R. Bechstein, M. Kitta, J. Schutte, A. Kuhnle, H. Onishi, Journal of Physical Chemistry C 113 (2009) 13199.
[207] Z. Ambrus, N. Balazs, T. Alapi, G. Wittmann, P. Sipos, A. Dombi, K. Mogyorosi, Applied Catalysis B 81 (2008) 27.
[208] L. Xiao, J.L. Zhang, Y. Cong, B.Z. Tian, F. Chen, M. Anpo, Catalysis Letters 111 (2006) 207.
[209] M.S. Nahar, K. Hasegawa, S. Kagaya, Chemosphere 65 (2006) 1976.
[210] X.H. Wang, J.G. Li., H. Kamiyama, Y. Moriyoshi, T. Ishigaki, Journal of Physical Chemistry B 110 (2006) 6804.
[211] X.H. Wang, J.G. Li., H. Kamiyama, T. Ishigaki, Thin Solid Films 506 (2006) 278.
[212] S. Karvinen, P. Hirva, T.A. Pakkanen, Journal of Molecular Structure-Theochem 626 (2003) 271.
[213] K. Lee, N.H. Lee, S.H. Shin, H.G. Lee, S.J. Kim, Materials Science and Engineering B 129 (2006) 109.
[214] M. Salmi, N. Tkachenko, R.J. Lamminmaki, S. Karvinen, V. Vehmanen, H. Lemmetyinen, Journal of Photochemistry and Photobiology A 175 (2005) 8.
[215] F. Gracia, J.P. Holgado, A. Caballero, A.R. Gonzalez-Elipe, Journal of Physical Chemistry B 108 (2004) 17466.
[216] (a) W.Y. Choi, A. Termin, M.R. Hoffmann, Journal of Physical Chemistry 98 (1994) 13669;
(b) J. Choi, H. Park, M.R. Hoffmann, Journal of Physical Chemistry C 114 (2010) 783.
[217] C.-C. Tsai, H. Teng, Applied Surface Science 254 (2008) 4912.
[218] J.C. Yu, G.S. Li., X.C. Wang, X.L. Hu., C.W. Leung, Z.D. Zhang, Chemical Communications (2006) 2717.
[219] T. Umebayashi, T. Yamaki, T. Sumita, S. Yamamoto, S. Tanaka, K. Asai, Nuclear Instruments & Methods in Physics Research B 206 (2003) 264.
[220] R.C.W. Lam, M.K.H. Leung, D.Y.C. Leung, L.L.P. Vrijmoed, W.C. Yam, S.P. Ng, Solar Energy Materials and Solar Cells 91 (2007) 54.
[221] J. Zhu, Z. Deng, F. Chen, J. Zhang, H. Chen, M. Anpo, J. Huang, L. Zhang, Applied Catalysis B 62 (2006) 329.
[222] T. Ikeda, T. Nomoto, K. Eda, Y. Mizutani, H. Kato, A. Kudo, H. Onishi, Journal of Physical Chemistry C 112 (2008) 1167.
[223] J.K. Zhou, M. Takeuchi, X.S. Zhao, A.K. Ray, M. Anpo, Catalysis Letters 106 (2006) 67.
[224] S. Klosek, D. Raftery, Journal of Physical Chemistry B 105 (2001) 2815.
[225] J.C.S. Wu, C.H. Chen, Journal of Photochemistry and Photobiology A 163 (2004) 509.
[226] G.L. Zhao, H. Kozuka, H. Lin, T. Yoko, Thin Solid Films 339 (1999) 123.
[227] D.H. Kim, D.-K. Choi, S.-J. Kim, K.S. Lee, Catalysis Communications 9 (2008) 654.
[228] A. Mattsson, M. Leideborg, K. Larsson, G. Westin, L. Osterlund, Journal of Physical Chemistry B 110 (2006) 1210.
[229] N.U. Zhanpeisov, K. Tsujimaru, A. Anpo, Research on Chemical Intermediates 30 (2004) 121.
[230] B. Xin, P. Wang, D. Ding, J. Liu, Z. Ren, H. Fu, Applied Surface Science 254 (2008) 2569.
[231] M.I. Franch, J. Peral, X. Domenech, R.F. Howe, J.A. Ayllon, Applied Catalysis B 55 (2005) 105.
[232] T. Umebayashi, T. Yamaki, H. Itoh, K. Asai, Journal of Physics and Chemistry of Solids 63 (2002) 1909.
[233] B. Sun, E.P. Reddy, P.G. Smirniotis, Environmental Science & Technology 39 (2005) 6251.
[234] R. Asahi, T. Morikawa, T. Ohwaki, K. Aoki, Y. Taga, Science 293 (2001) 269.
[235] Y. Aita, M. Komatsu, S. Yin, T. Sato, Journal of Solid State Chemistry 177 (2004) 3235.
[236] R. Asahi, T. Morikawa, Chemical Physics 339 (2007) 57.
[237] R. Bacsa, J. Kiwi, T. Ohno, P. Albers, V. Nadtochenko, Journal of Physical Chemistry B 109 (2005) 5994.
[238] W. Balcerski, S.Y. Ryu, M.R. Hoffmann, Journal of Physical Chemistry C 111 (2007) 15357.
[239] M. Batzill, E.H. Morales, U. Diebold, Physical Review Letters 96 (2006) 026103.
[240] M. Batzill, E.H. Morales, U. Diebold, Chemical Physics 339 (2007) 36.
[241] C. Belver, R. Bellod, S.J. Stewart, F.G. Requejo, M. Fernandez-Garcia, Applied Catalysis B 65 (2006) 309.
[242] R. Beranek, B. Neumann, S. Sakthivel, M. Janczarek, T. Dittrich, H. Tributsch, H. Kisch, Chemical Physics 339 (2007) 11.
[243] (a) S. Buzby, M.A. Barakat, H. Lin, C. Ni, S.A. Rykov, J.G. Chen, S.I. Shah, Journal of Vacuum Science & Technology B 24 (2006) 1210;
(b) A.K. Rumaiz, J.C. Woicik, E. Cockayne, H.Y. Lin, G.H. Jaffari, S.I. Shah, Applied Physics Letters 95 (2009) 262111.
[244] S.A. Chambers, S.H. Cheung, V. Shutthanandan, S. Thevuthasan, M.K. Bowman, A.G. Joly, Chemical Physics 339 (2007) 27.
[245] X. Chen, C. Burda, Journal of the American Chemical Society 130 (2008) 5018.
[246] X. Chen, P.-A. Glans, X. Qiu, S. Dayal, W.D. Jennings, K.E. Smith, C. Burda, J. Guo, Journal of Electron Spectroscopy and Related Phenomena 162 (2008) 67.
[247] X.B. Chen, Y.B. Lou, A.C.S. Samia, C. Burda, J.L. Gole, Advanced Functional Materials 15 (2005) 41.
[248] S.H. Cheung, P. Nachimuthu, A.G. Joly, M.H. Engelhard, M.K. Bowman, S.A. Chambers, Surface Science 601 (2007) 1754.
[249] C.Di. Valentin, G. Pacchioni, A. Selloni, Physical Review B 70 (2004) 085116.
[250] C.Di. Valentin, G. Pacchioni, A. Selloni, S. Livraghi, E. Giamello, Journal of Physical Chemistry B 109 (2005) 11414.
[251] C.Di. Valentin, E. Finazzi, G. Pacchioni, A. Selloni, S. Livraghi, M.C. Paganini, E. Giamello, Chemical Physics 339 (2007) 44.
[252] O. Diwald, T.L. Thompson, T. Zubkov, E.G. Goralski, S.D. Walck, J.T. Yates Jr., Journal of Physical Chemistry B 108 (2004) 6004.
[253] O. Diwald, T.L. Thompson, E.G. Goralski, S.D. Walck, J.T. Yates Jr., Journal of Physical Chemistry B 108 (2004) 52.
[254] C.X. Dong, A.P. Xian, E.H. Han, J.K. Shang, Journal of Materials Science 41 (2006) 6168.
[255] A.V. Emeline, X. Zhang, M. Jin, T. Murakami, A. Fujishima, Journal of Physical Chemistry B 110 (2006) 7409.
[256] A.V. Emeline, N.V. Sheremetyeva, N.V. Khomchenko, V.K. Ryabchuk, N. Serpone, Journal of Physical Chemistry C 111 (2007) 11456.
[257] C. Feng, Y. Wang, Z. Jin, J. Zhang, S. Zhang, Z. Wu, Z. Zhang, New Journal of Chemistry 32 (2008) 1038.
[258] E. Finazzi, C.Di. Valentin, A. Selloni, G. Pacchioni, Journal of Physical Chemistry C 111 (2007) 9275.
[259] H.B. Fu, L.W. Zhang, S.C. Zhang, Y.F. Zhu, J.C. Zhao, Journal of Physical Chemistry B 110 (2006) 3061.
[260] J. Graciani, L.J. Alvarez, J.A. Rodriguez, J.F. Sanz, Journal of Physical Chemistry C 112 (2008) 2624.
[261] T. Hirakawa, Y. Nosaka, Journal of Physical Chemistry C 112 (2008) 15818.
[262] T. Ihara, M. Miyoshi, Y. Iriyama, O. Matsumoto, S. Sugihara, Applied Catalysis B 42 (2003) 403.
[263] S. In, A. Orlov, F. Garcia, M. Tikhov, D.S. Wright, R.M. Lambert, Chemical Communications (2006) 4236.
[264] H. Irie, Y. Watanabe, K. Hashimoto, Journal of Physical Chemistry B 107 (2003) 5483.
[265] H. Irie, S. Washizuka, Y. Watanabe, T. Kako, K. Hashimoto, Journal of the Electrochemical Society 152 (2005) E351.
[266] H. Irie, S. Washizuka, N. Yoshino, K. Hashimoto, Chemical Communications (2003) 1298.
[267] S.K. Joung, T. Amemiya, M. Murabayashi, K. Itoh, Chemistry—A European Journal 12 (2006) 5526.
[268] S.K. Joung, T. Amemiya, M. Murabayashi, K. Itoh, Applied Catalysis A 312 (2006) 20.
[269] M. Kitano, K. Funatsu, M. Matsuoka, M. Ueshima, M. Anpo, Journal of Physical Chemistry B 110 (2006) 25266.
[270] K. Kobayakawa, Y. Murakami, Y. Sato, Journal of Photochemistry and Photobiology A 170 (2005) 177.
[271] Y. Kuroda, T. Mori, K. Yagi, N. Makihata, Y. Kawahara, M. Nagao, S. Kittaka, Langmuir 21 (2005) 8026.
[272] D. Li, N. Ohashi, S. Hishita, T. Kolodiazhnyi, H. Haneda, Journal of Solid State Chemistry 178 (2005) 3293.
[273] D. Li, H. Haneda, S. Hishita, N. Ohashi, Research on Chemical Intermediates 31 (2005) 331.
[274] D. Li, H. Haneda, S. Hishita, N. Ohashi, Materials Science and Engineering B 117 (2005) 67.
[275] Y. Liu, X. Chen, J. Li., C. Burda, Chemosphere 61 (2005) 11.
[276] S. Livraghi, M.C. Paganini, E. Giamello, A. Selloni, C.Di. Valentin, G. Pacchioni, Journal of the American Chemical Society 128 (2006) 15666.
[277] S. Livraghi, A. Votta, M.C. Paganini, E. Giamello, Chemical Communications (2005) 498.
[278] M.C. Long, W.M. Cai, Z.P. Wang, G.Z. Liu, Chemical Physics Letters 420 (2006) 71.
[279] Y. Liu, J. Li., X. Qiu, C. Burda, Water Science and Technology 54 (2006) 47.
[280] T. Lindgren, J. Lu, A. Hoel, C.G. Granqvist, G.R. Torres, S.E. Lindquist, Solar Energy Materials and Solar Cells 84 (2004) 145.
[281] J.M. Macak, A. Ghicov, R. Hahn, H. Tsuchiya, P. Schmuki, Journal of Materials Research 21 (2006) 2824.
[282] M. Maeda, T. Watanabe, Journal of the Electrochemical Society 153 (2006) C186.
[283] L. Mi, Y. Zhang, P.-N. Wang, Chemical Physics Letters 458 (2008) 341.
[284] S. Mozia, M. Tomaszewska, B. Kosowska, B. Grzmil, A.W. Morawski, K. Kalucki, Applied Catalysis B 55 (2005) 195.
[285] M. Mrowetz, W. Balcerski, A.J. Colussi, M.R. Hoffmann, Journal of Physical Chemistry B 108 (2004) 17269.
[286] (a) K. Naito, T. Tachikawa, M. Fujitsuka, T. Majima, Journal of Physical Chemistry C 112 (2008) 1048;
(b) T. Tachikawa, T. Majima, Chemical Society Reviews 39 (2010) 4802;
(c) K. Naito, T. Tachikawa, M. Fujitsuka, T. Majima, Journal of the American Chemical Society 131 (2009) 934.
[287] Y. Nakano, T. Morikawa, T. Ohwaki, Y. Taga, Chemical Physics 339 (2007) 20.
[288] A. Nambu, J. Graciani, J.A. Rodriguez, Q. Wu, E. Fujita, J.F. Sanz, Journal of Chemical Physics 125 (2006) 094706.
[289] Y. Nosaka, M. Matsushita, J. Nishino, A.Y. Nosaka, Science and Technology of Advanced Materials 6 (2005) 143.
[290] T. Ohsawa, I. Lyubinetsky, Y. Du, M.A. Henderson, V. Shutthanandan, S.A. Chambers, Physical Review B 79 (2009) 085401.
[291] T. Okato, T. Sakano, M. Obara, Physical Review B 72 (2005) 115124.

[292] E.A. Reyes-Garcia, Y.P. Sun, K. Reyes-Gil, D. Raftery, Journal of Physical Chemistry C 111 (2007) 2738.
[293] M. Sathish, B. Viswanathan, R.P. Viswanath, C.S. Gopinath, Chemistry of Materials 17 (2005) 6349.
[294] S. Sato, R. Nakamura, S. Abe, Applied Catalysis A 284 (2005) 131.
[295] S. Sakthivel, H. Kisch, Chemphyschem 4 (2003) 487.
[296] (a) Y. Suda, H. Kawasaki, T. Ueda, T. Ohshima, Thin Solid Films 453–54 (2004) 162;
(b) Y. Suda, H. Kawasaki, T. Ueda, T. Ohshima, Thin Solid Films 475 (2005) 337.
[297] M. D'arienzo, N. Siedl, A. Sternig, R. Scotti, F. Morazzoni, J. Bernardi, O. Diwald, Journal of Physical Chemistry C 114 (2010) 18067.
[298] H. Sun, Y. Bai, H. Liu, W. Jin, N. Xu, G. Chen, B. Xu, Journal of Physical Chemistry C 112 (2008) 13304.
[299] S.J. Stewart, M. Fernandez-Garcia, C. Belver, B.S. Mun, F.G. Requejo, Journal of Physical Chemistry B 110 (2006) 16482.
[300] T. Tachikawa, Y. Takai, S. Tojo, M. Fujitsuka, H. Irie, K. Hashimoto, T. Majima, Journal of Physical Chemistry B 110 (2006) 13158.
[301] I. Takahashi, D.J. Payne, R.G. Palgrave, R.G. Egdell, Chemical Physics Letters 454 (2008) 314.
[302] G.R. Torres, T. Lindgren, J. Lu, C.G. Granqvist, S.E. Lindquist, Journal of Physical Chemistry B 108 (2004) 5995.
[303] Y. Wang, C. Feng, Z. Jin, J. Zhang, J. Yang, S. Zhang, Journal of Molecular Catalysis A 260 (2006) 1.
[304] Z. Wang, W. Cai, X. Hong, X. Zhao, F. Xu, C. Cai, Applied Catalysis B 57 (2005) 223.
[305] H. Wang, J.P. Lewis, Journal of Physics-Condensed Matter 18 (2006) 421.
[306] Y. Wang, D.J. Doren, Solid State Communications 136 (2005) 186.
[307] M.S. Wong, H.P. Chou, T.S. Yang, Thin Solid Films 494 (2006) 244.
[308] Y. Yamamoto, S. Moribe, T. Ikoma, K. Akiyama, Q. Zhang, F. Saito, S. Tero-Kubota, Molecular Physics 104 (2006) 1733.
[309] K. Yang, Y. Dai, B. Huang, Journal of Physical Chemistry C 111 (2007) 12086.
[310] K. Yang, Y. Dai, B. Huang, S. Han, Journal of Physical Chemistry B 110 (2006) 24011.
[311] S.W. Yang, L. Gao, Journal of the American Ceramic Society 87 (2004) 1803.
[312] T.S. Yang, M.C. Yang, C.B. Shiu, W.K. Chang, M.S. Wong, Applied Surface Science 252 (2006) 3729.
[313] M.C. Yang, T.S. Yang, M.S. Wong, Thin Solid Films 469–470 (2004) 1.
[314] K. Yang, Y. Dai, B. Huang, M.-H. Whangbo, Journal of Physical Chemistry C 113 (2009) 2624.
[315] X.X. Yang, C.D. Cao, L. Erickson, K. Hohn, R. Maghirang, K. Klabunde, Journal of Catalysis 260 (2008) 128.
[316] S. Yin, Y. Aita, M. Komatsu, T. Sato, Journal of the European Ceramic Society 26 (2006) 2735.
[317] S. Yin, K. Ihara, M. Komatsu, Q.W. Zhang, F. Saito, T. Kyotani, T. Sato, Solid State Communications 137 (2006) 132.
[318] S. Yin, H. Yamaki, M. Komatsu, Q.W. Zhang, J.S. Wang, Q. Tang, F. Saito, T. Sato, Solid State Sciences 7 (2005) 1479.
[319] J. Yuan, M.X. Chen, J.W. Shi, W.F. Shangguan, International Journal of Hydrogen Energy 31 (2006) 1326.
[320] Z. Zhao, Q. Liu, Journal of Physics D 41 (2008) 025105.
[321] Y. Zhao, X. Qiu, C. Burda, Chemistry of Materials 20 (2008) 2629.
[322] T. Ohsawa, M.A. Henderson, S.A. Chambers, Journal of Physical Chemistry C 114 (2010) 6595.
[323] Y.Z. Li., D.S. Hwang, N.H. Lee, S.J. Kim, Chemical Physics Letters 404 (2005) 25.
[324] S. Sakthivel, M. Janczarek, H. Kisch, Journal of Physical Chemistry B 108 (2004) 19384.
[325] H. Kamisaka, T. Adachi, K. Yamashita, Journal of Chemical Physics 123 (2005) 084704.
[326] P. Gorska, A. Zaleska, E. Kowalska, T. Klimczuk, J.W. Sobczak, E. Skwarek, W. Janusz, J. Hupka, Applied Catalysis B 84 (2008) 440.
[327] S.U.M. Khan, M. Al-Shahry, W.B. Ingler, Science 297 (2002) 2243.
[328] K. Nagaveni, M.S. Hegde, N. Ravishankar, G.N. Subbanna, G. Madras, Langmuir 20 (2004) 2900.
[329] P.W. Chou, S. Treschev, P.H. Chung, C.L. Cheng, Y.H. Tseng, Y.J. Chen, M.S. Wong, Applied Physics Letters 89 (2006) 131919.
[330] S. Sakthivel, H. Kisch, Angewandte Chemie 42 (2003) 4908.
[331] C. Xu, R. Killmeyer, M.L. Gray, S.U.M. Khan, Applied Catalysis B 64 (2006) 312.
[332] W. Ren, Z. Ai, F. Jia, L. Zhang, X. Fan, Z. Zou, Applied Catalysis B 69 (2007) 138.
[333] J.H. Park, S. Kim, A.J. Bard, Nano Letters 6 (2006) 24.
[334] C.Di. Valentin, G. Pacchioni, A. Selloni, Chemistry of Materials 17 (2005) 6656.
[335] T. Tachikawa, S. Tojo, K. Kawai, M. Endo, M. Fujitsuka, T. Ohno, K. Nishijima, Z. Miyamoto, T. Majima, Journal of Physical Chemistry B 108 (2004) 19299.
[336] B. Neumann, P. Bogdanoff, H. Tributsch, S. Sakthivel, H. Kisch, Journal of Physical Chemistry B 109 (2005) 16579.
[337] K. Yang, Y. Dai, B. Huang, Journal of Physical Chemistry C 111 (2007) 18985.
[338] T. Ohno, M. Akiyoshi, T. Umebayashi, K. Asai, T. Mitsui, M. Matsumura, Applied Catalysis A 265 (2004) 115.
[339] J.C. Yu, W.K. Ho, J.G. Yu, H. Yip, P.K. Wong, J.C. Zhao, Environmental Science & Technology 39 (2005) 1175.
[340] T. Ohno, Water Science and Technology 49 (2004) 159.
[341] K. Demeestere, J. Dewulf, T. Ohno, P.H. Salgado, H. van Langenhove, Applied Catalysis B 61 (2005) 140.
[342] E.L.D. Hebenstreit, W. Hebenstreit, H. Geisler, S.N. Thornburg, C.A. Ventrice Jr., D.A. Hite, P.T. Sprunger, U. Diebold, Physical Review B 64 (2001) 115418.
[343] F.H. Tian, C.B. Liu, Journal of Physical Chemistry B 110 (2006) 17866.
[344] T. Umebayashi, T. Yamaki, H. Itoh, K. Asai, Applied Physics Letters 81 (2002) 454.
[345] T. Umebayashi, T. Yamaki, S. Yamamoto, A. Miyashita, S. Tanaka, T. Sumita, K. Asai, Journal of Applied Physics 93 (2003) 5156.
[346] Q.J. Yang, C. Xie, Z.L. Xu, Z.M. Gao, Y.G. Du, Journal of Physical Chemistry B 109 (2005) 5554.
[347] W.K. Ho, J.C. Yu, S.C. Lee, Journal of Solid State Chemistry 179 (2006) 1171.
[348] K. Yang, Y. Dai, B. Huang, M.-H. Whangbo, Chemistry of Materials 20 (2008) 6528.
[349] W. Ho, J.C. Yu, S. Lee, Chemical Communications (2006) 1115.
[350] X.T. Hong, Z.P. Wang, W.M. Cai, F. Lu, J. Zhang, Y.Z. Yang, N. Ma, Y.J. Liu, Chemistry of Materials 17 (2005) 1548.
[351] G. Liu, Z.G. Chen, C.L. Dong, Y.N. Zhao, F. Li, G.Q. Lu, H.M. Cheng, Journal of Physical Chemistry B 110 (2006) 20823.
[352] S. Tojo, T. Tachikawa, M. Fujitsuka, T. Majima, Journal of Physical Chemistry C 112 (2008) 14948.
[353] H. Park, W.Y. Choi, Journal of Physical Chemistry B 108 (2004) 4086.
[354] J. Xu, Y. Ao, D. Fu, C. Yuan, Applied Surface Science 254 (2008) 3033.
[355] J.F. He, Q.H. Liu, Z.H. Sun, W.S. Yan, G.B. Zhang, Z.M. Qi, P.S. Xu, Z.Y. Wu, S.Q. Wei, Journal of Physical Chemistry C 114 (2010) 6035.
[356] Q. Shi, D. Yang, Z. Jiang, J. Li, Journal of Molecular Catalysis B 43 (2006) 44.
[357] H. Geng, S.W. Yin, X. Yang, Z.G. Shuai, B.G. Liu, Journal of Physics-Condensed Matter 18 (2005) 87.
[358] K. Yang, Y. Dai, B. Huang, Physical Review B 76 (2007) 195201.
[359] A. Zaleska, J.W. Sobczak, E. Grabowska, J. Hupka, Applied Catalysis B 78 (2008) 92.
[360] M.A. Henderson, V. Shutthanandan, T. Ohsawa, S.A. Chambers, Proceedings of the SPIE 7770 (2010) 777007.
[361] S.A. Chambers, Journal of Physics-Condensed Matter 20 (2008) 264004.
[362] S.A. Chambers, Surface Science Reports 39 (2000) 105.
[363] S.A. Chambers, in: D.P. Woodruff (Ed.), The Chemical Physics of Solid Surfaces, New York, 2001, pp. 301–323.
[364] D. Li, H. Haneda, S. Hishita, N. Ohashi, Chemistry of Materials 17 (2005) 2596.
[365] J.G. Yu, M.H. Zhou, B. Cheng, X.J. Zhao, Journal of Molecular Catalysis A 246 (2006) 176.
[366] H. Kato, A. Kudo, Journal of Physical Chemistry B 106 (2002) 5029.
[367] H.Y. Liu, L. Gao, Journal of the American Ceramic Society 87 (2004) 1582.
[368] D. Noguchi, Y. Kawamata, T. Nagatomo, Journal of the Electrochemical Society 152 (2005) D124.
[369] C.C. Pan, J.C.S. Wu, Materials Chemistry and Physics 100 (2006) 102.
[370] Y. Gai, J. Li, S.-S. Li, J.-B. Xia, S.-H. Wei, Physical Review Letters 102 (2009) 036402.
[371] T. Morikawa, Y. Irokawa, T. Ohwaki, Applied Catalysis A 314 (2006) 123.
[372] T. Ohno, T. Tsubota, M. Toyofuku, R. Inaba, Catalysis Letters 98 (2004) 255.
[373] B.F. Gao, Y. Ma, Y. Cao, W.S. Yang, J.N. Yao, Journal of Physical Chemistry B 110 (2006) 14391.
[374] Y. Sakatani, H. Ando, K. Okusako, H. Koike, J. Nunoshige, T. Takata, J.N. Kondo, M. Hara, K. Domen, Journal of Materials Research 19 (2004) 2100.
[375] T. Rajh, O. Poluektov, A.A. Dubinski, G. Wiederrecht, M.C. Thurnauer, A.D. Trifunac, Chemical Physics Letters 344 (2001) 31.
[376] Y. Lei, L.D. Zhang, G.W. Meng, G.H. Li, X.Y. Zhang, C.H. Liang, W. Chen, S.X. Wang, Applied Physics Letters 78 (2001) 1125.
[377] Y. Lei, L.D. Zhang, Journal of Materials Research 16 (2001) 1138.
[378] K. Iijima, M. Goto, S. Enomoto, H. Kunugita, K. Ema, M. Tsukamoto, N. Ichikawa, H. Sakama, Journal of Luminescence 128 (2008) 911.
[379] I. Sildos, A. Suisalu, J. Aarik, T. Sekiya, S. Kurita, Journal of Luminescence 87–89 (2000) 290.
[380] F.M. Liu, T.M. Wang, Applied Surface Science 195 (2002) 284.
[381] M. Watanabe, T. Hayashi, H. Yagasaki, S. Sasaki, International Journal of Modern Physics B 15 (2001) 3997.
[382] M. Watanabe, T. Hayashi, Journal of Luminescence 112 (2005) 88.
[383] M. Watanabe, S. Sasaki, T. Hayashi, Journal of Luminescence 87–9 (2000) 1234.
[384] V. Kiisk, I. Sildos, A. Suisalu, J. Aarik, Thin Solid Films 400 (2001) 130.
[385] N. Nilius, N. Ernst, H.-J. Freund, Chemical Physics Letters 349 (2001) 351.
[386] Y. Tamaki, A. Furube, M. Murai, K. Hara, R. Katoh, M. Tachiya, Physical Chemistry Chemical Physics 9 (2007) 1453.
[387] T. Berger, M. Sterrer, O. Diwald, E. Knozinger, Chemphyschem 6 (2005) 2104.
[388] A.V. Emeline, A.V. Frolov, V.K. Ryabchuk, N. Serpone, Journal of Physical Chemistry B 107 (2003) 7109.
[389] Z.P. Jiang, H.Y. Wang, H. Huang, C.C. Cao, Chemosphere 56 (2004) 503.
[390] L. Gundlach, S. Felber, W. Storck, E. Galoppini, Q. Wei, F. Willig, Research on Chemical Intermediates 31 (2005) 39.
[391] L. Gundlach, R. Ernstorfer, F. Willig, Physical Review B 74 (2006) 035324.
[392] G.M. Turner, M.C. Beard, C.A. Schmuttenmaer, Journal of Physical Chemistry B 106 (2002) 11716.
[393] J. van de Lagemaat, A.J. Frank, Journal of Physical Chemistry B 105 (2001) 11194.
[394] T. Morishita, A. Hibara, T. Sawada, I. Tsuyumoto, Journal of Physical Chemistry B 103 (1999) 5984.
[395] A. Emeline, A. Salinaro, N. Serpone, Journal of Physical Chemistry B 104 (2000) 11202.

[396] M.A. Grela, M.A. Brusa, A.J. Colussi, Journal of Physical Chemistry B 101 (1997) 10986.
[397] M.A. Grela, M.A. Brusa, A.J. Colussi, Journal of Physical Chemistry B 103 (1999) 6400.
[398] M.A. Grela, A.J. Colussi, Journal of Physical Chemistry B 103 (1999) 2614.
[399] Y. Tamaki, A. Furube, R. Katoh, M. Murai, K. Hara, H. Arakawa, M. Tachiya, Comptes Rendus Chimie 9 (2006) 268.
[400] Y. Tamaki, A. Furube, M. Murai, K. Hara, R. Katoh, M. Tachiya, Journal of the American Chemical Society 128 (2006) 416.
[401] Q. Shen, K. Katayama, T. Sawada, M. Yamaguchi, Y. Kumagai, T. Toyoda, Chemical Physics Letters 419 (2006) 464.
[402] Q. Shen, K. Katayama, M. Yamaguchi, T. Sawada, T. Toyoda, Thin Solid Films 486 (2005) 15.
[403] J.M. Luttinger, W. Kohn, Physical Review 97 (1955) 869.
[404] L. Brus, Journal of Physical Chemistry 90 (1986) 2555.
[405] H. Lin, C.P. Huang, W. Li., C. Ni, S.I. Shah, Y.-H. Tseng, Applied Catalysis B 68 (2006) 1.
[406] N. Sakai, Y. Ebina, K. Takada, T. Sasaki, Journal of the American Chemical Society 126 (2004) 5851.
[407] D.V. Bavykin, S.N. Gordeev, A.V. Moskalenko, A.A. Lapkin, F.C. Walsh, Journal of Physical Chemistry B 109 (2005) 8565.
[408] R. van Grieken, J. Aguado, M.J. Lopez-Munoz, J. Marugan, Journal of Photochemistry and Photobiology A 148 (2002) 315.
[409] L. Zhao, J.G. Yu, Journal of Colloid and Interface Science 304 (2006) 84.
[410] B.J. Aronson, C.F. Blanford, A. Stein, Chemistry of Materials 9 (1997) 2842.
[411] J. Planelles, J.L. Movilla, Physical Review B 73 (2006) 235350.
[412] N. Serpone, D. Lawless, R. Khairutdinov, E. Pelizzetti, Journal of Physical Chemistry 99 (1995) 16655.
[413] L. Thulin, J. Guerra, Physical Review B 77 (2008) 195112.
[414] E. Yagi, R.R. Hasiguti, M. Aono, Physical Review B 54 (1996) 7945.
[415] E. Hendry, F. Wang, J. Shan, T.F. Heinz, M. Bonn, Physical Review B 69 (2004) 081101.
[416] E. Hendry, M. Koeberg, B. O'Regan, M. Bonn, Nano Letters 6 (2006) 755.
[417] Y. Furubayashi, N. Yamada, Y. Hirose, Y. Yamamoto, M. Otani, T. Hitosugi, T. Shimada, T. Hasegawa, Journal of Applied Physics 101 (2007) 093705.
[418] M.D. Stamate, Applied Surface Science 205 (2003) 353.
[419] A. Usami, Chemical Physics Letters 292 (1998) 223.
[420] I. Mora-Sero, J.A. Anta, T. Dittrich, G. Garcia-Belmonte, J. Bisquert, Journal of Photochemistry and Photobiology A 182 (2006) 280.
[421] A. Solbrand, A. Henningsson, S. Sodergren, H. Lindstrom, A. Hagfeldt, S.E. Lindquist, Journal of Physical Chemistry B 103 (1999) 1078.
[422] A.C. Fisher, L.M. Peter, E.A. Ponomarev, A.B. Walker, K.G.U. Wijayantha, Journal of Physical Chemistry B 104 (2000) 949.
[423] N. Kopidakis, E.A. Schiff, N.G. Park, J. van de Lagemaat, A.J. Frank, Journal of Physical Chemistry B 104 (2000) 3930.
[424] B. van der Zanden, A. Goossens, Journal of Physical Chemistry B 104 (2000) 7171.
[425] A. Usami, H. Ozaki, Journal of Physical Chemistry B 105 (2001) 4577.
[426] M.J. Cass, F.L. Qiu, A.B. Walker, A.C. Fisher, L.M. Peter, Journal of Physical Chemistry B 107 (2003) 113.
[427] J. Kruger, R. Plass, M. Grätzel, P.J. Cameron, L.M. Peter, Journal of Physical Chemistry B 107 (2003) 7536.
[428] K.D. Benkstein, N. Kopidakis, J. van de Lagemaat, A.J. Frank, Journal of Physical Chemistry B 107 (2003) 7759.
[429] S. Nakade, Y. Saito, W. Kubo, T. Kitamura, Y. Wada, S. Yanagida, Journal of Physical Chemistry B 107 (2003) 8607.
[430] S. Nakade, W. Kubo, Y. Saito, T. Kanzaki, T. Kitamura, Y. Wada, S. Yanagida, Journal of Physical Chemistry B 107 (2003) 14244.
[431] J. Bisquert, V.S. Vikhrenko, Journal of Physical Chemistry B 108 (2004) 2313.
[432] M.J. Cass, A.B. Walker, D. Martinez, L.M. Peter, Journal of Physical Chemistry B 109 (2005) 5100.
[433] I. Mora-Sero, T. Dittrich, A. Belaidi, G. Garcia-Belmonte, J. Bisquert, Journal of Physical Chemistry B 109 (2005) 14932.
[434] K. Hara, K. Miyamoto, Y. Abe, M. Yanagida, Journal of Physical Chemistry B 109 (2005) 23776.
[435] B.C. O'Regan, J.R. Durrant, Journal of Physical Chemistry B 110 (2006) 8544.
[436] L.Y. Liang, S.Y. Dai, L.H. Hu, F.T. Kong, W.W. Xu, K.J. Wang, Journal of Physical Chemistry B 110 (2006) 12404.
[437] L.M. Peter, A.B. Walker, G. Boschloo, A. Hagfeldt, Journal of Physical Chemistry B 110 (2006) 13694.
[438] J.A. Anta, I. Mora-Sero, T. Dittrich, J. Bisquert, Journal of Physical Chemistry C 111 (2007) 13997.
[439] J. Bisquert, Journal of Physical Chemistry C 111 (2007) 17163.
[440] J.A. Anta, J. Nelson, N. Quirke, Physical Review B 65 (2002) 125324.
[441] J. van de Lagemaat, N. Kopidakis, N.R. Neale, A.J. Frank, Physical Review B 71 (2005) 035304.
[442] T. Dittrich, I. Mora-Sero, G. Garcia-Belmonte, J. Bisquert, Physical Review B 73 (2006) 045407.
[443] S. Nakade, T. Kanzaki, Y. Wada, S. Yanagida, Langmuir 21 (2005) 10803.
[444] L. Dloczik, O. Ileperuma, I. Lauermann, L.M. Peter, E.A. Ponomarev, G. Redmond, N.J. Shaw, I. Uhlendorf, Journal of Physical Chemistry B 101 (1997) 10281.
[445] J. van de Lagemaat, N.G. Park, A.J. Frank, Journal of Physical Chemistry B 104 (2000) 2044.
[446] G. Boschloo, A. Hagfeldt, Journal of Physical Chemistry B 109 (2005) 12093.
[447] L.G.C. Rego, V.S. Batista, Journal of the American Chemical Society 125 (2003) 7989.
[448] S.G. Abuabara, L.G.C. Rego, V.S. Batista, Journal of the American Chemical Society 127 (2005) 18234.
[449] A. Wahl, J. Augustynski, Journal of Physical Chemistry B 102 (1998) 7820.
[450] N. Kopidakis, K.D. Benkstein, J. de van Lagemaat, A.J. Frank, Q. Yuan, E.A. Schiff, Physical Review B 73 (2006) 045326.
[451] J. van de Lagemaat, K. Zhu, K.D. Benkstein, A.J. Frank, Inorganica Chimica Acta 361 (2008) 620.
[452] J. Nelson, Physical Review B 59 (1999) 15374.
[453] J. Nelson, A.M. Eppler, I.M. Ballard, Journal of Photochemistry and Photobiology A 148 (2002) 25.
[454] A. Solbrand, H. Lindstrom, H. Rensmo, A. Hagfeldt, S.E. Lindquist, S. Sodergren, Journal of Physical Chemistry B 101 (1997) 2514.
[455] S. Kambe, S. Nakade, T. Kitamura, Y. Wada, S. Yanagida, Journal of Physical Chemistry B 106 (2002) 2967.
[456] H.G. Agrell, G. Boschloo, A. Hagfeldt, Journal of Physical Chemistry B 108 (2004) 12388.
[457] S.C. Ke, T.C. Wang, M.S. Wong, N.O. Gopal, Journal of Physical Chemistry B 110 (2006) 11628.
[458] H. Wittmer, S. Holten, H. Kliem, H.D. Breuer, Physica Status Solidi A 181 (2000) 461.
[459] Q. Shen, T. Toyoda, Thin Solid Films 438 (2003) 167.
[460] R. Könenkamp, Physical Review B 61 (2000) 11057.
[461] A.A. Eppler, I.N. Ballard, J. Nelson, Physica E 14 (2002) 197.
[462] P.T. Hsiao, Y.L. Tung, H.S. Teng, Journal of Physical Chemistry C 114 (2010) 6762.
[463] S. Nakade, S. Kambe, T. Kitamura, Y. Wada, S. Yanagida, Journal of Physical Chemistry B 105 (2001) 9150.
[464] S. Nakade, Y. Saito, W. Kubo, T. Kanzaki, T. Kitamura, Y. Wada, S. Yanagida, Journal of Physical Chemistry B 108 (2004) 1628.
[465] S. Tirosh, T. Dittrich, A. Ofir, L. Grinis, A. Zaban, Journal of Physical Chemistry B 110 (2006) 16165.
[466] V. Duzhko, V.Y. Timoshenko, F. Koch, T. Dittrich, Physical Review B 64 (2001) 075204.
[467] A.V. Emeline, N. Serpone, Journal of Physical Chemistry B 106 (2002) 12221.
[468] P.E. de Jongh, D. Vanmaekelbergh, Physical Review Letters 77 (1996) 3427.
[469] J.S. Salafsky, W.H. Lubberhuizen, E.v. Faassen, R.E.I. Schropp, Journal of Physical Chemistry B 102 (1998) 766.
[470] J.S. Salafsky, Physical Review B 59 (1999) 10885.
[471] A. Zaban, A. Meier, B.A. Gregg, Journal of Physical Chemistry B 101 (1997) 7985.
[472] F. Fabregat-Santiago, G. Garcia-Belmonte, J. Bisquert, A. Zaban, P. Salvador, Journal of Physical Chemistry B 106 (2002) 334.
[473] T.L. Thompson, J.T. Yates Jr., Journal of Physical Chemistry B 110 (2006) 7431.
[474] O. Byl, J.T. Yates Jr., Journal of Physical Chemistry B 110 (2006) 22966.
[475] N.A. Deskins, M. Dupuis, Physical Review B 75 (2007) 195212.
[476] N.A. Deskins, M. Dupuis, Journal of Physical Chemistry C 113 (2009) 346.
[477] S. Kerisit, N.A. Deskins, K.M. Rosso, M. Dupuis, Journal of Physical Chemistry C 112 (2008) 7678.
[478] P.E. de Jongh, D. Vanmaekelbergh, Journal of Physical Chemistry B 101 (1997) 2716.
[479] X.M. Qian, D.Q. Qin, Y.B. Bai, T.J. Li., X.Y. Tang, E.K. Wang, S.J. Dong, Journal of Solid State Electrochemistry 5 (2001) 562.
[480] G. Schlichthorl, N.G. Park, A.J. Frank, Journal of Physical Chemistry B 103 (1999) 782.
[481] W.J. Sun, C.R. Chenthamarakshan, K. Rajeshwar, Journal of Physical Chemistry B 106 (2002) 11531.
[482] J. van de Lagemaat, A.J. Frank, Journal of Physical Chemistry B 104 (2000) 4292.
[483] D. Nister, K. Keis, S.E. Lindquist, A. Hagfeldt, Solar Energy Materials and Solar Cells 73 (2002) 411.
[484] I. Mora-Sero, J. Bisquert, Nano Letters 3 (2003) 945.
[485] N.A. Deskins, R. Rousseau, M. Dupuis, Journal of Physical Chemistry C 113 (2009) 14583.
[486] J.M. Lantz, R.M. Corn, Journal of Physical Chemistry 98 (1994) 9387.
[487] N. Yu, J. Woods halley, Physical Review B 51 (1995) 4768.
[488] S. Ikeda, N. Sugiyama, S. Murakami, H. Kominami, Y. Kera, H. Noguchi, K. Uosaki, T. Torimoto, B. Ohtani, Physical Chemistry Chemical Physics 5 (2003) 778.
[489] G. Boschloo, D. Fitzmaurice, Journal of Physical Chemistry B 103 (1999) 2228.
[490] G.K. Boschloo, A. Goossens, Journal of Physical Chemistry 100 (1996) 19489.
[491] D.S. Warren, A.J. Mcquillan, Journal of Physical Chemistry B 108 (2004) 19373.
[492] Y. Fu, W.H. Cao, Journal of Applied Physics 100 (2006) 084324.
[493] Y.X. Weng, Y.Q. Wang, J.B. Asbury, H.N. Ghosh, T.Q. Lian, Journal of Physical Chemistry B 104 (2000) 93.
[494] G. Ramakrishna, H.N. Ghosh, A.K. Singh, D.K. Palit, J.P. Mittal, Journal of Physical Chemistry B 105 (2001) 12786.
[495] A.N.M. Green, R.E. Chandler, S.A. Haque, J. Nelson, J.R. Durrant, Journal of Physical Chemistry B 109 (2005) 142.
[496] I. Martini, J.H. Hodak, G.V. Hartland, Journal of Physical Chemistry B 103 (1999) 9104.
[497] H.N. Ghosh, Journal of Physical Chemistry B 103 (1999) 10382.
[498] N.W. Duffy, L.M. Peter, K.G.U. Wijayantha, Electrochemistry Communications 2 (2000) 262.

[499] G. Li, L. Chen, M.E. Graham, K.A. Gray, Journal of Molecular Catalysis A 275 (2007) 30.
[500] J. Bisquert, A. Zaban, P. Salvador, Journal of Physical Chemistry B 106 (2002) 8774.
[501] J.A. Anta, F. Casanueva, G. Oskam, Journal of Physical Chemistry B 110 (2006) 5372.
[502] N. Kopidakis, N.R. Neale, K. Zhu, J. van de Lagemaat, A.J. Frank, Applied Physics Letters 87 (2005) 202106.
[503] D.W. Bahnemann, M. Hilgendorff, R. Memming, Journal of Physical Chemistry B 101 (1997) 4265.
[504] T. Yoshihara, R. Katoh, A. Furube, Y. Tamaki, M. Murai, K. Hara, S. Murata, H. Arakawa, M. Tachiya, Journal of Physical Chemistry B 108 (2004) 3817.
[505] (a) R. Katoh, A. Huijser, K. Hara, T.J. Savenije, L.D.A. Siebbeles, Journal of Physical Chemistry C 111 (2007) 10741;
(b) R. Katoh, M. Murai, A. Furube, Chemical Physics Letters 461 (2008) 238.
[506] T. Asahi, A. Furube, H. Masuhara, Chemical Physics Letters 275 (1997) 234.
[507] K. Zhu, N. Kopidakis, N.R. Neale, J. van de Lagemaat, A.J. Frank, Journal of Physical Chemistry B 110 (2006) 25174.
[508] S.H. Szczepankiewicz, J.A. Moss, M.R. Hoffmann, Journal of Physical Chemistry B 106 (2002) 2922.
[509] A.M. Peiro, C. Colombo, G. Doyle, J. Nelson, A. Mills, J.R. Durrant, Journal of Physical Chemistry B 110 (2006) 23255.
[510] S.H. Szczepankiewicz, A.J. Colussi, M.R. Hoffmann, Journal of Physical Chemistry B 104 (2000) 9842.
[511] T.A. Konovalova, L.D. Kispert, V.V. Konovalov, Journal of Physical Chemistry B 103 (1999) 4672.
[512] A. Furube, T. Asahi, H. Masuhara, H. Yamashita, M. Anpo, Journal of Physical Chemistry B 103 (1999) 3120.
[513] Y. Nakaoka, Y. Nosaka, Journal of Photochemistry and Photobiology A 110 (1997) 299.
[514] C.A. Jenkins, D.M. Murphy, Journal of Physical Chemistry B 103 (1999) 1019.
[515] H. Uetsuka, H. Onishi, M.A. Henderson, J.M. White, Journal of Physical Chemistry B 108 (2004) 10621.
[516] H.L. Wang, J.J. He, G. Boschloo, H. Lindstrom, A. Hagfeldt, S.E. Lindquist, Journal of Physical Chemistry B 105 (2001) 2529.
[517] S.H. Szczepankiewicz, J.A. Moss, M.R. Hoffmann, Journal of Physical Chemistry B 106 (2002) 7654.
[518] D.C. Hurum, K.A. Gray, T. Rajh, M.C. Thurnauer, Journal of Physical Chemistry B 109 (2005) 977.
[519] C.P. Kumar, N.O. Gopal, T.C. Wang, M.S. Wong, S.C. Ke, Journal of Physical Chemistry B 110 (2006) 5223.
[520] A.A. Dubinski, G.D. Perekhodtsev, O.G. Poluektov, T. Rajh, M.C. Thurnauer, Journal of Physical Chemistry B 106 (2002) 938.
[521] N.M. Dimitrijevic, Z.V. Saponjic, B.M. Rabatic, O.G. Poluektov, T. Rajh, Journal of Physical Chemistry C 111 (2007) 14597.
[522] V. Shapovalov, E.V. Stefanovich, T.N. Truong, Surface Science 498 (2002) L103.
[523] P.M. Kowalski, M.F. Camellone, N.N. Nair, B. Meyer, D. Marx, Physical Review Letters 105 (2010) 146405.
[524] T. Miyagi, M. Kamei, T. Mitsuhashi, T. Ishigaki, A. Yamazaki, Chemical Physics Letters 390 (2004) 399.
[525] M. Kamei, T. Miyagi, T. Ishigaki, Chemical Physics Letters 407 (2005) 209.
[526] S. Wendt, P.T. Sprunger, E. Lira, G.K.H. Madsen, Z. Li, J.O. Hansen, J. Matthiesen, A. Blekinge-Rasmussen, E. Laegsgaard, B. Hammer, F. Besenbacher, Science 320 (2008) 1755.
[527] T. Minato, Y. Sainoo, Y. Kim, H. Kato, K. Aika, M. Kawai, J. Zhao, H. Petek, T. Huang, W. He, B. Wang, Z. Wang, Y. Zhao, J. Yang, J.G. Hou, Journal of Chemical Physics 130 (2009) 124502.
[528] D.P. Colombo, R.M. Bowman, Journal of Physical Chemistry 100 (1996) 18445.
[529] D.P. Colombo, R.M. Bowman, Journal of Physical Chemistry 99 (1995) 11752.
[530] D.E. Skinner, D.P. Colombo, J.J. Cavaleri, R.M. Bowman, Journal of Physical Chemistry 99 (1995) 7853.
[531] D.P. Colombo, K.A. Roussel, J. Saeh, D.E. Skinner, J.J. Cavaleri, R.M. Bowman, Chemical Physics Letters 232 (1995) 207.
[532] N.J. Cherepy, G.P. Smestad, M. Grätzel, J.Z. Zhang, Journal of Physical Chemistry B 101 (1997) 9342.
[533] K. Iwata, T. Takaya, H. Hamaguchi, A. Yamakata, T.A. Ishibashi, H. Onishi, H. Kuroda, Journal of Physical Chemistry B 108 (2004) 20233.
[534] X.J. Yang, N. Tamai, Physical Chemistry Chemical Physics 3 (2001) 3393.
[535] T. Tachikawa, S. Tojo, M. Fujitsuka, T. Sekino, T. Majima, Journal of Physical Chemistry B 110 (2006) 14055.
[536] R. Huber, S. Sporlein, J.E. Moser, M. Grätzel, J. Wachtveitl, Journal of Physical Chemistry B 104 (2000) 8995.
[537] A.I. Kuznetsov, O. Kameneva, L. Rozes, C. Sanchez, N. Bityurin, A. Kanaev, Chemical Physics Letters 429 (2006) 523.
[538] J. Rabani, K. Yamashita, K. Ushida, J. Stark, A. Kira, Journal of Physical Chemistry B 102 (1998) 1689.
[539] I.A. Shkrob, M.C. Sauer, Journal of Physical Chemistry B 108 (2004) 12497.
[540] A.I. Kuznetsov, O. Kameneva, A. Alexandrov, N. Bityurin, P. Marteau, K. Chhor, C. Sanchez, A. Kanaev, Physical Review E 71 (2005) 021403.
[541] M.A. Henderson, J.M. White, H. Uetsuka, H. Onishi, Journal of Catalysis 238 (2006) 153.
[542] T. Ohsawa, I.V. Lyubinetsky, M.A. Henderson, S.A. Chambers, Journal of Physical Chemistry C 112 (2008) 20050.
[543] J.M. White, M.A. Henderson, Journal of Physical Chemistry B 109 (2005) 12417.
[544] J.E. Kroeze, T.J. Savenije, J.M. Warman, Journal of the American Chemical Society 126 (2004) 7608.
[545] G. Schlichthorl, S.Y. Huang, J. Sprague, A.J. Frank, Journal of Physical Chemistry B 101 (1997) 8141.
[546] A.V. Barzykin, M. Tachiya, Journal of Physical Chemistry B 106 (2002) 4356.
[547] N. Beermann, G. Boschloo, A. Hagfeldt, Journal of Photochemistry and Photobiology A 152 (2002) 213.
[548] T. Hirakawa, Y. Nosaka, Langmuir 18 (2002) 3247.
[549] T. Berger, M. Sterrer, S. Stankic, J. Bernardi, O. Diwald, E. Knozinger, Materials Science and Engineering C 25 (2005) 664.
[550] A.L. Attwood, D.M. Murphy, J.L. Edwards, T.A. Egerton, R.W. Harrison, Research on Chemical Intermediates 29 (2003) 449.
[551] V. Iliev, D. Tomova, L. Bilyarska, A. Eliyas, L. Petrov, Applied Catalysis B 63 (2006) 266.
[552] O.I. Micic, Y.N. Zhang, K.R. Cromack, A.D. Trifunac, M.C. Thurnauer, Journal of Physical Chemistry 97 (1993) 7277.
[553] O.I. Micic, Y.N. Zhang, K.R. Cromack, A.D. Trifunac, M.C. Thurnauer, Journal of Physical Chemistry 97 (1993) 13284.
[554] R.F. Howe, M. Grätzel, Journal of Physical Chemistry 89 (1985) 4495.
[555] T. Rajh, A.E. Ostafin, O.I. Micic, D.M. Tiede, M.C. Thurnauer, Journal of Physical Chemistry 100 (1996) 4538.
[556] A.V. Emeline, L.G. Smirnova, G.N. Kuzmin, L.L. Basov, N. Serpone, Journal of Photochemistry and Photobiology A 148 (2002) 97.
[557] S. Yamazoe, K. Teramura, Y. Hitomi, T. Shishido, T. Tanaka, Journal of Physical Chemistry C 111 (2007) 14189.
[558] D.M. Martino, H. van Willigen, M.T. Spitler, Journal of Physical Chemistry B 101 (1997) 8914.
[559] T. Berger, M. Sterrer, O. Diwald, E. Knozinger, D. Panayotov, T.L. Thompson, J.T. Yates Jr., Journal of Physical Chemistry B 109 (2005) 6061.
[560] H. van't Spijker, B. O'Regan, A. Goossens, Journal of Physical Chemistry B 105 (2001) 7220.
[561] G. Franco, J. Gehring, L.M. Peter, E.A. Ponomarev, I. Uhlendorf, Journal of Physical Chemistry B 103 (1999) 692.
[562] A. Yamakata, T. Ishibashi, H. Onishi, Journal of Physical Chemistry B 105 (2001) 7258.
[563] M. Jakob, H. Levanon, P.V. Kamat, Nano Letters 3 (2003) 353.
[564] S. Eriksen, R.G. Egdell, Surface Science 180 (1987) 263.
[565] H. Ibach, D.L. Mills, Electron Energy Loss Spectroscopy and Surface Vibrations, Academic Press, New York, 1982.
[566] C.L. Pang, R. Lindsay, G. Thornton, Chemical Society Reviews 37 (2008) 2328.
[567] A.I. Kuznetsov, O. Kameneva, A. Alexandrov, N. Bityurin, K. Chhor, A. Kanaev, Journal of Physical Chemistry B 110 (2006) 435.
[568] N. Bityurin, A.I. Kuznetsov, A. Kanaev, Applied Surface Science 248 (2005) 86.
[569] T. Yoshihara, Y. Tamaki, A. Furube, M. Murai, K. Hara, R. Katoh, Chemical Physics Letters 438 (2007) 268.
[570] T. Berger, O. Diwald, E. Knozinger, M. Sterrer, J.T. Yates Jr., Physical Chemistry Chemical Physics 8 (2006) 1822.
[571] J.M. Coronado, A.J. Maira, A. Martinez-Arias, J.C. Conesa, J. Soria, Journal of Photochemistry and Photobiology A 150 (2002) 213.
[572] I.A. Shkrob, M.C. Sauer, D. Gosztola, Journal of Physical Chemistry B 108 (2004) 12512.
[573] T.L. Thompson, J.T. Yates Jr., Journal of Physical Chemistry B 109 (2005) 18230.
[574] P.V. Kamat, I. Bedja, S. Hotchandani, Journal of Physical Chemistry 98 (1994) 9137.
[575] M. Aono, R.R. Hasiguti, Physical Review B 48 (1993) 12406.
[576] N.D. Abazovic, M.I. Comor, M.D. Dramicanin, D.J. Jovanovic, S.P. Ahrenkiel, J.M. Nedeljkovic, Journal of Physical Chemistry B 110 (2006) 25366.
[577] K. Fujihara, S. Izumi, T. Ohno, M. Matsumura, Journal of Photochemistry and Photobiology A 132 (2000) 99.
[578] H.N. Ghosh, S. Adhikari, Langmuir 17 (2001) 4129.
[579] K. Hachiya, J. Kondoh, Physica B-Condensed Matter 334 (2003) 130.
[580] A. Imanishi, T. Okamura, N. Ohashi, R. Nakamura, Y. Nakato, Journal of the American Chemical Society 129 (2007) 11569.
[581] X. Li, K.H.A. Lau, D.H. Kim, W. Knoll, Langmuir 21 (2005) 5212.
[582] F. Montoncello, M.C. Carotta, B. Cavicchi, M. Ferroni, A. Giberti, V. Guidi, C. Malagu, G. Martinelli, F. Meinardi, Journal of Applied Physics 94 (2003) 1501.
[583] H. Nakajima, T. Mori, Q. Shen, T. Toyoda, Chemical Physics Letters 409 (2005) 81.
[584] R. Nakamura, T. Okamura, N. Ohashi, A. Imanishi, Y. Nakato, Journal of the American Chemical Society 127 (2005) 12975.
[585] Y. Nakato, H. Akanuma, Y. Magari, S. Yae, J.I. Shimizu, H. Mori, Journal of Physical Chemistry B 101 (1997) 4934.
[586] L. Qian, Z.S. Jin, S.Y. Yang, Z.L. Du, X.R. Xu, Chemistry of Materials 17 (2005) 5334.
[587] T. Sekiya, M. Tasaki, K. Wakabayashi, S. Kurita, Journal of Luminescence 108 (2004) 69.
[588] Y.C. Zhu, C.X. Ding, G.H. Ma, Z.L. Du, Journal of Solid State Chemistry 139 (1998) 124.
[589] Y.C. Zhu, C.X. Ding, Journal of Solid State Chemistry 145 (1999) 711.
[590] X.L. Wang, Z.C. Feng, J.Y. Shi, G.Q. Jia, S.A. Shen, J. Zhou, C. Li, Physical Chemistry Chemical Physics 12 (2010) 7083.
[591] M. Yoon, M. Seo, C. Jeong, J.H. Jang, K.S. Jeon, Chemistry of Materials 17 (2005) 6069.

[592] K. Miyashita, S. Kuroda, S. Tajima, K. Takehira, S. Tobita, H. Kubota, Chemical Physics Letters 369 (2003) 225.
[593] A. Yamakata, T. Ishibashi, H. Onishi, Chemical Physics 339 (2007) 133.
[594] H. Zhao, Q.L. Zhang, Y.X. Weng, Journal of Physical Chemistry C 111 (2007) 3762.
[595] H. Kominami, S. Murakami, Y. Kera, B. Ohtani, Catalysis Letters 56 (1998) 125.
[596] S.T. Martin, H. Herrmann, W.Y. Choi, M.R. Hoffmann, Journal of the Chemical Society-Faraday Transactions 90 (1994) 3315.
[597] S.T. Martin, H. Herrmann, M.R. Hoffmann, Journal of the Chemical Society-Faraday Transactions 90 (1994) 3323.
[598] A.G. Agrios, P. Pichat, Journal of Photochemistry and Photobiology A 180 (2006) 130.
[599] B. Ohtani, R.M. Bowman, D.P. Colombo, H. Kominami, H. Noguchi, K. Uosaki, Chemistry Letters (1998) 579.
[600] B. Ohtani, Y. Ogawa, S. Nishimoto, Journal of Physical Chemistry B 101 (1997) 3746.
[601] Y. Tachibana, J.E. Moser, M. Grätzel, D.R. Klug, J.R. Durrant, Journal of Physical Chemistry 100 (1996) 20056.
[602] Y.K. Du, J. Rabani, Journal of Physical Chemistry B 107 (2003) 11970.
[603] (a) Z. Zhang, J.T. Yates Jr., Journal of Physical Chemistry C 114 (2010) 3098; (b) Z. Zhang, J.T. Yates Jr., Journal of Physical Chemistry Letters 1 (2010) 2185.
[604] M.A. Grela, A.J. Colussi, Journal of Physical Chemistry 100 (1996) 18214.
[605] J.E. Evans, K.W. Springer, J.Z. Zhang, Journal of Chemical Physics 101 (1994) 6222.
[606] J.B. Asbury, R.J. Ellingson, H.N. Ghosh, S. Ferrere, A.J. Nozik, T.Q. Lian, Journal of Physical Chemistry B 103 (1999) 3110.
[607] J.B. Asbury, Y.-Q. Wang, E. Hao, H.N. Ghosh, T. Lian, Research on Chemical Intermediates 27 (2001) 393.
[608] R. Argazzi, C.A. Bignozzi, T.A. Heimer, F.N. Castellano, G.J. Meyer, Journal of the American Chemical Society 117 (1995) 11815.
[609] G. Benko, M. Hilgendorff, A.P. Yartsev, V. Sundstrom, Journal of Physical Chemistry B 105 (2001) 967.
[610] G. Benko, J. Kallioinen, J.E.I. Korppi-Tommola, A.P. Yartsev, V. Sundstrom, Journal of the American Chemical Society 124 (2002) 489.
[611] T.D.M. Bell, C. Pagba, M. Myahkostupov, J. Hofkens, P. Piotrowiak, Journal of Physical Chemistry B 110 (2006) 25314.
[612] P. Bonhote, J.E. Moser, R. Humphry-Baker, N. Vlachopoulos, S.M. Zakeeruddin, L. Walder, M. Grätzel, Journal of the American Chemical Society 121 (1999) 1324.
[613] C. Bauer, G. Boschloo, E. Mukhtar, A. Hagfeldt, Journal of Physical Chemistry B 106 (2002) 12693.
[614] C. Creutz, B.S. Brunschwig, N. Sutin, Journal of Physical Chemistry B 110 (2006) 25181.
[615] W.R. Duncan, W.M. Stier, O.V. Prezhdo, Journal of the American Chemical Society 127 (2005) 7941.
[616] W.R. Duncan, O.V. Prezhdo, Journal of the American Chemical Society 130 (2008) 9756.
[617] R.J. Ellingson, J.B. Asbury, S. Ferrere, H.N. Ghosh, J.R. Sprague, T.Q. Lian, A.J. Nozik, Journal of Physical Chemistry B 102 (1998) 6455.
[618] H.N. Ghosh, J.B. Asbury, Y.X. Weng, T.Q. Lian, Journal of Physical Chemistry B 102 (1998) 10208.
[619] B.A. Gregg, S.G. Chen, S. Ferrere, Journal of Physical Chemistry B 107 (2003) 3019.
[620] E. Galoppini, W.Z. Guo, W. Zhang, P.G. Hoertz, P. Qu, G.J. Meyer, Journal of the American Chemical Society 124 (2002) 7801.
[621] C.G. Garcia, A.K. Nakano, C.J. Kleverlaan, N.Y.M. Iha, Journal of Photochemistry and Photobiology A 151 (2002) 165.
[622] P.G. Hoertz, A. Staniszewski, A. Marton, G.T. Higgins, C.D. Incarvito, A.L. Rheingold, G.J. Meyer, Journal of the American Chemical Society 128 (2006) 8234.
[623] S.A. Haque, E. Palomares, B.M. Cho, A.N.M. Green, N. Hirata, D.R. Klug, J.R. Durrant, Journal of the American Chemical Society 127 (2005) 3456.
[624] M. Hilgendorff, V. Sundstrom, Chemical Physics Letters 287 (1998) 709.
[625] R. Huber, J.E. Moser, M. Grätzel, J. Wachtveitl, Journal of Physical Chemistry B 106 (2002) 6494.
[626] M. Ikeda, N. Koide, L. Han, A. Sasahara, H. Onishi, Journal of Physical Chemistry C 112 (2008) 6961.
[627] J.E. Kroeze, T.J. Savenije, J.M. Warman, Journal of Photochemistry and Photobiology A 148 (2002) 49.
[628] D. Kuciauskas, J.E. Monat, R. Villahermosa, H.B. Gray, N.S. Lewis, J.K. Mccusker, Journal of Physical Chemistry B 106 (2002) 9347.
[629] J. Kallioinen, G. Benko, P. Myllyperkio, L. Khriachtchev, B. Skarman, R. Wallenberg, M. Tuomikoski, J. Korppi-Tommola, V. Sundstrom, A.P. Yartsev, Journal of Physical Chemistry B 108 (2004) 6365.
[630] I. Kondov, M. Cizek, C. Benesch, H.B. Wang, M. Thoss, Journal of Physical Chemistry C 111 (2007) 11970.
[631] A.C. Khazraji, S. Hotchandani, S. Das, P.V. Kamat, Journal of Physical Chemistry B 103 (1999) 4693.
[632] M.O. Lenz, J. Wachtveitl, Journal of Physical Chemistry C 112 (2008) 11973.
[633] Y.F. Lu., D.J. Choi, J. Nelson, O.B. Yang, B.A. Parkinson, Journal of the Electrochemical Society 153 (2006) E131.
[634] L.Y. Luo, C.W. Chang, C.Y. Lin, E.W.G. Diau, Chemical Physics Letters 432 (2006) 452.
[635] D. Liu, P.V. Kamat, K.G. Thomas, K.J. Thomas, S. Das, M.V. George, Journal of Chemical Physics 106 (1997) 6404.
[636] F. Liu, G.J. Meyer, Journal of the American Chemical Society 127 (2005) 824.
[637] I. Martini, J.H. Hodak, G.V. Hartland, Journal of Physical Chemistry B 102 (1998) 607.
[638] I. Martini, J. Hodak, G.V. Hartland, P.V. Kamat, Journal of Chemical Physics 107 (1997) 8064.
[639] M. Nilsing, P. Persson, S. Lunell, L. Ojamaee, Journal of Physical Chemistry C 111 (2007) 12116.
[640] J. Pan, G. Benko, Y.H. Xu, T. Pascher, L.C. Sun, V. Sundstrom, T. Polivka, Journal of the American Chemical Society 124 (2002) 13949.
[641] S. Pelet, M. Grätzel, J.E. Moser, Journal of Physical Chemistry B 107 (2003) 3215.
[642] A. Petersson, M. Ratner, H.O. Karlsson, Journal of Physical Chemistry B 104 (2000) 8498.
[643] P. Piotrowiak, E. Galoppini, Q. Wei, G.J. Meyer, R. Wiewior, Journal of the American Chemical Society 125 (2003) 5278.
[644] P. Persson, R. Bergstrom, S. Lunell, Journal of Physical Chemistry B 104 (2000) 10348.
[645] P. Qu, D.W. Thompson, G.J. Meyer, Langmuir 16 (2000) 4662.
[646] G. Ramakrishna, A.K. Singh, D.K. Palit, H.N. Ghosh, Journal of Physical Chemistry B 108 (2004) 12489.
[647] S. Ramakrishna, F. Willig, V. May, Physical Review B 62 (2000) R16330.
[648] S. Ramakrishna, F. Willig, V. May, Journal of Chemical Physics 115 (2001) 2743.
[649] G. Ramakrishna, D.A. Jose, D.K. Kumar, A. Das, D.K. Palit, H.N. Ghosh, Journal of Physical Chemistry B 109 (2005) 15445.
[650] G. Ramakrishna, S. Verma, D.A. Jose, D.K. Kumar, A. Das, D.K. Palit, H.N. Ghosh, Journal of Physical Chemistry B 110 (2006) 9012.
[651] G. Ramakrishna, A.K. Singh, D.K. Palit, H.N. Ghosh, Journal of Physical Chemistry B 108 (2004) 4775.
[652] J. Rabani, K. Ushida, K. Yamashita, J. Stark, S. Gershuni, A. Kira, Journal of Physical Chemistry B 101 (1997) 3136.
[653] K.L. Sebastian, M. Tachiya, Journal of Chemical Physics 124 (2006) 064713.
[654] W. Stier, O.V. Prezhdo, Journal of Physical Chemistry B 106 (2002) 8047.
[655] J. Schnadt, J.N. O'Shea, L. Patthey, L. Kjeldgaard, J. Ahlund, K. Nilson, J. Schiessling, J. Krempasky, M. Shi, O. Karis, C. Glover, H. Siegbahn, N. Martensson, P.A. Bruhwiler, Journal of Chemical Physics 119 (2003) 12462.
[656] J. Schnadt, P.A. Bruhwiler, L. Patthey, J.N. O'Shea, S. Sodergren, M. Odelius, R. Ahuja, O. Karis, M. Bassler, P. Persson, H. Siegbahn, S. Lunell, N. Martensson, Nature 418 (2002) 620.
[657] L.C.T. Shoute, G.R. Loppnow, Journal of Chemical Physics 117 (2002) 842.
[658] C.X. She, J.C. Guo, T.Q. Lian, Journal of Physical Chemistry B 111 (2007) 6903.
[659] P.K. Sudeep, K. Takechi, P.V. Kamat, Journal of Physical Chemistry C 111 (2007) 488.
[660] C.X. She, N.A. Anderson, J.C. Guo, F. Liu, W.H. Goh, D.T. Chen, D.L. Mohler, Z.Q. Tian, J.T. Hupp, T.Q. Lian, Journal of Physical Chemistry B 109 (2005) 19345.
[661] D.V. Tsivlin, F. Willig, V. May, Physical Review B 77 (2008) 035319.
[662] Y. Tachibana, S.A. Haque, I.P. Mercer, J.R. Durrant, D.R. Klug, Journal of Physical Chemistry B 104 (2000) 1198.
[663] P.A. van Hal, M.P.T. Christiaans, M.M. Wienk, J.M. Kroon, R.A.J. Janssen, Journal of Physical Chemistry B 103 (1999) 4352.
[664] L.X. Wang, V. May, Journal of Chemical Physics 121 (2004) 8039.
[665] L.X. Wang, F. Willig, V. May, Journal of Chemical Physics 124 (2006) 014712.
[666] B. Wenger, M. Grätzel, J.-E. Moser, Journal of the American Chemical Society 127 (2005) 12150.
[667] X.J. Yang, Z.F. Dai, A. Miura, N. Tamai, Chemical Physics Letters 334 (2001) 257.
[668] C. Zimmermann, F. Willig, S. Ramakrishna, B. Burfeindt, B. Pettinger, R. Eichberger, W. Storck, Journal of Physical Chemistry B 105 (2001) 9245.
[669] B. Burfeindt, T. Hannappel, W. Storck, F. Willig, Journal of Physical Chemistry 100 (1996) 16463.
[670] Y.H. Wang, K. Hang, N.A. Anderson, T.Q. Lian, Journal of Physical Chemistry B 107 (2003) 9434.
[671] M. Haukka, P. Hirva, Surface Science 511 (2002) 373.
[672] A. Imanishi, H. Suzuki, K. Murakoshi, Y. Nakato, Journal of Physical Chemistry B 110 (2006) 21050.
[673] A. Imanishi, H. Suzuki, N. Ohashi, T. Ohta, Y. Nakato, Inorganica Chimica Acta 361 (2008) 778.
[674] S. Ushiroda, N. Ruzycki, Y. Lu, M.T. Spitler, B.A. Parkinson, Journal of the American Chemical Society 127 (2005) 5158.
[675] G. Ramakrishna, A.K. Singh, D.K. Palit, H.N. Ghosh, Journal of Physical Chemistry B 108 (2004) 1701.
[676] A. Furube, T. Asahi, H. Masuhara, H. Yamashita, M. Anpo, Research on Chemical Intermediates 27 (2001) 177.
[677] M. Salmi, N. Tkachenko, V. Vehmanen, R.J. Lamminmaki, S. Karvinen, H. Lemmetyinen, Journal of Photochemistry and Photobiology A 163 (2004) 395.
[678] T. Tachikawa, S. Tojo, M. Fujitsuka, T. Majima, Chemical Physics Letters 392 (2004) 50.
[679] D. Sporleder, D.P. Wilson, M.G. White, Journal of Physical Chemistry C 113 (2009) 13180.
[680] S.J. Garrett, V.P. Holbert, P.C. Stair, E. Weitz, Journal of Chemical Physics 100 (1994) 4626.
[681] S.H. Kim, P.C. Stair, E. Weitz, Journal of Chemical Physics 108 (1998) 5080.
[682] S.H. Kim, P.C. Stair, E. Weitz, Chemical Physics Letters 302 (1999) 511.
[683] S.H. Kim, P.C. Stair, E. Weitz, Surface Science 445 (2000) 177.
[684] P.R. Antoniewicz, Physical Review B 21 (1980) 3811.
[685] J.L. Ferry, W.H. Glaze, Journal of Physical Chemistry B 102 (1998) 2239.

[686] G. Grabner, R.M. Quint, Langmuir 7 (1991) 1091.
[687] D. Fitzmaurice, H. Frei, J. Rabani, Journal of Physical Chemistry 99 (1995) 9176.
[688] J.N. Clifford, E. Palomares, M.K. Nazeeruddin, M. Grätzel, J. Nelson, X. Li, N.J. Long, J.R. Durrant, Journal of the American Chemical Society 126 (2004) 5225.
[689] S.A. Haque, Y. Tachibana, R.L. Willis, J.E. Moser, M. Grätzel, D.R. Klug, J.R. Durrant, Journal of Physical Chemistry B 104 (2000) 538.
[690] S.A. Haque, Y. Tachibana, D.R. Klug, J.R. Durrant, Journal of Physical Chemistry B 102 (1998) 1745.
[691] M. Hilgendorff, V. Sundstrom, Journal of Physical Chemistry B 102 (1998) 10505.
[692] D. Kuciauskas, M.S. Freund, H.B. Gray, J.R. Winkler, N.S. Lewis, Journal of Physical Chemistry B 105 (2001) 392.
[693] I. Martini, J.H. Hodak, G.V. Hartland, Journal of Physical Chemistry B 102 (1998) 9508.
[694] S. Nakade, T. Kanzaki, W. Kubo, T. Kitamura, Y. Wada, S. Yanagida, Journal of Physical Chemistry B 109 (2005) 3480.
[695] S.G. Yan, J.S. Prieskorn, Y.J. Kim, J.T. Hupp, Journal of Physical Chemistry B 104 (2000) 10871.
[696] L. Zhang, J. Yang, L. Wang, G.Z. Yang, Y.X. Weng, Journal of Physical Chemistry B 107 (2003) 13688.
[697] Journal of Physical Chemistry 90 (16) (1986).
[698] J.J. He, H. Lindstrom, A. Hagfeldt, S.E. Lindquist, Journal of Physical Chemistry B 103 (1999) 8940.
[699] M. Borgstrom, E. Blart, G. Boschloo, E. Mukhtar, A. Hagfeldt, L. Hammarstrom, F. Odobel, Journal of Physical Chemistry B 109 (2005) 22928.
[700] H. Onishi, Springer Series in Chemical Physics 70 (2003) 75.
[701] M.A. Henderson, Journal of Physical Chemistry B 109 (2005) 12062.
[702] M.A. Henderson, Surface Science 602 (2008) 3188.
[703] R.T. Zehr, N.A. Deskins, M.A. Henderson, Journal of Physical Chemistry C 114 (2010) 16900.
[704] R.T. Zehr, M.A. Henderson, Surface Science 602 (2008) 2238.
[705] C.N. Rusu, J.T. Yates Jr., Journal of Physical Chemistry B 105 (2001) 2596.
[706] Y. Xu, W.K. Chen, S.H. Liu, M.J. Cao, J.Q. Li, Chemical Physics 331 (2007) 275.
[707] C.P. Leon, L. Kador, B. Peng, M. Thelakkat, Journal of Physical Chemistry B 110 (2006) 8723.
[708] K. Kilsa, E.I. Mayo, B.S. Brunschwig, H.B. Gray, N.S. Lewis, J.R. Winkler, Journal of Physical Chemistry B 108 (2004) 15640.
[709] R. Ernstorfer, L. Gundlach, S. Felber, W. Storck, R. Eichberger, F. Willig, Journal of Physical Chemistry B 110 (2006) 25383.
[710] H. Park, E. Bae, J.J. Lee, J. Park, W. Choi, Journal of Physical Chemistry B 110 (2006) 8740.
[711] M.J. Lundqvist, M. Nilsing, S. Lunell, B. Akermark, P. Persson, Journal of Physical Chemistry B 110 (2006) 20513.
[712] E. Bae, W. Choi, Journal of Physical Chemistry B 110 (2006) 14792.
[713] Y.X. Weng, L. Li, Y. Liu, L. Wang, G.Z. Yang, Journal of Physical Chemistry B 107 (2003) 4356.
[714] A.C. Lukaski, D.S. Muggli, Journal of Catalysis 223 (2004) 250.
[715] L.F. Liao, W.C. Wu, C.Y. Chen, J.L. Lin, Journal of Physical Chemistry B 105 (2001) 7678.
[716] W.C. Wu, C.C. Chuang, J.L. Lin, Journal of Physical Chemistry B 104 (2000) 8719.
[717] Z.Q. Yu, S.S.C. Chuang, Journal of Catalysis 246 (2007) 118.
[718] J.F. Fan, J.T. Yates Jr., Journal of the American Chemical Society 118 (1996) 4686.
[719] C.N. Rusu, J.T. Yates Jr., Journal of Physical Chemistry B 104 (2000) 12299.
[720] I. Lyubinetsky, Z.Q. Yu, M.A. Henderson, Journal of Physical Chemistry C 111 (2007) 4342.
[721] F. Arsac, D. Bianchi, J.M. Chovelon, C. Ferronato, J.M. Herrmann, Journal of Physical Chemistry A 110 (2006) 4202.
[722] F. Arsac, D. Bianchi, J.M. Chovellon, C. Ferronato, J.M. Herrmann, Journal of Physical Chemistry A 110 (2006) 4213.
[723] J.A. Byrne, B.R. Eggins, S. Linquette-Mailley, P.S.M. Dunlop, Analyst 123 (1998) 2007.
[724] K. Ishibashi, A. Fujishima, T. Watanabe, K. Hashimoto, Journal of Photochemistry and Photobiology A 134 (2000) 139.
[725] Y.X. Chen, S.Y. Yang, K. Wang, L.P. Lou, Journal of Photochemistry and Photobiology A 172 (2005) 47.
[726] R. Morelli, I.R. Bellobono, C.M. Chiodaroli, S. Alborghetti, Journal of Photochemistry and Photobiology A 112 (1998) 271.
[727] Y. Murakami, K. Endo, I. Ohta, A.Y. Nosaka, Y. Nosaka, Journal of Physical Chemistry C 111 (2007) 11339.
[728] P. Raja, A. Bozzi, H. Mansilla, J. Kiwi, Journal of Photochemistry and Photobiology A 169 (2005) 271.
[729] K. Ishibashi, A. Fujishima, T. Watanabe, K. Hashimoto, Electrochemistry Communications 2 (2000) 207.
[730] T. Hirakawa, H. Kominami, B. Ohtani, Y. Nosaka, Journal of Physical Chemistry B 105 (2001) 6993.
[731] P.F. Schwarz, N.J. Turro, S.H. Bossmann, A.M. Braun, A. Wahab, H. Durr, Journal of Physical Chemistry B 101 (1997) 7127.
[732] P. Salvador, Journal of Physical Chemistry C 111 (2007) 17038.
[733] I. Mora-Sero, T.L. Villarreal, J. Bisquert, A. Pitarch, R. Gomez, P. Salvador, Journal of Physical Chemistry B 109 (2005) 3371.
[734] Y. Nosaka, K. Koenuma, K. Ushida, A. Kira, Langmuir 12 (1996) 736.
[735] P. Kormali, T. Triantis, D. Dimotikali, A. Hiskia, E. Papaconstantinou, Applied Catalysis B 68 (2006) 139.
[736] Y. Nosaka, S. Komori, K. Yawata, T. Hirakawa, A.Y. Nosaka, Physical Chemistry Chemical Physics 5 (2003) 4731.
[737] J.T. Carneiro, T.J. Savenije, J.A. Moulijn, G. Mul, Journal of Physical Chemistry C 114 (2010) 327.
[738] S. Yamazaki, K. Hori, Catalysis Letters 59 (1999) 191.
[739] C. Minero, G. Mariella, V. Maurino, E. Pelizzetti, Langmuir 16 (2000) 2632.
[740] W. Kubo, T. Tatsuma, Applied Surface Science 243 (2005) 125.
[741] H. Haick, Y. Paz, Journal of Physical Chemistry B 105 (2001) 3045.
[742] T. Tatsuma, W. Kubo, A. Fujishima, Langmuir 18 (2002) 9632.
[743] J.S. Park, W. Choi, Langmuir 20 (2004) 11523.
[744] (a) J. Thiebaud, A. Parker, C. Fittschen, G. Vincent, O. Zahraa, P.-M. Marquaire, Journal of Physical Chemistry C 112 (2008) 2239;
(b) J. Thiebaud, F. Thévenet, C. Fittschen, Journal of Physical Chemistry C 114 (2010) 3082.
[745] Y. Kikuchi, K. Sunada, T. Iyoda, K. Hashimoto, A. Fujishima, Journal of Photochemistry and Photobiology A 106 (1997) 51.
[746] T. Tatsuma, S.-i. Tachibana, T. Miwa, D.A. Tryk, A. Fujishima, Journal of Physical Chemistry B 103 (1999) 8033.
[747] T. Tatsuma, S. Tachibana, A. Fujishima, Journal of Physical Chemistry B 105 (2001) 6987.
[748] H. Haick, Y. Paz, Chemphyschem 4 (2003) 617.
[749] K. Kawahara, Y. Ohko, T. Tatsuma, A. Fujishima, Physical Chemistry Chemical Physics 5 (2003) 4764.
[750] W. Kubo, T. Tatsuma, A. Fujishima, H. Kobayashi, Journal of Physical Chemistry B 108 (2004) 3005.
[751] K. Naito, T. Tachikawa, M. Fujitsuka, T. Majima, Journal of Physical Chemistry B 109 (2005) 23138.
[752] M.A. Henderson, Journal of Catalysis 256 (2008) 287.
[753] M.A. Henderson, Journal of Physical Chemistry C 112 (2008) 11433.
[754] V.P. Holbert, S.J. Garrett, P.C. Stair, E. Weitz, Surface Science 346 (1996) 189.
[755] S.J. Garrett, V.P. Holbert, P.C. Stair, E. Weitz, Journal of Chemical Physics 100 (1994) 4615.
[756] M. Shen, M.A. Henderson, Journal of Physical Chemistry C 115 (2011) 5886.
[757] J.M. White, M.A. Henderson, Journal of Physical Chemistry B 109 (2005) 14990.
[758] E. Carter, A.F. Carley, D.M. Murphy, ChemPhysChem 8 (2007) 113.
[759] A.L. Attwood, J.L. Edwards, C.C. Rowlands, D.M. Murphy, Journal of Physical Chemistry A 107 (2003) 1779.
[760] J.M. Coronado, J. Soria, Catalysis Today 123 (2007) 37.
[761] S. Upadhya, D.F. Ollis, Journal of Physical Chemistry B 101 (1997) 2625.
[762] A. Mills, J.S. Wang, D.F. Ollis, Journal of Physical Chemistry B 110 (2006) 14386.
[763] V. Loddo, M. Addamo, V. Augugliaro, L. Palmisano, A. Schiavello, E. Garrone, AIChE Journal 52 (2006) 2565.
[764] M. Salaices, B. Serrano, H.I. de Lasa, Industrial & Engineering Chemistry Research 40 (2001) 5455.
[765] C.Y. Wang, J. Rabani, D.W. Bahnemann, J.K. Dohrmann, Journal of Photochemistry and Photobiology A 148 (2002) 169.
[766] M. Bettoni, T. Del Giacco, C. Rol, G.V. Sebastiani, Journal of Photochemistry and Photobiology A 163 (2004) 481.
[767] C.J.G. Cornu, A.J. Colussi, M.R. Hoffmann, Journal of Physical Chemistry B 105 (2001) 1351.
[768] M. Corboz, I. Alxneit, G. Stoll, H.R. Tschudi, Journal of Physical Chemistry B 104 (2000) 10569.
[769] G.D. Lee, J.L. Falconer, Catalysis Letters 70 (2000) 145.
[770] D.S. Muggli, J.L. Falconer, Journal of Catalysis 191 (2000) 318.
[771] T.L. Thompson, D.A. Panayotov, J.T. Yates Jr., I. Martyanov, K. Klabunde, Journal of Physical Chemistry B 108 (2004) 17857.
[772] J. Zhuang, C.N. Rusu, J.T. Yates Jr., Journal of Physical Chemistry B 103 (1999) 6957.
[773] K. Yoshida, T. Nanbara, J. Yamasaki, N. Tanaka, Journal of Applied Physics 99 (2006) 084908.
[774] M.C. Blount, J.A. Buchholz, J.L. Falconer, Journal of Catalysis 197 (2001) 303.
[775] M. El-Maazawi, A.N. Finken, A.B. Nair, V.H. Grassian, Journal of Catalysis 191 (2000) 138.
[776] A. Linsebigler, G.Q. Lu, J.T. Yates Jr., Journal of Physical Chemistry 100 (1996) 6631.
[777] H. Idriss, P. Legare, G. Maire, Surface Science 515 (2002) 413.
[778] A. Sclafani, J.M. Herrmann, Journal of Physical Chemistry 100 (1996) 13655.
[779] C. Shu, N. Sukumar, C.P. Ursenbach, Journal of Chemical Physics 110 (1999) 10539.
[780] (a) C.N. Rusu, J.T. Yates Jr., Langmuir 13 (1997) 4311;
(b) Z. Zhang, J.T. Yates Jr., Journal of the American Chemical Society 132 (2010) 12804.
[781] G.Q. Lu, A. Linsebigler, J.T. Yates Jr., Journal of Chemical Physics 102 (1995) 4657.
[782] M.P. de Lara-Castells, J.L. Krause, Journal of Chemical Physics 118 (2003) 5098.
[783] H. Einaga, M. Harada, S. Futamura, T. Ibusuki, Journal of Physical Chemistry B 107 (2003) 9290.
[784] C.F. Lien, Y.F. Lin, Y.S. Lin, M.T. Chen, J.L. Lin, Journal of Physical Chemistry B 108 (2004) 18261.
[785] N. Bredemeyer, S. de Buhr, D. Hesse, Chemical Engineering & Technology 23 (2000) 527.
[786] M. Takeuchi, G. Martra, S. Coluccia, M. Anpo, Journal of Physical Chemistry C 111 (2007) 9811.

[787] E. Puzenat, P. Pichat, Journal of Photochemistry and Photobiology A 160 (2003) 127.
[788] A.A. Lisachenko, R.V. Mikhailov, L.L. Basov, B.N. Shelimov, M. Che, Journal of Physical Chemistry C 111 (2007) 14440.
[789] L. Xiao, A.N.M. Green, S.A. Haque, A. Mills, J.R. Durtant, Journal of Photochemistry and Photobiology A 162 (2004) 253.
[790] N. Serpone, J. Martin, S. Horikoshi, H. Hidaka, Journal of Photochemistry and Photobiology A 169 (2005) 235.
[791] S. Mezhenny, P. Maksymovych, T.L. Thompson, O. Diwald, D. Stahl, S.D. Walck, J.T. Yates Jr., Chemical Physics Letters 369 (2003) 152.
[792] Z. Dohnálek, I. Lyubinetsky, R. Rousseau, Progress in Surface Science 85 (2010) 161.
[793] P.M. Jayaweera, E.L. Quah, H. Idriss, Journal of Physical Chemistry C 111 (2007) 1764.
[794] U. Diebold, J. Lehman, T. Mahmoud, M. Kuhn, G. Leonardelli, W. Hebenstreit, M. Schmid, P. Varga, Surface Science 411 (1998) 137.
[795] Y. Du, N.A. Deskins, Z. Zhang, Z. Dohnálek, M. Dupuis, I. Lyubinetsky, Physical Review Letters 102 (2009) 096102.
[796] Y.G. Du, Z. Dohnálek, I. Lyubinetsky, Journal of Physical Chemistry C 112 (2008) 2649.
[797] Y.G. Du, N.A. Deskins, Z.R. Zhang, Z. Dohnálek, M. Dupuis, I. Lyubinetsky, Journal of Physical Chemistry C 113 (2009) 666.
[798] Z. Dohnálek, J. Kim, O. Bondarchuk, J.M. White, B.D. Kay, Journal of Physical Chemistry B 110 (2006) 6229.
[799] W.S. Epling, C.H.F. Peden, M.A. Henderson, U. Diebold, Surface Science 412/413 (1998) 333.
[800] G.A. Kimmel, N.G. Petrik, Physical Review Letters 100 (2008) 196102.
[801] L.-M. Liu, P. Crawford, P. Hu, Progress in Surface Science 84 (2009) 155.
[802] G.Q. Lu, A. Linsebigler, J.T. Yates Jr., Journal of Chemical Physics 102 (1995) 3005.
[803] J.M. Pan, B.L. Maschhoff, U. Diebold, T.E. Madey, Journal of Vacuum Science & Technology A 10 (1992) 2470.
[804] N.G. Petrik, Z. Zhang, Y. Du, Z. Dohnálek, I. Lyubinetsky, G.A. Kimmel, Journal of Physical Chemistry C 113 (2009) 12407.
[805] E. Wahlstrom, E.K. Vestergaard, R. Schaub, A. Ronnau, M. Vestergaard, E. Laegsgaard, I. Stensgaard, F. Besenbacher, Science 303 (2004) 511.
[806] S. Wendt, R. Schaub, J. Matthiesen, E.K. Vestergaard, E. Wahlstroem, M.D. Rasmussen, P. Thostrup, L.M. Molina, E. Laegsgaard, I. Stensgaard, B. Hammer, Besenbacher, Surface Science 598 (2005) 226.
[807] Z. Zhang, Y. Du, N.G. Petrik, G.A. Kimmel, I. Lyubinetsky, Z. Dohnálek, Journal of Physical Chemistry C 113 (2009) 1908.
[808] M. Li., W. Hebenstreit, U. Diebold, M.A. Henderson, D.R. Jennison, Faraday Discussions 114 (1999) 245.
[809] M. Li., W. Hebenstreit, L. Gross, U. Diebold, M.A. Henderson, D.R. Jennison, P.A. Schultz, M.P. Sears, Surface Science 437 (1999) 173.
[810] C.L. Pang, O. Bikondoa, D.S. Humphrey, A.C. Papageorgiou, G. Cabailh, R. Ithnin, Q. Chen, C.A. Muryn, H. Onishi, G. Thornton, Nanotechnology 17 (2006) 5397.
[811] C.M. Yim, C.L. Pang, G. Thornton, Physical Review Letters 104 (2010) 036806.
[812] Y. Du, N.A. Deskins, Z. Zhang, Z. Dohnálek, M. Dupuis, I. Lyubinetsky, Physical Chemistry Chemical Physics 12 (2010) 6337.
[813] A.C. Papageorgiou, N.S. Beglitis, C.L. Pang, G. Teobaldi, G. Cabailh, Q. Chen, A.J. Fisher, W.A. Hofer, G. Thornton, Proceedings of the National Academy of Sciences of the United States of America 107 (2010) 2391.
[814] A.A. Bonapasta, F. Filippone, Surface Science 577 (2005) 59.
[815] S. Chretien, H. Metiu, Journal of Chemical Physics 128 (2008) 044714.
[816] M.P. de Lara-Castells, A.O. Mitrushenkov, O. Roncero, J.L. Krause, Israel Journal of Chemistry 45 (2005) 59.
[817] M.P. de Lara-Castells, J.L. Krause, Chemical Physics Letters 354 (2002) 483.
[818] M.P. de Lara-Castells, J.L. Krause, Journal of Chemical Physics 115 (2001) 4798.
[819] K.N. Ding, J.Q. Li, Y.F. Zhang, W.F. Wang, Y. Li, Acta Chimica Sinica 61 (2003) 705.
[820] F. Filippone, G. Mattioli, A.A. Bonapasta, Catalysis Today 129 (2007) 169.
[821] F.M. Hossain, G.E. Murch, L. Sheppard, J. Nowotny, Advances in Applied Ceramics 106 (2007) 95.
[822] G. Mattioli, F. Filippone, A.A. Bonapasta, Journal of the American Chemical Society 128 (2006) 13772.
[823] D. Pillay, Y. Wang, G.S. Hwang, Journal of the American Chemical Society 128 (2006) 14000.
[824] Z.W. Qu, G.J. Kroes, Journal of Physical Chemistry B 110 (2006) 23306.
[825] M.D. Rasmussen, L.M. Molina, B. Hammer, Journal of Chemical Physics 120 (2004) 988.
[826] A. Tilocca, C. Di Valentin, A. Selloni, Journal of Physical Chemistry B 109 (2005) 20963.
[827] A. Tilocca, A. Selloni, Chemphyschem 6 (2005) 1911.
[828] X. Wu, A. Selloni, M. Lazzeri, S.K. Nayak, Physical Review B 68 (2003) 241402.
[829] Y. Wang, D. Pillay, G.S. Hwang, Physical Review B 70 (2004) 193410.
[830] C.J. Zhang, P.J.D. Lindan, Journal of Chemical Physics 121 (2004) 3811.
[831] N.U. Zhanpeisov, H. Fukumura, Journal of Physical Chemistry C 111 (2007) 16941.
[832] N.A. Deskins, R. Rousseau, M. Dupuis, Journal of Physical Chemistry C 114 (2010) 5891.
[833] M.J. Elser, T. Berger, D. Brandhuber, J. Bernardi, O. Diwald, E. Knozinger, Journal of Physical Chemistry B 110 (2006) 7605.
[834] S.J. Xu, J.Q. Shen, S. Chen, M.H. Zhang, T. Shen, Journal of Photochemistry and Photobiology B 67 (2002) 64.
[835] R. Nakamura, A. Imanishi, K. Murakoshi, Y. Nakato, Journal of the American Chemical Society 125 (2003) 7443.
[836] J.M. Coronado, A.J. Maira, J.C. Conesa, K.L. Yeung, V. Augugliaro, J. Soria, Langmuir 17 (2001) 5368.
[837] G.M. Liu, J.C. Zhao, H. Hidaka, Journal of Photochemistry and Photobiology A 133 (2000) 83.
[838] T. Hirakawa, Y. Nakaoka, J. Nishino, Y. Nosaka, Journal of Physical Chemistry B 103 (1999) 4399.
[839] H. Goto, Y. Hanada, T. Ohno, M. Matsumura, Journal of Catalysis 225 (2004) 223.
[840] Y. Nosaka, Y. Yamashita, H. Fukuyama, Journal of Physical Chemistry B 101 (1997) 5822.
[841] D.S. Muggli, J.L. Falconer, Journal of Catalysis 181 (1999) 155.
[842] L.F. Liao, C.F. Lien, D.L. Shieh, M.T. Chen, J.L. Lin, Journal of Physical Chemistry B 106 (2002) 11240.
[843] M.B. Hugenschmidt, L. Gamble, C.T. Campbell, Surface Science 302 (1994) 329.
[844] C. Di Valentin, Journal of Chemical Physics 127 (2007) 154705.
[845] R.A. Bennett, P. Stone, M. Bowker, Faraday Discussions 114 (1999) 267.
[846] R.A. Bennett, P. Stone, N.J. Price, M. Bowker, Physical Review Letters 82 (1999) 3831.
[847] H. Onishi, Y. Iwasawa, Physical Review Letters 76 (1996) 791.
[848] K.T. Park, M. Pan, V. Meunier, E.W. Plummer, Physical Review B 75 (2007) 245415.
[849] Z. Zhang, J. Lee, J.T. Yates Jr., R. Bechstein, E. Lira, J. Øhansen, S. Wendt, F. Besenbacher, Journal of Physical Chemistry C 114 (2010) 3059.
[850] M.A. Henderson, S. Otero-Tapia, M.E. Castro, Faraday Discussions 114 (1999) 313.
[851] M.A. Henderson, Journal of Physical Chemistry B 108 (2004) 18932.
[852] M.A. Henderson, Surface Science 355 (1996) 151.
[853] M.A. Henderson, Surface Science Reports 46 (2002) 5.
[854] K. Ishibashi, Y. Nosaka, K. Hashimoto, A. Fujishima, Journal of Physical Chemistry B 102 (1998) 2117.
[855] K. Ishibashi, A. Fujishima, T. Watanabe, K. Hashimoto, Journal of Physical Chemistry B 104 (2000) 4934.
[856] T. Tsuruta, M. Okuda, K. Katayama, Chemical Physics Letters 456 (2008) 47.
[857] S. Kataoka, M.I. Tejedor-Tejedor, J.M. Coronado, M.A. Anderson, Journal of Photochemistry and Photobiology A 163 (2004) 323.
[858] E. Carter, A.F. Carley, D.M. Murphy, Journal of Physical Chemistry C 111 (2007) 10630.
[859] Y. Nosaka, M. Nakamura, T. Hirakawa, Physical Chemistry Chemical Physics 4 (2002) 1088.
[860] A.V. Emeline, G.N. Kuzmin, D. Purevdorj, V.K. Ryabchuk, N. Serpone, Journal of Physical Chemistry B 104 (2000) 2989.
[861] J.J. He, J.C. Zhao, H. Hidaka, N. Serpone, Journal of the Chemical Society Faraday Transactions 94 (1998) 2375.
[862] J.H. Yu, J.R. Chen, C. Li., X.S. Wang, B.W. Zhang, H.Y. Ding, Journal of Physical Chemistry B 108 (2004) 2781.
[863] Z. Dohnálek, G.A. Kimmel, R.L. Ciolli, K.P. Stevenson, R.S. Smith, B.D. Kay, Journal of Chemical Physics 112 (2000) 5932.
[864] N.G. Petrik, G.A. Kimmel, Journal of Physical Chemistry Letters 1 (2010) 1758.
[865] N.G. Petrik, G.A. Kimmel, Journal of Physical Chemistry C 115 (2011) 152.
[866] G. Munuera, A. Navio, V. Rivesarnau, Journal of the Chemical Society-Faraday Transactions I 77 (1981) 2747.
[867] M.A. Brusa, Y.Di. Iorio, M.S. Churio, M.A. Grela, Journal of Molecular Catalysis A 268 (2007) 29.
[868] K. Hirakawa, T. Hirano, Chemistry Letters 35 (2006) 832.
[869] R. Konaka, E. Kasahara, W.C. Dunlap, Y. Yamamoto, K.C. Chien, M. Inoue, Redox Report 6 (2001) 319.
[870] R. Konaka, E. Kasahara, W.C. Dunlap, Y. Yamamoto, K.C. Chien, M. Inoue, Free Radical Biology and Medicine 27 (1999) 294.
[871] Y. Yamamoto, N. Imai, R. Mashima, R. Konaka, M. Inoue, W.C. Dunlap, Methods in Enzymology 319 (2000) 29.
[872] Y. Nosaka, T. Daimon, A.Y. Nosaka, Y. Murakami, Physical Chemistry Chemical Physics 6 (2004) 2917.
[873] T. Daimon, Y. Nosaka, Journal of Physical Chemistry C 111 (2007) 4420.
[874] T. Daimon, T. Hirakawa, M. Kitazawa, J. Suetake, Y. Nosaka, Applied Catalysis A 340 (2008) 169.
[875] A. Janczyk, E. Krakowska, G. Stochel, W. Macyk, Journal of the American Chemical Society 128 (2006) 15574.
[876] P.A. Babay, C.A. Emilio, R.E. Ferreyra, E.A. Gautier, R.T. Getter, M.I. Litter, Water Science and Technology 44 (2001) 179.
[877] G.R. Bamwenda, T. Uesigi, Y. Abe, K. Sayama, H. Arakawa, Applied Catalysis A 205 (2001) 117.
[878] A. Hameed, M.A. Gondal, Z.H. Yamani, A.H. Yahya, Journal of Molecular Catalysis A 227 (2005) 241.
[879] A. Mills, M.A. Valenzuela, Journal of Photochemistry and Photobiology A 165 (2004) 25.
[880] T. Ohno, K. Sarukawa, M. Matsumura, Journal of Physical Chemistry B 105 (2001) 2417.
[881] T. Tanaka, K. Teramura, K. Arakaki, T. Funabiki, Chemical Communications (2002) 2742.
[882] S. Yamazoe, T. Okumura, K. Teramura, T. Tanaka, Catalysis Today 111 (2006) 266.
[883] K. Teramura, T. Tanaka, T. Funabiki, Langmuir 19 (2003) 1209.

[884] P. Jacobson, S.C. Li, C. Wang, U. Diebold, Journal of Vacuum Science & Technology B 26 (2008) 2236.
[885] J. Arana, J.M. Dona-Rodriguez, C.G.i. Cabo, O. Gonzalez-Diaz, J.A. Herrera-Melian, J. Perez-Pena, Applied Catalysis B 53 (2004) 221.
[886] C.C. Chuang, C.C. Chen, J.L. Lin, Journal of Physical Chemistry B 103 (1999) 2439.
[887] C. Wang, D.W. Bahnemann, J.K. Dohrmann, Water Science and Technology 44 (2001) 279.
[888] C.Y. Zhou, Z.F. Ren, S.J. Tan, Z.B. Ma, X.C. Mao, D.X. Dai, H.J. Fan, X.M. Yang, J. LaRue, R. Cooper, A.M. Wodtke, Z. Wang, Z.Y. Li, B. Wang, J.L. Yang, J.G. Hou, Chemical Science 1 (2010) 575.
[889] T. Reztsova, C.H. Chang, J. Koresh, H. Idriss, Journal of Catalysis 185 (1999) 223.
[890] E. Piera, J.A. Ayllon, X. Domenech, J. Peral, Catalysis Today 76 (2002) 259.
[891] S.J. Hwang, D. Raftery, Catalysis Today 49 (1999) 353.
[892] J.M. Coronado, S. Kataoka, I. Tejedor-Tejedor, M.A. Anderson, Journal of Catalysis 219 (2003) 219.
[893] D.S. Muggli, K.H. Lowery, J.L. Falconer, Journal of Catalysis 180 (1998) 111.
[894] D.S. Muggli, J.T. Mccue, J.L. Falconer, Journal of Catalysis 173 (1998) 470.
[895] D.S. Muggli, S.A. Larson, J.L. Falconer, Journal of Physical Chemistry 100 (1996) 15886.
[896] F. Guzman, S.S.C. Chuang, Journal of American Chemical Society 132 (2010) 1502.
[897] S. Pilkenton, S.J. Hwang, D. Raftery, Journal of Physical Chemistry B 103 (1999) 11152.
[898] W.Z. Xu, D. Raftery, Journal of Physical Chemistry B 105 (2001) 4343.
[899] W.Z. Xu, D. Raftery, J.S. Francisco, Journal of Physical Chemistry B 107 (2003) 4537.
[900] D. Brinkley, T. Engel, Journal of Physical Chemistry B 104 (2000) 9836.
[901] D. Brinkley, T. Engel, Journal of Physical Chemistry B 102 (1998) 7596.
[902] D. Brinkley, T. Engel, Surface Science 415 (1998) L1001.
[903] C.P. Chang, J.N. Chen, M.C. Lu, Journal of Chemical Technology and Biotechnology 79 (2004) 1293.
[904] N. Sakaguchi, S. Matsuo, T. Kurisaki, T. Matsuo, H. Wakita, Research on Chemical Intermediates 32 (2006) 95.
[905] J. Kirchnerova, M.L.H. Cohen, C. Guy, D. Klvana, Applied Catalysis A 282 (2005) 321.
[906] F. Benoit-Marquie, U. Wilkenhoner, V. Simon, A.M. Braun, E. Oliveros, M.T. Maurette, Journal of Photochemistry and Photobiology A 132 (2000) 225.
[907] S. Preis, J.L. Falconer, Water Science and Technology 49 (2004) 141.
[908] S. Preis, J.L. Falconer, R. del Prado Asensio, N. Capdet santiago, A. Kachina, J. Kallas, Applied Catalysis B 64 (2006) 79.
[909] S. Preis, A. Kachina, N.C. Santiago, J. Kallas, Catalysis Today 101 (2005) 353.
[910] E.B. Azevedo, F. Radler de Aquino Neto, M. Dezotti, Applied Catalysis B 54 (2004) 165.
[911] A. Sobczynski, L. Duczmal, W. Zmudzinski, Journal of Molecular Catalysis A 213 (2004) 225.
[912] J. Chen, L. Eberlein, C.H. Langford, Journal of Photochemistry and Photobiology A 148 (2002) 183.
[913] G. Palmisano, M. Addamo, V. Augugliaro, T. Caronna, E. Garcia-Lopez, V. Loddo, L. Palmisano, Chemical Communications (2006) 1012.
[914] C. Hansch, A. Leo, R.W. Taft, Chemical Reviews 91 (1991) 165.
[915] X.J. Ye, D. Chen, J. Gossage, K.Y. Li, Journal of Photochemistry and Photobiology A 183 (2006) 35.
[916] Y. Ohko, D.A. Tryk, K. Hashimoto, A. Fujishima, Journal of Physical Chemistry B 102 (1998) 2699.
[917] T. Noguchi, A. Fujishima, P. Sawunyama, K. Hashimoto, Environmental Science and Technology 32 (1998) 3831.
[918] C.A. Jenkins, D.M. Murphy, C.C. Rowlands, T.A. Egerton, Journal of the Chemical Society-Perkin Transactions 2 (1997) 2479.
[919] X.Y. Li., G.H. Chen, Y. Po-Lock, C. Kutal, Journal of Chemical Technology and Biotechnology 78 (2003) 1246.
[920] M.A. Brusa, M.A. Grela, Journal of Physical Chemistry B 109 (2005) 1914.
[921] C.B. Almquist, P. Biswas, Applied Catalysis A 214 (2001) 259.
[922] P. Boarini, V. Carassiti, A. Maldotti, R. Amadelli, Langmuir 14 (1998) 2080.
[923] P. Du, J.A. Moulijn, G. Mul, Journal of Catalysis 238 (2006) 342.
[924] M.A. Gondal, A. Hameed, Z.H. Yamani, A. Arfaj, Chemical Physics Letters 392 (2004) 372.
[925] H. Yoshida, N. Matsushita, Y. Kato, T. Hattori, Journal of Physical Chemistry B 107 (2003) 8355.
[926] D.X. Shi, Y.Q. Feng, S.H. Zhong, Catalysis Today 98 (2004) 505.
[927] C. Hagglund, B. Kasemo, L. Osterlund, Journal of Physical Chemistry B 109 (2005) 10886.
[928] T. van der Meulen, A. Mattson, L. Osterlund, Journal of Catalysis 251 (2007) 131.
[929] M.D. Robbins, M.A. Henderson, Journal of Catalysis 238 (2006) 111.
[930] H. Kanai, M. Shono, K. Hamada, S. Imamura, Journal of Molecular Catalysis A 172 (2001) 25.
[931] C. Murata, H. Yoshida, J. Kumagai, T. Hattori, Journal of Physical Chemistry B 107 (2003) 4364.
[932] J. Shang, Y.G. Du, Z.L. Xu, Chemosphere 46 (2002) 93.
[933] S. Ikeda, Y. Kowata, K. Ikeue, M. Matsumura, B. Ohtani, Applied Catalysis, A: General 265 (2004) 69.
[934] K.I. Shimizu, T. Kaneko, T. Fujishima, T. Kodama, H. Yoshida, Y. Kitayama, Applied Catalysis A 225 (2002) 185.
[935] W. Wang, Y. Ku, Journal of Photochemistry and Photobiology A 159 (2003) 47.
[936] S. Zhang, Z. Zheng, J. Wang, J. Chen, Chemosphere 65 (2006) 2282.
[937] W.C. Wu, L.F. Liao, C.F. Lien, J.L. Lin, Physical Chemistry Chemical Physics 3 (2001) 4456.
[938] H. Park, W. Choi, Catalysis Today 101 (2005) 291.
[939] T.D. Bui, A. Kimura, S. Ikeda, M. Matsumura, Journal of American Chemical Society 132 (2010) 8453.
[940] M.C. Blount, J.L. Falconer, Journal of Catalysis 200 (2001) 21.
[941] M.C. Blount, J.L. Falconer, Applied Catalysis B 39 (2002) 39.
[942] G. Martra, S. Coluccia, L. Marchese, V. Augugliaro, V. Loddo, L. Palmisano, M. Schiavello, Catalysis Today 53 (1999) 695.
[943] L. Cao, Z. Gao, S.L. Suib, T.N. Obee, S.O. Hay, J.D. Freihaut, Journal of Catalysis 196 (2000) 253.
[944] A.J. Maira, J.M. Coronado, V. Augugliaro, K.L. Yeung, J.C. Conesa, J. Soria, Journal of Catalysis 202 (2001) 413.
[945] V. Augugliaro, S. Coluccia, V. Loddo, L. Marchese, G. Martra, L. Palmisano, M. Schiavello, Applied Catalysis B 20 (1998) 15.
[946] G. Marcì, M. Addamo, V. Augugliaro, S. Coluccia, E. Garcia-Lopez, V. Loddo, G. Martra, L. Palmisano, M. Schiavello, Journal of Photochemistry and Photobiology A 160 (2003) 105.
[947] R. Mendez-Roman, N. Cardona-Martinez, Catalysis Today 40 (1998) 353.
[948] T. Tachikawa, S. Tojo, M. Fujitsuka, T. Majima, Langmuir 20 (2004) 2753.
[949] T. Ohno, K. Tokieda, S. Higashida, M. Matsumura, Applied Catalysis A 244 (2003) 383.
[950] L. Hykrdova, J. Jirkovsky, G. Mailhot, M. Bolte, Journal of Photochemistry and Photobiology A 151 (2002) 181.
[951] B. Pal, M. Sharon, Journal of Molecular Catalysis A 160 (2000) 453.
[952] F. Soana, M. Sturini, L. Cermenati, A. Albini, Journal of the Chemical Society Perkins Transactions 2 (2000) 699.
[953] S. Wen, J.C. Zhao, G.Y. Sheng, J.M. Fu, P.A. Peng, Chemosphere 50 (2003) 111.
[954] A.V. Vorontsov, E.N. Savinov, E.N. Kurkin, O.D. Torbova, V.N. Parmon, Reaction Kinetics and Catalysis Letters 62 (1997) 83.
[955] S. Hwang, M.C. Lee, W. Choi, Applied Catalysis B 46 (2003) 49.
[956] A.V. Vorontsov, E.N. Savinov, G.B. Barannik, V.N. Troitsky, V.N. Parmon, Catalysis Today 39 (1997) 207.
[957] A. Linsebigler, C. Rusu, J.T. Yates Jr., Journal of the American Chemical Society 118 (1996) 5284.
[958] C. Rohmann, Y. Wang, M. Muhler, J. Metson, H. Idriss, C. Wöll, Chemical Physics Letters 460 (2008) 10.
[959] Y. Wang, C. Wöll, Surface Science 603 (2009) 1589.
[960] N.G. Petrik, G.A. Kimmel, Journal of Physical Chemistry Letters 1 (2010) 2508.
[961] J.R.S. Brownson, M.I. Tejedor-Tejedor, M.A. Anderson, Journal of Physical Chemistry B 110 (2006) 12494.
[962] D.S. Muggli, M.J. Backes, Journal of Catalysis 209 (2002) 105.
[963] L.L. Perissinotti, M.A. Brusa, M.A. Grela, Langmuir 17 (2001) 8422.
[964] B. Kraeutler, A.J. Bard, Journal of American Chemical Society 100 (1978) 2239.
[965] B. Kraeutler, A.J. Bard, Journal of the American Chemical Society 99 (1977) 7729.
[966] D.S. Muggli, J.L. Falconer, Journal of Catalysis 187 (1999) 230.
[967] J.N. Wilson, H. Idriss, Journal of Catalysis 214 (2003) 46.
[968] J.N. Wilson, H. Idriss, Journal of the American Chemical Society 124 (2002) 11284.
[969] E.L. Quah, J.N. Wilson, H. Idriss, Langmuir 26 (2010) 6411.
[970] L.F. Liao, C.F. Lien, J.L. Lin, Physical Chemistry Chemical Physics 3 (2001) 3831.
[971] M.J. Backes, A.C. Lukaski, D.S. Muggli, Applied Catalysis B 61 (2005) 21.
[972] D.S. Muggli, S.A. Keyser, J.L. Falconer, Catalysis Letters 55 (1998) 129.
[973] M.C. Blount, D.H. Kim, J.L. Falconer, Environmental Science & Technology 35 (2001) 2988.
[974] M.A. Henderson, unpublished.
[975] H. Uetsuka, C. Pang, A. Sasahara, H. Onishi, Langmuir 21 (2005) 11802.
[976] J.M. White, J. Szanyi, M.A. Henderson, Journal of Physical Chemistry B 108 (2004) 3592.
[977] G.S. Herman, M.R. Sievers, Y. Gao, Physical Review Letters 84 (2000) 3354.
[978] M. Lazzeri, A. Selloni, Physical Review Letters 87 (2001) 266105.
[979] Y. Liang, S.P. Gan, S.A. Chambers, E.I. Altman, Physical Review B 63 (2001) 235402.
[980] R.E. Tanner, A. Sasahara, Y. Liang, E.I. Altman, H. Onishi, Journal of Physical Chemistry B 106 (2002) 8211.
[981] P.Z. Araujo, C.B. Mendive, L.A.G. Rodenas, P.J. Morando, A.E. Regazzoni, M.A. Blesa, D. Bahnemann, Colloids and Surfaces A 265 (2005) 73.
[982] C.B. Mendive, D.W. Bahnemann, M.A. Blesa, Catalysis Today 101 (2005) 237.
[983] C.B. Mendive, T. Bredow, M.A. Blesa, D.W. Bahnemann, Physical Chemistry Chemical Physics 8 (2006) 3232.
[984] I. Dolamic, T. Burgi, Journal of Physical Chemistry B 110 (2006) 14898.
[985] I. Dolamic, T. Burgi, Journal of Catalysis 248 (2007) 268.
[986] Y.-C. Oh, X. Li, J.W. Cubbage, W.S. Jenks, Applied Catalysis B 54 (2004) 105.
[987] C. Guillard, Journal of Photochemistry and Photobiology A 135 (2000) 65.
[988] N. Serpone, J. Martin, S. Horikoshi, H. Hidaka, Journal of Photochemistry and Photobiology A 170 (2005) 51.
[989] P. Sawunyama, A. Fujishima, K. Hashimoto, Chemical Communications (1998) 2229.
[990] P. Sawunyama, A. Fujishima, K. Hashimoto, Langmuir 15 (1999) 3551.
[991] A.A. Ajmera, S.B. Sawant, V.G. Pangarkar, A. Beenackers, Chemical Engineering & Technology 25 (2002) 173.

[992] G.N. Ekstrom, A.J. Mcquillan, Journal of Physical Chemistry B 103 (1999) 10562.
[993] A.E. Regazzoni, P. Mandelbaum, M. Matsuyoshi, S. Schiller, S.A. Bilmes, M.A. Blesa, Langmuir 14 (1998) 868.
[994] J.C.S. Wong, A. Linsebigler, G.Q. Lu, J.F. Fan, J.T. Yates Jr., Journal of Physical Chemistry 99 (1995) 335.
[995] J. Borisch, S. Pilkenton, M.L. Miller, D. Raftery, J.S. Francisco, Journal of Physical Chemistry B 108 (2004) 5640.
[996] P. Calza, C. Minero, E. Pelizzetti, Journal of the Chemical Society Faraday Transactions 93 (1997) 3765.
[997] P. Calza, C. Minero, E. Pelizzetti, Environmental Science & Technology 31 (1997) 2198.
[998] M.T. Chen, C.F. Lien, L.F. Liao, J.L. Lin, Journal of Physical Chemistry B 107 (2003) 3837.
[999] W.Y. Choi, M.R. Hoffmann, Environmental Science & Technology 31 (1997) 89.
[1000] J. Stark, J. Rabani, Journal of Physical Chemistry B 103 (1999) 8524.
[1001] W.Y. Choi, M.R. Hoffmann, Journal of Physical Chemistry 100 (1996) 2161.
[1002] S. Yamazaki, A. Yoshida, H. Abe, Journal of Photochemistry and Photobiology A 169 (2005) 191.
[1003] C.V. Rice, D. Raftery, Chemical Communications (1999) 895.
[1004] S.J. Hwang, C. Petucci, D. Raftery, Journal of the American Chemical Society 120 (1998) 4388.
[1005] M. Kang, J.H. Lee, S.H. Lee, C.H. Chung, K.J. Yoon, K. Ogino, S. Miyata, S.J. Choung, Journal of Molecular Catalysis A 193 (2003) 273.
[1006] C.H. Hung, B.J. Marinas, Environmental Science & Technology 31 (1997) 1440.
[1007] J.S. Kim, K. Itoh, M. Murabayashi, Chemosphere 36 (1998) 483.
[1008] M.D. Driessen, A.L. Goodman, T.M. Miller, G.A. Zaharias, V.H. Grassian, Journal of Physical Chemistry B 102 (1998) 549.
[1009] S.-J. Hwang, C. Petucci, D. Raftery, Journal of the American Chemical Society 119 (1997) 7877.
[1010] S.K. Joung, T. Amemiya, M. Murabayashi, R. Cai, K. Itoh, Surface Science 598 (2005) 174.
[1011] S.-K. Joung, T. Amemiya, M. Murabayashi, K. Itoh, Journal of Photochemistry and Photobiology A 184 (2006) 273.
[1012] P.B. Amama, K. Itoh, M. Murabayashi, Applied Catalysis B 37 (2002) 321.
[1013] D. Chatterjee, S. Dasgupta, N.N. Rao, Solar Energy Materials and Solar Cells 90 (2006) 1013.
[1014] P.B. Amama, K. Itoh, M. Murabayashi, Journal of Molecular Catalysis A 217 (2004) 109.
[1015] S. Yamazaki, T. Tanimura, A. Yoshida, K. Hori, Journal of Physical Chemistry A 108 (2004) 5183.
[1016] P. Calza, C. Minero, A. Hiskia, E. Papacostantinou, E. Pelizzetti, Applied Catalysis B 21 (1999) 191.
[1017] L.F. Liao, C.F. Lien, M.T. Chen, Y.F. Lin, J.L. Lin, Physical Chemistry Chemical Physics 5 (2003) 1912.
[1018] W.C. Wu, L.F. Liao, J.S. Shiu, J.L. Lin, Physical Chemistry Chemical Physics 2 (2000) 4441.
[1019] R.T. Zehr, M.A. Henderson, Physical Chemistry Chemical Physics 12 (2010) 8084.
[1020] S. Luo, J.L. Falconer, Journal of Catalysis 185 (1999) 393.
[1021] W. Xu, D. Raftery, Journal of Catalysis 204 (2001) 110.
[1022] C. Lv, X. Wang, G. Agalya, M. Koyama, M. Kubo, A. Miyamoto, Applied Surface Science 244 (2005) 541.
[1023] F. Sunada, A. Heller, Environmental Science & Technology 32 (1998) 282.
[1024] P. Monneyron, M.H. Manero, J.N. Foussard, F. Benoit-Marquie, M.T. Maurette, Chemical Engineering Science 58 (2003) 971.
[1025] J.M. Coronado, M.E. Zorn, I. Tejedor-Tejedor, M.A. Anderson, Applied Catalysis B 43 (2003) 329.
[1026] C. Raillard, V. Hequet, P.Le. Cloirec, J. Legrand, Journal of Photochemistry and Photobiology A 163 (2004) 425.
[1027] T. Gierczak, J.B. Burkholder, S. Bauerle, A.R. Ravishankara, Chemical Physics 231 (1998) 229.
[1028] T.H. Wang, D.A. Dixon, Journal of Physical Chemistry C 114 (2010) 14083.
[1029] C.H. Ao, S.C. Lee, C.L. Mak, L.Y. Chan, Applied Catalysis B 42 (2003) 119.
[1030] S. Devahasdin, C. Fan, K.Y. Li, D.H. Chen, Journal of Photochemistry and Photobiology A 156 (2003) 161.
[1031] J.C.S. Wu, Y.-T. Cheng, Journal of Catalysis 237 (2006) 393.
[1032] K. Hashimoto, K. Wasada, M. Osaki, E. Shono, K. Adachi, N. Toukai, H. Kominami, Y. Kera, Applied Catalysis B 30 (2001) 429.
[1033] K. Hashimoto, K. Wasada, N. Toukai, H. Kominami, Y. Kera, Journal of Photochemistry and Photobiology A 136 (2000) 103.
[1034] T.H. Lim, S.M. Jeong, S.D. Kim, J. Gyenis, Journal of Photochemistry and Photobiology A 134 (2000) 209.
[1035] S. Yamazoe, T. Okumura, T. Tanaka, Catalysis Today 120 (2007) 220.
[1036] S. Yamazoe, T. Okumura, Y. Hitomi, T. Shishido, T. Tanaka, Journal of Physical Chemistry C 111 (2007) 11077.
[1037] C.C. Chuang, J.S. Shiu, J.L. Lin, Physical Chemistry Chemical Physics 2 (2000) 2629.
[1038] X. Zhu, S.R. Castleberry, M.A. Nanny, E.C. Butler, Environmental Science and Technology 39 (2005) 3784.
[1039] X. Zhu, M.A. Nanny, E.C. Butler, Journal of Photochemistry and Photobiology A 185 (2007) 289.
[1040] S. Kim, W. Choi, Environmental Science & Technology 36 (2002) 2019.
[1041] M.J. Lopez-Munoz, R. van Grieken, J. Aguado, J. Marugan, Catalysis Today 101 (2005) 307.
[1042] K. Chiang, R. Amal, T. Tran, Journal of Molecular Catalysis A 193 (2003) 285.
[1043] V. Augugliaro, J.B. Galvez, J.C. Vazquez, E.G. Lopez, V. Loddo, M.J.L. Munoz, S.M. Rodriguez, G. Marcì, L. Palmisano, M. Schiavello, J.S. Ruiz, Catalysis Today 54 (1999) 245.
[1044] V. Augugliaro, V. Loddo, G. Marcì, L. Palmisano, M.J. López-Muñozy, Journal of Catalysis 166 (1997) 272.
[1045] J.A. Pedraza-Avella, P. Acevedo-Pena, J.E. Pedraza-Rosas, Catalysis Today 133–135 (2008) 611.
[1046] C.C. Chuang, W.C. Wu, M.X. Lee, J.L. Lin, Physical Chemistry Chemical Physics 2 (2000) 3877.
[1047] M. Addamo, V. Augugliaro, S. Coluccia, M.G. Faga, E. Garcia-Lopez, V. Loddo, G. Marci, G. Martra, L. Palmisano, Journal of Catalysis 235 (2005) 209.
[1048] P. Davit, G. Martra, S. Coluccia, V. Augugliaro, E.G. Lopez, V. Loddo, G. Marci, L. Palmisano, M. Schiavello, Journal of Molecular Catalysis A 204 (2003) 693.
[1049] V. Augugliaro, S. Coluccia, E. Garcia-Lopez, V. Loddo, G. Marci, G. Martra, L. Palmisano, M. Schiavello, Topics in Catalysis 35 (2005) 237.
[1050] L.F. Liao, W.C. Wu, C.C. Chuang, J.L. Lin, Journal of Physical Chemistry B 105 (2001) 5928.
[1051] M. Hossain, M.M. Ameen, G.B. Raupp, Advances in Environmental Research 3 (1999).
[1052] A. Huang, L. Cao, J. Chen, F.-J. Spiess, S.L. Suib, T.N. Obee, S.O. Hay, J.D. Freihaut, Journal of Catalysis 188 (1999) 40.
[1053] J.A. Moss, S.H. Szczepankiewicz, E. Park, M.R. Hoffmann, Journal of Physical Chemistry B 109 (2005) 19779.
[1054] T.N. Obee, S. Satyapal, Journal of Photochemistry and Photobiology A 118 (1998) 45.
[1055] A. Kiselev, M. Andersson, A. Mattson, A. Shchukarev, S. Sjoeberg, A. Palmqvist, L. Oesterlund, Surface Science 584 (2005) 98.
[1056] A. Kiselev, A. Mattson, M. Andersson, A.E.C. Palmqvist, L. Osterlund, Journal of Photochemistry and Photobiology A 184 (2006) 125.
[1057] E.A. Kozlova, A.V. Vorontsov, Applied Catalysis B 63 (2006) 114.
[1058] K.E. O'Shea, S. Beightol, I. Garcia, M. Aguilar, D.V. Kalen, W.J. Cooper, Journal of Photochemistry and Photobiology A 107 (1997) 221.
[1059] Y.C. Oh, Y. Bao, W.S. Jenks, Journal of Photochemistry and Photobiology A 161 (2003) 69.
[1060] E.A. Kozlova, P.G. Smirniotis, A.V. Vorontsov, Journal of Photochemistry and Photobiology A 162 (2004) 503.
[1061] X.Z. Li, M.F. Hou, F.B. Li, H. Chua, Industrial & Engineering Chemistry Research 45 (2006) 487.
[1062] K. Demeestere, J. Dewulf, B. De Witte, H. van Langenhove, Applied Catalysis B 60 (2005) 93.
[1063] N. Gonzalez-Garcia, J.A. Ayllon, X. Domenech, J. Peral, Applied Catalysis, B: Environmental 52 (2004) 69.
[1064] M.C. Canela, R.M. Alberici, R.C.R. Sofia, M.N. Eberlin, W.F. Jardim, Environmental Science & Technology 33 (1999) 2788.
[1065] H. Nishikawa, Y. Takahara, Journal of Molecular Catalysis A 172 (2001) 247.
[1066] A.V. Vorontsov, E.V. Savinov, L. Davydov, P.G. Smirniotis, Applied Catalysis B 32 (2001) 11.
[1067] D.V. Kozlov, A.V. Vorontsov, P.G. Smirniotis, E.N. Savinov, Applied Catalysis B 42 (2003) 77.
[1068] M. Sokmen, D.W. Allen, A.T. Hewson, M.R. Clench, Journal of Photochemistry and Photobiology A 141 (2001) 63.
[1069] D. Panayotov, P. Kondratyuk, J.T. Yates Jr., Langmuir 20 (2004) 3674.
[1070] D.A. Panayotov, J.T. Yates Jr., Chemical Physics Letters 399 (2004) 300.
[1071] S.T. Han, H.L. Xi, X.Z. Fu, X.X. Wang, Z.X. Ding, Z.C. Lin, W.Y. Su, Acta Physico-Chimica Sinica 20 (2004) 296.
[1072] I.N. Martyanov, K.J. Klabunde, Environmental Science & Technology 37 (2003) 3448.
[1073] D.A. Panayotov, D.K. Paul, J.T. Yates Jr., Journal of Physical Chemistry B 107 (2003) 10571.
[1074] A.V. Vorontsov, C. Lion, E.N. Savinov, P.G. Smirniotis, Journal of Catalysis 220 (2003) 414.
[1075] G.M. Zuo, Z.X. Cheng, G.W. Li, L.Y. Wang, T. Miao, Environmental Science & Technology 39 (2005) 8742.
[1076] S. Kataoka, E. Lee, M.I. Tejedor-Tejedor, M.A. Anderson, Applied Catalysis, B: Environmental 61 (2005) 159.
[1077] L.Q. Jing, B.F. Xin, F.L. Yuan, B.Q. Wang, K.Y. Shi, W.M. Cai, H.G. Fu, Applied Catalysis A 275 (2004) 49.
[1078] J. Shang, Y.F. Zhu, Y.G. Du, Z.L. Xu, Journal of Solid State Chemistry 166 (2002) 395.
[1079] A.V. Vorontsov, A.A. Panchenko, E.N. Savinov, C. Lion, P.G. Smirniotis, Environmental Science & Technology 36 (2002) 5261.
[1080] A. Mills, M. Crow, J.S. Wang, I.P. Parkin, N. Boscher, Journal of Physical Chemistry C 111 (2007) 5520.
[1081] D. Wang, H. Noguchi, T. Kako, J. Ye, Research on Chemical Intermediates 31 (2005) 441.
[1082] M.C. Canela, R.M. Alberici, W.F. Jardim, Journal of Photochemistry and Photobiology A 112 (1998) 73.
[1083] S. Parra, J. Olivero, L. Pacheco, C. Pulgarin, Applied Catalysis B 43 (2003) 293.
[1084] V. Maurino, C. Minero, E. Pelizzetti, P. Piccinini, N. Serpone, H. Hidaka, Journal of Photochemistry and Photobiology A 109 (1997) 171.
[1085] N. San, A. Hatipoglu, G. Kocturk, Z. Cinar, Journal of Photochemistry and Photobiology A 146 (2002) 189.
[1086] A. Di Paola, V. Augugliaro, L. Palmisano, G. Pantaleo, E. Savinov, Journal of Photochemistry and Photobiology A 155 (2003) 207.
[1087] J. Theurich, M. Lindner, D.W. Bahnemann, Langmuir 12 (1996) 6368.

[1088] M. Moonsiri, P. Rangsunvigit, S. Chavadej, E. Gulari, Chemical Engineering Journal 97 (2004) 241.
[1089] A. Orlov, D.A. Jefferson, N. Macleod, R.M. Lambert, Catalysis Letters 92 (2004) 41.
[1090] G. Sivalingam, M.H. Priya, G. Madras, Applied Catalysis B 51 (2004) 67.
[1091] J. Krysa, G. Waldner, H. Mest'ankova, J. Jirkovsky, G. Grabner, Applied Catalysis B 64 (2006) 290.
[1092] A.K. Axelsson, L.J. Dunne, Journal of Photochemistry and Photobiology A 144 (2001) 205.
[1093] E. Soria, E. Roman, E.M. Williams, J.L. de Segovia, Surface Science 435 (1999) 543.
[1094] W. Langel, L. Menken, Surface Science 538 (2003) 1.
[1095] A.G. Thomas, W.R. Flavell, C.P. Chatwin, A.R. Kumarasinghe, S.M. Rayner, P.F. Kirkham, D. Tsoutsou, T.K. Johal, S. Patel, Surface Science 601 (2007) 3828.
[1096] G.J. Fleming, K. Adib, J.A. Rodriguez, M.A. Barteau, J.M. White, H. Idriss, Surface Science 602 (2008) 2029.
[1097] S. Koppen, O. Bronkalla, W. Langel, Journal of Physical Chemistry C 112 (2008) 13600.
[1098] M. Matsushita, T.H. Tran, A.Y. Nosaka, Y. Nosaka, Catalysis Today 120 (2007) 240.
[1099] H. Hidaka, S. Horikoshi, K. Ajisaka, J. Zhao, N. Serpone, Journal of Photochemistry and Photobiology A 108 (1997) 197.
[1100] T.H. Tran, A.Y. Nosaka, Y. Nosaka, Journal of Physical Chemistry B 110 (2006) 25525.
[1101] A.C. Lukaski, D.S. Muggli, Catalysis Letters 89 (2003) 129.
[1102] H. Tahiri, Y.A. Ichou, J.M. Herrmann, Journal of Photochemistry and Photobiology A 114 (1998) 219.
[1103] L.L. Lifongo, D.J. Bowden, P. Brimblecombe, Chemosphere 55 (2004) 467.
[1104] S. Kim, W. Choi, Journal of Physical Chemistry B 106 (2002) 13311.
[1105] F.X. Zhang, N.J. Guan, Y.Z. Li, X. Zhang, J.X. Chen, H.S. Zeng, Langmuir 19 (2003) 8230.
[1106] E. Stathatos, P. Lianos, Langmuir 16 (2000) 2398.
[1107] P.A.M. Hotsenpiller, J.D. Bolt, W.E. Farneth, J.B. Lowekamp, G.S. Rohrer, Journal of Physical Chemistry B 102 (1998) 3216.
[1108] J.B. Lowekamp, G.S. Rohrer, P.A.M. Hotsenpiller, J.D. Bolt, W.E. Farneth, Journal of Physical Chemistry B 102 (1998) 7323.
[1109] W.E. Farneth, R.S. Mclean, J.D. Bolt, E. Dokou, M.A. Barteau, Langmuir 15 (1999) 8569.
[1110] M.R.V. Sahyun, N. Serpone, Langmuir 13 (1997) 5082.
[1111] Y. Yamamoto, K. Nakajima, T. Ohsawa, Y. Matsumoto, H. Konuma, Japanese Journal of Applied Physics 2 44 (2005) L511.
[1112] T. Torimoto, N. Nakamura, S. Ikeda, B. Ohtani, Physical Chemistry Chemical Physics 4 (2002) 5910.
[1113] E. Szabo-Bardos, H. Czili, A. Horvath, Journal of Photochemistry and Photobiology A 154 (2003) 195.
[1114] T. Sano, N. Negishi, D. Mas, K. Takeuchi, Journal of Catalysis 194 (2000) 71.
[1115] X. He, X. Zhao, B. Liu, Applied Surface Science 254 (2008) 1705.
[1116] D. Guin, S.V. Manorama, J.N.L. Latha, S. Singh, Journal of Physical Chemistry C 111 (2007) 13393.
[1117] S.C. Chan, M.A. Barteau, Langmuir 21 (2005) 5588.
[1118] V. Vamathevan, R. Amal, D. Beydoun, G. Low, S. Mcevoy, Journal of Photochemistry and Photobiology A 148 (2002) 233.
[1119] K. Rajeshwar, C.R. Chenthamarakshan, Y. Ming, W.J. Sun, Journal of Electroanalytical Chemistry 538 (2002) 173.
[1120] C.Y. Wang, C.Y. Liu, X. Zheng, J. Chen, T. Shen, Colloids and Surfaces A 131 (1998) 271.
[1121] T. Soejima, H. Tada, T. Kawahara, S. Ito, Langmuir 18 (2002) 4191.
[1122] S. Somasundaram, Y. Ming, C.R. Chenthamarakshan, Z.A. Schelly, K. Rajeshwar, Journal of Physical Chemistry B 108 (2004) 4784.
[1123] I.A. Ruvarac-Bugarcic, Z.V. Saponjic, S. Zec, T. Rajh, J.M. Nedeljkovic, Chemical Physics Letters 407 (2005) 110.
[1124] V.N.H. Nguyen, R. Amal, D. Beydoun, Chemical Engineering Science 58 (2003) 4429.
[1125] K. Kabra, R. Chaudhary, R.L. Sawhney, Environmental Progress 27 (2008) 487.
[1126] J.J. Testa, M.A. Grela, M.I. Litter, Langmuir 17 (2001) 3515.
[1127] J.J. Testa, M.A. Grela, M.I. Litter, Environmental Science & Technology 38 (2004) 1589.
[1128] T. Aarthi, G. Madras, Catalysis Communications 9 (2008) 630.
[1129] J. Gimenez, M.A. Aguado, S. Cerveramarch, Journal of Molecular Catalysis A 105 (1996) 67.
[1130] S. Goeringer, C.R. Chenthamarakshan, K. Rajeshwar, Electrochemistry Communications 3 (2001) 290.
[1131] O. Horvath, E. Bodnar, J. Hegyi, Colloids and Surfaces a-Physicochemical and Engineering Aspects 265 (2005) 135.
[1132] X.R. Xu, H.B. Li, J.D. Gu, Environmental Technology 28 (2007) 1055.
[1133] H.X. Fu, G.X. Lu, S.B. Li, Journal of Photochemistry and Photobiology A 114 (1998) 81.
[1134] X.L. Wang, S.O. Pehkonen, A.K. Ray, Industrial & Engineering Chemistry Research 43 (2004) 1665.
[1135] R. Vinu, G. Madras, Environmental Science & Technology 42 (2008) 913.
[1136] S.G. Schrank, H.J. Jose, R. Moreira, Journal of Photochemistry and Photobiology A 147 (2002) 71.
[1137] M. Alam, R.A. Montalvo, Metallurgical and Materials Transactions B 29 (1998) 95.
[1138] C.R. Chenthamarakshan, K. Rajeshwar, Langmuir 16 (2000) 2715.
[1139] G. Colon, M.C. Hidalgo, J.A. Navio, Journal of Photochemistry and Photobiology A 138 (2001) 79.
[1140] G. Colon, M.C. Hidalgo, J.A. Navio, Langmuir 17 (2001) 7174.
[1141] K. Kabra, R. Chaudhary, R.L. Sawhney, Journal of Hazardous Materials 155 (2008) 424.
[1142] K. Kabra, R. Chaudhary, R.L. Sawhney, Journal of Hazardous Materials 149 (2007) 680.
[1143] S. Sanuki, K. Nakagawa, T. Kato, S. Nagaoka, H. Majima, Materials Transactions 43 (2002) 3247.
[1144] J.K. Yang, A.P. Davis, Environmental Science & Technology 34 (2000) 3789.
[1145] M.J. Lopez-Munoz, J. Aguado, B. Ruperez, Research on Chemical Intermediates 33 (2007) 377.
[1146] K. Akamatsu, A. Kimura, H. Matsubara, S. Ikeda, H. Nawafune, Langmuir 21 (2005) 8099.
[1147] N.S. Foster, R.D. Noble, C.A. Koval, Environmental Science & Technology 27 (1993) 350.
[1148] Y.Y. Wang, C.C. Wan, Journal of Photochemistry and Photobiology A 79 (1994) 203.
[1149] L.X. Chen, T. Rajh, Z.Y. Wang, M.C. Thurnauer, Journal of Physical Chemistry B 101 (1997) 10688.
[1150] T. Kanki, H. Yoneda, N. Sano, A. Toyoda, C. Nagai, Chemical Engineering Journal 97 (2004) 77.
[1151] S. Yamazaki, S. Iwai, J. Yano, H. Taniguchi, Journal of Physical Chemistry A 105 (2001) 11285.
[1152] X.L. Wang, S.O. Pehkonen, A.K. Ray, Electrochimica Acta 49 (2004) 1435.
[1153] M.A. Aguado, S. Cerveramarch, J. Gimenez, Chemical Engineering Science 50 (1995) 1561.
[1154] W.Y. Lin, K. Rajeshwar, Journal of the Electrochemical Society 144 (1997) 2751.
[1155] F. Forouzan, T.C. Richards, A.J. Bard, Journal of Physical Chemistry 100 (1996) 18123.
[1156] L. Murruni, F. Conde, G. Leyva, M.I. Litter, Applied Catalysis B 84 (2008) 563.
[1157] T. Ohno, K. Sarukawa, M. Matsumura, New Journal of Chemistry 26 (2002) 1167.
[1158] K. Teramura, S.-i. Okuoka, S. Yamazoe, K. Kato, T. Shishido, T. Tanaka, Journal of Physical Chemistry C 112 (2008) 8495.
[1159] V. Eliet, G. Bidoglio, Environmental Science & Technology 32 (1998) 3155.
[1160] J. Chen, D.F. Ollis, W.H. Rulkens, H. Bruning, Colloids and Surfaces a-Physicochemical and Engineering Aspects 151 (1999) 339.
[1161] E. Selli, V. Eliet, M.R. Spini, G. Bidoglio, Environmental Science & Technology 34 (2000) 3742.
[1162] C.N. Rusu, J.T. Yates Jr., Journal of Physical Chemistry B 104 (2000) 1729.
[1163] M. Takeuchi, H. Yamashita, M. Matsuoka, M. Anpo, T. Hirao, N. Itoh, N. Iwamoto, Catalysis Letters 66 (2000) 185.
[1164] H. Yamashita, Y. Ichihashi, M. Anpo, M. Hashimoto, C. Louis, M. Che, Journal of Physical Chemistry 100 (1996) 16041.
[1165] J.L. Zhang, M. Minagawa, M. Matsuoka, H. Yamashita, M. Anpo, Catalysis Letters 66 (2000) 241.
[1166] A. Kudo, H. Nagayoshi, Catalysis Letters 52 (1998) 109.
[1167] R.J. Gustafsson, A. Orlov, P.T. Griffiths, R.A. Cox, R.M. Lambert, Chemical Communications (2006) 3936.
[1168] Y.X. Li, F. Wasgestian, Journal of Photochemistry and Photobiology A 112 (1998) 255.
[1169] H. Shibata, N. Noda, Y. Ogura, K. Sogabe, Y. Sawa, Bioscience Biotechnology and Biochemistry 64 (2000) 1751.
[1170] K.T. Ranjit, B. Viswanathan, T.K. Varadarajan, Journal of Materials Science Letters 15 (1996) 874.
[1171] O.V. Makarova, T. Rajh, M.C. Thurnauer, A. Martin, P.A. Kemme, D. Cropek, Environmental Science & Technology 34 (2000) 4797.
[1172] S.O. Flores, O. Rios-Bernij, M.A. Valenzuela, I. Cordova, R. Gomez, R. Gutierrez, Topics in Catalysis 44 (2007) 507.
[1173] J.L. Ferry, W.H. Glaze, Langmuir 14 (1998) 3551.
[1174] V. Brezova, A. Blazkova, I. Surina, B. Havlinova, Journal of Photochemistry and Photobiology A 107 (1997) 233.
[1175] V. Brezova, P. Tarabek, D. Dvoranova, A. Stasko, S. Biskupic, Journal of Photochemistry and Photobiology A 155 (2003) 179.
[1176] E. Kikuchi, H. Sakamoto, Journal of the Electrochemical Society 147 (2000) 4589.
[1177] V.N.H. Nguyen, D. Beydoun, R. Amal, Journal of Photochemistry and Photobiology A 171 (2005) 113.
[1178] S. Sanuki, T. Kojima, K. Arai, S. Nagaoka, H. Majima, Metallurgical and Materials Transactions B 30 (1999) 15.
[1179] T. Tan, D. Beydoun, R. Amal, Journal of Photochemistry and Photobiology A 159 (2003) 273.
[1180] T.T.Y. Tan, C.K. Yip, D. Beydoun, R. Amal, Chemical Engineering Journal 95 (2003) 179.
[1181] T.T.Y. Tan, D. Beydoun, R. Amal, Journal of Physical Chemistry B 107 (2003) 4296.
[1182] T.T.Y. Tan, D. Beydoun, R. Amal, Journal of Molecular Catalysis A 202 (2003) 73.
[1183] R.L. Calhoun, K. Winkelmann, G. Mills, Journal of Physical Chemistry B 105 (2001) 9739.
[1184] D. Mas, P. Pichat, C. Guillard, Research on Chemical Intermediates 23 (1997) 275.
[1185] S. Weaver, G. Mills, Journal of Physical Chemistry B 101 (1997) 3769.
[1186] M. Anpo, H. Yamashita, Y. Ichihashi, Y. Fujii, M. Honda, Journal of Physical Chemistry B 101 (1997) 2632.

[1187] D. Behar, J. Rabani, Journal of Physical Chemistry B 110 (2006) 8750.
[1188] Y.L. Chen, D.Z. Li, X.C. Wang, X.X. Wang, X.Z. Fu, Chemical Communications (2004) 2304.
[1189] T. Chen, Z.H. Feng, G.P. Wu, J.Y. Shi, G.J. Ma, P.L. Ying, C. Li, Journal of Physical Chemistry C 111 (2007) 8005.
[1190] K. Chiang, T.M. Lim, L. Tsen, C.C. Lee, Applied Catalysis A 261 (2004) 225.
[1191] H. Einaga, M. Harada, Langmuir 21 (2005) 2578.
[1192] C.A. Emilio, M.I. Litter, M. Kunst, M. Bouchard, C. Colbeau-Justin, Langmuir 22 (2006) 3606.
[1193] G. Facchin, G. Carturan, R. Campostrini, S. Gialanella, L. Lutterotti, L. Armelao, G. Marci, L. Palmisano, A. Sclafani, Journal of Sol-Gel Science and Technology 18 (2000) 29.
[1194] J.L. Falconer, K.A. Magrini-Bair, Journal of Catalysis 179 (1998) 171.
[1195] A. Furube, T. Asahi, H. Masuhara, H. Yamashita, M. Anpo, Chemical Physics Letters 336 (2001) 424.
[1196] H. Haick, Y. Paz, Journal of Physical Chemistry B 107 (2003) 2319.
[1197] M. Harada, H. Einaga, Catalysis Communications 5 (2004) 63.
[1198] K. Hiehata, A. Sasahara, H. Onishi, Nanotechnology 18 (2007) 084007.
[1199] D. Hufschmidt, D. Bahemann, J.J. Testa, C.A. Emilio, M.I. Litter, Journal of Photochemistry and Photobiology A 148 (2002) 223.
[1200] Z. Kasarevic-Popovic, D. Behar, J. Rabani, Journal of Physical Chemistry B 108 (2004) 20291.
[1201] V. Keller, P. Bernhardt, F. Garin, Journal of Catalysis 215 (2003) 129.
[1202] J.C. Kennedy III, A.K. Datye, Journal of Catalysis 179 (1998) 375.
[1203] S.C. Kim, M.C. Heo, S.H. Hahn, C.W. Lee, J.H. Joo, J.S. Kim, I.-K. Yoo, E.J. Kim, Materials Letters 59 (2005) 2059.
[1204] J.S. Lee, W.Y. Choi, Journal of Physical Chemistry B 109 (2005) 7399.
[1205] J.S. Lee, H.W. Park, W.Y. Choi, Environmental Science & Technology 36 (2002) 5462.
[1206] J.S. Lee, W.Y. Choi, Environmental Science & Technology 38 (2004) 4026.
[1207] S.K. Lee, A. Mill's, Platinum Metals Review 47 (2003) 61.
[1208] Q.Y. Li, K. Wang, S.L. Zhang, M. Zhang, H.J. Yang, Z.S. Jin, Journal of Molecular Catalysis A 258 (2006) 83.
[1209] F.B. Li, X.Z. Li, Chemosphere 48 (2002) 1103.
[1210] H. Nakajima, T. Mori, M. Watanabe, Journal of Applied Physics 96 (2004) 925.
[1211] Y. Nosaka, M. Kishimoto, J. Nishino, Journal of Physical Chemistry B 102 (1998) 10279.
[1212] B. Ohtani, K. Iwai, S. Nishimoto, S. Sato, Journal of Physical Chemistry B 101 (1997) 3349.
[1213] H.W. Park, J.S. Lee, W.Y. Choi, Catalysis Today 111 (2006) 259.
[1214] K.T. Ranjit, T.K. Varadarajan, B. Viswanathan, Journal of Photochemistry and Photobiology A 96 (1996) 181.
[1215] T. Sano, N. Negishi, K. Uchino, J. Tanaka, S. Matsuzawa, K. Takeuchi, Journal of Photochemistry and Photobiology A 160 (2003) 93.
[1216] H. Selcuk, W. Zaltner, J.J. Sene, M. Bekbolet, M.A. Anderson, Journal of Applied Electrochemistry 34 (2004) 653.
[1217] M.K.I. Senevirathna, P. Pitigala, K. Tennakone, Solar Energy Materials and Solar Cells 90 (2006) 2918.
[1218] W. Shangguan, A. Yoshida, M.X. Chen, Solar Energy Materials and Solar Cells 80 (2003) 433.
[1219] L. Shivalingappa, J. Sheng, T. Fukami, Vacuum 48 (1997) 413.
[1220] V. Subramanian, E. Wolf, P.V. Kamat, Journal of Physical Chemistry B 105 (2001) 11439.
[1221] B. Sun, A.V. Vorontsov, P.G. Smirniotis, Langmuir 19 (2003) 3151.
[1222] M. Takeuchi, K. Tsujimaru, K. Sakamoto, M. Matsuoka, H. Yamashita, M. Anpo, Research on Chemical Intermediates 29 (2003) 619.
[1223] A.V. Vorontsov, I.V. Stoyanova, D.V. Kozlov, V.I. Simagina, E.N. Savinov, Journal of Catalysis 189 (2000) 360.
[1224] A.V. Vorontsov, V.P. Dubovitskaya, Journal of Catalysis 221 (2004) 102.
[1225] C.Y. Wang, R. Pagel, D.W. Bahnemann, J.K. Dohrmann, Journal of Physical Chemistry B 108 (2004) 14082.
[1226] A. Yamakata, T.A. Ishibashi, H. Onishi, Journal of Photochemistry and Photobiology A 160 (2003) 33.
[1227] A. Yamakata, T. Ishibashi, H. Onishi, Journal of Physical Chemistry B 106 (2002) 9122.
[1228] Y.Z. Yang, C.H. Chang, H. Idriss, Applied Catalysis B 67 (2006) 217.
[1229] C. Young, T.M. Lim, K. Chiang, R. Amal, Water Science and Technology 50 (2004) 251.
[1230] W. Zhao, C.C. Chen, X.Z. Li, J.C. Zhao, H. Hidaka, N. Serpone, Journal of Physical Chemistry B 106 (2002) 5022.
[1231] M. Zhang, Z.S. Jin, J.W. Zhang, Z.J. Zhang, H.X. Dang, Journal of Molecular Catalysis A 225 (2005) 59.
[1232] A.V. Vorontsov, E.N. Savinov, Z.S. Jin, Journal of Photochemistry and Photobiology A 125 (1999) 113.
[1233] H. Kominami, A. Furusho, S. Murakami, H. Inoue, Y. Kera, B. Ohtani, Catalysis Letters 76 (2001) 31.
[1234] H. Keskinen, J.M. Makela, M. Aromaa, J. Keskinen, S. Areva, C.V. Teixeira, J.B. Rosenholm, V. Pore, M. Ritala, M. Leskela, M. Raulio, M.S. Salkinoja-Salonen, E. Levanen, T. Mantyla, Catalysis Letters 111 (2006) 127.
[1235] X.F. You, F. Chen, J.L. Zhang, M. Anpo, Catalysis Letters 102 (2005) 247.
[1236] J. Sa, M. Fernandez-Garcia, J.A. Anderson, Catalysis Communications 9 (2008) 1991.
[1237] C.C. Su, C.H. Liao, J.D. Wang, C.M. Chiu, B.J. Chen, Catalysis Today 97 (2004) 71.
[1238] S. Rengaraj, X.Z. Li, Journal of Molecular Catalysis A 243 (2006) 60.
[1239] H. Tran, J. Scott, K. Chiang, R. Amal, Journal of Photochemistry and Photobiology A 183 (2006) 41.
[1240] T. Hirakawa, P.V. Kamat, Journal of the American Chemical Society 127 (2005) 3928.
[1241] S.X. Liu, Z.P. Qu, X.W. Han, C.L. Sun, Catalysis Today 93–95 (2004) 877.
[1242] P.D. Cozzoli, M.L. Curri, A. Agostiano, Chemical Communications (2005) 3186.
[1243] C. He, Y. Yu, X.F. Hu, A. Larbot, Applied Surface Science 200 (2002) 239.
[1244] B.F. Xin, Z.Y. Ren, H.Y. Hu, X.Y. Zhang, C.L. Dong, K.Y. Shi, L.Q. Jing, H.G. Fu, Applied Surface Science 252 (2005) 2050.
[1245] B.F. Xin, L.Q. Jing, Z.Y. Ren, B.Q. Wang, H.G. Fu, Journal of Physical Chemistry B 109 (2005) 2805.
[1246] P.D. Cozzoli, E. Fanizza, R. Comparelli, M.L. Curri, A. Agostiano, D. Laub, Journal of Physical Chemistry B 108 (2004) 9623.
[1247] S. Kato, Y. Hirano, M. Iwata, T. Sano, K. Takeuchi, S. Matsuzawa, Applied Catalysis B: Environmental 57 (2005) 109.
[1248] H. Einaga, Reaction Kinetics and Catalysis Letters 88 (2006) 357.
[1249] A. Dobosz, A. Sobczynski, Water Research 37 (2003) 1489.
[1250] C.C. Chang, C.K. Lin, C.C. Chan, C.S. Hsu, C.Y. Chen, Thin Solid Films 494 (2006) 274.
[1251] A. Kumar, N. Mathur, Applied Catalysis A 275 (2004) 189.
[1252] H. Tada, T. Ishida, A. Takao, S. Ito, Langmuir 20 (2004) 7898.
[1253] F. Zhang, R. Jin, J. Chen, C. Shao, W. Gao, L. Li, N. Guan, Journal of Catalysis 232 (2005) 424.
[1254] F.X. Zhang, Y. Pi, J. Cui, Y.L. Yang, X. Zhang, N.J. Guan, Journal of Physical Chemistry C 111 (2007) 3756.
[1255] H. Tada, T. Ishida, A. Takao, S. Ito, S. Mukhopadhyay, T. Akita, K. Tanaka, H. Kobayashi, Chemphyschem 6 (2005) 1537.
[1256] J.L. Gong, C.B. Mullins, Accounts of Chemical Research 42 (2009) 1063.
[1257] H.J. Freund, G. Pacchioni, Chemical Society Reviews 37 (2008) 2224.
[1258] C.W. Corti, R.J. Holliday, D.T. Thompson, Topics in Catalysis 44 (2007) 331.
[1259] S. Panigrahi, S. Basu, S. Praharaj, S. Pande, S. Jana, A. Pal, S.K. Ghosh, T. Pal, Journal of Physical Chemistry C 111 (2007) 4596.
[1260] G.J. Hutchings, M. Brust, H. Schmidbaur, Chemical Society Reviews 37 (2008) 1759.
[1261] B.K. Min, C.M. Friend, Chemical Reviews 107 (2007) 2709.
[1262] A.S.K. Hashmi, G.J. Hutchings, Angewandte Chemie-International Edition 45 (2006) 7896.
[1263] V. Iliev, D. Tomova, R. Todorovska, D. Oliver, L. Petrov, D. Todorovsky, M. Uzunova-Bujnova, Applied Catalysis A 313 (2006) 115.
[1264] A. Dawson, P.V. Kamat, Journal of Physical Chemistry B 105 (2001) 960.
[1265] I.M. Arabatzis, T. Stergiopoulos, D. Andreeva, S. Kitova, S.G. Neophytides, P. Falaras, Journal of Catalysis 220 (2003) 127.
[1266] R.S. Sonawane, M.K. Dongare, Journal of Molecular Catalysis A 243 (2006) 68.
[1267] V. Subramanian, E.E. Wolf, P.V. Kamat, Journal of the American Chemical Society 126 (2004) 4943.
[1268] G. Wu, T. Chen, W. Su, G. Zhou, X. Zong, Z. Lei, C. Li, International Journal of Hydrogen Energy 33 (2008) 1243.
[1269] V. Iliev, D. Tomova, L. Bilyarska, G. Tyuliev, Journal of Molecular Catalysis A 263 (2007) 32.
[1270] F.B. Li, X.Z. Li, Applied Catalysis A 228 (2002) 15.
[1271] N. Chandrasekharan, P.V. Kamat, Journal of Physical Chemistry B 104 (2000) 10851.
[1272] B. Tian, J. Zhang, T. Tong, F. Chen, Applied Catalysis B 79 (2008) 394.
[1273] T. Garcia, B. Solsona, D. Cazorla-Amoros, A. Linares-Solano, S.H. Taylor, Applied Catalysis B: Environmental 62 (2006) 66.
[1274] S. Jin, F. Shiraishi, Chemical Engineering Journal 97 (2004) 203.
[1275] F. Shiraishi, T. Nakasako, Z.Z. Hua, Journal of Physical Chemistry A 107 (2003) 11072.
[1276] M. Bowker, D. James, P. Stone, R. Bennett, N. Perkins, L. Millard, J. Greaves, A. Dickinson, Journal of Catalysis 217 (2003) 427.
[1277] A. Dickinson, D. James, N. Perkins, T. Cassidy, M. Bowker, Journal of Molecular Catalysis A 146 (1999) 211.
[1278] T. Sano, S. Kutsuna, N. Negishi, K. Takeuchi, Journal of Molecular Catalysis A 189 (2002) 263.
[1279] C. Belver, M.J. Lopez-Munoz, J.M. Coronado, J. Soria, Applied Catalysis B 46 (2003) 497.
[1280] H. Einaga, T. Ibusuki, S. Futamura, Environmental Science and Technology 38 (2004) 285.
[1281] H. Einaga, S. Futamura, T. Ibusuki, Chemistry Letters (2001) 582.
[1282] J. Rasko, F. Solymosi, Journal of Physical Chemistry 98 (1994) 7147.
[1283] J. Rasko, Z. Szabo, T. Bansagi, F. Solymosi, Physical Chemistry Chemical Physics 3 (2001) 4437.
[1284] Y. Kohno, T. Yamamoto, T. Tanaka, T. Funabiki, Journal of Molecular Catalysis A: Chemical 175 (2001) 173.
[1285] H. Tsuji, T. Sagimori, K. Kurita, Y. Gotoh, J. Ishikawa, Surface & Coatings Technology 158 (2002) 208.
[1286] J. Zhou, Y.C. Kang, D.A. Chen, Journal of Physical Chemistry B 107 (2003) 6664.
[1287] Slamet, H.W. Nasution, E. Purnama, S. Kosela, J. Gunlazuardi, Catalysis Communications 6 (2005) 313.
[1288] I.H. Tseng, J.C.S. Wu, Catalysis Today 97 (2004) 113.
[1289] N.L. Wu, M.S. Lee, International Journal of Hydrogen Energy 29 (2004) 1601.
[1290] W. Chu, W.K. Choy, T.Y. So, Journal of Hazardous Materials 141 (2007) 86.
[1291] R.A. Doong, C.H. Chen, R.A. Maithreepala, S.M. Chang, Water Research 35 (2001) 2873.

[1292] K.A. Halhouli, Journal of Photochemistry Photobiology A: Chemistry 200 (2008) 421.
[1293] H.S. Son, S.J. Lee, I.H. Cho, K.D. Zoh, Chemosphere 57 (2004) 309.
[1294] J. Chen, D.F. Ollis, W.H. Rulkens, H. Bruning, Water Research 33 (1999) 661.
[1295] R.J. Candal, W.A. Zeltner, M.A. Anderson, Environmental Science & Technology 34 (2000) 3443.
[1296] K.H. Wang, Y.H. Hsieh, C.H. Wu, C.Y. Chang, Chemosphere 40 (2000) 389.
[1297] D.H. Kim, M.A. Anderson, Journal of Photochemistry and Photobiology A 94 (1996) 221.
[1298] H. Noguchi, A. Nakajima, T. Watanabe, K. Hashimoto, Water Science and Technology 46 (2002) 27.
[1299] L.D. Lau, R. Rodriguez, S. Henery, D. Manuel, L. Schwendiman, Environmental Science & Technology 32 (1998) 670.
[1300] S.G. Botta, D.J. Rodriguez, A.G. Leyva, M.I. Litter, Catalysis Today 76 (2002) 247.
[1301] I.N. Martyanov, E.N. Savinov, V.N. Parmon, Kinetics and Catalysis 38 (1997) 70.
[1302] A. Piscopo, D. Robert, J.V. Weber, Applied Catalysis B 35 (2001) 117.
[1303] R. Vargas, O. Nunez, Journal of Molecular Catalysis A 300 (2009) 65.
[1304] J. Bangun, A.A. Adesina, Applied Catalysis A 175 (1998) 221.
[1305] M.L. Canel, J.A. Santaballa, E. Vulliet, Journal of Photochemistry and Photobiology A 175 (2005) 192.
[1306] C.J.G. Cornu, A.J. Colussi, M.R. Hoffmann, Journal of Physical Chemistry B 107 (2003) 3156.
[1307] V.V. Matylitsky, M.O. Lenz, J. Wachtveitl, Journal of Physical Chemistry B 110 (2006) 8372.
[1308] B. Enright, G. Redmond, D. Fitzmaurice, Journal of Physical Chemistry 98 (1994) 6195.
[1309] L.A. Lyon, J.T. Hupp, Journal of Physical Chemistry B 103 (1999) 4623.
[1310] P. Qu, G.J. Meyer, Langmuir 17 (2001) 6720.
[1311] T.N. Obee, R.T. Brown, Environmental Science & Technology 29 (1995) 1223.
[1312] S.B. Kim, H.T. Jang, S.C. Hong, Journal of Industrial and Engineering Chemistry 8 (2002) 156.
[1313] L.X. Cao, F.J. Spiess, A.M. Huang, S.L. Suib, T.N. Obee, S.O. Hay, J.D. Freihaut, Journal of Physical Chemistry B 103 (1999) 2912.
[1314] L. Cao, A. Huang, F.-J. Spiess, S.L. Suib, Journal of Catalysis 188 (1999) 48.
[1315] P.B. Amama, K. Itoh, M. Murabayashi, Journal of Molecular Catalysis A 176 (2001) 165.
[1316] C.H. Ao, S.C. Lee, J.Z. Yu, J.H. Xu, Applied Catalysis B 54 (2004) 41.
[1317] K.E. O'Shea, S.H. Jannach, I. Garcia, Journal of Photochemistry and Photobiology A 122 (1999) 127.
[1318] M. Addamo, V. Augugliaro, S. Coluccia, A. Di Paola, E. Garcia-Lopez, V. Loddo, G. Marci, G. Martra, L. Palmisano, International Journal of Photoenergy (2006) 39182.
[1319] J. Wan-Kuen, K.H. Park, Chemosphere 57 (2004) 555.
[1320] G. Lu, A. Linsebigler, J.T. Yates Jr., Journal of Physical Chemistry 99 (1995) 7626.
[1321] T. Sano, N. Negishi, K. Takeuchi, S. Matsuzawa, Solar Energy 77 (2004) 543.
[1322] X.Z. Fu, L.A. Clark, W.A. Zeltner, M.A. Anderson, Journal of Photochemistry and Photobiology A 97 (1996) 181.
[1323] M.A. Henderson, Langmuir 21 (2005) 3443.
[1324] C.L. Olson, Journal of Physical Chemistry B 110 (2006) 9619.
[1325] T. Guo, Z. Bai, C. Wu, T. Zhu, Applied Catalysis B 79 (2008) 171.
[1326] M.M. Ameen, G.B. Raupp, Journal of Catalysis 184 (1999) 112.
[1327] H. Einaga, S. Futamura, T. Ibusuki, Applied Catalysis B 38 (2002) 215.
[1328] J.G. Yu, H.G. Yu, B. Cheng, M.H. Zhou, X.J. Zhao, Journal of Molecular Catalysis A 253 (2006) 112.
[1329] N.C. Lee, W.Y. Choi, Journal of Physical Chemistry B 106 (2002) 11818.
[1330] J. Sun, L. Gao, Q.H. Zhang, Journal of the American Ceramic Society 86 (2003) 1677.
[1331] P. Du, A. Bueno-Lopez, M. Verbaas, A.R. Almeida, M. Makkee, J.A. Moulijn, G. Mul, Journal of Catalysis 260 (2008) 75.
[1332] Z. Ding, G.Q. Lu, P.F. Greenfield, Journal of Physical Chemistry B 104 (2000) 4815.
[1333] H. Einaga, S. Futamura, T. Ibusuki, Physical Chemistry Chemical Physics 1 (1999) 4903.
[1334] K. Kakinoki, K. Yamane, R. Teraoka, M. Otsuka, Y. Matsuda, Journal of Pharmaceutical Sciences 93 (2004) 582.
[1335] H.S. Wahab, T. Bredow, S.M. Aliwi, Chemical Physics 353 (2008) 93.
[1336] H.J. Kim, Y.G. Shul, H.S. Han, Topics in Catalysis 35 (2005) 287.
[1337] M. Machida, K. Norimoto, T. Watanabe, K. Hashimoto, A. Fujishima, Journal of Materials Science 34 (1999) 2569.
[1338] K.Y. Jung, S.B. Park, Journal of Photochemistry and Photobiology A 127 (1999) 117.
[1339] P. Cheng, M.P. Zheng, Y.P. Jin, Q. Huang, M.Y. Gu, Materials Letters 57 (2003) 2989.
[1340] I.N. Martyanov, K.J. Klabunde, Journal of Catalysis 225 (2004) 408.
[1341] Z.J. Li, B. Hou, Y. Xu, D. Wu, Y.H. Sun, Journal of Colloid and Interface Science 288 (2005) 149.
[1342] J. Zhang, M.J. Li, Z.C. Feng, J. Chen, C. Li, Journal of Physical Chemistry B 110 (2006) 927.
[1343] M. Hirano, C. Nakahara, K. Ota, O. Tanaike, M. Inagaki, Journal of Solid State Chemistry 170 (2003) 39.
[1344] K.Y. Jung, S.B. Park, Materials Letters 58 (2004) 2897.
[1345] B.T. Lee, J.K. Han, A.K. Gain, K.H. Lee, F. Saito, Materials Letters 60 (2006) 2101.
[1346] D.G. Shchukin, J.H. Schattka, M. Antonietti, R.A. Caruso, Journal of Physical Chemistry B 107 (2003) 952.
[1347] J.H. Schattka, D.G. Shchukin, J.G. Jia, M. Antonietti, R.A. Caruso, Chemistry of Materials 14 (2002) 5103.
[1348] J.-J. Zou, B. Zhu, L. Wang, X. Zhang, Z. Mi, Journal of Molecular Catalysis A 286 (2008) 63.
[1349] X.F. Yu, N.Z. Wu, H.Z. Huang, Y.C. Xie, Y.Q. Tang, Journal of Materials Chemistry 11 (2001) 3337.
[1350] M.S.P. Francisco, V.R. Mastelaro, Chemistry of Materials 14 (2002) 2514.
[1351] K.K. Akurati, A. Vital, R. Hany, B. Bommer, T. Graule, M. Winterer, International Journal of Photoenergy 7 (2005) 153.
[1352] J. Yang, D. Li, X. Wang, X.J. Yang, L.D. Lu, Journal of Solid State Chemistry 165 (2002) 193.
[1353] Y. Gnatyuk, N. Smirnova, A. Eremenko, V. Ilyin, Adsorption Science & Technology 23 (2005) 497.
[1354] J.G. Yu, J.C. Yu, X.J. Zhao, Journal of Sol-Gel Science and Technology 24 (2002) 95.
[1355] C. Anderson, A.J. Bard, Journal of Physical Chemistry B 101 (1997) 2611.
[1356] S.W. Ahn, L. Kevan, Journal of the Chemical Society Faraday Transactions 94 (1998) 3147.
[1357] X. Zhang, F. Zhang, K.Y. Chan, Applied Catalysis A 284 (2005) 193.
[1358] S.S. Hong, M.S. Lee, S.S. Park, G.D. Lee, Catalysis Today 87 (2003) 99.
[1359] C.Y. Kuo, S.Y. Lu, Journal of Materials Research 21 (2006) 2290.
[1360] Y.M. Xu, W. Zheng, W.P. Liu, Journal of Photochemistry and Photobiology A 122 (1999) 57.
[1361] Y.Z. Li, S.J. Kim, Journal of Physical Chemistry B 109 (2005) 12309.
[1362] O.K. Park, Y.S. Kang, B.G. Jo, Journal of Industrial and Engineering Chemistry 10 (2004) 733.
[1363] V. Loddo, G. Marci, L. Palmisano, A. Sclafani, Materials Chemistry and Physics 53 (1998) 217.
[1364] L.C. Lei, H.P. Chu, X.J. Hu, P.L. Yue, Industrial & Engineering Chemistry Research 38 (1999) 3381.
[1365] B.N. Shelimov, N.N. Tolkachev, O.P. Tkachenko, G.N. Baeva, K.V. Klementiev, A.Y. Stakheev, V.B. Kazansky, Journal of Photochemistry and Photobiology A 195 (2008) 81.
[1366] Q. Zhang, W. Fan, L. Gao, Applied Catalysis B 76 (2007) 168.
[1367] E. Vaisman, R.L. Cook, C.H. Langford, Journal of Physical Chemistry B 104 (2000) 8679.
[1368] K.V.S. Rao, B. Srinivas, M. Subrahmanyam, Catalysis Letters 90 (2003) 95.
[1369] Y.H. Hsien, C.F. Chang, Y.H. Chen, S. Cheng, Applied Catalysis B 31 (2001) 241.
[1370] F.F. Li, Y.S. Jiang, L.X. Yu, Z.W. Yang, T.Y. Hou, S.M. Sun, Applied Surface Science 252 (2005) 1410.
[1371] X.S. Liu, K.K. Lu, J.K. Thomas, Journal of the Chemical Society-Faraday Transactions 89 (1993) 1861.
[1372] J.L. Zhang, Y. Hu, M. Matsuoka, H. Yamashita, M. Minagawa, H. Hidaka, M. Anpo, Journal of Physical Chemistry B 105 (2001) 8395.
[1373] T.A. Egerton, I.R. Tooley, Journal of Materials Chemistry 12 (2002) 1111.
[1374] T.A. Egerton, N.J. Everall, I.R. Tooley, Langmuir 21 (2005) 3172.
[1375] U. Gesenhues, Journal of Photochemistry and Photobiology A 139 (2001) 243.
[1376] S.-T. Bae, H. Shin, J.Y. Kim, H.S. Jung, K.S. Hong, Journal of Physical Chemistry C 112 (2008) 9937.
[1377] A.M. El-Toni, S. Yin, T. Sato, Journal of Colloid and Interface Science 300 (2006) 123.
[1378] H. Nishiguchi, J.L. Zhang, M. Anpo, H. Masuhara, Journal of Physical Chemistry B 105 (2001) 3218.
[1379] H. Ichiura, T. Kitaoka, H. Tanaka, Chemosphere 51 (2003) 855.
[1380] H. Tada, M. Yamamoto, S. Ito, Langmuir 15 (1999) 3699.
[1381] H. Tada, M. Yamamoto, S. Ito, Journal of the Electrochemical Society 147 (2000) 613.
[1382] T. Kamegawa, T.-H. Kim, J. Morishima, M. Matsuoka, M. Anpo, Catalysis Letters 129 (2009) 7.
[1383] C.S. Yang, C.J. Chen, Applied Catalysis A 294 (2005) 40.
[1384] S. Cao, K.L. Yeung, P.-L. Yue, Applied Catalysis B 76 (2007) 64.
[1385] J.H. Pan, W.I. Lee, Chemistry of Materials 18 (2006) 847.
[1386] C. Martin, G. Solana, V. Rives, G. Marci, L. Palmisano, A. Sclafani, Catalysis Letters 49 (1997) 235.
[1387] S. Yamazoe, Y. Hitomi, T. Shishido, T. Tanaka, Journal of Physical Chemistry C 112 (2008) 6869.
[1388] L.J. Zhou, S.S. Yan, B.Z. Tian, J.L. Zhang, M. Anpo, Materials Letters 60 (2006) 396.
[1389] H.S. Jung, J.K. Lee, M. Nastasi, J.R. Kim, S.W. Lee, J.Y. Kim, J.S. Park, K.S. Hong, H. Shin, Applied Physics Letters 88 (2006) 013107.
[1390] M.S. Vohra, J.S. Lee, W.Y. Choi, Journal of Applied Electrochemistry 35 (2005) 757.
[1391] I. Othman, R.M. Mohamed, F.M. Ibrahem, Journal of Photochemistry and Photobiology A 189 (2007) 80.
[1392] K. Chiang, R. Amal, T. Tran, Advances in Environmental Research 6 (2002) 471.
[1393] T. Tatsuma, S. Saitoh, P. Ngaotrakanwiwat, Y. Ohko, A. Fujishima, Langmuir 18 (2002) 7777.
[1394] T. Tatsuma, S. Saitoh, Y. Ohko, A. Fujishima, Chemistry of Materials 13 (2001) 2838.
[1395] T. Tatsuma, S. Takeda, S. Saitoh, Y. Ohko, A. Fujishima, Electrochemistry Communications 5 (2003) 793.

[1396] Y. Takahashi, P. Ngaotrakanwiwat, T. Tatsuma, Electrochimica Acta 49 (2004) 2025.
[1397] P. Ngaotrakanwiwat, T. Tatsuma, Journal of Electroanalytical Chemistry 573 (2004) 263.
[1398] D. Beydoun, R. Amal, Materials Science and Engineering B 94 (2002) 71.
[1399] D. Beydoun, R. Amal, G. Low, S. Mcevoy, Journal of Molecular Catalysis A 180 (2002) 193.
[1400] D. Beydoun, R. Amal, G.K.C. Low, S. Mcevoy, Journal of Physical Chemistry B 104 (2000) 4387.
[1401] A.O. Ibhadon, G.M. Greenway, Y. Yue, P. Falaras, D. Tsoukleris, Journal of Photochemistry and Photobiology A 197 (2008) 321.
[1402] M. Kang, S.J. Choung, J.Y. Park, Catalysis Today 87 (2003) 87.
[1403] B. Pal, M. Sharon, G. Nogami, Materials Chemistry and Physics 59 (1999) 254.
[1404] I.H. Tseng, W.-C. Chang, J.C.S. Wu, Applied Catalysis B 37 (2002) 37.
[1405] Y. Bessekhouad, D. Robert, J.V. Weber, Catalysis Today 101 (2005) 315.
[1406] J.P. Yasomanee, J. Bandara, Solar Energy Materials and Solar Cells 92 (2008) 348.
[1407] W. Siripala, A. Ivanovskaya, T.F. Jaramillo, S.H. Baeck, E.W. Mcfarland, Solar Energy Materials and Solar Cells 77 (2003) 229.
[1408] M.K.I. Senevirathna, P. Pitigala, K. Tennakone, Journal of Photochemistry and Photobiology A 171 (2005) 257.
[1409] Z. Jin, X. Zhang, Y. Li, S. Li, G. Lu, Catalysis Communications 8 (2007) 1267.
[1410] T.L. Hsiung, H.P. Wang, Y.-M. Lu, M.C. Hsiao, Radiation Physics and Chemistry 75 (2006) 2054.
[1411] J. Bandara, C.P.K. Udawatta, C.S.K. Rajapakse, Photochemical & Photobiological Sciences 4 (2005) 857.
[1412] D. Chen, H. Zhang, S. Hu, J. Li, Journal of Physical Chemistry C 112 (2008) 117.
[1413] S.J. Wang, G. Cheng, X.H. Jiang, Y.C. Li, Y.B. Huang, Z.L. Du, Applied Physics Letters 88 (2006) 212108.
[1414] S. Somasundaram, N. Tacconi, C.R. Chenthamarakshan, K. Rajeshwar, N.R. de Tacconi, Journal of Electroanalytical Chemistry 577 (2005) 167.
[1415] M. Miyauchi, A.K. Nakajima, T. Watanabe, K. Hashimoto, Chemistry of Materials 14 (2002) 4714.
[1416] K.K. Akurati, A. Vital, J.-P. Dellemann, K. Michalow, T. Graule, D. Ferri, A. Baiker, Applied Catalysis B 79 (2008) 53.
[1417] T. He, Y. Ma, Y. Cao, X.L. Hu, H.M. Liu, G.J. Zhang, W.S. Yang, J.N. Yao, Journal of Physical Chemistry B 106 (2002) 12670.
[1418] I. Shiyanovskaya, M. Hepel, Journal of the Electrochemical Society 145 (1998) 3981.
[1419] H. Ohsaki, N. Kanai, Y. Fukunaga, M. Suzuki, T. Watanabe, K. Hashimoto, Thin Solid Films 502 (2006) 138.
[1420] A. Hattori, Y. Tokihisa, H. Tada, S. Ito, Journal of the Electrochemical Society 147 (2000) 2279.
[1421] S.F. Chen, L. Chen, S. Gao, G.Y. Cao, Materials Chemistry and Physics 98 (2006) 116.
[1422] T. Kawahara, Y. Konishi, H. Tada, N. Tohge, S. Ito, Langmuir 17 (2001) 7442.
[1423] H. Nur, Misnon II, L.K. Wei, International Journal of Photoenergy (2007) 98548.
[1424] M. Okada, K. Tajima, Y. Yamada, K. Yoshimura, Vacuum 83 (2008) 688.
[1425] H.-H. Ou, S.-L. Lo, C.-H. Wu, Journal of Hazardous Materials 137 (2006) 1362.
[1426] L.Y. Shi, Y. Zhang, D.Y. Fang, C.Z. Li, H.C. Gu, Journal of Materials Synthesis and Processing 7 (1999) 357.
[1427] H. Tada, A. Hattori, Y. Tokihisa, K. Imai, N. Tohge, S. Ito, Journal of Physical Chemistry B 104 (2000) 4585.
[1428] P.B. Amama, K. Itoh, M. Murabayashi, Journal of Materials Science 39 (2004) 4349.
[1429] B.S. Liu, X.J. Zhao, N.Z. Zhang, Q.N. Zhao, X. He, J.Y. Feng, Surface Science 595 (2005) 203.
[1430] A.C. Tuan, T.C. Kaspar, T. Droubay, J.W. Rogers, S.A. Chambers, Applied Physics Letters 83 (2003) 3734.
[1431] M.D. Hernandez-Alonso, I. Tejedor-Tejedor, J.M. Coronado, J. Soria, M.A. Anderson, Thin Solid Films 502 (2006) 125.
[1432] M.M. Mohamed, I. Othman, R.M. Mohamed, Journal of Photochemistry and Photobiology A 191 (2007) 153.
[1433] Y. Matsumoto, M. Noguchi, T. Matsunaga, Journal of Physical Chemistry B 103 (1999) 7190.
[1434] D. Panayotov, J.T. Yates Jr., Chemical Physics Letters 381 (2003) 154.
[1435] G.H. Li, N.M. Dimitrijevic, L. Chen, T. Rajh, K.A. Gray, Journal of Physical Chemistry C 112 (2008) 19040.
[1436] J. Bandara, S.S. Kuruppu, U.W. Pradeep, Colloids and Surfaces A 276 (2006) 197.
[1437] S. Li, Z. Ma, J. Zhang, J. Liu, Catalysis Communications 9 (2008) 1482.
[1438] M. Sanchez-Agudo, L. Soriano, R. Fernandez-Jimenez, A. Gutierrez, M. Abbate, S. Wiklund, J.M. Sanz, Surface Science 566 (2004) 515.
[1439] M. Sanchez-Agudo, L. Soriano, C. Quiros, M. Abbate, L. Roca, J. Avila, J.M. Sanz, Langmuir 17 (2001) 7339.
[1440] M. Sanchez-Agudo, L. Soriano, C. Quiros, L. Roca, V. Perez-Dieste, J.M. Sanz, Surface Science 507 (2002) 672.
[1441] F. Fabregat-Santiago, J. Garcia-Canadas, E. Palomares, J.N. Clifford, S.A. Haque, J.R. Durrant, G. Garcia-Belmonte, J. Bisquert, Journal of Applied Physics 96 (2004) 6903.
[1442] X.T. Zhang, H.W. Liu, T. Taguchi, Q.B. Meng, O. Sato, A. Fujishima, Solar Energy Materials and Solar Cells 81 (2004) 197.
[1443] E. Palomares, J.N. Clifford, S.A. Haque, T. Lutz, J.R. Durrant, Chemical Communications 2002 (1464) 1465.
[1444] B.C. O'Regan, S. Scully, A.C. Mayer, E. Palomares, J. Durrant, Journal of Physical Chemistry B 109 (2005) 4616.
[1445] E. Palomares, J.N. Clifford, S.A. Haque, T. Lutz, J.R. Durrant, Journal of the American Chemical Society 125 (2003) 475.
[1446] J. Bandara, U.W. Pradeep, R. Bandara, Journal of Photochemistry and Photobiology A 170 (2005) 273.
[1447] J.A. He, R. Mosurkal, L.A. Samuelson, L. Li, J. Kumar, Langmuir 19 (2003) 2169.
[1448] Z.S. Wang, C.H. Huang, Y.Y. Huang, Y.J. Hou, P.H. Xie, B.W. Zhang, H.M. Cheng, Chemistry of Materials 13 (2001) 678.
[1449] Y. Zhao, C. Li, X. Liu, F. Gu, H.L. Du, L. Shi, Applied Catalysis B 79 (2008) 208.
[1450] N.G. Park, M.G. Kang, K.M. Kim, K.S. Ryu, S.H. Chang, D.K. Kim, J. van de Lagemaat, K.D. Benkstein, A.J. Frank, Langmuir 20 (2004) 4246.
[1451] M. Bideau, B. Claudel, L. Faure, H. Kazouan, Journal of Photochemistry and Photobiology A 67 (1992) 337.
[1452] M. Bideau, B. Claudel, L. Faure, H. Kazouan, Journal of Photochemistry and Photobiology A 61 (1991) 269.
[1453] J. Arana, C. Fernandez Rodriguez, O. Gonzalez Diaz, J.A. Herrera Melian, J. Perez Pena, Catalysis Today 101 (2005) 261.
[1454] H. Yamashita, H. Nishiguchi, N. Kamada, M. Anpo, Y. Teraoka, H. Hatano, S. Ehara, K. Kikui, L. Palmisano, A. Sclafani, M. Schiavello, M.A. Fox, Research on Chemical Intermediates 20 (1994) 815.
[1455] M.I. Franch, J.A. Ayllon, J. Peral, X. Domenech, Catalysis Today 101 (2005) 245.
[1456] V. Maurino, C. Minero, E. Pelizzetti, G. Mariella, A. Arbezzano, F. Rubertelli, Research on Chemical Intermediates 33 (2007) 319.
[1457] Y. Mu, H.Q. Yu, J.C. Zheng, S.J. Zhang, Journal of Photochemistry and Photobiology A 163 (2004) 311.
[1458] E. Piera, M.I. Tejedor-Tejedor, M.E. Zorn, M.A. Anderson, Applied Catalysis B 46 (2003) 671.
[1459] M.I. Franch, J. Peral, X. Domenech, J.A. Ayllon, Chemical Communications 2005 (1851) 1853.
[1460] N. Murakami, T. Chiyoya, T. Tsubota, T. Ohno, Applied Catalysis, A: General 348 (2008) 148.
[1461] C.C. Chen, X.Z. Li, W.H. Ma, J.C. Zhao, H. Hidaka, N. Serpone, Journal of Physical Chemistry B 106 (2002) 318.
[1462] C.A. Kelly, F. Farzad, D.W. Thompson, J.M. Stipkala, G.J. Meyer, Langmuir 15 (1999) 7047.
[1463] S. Pelet, J.E. Moser, M. Grätzel, Journal of Physical Chemistry B 104 (2000) 1791.
[1464] P.K. Surolia, R.J. Tayade, R.V. Jasra, Industrial & Engineering Chemistry Research 46 (2007) 6196.
[1465] M. Krichevskaya, S. Preis, Journal of Advanced Oxidation Technologies 6 (2003) 150.
[1466] N.N. Lichtin, M. Avudaithai, E. Berman, A. Grayfer, Solar Energy 56 (1996) 377.
[1467] J. Arana, J.M.D. Rodriguez, O.G. Diaz, J.A.H. Melian, C.F. Rodriguez, J.P. Pena, Applied Catalysis A 299 (2006) 274.
[1468] Y. Kohno, T. Yamamoto, T. Tanaka, T. Funabiki, Journal of Molecular Catalysis A 175 (2001) 173.
[1469] C.P. Chang, J.N. Chen, M.C. Lu, H.Y. Yang, Chemosphere 58 (2005) 1071.
[1470] H.Y. Chen, O. Zahraa, M. Bouchy, Journal of Photochemistry and Photobiology A 108 (1997) 37.
[1471] H.-c. Liang, X.-z. Li, Y.-h. Yang, K.-h. Sze, Chemosphere 73 (2008) 805.
[1472] M. Lindner, D.W. Bahnemann, B. Hirthe, W.D. Griebler, Journal of Solar Energy Engineering-Transactions of the ASME 119 (1997) 120.
[1473] Y. Cao, W.S. Yang, Y.M. Chen, H. Du, P. Yue, Applied Surface Science 236 (2004) 223.
[1474] C.Y. Wu, Y.H. Yue, X.Y. Deng, W.M. Hua, Z. Gao, Catalysis Today 93–95 (2004) 863.
[1475] G. Wu, T. Chen, X. Zong, H. Yan, G. Ma, X. Wang, Q. Xu, D. Wang, Z. Lei, C. Li, Journal of Catalysis 253 (2008) 225.
[1476] J.C. Yu, L.Z. Zhang, Z. Zheng, J.C. Zhao, Chemistry of Materials 15 (2003) 2280.
[1477] L. Korosi, I. Dekany, Colloids and Surfaces A 280 (2006) 146.
[1478] X. Deng, Y. Yue, Z. Gao, Applied Catalysis B 39 (2002) 135.
[1479] E. Barraud, F. Bosc, D. Edwards, N. Keller, V. Keller, Journal of Catalysis 235 (2005) 318.
[1480] A. Nakajima, H. Obata, Y. Kameshima, K. Okada, Catalysis Communications 6 (2005) 716.
[1481] D.S. Muggli, L.F. Ding, M.J. Odland, Catalysis Letters 78 (2002) 23.
[1482] G. Colon, M.C. Hidalgo, G. Munuera, I. Ferino, M.G. Cutrufello, J.A. Navio, Applied Catalysis B 63 (2006) 45.
[1483] G. Colon, J.M. Sanchez-Espana, M.C. Hidalgo, J.A. Navio, Journal of Photochemistry and Photobiology A 179 (2006) 20.
[1484] R. Gomez, T. Lopez, E. Ortis-Islas, J. Navarrete, E. Sanchez, F. Tzompanztzi, X. Bokhimi, Journal of Molecular Catalysis A 193 (2003) 217.
[1485] X.C. Wang, J.C. Yu, P. Liu, X.X. Wang, W.Y. Su, X.Z. Fu, Journal of Photochemistry and Photobiology A 179 (2006) 339.
[1486] V. Maurino, C. Minero, G. Mariella, E. Pelizzetti, Chemical Communications (2005) 2627.
[1487] C. Minero, G. Mariella, V. Maurino, D. Vione, E. Pelizzetti, Langmuir 16 (2000) 8964.
[1488] M. Mrowetz, E. Selli, Physical Chemistry Chemical Physics 7 (2005) 1100.
[1489] J.W. Tang, H.D. Quan, J.H. Ye, Chemistry of Materials 19 (2007) 116.
[1490] A. Nakajima, M. Tanaka, Y. Kameshima, K. Okada, Journal of Photochemistry and Photobiology A 167 (2004) 75.
[1491] H. Kim, W. Choi, Applied Catalysis B 69 (2007) 127.
[1492] M. Mrowetz, E. Selli, New Journal of Chemistry 30 (2006) 108.

[1493] J. Wiszniowski, D. Robert, J. Surmacz-Gorska, K. Miksch, J.V. Weber, International Journal of Photoenergy 5 (2003) 69.
[1494] O. D'Hennezel, D.F. Ollis, Helvetica Chimica Acta 84 (2001) 3511.
[1495] S. Horikoshi, T. Miura, M. Kajitani, H. Hidaka, N. Serpone, Journal of Photochemistry and Photobiology A 194 (2008) 189.
[1496] M. Ohtaki, H. Sato, H. Fujii, K. Eguchi, Journal of Molecular Catalysis A 155 (2000) 121.
[1497] J.A. Treadway, J.A. Moss, T.J. Meyer, Inorganic Chemistry 38 (1999) 4386.
[1498] A. Kumar, A.K. Jain, Journal of Molecular Catalysis A 165 (2001) 265.
[1499] Y. Bessekhouad, D. Robert, J. Weber, Journal of Photochemistry and Photobiology A 163 (2004) 569.
[1500] Y. Bessekhouad, N. Chaoui, M. Trzpit, N. Ghazzal, D. Robert, J.V. Weber, Journal of Photochemistry and Photobiology A 183 (2006) 218.
[1501] J.C. Kim, J. Choi, Y.B. Lee, J.H. Hong, J.I. Lee, J.W. Yang, Chemical Communications (2006) 5024.
[1502] G.M. Liu, T. Schulmeyer, A. Thissen, A. Klein, W. Jaegermann, Applied Physics Letters 82 (2003) 2269.
[1503] J.C. Yu, L. Wu, J. Lin, P.S. Li, Q. Li, Chemical Communications 2003 (1552) 1553.
[1504] J.L. Blackburn, D.C. Selmarten, A.J. Nozik, Journal of Physical Chemistry B 107 (2003) 14154.
[1505] H. Fujii, M. Ohtaki, K. Eguchi, H. Arai, Journal of Molecular Catalysis A 129 (1998) 61.
[1506] J.S. Jang, W. Li., S.H. Oh, J.S. Lee, Chemical Physics Letters 425 (2006) 278.
[1507] N. Serpone, P. Maruthamuthu, P. Pichat, E. Pelizzetti, H. Hidaka, Journal of Photochemistry and Photobiology A 85 (1995) 247.
[1508] L. Wu, J.C. Yu, X.Z. Fu, Journal of Molecular Catalysis A 244 (2006) 25.
[1509] T. Hirai, K. Suzuki, I. Komasawa, Journal of Colloid and Interface Science 244 (2001) 262.
[1510] M.G. Kang, H.E. Han, K.J. Kim, Journal of Photochemistry and Photobiology A 125 (1999) 119.
[1511] L.M. Peter, K.G.U. Wijayantha, D.J. Riley, J.P. Waggett, Journal of Physical Chemistry B 107 (2003) 8378.
[1512] D. Chatterjee, A. Mahata, Journal of Photochemistry and Photobiology A 153 (2002) 199.
[1513] K.T. Ranjit, I. Willner, S. Bossmann, A. Braun, Journal of Physical Chemistry B 102 (1998) 9397.
[1514] Y. Nakanishi, T. Imae, Journal of Colloid and Interface Science 297 (2006) 122.
[1515] A.J. Morris, G.J. Meyer, Journal of Physical Chemistry C 112 (2008) 18224.
[1516] P.F. Fu, Y. Luan, X.G. Dai, Journal of Molecular Catalysis A 221 (2004) 81.
[1517] W. Fan, L. Gao, J. Sun, Journal of the American Ceramic Society 89 (2006) 731.
[1518] X.-H. Xia, Z.-J. Jia, Y. Yu, Y. Liang, Z. Wang, L.-L. Ma, Carbon 45 (2007) 717.
[1519] W. Wang, P. Serp, P. Kalck, J.L. Faria, Journal of Molecular Catalysis A: Chemical 235 (2005) 194.
[1520] Y. Yu, J.C. Yu, J.G. Yu, Y.C. Kwok, Y.K. Che, J.C. Zhao, L. Ding, W.K. Ge, P.K. Wong, Applied Catalysis A 289 (2005) 186.
[1521] C. Dechakiatkrai, J. Chen, C. Lynam, S. Phanichphant, G.G. Wallace, Journal of the Electrochemical Society 154 (2007) A407.
[1522] G. Benko, B. Skarman, R. Wallenberg, A. Hagfeldt, V. Sundstrom, A.P. Yartsev, Journal of Physical Chemistry B 107 (2003) 1370.
[1523] P.C. Angelome, L. Andrini, M.E. Calvo, F.G. Requejo, S.A. Bilmes, G. Soler-Illia, Journal of Physical Chemistry C 111 (2007) 10886.
[1524] J.M. Wu, B. Huang, Y.H. Zeng, Thin Solid Films 497 (2006) 292.
[1525] M. Maeda, T. Watanabe, Thin Solid Films 489 (2005) 320.
[1526] R. Beranek, H. Tsuchiya, T. Sugishima, J.M. Macak, L. Taveira, S. Fujimoto, H. Kisch, P. Schmuki, Applied Physics Letters 87 (2005) 243114.
[1527] M.S. Lee, G.D. Lee, C.S. Ju, S.S. Hong, Solar Energy Materials and Solar Cells 88 (2005) 389.
[1528] J.T. Jiu, F.M. Wang, M. Adachi, Materials Letters 58 (2004) 3915.
[1529] K.L. Yeung, A.J. Maira, J. Stolz, E. Hung, N.K.C. Ho, A.C. Wei, J. Soria, K.J. Chao, Journal of Physical Chemistry B 106 (2002) 4608.
[1530] H. Kominami, S. Murakami, J. Kato, Y. Kera, B. Ohtani, Journal of Physical Chemistry B 106 (2002) 10501.
[1531] T. Hamaguchi, M. Uno, S. Yamanaka, Journal of Photochemistry and Photobiology A 173 (2005) 99.
[1532] J.F. Porter, Y.G. Li, C.K. Chan, Journal of Materials Science 34 (1999) 1523.
[1533] M. Inagaki, R. Nonaka, B. Tryba, A.W. Morawski, Chemosphere 64 (2006) 437.
[1534] M. Inagaki, Y. Nakazawa, M. Hirano, Y. Kobayashi, M. Toyoda, International Journal of Inorganic Materials 3 (2001) 809.
[1535] Y.L. Choi, S.H. Kim, Y.S. Song, D.Y. Lee, Journal of Materials Science 39 (2004) 5695.
[1536] S. Ito, S. Inoue, H. Kawada, M. Hara, M. Iwasaki, H. Tada, Journal of Colloid and Interface Science 216 (1999) 59.
[1537] Y. Zhang, J. Li, J. Wang, Chemistry of Materials 18 (2006) 2917.
[1538] A.V. Vorontsov, A.A. Altynnikov, E.N. Savinov, E.N. Kurkin, Journal of Photochemistry and Photobiology A 144 (2001) 193.
[1539] Q. Zhang, L. Gao, J. Guo, Applied Catalysis B 26 (2000) 207.
[1540] L. Zhao, Y. Yu, L.X. Song, X.F. Hu, A. Larbot, Applied Surface Science 239 (2005) 285.
[1541] C.H. Cho, D.K. Kim, D.H. Kim, Journal of the American Ceramic Society 86 (2003) 1138.
[1542] L. Gao, Q.H. Zhang, Scripta Materialia 44 (2001) 1195.
[1543] A.G. Thomas, W.R. Flavell, A.K. Mallick, A.R. Kumarasinghe, D. Tsoutsou, N. Khan, C. Chatwin, S. Rayner, G.C. Smith, R.L. Stockbauer, S. Warren, T.K. Johal, S. Patel, D. Holland, A. Taleb, F. Wiame, Physical Review B 75 (2007) 035105.
[1544] M. Addamo, M. Bellardita, A. Di Paola, L. Palmisano, Chemical Communications (2006) 4943.
[1545] M. Andersson, L. Osterlund, S. Ljungstrom, A. Palmqvist, Journal of Physical Chemistry B 106 (2002) 10674.
[1546] S.J. Kim, H.G. Lee, S.J. Kim, J.K. Lee, E.G. Lee, Applied Catalysis A 242 (2003) 89.
[1547] S.J. Kim, J.K. Lee, E.G. Lee, H.G. Lee, S.J. Kim, K.S. Lee, Journal of Materials Research 18 (2003) 729.
[1548] L. Lucarelli, V. Nadtochenko, J. Kiwi, Langmuir 16 (2000) 1102.
[1549] J.S. Song, H.J. Kim, B.K. Koo, D.Y. Lee, W.J. Lee, S.J. Kim, Smart Materials & Structures 15 (2006) S65.
[1550] J. Sun, L. Gao, Q.H. Zhang, Acta Chimica Sinica 61 (2003) 74.
[1551] Q.H. Zhang, L. Gao, S. Zheng, Acta Chimica Sinica 59 (2001) 1909.
[1552] Q.H. Zhang, L. Gao, J.K. Guo, Journal of Inorganic Materials 15 (2000) 556.
[1553] A.S. Barnard, P. Zapol, Physical Review B 70 (2004) 235403.
[1554] S. Yin, H. Hasegawa, D. Maeda, M. Ishitsuka, T. Sato, Journal of Photochemistry and Photobiology A 163 (2004) 1.
[1555] J. Ryu, W. Choi, Environmental Science & Technology 42 (2008) 294.
[1556] R.R. Bacsa, J. Kiwi, Applied Catalysis B 16 (1998) 19.
[1557] D.L. Jiang, S.Q. Zhang, H.J. Zhao, Environmental Science & Technology 41 (2007) 303.
[1558] K.Y. Jung, S.B. Park, H.D. Jang, Catalysis Communications 5 (2004) 491.
[1559] T. Kawahara, Y. Konishi, H. Tada, N. Tohge, J. Nishii, S. Ito, Angewandte Chemie 41 (2002) 2811.
[1560] T. Kawahara, T. Ozawa, M. Iwasaki, H. Tada, S. Ito, Journal of Colloid and Interface Science 267 (2003) 377.
[1561] Y.V. Kolen'ko, B.R. Churagulov, M. Kunst, L. Mazerolles, C. Colbeau-Justin, Applied Catalysis B 54 (2004) 51.
[1562] G. Li, S. Ciston, Z.V. Saponjic, L. Chen, N.M. Dimitrijevic, T. Rajh, K.A. Gray, Journal of Catalysis 253 (2008) 105.
[1563] T. Sato, M. Taya, Biochemical Engineering Journal 28 (2006) 303.
[1564] B. Sun, P.G. Smirniotis, Catalysis Today 88 (2003) 49.
[1565] M.C. Yan, F. Chen, J.L. Zhang, M. Anpo, Journal of Physical Chemistry B 109 (2005) 8673.
[1566] L. Zhao, M. Han, J. Lian, Thin Solid Films 516 (2008) 3394.
[1567] M.A. Behnajady, N. Modirshahla, M. Shokri, H. Elham, A. Zeininezhad, Journal of Environmental Science and Health A 43 (2008) 460.
[1568] A. Bojinova, R. Kralchevska, I. Poulios, C. Dushkin, Materials Chemistry and Physics 106 (2007) 187.
[1569] A.K. Datye, G. Riegel, J.R. Bolton, M. Huang, M.R. Prairie, Journal of Solid State Chemistry 115 (1995) 236.
[1570] D. Gumy, S.A. Giraldo, J. Rengifo, C. Pulgarin, Applied Catalysis B 78 (2008) 19.
[1571] T. Ohno, K. Sarukawa, K. Tokieda, M. Matsumura, Journal of Catalysis 203 (2001) 82.
[1572] J.L. Zhang, H.S. Xu, H.J. Chen, M. Anpo, Research on Chemical Intermediates 29 (2003) 839.
[1573] E. Asari, R. Souda, Surface Science 486 (2001) 203.
[1574] L. Jing, S. Li, S. Song, L. Xue, H. Fu, Solar Energy Materials and Solar Cells 92 (2008) 1030.
[1575] R.K. Wahi, W.W. Yu, Y.P. Liu, M.L. Mejia, J.C. Falkner, W. Nolte, V.L. Colvin, Journal of Molecular Catalysis A 242 (2005) 48.
[1576] J. Zhang, Q. Xu, Z. Feng, M. Li, C. Li, Angewandte Chemie 47 (2008) 1766.
[1577] R. Shao, C.M. Wang, D.E. Mccready, T.C. Droubay, S.A. Chambers, Surface Science 601 (2007) 1582.
[1578] N.A. Deskins, S. Kerisit, K.M. Rosso, M. Dupuis, Journal of Physical Chemistry C 111 (2007) 9290.
[1579] T. Hirakawa, K. Yawata, Y. Nosaka, Applied Catalysis A 325 (2007) 105.
[1580] Y.H. Tseng, H.Y. Lin, C.S. Kuo, Y.Y. Li, C.P. Huang, Reaction Kinetics and Catalysis Letters 89 (2006) 63.
[1581] X.H. Tang, Y. Zhang, G.F. Yin, D.L. Zhou, H. Liu, C.Q. Zheng, Rare Metal Materials and Engineering 33 (2004) 864.
[1582] Y.M. Sung, J.K. Lee, W.S. Chae, Crystal Growth & Design 6 (2006) 805.
[1583] S. Bakardjieva, J. Subrt, V. Stengl, M.J. Dianez, M.J. Sayagues, Applied Catalysis B 58 (2005) 193.
[1584] G.J. Yang, C.J. Li, F. Han, X.C. Huang, Journal of Vacuum Science & Technology B 22 (2004) 2364.
[1585] G. Li, N.M. Dimitrijevic, L. Chen, J.M. Nichols, T. Rajh, K.A. Gray, Journal of the American Chemical Society 130 (2008) 5402.
[1586] T.B. Ghosh, S. Dhabal, A.K. Datta, Journal of Applied Physics 94 (2003) 4577.
[1587] S. Bakardjieva, V. Stengl, L. Szatmary, J. Subrt, J. Lukac, N. Murafa, D. Niznansky, K. Cizek, J. Jirkovsky, N. Petrova, Journal of Materials Chemistry 16 (2006) 1709.
[1588] A. Di Paola, M. Addamo, M. Bellardita, E. Cazzanelli, L. Palmisano, Thin Solid Films 515 (2007) 3527.
[1589] S.R. Hall, V.M. Swinerd, F.N. Newby, A.M. Collins, S. Mann, Chemistry of Materials 18 (2006) 598.
[1590] H. Kominami, Y. Ishii, M. Kohno, S. Konishi, Y. Kera, B. Ohtani, Catalysis Letters 91 (2003) 41.
[1591] H. Kominami, J. Kato, S. Murakami, Y. Ishii, M. Kohno, K. Yabutani, T. Yamamoto, Y. Kera, M. Inoue, T. Inui, B. Ohtani, Catalysis Today 84 (2003) 181.
[1592] J.G. Li., C.C. Tang, D. Li, H. Haneda, T. Ishigaki, Journal of the American Ceramic Society 87 (2004) 1358.

[1593] T. Lopez, R. Gomez, E. Sanchez, F. Tzompantzi, L. Vera, Journal of Sol-Gel Science and Technology 22 (2001) 99.
[1594] C.A. Nolph, D.E. Sievers, S. Kaewgun, C.J. Kucera, D.H. Mckinney, J.P. Rientjes, J.L. White, R. Bhave, B.I. Lee, Catalysis Letters 117 (2007) 102.
[1595] Z.W. Qu, G.J. Kroes, Journal of Physical Chemistry C 111 (2007) 16808.
[1596] S. Hamad, C.R.A. Catlow, S.M. Woodley, S. Lago, J.A. Mejias, Journal of Physical Chemistry B 109 (2005) 15741.
[1597] T. Albaret, F. Finocchi, C. Noguera, Applied Surface Science 145 (1999) 672.
[1598] Y. Shiraishi, M. Morishita, T. Hirai, Chemical Communications (2005) 5977.
[1599] F. Amano, T. Yamaguchi, T. Tanaka, Journal of Physical Chemistry B 110 (2006) 281.
[1600] L. Yuliati, H. Itoh, H. Yoshida, Studies in Surface Science and Catalysis 172 (2007) 457.
[1601] H. Yamashita, S. Nishio, I. Katayama, N. Nishiyama, H. Fujii, Catalysis Today 111 (2006) 254.
[1602] H. Yamashita, M. Honda, M. Harada, Y. Ichihashi, M. Anpo, T. Hirao, N. Itoh, N. Iwamoto, Journal of Physical Chemistry B 102 (1998) 10707.
[1603] H. Yamashita, S. Kawasaki, Y. Ichihashi, M. Harada, M. Takeuchi, M. Anpo, G. Stewart, M.A. Fox, C. Louis, M. Che, Journal of Physical Chemistry B 102 (1998) 5870.
[1604] Y. Shioya, K. Ikeue, M. Ogawa, M. Anpo, Applied Catalysis A: General 254 (2003) 251.
[1605] S. Dohshi, M. Takeuchi, M. Anpo, Catalysis Today 85 (2003) 199.
[1606] T. Tanaka, K. Teramura, T. Yamamoto, S. Takenaka, S. Yoshida, T. Funabiki, Journal of Photochemistry and Photobiology A 148 (2002) 277.
[1607] T. Ban, S. Kondoh, Y. Ohya, Y. Takahashi, Physical Chemistry Chemical Physics 1 (1999) 5745.
[1608] J. Klaas, G. Schulzekloff, N.I. Jaeger, Journal of Physical Chemistry B 101 (1997) 1305.
[1609] M.S. Hamdy, O. Berg, J.C. Jansen, T. Maschmeyer, J.A. Moulijn, G. Mul, Chemistry—a European Journal 12 (2005) 620.
[1610] S. Zheng, L. Gao, Q.H. Zhang, W.P. Zhang, J.K. Guo, Journal of Materials Chemistry 11 (2001) 578.
[1611] S. Zheng, L.A. Gao, Q.H. Zhang, J.K. Guo, Journal of Materials Chemistry 10 (2000) 723.
[1612] A. Orlov, Q.Z. Zhai, J. Klinowski, Journal of Materials Science 41 (2006) 2187.
[1613] M. Morishita, Y. Shiraishi, T. Hirai, Journal of Physical Chemistry B 110 (2006) 17898.
[1614] Y. Shiraishi, N. Saito, T. Hirai, Journal of the American Chemical Society 127 (2005) 8304.
[1615] M. Anpo, J.M. Thomas, Chemical Communications (2006) 3273.
[1616] K. Ikeue, H. Yamashita, M. Anpo, Electrochemistry 70 (2002) 402.
[1617] K. Ikeue, H. Yamashita, T. Takewaki, M.E. Davis, M. Anpo, Journal of Synchrotron Radiation 8 (2001) 602.
[1618] K. Ikeue, H. Mukai, H. Yamashita, S. Inagaki, M. Matsuoka, M. Anpo, Journal of Synchrotron Radiation 8 (2001) 640.
[1619] K. Ikeue, S. Nozaki, M. Ogawa, M. Anpo, Catalysis Today 74 (2002) 241.
[1620] H. Yamashita, Y. Fujii, Y. Ichihashi, S.G. Zhang, K. Ikeue, D.R. Park, K. Koyano, T. Tatsumi, M. Anpo, Catalysis Today 45 (1998) 221.
[1621] M. Anpo, H. Yamashita, K. Ikeue, Y. Fujii, S.G. Zhang, Y. Ichihashi, D.R. Park, Y. Suzuki, K. Koyano, T. Tatsumi, Catalysis Today 44 (1998) 327.
[1622] H. Yamashita, K. Ikeue, T. Takewaki, M. Anpo, Topics in Catalysis 18 (2002) 95.
[1623] Y. Hu, G. Martra, J.L. Zhang, S. Higashimoto, S. Coluccia, M. Anpo, Journal of Physical Chemistry B 110 (2006) 1680.
[1624] J.L. Zhang, M. Matsuoka, H. Yamashita, M. Anpo, Journal of Synchrotron Radiation 8 (2001) 637.
[1625] H. Yamashita, Y. Ichihashi, S.G. Zhang, Y. Matsumura, Y. Souma, T. Tatsumi, M. Anpo, Applied Surface Science 121 (1997) 305.
[1626] A.S. Barnard, S. Erdin, Y. Lin, P. Zapol, J.W. Halley, Physical Review B 73 (2006) 205405.
[1627] H.G. Yang, C.H. Sun, S.Z. Qiao, J. Zou, G. Liu, S.C. Smith, H.M. Cheng, G.Q. Lu, Nature 453 (2008) 638.
[1628] Y. Alivov, Z.Y. Fan, Journal of Physical Chemistry C 113 (2009) 12954.
[1629] J.Y. Kim, S.B. Choi, D.W. Kim, S. Lee, H.S. Jung, J.-K. Lee, K.S. Hong, Langmuir 24 (2008) 4316.
[1630] D.L. Liao, B.Q. Liao, Journal of Photochemistry and Photobiology A 187 (2007) 363.
[1631] S.W. Yang, L. Gao, Journal of the American Ceramic Society 88 (2005) 968.
[1632] N. Balazs, K. Mogyorosi, D.F. Sranko, A. Pallagi, T. Alapi, A. Oszko, A. Dombi, P. Sipos, Applied Catalysis B 84 (2008) 365.
[1633] C.H. Cho, M.H. Han, D.H. Kim, D.K. Kim, Materials Chemistry and Physics 92 (2005) 104.
[1634] C.B. Almquist, P. Biswas, Journal of Catalysis 212 (2002) 145.
[1635] N.Q. Wu, J. Wang, D. Tafen, H. Wang, J.G. Zheng, J.P. Lewis, X.G. Liu, S.S. Leonard, A. Manivannan, Journal of American Chemical Society 132 (2010) 6679.
[1636] H. Zhang, B. Chen, J.F. Banfield, Physical Chemistry Chemical Physics 11 (2009) 2553.
[1637] V. Swamy, D. Menzies, B.C. Muddle, A. Kuznetsov, L.S. Dubrovinsky, Q. Dai, V. Dmitriev, Applied Physics Letters 88 (2006) 243103.
[1638] K.Y. Jung, S. Bin park, S.K. Ihm, Applied Catalysis A 224 (2002) 229.
[1639] V. Cohen-Yaniv, N. Narkis, R. Armon, Water Science and Technology 58 (2008) 247.
[1640] I. Arslan, I.A. Balcioglu, D.W. Bahnemann, Water Science and Technology 44 (2001) 171.
[1641] D. Gumy, A.G. Rincon, R. Hajdu, C. Pulgarin, Solar Energy 80 (2006) 1376.
[1642] W.S. Kuo, Journal of Environmental Science and Health Part A 35 (2000) 419.
[1643] A. Rachel, M. Subrahmanyam, P. Boule, Applied Catalysis B 37 (2002) 301.
[1644] A.D. Modestov, O. Lev, Journal of Photochemistry and Photobiology A 112 (1998) 261.
[1645] S. Parra, S.E. Stanca, I. Guasaquillo, K.R. Thampi, Applied Catalysis B 51 (2004) 107.
[1646] T.A. Egerton, I.R. Tooley, Journal of Physical Chemistry B 108 (2004) 5066.
[1647] S.U. Geissen, W. Xi, A. Weidemeyer, A. Vogelpohl, L. Bousselmi, A. Ghrabi, A. Ennabll, Water Science and Technology 44 (2001) 245.
[1648] D.S. Kim, S.J. Han, S.-Y. Kwak, Journal of Colloid and Interface Science 316 (2007) 85.
[1649] D.S. Kim, S.-Y. Kwak, Applied Catalysis A 323 (2007) 110.
[1650] M.A. Carreon, S.Y. Choi, M. Mamak, N. Chopra, G.A. Ozin, Journal of Materials Chemistry 17 (2007) 82.
[1651] A. Ghicov, P. Schmuki, Chemical Communications (2009) 2791.
[1652] M. Paulose, K. Shankar, S. Yoriya, H.E. Prakasam, O.K. Varghese, G.K. Mor, T.A. Latempa, A. Fitzgerald, C.A. Grimes, Journal of Physical Chemistry B 110 (2006) 16179.
[1653] A. Tsujiko, T. Kisumi, Y. Magari, K. Murakoshi, Y. Nakato, Journal of Physical Chemistry B 104 (2000) 4873.
[1654] T. Kisumi, A. Tsujiko, K. Murakoshi, Y. Nakato, Journal of Electroanalytical Chemistry 545 (2003) 99.
[1655] B.J. Morgan, G.W. Watson, Surface Science 601 (2007) 5034.
[1656] J.C. Woicik, E.J. Nelson, L. Kronik, M. Jain, J.R. Chelikowsky, D. Heskett, L.E. Berman, G.S. Herman, Physical Review Letters 89 (2002) 077401.
[1657] L.D. Finkelstein, E.Z. Kurmaev, M.A. Korotin, A. Moewes, B. Schneider, S.M. Butorin, J.H. Guo, J. Nordgren, D. Hartmann, M. Neumann, D.L. Ederer, Physical Review B 60 (1999) 2212.
[1658] A.T. Paxton, L. Thien-Nga, Physical Review B 57 (1998) 1579.
[1659] M.M. Islam, T. Bredow, A. Gerson, Physical Review B 76 (2007) 045217.
[1660] P.M. Kowalski, B. Meyer, D. Marx, Physical Review B 79 (2009) 115410.
[1661] A.G. Thomas, W.R. Flavell, A.R. Kumarasinghe, A.K. Mallick, D. Tsoutsou, G.C. Smith, R. Stockbauer, S. Patel, M. Grätzel, R. Hengerer, Physical Review B 67 (2003) 035110.
[1662] J. Nerlov, Q.F. Ge, P.J. Moller, Surface Science 348 (1996) 28.
[1663] K.C. Prince, V.R. Dhanak, P. Finetti, J.F. Walsh, R. Davis, C.A. Muryn, H.S. Dhariwal, G. Thornton, G. vanderLaan, Physical Review B 55 (1997) 9520.
[1664] R. Heise, R. Courths, S. Witzel, Solid State Communications 84 (1992) 599.
[1665] Z.M. Zhang, S.P. Jeng, V.E. Henrich, Physical Review B 43 (1991) 12004.
[1666] V.S. Lusvardi, M.A. Barteau, J.G. Chen, J. Eng Jr., B. Fruhberger, A. Teplyakov, Surface Science 397 (1998) 237.
[1667] J. Purton, D.W. Bullett, P.M. Oliver, S.C. Parker, Surface Science 336 (1995) 166.
[1668] H. Perron, C. Domain, J. Roques, R. Drot, E. Simoni, H. Catalette, Theoretical Chemistry Accounts 117 (2007) 565.
[1669] P.J. Møller, S.A. Komolov, E.F. Lazneva, Journal of Physics-Condensed Matter 12 (2000) 7705.
[1670] R. Brydson, B.G. Williams, W. Engel, H. Sauer, E. Zeitler, J.M. Thomas, Solid State Communications 64 (1987) 609.
[1671] A.K. See, R.A. Bartynski, Journal of Vacuum Science & Technology A 10 (1992) 2591.
[1672] A.K. See, M. Thayer, R.A. Bartynski, Physical Review B 47 (1993) 13722.
[1673] J.W. Bullard, M.J. Cima, Langmuir 22 (2006) 10264.
[1674] R. Nakamura, N. Ohashi, A. Imanishi, T. Osawa, Y. Matsumoto, H. Koinuma, Y. Nakato, Journal of Physical Chemistry B 109 (2005) 1648.
[1675] A. Imanishi, E. Tsuji, Y. Nakato, Journal of Physical Chemistry C 111 (2007) 2128.
[1676] W. Hebenstreit, N. Ruzycki, G.S. Herman, Y. Gao, U. Diebold, Physical Review B 62 (2000) R16334.
[1677] Y. He, O. Dulub, H. Cheng, A. Selloni, U. Diebold, Physical Review Letters 102 (2009) 106105.
[1678] A. Sasahara, T.C. Droubay, S.A. Chambers, H. Uetsuka, H. Onishi, Nanotechnology 16 (2005) S18.
[1679] A. Sandell, B. Sanyal, L.E. Walle, J.H. Richter, S. Plogmaker, P.G. Karlsson, A. Borg, P. Uvdal, Physical Review B 78 (2008) 075113.
[1680] R. Hengerer, L. Kavan, P. Krtil, M. Grätzel, Journal of the Electrochemical Society 147 (2000) 1467.
[1681] J. Blomquist, L.E. Walle, P. Uvdal, A. Borg, A. Sandell, Journal of Physical Chemistry C 112 (2008) 16616.
[1682] X.Q. Gong, A. Selloni, Journal of Catalysis 249 (2007) 134.
[1683] G.S. Herman, Z. Dohnálek, N. Ruzycki, U. Diebold, Journal of Physical Chemistry B 107 (2003) 2788.
[1684] G. Mattioli, F. Filippone, R. Caminiti, A.A. Bonapasta, Journal of Physical Chemistry C 112 (2008) 13579.
[1685] K.J. Hameeuw, G. Cantele, D. Ninno, F. Trani, G. Iadonisi, Journal of Chemical Physics 124 (2006) 024708.
[1686] A. Kiejna, T. Pabisiak, S.W. Gao, Journal of Physics-Condensed Matter 18 (2006) 4207.
[1687] S.J. Thompson, S.P. Lewis, Physical Review B 73 (2006) 073403.
[1688] A. Verdini, M. Sambi, F. Bruno, D. Cvetko, M.D. Negra, R. Gotter, L. Floreano, A. Morgante, G.A. Rizzi, G. Granozzi, Surface Review Letters 6 (1999) 1201.
[1689] X.-G. Ma, C.-Q. Tang, X.-H. Yang, Surface Review and Letters 13 (2006) 825.
[1690] S.P. Bates, G. Kresse, M.J. Gillan, Surface Science 385 (1997) 386.
[1691] M. Calatayud, C. Minot, Surface Science 552 (2004) 169.
[1692] T. Bredow, G. Pacchioni, Chemical Physics Letters 355 (2002) 417.
[1693] C.J. Calzado, N.C. Hernandez, J.F. Sanz, Physical Review B 77 (2008) 045118.

[1694] K. Hameeuw, G. Cantele, D. Ninno, F. Trani, G. Iadonisi, Physica Status Solidi A 203 (2006) 2219.
[1695] P.J.D. Lindan, N.M. Harrison, M.J. Gillan, J.A. White, Physical Review B 55 (1997) 15919.
[1696] W.C. Mackrodt, E.A. Simson, N.M. Harrison, Surface Science 384 (1997) 192.
[1697] M. Nolan, S.D. Elliott, J.S. Mulley, R.A. Bennett, M. Basham, P. Mulheran, Physical Review B 77 (2008) 235424.
[1698] J. Oviedo, M.A. San miguel, J.F. Sanz, Journal of Chemical Physics 121 (2004) 7427.
[1699] T. Pabisiak, A. Kiejna, Solid State Communications 144 (2007) 324.
[1700] M. Ramamoorthy, R.D. Kingsmith, D. Vanderbilt, Physical Review B 49 (1994) 7709.
[1701] G.U. Von Oertzen, A.R. Gerson, International Journal of Quantum Chemistry 106 (2006) 2054.
[1702] S.-G. Wang, X.-D. Wen, D.-B. Cao, Y.-W. Li, J. Wang, H. Jiao, Surface Science 577 (2005) 69.
[1703] S. Kodaira, Y. Sakisaka, T. Maruyama, Y. Haruyama, Y. Aiura, H. Kato, Solid State Communications 89 (1994) 9.
[1704] P. Kruger, S. Bourgeois, B. Domenichini, H. Magnan, D. Chandesris, P. Le Fevre, A.M. Flank, J. Jupille, L. Floreano, A. Cossaro, A. Verdini, A. Morgante, Physical Review Letters 100 (2008) 055501.
[1705] O. Dulub, C. Di Valentin, A. Selloni, U. Diebold, Surface Science 600 (2006) 4407.
[1706] X.-Q. Gong, N. Khorshidi, A. Stierle, V. Vonk, C. Ellinger, H. Dosch, H. Cheng, A. Selloni, Y. He, O. Dulub, U. Diebold, Surface Science 603 (2009) 138.
[1707] T.J. Beck, A. Klust, M. Batzill, U. Diebold, C.Di. Valentin, A. Selloni, Physical Review Letters 93 (2004) 036104.
[1708] H. Cheng, A. Selloni, Journal of Chemical Physics 131 (2009) 054703.
[1709] S.-C. Li, O. Dulub, U. Diebold, Journal of Physical Chemistry C 112 (2008) 16166.
[1710] M. Batzill, K. Katsiev, D.J. Gaspar, U. Diebold, Physical Review B 66 (2002) 235401.
[1711] X.-Q. Gong, A. Selloni, M. Batzill, U. Diebold, Nature Materials 5 (2006) 665.
[1712] C. Di Valentin, A. Tilocca, A. Selloni, T.J. Beck, A. Klust, M. Batzill, Y. Losovyj, U. Diebold, Journal of the American Chemical Society 127 (2005) 9895.
[1713] C.D. Lane, N.G. Petrik, T.M. Orlando, G.A. Kimmel, Journal of Physical Chemistry C 111 (2007) 16319.
[1714] G. Ketteler, S. Yamamoto, H. Bluhm, K. Andersson, D.E. Starr, D.F. Ogletree, H. Ogasawara, A. Nilsson, M. Salmeron, Journal of Physical Chemistry C 111 (2007) 8278.
[1715] R.L. Kurtz, R. Stockbauer, T.E. Madey, E. Roman, J.L. Desegovia, Surface Science 218 (1989) 178.
[1716] S.-C. Li, Z. Zhang, D. Sheppard, B.D. Kay, J.M. White, Y. Du, I. Lyubinetsky, G. Henkelman, Z. Dohnálek, Journal of the American Chemical Society 130 (2008) 9080.
[1717] B. Hammer, S. Wendt, F. Besenbacher, Topics in Catalysis 53 (2010) 423.
[1718] A. Valdes, Z.W. Qu, G.J. Kroes, J. Rossmeisl, J.K. Norskov, Journal of Physical Chemistry C 112 (2008) 9872.
[1719] P.J.D. Lindan, C.J. Zhang, Physical Review B 72 (2005) 075439.
[1720] R. Nakamura, Y. Nakato, Journal of the American Chemical Society 126 (2004) 1290.
[1721] H. Cheng, A. Selloni, Langmuir 26 (2010) 11518.
[1722] A. Valdes, G.J. Kroes, Journal of Physical Chemistry C 114 (2010) 1701.
[1723] Y.X. Li, G.X. Lu, S.B. Li, Chemosphere 52 (2003) 843.
[1724] C.L. Perkins, M.A. Henderson, unpublished results.
[1725] J.T. Yates Jr., Private communication.
[1726] P. Usubharatana, D. Mcmartin, A. Veawab, P. Tontiwachwuthikul, Industrial & Engineering Chemistry Research 45 (2006) 2558.
[1727] K. Koci, L. Obalova, Z. Lacny, Chemical Papers 62 (2008) 1.
[1728] J. Rasko, Catalysis Letters 56 (1998) 11.
[1729] F. Saladin, I. Alxneit, Journal of the Chemical Society Faraday Transactions 93 (1997) 4159.
[1730] M. Anpo, H. Yamashita, Y. Ichihashi, S. Ehara, Journal of Electroanalytical Chemistry 396 (1995) 21.
[1731] W.Y. Lin, H.X. Han, H. Frei, Journal of Physical Chemistry B 108 (2004) 18269.
[1732] N. Ulagappan, H. Frei, Journal of Physical Chemistry A 104 (2000) 7834.
[1733] Y. Ku, W.H. Lee, W.Y. Wang, Journal of Molecular Catalysis A 212 (2004) 191.
[1734] J.C.S. Wu, H.M. Lin, C.L. Lai, Applied Catalysis A 296 (2005) 194.
[1735] G. Guan, T. Kida, A. Yoshida, Applied Catalysis B 41 (2003) 387.
[1736] N. Sasirekha, S.J.S. Basha, K. Shanthi, Applied Catalysis B 62 (2006) 169.
[1737] A. Sclafani, L. Palmisano, G. Farneti, Chemical Communications (1997) 529.
[1738] I.H. Tseng, J.C.S. Wu, H.-Y. Chou, Journal of Catalysis 221 (2004) 432.
[1739] X.T. Wang, S.H. Zhong, X.F. Xiao, Journal of Molecular Catalysis A 229 (2005) 87.
[1740] T. Mizuno, K. Adachi, K. Ohta, A. Saji, Journal of Photochemistry and Photobiology A 98 (1996) 87.
[1741] S. Kaneco, H. Kurimoto, K. Ohta, T. Mizuno, A. Saji, Journal of Photochemistry and Photobiology A 109 (1997) 59.
[1742] Y. Kohno, H. Hayashi, S. Takenaka, T. Tanaka, T. Funabiki, S. Yoshida, Journal of Photochemistry and Photobiology A 126 (1999) 117.
[1743] G.R. Dey, A.D. Belapurkar, K. Kishore, Journal of Photochemistry and Photobiology A 163 (2004) 503.
[1744] C.-C. Lo, C.-H. Hung, C.-S. Yuan, J.-F. Wu, Solar Energy Materials and Solar Cells 91 (2007) 1765.
[1745] M. Subrahmanyam, S. Kaneco, N. Alonso-Vante, Applied Catalysis B 23 (1999) 169.
[1746] T. Tachikawa, S. Tojo, M. Fujitsuka, T. Majima, Langmuir 20 (2004) 9441.
[1747] P.C. Maness, S. Smolinski, D.M. Blake, Z. Huang, E.J. Wolfrum, W.A. Jacoby, Applied and Environmental Microbiology 65 (1999) 4094.
[1748] P. Amezaga-Madrid, R. Silveyra-Morales, L. Cordoba-Fierro, G.V. Nevarez-Moorillon, M. Miki-Yoshida, E. Orrantia-Borunda, F.J. Solis, Journal of Photochemistry and Photobiology B 70 (2003) 45.
[1749] M. Cho, H.M. Chung, W.Y. Choi, J.Y. Yoon, Applied and Environmental Microbiology 71 (2005) 270.
[1750] M. Cho, H. Chung, W. Choi, J. Yoon, Water Research 38 (2004) 1069.
[1751] S. Matsuo, Y. Anraku, S. Yamada, T. Honjo, T. Matsuo, H. Wakita, Journal of Environmental Science and Health A 36 (2001) 1419.
[1752] J.M. Coronado, J. Soria, J.C. Conesa, R. Bellod, C. Adan, H. Yamaoka, V. Loddo, V. Augugliaro, Topics in Catalysis 35 (2005) 279.
[1753] K. Sunada, T. Watanabe, K. Hashimoto, Journal of Photochemistry and Photobiology A 156 (2003) 227.
[1754] K. Sunada, T. Watanabe, K. Hashimoto, Environmental Science & Technology 37 (2003) 4785.
[1755] Z.X. Lu, L. Zhou, Z.L. Zhang, W.L. Shi, Z.X. Xie, H.Y. Xie, D.W. Pang, P. Shen, Langmuir 19 (2003) 8765.
[1756] L.A. Lawton, P.K.J. Robertson, B.J.P.A. Cornish, I.L. Marr, M. Jaspars, Journal of Catalysis 213 (2003) 109.
[1757] V. Keller, N. Keller, M.J. Ledoux, M.-C. Lett, Chemical Communications (2005) 2918.
[1758] T.A. Egerton, S.A.M. Kosa, P.A. Christensen, Physical Chemistry Chemical Physics 8 (2006) 398.
[1759] H.M. Coleman, C.P. Marquis, J.A. Scott, S.S. Chin, R. Amal, Chemical Engineering Journal 113 (2005) 55.
[1760] M. Bekbolet, Water Science and Technology 35 (1997) 95.
[1761] N. Kashige, Y. Kakita, Y. Nakashima, F. Miake, K. Watanabe, Current Microbiology 42 (2001) 184.
[1762] N.P. Huang, M.H. Xu, C.W. Yuan, R.R. Yu, Journal of Photochemistry and Photobiology A 108 (1997) 229.
[1763] D. Gumy, C. Morais, P. Bowen, C. Pulgarin, S. Giraldo, R. Hajdu, J. Kiwi, Applied Catalysis B 63 (2006) 76.
[1764] G. Rajagopal, S. Maruthamuthu, S. Mohanan, N. Palaniswamy, Colloids and Surfaces B 51 (2006) 107.
[1765] A.-G. Rincon, C. Pulgarin, Applied Catalysis B 49 (2004) 99.
[1766] A.-G. Rincon, C. Pulgarin, Applied Catalysis B 51 (2004) 283.
[1767] A.G. Rincon, C. Pulgarin, N. Adler, P. Peringer, Journal of Photochemistry and Photobiology A 139 (2001) 233.
[1768] C. Sichel, J. Blanco, S. Malato, P. Fernandez-Ibanez, Journal of Photochemistry and Photobiology A 189 (2007) 239.
[1769] M. Sokmen, F. Candan, Z. Sumer, Journal of Photochemistry and Photobiology A 143 (2001) 241.
[1770] J. Wist, J. Sanabria, C. Dierolf, W. Torres, C. Pulgarin, Journal of Photochemistry and Photobiology A 147 (2002) 241.
[1771] M.S. Wong, W.C. Chu, D.S. Sun, H.S. Huang, J.H. Chen, P.J. Tsai, N.T. Lin, M.S. Yu, S.F. Hsu, S.L. Wang, H.H. Chang, Applied and Environmental Microbiology 72 (2006) 6111.
[1772] A. Vohra, D.Y. Goswami, D.A. Deshpande, S.S. Block, Applied Catalysis B 65 (2006) 57.
[1773] M.H. Xu, N.P. Huang, Z.D. Xiao, Z.H. Lu, Supramolecular Science 5 (1998) 449.
[1774] H. Zheng, P.C. Maness, D.M. Blake, E.J. Wolfrum, S.L. Smolinski, W.A. Jacoby, Journal of Photochemistry and Photobiology A 130 (2000) 163.
[1775] V.A. Nadtochenko, A.G. Rincon, S.E. Stanca, J. Kiwi, Journal of Photochemistry and Photobiology A 169 (2005) 131.
[1776] V. Nadtochenko, N. Denisov, O. Sarkisov, D. Gumy, C. Pulgarin, J. Kiwi, Journal of Photochemistry and Photobiology A 181 (2006) 401.
[1777] J. Kiwi, V. Nadtochenko, Journal of Physical Chemistry B 108 (2004) 17675.
[1778] J. Kiwi, V. Nadtochenko, Langmuir 21 (2005) 4631.
[1779] C.Y. Wang, H. Groenzin, M.J. Shultz, Langmuir 19 (2003) 7330.
[1780] T. Zubkov, D. Stahl, T.L. Thompson, D. Panayotov, O. Diwald, J.T. Yates Jr., Journal of Physical Chemistry B 109 (2005) 15454.
[1781] M. Takeuchi, K. Sakamoto, G. Martra, S. Coluccia, M. Anpo, Journal of Physical Chemistry B 109 (2005) 15422.
[1782] J.M. White, J. Szanyi, M.A. Henderson, Journal of Physical Chemistry B 107 (2003) 9029.
[1783] M. Miyauchi, A. Nakajima, A. Fujishima, K. Hashimoto, T. Watanabe, Chemistry of Materials 12 (2000) 3.
[1784] A. Nakajima, S. Koizumi, T. Watanabe, K. Hashimoto, Journal of Photochemistry and Photobiology A 146 (2001) 129.
[1785] A. Nakajima, S. Koizumi, T. Watanabe, K. Hashimoto, Langmuir 16 (2000) 7048.
[1786] R. Wang, N. Sakai, A. Fujishima, T. Watanabe, K. Hashimoto, Journal of Physical Chemistry B 103 (1999) 2188.
[1787] R. Wang, K. Hashimoto, A. Fujishima, M. Chikuni, E. Kojima, A. Kitamura, M. Shimohigoshi, T. Watanabe, Nature 388 (1997) 431.
[1788] T. Watanabe, A. Nakajima, R. Wang, M. Minabe, S. Koizumi, A. Fujishima, K. Hashimoto, Thin Solid Films 351 (1999) 260.

[1789] R. Wang, K. Hashimoto, A. Fujishima, M. Chikuni, E. Kojima, A. Kitamura, M. Shimohigoshi, T. Watanabe, Advanced Materials 10 (1998) 135.
[1790] K.R. Denison, C. Boxall, Langmuir 23 (2007) 4358.
[1791] A.Y. Nosaka, E. Kojima, T. Fujiwara, H. Yagi, H. Akutsu, Y. Nosaka, Journal of Physical Chemistry B 107 (2003) 12042.
[1792] Z.Z. Gu, A. Fujishima, O. Sato, Applied Physics Letters 85 (2004) 5067.
[1793] A. Hattori, T. Kawahara, T. Uemoto, F. Suzuki, H. Tada, S. Ito, Journal of Colloid and Interface Science 232 (2000) 410.
[1794] R.D. Sun, A. Nakajima, A. Fujishima, T. Watanabe, K. Hashimoto, Journal of Physical Chemistry B 105 (2001) 1984.
[1795] N. Sakai, A. Fujishima, T. Watanabe, K. Hashimoto, Journal of Physical Chemistry B 105 (2001) 3023.
[1796] N. Sakai, A. Fujishima, T. Watanabe, K. Hashimoto, Journal of Physical Chemistry B 107 (2003) 1028.
[1797] T. Shibata, H. Irie, K. Hashimoto, Journal of Physical Chemistry B 107 (2003) 10696.
[1798] K. Seki, M. Tachiya, Journal of Physical Chemistry B 108 (2004) 4806.
[1799] N. Sakai, K. Fukuda, T. Shibata, Y. Ebina, K. Takada, T. Sasaki, Journal of Physical Chemistry B 110 (2006) 6198.
[1800] N. Sakai, R. Wang, A. Fujishima, T. Watanabe, K. Hashimoto, Langmuir 14 (1998) 5918.
[1801] A. Nakajima, K. Hashimoto, T. Watanabe, K. Takai, G. Yamauchi, A. Fujishima, Langmuir 16 (2000) 7044.
[1802] H.Y. Lee, Y.H. Park, K.H. Ko, Langmuir 16 (2000) 7289.
[1803] N. Stevens, C.I. Priest, R. Sedev, J. Ralston, Langmuir 19 (2003) 3272.
[1804] Y.F. Gao, Y. Masuda, K. Koumoto, Langmuir 20 (2004) 3188.
[1805] A. Kanta, R. Sedev, J. Ralston, Langmuir 21 (2005) 2400.
[1806] X.T. Zhang, M. Jin, Z.Y. Liu, S. Nishimoto, H. Saito, T. Murakami, A. Fujishima, Langmuir 22 (2006) 9477.
[1807] S. Yamamoto, S. Nagata, A. Takayama, M. Yoshikawa, Nuclear Instruments & Methods in Physics Research B 249 (2006) 374.
[1808] M. Miyauchi, N. Kieda, S. Hishita, T. Mitsuhashi, A. Nakajima, T. Watanabe, K. Hashimoto, Surface Science 511 (2002) 401.
[1809] L. Sirghi, Y. Hatanaka, Surface Science 530 (2003) L323.
[1810] K. Katsumata, A. Nakajima, H. Yoshikawa, T. Shiota, N. Yoshida, T. Watanabe, Y. Kameshima, K. Okada, Surface Science 579 (2005) 123.
[1811] S. Kataoka, M.A. Anderson, Thin Solid Films 446 (2004) 232.
[1812] H. Irie, S. Washizuka, K. Hashimoto, Thin Solid Films 510 (2006) 21.
[1813] S. Dohshi, M. Anpo, S. Okuda, T. Kojima, Topics in Catalysis 35 (2005) 327.
[1814] G. Hyett, M. Green, I.P. Parkin, Journal of the American Chemical Society 128 (2006) 12147.
[1815] Z.Y. Jiang, C.Q. Lu, H. Wu, Industrial & Engineering Chemistry Research 44 (2005) 4165.
[1816] B. Pal, S. Ikeda, H. Kominami, Y. Kera, B. Ohtani, Journal of Catalysis 217 (2003) 152.
[1817] S.D. Senanayake, H. Idriss, Proceedings of the National Academy of Sciences 103 (2006) 1194.
[1818] A. Maldotti, R. Amadelli, L. Samiolo, A. Molinari, A. Penoni, S. Tollari, S. Cenini, Chemical Communications (2005) 1749.
[1819] M.V.B. Zanoni, J.J. Sene, H. Selcuk, M.A. Anderson, Environmental Science & Technology 38 (2004) 3203.
[1820] C.C. Wang, C.C. Chen, Applied Catalysis A 293 (2005) 171.
[1821] C.C. Chen, C.C. Wang, Journal of Sol-Gel Science and Technology 40 (2006) 31.
[1822] H. Yoshida, C. Murata, T. Hattori, Chemical Communications 1999 (1551) 1552.
[1823] T. Ohno, K. Nakabeya, M. Matsumura, Journal of Catalysis 176 (1998) 76.
[1824] X.Y. Li, C. Kutal, Journal of Materials Science Letters 21 (2002) 1525.
[1825] S. Higashida, A. Harada, R. Kawakatsu, N. Fujiwara, M. Matsumura, Chemical Communications (2006) 2804.
[1826] K.V.S. Rao, B. Srinivas, P. Boule, M. Subrahmanyam, Journal of Chemical Technology and Biotechnology 77 (2002) 568.
[1827] G. Palmisano, E. Garcia-Lopez, G. Marci, V. Loddo, S. Yurdakal, V. Augugliaro, L. Palmisano, Chemical Communications 46 (2010) 7074.
[1828] M.E. Monge, C. George, B. D'Anna, J.F. Doussin, A. Jammoul, J. Wang, G. Eyglunent, G. Solignac, V. Daele, A. Mellouki, Journal of the American Chemical Society 132 (2010) 8234.
[1829] R. Cai, Y. Kubota, A. Fujishima, Journal of Catalysis 219 (2003) 214.
[1830] A.V. Bandura, J.D. Kubicki, Journal of Physical Chemistry B 107 (2003) 11072.
[1831] D. Vione, V. Maurino, C. Minero, M. Vincenti, E. Pelizzetti, Chemosphere 44 (2001) 237.
[1832] D. Vione, V. Maurino, C. Minero, E. Pelizzetti, Chemosphere 45 (2001) 903.
[1833] C. Damm, D. Voltzke, H.P. Abicht, G. Israel, Journal of Photochemistry and Photobiology A 174 (2005) 171.
[1834] X.Y. Ni, J. Ye, C. Dong, Journal of Photochemistry and Photobiology A 181 (2006) 19.
[1835] C. Damm, Journal of Photochemistry and Photobiology A 181 (2006) 297.
[1836] D. Yang, X. Ni, W. Chen, Z. Weng, Journal of Photochemistry and Photobiology A 195 (2008) 323.
[1837] S. Kuwabata, H. Yamauchi, H. Yoneyama, Langmuir 14 (1998) 1899.
[1838] D.G. Shchukin, H. Mohwald, Langmuir 21 (2005) 5582.
[1839] Y. Kato, N. Matsushita, H. Yoshida, T. Hattori, Catalysis Communications 3 (2002) 99.
[1840] T. Caronna, C. Gambarotti, L. Palmisano, C. Punta, F. Recupero, Chemical Communications (2003) 2350.
[1841] L. Cermenati, C. Richter, A. Albini, Chemical Communications (1998) 805.
[1842] B.M. Reddy, I. Ganesh, A. Khan, Journal of Molecular Catalysis A 223 (2004) 295.
[1843] R.R. Kuntz, Journal of Photochemistry and Photobiology A 108 (1997) 215.
[1844] K. Schoumacher, C. Geantet, M. Lacroix, E. Puzenat, C. Guillard, J.M. Herrmann, Journal of Photochemistry and Photobiology A 152 (2002) 147.
[1845] S. Ghosh-Mukerji, H. Haick, M. Schvartzman, Y. Paz, Journal of the American Chemical Society 123 (2001) 10776.
[1846] S. Gershuni, N. Itzhak, J. Rabani, Langmuir 15 (1999) 1141.
[1847] T. Ohno, Y. Masaki, S. Hirayama, M. Matsumura, Journal of Catalysis 204 (2001) 163.